

Diss. ETH No. 18912

Coherent Cooperative Relaying in Low Mobility Wireless Multiuser Networks

A dissertation submitted to the
ETH ZURICH

for the degree of
Doctor of Sciences (Dr. sc. ETH Zürich)

presented by
STEFAN BERGER
Dipl.-Ing., Technische Universität München
born June 22, 1978
citizen of Germany

accepted on the recommendation of
Prof. Dr.-Ing. A. Wittneben, examiner
Prof. Dr.-Ing. A. Klein, co-examiner

2010

Abstract

In this thesis, several important aspects of cooperative wireless multiuser networks are investigated. These include *hardware imperfections*, *channel estimation*, *distributed phase synchronization*, *gain allocation*, and *practical demonstration*. The focus lies on coherent two-hop relaying networks where several amplify-and-forward (AF) relays assist the communication between multiple source-destination pairs. In these type of networks the signals from all relays are to add up coherently at the destination antennas. By choosing the gain factors in a smart way, a *spatial multiplexing gain*, *distributed diversity gain* and an *antenna gain* can thus be achieved. This allows multiple source-destination pairs to efficiently communicate concurrently on the same physical channel.

Hardware imperfections obviously degrade the overall system performance. In this work, impairments of the radio frequency (RF) hardware that are have a special impact on AF relaying networks are identified and investigated. Specifically, *local oscillator (LO) frequency offsets*, *LO phase noise*, and *I/Q imbalance* at the relays are discussed. A special focus lies on the comparison between frequency division duplexing (FDD) and time division duplexing (TDD) relays because it turns out that they are affected differently by the LO imperfections. Important design guidelines for the implementation of a practical cooperative network employing either type of relays are derived.

For coherent relaying schemes the gain factors have to be computed from instantaneous channel state information (CSI) that takes the current phases of the channel coefficients into account. If this type of information is not available or outdated, the unknown phase shifts due to the propagation delays prevent the signals from the relays to add up coherently at the destination antennas. Another important mechanism that may destroy coherency is that the LO phases of the nodes introduce phase shifts to the channel estimates. This leads to the key observation that the direction in which a channel between two wireless nodes is measured has an impact on the estimate if the nodes are not phase synchronous. Based on this insight, phase synchronization requirements for coherent relaying networks are found. Several channel estimation protocols are then identified that differ in the direction in which the individual point-to-point channels in a wireless two-hop network are measured. They are

investigated regarding the effort required to measure all channel coefficients and the quality of the estimates in the presence of additive noise and phase noise.

The analysis of the phase synchronization requirements reveals that in some cases a global phase reference is required for a certain set of nodes in order to allow for coherent forwarding. A very simple phase synchronization scheme is presented that provides a set of relays with a common LO phase. It is compared in detail to a similar scheme found in literature. Furthermore, the phase error resulting from imperfect synchronization due to additive noise and phase noise is characterized.

Two coherent beamforming schemes, namely multiuser zero-forcing (MUZF) and multiuser minimum mean squared error (MMSE) relaying, are then presented. The gain factors are derived in the presence of unknown and random LO phase offsets at all nodes. While inter-user interference is completely suppressed for MUZF, the multiuser MMSE relaying scheme minimizes the MMSE of the received symbols at all destinations. Both schemes exhibit a distributed spatial multiplexing gain by allowing multiple source-destination pairs to communicate concurrently on the same physical channel. The impact of *noisy CSI*, *phase noise*, and *phase synchronization errors* at the relays on the performance of both relaying schemes is also discussed.

Finally, a real-world demonstrator for distributed wireless communication networks, that is called RACoon Lab and is available at the Wireless Communications Group at ETH Zurich, is introduced. It was used to implement MUZF relaying on a practical two-hop relaying network with two source-destination pairs and three relays. The performance results show that even in the presence of hardware imperfections encountered in any practical system (e.g. additive noise, phase noise, interference, frequency offsets, etc.), a promising inter-user interference rejection capability can be observed.

Kurzfassung

In dieser Arbeit werden verschiedene wichtige Aspekte von kooperativen, drahtlosen Mehrnutzer-Netzwerken untersucht. Betrachtet werden *Hardware-Imperfektionen*, die *Kanalmessung*, *Phasensynchronisierung* von verteilten Knoten, die *Berechnung von komplexwertigen Verstärkungsfaktoren der Relays* sowie ein praktischer *Demonstrator*. Der Fokus liegt bei kohärenten zwei-Hop Netzwerken bei denen so genannte „amplify-and-forward (AF)“ Relays die Kommunikation zwischen mehreren Sendern und Empfängern unterstützen. Bei dieser Art von Relays werden die Empfangssignale linear gefiltert aber nicht dekodiert bevor sie weitergesendet werden. Charakteristisch für die untersuchten Netzwerke ist, dass sich die Signale der Relays kohärent an den Antennen der Empfänger überlagern. Indem die komplexwertigen Verstärkungsfaktoren geschickt gewählt werden, können eine *räumliche Mehrfachnutzung des Kanals*, sowie ein *verteilter Diversitäts- und Antennengewinn* erzielt werden. Das erlaubt mehreren Nutzern effektiv auf demselben physikalischen Kanal zu kommunizieren.

Hardware-Imperfektionen vermindern die Leistungsfähigkeit des gesamten Netzwerkes. In dieser Arbeit werden Imperfektionen in der Hochfrequenz (HF)-Hardware betrachtet, die einen speziellen Einfluss auf Netzwerke mit AF-Relays besitzen. Im Speziellen werden *Frequenzabweichungen der Lokaloszillatoren*, *Phasenrauschen* und *I/Q Ungleichgewicht* diskutiert. Besonderes Gewicht erhält dabei der Vergleich zwischen Frequenzduplex und Zeitduplex Relays, weil beide Arten unterschiedlich unter den betrachteten Imperfektionen der Lokaloszillatoren leiden. Es werden daraus wichtige Richtlinien für die Implementierung praktischer Systeme abgeleitet.

Die Verstärkungsfaktoren in verteilten Systemen, bei denen die Signale sich kohärent an den Empfängern überlagern sollen, müssen aus aktueller Kanalinformation berechnet werden. Das ist unerlässlich, damit die derzeitigen Phasen der Kanalkoeffizienten berücksichtigt werden. Sollte diese Art von Kanalschätzung nicht zur Verfügung stehen oder veraltet sein, werden die Phasendrehungen, die durch die unbekanntenen Ausbreitungswege der unterschiedlichen Signale entstehen, eine kohärente Überlagerung verhindern. Der Einfluss der Lokaloszillatorphasen auf die Kanalschätzungen ist ein weiterer, wichtiger Mechanismus,

der dies unmöglich machen kann. Das führt zu der Schlüsselbeobachtung, dass die Richtung der Kanalmessung zwischen zwei Knoten, die nicht phasensynchron sind, einen Einfluss auf die Schätzung besitzt. Basierend auf dieser Erkenntnis werden Anforderungen an die Phasensynchronisierung in verteilten Netzwerken erarbeitet. Des Weiteren werden mehrere Kanalschätzprotokolle untersucht, die sich durch die Richtung, in der die einzelnen Punkt-zu-Punkt Kanäle gemessen werden, unterscheiden. Sie werden bezüglich des benötigten Aufwandes und der Qualität ihrer Kanalschätzungen in Gegenwart von additivem Rauschen und Phasenrauschen verglichen.

Die Analyse der Anforderungen an die Phasensynchronisierung enthüllt, dass bestimmte Gruppen von Knoten in manchen Fällen eine gemeinsame Phasenreferenz benötigen, damit eine kohärente Überlagerung der Signale an den Empfängern möglich ist. Es wird ein sehr einfaches Verfahren vorgestellt, mit dem sich eine solche gemeinsame Phasenreferenz bei verteilten Relay-Knoten erreichen lässt. Ein Vergleich mit einem ähnlichen Verfahren aus der Literatur beleuchtet die jeweiligen Vor- und Nachteile. Des Weiteren wird der Phasenfehler durch fehlerbehaftete Phasensynchronisierung aufgrund von additivem Rauschen und Phasenrauschen charakterisiert.

Danach werden zwei Methoden zur Berechnung der Verstärkungsfaktoren an den Relays präsentiert. Diese heissen „multiuser zero-forcing (MUZF) relaying“ und „multiuser minimum mean squared error (MMSE) relaying“. Die Verstärkungsfaktoren werden unter Berücksichtigung unbekannter und zufälliger Lokalszillatorphasen hergeleitet. Während „MUZF relaying“ jegliche Interferenz zwischen den Nutzern unterdrückt, wird der minimale mittlere quadratische Fehler (MMSE) aller Empfangssignale bei „MMSE relaying“ minimiert. Beide Verfahren erlauben eine effektive räumliche Mehrfachnutzung des Kanals für alle Nutzer. Des Weiteren wird der Einfluss von *verrauschter Kanalinformation*, *Phasenrauschen* und *Phasensynchronisierungsfehler* auf die Leistungsfähigkeit beider Methoden untersucht.

Schliesslich wird noch eine praktische Messeinrichtung, das so gennante „RACooN Lab“, vorgestellt. Es befindet sich am Institut für Kommunikationstechnik an der ETH Zürich und eignet sich als Demonstrator für verteilte, drahtlose Kommunikationsnetze. Das RACooN Lab wurde verwendet, um „MUZF relaying“ in einem realen zwei-Hop Netzwerk mit zwei Sender-Empfänger-Pärchen und drei Relays zu implementieren. Die Messergebnisse zeigen, dass bei realen Ausbreitungskanälen und selbst in Gegenwart von praktischen Hardware-Imperfektionen, wie z.B. additivem Rauschen, Phasenrauschen, Interferenz und Frequenzfehlern, eine vielversprechende Unterdrückung der Mehrnutzerinterferenz beobachtet werden kann.

Contents

Abstract	i
Kurzfassung	iii
1 Introduction	1
1.1 Relaying Schemes	4
1.1.1 Distributed Space-Time Codes	6
1.1.2 Relay Selection	7
1.1.3 Beamforming	10
1.1.4 Two-Way Relaying	12
1.2 Capacity Scaling	13
1.3 Diversity-Multiplexing Tradeoff	15
1.4 Hardware Imperfections	15
1.5 Real-World Demonstrators	16
1.6 Contribution and Outline	18
2 System Model	23
2.1 System Topology	24
2.2 Channel Model	25
2.3 Local Oscillator Phases and Equivalent Channels	26
2.4 Traffic Patterns and Input/Output Relation	27
2.5 Reference Scenario and Definition of the SNR	31
2.6 Average Sum Rate	31
3 Implementation Issues	33
3.1 Relay Block Diagram	34
3.2 LO Imperfections	36
3.2.1 LO Frequency Offset	36
3.2.1.1 Sampling Time Offset	36

3.2.1.2	Carrier Frequency Offset	37
3.2.1.3	Timing Error	37
3.2.2	Phase Noise	40
3.2.3	Impact on AF Relaying	43
3.2.3.1	Frequency and Phase Error	43
3.2.3.2	Comparison Between FDD and TDD Relays	46
3.2.3.3	Network Synchronization Error	51
3.3	I/Q Imbalance	57
3.3.1	Transmitter Imbalance	59
3.3.2	Receiver Imbalance	61
3.3.3	Equivalent Baseband System Model	62
3.3.4	Impact on Signal Quality	65
3.3.4.1	Signal Power	66
3.3.4.2	Interference Power	69
3.3.4.3	Noise Power	73
4	Channel Estimation	81
4.1	Channel Estimation and Dissemination	82
4.2	Coherent Distributed Beamforming	84
4.2.1	Single-User System	85
4.2.2	Multi-User System	87
4.2.3	Required Phase Synchronization for $S \rightarrow D / S \rightarrow R / R \rightarrow D$	90
4.2.4	Required Phase Synchronization for $S \rightarrow D / S \leftarrow R / R \leftarrow D$	90
4.2.5	Required Phase Synchronization for $S \rightarrow D / S \rightarrow R / R \leftarrow D$	93
4.2.6	Required Phase Synchronization for $S \rightarrow D / S \leftarrow R / R \rightarrow D$	95
4.2.7	Required Phase Synchronization for $S \leftarrow D / S \rightarrow R / R \rightarrow D$	97
4.2.8	Required Phase Synchronization for $S \leftarrow D / S \leftarrow R / R \leftarrow D$	100
4.2.9	Required Phase Synchronization for $S \leftarrow D / S \rightarrow R / R \leftarrow D$	100
4.2.10	Required Phase Synchronization for $S \leftarrow D / S \leftarrow R / R \rightarrow D$	103
4.2.11	Summary of Results	105
4.3	Channel Update Rate	106
4.4	Channel Estimation Protocols	106
4.4.1	Performance Measure	110
4.4.2	Compound Channel Estimates and Required Number of Channel Uses	111
4.4.3	Impact of Noise	115
4.4.3.1	Distributed Phase Synchronization Scheme	116

4.4.3.2	Single-Hop Channel Estimates: Protocol A1	117
4.4.3.3	Single-Hop Channel Estimates: Protocol B1	118
4.4.3.4	Channel Estimation Error: Equivalent Two-Hop Channels	121
4.4.3.5	Channel Estimation Error: Single-Hop Channels	125
4.4.3.6	Application Example	126
4.4.4	Performance Comparison	132
5	Distributed Phase Synchronization	137
5.1	Relay Phase Noise	138
5.1.1	Phase Beacon at the Relays	139
5.1.2	Phase Error	140
5.2	Distributed Phase Synchronization Schemes	141
5.2.1	Slave-Based Scheme	142
5.2.2	Master-Based Scheme	144
5.2.3	Comparison	145
5.2.3.1	Application Example	146
5.2.3.2	Simulation Results	149
5.2.4	Phase Error	156
5.2.4.1	Phase Error Due to Estimation Noise	157
5.2.4.2	Phase Error Due to Phase Noise	161
5.2.4.3	Joint Phase Error	163
6	Gain Allocation Schemes	165
6.1	Transmit Power Constraint	167
6.2	Multuser Zero-Forcing Relaying	168
6.2.1	Traffic Pattern III	170
6.2.1.1	Channel Estimation Protocol A1	172
6.2.1.2	Channel Estimation Protocol B1	173
6.2.2	Traffic Pattern IV	175
6.2.2.1	Channel Estimation Protocol A1	178
6.2.2.2	Channel Estimation Protocol B1	179
6.2.3	Impact of Phase Estimation Error	179
6.2.4	Simulation Results	183
6.3	Multuser MMSE Relaying	188
6.3.1	Linear Relaying, Generic Case	190
6.3.2	Linear Relaying, Special Case	193

6.3.3	Linear Distributed Antenna System, Generic Case	197
6.3.4	Linear Distributed Antenna System, Special Case	199
6.3.5	Impact of Phase Noise	201
6.3.6	Simulation Results	203
6.3.6.1	Linear Relaying (LinRel)	204
6.3.6.2	Linear Relaying (LDAS)	207
6.4	Impact of Relay Imperfections	212
6.4.1	Noisy CSI	213
6.4.2	Phase Noise	217
6.4.3	Phase Synchronization Error	218
7	The RACooN Lab	223
7.1	General Description	224
7.1.1	Baseband Processing	227
7.1.2	System Operation	227
7.1.3	Real-Time Features	228
7.2	System Characteristics	229
7.2.1	Transmit Power	229
7.2.2	Analog Gain Control	231
7.2.3	Imperfections	232
7.2.3.1	Inherent Delay	232
7.2.3.2	LO Phase Noise and Frequency Offset	234
7.3	Channel Measurements	240
7.3.1	Measurement Scenario	240
7.3.2	RACooN Setup	242
7.3.3	Measurement Results	244
7.3.3.1	rms Delay Spread	245
7.3.3.2	Coherence Bandwidth	253
7.4	RACooN Demonstrator	257
7.4.1	System Setup	257
7.4.2	Transmission Cycle	257
7.4.3	Results	261
8	Conclusions and Outlook	269
A	Appendix	273

A.1	Proof of (4.163)	273
A.2	pdf of a Function of a Random Variable	283
A.3	pdf of a Function of Two Random Variables	284
A.4	Multiuser Zero-Forcing Relaying Example	285
A.5	Matrix Derivatives	287
A.5.1	Derivatives of Traces	287
A.5.2	Derivatives of Matrix Inverses	288
A.6	Matrix Equivalencies	288
A.7	Synthesis of a Diagonal Matrix	288
A.8	Derivative Used in Linear Relaying Scenario	289
A.8.1	Summand 1	289
A.8.2	Summand 2 and 3	290
A.8.3	Summand 4	290
A.8.4	Summand 5	291
A.8.5	Derivative of $\tilde{\mathbf{g}}$ with respect to μ	291
A.8.6	Final Result	292
A.9	Derivative Used in LDAS Scenario	294
A.10	RACooN Channel Measurements	297
A.10.1	rms Delay Spread	297
A.10.2	Coherence Bandwidth	297
Acronyms		305
Notation		309
Frequently Used Symbols		313
Bibliography		315

Chapter 1

Introduction

Two major trends can currently be identified in the field of wireless communications. The first one is that the number of devices communicating over the air will increase. Even today, people use cell phones, laptops, wireless headsets, PDAs, and so on. The node density in a typical wireless network environment is therefore likely to increase drastically in the near future. As a consequence, significantly more active nodes will have to compete for a common wireless channel in cellular as well as access or ad hoc networks. Secondly, the general trend of reducing size of handheld devices will drive the need for higher carrier frequencies. This allows for smaller antennas, saving precious space in a mobile terminal or allowing to house multiple antennas on the same space. Employing more than one antenna at both the transmitting and the receiving terminal, also known as multiple-input multiple-output (MIMO) communication, has been shown to provide large benefits with respect to system performance. Under certain channel conditions, MIMO systems allow multiple independent data streams to be transmitted simultaneously over the same physical channel (spatial multiplexing). This leads to an improvement of the spectral efficiency. The system capacity has been shown to increase linearly with the minimum of the number of source-destination antennas [1–4]. Furthermore, spatial diversity can be exploited to increase the link reliability, making the communication more robust against random channel fluctuations known as fading [5]. And finally, an array gain increases the coverage range by increasing the receive signal-to-noise ratio (SNR). This is achieved by combining the signal from multiple antennas coherently [5].

There are, however, two inherent problems that arise. The first one is that increasing the number of devices in radio range of each other also increases the amount of interference due to the broadcast nature of the wireless channel. If multiple users have to share the same physical channel, the data rate for each user is limited by the amount of interference created

by all other users. The second problem is that higher carrier frequencies will make the wireless channel becomes more and more line-of-sight. This means that the number of relevant scatterers decreases and the channel becomes rank-deficient. In order to exploit the linear scaling of data rate offered by MIMO technology, it is, however, crucial that the propagation channel has full rank. In order to alleviate these problems, future wireless communication systems will have to be built for cooperation rather than for mere coexistence. Cooperative communication is thus a hot topic of current research and many people believe it to be the next big step after MIMO systems.

The basic idea is that multiple autonomous nodes cooperate in order to increase the link quality, reliability and data rate not only of the whole system but also for each individual user. The general relay channel describes the situation where one source transmits to one destination while a single relay assists. It was first investigated in [6] but its capacity is still unknown. Moreover, there is even no cooperation strategy known that works best for this general case. A straightforward way of cooperation is that one or more nodes in a wireless network act as relays to increase the coverage range of a transmitter by increasing the receive SNR. Multiple users can furthermore exploit the inherent spatial diversity of the network by assisting each other in the communication. This provides robustness against fading and is called (user) cooperative diversity. It was introduced in [7–9]. An overview of several cooperative diversity protocols for wireless networks can be found in [10]. In [11] the authors show that the use of simple relays as 'active scatterers' can recover spatial multiplexing gain for MIMO communication systems in poor scattering environments. In more sophisticated networks, the communication between one or more source-destination pairs is assisted by a set of terminals that form a virtual array. Either user nodes or other dedicated devices act as relays and assist the communication between sources and destinations. This approach is promising to even supersede conventional MIMO systems with respect to diversity and spatial multiplexing gain especially in unfavorable channel conditions. In literature, cooperative networks are often classified as follows:

- **Relay network:** A single source-destination pair communicates with the help of one or more relay terminals. The relays are allowed to have different complexity (e.g. different number of antennas) than source and destination. A 'MIMO relay network' comprises a single multi-antenna source-destination pair and at least one multi-antenna relay.
- **Sensory network:** Sensory networks comprise a single source-destination pair and multiple relays, where it is often assumed that the source and all relays are of equal complexity [12, 13]. There is only one active transmitter at any time.

-
- **Ad hoc network:** An ad hoc network consists of dedicated relay nodes and multiple source-destination pairs that communicate simultaneously [12]. The relays cooperate to assist the communication in the network. In an ad-hoc network the relay terminals might also have own data to transmit. This notion has been investigated for example in [8,9], where the data to be forwarded is decoded and combined with the own data of the relay before re-encoding and transmitting the combined signal. Since there are multiple source-destination pairs that want to communicate, these networks are also called 'interference relay networks'.

The performance gains of point-to-point MIMO systems over single-input-single-output (SISO) systems have been mentioned above. The spectral efficiency can be increased by a spatial multiplexing gain, the link reliability by a spatial diversity gain, and the receive SNR by an array gain. These gains can also be achieved in a distributed wireless network.

- **Spatial Diversity:** Due to the spatial separation of the nodes, distributed wireless networks inherently exhibit spatial diversity [14]. It has been shown that the maximum achievable diversity in a network featuring single-antenna terminals is in the order of cooperating nodes [7]. Cooperative communication schemes can exploit the diversity to mitigate fading and increase the outage rate, thus making the communication more robust against deep fades. Basic protocols and user cooperation strategies for single-antenna relay networks that achieve a distributed diversity gain are developed and analyzed in [7, 10, 14]. In [15–18] the authors consider an ad hoc network in a slow-fading environment. They propose to introduce random phase offsets at the relays in order to create a time varying channel. Together with an adaptive scheduling algorithm, the outage aggregate throughput can be thus be increased. In [19] the authors investigate the diversity gains of different relaying schemes in MIMO relay networks. Outage probability expressions for various types of cooperative networks, system configurations, and transmission schemes are derived in [20–23].
- **Distributed Spatial Multiplexing:** In a wireless ad hoc network, a distributed spatial multiplexing gain can be realized by allowing multiple source-destination pairs to communicate concurrently on the same physical channel. This increases the data rate of a wireless system without requiring additional bandwidth or transmit power. A cooperative network with $2N$ users, i.e., N source-destination pairs and no dedicated relays, exhibits a spatial multiplexing gain of at most $\frac{N}{2}$ [24]. In [11,25,26] it has been shown how this multiplexing gain can be achieved in a network with dedicated relays. Multiple source-destination links can be orthogonalized in a completely distributed manner, allowing them to communicate concurrently on the same physical channel.

- **Distributed Array Gain:** If the signals from multiple relays add up coherently at the destination antennas, the receive SNR increases. This gain is called distributed array gain (e.g. [11,12]).

1.1 Relaying Schemes

Relaying schemes are concepts for the practical implementation of cooperative wireless networks. They describe the signal processing at the relay nodes, the network organization and the traffic pattern. For the networks considered in this work, all nodes are assigned to any of the following groups:

- Sources
- Relays
- Destinations

The sources are the data sources, the destinations the data sinks and the relay terminals assist the communication between them. In literature, the relays are classified as either 'full-duplex' or 'half-duplex'. Full-duplex relays can transmit and receive simultaneously, whereas half-duplex relays cannot. For example, the nodes in full-duplex frequency division duplex (FDD) systems transmit and receive signals at the same time but use different frequency channels. For half-duplex relays, one transmission cycle is divided into time slots. In one time slot they receive the signals from the sources and in the next they retransmit a processed version of their received signals. For these relaying schemes there has to exist a time-frame structure within the network so that all nodes can operate in a cooperative manner. There are several relaying strategies that exhibit fundamentally different approaches to forwarding. The most important ones are

- amplify-and-forward (AF),
- decode-and-forward (DF),
- and compress-and-forward (CF).

AF and DF relaying protocols have first been proposed in [10].

AF relays retransmit their received signals after multiplication with a complex-valued scaling factor. These scaling factors are called 'gain factors' and the matrix comprising all gain factors of all relays is the 'gain matrix'. Accordingly, the computation of the gain factors will in this work be called 'gain allocation'. Complex-valued gain factors realize an amplitude scaling and phase rotation of the received signal. In case the relays employ multiple

antennas, they can forward a linear combination of their received signals from all antennas. As the received signal is not decoded by the relays to recover the data, AF relaying is also said to be 'non-regenerative'. The relays neither need knowledge of the used codebooks nor of the modulation alphabets. They are thus suited to operate in wireless ad-hoc networks that comprise many heterogeneous devices.

Inevitably, AF relays forward not only the desired signal but also noise. In multihop networks, where the communication between sources and destinations is conducted via several layers of relays, the noise is accumulated with increasing number of hops [27]. This leads to an SNR loss that degrades the performance. However, AF relays are generally assumed to exhibit a rather low hardware complexity because they do not need to decode the signal from the sources. This means that even single-antenna relays, which cannot separate the streams of multiple sources, can assist the communication between multiple source-destination pairs. This makes them an interesting option for practical realizations of cooperative networks.

DF relays fully decode and re-encode their received signal prior to retransmission. For this reason, they are also called 'regenerative'. These kind of relays are not transparent to coding or modulation because they have to decode the signal. This means that the sources have to transmit at a rate so that all relays can decode. In the presence of multiple sources, DF relays are furthermore required to have enough antennas so that they can separate the data streams. The necessary signal processing is generally more complex than for AF relays. However, the retransmitted data is mostly assumed to be perfectly recovered at the relays and thus noiseless. [28] provides an overview over various regenerative relaying strategies. The authors examine two-hop as well as multi-hop relaying protocols and provide a framework for the investigated schemes. In terms of sum rate, DF relaying is close to optimal when the source-relay channel is excellent, which is practically the case when sources and relays are physically close or when dedicated relays are placed intentionally in a way that a good connection to the source is ensured. Note that DF relays are generally half-duplex nodes because the codeword has to be received completely before it can be decoded.

Finally, **CF relays** do not decode the source signal. They use their observations in a different way. The received signal is quantized (and possibly compressed) and then forwarded to the destination [29]. This type of protocol is also called 'quantize-and-forward'. CF relays are most efficient in cases where the source-relay and the source-destination channels are of comparable quality and the relay-destination link is good. In this situation, the relay may not be able to decode the source signal but nevertheless has an independent signal observation that can be used to assist the decoding at the destination. DF and CF strategies for relay networks are developed in [29]. Considering full-duplex terminals, the authors evolve capacity

theorems and provide achievable rates and rate regions for a number of wireless channel models.

Apart from the relaying scheme, it makes sense to distinguish between 'coherent' and 'non-coherent' forwarding. Coherent forwarding schemes refer to protocols where the signals from multiple relays add up coherently at the destination antennas. This generally requires instantaneous channel state information (CSI) in order to compute the gain factors. In this context *local CSI* at a relay refers to the case where the relay knows its own local channel coefficients (from the sources and to the destinations). In contrast to that, *global CSI* means the knowledge of all channel coefficients. The relays only require little (e.g. second order statistics or amplitude information) or no CSI for non-coherent forwarding schemes. Note that neither a distributed array gain nor a spatial multiplexing gain can be achieved if the signals do not combine coherently at the destination antennas. It is often believed that perfect instantaneous CSI is required to compute the gain factors for coherent relaying schemes. However, in the context of distributed AF relaying, this assumption has to be adapted. In some cases, the presence of an unknown and random phase offset on the channel estimates has no impact on the system performance. It makes sense to call those schemes 'coherent', even if perfect CSI is not available (cf. Chapter 4 in this work).

In literature, people furthermore distinguish between *orthogonal* and *non-orthogonal* forwarding. Orthogonal forwarding refers to all schemes where the relays transmit on orthogonal subchannels to the destinations. The group of schemes where all relays transmit on the same subchannel is referred to as non-orthogonal forwarding. They can achieve a diversity gain, a distributed spatial multiplexing gain, and a distributed array gain.

1.1.1 Distributed Space-Time Codes

In cooperative networks, space-time codes can be implemented in a distributed fashion. To this end, the relays have to encode their received signals prior to retransmission so that a space-time code is generated at the receiver. No CSI is required at the relays but the destination has to have global CSI, i.e., it has to know all source/relay and relay/destination channels. Cooperative protocols that apply the idea of space-time coding originally devised for multiple-antenna systems to the problem of communication over a distributed wireless relay network are analyzed in [7,30–39]:

In [7] space-time coded cooperative diversity protocols are developed and analyzed. All relays that can decode the message from the source apply a suitable space-time code to their

transmit signals. It is shown that these protocols achieve the full spatial diversity corresponding to the number of cooperating nodes even if not all relays are able to decode. In [30] the authors analyze a network with a single source-destination pair, where an Alamouti-based space-time coding is realized by the relays. The authors of [31] investigate several distributed space-time codes for DF relays. They consider distributed orthogonal space-time codes, full-rate/full diversity codes, and V-BLAST codes (e.g. [32]) and compare the network performance to conventional non-cooperative protocols. In [33] the authors consider a wireless sensory network with AF relays. They propose the use of linear dispersion codes, where the transmit signal from each relay is a linear combination of the received signal and its conjugate. Outage analysis shows that the full spatial diversity can be achieved.

Distributed space-time coding was generalized to networks with multi-antenna nodes in [34]. In [35] the authors use real orthogonal, complex orthogonal, and quasi-orthogonal designs to develop distributed space-time codes. An extension to the work of [33] is presented in [36]. While synchronous networks are considered in [33], the authors of [36] investigate space-time coding for asynchronous networks. Assuming imperfect CSI at the receiver, the authors of [37] propose a differential space-time transmission scheme at the transmitter that is combined with selection combining and antenna selection. A differential transmission scheme that requires no CSI at relays and destination is proposed in [38]. Compared to coherent distributed space-time coding, the differential scheme is shown to lose 3 dB SNR. Codes that are designed to minimize the upper bound of the average pairwise error probability are finally presented in [39].

1.1.2 Relay Selection

A topic that has attracted large interest within the field of cooperative communications is 'relay selection' or 'opportunistic relaying'. One or more nodes are selected from the whole set of potential relays to forward data from source to destination. It has been shown in [40] that a simple selection scheme, where only one relay at a time assists the communication between a source-destination pair, can achieve full spatial diversity in the order of the total number of cooperating nodes. In terms of receive SNR, relay selection is, however, suboptimal because it cannot achieve a distributed array gain. Cooperative strategies, where all available relays forward their signals on orthogonal channels and the destination uses maximum ratio combining (MRC), achieves full diversity and is optimal in the sense of receive SNR. However, these repetition-based schemes obviously suffer from a loss in spectral efficiency because the number of required channel uses increases linearly with the number of transmitting nodes. In

contrast to that, relay selection can provide diversity without sacrificing the achievable rate. Furthermore, in AF networks these schemes have been shown to outperform repetition-based scheduling in terms of average throughput, outage probability, and error probability at the cost of a small amount of feedback [41,42].

Selecting the optimal subset of relays from all candidate nodes is a very difficult task. It is affected by many parameters that have impact on the system performance. A simple but suboptimal way to tackle the problem is to pick a single *best* relay among the whole set of candidates to forward the signal from the source (e.g. [40,43–48]):

In [43] the authors use the average receive SNR or the relay-destination channel as indicator for the best relay. They present a timer-based approach to select this relay in a completely decentralized way. The authors furthermore point out that their scheme exhibits exactly the same diversity-multiplexing tradeoff (DMT) as the space-time coded protocol presented in [7]. Due to propagation delays and timing offsets, there is, however, a non-zero probability that more than one relay is selected as best relay. In [40] the same authors analyze this probability. It is shown in [44] that under a sum power constraint, opportunistic DF relaying exhibits the same outage behavior as the optimal DF strategy that utilizes all potential relays. The authors of [45] investigate a scheme where the relay is selected based on the quality of the source-relay link only. They provide a closed-form approximation of the probability density function (pdf) of the received SNR. In [46] the outage probability and probability of error are derived for beamforming with unlimited feedback. The authors compare these expressions with the ones corresponding to the selection schemes [41,42] to find the performance gap between beamforming with distributed MRC and relay selection. Finally, in [47,48] the focus lies on the outage probability of opportunistic DF relaying. While [47] considers Nakagami fading channels, the authors of [48] concentrate on co-channel interferences with unequal power under the Rayleigh fading channels.

Cooperative protocols where the relay always forwards the signal from the source suffer from a loss of spectral efficiency because there is no need to forward the information if the destination is able to decode the signal from the direct link. In [49–51] cooperative protocols are investigated, where a relay is picked to support the source-destination pair only when necessary. Compared to traditional relay selection schemes, these strategies achieve a higher bandwidth efficiency. The authors of [50] investigate selection relaying in a network scenario with multiple simultaneous transmissions. They analyze the outage probability of a simple and completely distributed relay selection scheme that requires some feedback. The relays are only active to improve the reliability of the network when required, i.e., when the channel conditions are bad. Their analysis is similar to [44] but they consider a network

setting, where a single relay may support multiple source nodes. In [51] the authors finally discuss the performance of opportunistic relaying protocols that employ simple packet level feedback and strictly orthogonal transmissions. The feedback allows to decide when it is beneficial to forward the signal and when not.

In [51–55] the notion of relay selection is generalized by allowing more than one relay to assist a source-destination pair. A diversity multiplexing tradeoff analysis for this kind of schemes is provided in [51]. The authors of [52] study the impact of CSI on the design of cooperative transmission protocols employing DF relays. They assume that the source possesses different amount of CSI and decides which subset of nodes should forward their signals to the destination. Explicit expressions of the outage probability are developed for three cooperative protocols that differ in the amount of available CSI at the source node. In [54] the authors consider the problem of selecting a subset of relays that maximizes the overall throughput. They determine the network diversity that is achieved by the selected set and use this as a performance benchmark. Since the original problem is very difficult, the authors increase the tractability by assuming that the relays employ partial DF relaying. They then provide relay selection strategies that are based on further simplifications but yield near-optimum expected rates for small number of selected relays. Finally, the authors of [55] consider networks with parallel AF relays. They propose several relay selection schemes that are suboptimal with respect to receive SNR but achieve full diversity. In contrast to an exhaustive search delivering the optimal subset, the complexity of the proposed schemes increases only linearly with the number of relays.

The relay selection schemes that have been considered so far mostly neglected the overhead required to obtain CSI. For fading channels a lot of energy may, however, be required to feedback CSI reliably to the relays. The authors of [56] consider a cooperative wireless network where a set of DF relays forwards the information in parallel from source to destination. They transmit training sequences to the destination and cooperate based on CSI feedback. The energy consumption of the whole network is analyzed for the case that the number of active relays varies with time as the channel changes. The authors propose the optimal scheme in terms of energy consumption that selects a certain subset of relays. There exists a tradeoff between the energy consumption for data transmission and the overhead for CSI acquisition: Decreasing the energy consumption for data transmission by using more (potential) relays increases the overhead for CSI acquisition and vice versa.

1.1.3 Beamforming

Coherent AF relaying schemes use instantaneous channel information to compute the gain factors such that the signals from all relays add up coherently at the destinations. In [11,25,26] it has been shown that a finite number of relays can completely orthogonalize multiple source-destination pairs in space. Apart from a distributed diversity and array gain, these schemes are able to provide a distributed spatial multiplexing gain. The sum rate of the whole network can thus scale linearly with the number of multiplexed streams.

A lot of work has been done in the field of MIMO AF relay networks [57–65]: The gain matrix that maximizes the capacity between source and destination is found in [57,58]. The work in [59] is based on [57,58] and jointly optimizes the precoding matrix at the source and the gain matrix at the relays. The authors of [57] extend their work by comparing their scheme to a selection of other relaying protocols in [60]. A scheme that combines direct transmission from source to destination with transmission over the relay is investigated in [61]. In [62] a relay network with multiple relays that employ an arbitrary number of antennas is considered. The gain factors of all relays are jointly optimized using the generalized singular value decomposition (SVD). In [63–65] the authors consider the same scenario as in [57,58,60]. A joint optimization of the gain matrix at the relay and the decoding matrix at the destination such that the mean squared error (MSE) of the received symbols is minimized is presented in [63]. In [64,65] the authors investigate gain allocation schemes for the case of partial CSI at the relays.

Gain allocation schemes for ad hoc and sensor networks have been presented in [12,25,66–89]: In [25,66] the authors consider an ad hoc network with multiple single-antenna source-destination pairs and either multiple single-antenna relays or a single multi-antenna relay. The gain factors are computed such that all source-destination pairs are orthogonalized, i.e., inter-user interference is completely suppressed. The scheme is called multiuser zero-forcing (MUZF) relaying and is able to achieve full spatial multiplexing gain. Another scheme where the relays orthogonalize multiple source-destination pairs is presented in [12]. The impact of noisy CSI on MUZF relaying has been investigated in [67,68] and the extension to relays that can exchange received signals in an arbitrary fashion is presented in [69]. In [70] the authors propose several optimization functions to determine the gain factors for the case that there are more relays than necessary to orthogonalize the source-destination pairs. They are optimized with respect to average sum rate, diversity, and fairness. In most of the cases, there exists no closed-form solutions so that the relay gains are found using numerical optimization techniques. The concept of MUZF relaying has been extended to multi-hop wireless networks in [71]. A distributed gradient based gain allocation scheme

that is capable of orthogonalizing multiple source-destination pairs in space is presented in [72].

In [73–75] minimum mean squared error (MMSE)-based gain allocation schemes are presented. The authors of [73] consider an ad-hoc network with multiple source-destination pairs and either several single-antenna relays or one relay with multiple antennas. The scheme is shown to exhibit a diversity gain as well as a distributed spatial multiplexing gain. In [74,75] a slightly different scenario is considered. There, the network comprises a single multi-antenna source-destination pair and several multi-antenna relays. The authors of [76] consider the same system model as in [90], i.e., a single source-destination pair and one relay, and propose a gain allocation scheme based on QR decomposition and phase control at the relays. It is shown to provide a distributed array gain and a receive array gain while maintaining maximum spatial multiplexing gain. The authors compare the ergodic capacity of their scheme with zero-forcing (ZF) relaying and simple AF relaying as described in [90]. In the succeeding work [77] they combine the scheme presented in [76] with ZF in the source-relay or the relay-destination link. Finally, in [78], the authors analyze the capacity and achievable gains of their proposed schemes.

The impact of noise correlation (e.g. due to common interference or noise accumulation from previous hops) on the performance of relay networks with multiple sources, multiple relays and a single common destination are investigated in [79]. The authors present a closed-form expression for the relay gains that maximize the rate. They find that noise correlation is beneficial, even if there is no knowledge about the correlation structure. However, knowledge of the correlation can greatly improve the performance. In [80] the authors consider an ad hoc network where multiple AF relays assisting the communication between several source-destination pairs. They propose to build clusters of relays to reduce the overall amount of overhead required to disseminate CSI among the relays. The gain factors that maximize the minimum link rate are found with the help of semidefinite programming. Similarly, in [81] the authors consider dividing the relays into two sets with different amount of CSI and analyze the resulting network performance compared to the case where all relays possess global CSI. A gain allocation scheme for an ad hoc network with AF relays that is robust against relay phase noise is proposed in [82]. The authors use semidefinite programming to find gain factors in a way that the system performance becomes robust against phase fluctuations of the local oscillators (LOs) of the relays. In [83] the authors decompose the two-hop relay channel into a cascade of MIMO X networks¹. Based on this view, they investigate corresponding signaling schemes, interference alignment, and relay selection. A

¹In a MIMO X network, every transmitting node has a message for every receiving node [91].

low-complexity relaying scheme, where the destinations only estimate the channel phases is presented in [84]. After the relays have forwarded their signals on orthogonal subchannels, the destinations use equal gain combining (EGC) to combine the signals. In [85] the authors study beamforming approaches for the case that only second order statistics of the channels are known. The authors of [86] propose a beamforming and power allocation algorithm that achieves a distributed diversity gain and is based on local CSI at the relays only. A gain allocation scheme that minimizing both the noise and interference at each destination node is proposed in [87]. The gain factors are not available in closed-form, but can be found by interior point methods. The relay gains in [88] are optimized jointly to maximize the received SNR with both individual and total power constraint at the relays. The considered problem is similar to [85], but with perfect CSI at the relays. The authors propose a distribute algorithm that allows each relay to compute its own gain factor locally. Finally, in [89], three detectors for sensory networks are proposed and compared: a channel inversion type detector, a MRC type detector, and a biased maximum likelihood (ML) detector.

1.1.4 Two-Way Relaying

The typical approach to orthogonalize channel resources for half-duplex relays is to use time division duplex (TDD). Reception and retransmission at the relays are orthogonalized by the use of two orthogonal time slots. Hence, a bidirectional transmission between two nodes via one half-duplex relay requires four time slots to exchange only two messages. To increase the spectral efficiency of such a bidirectional communication, the authors of [92] propose a scheme - known as 'two-way relaying' - that reduces the number of time slots to from four to two: In the first time slot both users transmit their messages simultaneously to the relay (multiple access phase) and in the second time slot the relay transmits a combined version of its two received signals to both nodes (broadcast phase). Since each user node knows its own transmitted signal it can subtract the back-propagated *self-interference* prior to decoding. In a full-duplex FDD system, the transmission from the nodes to the relay and from the relay back to the nodes would take place at the same time, but on different frequency channels.

In [93] the authors provide achievable rate regions of the two-way relay channel for different cooperation strategies. Spectrally efficient communication protocols where a relay assists the bidirectional communication between one or more source-destination pairs are proposed in [66]. The impact of transmit CSI at the relay on the performance of two-way relaying is investigated in [94]. The authors extend the scheme of [92] by considering a network, where both users and the relay are equipped with multiple antennas. Two relaying

schemes are compared: 1) the relay uses superposition coding and 2) the relay combines both messages on bit-level using the XOR² operation. They authors find that when transmit CSI is used by the relay, the XOR-based scheme always leads to higher minimum user rates than the superposition coding based scheme. Capacity regions and achievable sum rates of coded bidirectional communication for half-duplex relays and various DF protocols are derived in [95,96]. The authors of [97] investigate the use of network coding for bi-directional communication with AF relays. A two-way relaying system with two users and an AF relay is analyzed in [98]. The authors derive upper and lower bounds of the average sum rate and find the optimal power allocation for the case that links between the users and the relay are not equally strong. Furthermore, they consider the case where both users are equipped with two antennas while the relays still employs only one antenna. It is shown that both users can achieve a diversity order of two when using the Alamouti space-time block code. In [99] the authors consider the case where the bidirectional communication between a single source-destination pair is assisted by multiple relays. The relays encode their signals using a distributed linear dispersion code before retransmission. Relaying protocols that use two, three, and four time slots for one full transmission cycle, i.e., the exchange of two messages between both users, are subsequently compared.

1.2 Capacity Scaling

The capacity scaling of cooperative communication networks indicates how many spatial data streams it can support. This is an interesting aspect because it directly relates to the supported data rate for each user. Early capacity scaling results for cooperative networks were obtained for static topologies where the density of nodes per area is constant. It was found that the capacity of *sensory networks* scales linearly with the logarithm of the number of users [100]. For *ad hoc networks* it has been shown that the total network capacity increases linearly with the square root of the number of nodes [101–104]. Both results were discouraging because they implied that the individual data rate for each user tends to zero if the number of users is increases. In [105] it was, however, found that for mobile users the total capacity scales linearly with the number of users. The per-user capacity thus stays constant for increasing number of nodes.

Asymptotic scaling laws for relay networks with multi-antenna terminals are presented in [11,90] for time-synchronous nodes and in [106] for asynchronous nodes. The authors

²Exclusive OR.

consider a MIMO relay network where the relays possess local CSI, i.e., they know their local channels to the source and the destination. It is shown that, asymptotically in the number of relays and the number of relay antennas, the network capacity scales linearly with the number of multiplexed streams and logarithmically with the total number of relay antennas. This shows that both a *multiplexing gain* and a *distributed array gain* are achieved. For the case that each relay employs a finite number of antennas, the distributed array gain only corresponds to the number of relays. Furthermore, the authors consider a relay network with a single multi-antenna source-destination pair and multiple relay terminals that have no CSI. It is shown that, again asymptotically in the number of relays, the network can be turned into a point-to-point MIMO link even with single-antenna relays. Consequently, the capacity scales linearly with the number of multiplexed streams and logarithmically with the SNR. The authors of [107,108] investigate the mutual information of a MIMO relay channel without direct link for the case that the number of relay antennas goes to infinity. They find the cumulants of the mutual information for the case of flat Rayleigh fading and a single AF MIMO relay. In [109] and its extension [110] source and relay precoders that optimize upper and lower bounds on the Gaussian MIMO relay channel capacity are derived for the case that full CSI is available.

A different approach to the problem of capacity scaling in *ad hoc* and *sensory wireless networks* can be found in [12,111,112]. The authors investigate the power efficiency in order to find out how much power the nodes have to spend in order to maintain the same rate as in a single-user system. In [113] the power efficiency is defined as the ratio between the capacity (data rate) of the channel and the transmit power (energy rate). For ad hoc networks, where multiple source-destination pairs communicate concurrently with the help of a set of relays, the power efficiency is defined as the ratio between the sum of the mutual information and the total power consumption of the network [12]. It is shown that by increasing the number of nodes in the network, each user has to expend less power in order to support the same rate.

An interference network with two source-destination pairs and one full-duplex DF relay is considered in [114,115]. The authors provide an achievable rate region for the case that both sources have messages for both destinations [114] and the case where each source only has a message for its belonging destination [115]. In [116] the spatial multiplexing gain, which characterizes the capacity scaling behavior, is investigated for the K -user interference channel with a single MIMO relay. The authors show that the capacity scales with no more than $\frac{K}{2}$ and find that at high SNR the direct link does not provide any additional degrees of freedom. A similar scenario as in [116] is considered in [117]. However, the relay can now observe the signal from one source only. The authors derive and analyze the achievable

rate region for this case. Finally, in [118] sensory networks with either DF or AF relays are investigated. The authors find closed-form expressions of the ergodic capacity for the case that the relays forward on orthogonal channels to the destination. Capacity scaling for non-regenerative multihop ad hoc networks is investigated in [119].

1.3 Diversity-Multiplexing Tradeoff

In MIMO wireless networks, a diversity gain and a spatial multiplexing gain can be obtained simultaneously. But there is a fundamental tradeoff between how much of each type of gain any coding scheme can extract [120,121]. The concept of DMT has been extended and investigated for cooperative wireless networks (e.g. [7,10,122–126]). In [122] the authors propose protocols for several types of relay channels and characterize them using the DMT. The half-duplex relay channel with multiple AF or DF relays, the cooperative broadcast channel, and the symmetric multiple access scenario are considered. Furthermore, the authors propose a new protocol called 'dynamic DF', where the relay terminal listens to the source until it can decode the message. It then re-encodes the message using an independent Gaussian codebook and transmits it during the rest of the codeword. A static and a dynamic DF protocol are proposed for the single-relay channel in [123]. The dynamic DF protocol is based on the one presented in [122] but uses superposition coding. Both protocols are analyzed with respect to the DMT. Finally, the static DF protocol is extended to the case of multiple relays. In [124] the authors consider an ad hoc network with multiple sources, relays, and destinations. They examine the DMT for different network configurations and forwarding protocols. It is shown that for full CSI at the relay, the CF protocol achieves the DMT upper bound for half-duplex as well as full-duplex relays in a MIMO relaying network. A cooperative network with a multi-antenna source-destination pair and several single-antenna AF relays is considered in [125]. The authors use the protocol described in [34] to find the achievable DMT for this network. Finally, the authors of [126] derive the fundamental DMT for a MIMO relaying network with either a full-duplex or a half-duplex relay. They show that DF achieves the optimal DMT in case the relay is full-duplex. For a half-duplex relay, the dynamic DF protocol proposed in [122] is shown to achieve the optimal DMT.

1.4 Hardware Imperfections

In order to build practical systems it is crucial to identify and understand the implications of imperfect hardware on the system performance. This allows to

1. assess the performance of devised algorithms and protocols under more realistic conditions and
2. to design algorithms, protocols, and schemes to mitigate the degrading effects of practical hardware imperfections.

Understanding hardware imperfections and their impact on the performance of practical systems is an important step towards building them. A good overview of some of the most important impairments of the analog radio frequency (RF) hardware in a wireless communication system is given in [127]. The authors discuss the mechanisms behind aperture and clock jitter, phase noise, I/Q imbalance, and non-linearity of the high power amplifier and their effects on the system performance. Further hardware imperfections commonly discussed in current literature include carrier frequency and time synchronization offsets. Both are the result of LO frequency errors because the carrier frequency as well as the signal clock are derived from the local LO reference. Due to hardware imperfections, practical LOs oscillate at a frequency that is slightly different from the desired one. In networks with multiple distributed nodes this leads to individual carrier frequency offsets and the timing of the nodes will drift apart over time. In order to allow for efficient communication, a frequent time and frequency synchronization is therefore generally required.

Methods for distributed carrier frequency synchronization in cooperative wireless networks are discussed for example in [128, 129]. The impact of carrier frequency offsets on the network performance is investigated in [130–137]. The authors of [138] discuss time synchronization in distributed networks with DF relays and in [139–141] time synchronization errors in cooperative networks are analyzed. The individual distances between multiple distributed nodes have a similar impact on system design and performance as time synchronization errors because they lead to different propagation delays (e.g. [142–145]). Finally, the joint impact of time and frequency synchronization errors are discussed for example in [146–149].

1.5 Real-World Demonstrators

Although the field of cooperative communication has drawn a lot of attention, most results are of theoretical nature. There has not been much work on real-world demonstrators and practical implementations. Only a few institutions possess the measurement hardware with which cooperative wireless networks can be demonstrated. The most prominent are:

- **MIT's Commodity Hardware Demonstrator:** This is a low-complexity cooperative diversity demonstrator that has been built with commodity hardware at the Massachusetts Institute of Technology (MIT) in 2006 [150]. A low-cost embedded, software defined radio was designed and implemented with cheap hardware. In the conducted experiments, three relay nodes assisted the communication between a single source-destination pair in an indoor environment. The simple opportunistic relaying protocol proposed in [40] was implemented. The experiments confirmed that the reliability of the data transfer improved compared to conventional (non-cooperative) communication.
- **OpenAirInterface:** The Mobile Communications Department at EURECOM created a project named 'OpenAirInterface' [151]. It comprises a platform that can be used to conduct real-time experiments in realistic cellular and mesh network topologies. The architecture configuration that can be used for measurements in cooperative mesh networks is called 'OpenAirMesh' [152]. It is built to perform experiments in WiMAX and UMTS LTE like networks and employs a MIMO-OFDMA physical layer. The current terminals operate at a carrier frequency of 1.9 GHz – 1.92 GHz and support a bandwidth of 5 MHz. Two transmit/receive antennas can be employed. A planned extension to the current hardware comprises a new RF chain with a tuning range of 180 MHz – 8 GHz and a maximum baseband channel bandwidth of 20 MHz. Furthermore, four antennas will be supported. Application examples for OpenAirMesh are [152]:
 - Investigation of the practicality of interference aware scheduling and interference cancellation.
 - Investigation of practical issues connected to the realization of wireless distributed relaying, e.g. synchronization.
 - Demonstration of broadband ad hoc communication systems and of collaborative communication in a sensor network.
- **Easy-C Project:** The EASY-C project is a research project that aims at developing key technologies for the next generation of cellular networks [153]. It is funded by the German Federal Ministry for Education and Research and is led by Deutsche Telekom, Vodafone, the Vodafone Chair Mobile Communications Systems at Technische Universität Dresden, and the Fraunhofer Institute for Communications, Heinrich-Hertz Institute. One part of the project is the development of a cellular testbed [154] to implement and evaluate multi-antenna techniques and multi-cell signal processing such as

cooperative and non-cooperative relaying, interference coordination and interference cancellation. The physical layer of the testbed is based on 3GPP LTE project [155]. It will be operated in FDD mode at 2.67GHz – 2.69GHz for the downlink and 2.52GHz – 2.54 GHz for the uplink.

- **RACooN Lab:** The RACooN Lab is a measurement laboratory that is available at the Institute for Communication Technology at ETH Zurich [156]. It can be used to
 - measure (distributed) MIMO channels without antenna switching,
 - emulate and evaluate the performance of distributed wireless networks.

Chapter 7 of this Thesis elaborates on the RACooN Lab and presents experiments that have been conducted (see also [157]).

1.6 Contribution and Outline

In this work, several important aspects of wireless relaying networks are investigated. The focus lies on ad hoc networks with AF relays. In the most general case there are multiple source-destination pairs and several relays to assist the communication. Chapter 2 presents the overall system model and notation that will be used throughout this work. The system topology and channel model are introduced in Sections 2.1 and 2.2, respectively. Section 2.3 discussed the impact of unknown LO phases on the signaling. The 'equivalent' channels are defined as the concatenation of propagation channels and phase rotations due to LO phase offsets of the nodes. In Section 2.4 four traffic patterns and the corresponding input/output relations are presented. They differ in the utilization of the direct link between sources and destinations. A reference scenario for which the system SNR is defined is introduced in Section 2.5. The average sum rate acts as an important figure of merit in subsequent chapters because it reflects the overall system performance. For the sake of completeness it is shortly introduced in Section 2.6.

Chapter 3 investigates hardware imperfections at the relays in cooperative, wireless two-hop networks. The focus lies on AF relaying, where the received signals are retransmitted after linear filtering. A selection of the most important RF impairments that have a special impact on two-hop relaying systems will be discussed. These are *LO frequency offsets*, *LO phase noise*, and *I/Q imbalance*. Section 3.1 introduces the block diagram of a relay, highlighting the hardware components that are affected by the considered LO imperfections. It forms the basis for Section 3.2, where a detailed discussion of the performance of AF relaying in the presence of LO frequency errors and phase noise is presented. The former leads

to a sampling time and carrier frequency offset. Both effects are studied in Section 3.2.1. Network timing is another important aspect that is affected by an LO frequency error. The reduction of the overall data rate in the presence of a network timing error is also analyzed in Section 3.2.1. Section 3.2.2 deals with phase noise at the relay. A model that is commonly used to describe the random phase variations of an LO is the so-called *Wiener phase noise*. It characterizes the phase fluctuation of a free-running oscillator that is perturbed by white noise as Wiener-Lévy process. The phase increments are independent, zero-mean, Gaussian random variables with a variance that increases linearly with the time between two observations. In Section 3.2.3 the impact of the LO phase and frequency errors on the input/output relation of two-hop AF relaying is investigated. It turns out that FDD and TDD relays are affected differently by the LO impairments. The implications of the presented imperfections for both types of relays are analyzed in detail. This leads to important design guidelines for the implementation of a practical cooperative network. The results of Section 3.2 have been published at VTC Spring 2010 [158]. Section 3.3 finally investigates the impact of I/Q imbalance at a relay on the signal at the destination. The received signal, self-interference, and noise power are discussed qualitatively.

Channel estimation in an ad hoc network is investigated in Chapter 4. In Section 4.1 it will be shown that the direction in which the channels are measured has an impact on the estimates (even if they are noiseless). Based on this observation, it turns out in Section 4.2 that in some cases a global phase reference is required for a certain set of nodes in order to allow for coherent forwarding. The following question is answered: *Which nodes in a two-hop relaying network require a global phase reference so that coherent distributed beamforming is possible?* To this end, a framework is derived to determine the phase synchronization requirements. All four traffic patterns introduced in Section 2.4 are investigated regarding this issue for the case that the single-hop channels are estimated in different directions. The results of this section have been presented at Globecom 2009 [159]. Thoughts on the channel update rate are given in 4.3. In Section 4.4 four channel estimation protocols that obtain global CSI in a two-hop network without direct link are identified. They differ in the direction in which the single-hop channels are measured. The quality of their estimates in the presence of additive signal noise and phase noise is compared with respect to the accuracy of the gain factors that can be computed from them.

Chapter 5 discusses the phase synchronization of the relays in a distributed wireless network. Section 5.1 shows how a common beacon signal can alleviate the degrading effect of relay phase noise on the network performance. In Section 5.2 phase noise is then disregarded. A simple scheme to provide a global phase reference for multiple relays is presented

in Section 5.2.1. It was first published at SPAWC 2007 [160] and is based on a master/slave architecture where one node is assigned master, all others are slaves. The impact of additive noise and phase noise on the quality of the phase synchronization and on the performance of MUZF relaying has then been studied in [133]. A slightly different approach than [160] has been presented by other authors in [161]. The scheme is shortly revisited in Section 5.2.2 for the sake of completeness. It is also based on a master/slave architecture but has the disadvantage that neither frequency nor antenna diversity can be exploited. Based on a simple example with a single source, multiple relays and a remote destination, the performance of both schemes is compared in Section 5.2.3. Section 5.2.4 finally evaluates the phase error resulting from an imperfect phase synchronization (due to phase noise and additive signal noise) with the scheme of [160]. It turns out that it can be modelled as a Gaussian random variable for SNR values that are relevant for practical applications. The results of Section 5.2.4 have originally been published at Globecom 2007 [133].

Two gain allocation schemes for coherent, wireless relaying in ad hoc networks with single-antenna source-destination pairs are presented in Chapter 6. All relays are subject to an instantaneous sum transmit power constraint, which is introduced in Section 6.1. In Section 6.2 the first gain allocation scheme, called MUZF relaying, is presented. It orthogonalizes all source-destination pairs in space. The gain factors are computed for two of the four traffic patterns introduced in Section 2.4 and different channel estimation protocols discussed in Section 4.4. The concepts originally presented in [25,69] are extended in the sense that the unknown and random LO phases of all nodes are taken into account. Section 6.3 then presents multiuser MMSE relaying as published at Asilomar Conference on Signals, Systems & Computers in 2005 [73]. The gain factors are computed such that the MMSE of the received symbols at all destinations is minimized. Numerical simulation results of the impact of relay imperfections on the performance on MUZF and multiuser MMSE relaying are presented in Section 6.4. The discussed imperfections are noisy CSI, relay phase noise, and a phase synchronization error (in those cases where a phase synchronization is required).

Chapter 7 finally introduces the RACooN Lab, which is a real-world demonstrator for distributed wireless networks. A general description of the equipment is provided in Section 7.1. It explains the basic functionality and gives an overview over important system characteristics. Some basics about system operation and features are also provided. In Section 7.2 some selected system characteristics are explained in more detail. The system transmit power and a switchable analog power gain are highlighted in Sections 7.2.1 and 7.2.2, respectively. Section 7.2.3 discusses the implications of a selection of hardware imperfections on the system operation. The focus lies on an inherent system delay and LO phase noise. Both effects

have to be taken into account in order to produce reliable measurement results. Section 7.3 presents the result of a channel measurement campaign that has been conducted in a typical laboratory environment. The RACooN Lab is able to measure 'real' MIMO channels, i.e., no antenna switching or time duplexing is necessary. The scenario consisted of four receivers and four transmitters and represented a network with two source-destination pairs (transmitters) and four relays (receivers), where all channels are estimated at the relays. Concatenating two point-to-point channels delivers the compound source-destination channel. The measured channel impulse responses have been used to evaluate the performance of MUZF relaying in a real-world environment. This work was published at VTC Spring 2005 [162]. The root-mean-square (rms) delay spread and coherence bandwidth are furthermore computed from the estimated two-hop channel transfer functions. This knowledge is then used in Section 7.4, where the implementation of MUZF relaying on the RACooN Lab is described. The results show its interference rejection capabilities on a real-world demonstrator, i.e., in the presence of hardware imperfections and without a global phase reference. The results have originally been published in at PIMRC 2008 [157].

Chapter 2

System Model

This chapter introduces the overall system model and the notation that will be used in this work. Consider a distributed wireless multi-user network, where multiple source-destination pairs communicate with the help of dedicated AF relay terminals. The system topology is presented in **Section 2.1**. In **Section 2.2** the channel matrices and the model for all point-to-point channels are introduced. In a distributed wireless network it makes sense to assume that each terminal employs its own, independent LO. Consequently, each LO exhibits an unknown and random phase offset with respect to a global reference. **Section 2.3** introduces these phase offsets to the system model. They enter the signal during the mixing operations (e.g. [163]) and can therefore be included into the channel. Throughout this work, the combination of propagation channel coefficient and phase rotation due to LO phase offsets will be called equivalent channel.

Four different traffic patterns are identified in **Section 2.4**. They differ in the utilization of the direct link between sources and destinations. The input/output relation for all four traffic patterns turns out to be independent of the LO phases of the relays under the following assumptions:

1. The gain matrix is fixed.
2. The LO phase offsets at the relay terminals remain constant during the time between reception and retransmission.
3. All antennas at a relay have the same phase reference.

The second requirement is related to phase noise. It states that the phase jitter at the LOs has to be negligible during the time between reception and retransmission of the signal at the relays. The last requirement will probably be met in most relaying scenarios because it is likely that each terminal has only one LO.

In order to be able to compare the performance of different channel estimation protocols, gain allocation schemes or traffic patterns, it is necessary to define the SNR of the system. This is done in **Section 2.5**. Since additive noise perturbs the signal at the relays as well as at the destination, there is no closed-form expression for the SNR in the generic two-hop network. Instead, a simple reference scenario is introduced. The system SNR is then defined based on this reference scenario. Finally, the average sum rate, which will be an important figure of merit for the gain allocation schemes discussed in Chapter 6 is introduced in **Section 2.6**.

2.1 System Topology

Consider a distributed wireless network where the same number of sources and destinations communicate with the help of N_R linear AF relay nodes. Each source wants to communicate with a single, dedicated destination terminal, together forming a source-destination pair. All in all there are N_{SD} source-destination pairs. The sources operate in spatial multiplexing mode, i.e., all data streams are mutually independent. It is assumed that the relays are not able to transmit and receive at the same time (*half-duplex constraint*). Consequently, a transmission cycle consists of two time slots: one for the 'first-hop' transmission from the sources to all relays and one for the 'second-hop' transmission from the relays to the destinations. Additionally, the 'direct link' constitutes the transmission from the sources to the destinations (see Fig. 2.1). Without going further into detail, it is assumed that the nodes are synchronized on a time slot basis. Papers addressing the issue of synchronizing multiple distributed nodes in a wireless network are for example [164, 165]. The achieved accuracy in networks of about 40 to 60 nodes is a couple of microseconds. The number of antennas employed by source k , relay l , and destination m are denoted by M_{S_k} , M_{R_l} , and M_{D_m} , respectively. Consequently, the total number of source, relay, and destination antennas is

$$M_S = \sum_{k=1}^{N_{SD}} M_{S_k}, \quad M_R = \sum_{l=1}^{N_R} M_{R_l}, \quad \text{and} \quad M_D = \sum_{m=1}^{N_{SD}} M_{D_m}, \quad (2.1)$$

respectively. The relays coherently amplify the signals they receive from the sources by multiplying them with complex gain factors prior to retransmission. All gain factors are collected in the gain matrix $\mathbf{G} \in \mathbb{C}^{M_R \times M_R}$. The structure of \mathbf{G} is determined by the cooperation between relay antennas, where 'cooperation' means the exchange of received signals. When, for example, relay antenna j is aware of the receive signal of relay antenna i , the entry $\mathbf{G}[i, j]$ may be nonzero. If there is no cooperation between two relay antennas

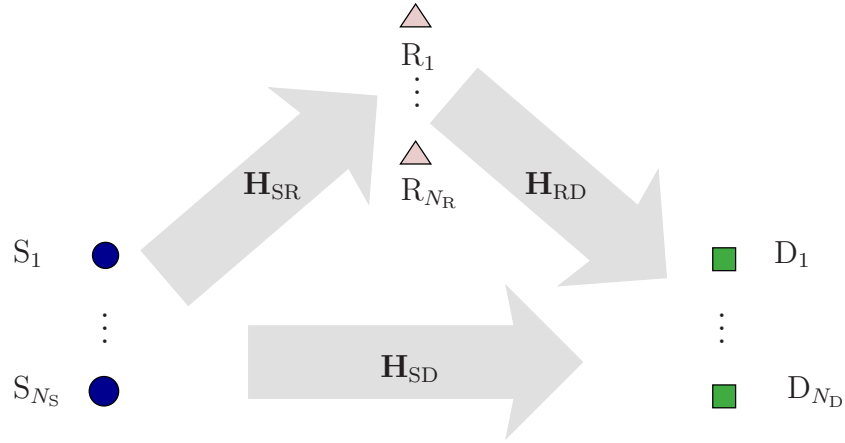


Fig. 2.1: Two-hop system configuration with half-duplex relays.

the corresponding entries of the gain matrix are zero. For the rest of this work it is assumed that all antennas belonging to the same relay are able to exchange data while there is no data exchange between relays. Consequently, the gain matrix is block diagonal. In the special case that all relays employ a single antenna only \mathbf{G} is diagonal.

2.2 Channel Model

All channels are assumed to be mutually independent and frequency flat. They are subject to *Rayleigh fading*, i.e., the channel coefficients are complex Gaussian random variables with circular symmetric probability density function. The whole system features three different propagation channels with the following coefficients:

- $\mathbf{H}_{\text{SR}}[l, k] = h_{\text{S}_k\text{R}_l} \sim \mathcal{CN}(0, \sigma_h^2)$: Channel coefficient from source antenna $k \in \{1, \dots, M_{\text{S}}\}$ to relay antenna $l \in \{1, \dots, M_{\text{R}}\}$
- $\mathbf{H}_{\text{RD}}[m, l] = h_{\text{R}_l\text{D}_m} \sim \mathcal{CN}(0, \sigma_h^2)$: Channel coefficient from relay antenna l to destination antenna $m \in \{1, \dots, M_{\text{D}}\}$
- $\mathbf{H}_{\text{SD}}[m, k] = h_{\text{S}_k\text{D}_m} \sim \mathcal{CN}(0, \sigma_h^2)$: Channel coefficient from source antenna k to destination antenna m

The matrices $\mathbf{H}_{\text{SR}} \in \mathbb{C}^{M_{\text{R}} \times M_{\text{S}}}$ and $\mathbf{H}_{\text{RD}} \in \mathbb{C}^{M_{\text{D}} \times M_{\text{R}}}$ are the first-hop and second-hop channel matrices, respectively. $\mathbf{H}_{\text{SD}} \in \mathbb{C}^{M_{\text{D}} \times M_{\text{S}}}$ denotes the direct link channel matrix. The propagation environment is assumed to be quasi-static, i.e., the channels are constant during at least

one transmission cycle while different channel realizations are mutually independent (block fading).

2.3 Local Oscillator Phases and Equivalent Channels

All terminals in the system as shown in Fig. 2.1 are independent, stand-alone nodes. It is sensible to assume that each of them employs its own LO that exhibits an unknown and random phase offset with respect to a global reference. Assume that the nodes A and B employ a single antenna only and their LOs are mutually independent. Let h be the complex-valued coefficient of the frequency-flat propagation channel between them. The LO phase offsets of nodes A and B at a certain point in time are denoted by φ_A and φ_B , respectively. Then, the 'equivalent channel coefficient' from A to B is

$$\tilde{h}_{AB} = h_{AB} e^{j(\varphi_A - \varphi_B)}. \quad (2.2)$$

It comprises the propagation channel as well as the phase rotations due to the LO phase offsets of the nodes. The latter are introduced to the signal during the mixing operation. With positive sign when mixing from baseband to passband and with negative sign when mixing from passband to baseband (e.g. [163]).

Consider now the system configuration depicted in Fig. 2.1 and let φ_{S_k} , φ_{R_l} , and φ_{D_m} denote the current LO phase offset of source antenna k , relay antenna l , and destination antenna m , respectively. The equivalent channel coefficients from source antenna k to destination antenna m , from source antenna k to relay antenna l , and from relay antenna l to destination antenna m are then given by

$$\tilde{h}_{S_k D_m} = h_{S_k D_m} e^{j(\varphi_{S_k} - \varphi_{D_m})}, \quad (2.3)$$

$$\tilde{h}_{S_k R_l} = h_{S_k R_l} e^{j(\varphi_{S_k} - \varphi_{R_l})}, \quad (2.4)$$

$$\text{and } \tilde{h}_{R_l D_m} = h_{R_l D_m} e^{j(\varphi_{R_l} - \varphi_{D_m})}, \quad (2.5)$$

respectively. With the diagonal matrices

$$\Phi_S := \text{diag} \left(e^{j\varphi_{S_1}}, \dots, e^{j\varphi_{S_{N_{SD}}} \right), \quad (2.6)$$

$$\Phi_R := \text{diag} \left(e^{j\varphi_{R_1}}, \dots, e^{j\varphi_{S_{N_R}}} \right), \quad (2.7)$$

$$\text{and } \Phi_D := \text{diag} \left(e^{j\varphi_{D_1}}, \dots, e^{j\varphi_{D_{N_{SD}}} \right), \quad (2.8)$$

the 'equivalent channel matrices' are defined as

$$\tilde{\mathbf{H}}_{\text{SD}} := \Phi_{\text{D}}^{\text{H}} \mathbf{H}_{\text{SD}} \Phi_{\text{S}}, \quad (2.9)$$

$$\tilde{\mathbf{H}}_{\text{SR}} := \Phi_{\text{R}}^{\text{H}} \mathbf{H}_{\text{SR}} \Phi_{\text{S}}, \quad (2.10)$$

$$\text{and } \tilde{\mathbf{H}}_{\text{RD}} := \Phi_{\text{D}}^{\text{H}} \mathbf{H}_{\text{RD}} \Phi_{\text{R}}. \quad (2.11)$$

They comprise the channel matrices as well as the phase rotations due to the LO phases of the respective transmitter and receiver.

2.4 Traffic Patterns and Input/Output Relation

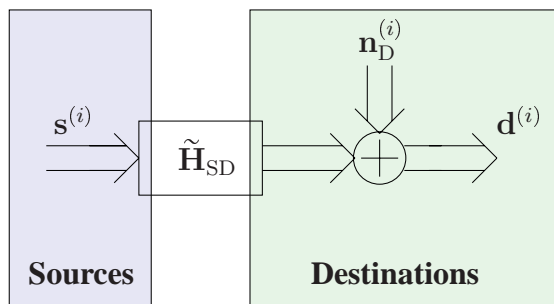
Due to the half-duplex constraint, a two-hop transmission cycle requires two time slots. Let $\mathbf{s}^{(i)} \in \mathbb{C}^{M_{\text{S}}}$ denote the vector comprising the transmit symbols of all source antennas in time slot $i \in \{1, 2\}$. It is assumed that the sources do not have any channel knowledge and distribute their transmit power equally among all M_{S} antennas. Since they are in spatial multiplexing mode, the covariance matrix of the transmit vector is $\mathbb{E}_{\mathbf{s}} [\mathbf{s}^{(i)} \mathbf{s}^{(i)\text{H}}] = \sigma_{\text{s}}^2 \mathbf{I}_{M_{\text{S}}}$. The total transmit power of all sources is then given by

$$P_{\text{S}} = M_{\text{S}} \sigma_{\text{s}}^2. \quad (2.12)$$

Fig. 2.2 shows block diagrams of the direct link and the two-hop link between sources and destinations. The vectors $\mathbf{n}_{\text{R}}^{(i)} \sim \mathcal{CN}(\mathbf{0}, \sigma_{n_{\text{R}}}^2 \mathbf{I}_{N_{\text{R}}})$ and $\mathbf{n}_{\text{D}}^{(i)} \sim \mathcal{CN}(\mathbf{0}, \sigma_{n_{\text{D}}}^2 \mathbf{I}_{N_{\text{SD}}})$ comprise the additive white Gaussian noise (AWGN) samples in time slot i at the relays and destinations, respectively. In the following, four two-hop traffic patterns are described within the framework of the system model. They differ in the utilization of the direct link.

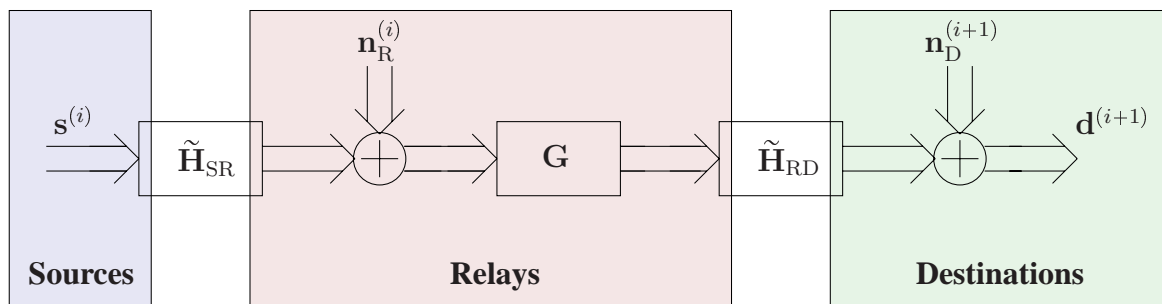
- **Traffic Pattern I:** In the first time slot, the sources transmit to all relays and destinations. In the second time slot, the sources and relays transmit to the destinations.
- **Traffic Pattern II:** The sources transmit to relays and destinations in the first time slot. While the relays retransmit in the second time slot, the sources are silent. This traffic pattern might be used in a scenario where the sources receive data from other terminals in the second time slot and are thus not able to transmit.
- **Traffic Pattern III:** In the first time slot, the sources transmit only to the relays. In the second time slot, both the sources and relays transmit to the destinations. This traffic pattern might be used in a scenario where the destinations transmit data to other terminals in the first time slot thus not being able to receive.

Direct Link



Direct link channel

Two-Hop Link



First-hop channel

Second-hop channel

Fig. 2.2: Block diagram of the direct link and the two-hop link between sources and destinations.

Table 2.1: Summary of traffic patterns I – IV; $A \rightarrow B$ denotes the case that terminal A transmits to B.

Traffic Pattern	Time slot 1	Time slot 2
I	$S \rightarrow \{R, D\}$	$\{S, R\} \rightarrow D$
II	$S \rightarrow \{R, D\}$	$R \rightarrow D$
III	$S \rightarrow R$	$\{S, R\} \rightarrow D$
IV	$S \rightarrow R$	$R \rightarrow D$

- **Traffic Pattern IV:** The direct link is not utilized at all. This corresponds to pure two-hop relaying which may be relevant for situations where the source-destination link is blocked.

Note that traffic patterns II and III were first proposed in [10] and [166], respectively. Traffic pattern I was later introduced in [167]. Table 2.1 summarizes all four traffic patterns. Subsequently, the input/output relation for traffic pattern I is derived. The input/output relations for traffic patterns II – IV can be readily computed from the result.

In the first time slot, the symbols in $\mathbf{s}^{(1)}$ are transmitted over the equivalent first-hop channel and the equivalent direct link channel to the relays and destinations, respectively. The vectors of received symbols at relays and destinations are

$$\mathbf{r} = \tilde{\mathbf{H}}_{SR}\mathbf{s}^{(1)} + \mathbf{n}_R^{(1)} \quad (2.13)$$

$$\text{and } \mathbf{d}_I^{(1)} = \tilde{\mathbf{H}}_{SD}\mathbf{s}^{(1)} + \mathbf{n}_D^{(1)}. \quad (2.14)$$

Prior to retransmission, \mathbf{r} is multiplied with the gain matrix \mathbf{G} . In the second time slot, the relay transmit signal is passed through the equivalent second-hop channel to the destinations while the sources transmit $\mathbf{s}^{(2)}$. The received signals at the destinations in time slot two are stacked in the vector

$$\begin{aligned} \mathbf{d}_I^{(2)} &= \tilde{\mathbf{H}}_{RD}\mathbf{G}\mathbf{r} + \tilde{\mathbf{H}}_{SD}\mathbf{s}^{(2)} + \mathbf{n}_D^{(2)} = \\ &= \tilde{\mathbf{H}}_{RD}\mathbf{G}\left(\tilde{\mathbf{H}}_{SR}\mathbf{s}^{(1)} + \mathbf{n}_R^{(1)}\right) + \tilde{\mathbf{H}}_{SD}\mathbf{s}^{(2)} + \mathbf{n}_D^{(2)}. \end{aligned} \quad (2.15)$$

The matrix

$$\tilde{\mathbf{H}}_{SRD} = \tilde{\mathbf{H}}_{RD}\mathbf{G}\tilde{\mathbf{H}}_{SR} \quad (2.16)$$

is called 'equivalent two-hop' channel matrix. It describes the two-hop channel from the sources via the relays to the destinations¹. Assume that the carrier phase offset is the same for all antennas of a relay because a single LO is employed to provide all oscillations. If the relay phases are furthermore constant for the duration of the whole transmission cycle (comprising two time slots), the relay phase matrices Φ_R and Φ_R^H in $\tilde{\mathbf{H}}_{\text{SRD}}$ cancel and the equivalent two-hop channel matrix becomes

$$\tilde{\mathbf{H}}_{\text{SRD}} = \Phi_D^H \mathbf{H}_{\text{RD}} \mathbf{G} \mathbf{H}_{\text{SR}} \Phi_S. \quad (2.17)$$

A discussion of the impact of a frequency offset and phase noise at the relays on the equivalent channel between sources and destinations is given in Chapter 3.

The input/output relation for traffic patterns II – IV are derived from (2.14) and (2.15) by setting either $\mathbf{s}^{(2)}$ or $\mathbf{d}^{(1)}$ or both to zero:

- **Traffic Pattern II:** For traffic pattern II, the direct link is only used in the first time slot. Since the sources are silent in the second time slot, i.e. $\mathbf{s}^{(2)} = \mathbf{0}$, the destinations receive

$$\mathbf{d}_{\text{II}}^{(1)} = \tilde{\mathbf{H}}_{\text{SD}} \mathbf{s}^{(1)} + \mathbf{n}_{\text{D}}^{(1)} \quad (2.18)$$

$$\mathbf{d}_{\text{II}}^{(2)} = \tilde{\mathbf{H}}_{\text{RD}} \mathbf{G} \left(\tilde{\mathbf{H}}_{\text{SR}} \mathbf{s}^{(1)} + \mathbf{n}_{\text{R}}^{(1)} \right) + \mathbf{n}_{\text{D}}^{(2)} \quad (2.19)$$

in the first and second time slot, respectively.

- **Traffic Pattern III:** For traffic pattern III, the destinations do not receive in the first time slot. This means that the direct link is only used in the second time slot. Consequently, $\mathbf{d}_{\text{III}}^{(1)} = \mathbf{0}$ and $\mathbf{d}_{\text{III}}^{(2)}$ is the same as $\mathbf{d}_{\text{I}}^{(2)}$ in (2.15):

$$\mathbf{d}_{\text{III}}^{(1)} = \mathbf{0} \quad (2.20)$$

$$\mathbf{d}_{\text{III}}^{(2)} = \tilde{\mathbf{H}}_{\text{RD}} \mathbf{G} \left(\tilde{\mathbf{H}}_{\text{SR}} \mathbf{s}^{(1)} + \mathbf{n}_{\text{R}}^{(1)} \right) + \tilde{\mathbf{H}}_{\text{SD}} \mathbf{s}^{(2)} + \mathbf{n}_{\text{D}}^{(2)} \quad (2.21)$$

- **Traffic Pattern IV:** The direct link is not used at all for traffic pattern IV. Consequently, the input/output relation is derived from (2.14) and (2.15) by setting $\mathbf{d}_{\text{IV}}^{(1)} = \mathbf{0}$ and $\mathbf{s}^{(2)} = \mathbf{0}$:

$$\mathbf{d}_{\text{IV}}^{(1)} = \mathbf{0} \quad (2.22)$$

$$\mathbf{d}_{\text{IV}}^{(2)} = \tilde{\mathbf{H}}_{\text{RD}} \mathbf{G} \left(\tilde{\mathbf{H}}_{\text{SR}} \mathbf{s}^{(1)} + \mathbf{n}_{\text{R}}^{(1)} \right) + \mathbf{n}_{\text{D}}^{(2)} \quad (2.23)$$

¹Please recall that the transmission from sources via relays to destination requires two time slots.

2.5 Reference Scenario and Definition of the SNR

The average receive SNR of the network is defined by introducing a very simple reference scenario. It comprises M_S single-antenna source-destination pairs that communicate in a TDD manner. The instantaneous SNR in each time slot is given by

$$\text{SNR} = \frac{\mathbb{E}_s [|h \cdot s|^2]}{\mathbb{E}_n [|n|^2]} = \frac{|h|^2 \cdot 2\sigma_s^2}{\sigma_n^2}, \quad (2.24)$$

where $h \sim \mathcal{CN}(0, \sigma_h^2)$, $s \sim \mathcal{CN}(0, 2\sigma_s^2)$, and $n \sim \mathcal{CN}(0, \sigma_n^2)$ are the channel coefficient, the transmit symbol and the AWGN noise sample, respectively. Note that the factor 2 in the variance of s is used for normalization. The average receive SNR is then

$$\overline{\text{SNR}} = \mathbb{E}_h [\text{SNR}] = \frac{2\sigma_h^2 \sigma_s^2}{\sigma_n^2}. \quad (2.25)$$

The value for σ_s^2 leading to a certain $\overline{\text{SNR}}$ in (2.25) is then used in the multi-user scenarios to deliver a value of the respective figure of merit at this average SNR. One transmission cycle of the reference system, i.e. M_S time slots, then consumes a total transmit power of $M_S \cdot 2\sigma_s^2 := 2P_S$.

2.6 Average Sum Rate

Let $\mathbf{R}_X^{(s)}$, $\mathbf{R}_X^{(i)}$, and $\mathbf{R}_X^{(n)}$ denote the signal-, interference-, and noise covariance matrices at a certain destination m for traffic pattern $X \in \{\text{I, II, III, IV}\}$. Then, the mutual information for this source-destination pair is [168]

$$I_X = \frac{1}{2} \log_2 \det \left(\mathbf{I}_{M_{D_m}} + \left(\mathbf{R}_X^{(i)} + \mathbf{R}_X^{(n)} \right)^{-1} \mathbf{R}_X^{(s)} \right). \quad (2.26)$$

The pre-log factor $\frac{1}{2}$ comes from the fact that a two-hop transmission cycle comprises two time slots. Averaging the mutual information over the channel realizations delivers the average rate for source-destination pair m . The sum of the average rates for all source-destination pairs finally yields the *average sum rate*.

Chapter 3

Implementation Issues

Wireless communication systems exhibit an inherent dilemma. A high network performance is desirable while at the same time the mobile devices are supposed to be cheap and have a low power consumption. In particular, for relays and sensors in cooperative networks, price and battery life are crucial design goals. However, cheaper hardware components generally suffer from more severe impairments that in turn lead to a performance degradation. In order to build practical systems it is thus important to identify and understand the implications of imperfect hardware on the network. This allows to assess the performance of devised algorithms and protocols under more realistic conditions and to design methods to mitigate the perturbing effects of practical hardware components. Understanding hardware imperfections and their impact on the performance of a practical system is therefore an important step towards building it.

In this chapter the impact of hardware imperfections at the relays on cooperative, wireless two-hop networks is investigated. The focus lies on AF relaying, where the received signals are retransmitted after linear filtering. A selection of the most important RF impairments that have a special impact on two-hop relaying systems is discussed in the following. These are *LO frequency offsets*, *LO phase noise*, and *I/Q imbalance*. While TDD relays orthogonalize the first-hop and second-hop links in time (half-duplex), FDD relays orthogonalize them in frequency (full-duplex). For this reason, both types of relays introduce different errors to their forwarded signals. It turns out that networks employing half-duplex relays mainly suffer from phase noise during the time between reception and retransmission. In contrast to that, full-duplex relays introduce frequency offsets to the forwarded signals. They furthermore suffer from phase noise during the time between channel estimation and data transmission. If their forwarded signals are to combine coherently at the destination antennas, FDD relays require a global phase reference or frequent channel estimation even the propagation environment remains constant.

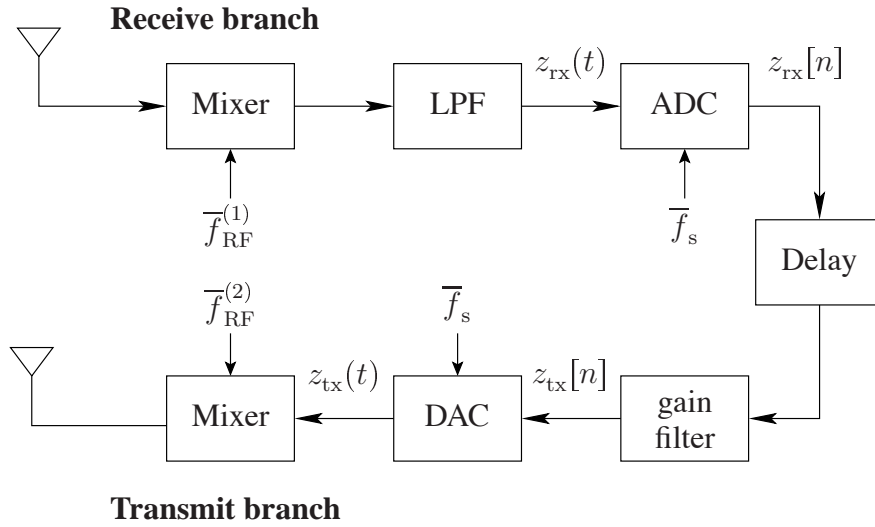


Fig. 3.1: Schematic of an AF relay with a single antenna.

The rest of this chapter is organized as follows: Section 3.1 introduces the relay block diagram and notation for Section 3.2, where the impact of an LO frequency offset and phase noise at the relay on the system performance is investigated. Section 3.3 then discusses I/Q imbalance at the relay and analyses its impact on the received signal at the destination.

3.1 Relay Block Diagram

Consider a simple distributed network with a single source-destination pair and one AF relay. For the introduction of the system model it is assumed that all hardware components are perfect (reference system). The nominal parameters of the reference system are in the following indicated by an overline (e.g. \bar{f}_s denotes the reference sampling frequency). Fig. 3.1 shows a schematic of the relay, where all components that are not affected by the discussed imperfections are omitted. These are, e.g., the preselection filter, low noise amplifier (LNA) and baseband amplifiers in the receive branch and the power amplifier and bandpass transmit filter in the transmit branch. The two depicted antennas represent the same physical antenna that is used for both reception and transmission. A direct conversion architecture is assumed in both the receive and transmit branch because it is of less complexity and exhibits a lower power consumption than super-heterodyne architectures (e.g. [169]). These two properties are important qualities of simple relays in ad-hoc or sensor networks.

The following investigations are based on the assumption that all oscillations in a node are generated by its LO. The carrier frequency in the first-hop transmission from source to

relay is denoted by $\bar{f}_{\text{RF}}^{(1)}$ and the carrier frequency in the second-hop transmission from relay to destination by $\bar{f}_{\text{RF}}^{(2)}$. The LO of the relay runs at frequency \bar{f}_{LO} and is used to generate both carrier frequencies locally using frequency synthesizers with parameters $c_{\text{RF}}^{(1)}$ and $c_{\text{RF}}^{(2)}$ (e.g. [170]):

$$\bar{f}_{\text{RF}}^{(1)} = c_{\text{RF}}^{(1)} \cdot \bar{f}_{\text{LO}}, \quad c_{\text{RF}}^{(1)} \in \mathbb{Q}, \quad (3.1)$$

$$\bar{f}_{\text{RF}}^{(2)} = c_{\text{RF}}^{(2)} \cdot \bar{f}_{\text{LO}}, \quad c_{\text{RF}}^{(2)} \in \mathbb{Q}. \quad (3.2)$$

The mixer in the receive branch uses $\bar{f}_{\text{RF}}^{(1)}$ to shift the signal from passband to baseband. Low-pass filtering of the mixer output delivers the continuous-time complex baseband signal $z_{\text{rx}}(t)$. It is sampled in the analog to digital converter (ADC) at a rate of

$$\bar{f}_s = c_s \cdot \bar{f}_{\text{LO}}, \quad c_s \in \mathbb{Q} \quad (3.3)$$

The resulting complex baseband samples are $z_{\text{rx}}[n] = z_{\text{rx}}(n\bar{T}_s)$, where $\bar{T}_s = 1/\bar{f}_s$. The subsequent delay will be called 'processing time'. It represents the total time between reception and retransmission and is defined as integer multiple of the sampling period \bar{T}_s , i.e.

$$\bar{T}_p := p \cdot \bar{T}_s, \quad p \in \mathbb{N}. \quad (3.4)$$

For full-duplex FDD relays, \bar{T}_p is zero and for half-duplex TDD relays it represents the orthogonalization of first-hop and second-hop transmission in time. The samples are subsequently fed to the discrete-time digital gain filter with impulse response

$$g[n] = \sum_{q=1}^Q g_q \delta[n - q]. \quad (3.5)$$

The computation of the complex-valued filter coefficients g_q is subject to system design and not treated in this chapter. Note, however, that the filter coefficients depend on the sampling rate. Filtering with the pulse shape $a(t)$ in the digital to analog converter (DAC) yields the continuous-time transmit signal $z_{\text{tx}}(t)$. The impulse response of the discrete-time digital gain filter, i.e. $g[n]$, and $a(t)$ can be combined into a single filter with continuous-time impulse response

$$g_a(t) = g[n] * a(t). \quad (3.6)$$

Finally, the signal $z_{\text{tx}}(t)$ is shifted from baseband to the carrier frequency $\bar{f}_{\text{RF}}^{(2)}$ in the up-

conversion mixer. For TDD relays the carrier frequencies of both links are identical, i.e. $\bar{f}_{\text{RF}}^{(1)} = \bar{f}_{\text{RF}}^{(2)}$, and for FDD relays they are different, i.e. $\bar{f}_{\text{RF}}^{(1)} \neq \bar{f}_{\text{RF}}^{(2)}$.

3.2 LO Imperfections

Several impairments are caused by the frequency offset and phase noise of an imperfect LO at an AF relay. In Section 3.2.1 the *sampling time offset*, *carrier frequency offset*, and *timing error* resulting from an LO frequency offset are introduced and discussed. LO phase noise is investigated in Section 3.2.2 and in Section 3.2.3 the impact of these imperfections on AF relaying is treated. Some of the results presented in this section have originally been published in [158].

3.2.1 LO Frequency Offset

In the following it is assumed that the LO frequency at the relay can be written as

$$f_{\text{LO}} = \bar{f}_{\text{LO}} (1 + \epsilon), \quad (3.7)$$

where $\epsilon \in \mathbb{R}$ is a measure for its frequency inaccuracy.

3.2.1.1 Sampling Time Offset

A sampling time offset occurs in the ADC of the receive chain. It can be split into a constant component, a random offset (jitter), and a sampling frequency offset. It turns out that neither a constant sampling time offset nor a sampling frequency offset at the relay have an impact on its retransmitted signal (as long as the sampling theorem is fulfilled). Jitter, however, leads to random amplitude errors in the digital signal and thus reduces the achievable SNR of the ADC (see e.g. [127] and references therein).

Assume that the sampling clock is derived by up-converting the local reference oscillation of frequency f_{LO} by the factor c_s . The sampling frequency is then given by

$$f_s = c_s \cdot f_{\text{LO}} = (1 + \epsilon) \bar{f}_s. \quad (3.8)$$

It has to be chosen large enough to guarantee that the sampling theorem is fulfilled in the presence of an LO frequency offset. Let furthermore ν denote a constant sampling time

offset. In the absence of jitter, the complex baseband receive signal $z_{\text{rx}}(t)$ is thus sampled at time instances $nT_s + \nu$, where $T_s = 1/f_s$ and $n \in \mathbb{N}$. The (periodic) frequency spectrum of the resulting discrete-time signal $z_{\text{rx}}[n] = z_{\text{rx}}(nT_s - \nu)$ is given by

$$Z_{\text{rx}}[k] = \sum_{k=-\infty}^{\infty} Z_{\text{rx}}\left(f - \frac{k}{T_s}\right) e^{-j2\pi\nu\frac{k}{T_s}}, \quad (3.9)$$

where $Z_{\text{rx}}(f)$ is the Fourier transform of $z_{\text{rx}}(t)$. Equation (3.9) reveals that the constant sampling time offset leads to a shift of the signal phase by $-2\pi\nu\frac{k}{T_s}$. For $k = 0$, i.e. in baseband, this phase shift is zero. Since the gain filter $g_a(t)$ given in (3.6) possesses a low-pass characteristic, the sampling time offset ν does not change the transmit signal of the relay. Furthermore, the continuous-time signal can be perfectly reconstructed from the sampled signal as long as f_s fulfills the sampling theorem.

3.2.1.2 Carrier Frequency Offset

Since the carrier frequencies used in the mixers are generated from f_{LO} , they are given by

$$f_{\text{RF}}^{(1)} = c_{\text{RF}}^{(1)} \cdot f_{\text{LO}} = \bar{f}_{\text{RF}}^{(1)} (1 + \epsilon) \quad (3.10)$$

$$f_{\text{RF}}^{(2)} = c_{\text{RF}}^{(2)} \cdot f_{\text{LO}} = \bar{f}_{\text{RF}}^{(2)} (1 + \epsilon), \quad (3.11)$$

where $c_{\text{RF}}^{(1)}$ and $c_{\text{RF}}^{(2)}$ are the same as in (3.1) and (3.2). With respect to the references $\bar{f}_{\text{RF}}^{(1)}$ and $\bar{f}_{\text{RF}}^{(2)}$, the locally generated carriers thus exhibit a frequency error of $\epsilon\bar{f}_{\text{RF}}^{(1)}$ and $\epsilon\bar{f}_{\text{RF}}^{(2)}$.

3.2.1.3 Timing Error

In order to operate multiple distributed nodes in a cooperative scheme, they have to follow a predefined schedule. Each participating terminal has to know when to transmit and when to receive. This requires a time synchronization on a time slot basis and a specified transmission cycle. In the presence of LO frequency offsets, the clock reference will be different for each node in the network. As a consequence, the timing drifts apart so that guard intervals at the beginning and at the end of each transmit burst have to be inserted. Furthermore, a regular resynchronization of the network becomes necessary in order to maintain proper operation.

Time synchronization in a distributed network is a difficult task that is out of the scope of the present work. So, without elaborating, it is assumed that perfect time synchronization of all nodes in the network is achieved at a certain point in time. The network has to agree

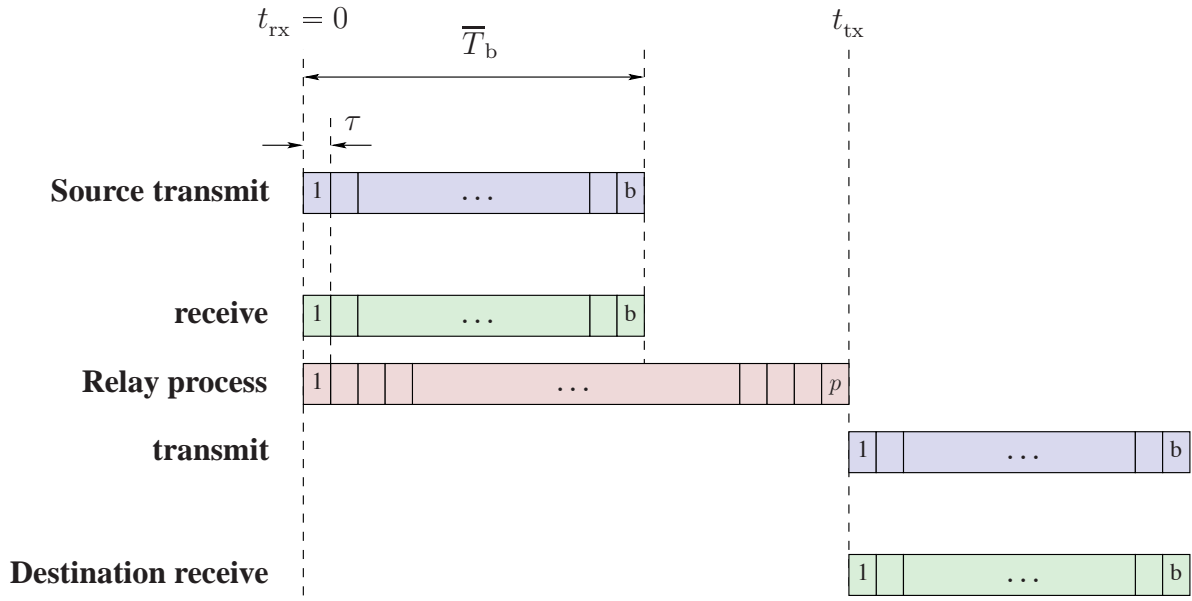


Fig. 3.2: Time chart for a two-hop traffic pattern with a single relay.

on a reference burst length \bar{T}_b and a relay processing time \bar{T}_p (as defined in (3.4)) in order to operate in a two-hop traffic pattern that comprises first-hop and second-hop transmission. The processing time has to be chosen large enough that all relays have finished processing their received data and are ready to retransmit. This also includes the time necessary for the relays to switch from receive to transmit mode and any inherent system delay.

Assume that the reference burst length and processing time are defined as integer multiples of the reference sampling period \bar{T}_s , i.e.

$$\bar{T}_b := b \cdot \bar{T}_s, \quad b \in \mathbb{N} \quad (3.12)$$

$$\bar{T}_p := p \cdot \bar{T}_s, \quad p \in \mathbb{N}. \quad (3.13)$$

In Fig. 3.2, the corresponding time chart for a perfectly synchronized network with a single source-destination pair and one relay is depicted. Starting from time $t_{rx} := 0$ the source transmits its burst to the relay. At time $t_{rx} + \bar{T}_b$ the first-hop transmission is completed. The relay has to finalize all signal processing until $t_{tx} = \bar{T}_p$. From t_{tx} until $t_{tx} + \bar{T}_b$ it retransmits its processed data to the destination. For *full-duplex relays*, the processing time is zero, i.e. $t_{tx} = t_{rx}$, and for *half duplex relays*, the processing time is at least as large as the burst length, i.e. $t_{tx} \geq t_{rx} + \bar{T}_b$.

In the presence of an LO frequency offset, the sampling period at the relay is $T_s = 1/f_s$ instead of $\bar{T}_s = 1/\bar{f}_s$, where the actual and the nominal sampling frequencies f_s and \bar{f}_s are

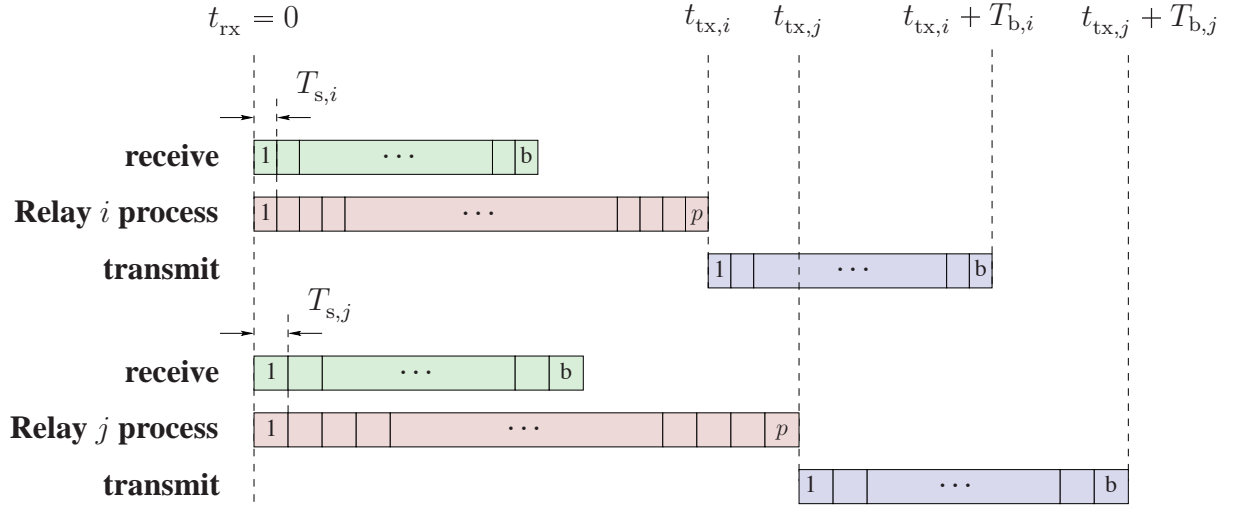


Fig. 3.3: Time chart for signal reception, processing, and retransmission at two relays.

given in (3.8) and (3.3), respectively. Consequently, the burst and processing times used by the relay are

$$T_b = b \cdot T_s = \frac{\bar{T}_b}{1 + \epsilon} \quad (3.14)$$

$$T_p = p \cdot T_s = \frac{\bar{T}_p}{1 + \epsilon}. \quad (3.15)$$

The timing of distributed nodes drifts apart if their LOs exhibit frequency offsets with respect to each other. Fig. 3.3 depicts a situation where the timing of two relays, namely relay i and j , drifts apart due to an offset in their respective sampling periods $T_{s,i}$ and $T_{s,j}$. In the following, the maximum timing error between any two relays that occurs within a single transmission cycle is derived as a function of \bar{T}_b and \bar{T}_p and the LO frequency inaccuracy parameter ϵ .

Consider a cooperative network with multiple relay nodes, where ϵ_l denotes the frequency inaccuracy parameter of relay l and $T_{s,l}$ the corresponding sampling period. Assume further and without loss of generality that relay i represents the relay with the fastest clock in the network and relay j the relay with the slowest clock. This means that

$$T_{s,i} = \min_l \{T_{s,l}\} \quad (3.16)$$

$$T_{s,j} = \max_l \{T_{s,l}\} \quad (3.17)$$

and thus

$$\epsilon_i = \max_l \{\epsilon_l\} \quad (3.18)$$

$$\epsilon_j = \min_l \{\epsilon_l\}. \quad (3.19)$$

The maximum synchronization error per transmission cycle is then given by

$$\begin{aligned} \Delta t_{i,j} &= (t_{\text{tx},j} + T_{\text{b},j}) - (t_{\text{tx},i} + T_{\text{b},i}) = \\ &= (b + p) (T_{\text{s},j} - T_{\text{s},i}) = \\ &= \bar{T}_s (b + p) \left(\frac{1}{1 + \epsilon_j} - \frac{1}{1 + \epsilon_i} \right). \end{aligned} \quad (3.20)$$

A time synchronization drift not only leads to an increasing synchronization mismatch between the nodes but also introduces different delays for the signal travelling via different relays. The delay difference that signals travelling via relay i and j experience is

$$t_{\text{tx},j} - t_{\text{tx},i} = \bar{T}_s p \left(\frac{1}{1 + \epsilon_j} - \frac{1}{1 + \epsilon_i} \right). \quad (3.21)$$

The equivalent two-hop channel (being the sum of all individual two-hop channels) becomes frequency-selective if the delay difference becomes comparable to the baseband symbol duration. Note that the severity of the frequency-selectivity is not influenced by the accumulated time synchronization error.

The 802.11-2007 wireless LAN MAC and PHY specifications [171] require an accuracy for the baseband frequency of 20 ppm. In a network comprising nodes that exhibit this accuracy, the maximum relative time shift per transmission cycle occurs if $\epsilon_i = \frac{20}{10^6}$ and $\epsilon_j = -\frac{20}{10^6}$. In this case, the relative timing error is given by

$$\frac{\Delta t_{i,j}}{\bar{T}_s} = (b + p) \frac{40}{10^6}. \quad (3.22)$$

This means that after $10^6/40 = 25\,000$ time intervals of length \bar{T}_s , the timing difference between any two nodes in the network is at maximum equal to \bar{T}_s .

3.2.2 Phase Noise

The output of any practical oscillator is subject to random fluctuations: Phase noise represents a time-varying drift of the LO phase from its reference. A model that is commonly used

to describe these phase variations is the so-called *Wiener phase noise*. It characterizes the phase fluctuation of a free-running oscillator that is perturbed by white noise as Wiener-Lévy process. The phase increments are modeled as independent zero-mean Gaussian random variables with a variance that increases linearly with the time between two observations.

In [172] the authors provide a framework to model phase noise in oscillators. For the sake of self-containedness, a short summary of their main results is presented here. This provides some background on Wiener phase noise, which will be used to model LO phase noise throughout this work. Let $x(t)$ denote the perfectly periodic signal of an unperturbed oscillator. If this oscillator is perturbed by noise, its output becomes a stationary stochastic process described by

$$x'(t) = x(t + \alpha(t)), \quad (3.23)$$

where $\alpha(t)$ is a changing time shift or phase deviation in the periodic output of the oscillator. The phase shift at the oscillator frequency f_{LO} that is the result of the time shift $\alpha(t)$ is given by

$$\phi(t) = 2\pi f_{LO}\alpha(t). \quad (3.24)$$

For the case that the perturbation is white noise, the authors of [172] show that, asymptotically in t , $\alpha(t)$ becomes a Gaussian random variable with constant mean m and variance ct . The scalar c is a real-valued hardware constant characterizing the oscillator quality in terms of phase stability. The power spectrum of the perturbed oscillator is then a Lorentzian¹ about each harmonic. It is furthermore shown that, asymptotically with time, the time shifts $\alpha(t)$ and $\alpha(t + \tau)$ at time instances t and $t + \tau \geq t$ are jointly Gaussian. Consequently, the phase increment between t and $t + \tau$ is normally distributed with zero mean and variance

$$\begin{aligned} \text{E} [(\phi(t + \tau) - \phi(t))^2] &= 4\pi^2 f_{LO}^2 \cdot \text{E} [(\alpha(t + \tau) - \alpha(t))^2] = \\ &= 4\pi^2 f_{LO}^2 \cdot c\tau. \end{aligned} \quad (3.26)$$

¹The Lorentzian function is defined as

$$L(x) = \frac{1}{\pi} \frac{\gamma}{(x - x_0)^2 + \gamma^2}, \quad (3.25)$$

where x_0 is the center and γ the scale parameter which specifies the half-width at half-maximum (corresponding to the *single-sided 3dB bandwidth* when the Lorentzian shape is in the frequency domain). The pdf of a Cauchy distribution (e.g. [173]) is a Lorentzian function.

The *phase noise variance* is defined as

$$\sigma_{\text{pn}}^2 = 4\pi^2 f_{\text{LO}}^2 c \left[\frac{\text{rad}^2}{\text{s}} \right]. \quad (3.27)$$

In practical hardware specifications, the constant c (in [$\text{s}^2 \text{ Hz}$]) is unfortunately not directly available. Instead, the decay of the oscillator power spectral density around the first harmonic is often used to describe the oscillator performance. This decay is characterized by the parameter $\mathcal{L}(f_m)$ [dBc/Hz], where f_m is the frequency offset with respect to f_{LO} . For small values of c and for $0 \leq f_m \ll f_c$, it can be approximated by (cf. [172])

$$\mathcal{L}(f_m) \approx 10 \log_{10} \left(\frac{1}{\pi} \cdot \frac{\pi f_c^2 c}{\pi^2 f_c^4 c^2 + f_m^2} \right). \quad (3.28)$$

The argument of the logarithm in (3.28) is a Lorentzian function. Thus, the single-sided 3dB bandwidth of the perturbed oscillator output signal is

$$\Delta f_{3 \text{ dB}} = \pi f_c^2 c. \quad (3.29)$$

For $\Delta f_{3 \text{ dB}} \ll f_m \ll f_c$, (3.28) can be further approximated by

$$\mathcal{L}(f_m) \approx 10 \log_{10} \left(\left(\frac{f_c}{f_m} \right)^2 c \right). \quad (3.30)$$

Solving (3.30) for c delivers

$$c = 10^{\frac{\mathcal{L}(f_m)}{10}} \cdot \left(\frac{f_m}{f_c} \right)^2, \quad (3.31)$$

which can be used to calculate the phase noise variance σ_{pn}^2 from the frequency characterization of a free-running LO. For voltage controlled oscillators (VCOs) running at around 5GHz typical values for $\mathcal{L}(1 \text{ MHz})$ are found to be between -110 dBc and -130 dBc (see e.g. [174] or [175] and references therein). Fig. 3.4 shows the resulting phase noise variance σ_{pn}^2 these oscillators exhibit. The three curves correspond to the same value of c but are plotted for different time increments (1 s, 1 ms, and 1 μs). Typical values of σ_{pn}^2 are hence between $4 \text{ rad}^2/\text{s}$ and $400 \text{ rad}^2/\text{s}$. Note that the Wiener phase noise model represents a worst-case for the phase error introduced at the relays because it is not bounded. Techniques that limit the phase variation within certain bounds (e.g. using a phase-locked-loop (PLL)) generally reduce the phase error (e.g. [176]). [177] provides a summary of phase noise models for two

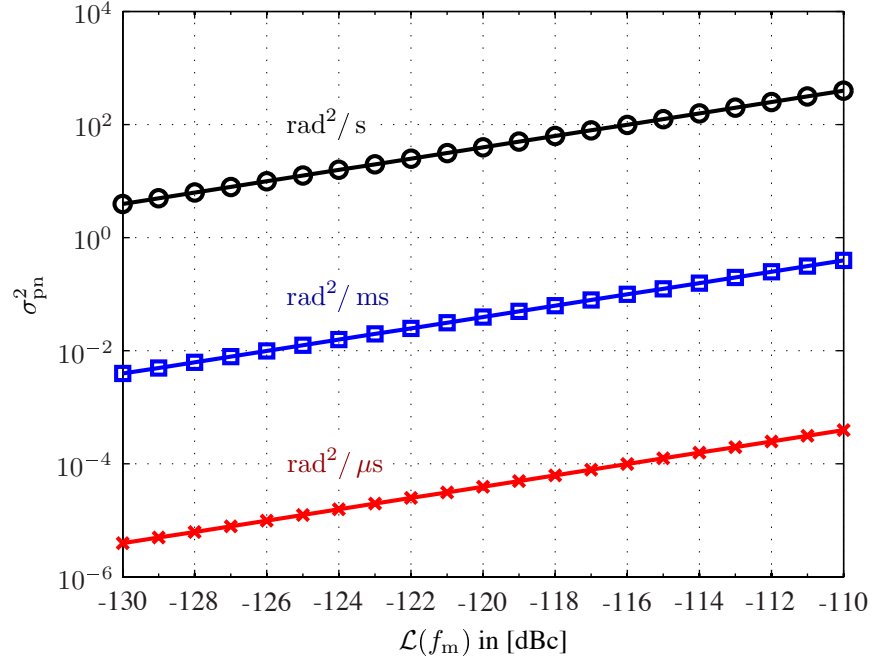


Fig. 3.4: Phase noise variance σ_{pn}^2 vs. $\mathcal{L}(f_m)$ at $f_m = 1$ MHz for typical LOs with $f_{LO} = 5$ GHz.

practical realizations of the LO, i.e., when the LO is realized as free-running oscillator and as a PLL synthesizer.

3.2.3 Impact on AF Relaying

In this section, the impact of LO frequency offsets and phase noise on AF relaying is investigated. Since the focus lies on hardware imperfections at the relays both the source and destination nodes are assumed to possess perfect hardware components. In Section 3.2.3.1 the phase and frequency errors that occur at a relay with imperfect LO are investigated. It turns out that FDD and TDD relays introduces different errors to their forwarded signals. A comparison between both types of relays is presented in Section 3.2.3.2. Finally, Section 3.2.3.3 discusses the impact of a timing error on the overall data rate of the network.

3.2.3.1 Frequency and Phase Error

Sections 3.2.1 and 3.2.2 introduced the frequency offset and phase noise an imperfect LO exhibits. At an AF relay they lead to a frequency and phase error of the retransmitted signal.

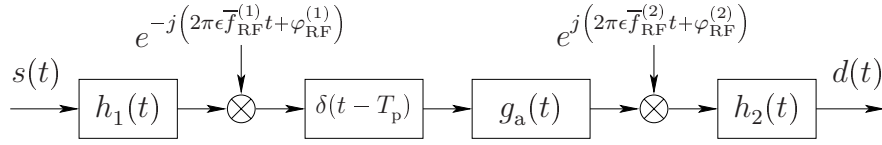


Fig. 3.5: Complex baseband block diagram.

In this section, these two perturbances are quantified. To this end, the following assumptions are made:

- There is neither thermal noise nor quantization noise (so that the effect of the LO imperfections can be isolated).
- All nodes exhibit a perfect time slot synchronization at the beginning of the transmission cycle.
- The sampling theorem is always fulfilled.

Consider the analog system model depicted in Fig. 3.5. It shows the complex-baseband block diagram of the transmission between source and destination via an AF relay. The *carrier frequency offsets*, *LO phase noise*, and the *timing error* are taken into account. $s(t)$ denotes the complex baseband transmit signal of the source and $d(t)$ the complex baseband receive signal of the destination. The equivalent low-pass first-hop and second-hop channels are characterized by their impulse responses $h_1(t)$ and $h_2(t)$, respectively. They are assumed to remain constant for a whole transmission cycle (block-fading). Since the carrier frequencies are generated from the LO as given in (3.10) and (3.11), the RF phases at reception and retransmission time are $\varphi_{\text{RF}}^{(1)} = c_{\text{RF}}^{(1)}\varphi_{\text{LO}}^{(1)}$ and $\varphi_{\text{RF}}^{(2)} = c_{\text{RF}}^{(2)}\varphi_{\text{LO}}^{(2)}$, respectively. They are assumed to remain constant for the duration of a whole data burst. Using the Wiener phase noise model, the phase difference $\Delta\varphi = \varphi_{\text{LO}}^{(2)} - \varphi_{\text{LO}}^{(1)}$ is a zero-mean Gaussian random variable with variance $\sigma_{\text{pn}}^2 T_p$, i.e.

$$\Delta\varphi \sim \mathcal{N}(0, \sigma_{\text{pn}}^2 T_p). \quad (3.32)$$

The frequency spectrum of the received signal at the destination is

$$D(f) = H_2(f)H_1\left(f - \epsilon\bar{f}_{\text{RF}}^{(2)} + \epsilon\bar{f}_{\text{RF}}^{(1)}\right)G_a\left(f - \epsilon\bar{f}_{\text{RF}}^{(2)}\right) \cdot e^{-j2\pi(f - \epsilon\bar{f}_{\text{RF}}^{(2)})T_p} e^{j(\varphi_{\text{RF}}^{(2)} - \varphi_{\text{RF}}^{(1)})} S\left(f - \epsilon\bar{f}_{\text{RF}}^{(2)} + \epsilon\bar{f}_{\text{RF}}^{(1)}\right), \quad (3.33)$$

where $S(f) = \mathcal{F}\{s(t)\}$, $H_1(f) = \mathcal{F}\{h_1(t)\}$, $H_2(f) = \mathcal{F}\{h_2(t)\}$, $G_a(f) = \mathcal{F}\{g_a(t)\}$, and $D(f) = \mathcal{F}\{d(t)\}$. The following signal impairments can be identified in $D(f)$:

Frequency Error: A total frequency error of

$$\Delta f = \left(\bar{f}_{\text{RF}}^{(2)} - \bar{f}_{\text{RF}}^{(1)} \right) \epsilon, \quad (3.34)$$

is introduced to the signal at the relay as a result of downconversion (reception) and upconversion (retransmission). For TDD relays the frequency error vanishes, i.e. $\Delta f = 0$, because $\bar{f}_{\text{RF}}^{(2)} = \bar{f}_{\text{RF}}^{(1)}$. However, for FDD relays it generally holds that $|\Delta f| > 0$ because $\bar{f}_{\text{RF}}^{(2)} \neq \bar{f}_{\text{RF}}^{(1)}$.

Phase Error: Both phase noise and the timing error lead to a phase error in the received signal at the destination. The *phase error due to phase noise* is

$$\psi_{\text{pn}} = \varphi_{\text{RF}}^{(2)} - \varphi_{\text{RF}}^{(1)} = \left(c_{\text{RF}}^{(2)} - c_{\text{RF}}^{(1)} \right) \varphi_{\text{LO}}^{(1)} + c_{\text{RF}}^{(2)} \Delta \varphi, \quad (3.35)$$

where $\Delta \varphi = \varphi_{\text{LO}}^{(2)} - \varphi_{\text{LO}}^{(1)}$ is the phase change of the LO during the processing time (cf. (3.32)). We have

$$\psi_{\text{pn}}^{(\text{TDD})} = c_{\text{RF}} \Delta \varphi \quad (3.36)$$

for TDD relays because $c_{\text{RF}}^{(2)} = c_{\text{RF}}^{(1)} := c_{\text{RF}}$. Equation (3.36) reveals that the severity of the phase error is determined by the processing time T_p . In order to keep it small, T_p has to be kept small. For FDD relays we have

$$\psi_{\text{pn}}^{(\text{FDD})} = \left(c_{\text{RF}}^{(2)} - c_{\text{RF}}^{(1)} \right) \varphi_{\text{LO}}^{(1)} \quad (3.37)$$

because $T_p = 0$. In this case, the phase error introduced to the signal depends on the current LO phase of the relay. If the channel measurement is performed in the same traffic pattern as the data transmission, $\psi_{\text{pn}}^{(\text{FDD})}$ is implicitly included in the channel estimates and thus compensated by the gain filter as long as the LO phase remains constant. However, $\varphi_{\text{LO}}^{(1)}$ changes in the presence of phase noise. In case the forwarded signals of multiple FDD relays are to combine coherently at the destination antennas, they require a global phase reference or frequent channel estimation (to take the current LO phases into account) even if the propagation environment remains constant. Note that $\psi_{\text{pn}}^{(\text{FDD})}$ can be kept small by keeping the frequency separation $\left(c_{\text{RF}}^{(2)} - c_{\text{RF}}^{(1)} \right)$ small.

The *phase error due to timing error* is derived from the phase offset introduced by the processing time, i.e.

$$\psi_{\text{T}}(f) = -2\pi \left(f - \bar{f}_{\text{RF}}^{(2)} \right) T_p. \quad (3.38)$$

Compared to the signal that is forwarded by a relay with perfect LO, $\psi_T(f)$ exhibits an error of

$$\begin{aligned}\Delta\psi_T(f) &= \psi_T(f) - (-2\pi f\bar{T}_p) = \\ &= 2\pi f\bar{T}_p \frac{\epsilon}{1+\epsilon} + 2\pi \bar{f}_{\text{RF}}^{(2)} \bar{T}_p \frac{\epsilon}{1+\epsilon}.\end{aligned}\quad (3.39)$$

Note that the first summand in (3.39) is a function of the frequency f . In the presence of multiple relays with different processing times this leads to an increased frequency-selectivity of the compound source-relay-destination channel. For a TDD relay $|\Delta\psi_T(f)| > 0$ whereas we have $\Delta\psi_T(f) = 0$ for a FDD relay because $\bar{T}_p = 0$. Since ϵ is likely to change slowly compared to the propagation environment, $\Delta\psi_T(f)$ will be taken into account by the channel estimates if the measurement procedure follows the same traffic pattern as the data transmission. It is thus compensated by the gain filters if they are computed from these estimates.

3.2.3.2 Comparison Between FDD and TDD Relays

While TDD relays orthogonalize the first-hop and second-hop links in time (half-duplex), FDD relays orthogonalize them in frequency (full-duplex). For this reason, both types of relays introduce different errors to their forwarded signals. We have seen in Section 3.2.3.1 that networks employing half-duplex relays mainly suffer from phase noise during the time between reception and retransmission. In contrast to that, full-duplex relays introduce frequency offsets to the forwarded signals and suffer from phase noise during the time between channel estimation and data transmission. If their forwarded signals are to combine coherently at the destination antennas, FDD relays require a global phase reference or frequent channel estimation even if the propagation environment remains constant.

In this section the severity of the errors that are introduced by both types of relays are compared. Monte-Carlo simulations were performed to assess the performance of a multiuser network employing either TDD or FDD relays with imperfect LOs.

System Parameters: The investigated network comprises N_{SD} source-destination pairs and N_{R} relays. Each node is equipped with a single antenna only. The system parameters are chosen according to the IEEE 802.11n standard: All nodes employ orthogonal frequency division multiplexing (OFDM) modulation with 65 equally spaced subcarriers, out of which 57 are used for data transmission. The gain filter at each relay realizes a complex-valued scaling factor for every frequency-flat data subchannel. The user bandwidth is 20 MHz and the OFDM symbol duration including cyclic prefix is 4 μs . For TDD relaying the nominal

carrier frequencies for both the first-hop and the second-hop link are $\bar{f}_{\text{RF}}^{(1)} = \bar{f}_{\text{RF}}^{(2)} = 5.5$ GHz. The nominal carrier frequencies for FDD relaying are $\bar{f}_{\text{RF}}^{(1)} = 5.5$ GHz and $\bar{f}_{\text{RF}}^{(2)} = 5.6$ GHz. The HIPERLAN B channel model [178] is used to generate realizations of the frequency-selective blockfading radio channels between all nodes. It corresponds to an office environment with large delay spread. The gain factors are computed such that the source-destination pairs are completely orthogonalized in space (MUZF relaying, cf. [25] and Section 6.2). To this end, the signals from all relays have to add coherently at the destination antennas. For all simulation results the number of relays is $N_{\text{R}} = N_{\text{SD}}(N_{\text{SD}} - 1) + 1$, which is the minimum number of relays than can orthogonalize all source-destination pairs [25].

Figure of Merit: All first and second-hop channel coefficients are assumed to be measured at $t = 0$ and $t = T_{\text{p}}$, respectively. Please recall that for FDD relays $T_{\text{p}} = 0$. For TDD relays the estimates of the second-hop channels take the phase offset due to timing error (cf. (3.39)) into account. In order to investigate the impact of imperfect LOs at the relays on the network performance it is assumed that the channel estimates are noiseless but subject to frequency and phase errors from the relays. The gain filters are then computed from these estimates and the average signal-to-interference ratio (SIR) is evaluated for a data transmission at $t = T_{\text{p}} + T_{\text{d}}$, where T_{d} represents the time between channel estimation and data transmission. This figure of merit reflects the accuracy with which the relays orthogonalize the source-destination pairs and is thus a direct indicator for the severity of the phase and frequency errors. Let

$$h_{m,k}^{(i)} = \sum_{l=1}^{N_{\text{R}}} h_{m,l}^{(i)} g_l^{(i)} h_{l,k}^{(i)} \quad (3.40)$$

denote the equivalent channel coefficient of subchannel i between source k and destination m , where $h_{l,k}^{(i)}$ and $h_{m,l}^{(i)}$ are the respective source-relay and relay-destination channels. The instantaneous SIR on subchannel i at destination m is then given by

$$\text{SIR}_m^{(i)} = \frac{|h_{m,m}^{(i)}|^2}{\left| \sum_{k=1, k \neq m}^{N_{\text{SD}}} h_{m,k}^{(i)} \right|^2}. \quad (3.41)$$

Averaging $\text{SIR}_m^{(i)}$ over 10000 channel realizations, all subchannels, and all destinations yields the average SIR that is used in the following.

Simulation Results: Fig. 3.6 shows the average SIR versus the frequency uncertainty for different number of source-destination pairs and relays. There is no phase noise, i.e. $\sigma_{\text{pn}}^2 = 0$,

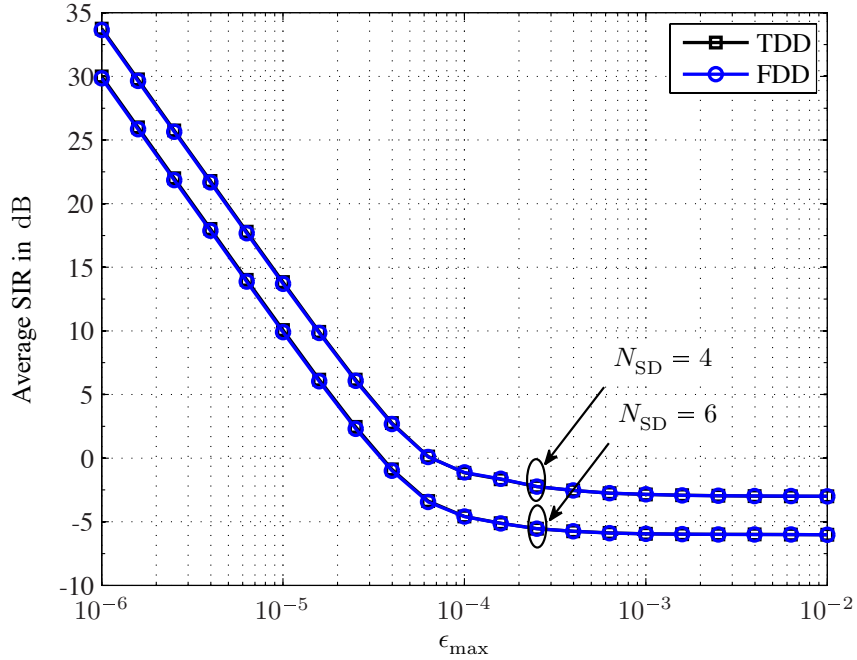


Fig. 3.6: Average SIR vs. frequency uncertainty for $\sigma_{\text{pn}}^2 = 0$.

which makes the results independent of T_p and T_d . For each relay and channel realization the frequency uncertainty parameter ϵ was randomly drawn from a uniform distribution $\epsilon \sim \mathcal{U}(-\epsilon_{\text{max}}, \epsilon_{\text{max}})$. The SIR degrades for increasing frequency uncertainty and saturates at a point that corresponds to noncoherent forwarding, i.e., amplitude scaling at the relays without phase rotation. The figure also reveals that the frequency error degrades the SIR equally for TDD and FDD relays for the used channel model and the depicted values for ϵ_{max} .

Fig. 3.7 shows the average SIR as a function of the time \bar{T}_d between channel estimation and data transmission for $\epsilon_{\text{max}} = 0$. The frequency error (3.34) as well as the phase error due to timing error (3.39) vanish in this case. The phase error due to phase noise is the only remaining signal perturbation. Note that for TDD relays it is independent of T_d (see (3.36)). In order to compute the crossing point between the performance of TDD and FDD relays (indicated by the dashed line) it suffices to look at a single source-destination pair and one relay. Let \hat{h}_1 and \hat{h}_2 denote the estimates of the source-relay and relay-destination channel coefficients. They are given by

$$\hat{h}_1 = h_1 e^{-j\varphi_1} \quad (3.42)$$

$$\hat{h}_2 = h_2 e^{j\varphi_2}, \quad (3.43)$$

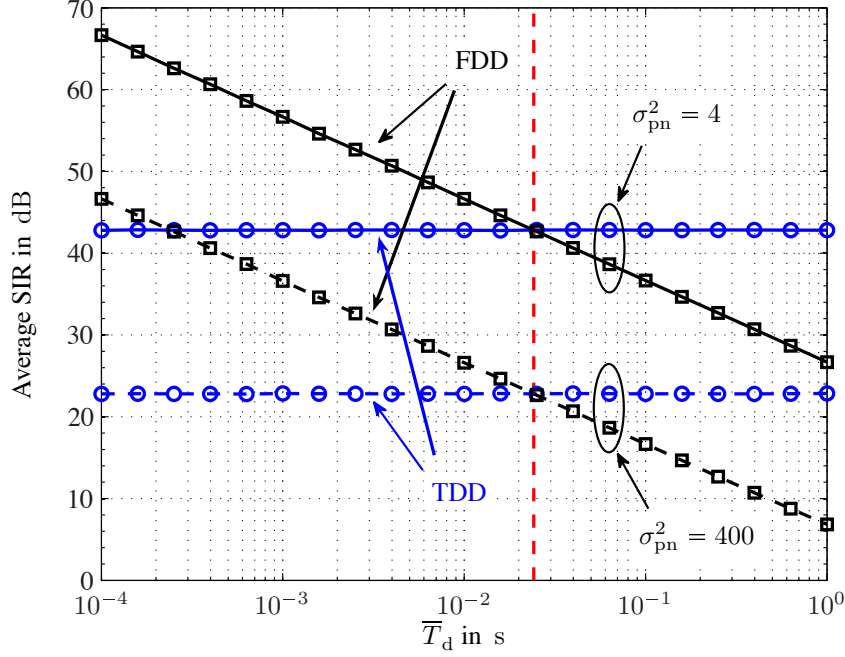


Fig. 3.7: Average SIR vs. \bar{T}_d for $N_{SD} = 4$, $\epsilon_{\max} = 0$, and $\bar{T}_p = 4 \mu\text{s}$.

where $\varphi_1 = c_{\text{RF}}^{(1)} \cdot \varphi_{\text{LO}}^{(1)}$ is the RF phase and $\varphi_{\text{LO}}^{(1)}$ the LO phase of the relay at $t = 0$ and $\varphi_2 = c_{\text{RF}}^{(2)} \cdot \varphi_{\text{LO}}^{(2)}$ the RF phase and $\varphi_{\text{LO}}^{(2)}$ the LO phase of the relay at $t = \bar{T}_p$. The gain factor is computed from \hat{h}_1 and \hat{h}_2 , i.e. $g = f(\hat{h}_1, \hat{h}_2)$. Hence, the *desired* equivalent two-hop channel coefficient is

$$\hat{h}_{\text{eq}} = \hat{h}_2 \cdot g \cdot \hat{h}_1. \quad (3.44)$$

At time $t = \bar{T}_p + T_d$ the source transmits data over the first-hop channel h'_1 to the relay and the relay retransmits the data over the second-hop channel h'_2 to the destination at time $t = 2\bar{T}_p + T_d$. The channel coefficients are now given by

$$h'_1 = h_1 e^{-j\varphi'_1} \quad (3.45)$$

$$h'_2 = h_2 e^{j\varphi'_2}, \quad (3.46)$$

where $\varphi'_1 = c_{\text{RF}}^{(1)} \cdot \varphi_{\text{LO}}^{(1)'}$ is the RF phase and $\varphi_{\text{LO}}^{(1)'}$ the LO phase of the relay at $t = \bar{T}_p + T_d$ and $\varphi'_2 = c_{\text{RF}}^{(2)} \cdot \varphi_{\text{LO}}^{(2)'}$ is the RF phase and $\varphi_{\text{LO}}^{(2)'}$ the LO phase of the relay at $t = 2\bar{T}_p + T_d$.

The equivalent source-destination channel is then

$$\begin{aligned} h'_{\text{eq}} &= \hat{h}'_2 \cdot g \cdot \hat{h}'_1 = \\ &= h_2 g h_1 \cdot e^{j(\varphi'_2 - \varphi'_1)}. \end{aligned} \quad (3.47)$$

Since $h_1 = \hat{h}_1 e^{j\varphi_1}$ (see (3.42)) and $h_2 = \hat{h}_2 e^{-j\varphi_2}$ (see (3.43)), h'_{eq} can be written as

$$\begin{aligned} h'_{\text{eq}} &= \hat{h}_2 e^{-j\varphi_2} g \hat{h}_1 e^{j\varphi_1} \cdot e^{j(\varphi'_2 - \varphi'_1)} = \\ &= \hat{h}_2 g \hat{h}_1 \cdot e^{j(\varphi'_2 - \varphi'_1 - \varphi_2 + \varphi_1)} = \\ &= \hat{h}_{\text{eq}} \cdot e^{j(\varphi'_2 - \varphi'_1 - \varphi_2 + \varphi_1)}. \end{aligned} \quad (3.48)$$

Note that \hat{h}_{eq} is the *desired* channel coefficient while h'_{eq} is the *actual* one. In the presence of phase noise the phase error $\varphi'_2 - \varphi'_1 - \varphi_2 + \varphi_1$ is generally nonzero. For **TDD relays** it becomes

$$\begin{aligned} \psi_{\text{pn},l}^{(\text{TDD})} &:= \varphi'_2 - \varphi'_1 - \varphi_2 + \varphi_1 = \\ &= c_{\text{RF}} \cdot \varphi_{\text{LO}}^{(2)'} - c_{\text{RF}} \cdot \varphi_{\text{LO}}^{(1)'} - c_{\text{RF}} \cdot \varphi_{\text{LO}}^{(2)} + c_{\text{RF}} \cdot \varphi_{\text{LO}}^{(1)} = \\ &= c_{\text{RF}} \left(\varphi_{\text{LO}}^{(2)'} - \varphi_{\text{LO}}^{(1)'} - \left(\varphi_{\text{LO}}^{(2)} - \varphi_{\text{LO}}^{(1)} \right) \right) = \\ &= c_{\text{RF}} (\Delta\varphi' - \Delta\varphi) \end{aligned} \quad (3.49)$$

because $c_{\text{RF}}^{(1)} = c_{\text{RF}}^{(2)} := c_{\text{RF}}$. For the Wiener phase noise model the phase changes due to phase noise are $\Delta\varphi' \sim \mathcal{N}(0, \sigma_{\text{pn}}^2 \bar{T}_p)$ and $\Delta\varphi \sim \mathcal{N}(0, \sigma_{\text{pn}}^2 \bar{T}_p)$ (see (3.32)). They are mutually independent and thus

$$\psi_{\text{pn},l}^{(\text{TDD})} \sim \mathcal{N}(0, 2c_{\text{RF}}^2 \sigma_{\text{pn}}^2 \bar{T}_p). \quad (3.50)$$

For **FDD relays** the processing time is zero, i.e. $\bar{T}_p = 0$. This means that $\varphi_{\text{LO}}^{(1)} = \varphi_{\text{LO}}^{(2)} := \varphi_{\text{LO}}$ and $\varphi_{\text{LO}}^{(1)'} = \varphi_{\text{LO}}^{(2)'} := \varphi'_{\text{LO}}$. The phase error is in this case

$$\begin{aligned} \psi_{\text{pn},l}^{(\text{FDD})} &:= \varphi'_2 - \varphi'_1 - \varphi_2 + \varphi_1 = \\ &= c_{\text{RF}}^{(2)} \cdot \varphi'_{\text{LO}} - c_{\text{RF}}^{(1)} \cdot \varphi'_{\text{LO}} - c_{\text{RF}}^{(2)} \cdot \varphi_{\text{LO}} + c_{\text{RF}}^{(1)} \cdot \varphi_{\text{LO}} = \\ &= \left(c_{\text{RF}}^{(2)} - c_{\text{RF}}^{(1)} \right) (\varphi'_{\text{LO}} - \varphi_{\text{LO}}) = \\ &= \left(c_{\text{RF}}^{(2)} - c_{\text{RF}}^{(1)} \right) \cdot \Delta\varphi_{\text{LO}}, \end{aligned} \quad (3.51)$$

where $\Delta\varphi_{\text{LO}}$ is the phase change during the time between channel estimation and data trans-

mission. In analogy to (3.32) it is a zero-mean Gaussian random variable with variance $\left(c_{\text{RF}}^{(2)} - c_{\text{RF}}^{(1)}\right)^2 \sigma_{\text{pn}}^2 T_{\text{data}}$, i.e.

$$\psi_{\text{pn},l}^{(\text{FDD})} \sim \mathcal{N}\left(0, \left(c_{\text{RF}}^{(2)} - c_{\text{RF}}^{(1)}\right)^2 \sigma_{\text{pn}}^2 T_{\text{d}}\right). \quad (3.52)$$

For TDD relays $\psi_{\text{pn},l}^{(\text{TDD})}$ depends on \bar{T}_{p} , i.e. the processing time, but not on T_{d} , i.e. the time between channel estimation and data transmission. For FDD relays $\psi_{\text{pn},l}^{(\text{FDD})}$ depends on T_{d} but not on \bar{T}_{p} . The severity of the phase error introduced by both types of relays is equal if

$$2c_{\text{RF}}^2 \sigma_{\text{pn}}^2 \bar{T}_{\text{p}} = \left(c_{\text{RF}}^{(2)} - c_{\text{RF}}^{(1)}\right)^2 \sigma_{\text{pn}}^2 T_{\text{d}}. \quad (3.53)$$

Solving for T_{d} delivers

$$T_{\text{d}} = 2 \left(\frac{c_{\text{RF}}}{c_{\text{RF}}^{(2)} - c_{\text{RF}}^{(1)}} \right)^2 \bar{T}_{\text{p}}. \quad (3.54)$$

The lines in Fig. 3.7 consequently cross at

$$T_{\text{d}} = 2 \left(\frac{c_{\text{RF}}}{c_{\text{RF}}^{(2)} - c_{\text{RF}}^{(1)}} \right)^2 \cdot T_{\text{p}} = 24.2 \text{ ms} \quad (3.55)$$

for the chosen set of parameters. This point is indicated by the dashed red line. Note in particular that (3.54) is independent of σ_{pn}^2 and the number of relays!

Finally, Fig. 3.8 shows the degradation of the average SIR versus \bar{T}_{p} for TDD relays and the case that $\epsilon_{\text{max}} = 0$. The left-most point corresponds to $\bar{T}_{\text{p}} = 4 \mu\text{s}$, i.e., a transmission frame comprises exactly one OFDM symbol. Efficient orthogonalization of all source-destination pairs obviously requires stable LOs at the relays, i.e. small σ_{pn}^2 , or short processing times, i.e. small \bar{T}_{p} .

3.2.3.3 Network Synchronization Error

We have seen in Section 3.2.1.3 that an LO frequency offset leads to an accumulating timing error. This in turn reduces the usable section of each data burst in a network because guard intervals have to be inserted. In this section the resulting reduction of the effective data rate for a cooperative relaying network is investigated. Consider to this end a two-hop network with a single source-destination pair and multiple TDD relays.

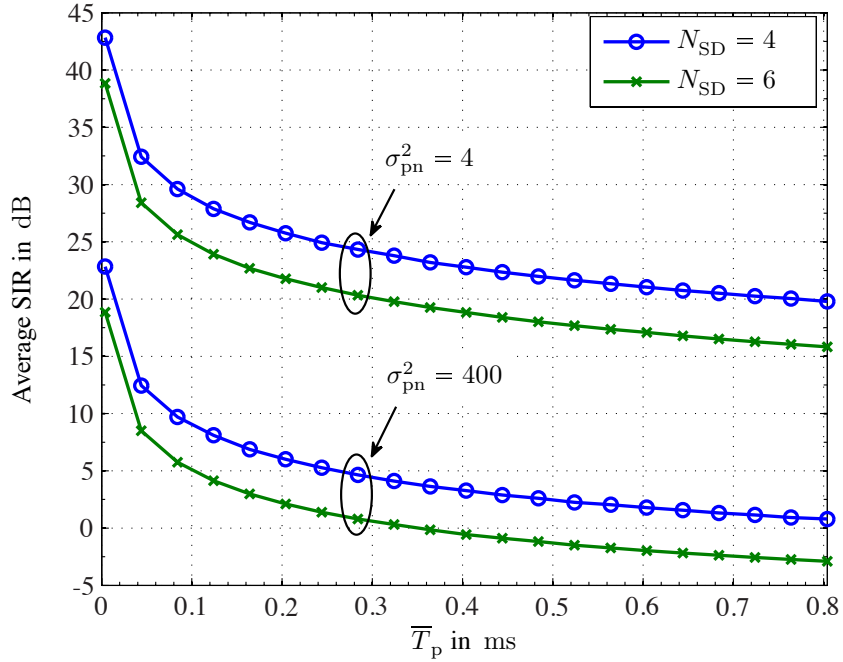


Fig. 3.8: Average SIR vs. \bar{T}_p for TDD relays, where $\epsilon_{\max} = 0$.

The nominal start (reference timing) of the first and second time slot of a transmission cycle is denoted by t_1 and t_2 , respectively. The source node exhibits the timing offset Δt_S and thus starts transmitting at time $t_1 + \Delta t_S$. The destination exhibits the timing offset Δt_D and starts receiving at time $t_2 + \Delta t_D$. Assume without loss of generality the relay i exhibits the fastest clock of all relays and relay j the slowest. They start their respective transmission cycles at times $t_1 + \Delta t_{R,i}$ and $t_1 + \Delta t_{R,j}$, where

$$\Delta t_{R,i} = \min_l \{\Delta t_{R,l}\}, \quad l \in \{1, \dots, N_R\} \quad (3.56)$$

$$\Delta t_{R,j} = \max_l \{\Delta t_{R,l}\}, \quad l \in \{1, \dots, N_R\}. \quad (3.57)$$

An exemplary time chart of the described situation is depicted in Fig. 3.9. It is assumed that the incremental timing error is negligible, i.e. $T_p \approx \bar{T}_p$ and $T_b \approx \bar{T}_b$ for all relays. Note that all timing offsets can be negative. In the following the first-hop (source-to-relays) and second-hop (relays-to-destination) transmission are investigated in detail:

- **First-hop transmission:** The source transmits its data from $t_{S,\text{begin}} := t_1 + \Delta t_S$ until $t_{S,\text{end}} := t_1 + \Delta t_S + \bar{T}_b$. Consequently, relay l receives a useful signal from

$$t_{1,\text{begin}}^{(l)} := \max \{t_{S,\text{begin}}, t_1 + \Delta t_{R,l}\} \quad (3.58)$$

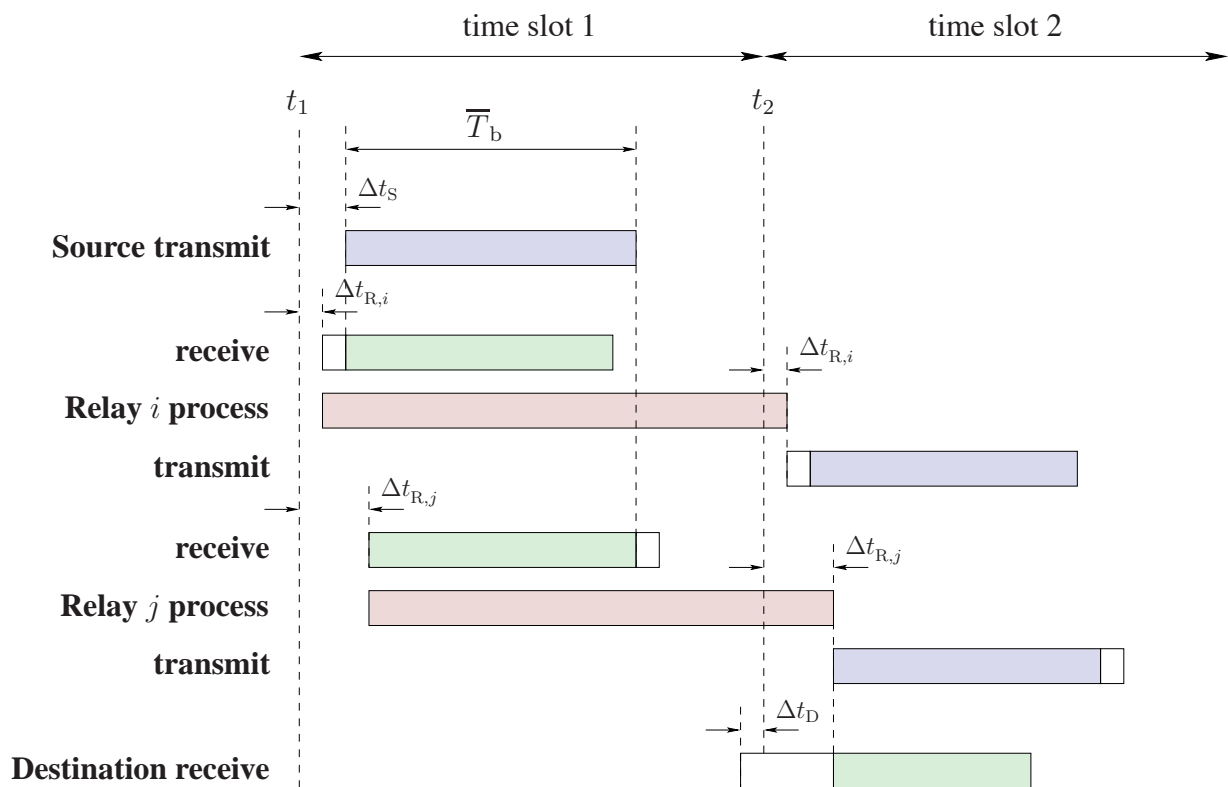


Fig. 3.9: Example of a time chart for signal reception, processing, and retransmission in the presence of a time synchronization error.

until

$$t_{1,\text{end}}^{(l)} := \min \{t_{\text{S,end}}, t_1 + \Delta t_{\text{R},l} + \bar{T}_b\}. \quad (3.59)$$

The *useful* part of the received burst at each relay is indicated as green rectangle in Fig. 3.9 and the *useless* part as white rectangle.

- **Second-hop transmission:** In Sections 6.2 and 6.3, two coherent multiuser gain allocation schemes are presented that allow multiple source-destination pairs to communicate concurrently on the same physical channel. This is achieved by computing the gain factors of the relays such that multiuser interference (MUI) is suppressed at all nonbelonging destinations. However, the schemes only work while all relay terminals retransmit their data bursts. Consequently, the destinations receive a useful signal only during that time. The relay with the slowest clock, i.e. relay j , starts retransmitting useful data at

$$\begin{aligned} t_{2,\text{begin}}^{\text{max}} &= \max_l \{t_{1,\text{begin}}^{(l)}\} + \bar{T}_p = \\ &= t_{1,\text{begin}}^{(j)} + \bar{T}_p. \end{aligned} \quad (3.60)$$

The relay with the fastest clock, i.e. relay i , stops transmitting useful data at

$$\begin{aligned} t_{2,\text{end}}^{\text{min}} &= \min_l \{t_{1,\text{end}}^{(l)}\} + \bar{T}_p = \\ &= t_{1,\text{end}}^{(i)} + \bar{T}_p. \end{aligned} \quad (3.61)$$

The destination can thus only receive a useful signal from $t_{2,\text{begin}}^{(\text{max})}$ to $t_{2,\text{end}}^{(\text{min})}$. Taking its own time synchronization shift into account, it is in receive mode from $t_2 + \Delta t_D$ until $t_2 + \Delta t_D + \bar{T}_b$. Consequently, the destination receives useful data from

$$t_{\text{D,begin}} := \max \left\{ t_2 + \Delta t_D, t_{2,\text{begin}}^{(\text{max})} \right\} \quad (3.62)$$

until

$$t_{\text{D,end}} := \min \left\{ t_2 + \Delta t_D + \bar{T}_b, t_{2,\text{end}}^{(\text{min})} \right\}. \quad (3.63)$$

In order to transmit the whole data burst successfully, the source has to use a guard interval at the beginning (pre-guard) and at the end (post-guard) of each burst. Their respective lengths are denoted by $t_{\text{g,pre}}$ and $t_{\text{g,post}}$, respectively. This means that it starts transmitting useful

data at

$$t_{S,\text{begin}} := t_1 + \Delta t_S + t_{g,\text{pre}} \quad (3.64)$$

and stops transmitting useful data at

$$t_{S,\text{end}} := t_1 + \Delta t_S + T_b - t_{g,\text{post}}. \quad (3.65)$$

For the destination to be able to receive the whole burst of useful data, it is required that

$$t_{g,\text{pre}} \geq \max \{ \Delta t_{R,j} - \Delta t_S, 0 \} \quad (3.66)$$

$$\text{and } t_{2,\text{begin}}^{(\max)} \geq t_2 + \Delta t_D \quad (3.67)$$

for the pre-guard and

$$t_{g,\text{post}} \geq \max \{ \Delta t_S - \Delta t_{R,i}, 0 \} \quad (3.68)$$

$$\text{and } t_{2,\text{end}}^{(\min)} \leq t_2 + \Delta t_D + T_b \quad (3.69)$$

for the post-guard. For the following considerations it is assumed that the guard intervals are chosen to have the smallest possible duration that still fulfills the requirements (3.66)–(3.69).

- **Pre-Guard:** Requirement (3.66) can be interpreted as follows: If $\Delta t_S \geq \Delta t_{R,j}$, no pre-guard is required, i.e. $t_{g,\text{pre}} = 0$. However, if $\Delta t_S < \Delta t_{R,j}$, then $t_{g,\text{pre}} = \Delta t_{R,j} - \Delta t_S$. Requirement (3.67) states that the destination has to be in receive mode at the time the slowest relay starts retransmitting useful data.

Inserting (3.60), (3.58), and (3.64) consecutively into (3.67) delivers

$$\begin{aligned} t_{1,\text{begin}}^{(j)} + \bar{T}_b + \bar{T}_p &\geq t_2 + \Delta t_D \\ \max \{ t_{S,\text{begin}}, t_1 + \Delta t_{R,j} \} + \bar{T}_p &\geq t_2 + \Delta t_D \\ \max \{ t_1 + \Delta t_S + t_{g,\text{pre}}, t_1 + \Delta t_{R,j} \} + \bar{T}_p &\geq t_2 + \Delta t_D \\ \max \{ \Delta t_S + t_{g,\text{pre}}, \Delta t_{R,j} \} + t_1 + \bar{T}_p &\geq t_2 + \Delta t_D \\ \max \{ \Delta t_S + t_{g,\text{pre}}, \Delta t_{R,j} \} &\geq \Delta t_D, \end{aligned} \quad (3.70)$$

where $t_1 + \bar{T}_p = t_2$ was used. If $\Delta t_{R,j} \geq \Delta t_D$, a pre-guard is not required, i.e. $t_{g,\text{pre}} = 0$, because (3.70) is always fulfilled. However, if $\Delta t_{R,j} < \Delta t_D$, the pre-guard

has to be large enough so that

$$\Delta t_S + t_{g,\text{pre}} \geq \Delta t_D. \quad (3.71)$$

The smallest possible $t_{g,\text{pre}}$ fulfilling (3.71) obviously is

$$t_{g,\text{pre}} = \Delta t_D - \Delta t_S. \quad (3.72)$$

- **Post-Guard:** Requirement (3.68) can be interpreted as follows: If $\Delta t_{R,i} \geq \Delta t_S$, no post-guard is required, i.e. $t_{g,\text{post}} = 0$. However, if $\Delta t_{R,i} < \Delta t_S$, then $t_{g,\text{post}} = \Delta t_S - \Delta t_{R,i}$. Requirement (3.69) states that the destination has to be in receive mode at least as long as the fastest relay retransmits useful data.

Inserting (3.61), (3.59), and (3.65) consecutively into (3.69) delivers

$$\begin{aligned} t_{2,\text{end}}^{(\min)} &\leq t_2 + \Delta t_D + \bar{T}_b \\ t_{1,\text{end}}^{(i)} + T_p &\leq t_2 + \Delta t_D + T_b \\ \min \{t_{S,\text{end}}, t_1 + \Delta t_{R,i} + \bar{T}_b\} + T_p &\leq t_2 + \Delta t_D + \bar{T}_b \\ \min \{t_1 + \Delta t_S + T_b - t_{g,\text{post}}, t_1 + \Delta t_{R,i} + \bar{T}_b\} + \bar{T}_p &\leq t_2 + \Delta t_D + \bar{T}_b \\ \min \{\Delta t_S + \bar{T}_b - t_{g,\text{post}}, \Delta t_{R,i} + \bar{T}_b\} + t_1 + \bar{T}_p &\leq t_2 + \Delta t_D + \bar{T}_b \\ \min \{\Delta t_S - t_{g,\text{post}}, \Delta t_{R,i}\} &\leq \Delta t_D, \end{aligned} \quad (3.73)$$

where $t_1 + \bar{T}_p = t_2$ was used. If $\Delta t_{R,i} \leq \Delta t_D$, a post-guard is not required, i.e. $t_{g,\text{post}} = 0$. However, if $\Delta t_{R,i} > \Delta t_D$, the post-guard has to be large enough so that

$$\Delta t_S - t_{g,\text{post}} \leq \Delta t_D. \quad (3.74)$$

The smallest possible $t_{g,\text{pre}}$ fulfilling (3.74) obviously is

$$t_{g,\text{pre}} = \Delta t_S - \Delta t_D. \quad (3.75)$$

Summarizing the requirements for pre- and post-guard delivers the following, simple rules:

$$t_{g,\text{pre}} = \begin{cases} \Delta t_D - \Delta t_S & , \Delta t_{R,j} < \Delta t_D \\ \Delta t_{R,j} - \Delta t_S & , \Delta t_S < \Delta t_{R,j} \\ 0 & , \Delta t_D \leq \Delta t_{R,j} \leq \Delta t_S \end{cases} \quad (3.76)$$

$$t_{g,\text{post}} = \begin{cases} \Delta t_S - \Delta t_D & , \Delta t_{R,i} > \Delta t_D \\ \Delta t_S - \Delta t_{R,i} & , \Delta t_S > \Delta t_{R,i} \\ 0 & , \Delta t_S \leq \Delta t_{R,i} \leq \Delta t_D \end{cases} \quad (3.77)$$

Let γ denote the effective relative data rate. It is defined as

$$\gamma = \frac{\max\{\bar{T}_b - t_{g,\text{pre}} - t_{g,\text{post}}, 0\}}{\bar{T}_b}, \quad (3.78)$$

where $0 \leq \gamma \leq 1$. Consider the following worst-case scenario:

- $\Delta t_{R,i} = -\Delta t_{R,j}$
- $\Delta t_S = -\Delta t_D$

In this case, the following two definitions are used: $|\Delta t_{R,i}| = |\Delta t_{R,j}| := \Delta t_R$ and $|\Delta t_S| = |\Delta t_D| := \Delta t_{SD}$. Fig. 3.10 shows the effective relative data rate γ for different timing accuracies. For $\frac{|\Delta t_R|}{\bar{T}_b} \leq \frac{1}{2}$, the effective relative data rate γ is zero. Increasing the timing accuracy of either the relays or of source and destination does not deliver a gain. The data rate only increases if the timing accuracy of all nodes in the network increases. This behavior leads to the flat regions of the curves in Fig. 3.10. The worst timing accuracy that is currently present in a network, i.e. $\max\{|\Delta t_R|, |\Delta t_{SD}|\}$, thus represents a limiting factor to the data rate.

3.3 I/Q Imbalance

In practical transceivers the relative differences between all the analog components of the quadrature frontend lead to a mismatch between amplitude and phase of the in-phase and quadrature phase signal branches. At the transmitter these are the up-conversion mixers, DACs, and lowpass filters. At the receiver, these are the downconversion mixers, filters, amplifiers, and ADCs (e.g. [179–181]). In theory, an infinite image rejection is provided if the signal amplitude in the I- and the Q-branch of the signal processing path is equal and the phase difference is exactly 90 degrees. However, a perfect match between the I- and

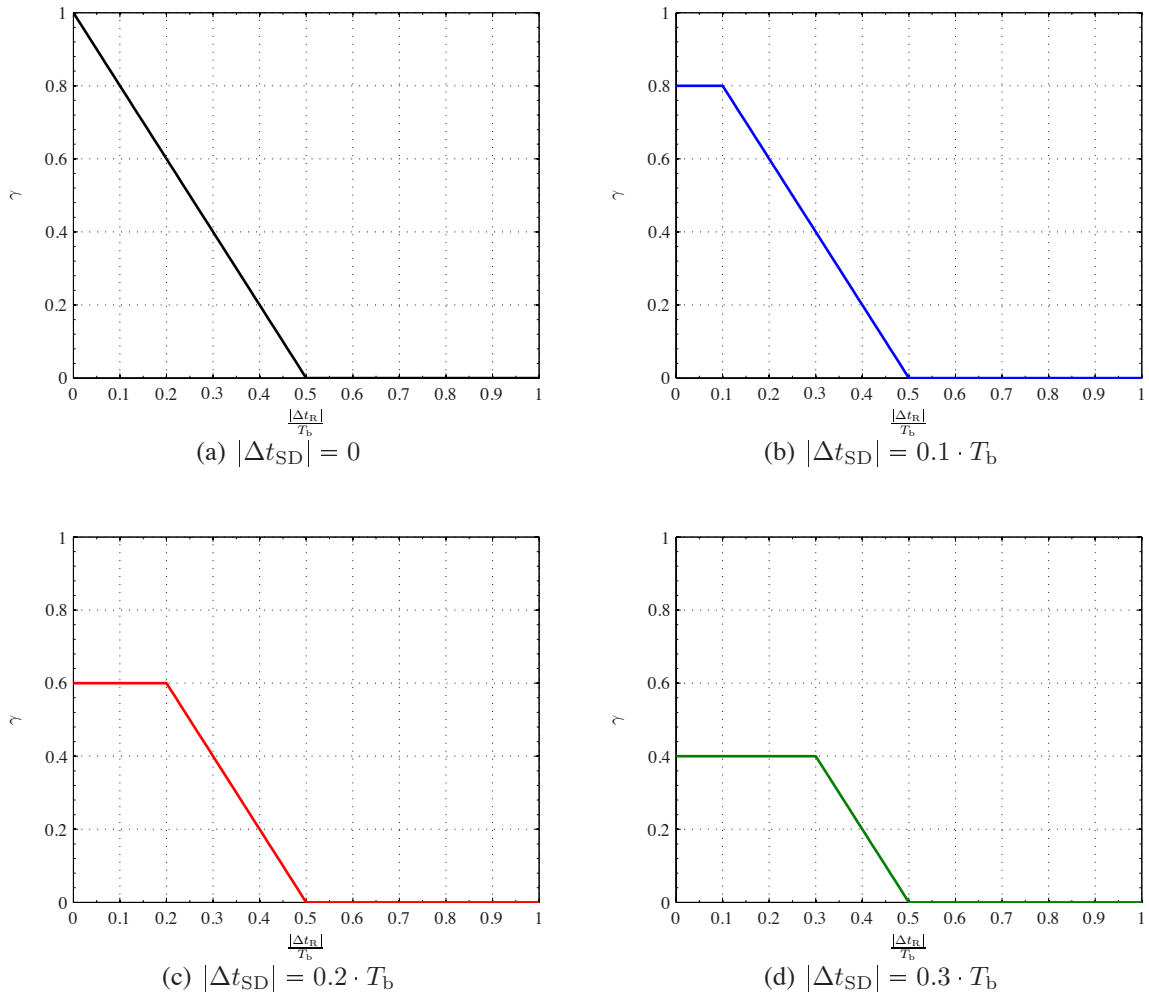


Fig. 3.10: Effective relative data rate γ for different values of the source-destination timing accuracy.

the Q-branch is not feasible in a practical hardware implementation due to the limited accuracy of the analog components. These unavoidable mismatches, known as I/Q imbalance, significantly degrade the image rejection capability of any I/Q signal processing architecture.

In this section, a simple network with one source-destination pair and a single relay is considered. The aim is to investigate the degradation of the signal quality due to I/Q imbalance at the relay. To this end, it is assumed that the quadrature modulator at the source and the demodulator at the destination are perfectly matched. The considered scenario could represent a simple cooperative network employing opportunistic relaying or relay selection (cf. Section 1.1.2), where a single node is chosen from a set of potential relays to assist the communication between the source-destination pair. The I/Q imbalance will be modeled as for example in [127, 182]. The notation is introduced for a simple SISO point-to-point transmission in Sections 3.3.1 and 3.3.2, where an equivalent baseband model is presented that takes the I/Q mismatch into account. Section 3.3.3 extends the simple point-to-point model to a two-hop scenario with a single source-destination pair and one relay. Finally, in Section 3.3.4, the impact of the I/Q mismatch at the relay on the received signal at the destination is investigated. Expressions for the expected signal, interference and noise power are derived.

3.3.1 Transmitter Imbalance

Fig. 3.11 shows the block diagram of the quadrature modulator of the transmitter suffering from amplitude and phase mismatch between the in-phase and quadrature branches. The digital equivalent baseband transmit signal $z_S[n] = x_S[n] + jy_S[n]$ is split into its real (in-phase) and imaginary (quadrature) component. Digital-to-analog conversion delivers the corresponding continuous-time baseband signals $x_S(t)$ and $y_S(t)$. They are up-converted to the carrier frequency f_c by the mixer. The I/Q mismatch comprises the amplitude and phase imbalance λ_S and ρ_S , respectively. The joint signal is scaled by a factor $\eta_S \in \mathbb{Q}$ that is introduced to the model in order to make the power of the transmit signal independent of λ_S . This normalization will later be useful to assess the signal degradation due to I/Q imbalance.

Let $x_S[n]$ and $y_S[n]$ be mutually independent, zero-mean, complex Gaussian random variables with variance $\frac{1}{2}\sigma_S^2$ each. The scaling factor η_S is in this case chosen such that

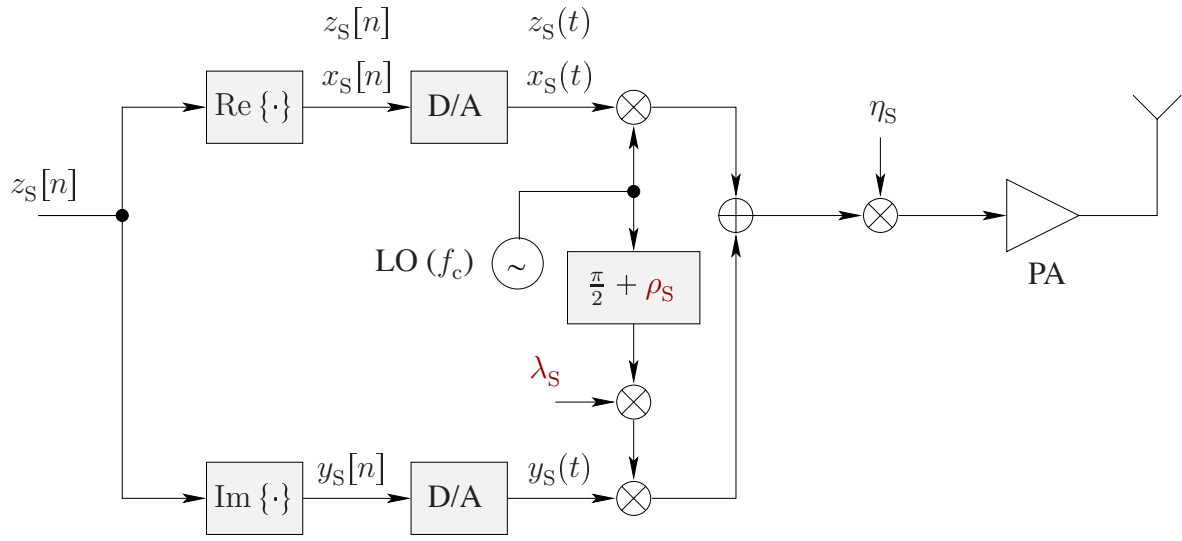


Fig. 3.11: Quadrature modulator suffering from I/Q imbalance.

$E_n [|z_S[n]|^2] = \sigma_S^2$. Consequently,

$$\begin{aligned} E_n [|z_S[n]|^2] &= E_n [|\eta_S (x_S[n] + j\lambda_S y_S[n])|^2] = \\ &= \eta_S^2 \left(\frac{\sigma_S^2}{2} + \lambda_S^2 \frac{\sigma_S^2}{2} \right) = \sigma_S^2, \end{aligned} \quad (3.79)$$

and

$$\eta_S = \sqrt{\frac{2}{1 + \lambda_S^2}}. \quad (3.80)$$

The analytic transmit signal can be written as (e.g. [183])

$$\begin{aligned} s(t) &= \eta_S \cdot (k_{S,1} z_S(t) + k_{S,2} z_S^*(t)) \cdot e^{j2\pi f_c t} := \\ &:= \bar{z}_S(t) e^{j2\pi f_c t}, \end{aligned} \quad (3.81)$$

where $\bar{z}_S(t)$ is the baseband signal in an equivalent system with perfectly matched I/Q modulator and

$$k_{S,1} = \frac{1 + \lambda_S e^{j\rho_S}}{2} \quad (3.82)$$

$$k_{S,2} = \frac{1 - \lambda_S e^{j\rho_S}}{2}. \quad (3.83)$$

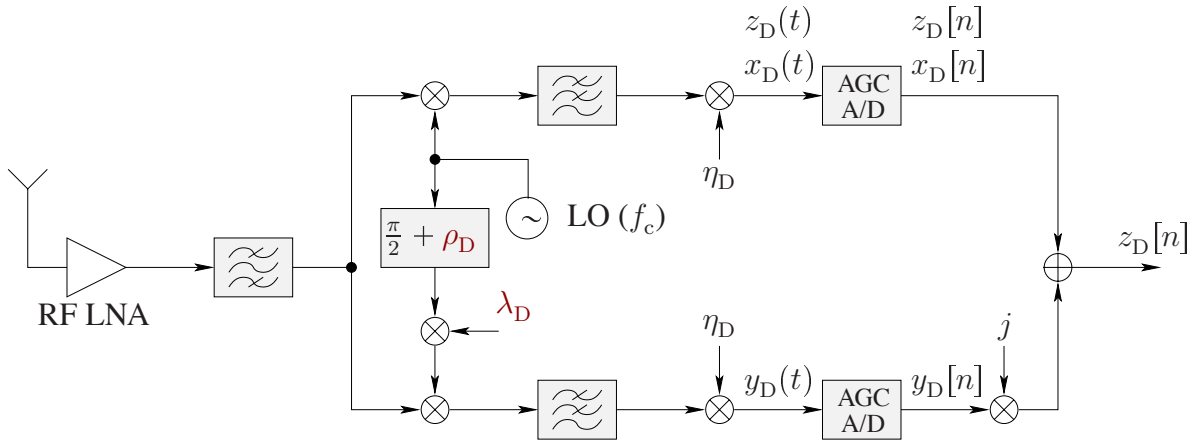


Fig. 3.12: Quadrature demodulator suffering from I/Q imbalance.

3.3.2 Receiver Imbalance

In analogy to Section 3.3.1, Fig. 3.12 depicts the block diagram of the quadrature demodulator of the receiver suffering from amplitude and phase mismatch between the in-phase and quadrature branches. The receive signal is amplified in the LNA and bandpass-filtered. The resulting signal is fed into the quadrature demodulator where it is downconverted to baseband yielding $r(t) = r_I(t) + jr_Q(t)$. The I/Q mismatch now comprises the amplitude and phase imbalance λ_D and ρ_D , respectively. After low-pass filtering, the baseband in-phase and quadrature components are scaled with the factor $\eta_D \in \mathbb{Q}$. In analogy to the previous section, this factor is introduced to the model in order to make the power of the baseband receive signal independent of λ_D . It is given by

$$\eta_D = \sqrt{\frac{2}{1 + \lambda_D^2}}. \quad (3.84)$$

The complex baseband signal $z_D(t) = x_D(t) + jy_D(t)$ can be written as (e.g. [183])

$$z_D(t) = \eta_D \cdot (k_{D,1} \bar{z}_D(t) + k_{D,2} \bar{z}_D^*(t)), \quad (3.85)$$

where $\bar{z}_D(t)$ is the result of perfect downconversion, i.e., mixing without I/Q mismatch. It is given by

$$\bar{z}_D(t) = r(t) \cdot e^{-j2\pi f_c t}, \quad (3.86)$$

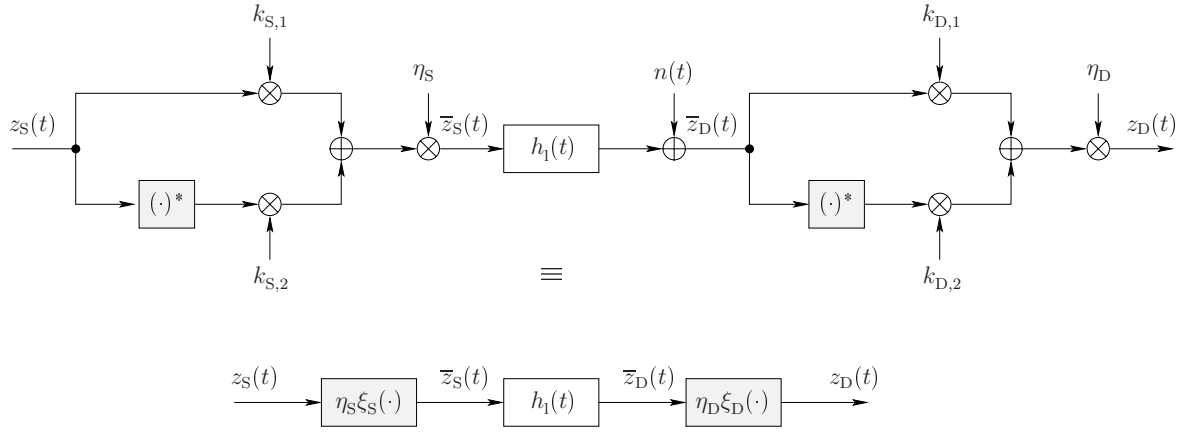


Fig. 3.13: Equivalent baseband transceiver model.

where $r(t)$ is the analytic receive signal. The parameters $k_{D,1}$ and $k_{D,2}$ are

$$k_{D,1} = \frac{1 + \lambda_D e^{-j\rho_D}}{2} \quad (3.87)$$

$$k_{D,2} = \frac{1 - \lambda_D e^{j\rho_D}}{2}. \quad (3.88)$$

The resulting signal $z_D(t)$ is finally transferred to the digital domain by an ADC with automatic gain control (AGC).

3.3.3 Equivalent Baseband System Model

Using (3.81) and (3.85), the transmission between a transmitter and receiver suffering from I/Q imbalance can be described by an equivalent, perfect transceiver pair. The resulting equivalent baseband transceiver model is depicted in Fig. 3.13, where $h_1(t)$ denotes the impulse response of the equivalent low-pass channel. Additive signal noise $n(t)$ is furthermore assumed to be present at the destination. Finally, the functions

$$\xi_S(z_S(t)) = k_{S,1}z_S(t) + k_{S,2}z_S^*(t) \quad (3.89)$$

$$\xi_D(\bar{z}_D(t)) = k_{D,1}\bar{z}_D(t) + k_{D,2}\bar{z}_D^*(t) \quad (3.90)$$

are defined for brevity of notation. The transmission between source and relay and between relay and destination can then be described as in Fig. 3.14. The block diagram of the single relay can furthermore be easily derived from Figs. 3.11 and 3.12. It is shown in Fig. 3.15. In

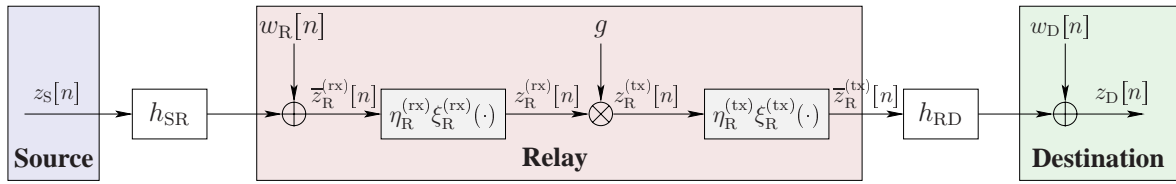


Fig. 3.14: Discrete-time equivalent baseband system model for the two-hop transmission from source to destination via a single relay that exhibits I/Q imbalance.

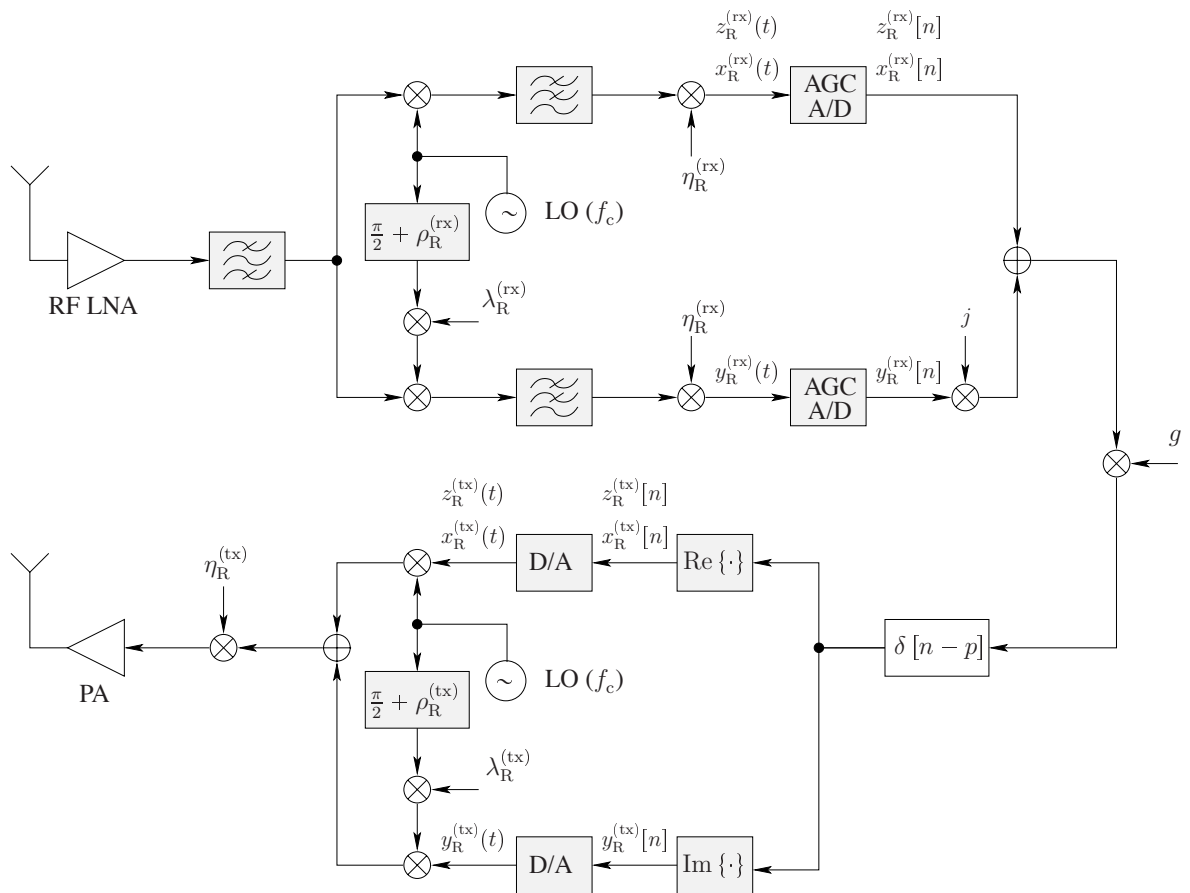


Fig. 3.15: AF relay with quadrature modulator.

analogy to (3.89) and (3.90) the functions $\eta_R^{(rx)} \xi_R^{(rx)}(\cdot)$ and $\eta_R^{(tx)} \xi_R^{(tx)}(\cdot)$ are defined as

$$\eta_R^{(rx)} \xi_R^{(rx)}(f[n]) = \eta_R^{(rx)} \left(k_{R,1}^{(rx)} f[n] + k_{R,2}^{(rx)} f^*[n] \right) \quad (3.91)$$

$$\eta_R^{(tx)} \xi_R^{(tx)}(f[n]) = \eta_R^{(tx)} \left(k_{R,1}^{(tx)} f[n] + k_{R,2}^{(tx)} f^*[n] \right), \quad (3.92)$$

where

$$k_{R,1}^{(rx)} = \frac{1 + \lambda_R^{(rx)} e^{-j\rho_R^{(rx)}}}{2} \quad (3.93)$$

$$k_{R,2}^{(rx)} = \frac{1 - \lambda_R^{(rx)} e^{j\rho_R^{(rx)}}}{2} \quad (3.94)$$

$$k_{R,1}^{(tx)} = \frac{1 + \lambda_R^{(tx)} e^{j\rho_R^{(tx)}}}{2} \quad (3.95)$$

$$k_{R,2}^{(tx)} = \frac{1 - \lambda_R^{(tx)} e^{-j\rho_R^{(tx)}}}{2}. \quad (3.96)$$

The scaling factors used to preserve the signal power are now given by

$$\eta_R^{(rx)} = \sqrt{\frac{2}{1 + \lambda_R^{(rx)2}}} \quad (3.97)$$

$$\eta_R^{(tx)} = \sqrt{\frac{2}{1 + \lambda_R^{(tx)2}}}. \quad (3.98)$$

Consequently, the received signal at the destination is

$$\begin{aligned} z_D[n] &= h_{RD} \cdot \eta_R^{(tx)} \xi_R^{(tx)} \left(g \eta_R^{(rx)} \xi_R^{(rx)} (h_{SR} \cdot z_S[n]) \right) = \\ &= h_{RD} \cdot \eta_R^{(tx)} k_{R,1}^{(tx)} \cdot g \eta_R^{(rx)} k_{R,1}^{(rx)} \cdot h_{SR} z_S[n] + && \text{[signal]} \\ &+ h_{RD} \cdot \eta_R^{(tx)} k_{R,1}^{(tx)} \cdot g \eta_R^{(rx)} k_{R,2}^{(rx)} \cdot h_{SR}^* z_S^*[n] + && \text{[interference]} \\ &+ h_{RD} \cdot \eta_R^{(tx)} k_{R,2}^{(tx)} \cdot g^* \eta_R^{(rx),*} k_{R,1}^{(rx),*} \cdot h_{SR}^* z_S^*[n] + && \text{[interference]} \\ &+ h_{RD} \cdot \eta_R^{(tx)} k_{R,2}^{(tx)} \cdot g^* \eta_R^{(rx),*} k_{R,2}^{(rx),*} \cdot h_{SR} z_S[n]. && \text{[interference]} \end{aligned} \quad (3.99)$$

Apart from the useful signal

$$z_{D,\text{signal}}[n] = h_{RD} \cdot \eta_R^{(tx)} k_{R,1}^{(tx)} \cdot g \eta_R^{(rx)} k_{R,1}^{(rx)} \cdot h_{SR} z_S[n] \quad (3.100)$$

it comprises a self-interference part

$$\begin{aligned}
 z_{D,\text{interference}}[n] &= h_{RD} \cdot \eta_R^{(\text{tx})} k_{R,1}^{(\text{tx})} \cdot g \eta_R^{(\text{rx})} k_{R,2}^{(\text{rx})} \cdot h_{SR}^* z_S^*[n] + \\
 &\quad + h_{RD} \cdot \eta_R^{(\text{tx})} k_{R,2}^{(\text{tx})} \cdot g^* \eta_R^{(\text{rx}),*} k_{R,1}^{(\text{rx}),*} \cdot h_{SR}^* z_S^*[n] + \\
 &\quad + h_{RD} \cdot \eta_R^{(\text{tx})} k_{R,2}^{(\text{tx})} \cdot g^* \eta_R^{(\text{rx}),*} k_{R,2}^{(\text{rx}),*} \cdot h_{SR} z_S[n]
 \end{aligned} \tag{3.101}$$

that is due to the I/Q imbalance. A plausibility check, i.e., $\lambda_R^{(\text{rx})} = \lambda_R^{(\text{tx})} = 1$ and $\rho_R^{(\text{rx})} = \rho_R^{(\text{tx})} = 0$, delivers

$$\eta_R^{(\text{rx})} = \eta_R^{(\text{tx})} = 1 \tag{3.102}$$

$$k_{R,1}^{(\text{rx})} = k_{R,1}^{(\text{tx})} = 1 \tag{3.103}$$

$$k_{R,2}^{(\text{rx})} = k_{R,2}^{(\text{tx})} = 0. \tag{3.104}$$

Equation (3.99) becomes in this case

$$z_D = h_{RD} g h_{SR} \cdot z_S[n], \tag{3.105}$$

which is the received signal for the case that there is no I/Q mismatch. Finally, the noise part comprises the forwarded relay noise plus noise at the destination. It is given by

$$\begin{aligned}
 n_D[n] &= h_{RD} \cdot \eta_R^{(\text{tx})} \xi_{SR}^{(\text{tx})} \left(g \eta_R^{(\text{rx})} \xi_{SR}^{(\text{rx})} (h_{SR} \cdot w_R[n]) \right) + w_D[n] = \\
 &= h_{RD} h_{SR} \eta_R^{(\text{tx})} \left(g \eta_R^{(\text{rx})} k_{R,1}^{(\text{rx})} k_{R,1}^{(\text{tx})} + g^* \eta_R^{(\text{rx}),*} k_{R,2}^{(\text{rx}),*} k_{R,2}^{(\text{tx})} \right) w_R[n] + \\
 &\quad + h_{RD} h_{SR}^* \eta_R^{(\text{tx})} \left(g \eta_R^{(\text{rx})} k_{R,2}^{(\text{rx})} k_{R,1}^{(\text{tx})} + g^* \eta_R^{(\text{rx}),*} k_{R,1}^{(\text{rx}),*} k_{R,2}^{(\text{tx})} \right) w_R^*[n] + \\
 &\quad + w_D[n],
 \end{aligned} \tag{3.106}$$

where $w_R[n] \sim \mathcal{CN}(0, \sigma_n^2)$ and $w_D[n] \sim \mathcal{CN}(0, \sigma_n^2)$ are AWGN noise samples.

3.3.4 Impact on Signal Quality

A mismatch between in-phase and quadrature phase branches at the relay leads to a degradation of the signal quality at the destination. In this section, the impact on the expected signal and noise power as well as the generated self-interference are computed. From there, design goals can be derived for a practical hardware implementation, that lead to a specified amount of self-interference or noise power at the destination.

3.3.4.1 Signal Power

The signal part arriving at the destination is given in (3.100):

$$z_{D,\text{signal}}[n] = h_{\text{RD}} \cdot \eta_{\text{R}}^{(\text{tx})} k_{\text{R},1}^{(\text{tx})} \cdot g \eta_{\text{R}}^{(\text{rx})} k_{\text{R},1}^{(\text{rx})} \cdot h_{\text{SR}} z_{\text{S}}[n] \quad (3.107)$$

The expected signal power is consequently

$$\begin{aligned} P_{\text{s}} &= \text{E} \left[\left| h_{\text{RD}} \cdot \eta_{\text{R}}^{(\text{tx})} k_{\text{R},1}^{(\text{tx})} \cdot g \eta_{\text{R}}^{(\text{rx})} k_{\text{R},1}^{(\text{rx})} \cdot h_{\text{SR}} z_{\text{S}}[n] \right|^2 \right] = \\ &= |h_{\text{RD}}|^2 |h_{\text{SR}}|^2 |g|^2 \cdot \left| \eta_{\text{R}}^{(\text{rx})} \right|^2 \left| \eta_{\text{R}}^{(\text{tx})} \right|^2 \left| k_{\text{R},1}^{(\text{rx})} \right|^2 \left| k_{\text{R},1}^{(\text{tx})} \right|^2 \cdot \sigma_{\text{s}}^2. \end{aligned} \quad (3.108)$$

The component depending on the I/Q imbalance parameters $\lambda_{\text{R}}^{(\text{rx})}$, $\lambda_{\text{R}}^{(\text{tx})}$, $\rho_{\text{R}}^{(\text{rx})}$, and $\rho_{\text{R}}^{(\text{tx})}$ is

$$\begin{aligned} \left| \eta_{\text{R}}^{(\text{rx})} \right|^2 \left| \eta_{\text{R}}^{(\text{tx})} \right|^2 \left| k_{\text{R},1}^{(\text{rx})} \right|^2 \left| k_{\text{R},1}^{(\text{tx})} \right|^2 &= \\ &= \frac{2}{1 + \lambda_{\text{R}}^{(\text{rx})2}} \cdot \frac{2}{1 + \lambda_{\text{R}}^{(\text{tx})2}} \cdot \frac{\left| 1 + \lambda_{\text{R}}^{(\text{rx})} e^{-j\rho_{\text{R}}^{(\text{rx})}} \right|^2}{4} \cdot \frac{\left| 1 + \lambda_{\text{R}}^{(\text{tx})} e^{j\rho_{\text{R}}^{(\text{tx})}} \right|^2}{4} = \\ &= \frac{1}{4} \cdot \frac{\left| 1 + \lambda_{\text{R}}^{(\text{rx})} e^{-j\rho_{\text{R}}^{(\text{rx})}} \right|^2}{1 + \lambda_{\text{R}}^{(\text{rx})2}} \cdot \frac{\left| 1 + \lambda_{\text{R}}^{(\text{tx})} e^{j\rho_{\text{R}}^{(\text{tx})}} \right|^2}{1 + \lambda_{\text{R}}^{(\text{tx})2}} = \\ &= \frac{1}{4} \cdot \frac{1 + \lambda_{\text{R}}^{(\text{rx})2} + \lambda_{\text{R}}^{(\text{rx})} \left(e^{-j\rho_{\text{R}}^{(\text{rx})}} + e^{j\rho_{\text{R}}^{(\text{rx})}} \right)}{1 + \lambda_{\text{R}}^{(\text{rx})2}} \cdot \frac{1 + \lambda_{\text{R}}^{(\text{tx})2} + \lambda_{\text{R}}^{(\text{tx})} \left(e^{j\rho_{\text{R}}^{(\text{tx})}} + e^{-j\rho_{\text{R}}^{(\text{tx})}} \right)}{1 + \lambda_{\text{R}}^{(\text{tx})2}} = \\ &= \frac{1}{4} \cdot \left(1 + \frac{2\lambda_{\text{R}}^{(\text{rx})} \cos(\rho_{\text{R}}^{(\text{rx})})}{1 + \lambda_{\text{R}}^{(\text{rx})2}} \right) \cdot \left(1 + \frac{2\lambda_{\text{R}}^{(\text{tx})} \cos(\rho_{\text{R}}^{(\text{tx})})}{1 + \lambda_{\text{R}}^{(\text{tx})2}} \right). \end{aligned} \quad (3.109)$$

For the sake of a better visualization of the results, it is assumed that $\lambda_{\text{R}}^{(\text{rx})} = \lambda_{\text{R}}^{(\text{tx})} := \lambda_{\text{R}}$ and $\rho_{\text{R}}^{(\text{rx})} = \rho_{\text{R}}^{(\text{tx})} := \rho_{\text{R}}$. The power of the signal part is then

$$\begin{aligned} P_{\text{s}} &= \frac{1}{4} |h_{\text{RD}}|^2 |h_{\text{SR}}|^2 |g|^2 \cdot \left(1 + \frac{2\cos(\rho_{\text{R}})}{\frac{1}{\lambda_{\text{R}}} + \lambda_{\text{R}}} \right) \cdot \left(1 + \frac{2\cos(\rho_{\text{R}})}{\frac{1}{\lambda_{\text{R}}} + \lambda_{\text{R}}} \right) \cdot \sigma_{\text{s}}^2 = \\ &= \frac{1}{4} |h_{\text{RD}}|^2 |h_{\text{SR}}|^2 |g|^2 \cdot \left(1 + \frac{2\cos(\rho_{\text{R}})}{\frac{1}{\lambda_{\text{R}}} + \lambda_{\text{R}}} \right)^2 \cdot \sigma_{\text{s}}^2. \end{aligned} \quad (3.110)$$

In order to separate the impact of amplitude and phase mismatch, two cases are considered:

1. **Amplitude uncertainty:** In order to extract the impact of amplitude uncertainty λ_{R}

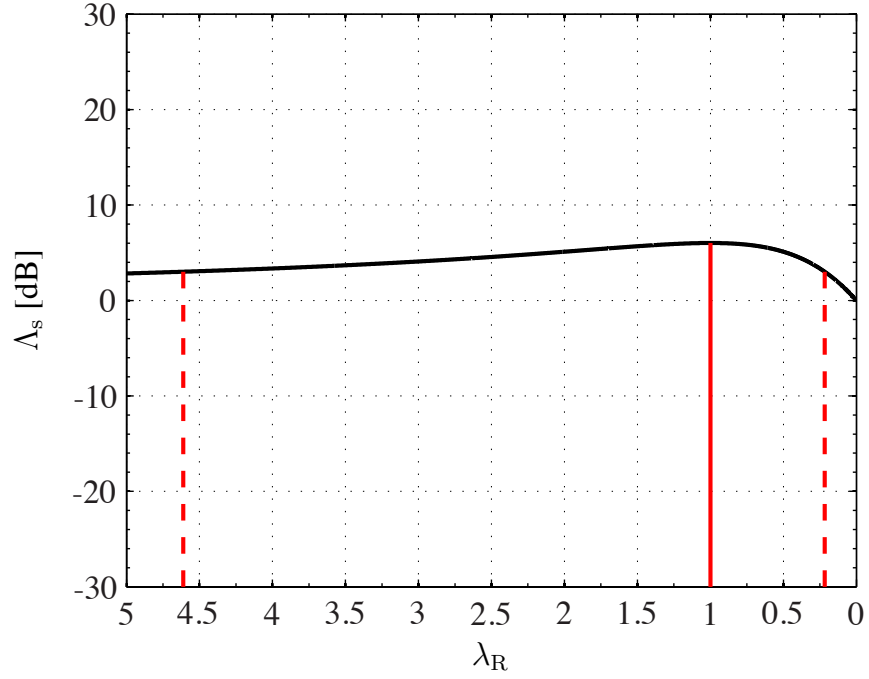


Fig. 3.16: Dependence of the signal power on the amplitude mismatch λ_R .

on the signal power, the phase of in-phase and quadrature branch are assumed to be perfectly matched, i.e. $\rho_R = 0$. The signal power is in this case

$$P_s = \frac{1}{4} |h_{RD}|^2 |h_{SR}|^2 |g|^2 \cdot \left(1 + \frac{2}{\frac{1}{\lambda_R} + \lambda_R}\right)^2 \cdot \sigma_s^2. \quad (3.111)$$

The term depending on λ_R is

$$\Lambda_s := \left(1 + \frac{2}{\frac{1}{\lambda_R} + \lambda_R}\right)^2. \quad (3.112)$$

In Fig. 3.16 Λ_s is plotted versus the amplitude mismatch λ_R . The maximum signal power is achieved at $\lambda_R = 1$. It is reduced by a factor of $\beta \in \mathbb{Q}$ for

$$\lambda_R = \frac{1 \pm \sqrt{1 - \left(2\sqrt{\frac{1}{\beta}} - 1\right)^2}}{2\sqrt{\frac{1}{\beta}} - 1}. \quad (3.113)$$

Example: An amplitude mismatch of $\lambda_R^{(1)} \approx 4.61$ or $\lambda_R^{(2)} \approx 0.22$ leads to a reduction of the signal power by 3 dB, i.e. $\beta = 2$. The values are plotted as dashed lines in

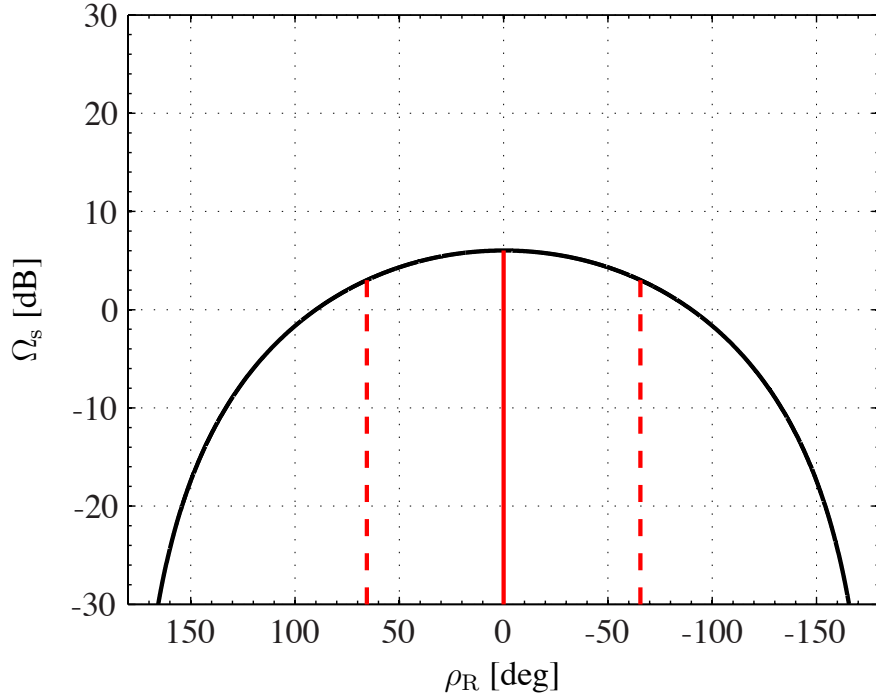


Fig. 3.17: Dependence of the signal power on the phase mismatch ρ_R .

Fig. 3.16. $\lambda_R^{(1)}$ and $\lambda_R^{(2)}$ are readily obtained by inserting $\beta = 2$ into (3.113).

2. **Phase uncertainty:** In order to extract the impact of phase uncertainty ρ_R on the signal power, the amplitude mismatch is assumed to be negligible, i.e. $\lambda_R = 1$. The signal power then is

$$P_s = \frac{1}{4} |h_{RD}|^2 |h_{SR}|^2 |g|^2 \cdot (1 + \cos(\rho_R))^2 \cdot \sigma_s^2. \quad (3.114)$$

In Fig. 3.17 the term depending on the phase imbalance ρ_R , i.e.

$$\Omega_s := (1 + \cos(\rho_R))^2 \quad (3.115)$$

is plotted versus ρ_R . Maximum signal power is achieved at $\rho_R = 0$. It is reduced by a factor of β for

$$\rho_R = \arccos\left(2\sqrt{\frac{1}{\beta}} - 1\right). \quad (3.116)$$

Example: A phase mismatch of $\rho_R \approx \pm 1.14$ (corresponding to ± 65.53 deg) results in a reduction of the signal power by 3 dB, i.e. $\beta = 2$. The dashed lines in Fig. 3.17 indicate the corresponding values.

3.3.4.2 Interference Power

The expected self-interference power at the destination is given by

$$P_i = \mathbb{E} \left[|z_{\text{D,interference}}[n]|^2 \right], \quad (3.117)$$

where (see (3.101))

$$\begin{aligned} z_{\text{D,interference}}[n] = & h_{\text{RD}} \eta_{\text{R}}^{(\text{tx})} \left(k_{\text{R},1}^{(\text{tx})} g \eta_{\text{R}}^{(\text{rx})} k_{\text{R},2}^{(\text{rx})} + k_{\text{R},2}^{(\text{tx})} g^* \eta_{\text{R}}^{(\text{rx},*)} k_{\text{R},1}^{(\text{rx},*)} \right) h_{\text{SR}}^* z_{\text{S}}^*[n] + \\ & + h_{\text{RD}} \eta_{\text{R}}^{(\text{tx})} \cdot k_{\text{R},2}^{(\text{tx})} g^* \eta_{\text{R}}^{(\text{rx},*)} k_{\text{R},2}^{(\text{rx},*)} \cdot h_{\text{SR}} z_{\text{S}}[n]. \end{aligned} \quad (3.118)$$

Since $z_{\text{S}}[n]$ is assumed to be a complex normal random variable, i.e. $z_{\text{S}}[n] \sim \mathcal{CN}(0, \sigma_{\text{s}}^2)$, the interference power is given by

$$\begin{aligned} P_i = & \left| h_{\text{RD}} \eta_{\text{R}}^{(\text{tx})} \eta_{\text{R}}^{(\text{rx})} \left(g k_{\text{R},1}^{(\text{tx})} k_{\text{R},2}^{(\text{rx})} + g^* k_{\text{R},2}^{(\text{tx})} k_{\text{R},1}^{(\text{rx},*)} \right) h_{\text{SR}}^* \right|^2 \sigma_{\text{s}}^2 + \\ & + \left| h_{\text{RD}} \eta_{\text{R}}^{(\text{tx})} \eta_{\text{R}}^{(\text{rx})} \cdot g^* k_{\text{R},2}^{(\text{tx})} k_{\text{R},2}^{(\text{rx},*)} \cdot h_{\text{SR}} \right|^2 \sigma_{\text{s}}^2, \end{aligned} \quad (3.119)$$

where the fact that $\eta_{\text{R}}^{(\text{rx})} \in \mathbb{R}$ was used. The first summand of (3.119) is

$$\begin{aligned} & \left| h_{\text{RD}} \eta_{\text{R}}^{(\text{tx})} \eta_{\text{R}}^{(\text{rx})} \left(g k_{\text{R},1}^{(\text{tx})} k_{\text{R},2}^{(\text{rx})} + g^* k_{\text{R},2}^{(\text{tx})} k_{\text{R},1}^{(\text{rx},*)} \right) h_{\text{SR}}^* \right|^2 \sigma_{\text{s}}^2 = \\ & = |h_{\text{RD}}|^2 |h_{\text{SR}}|^2 \frac{2}{1 + \lambda_{\text{R}}^{(\text{rx})2}} \frac{2}{1 + \lambda_{\text{R}}^{(\text{tx})2}} \cdot \\ & \cdot \left| g \frac{1 - \lambda_{\text{R}}^{(\text{rx})} e^{j\rho_{\text{R}}^{(\text{rx})}}}{2} \frac{1 + \lambda_{\text{R}}^{(\text{tx})} e^{j\rho_{\text{R}}^{(\text{tx})}}}{2} + g^* \frac{1 + \lambda_{\text{R}}^{(\text{rx})} e^{j\rho_{\text{R}}^{(\text{rx})}}}{2} \frac{1 - \lambda_{\text{R}}^{(\text{tx})} e^{j\rho_{\text{R}}^{(\text{tx})}}}{2} \right|^2 \sigma_{\text{s}}^2. \end{aligned} \quad (3.120)$$

In order to better visualize the results, it is assumed that $\lambda_R^{(\text{rx})} = \lambda_R^{(\text{tx})} := \lambda_R$ and $\rho_R^{(\text{rx})} = \rho_R^{(\text{tx})} := \rho_R$ (as in Section 3.3.4.1). Thus,

$$\begin{aligned}
 & \left| h_{\text{RD}} \eta_{\text{R}}^{(\text{tx})} \eta_{\text{R}}^{(\text{rx})} \left(g k_{\text{R},1}^{(\text{tx})} k_{\text{R},2}^{(\text{rx})} + g^* k_{\text{R},2}^{(\text{tx})} k_{\text{R},1}^{(\text{rx},*)} \right) h_{\text{SR}}^* \right|^2 \sigma_s^2 = \\
 & = |h_{\text{RD}}|^2 |h_{\text{SR}}|^2 \frac{2}{1 + \lambda_R^2} \frac{2}{1 + \lambda_R^2} \cdot \\
 & \quad \cdot \left| g \cdot \frac{1 - \lambda_R e^{j\rho_R}}{2} \frac{1 + \lambda_R e^{j\rho_R}}{2} + g^* \cdot \frac{1 + \lambda_R e^{j\rho_R}}{2} \frac{1 - \lambda_R e^{j\rho_R}}{2} \right|^2 \sigma_s^2 = \\
 & = \frac{1}{4} |h_{\text{RD}}|^2 |h_{\text{SR}}|^2 \frac{1}{(1 + \lambda_R^2)^2} |1 - \lambda_R e^{j\rho_R}|^2 |1 + \lambda_R e^{j\rho_R}|^2 |g + g^*|^2 \sigma_s^2 = \\
 & = \frac{1}{4} |h_{\text{RD}}|^2 |h_{\text{SR}}|^2 \frac{1 + \lambda_R^2 - 2\lambda_R \cos(\rho_R)}{1 + \lambda_R^2} \cdot \frac{1 + \lambda_R^2 + 2\lambda_R \cos(\rho_R)}{1 + \lambda_R^2} (g + g^*)^2 \sigma_s^2 = \\
 & = \frac{1}{4} |h_{\text{RD}}|^2 |h_{\text{SR}}|^2 \left(1 - \frac{2\cos(\rho_R)}{\frac{1}{\lambda_R} + \lambda_R} \right) \left(1 + \frac{2\cos(\rho_R)}{\frac{1}{\lambda_R} + \lambda_R} \right) (g + g^*)^2 \sigma_s^2. \quad (3.121)
 \end{aligned}$$

The second summand of (3.119) is

$$\begin{aligned}
 & \left| h_{\text{RD}} \eta_{\text{R}}^{(\text{tx})} \eta_{\text{R}}^{(\text{rx})} \cdot g^* k_{\text{R},2}^{(\text{tx})} k_{\text{R},2}^{(\text{rx},*)} \cdot h_{\text{SR}} \right|^2 \sigma_s^2 = \\
 & = |h_{\text{RD}}|^2 |h_{\text{SR}}|^2 |g|^2 \frac{2}{1 + \lambda_R^{(\text{rx})2}} \frac{2}{1 + \lambda_R^{(\text{tx})2}} \cdot \left| \frac{1 - \lambda_R^{(\text{rx})} e^{j\rho_R^{(\text{rx})}}}{2} \right|^2 \left| \frac{1 - \lambda_R^{(\text{tx})} e^{-j\rho_R^{(\text{tx})}}}{2} \right|^2 \sigma_s^2. \quad (3.122)
 \end{aligned}$$

With $\lambda_R^{(\text{rx})} = \lambda_R^{(\text{tx})} := \lambda_R$ and $\rho_R^{(\text{rx})} = \rho_R^{(\text{tx})} := \rho_R$ equation (3.122) simplifies to

$$\begin{aligned}
 & \left| h_{\text{RD}} \eta_{\text{R}}^{(\text{tx})} \eta_{\text{R}}^{(\text{rx})} \cdot g^* k_{\text{R},2}^{(\text{tx})} k_{\text{R},2}^{(\text{rx},*)} \cdot h_{\text{SR}} \right|^2 \sigma_s^2 = \\
 & = \frac{1}{4} |h_{\text{RD}}|^2 |h_{\text{SR}}|^2 |g|^2 \left(\frac{1}{1 + \lambda_R^2} \right)^2 \cdot |1 - \lambda_R e^{j\rho_R}|^2 |1 - \lambda_R e^{-j\rho_R}|^2 \sigma_s^2 = \\
 & = \frac{1}{4} |h_{\text{RD}}|^2 |h_{\text{SR}}|^2 |g|^2 \left(\frac{1}{1 + \lambda_R^2} \right)^2 (1 + \lambda_R^2 - 2\lambda_R \cos(\rho_R))^2 \sigma_s^2 = \\
 & = \frac{1}{4} |h_{\text{RD}}|^2 |h_{\text{SR}}|^2 |g|^2 \left(\frac{1 + \lambda_R^2 - 2\lambda_R \cos(\rho_R)}{1 + \lambda_R^2} \right)^2 \sigma_s^2 = \\
 & = \frac{1}{4} |h_{\text{RD}}|^2 |h_{\text{SR}}|^2 |g|^2 \left(1 - \frac{2\cos(\rho_R)}{\frac{1}{\lambda_R} + \lambda_R} \right)^2 \sigma_s^2. \quad (3.123)
 \end{aligned}$$

Adding up (3.121) and (3.123) yields the interference power

$$\begin{aligned}
 P_i &= \frac{1}{4} |h_{RD}|^2 |h_{SR}|^2 \left(1 - \frac{2\cos(\rho_R)}{\frac{1}{\lambda_R} + \lambda_R} \right) \left(1 + \frac{2\cos(\rho_R)}{\frac{1}{\lambda_R} + \lambda_R} \right) (g + g^*)^2 \sigma_s^2 + \\
 &\quad + \frac{1}{4} |h_{RD}|^2 |h_{SR}|^2 |g|^2 \left(1 - \frac{2\cos(\rho_R)}{\frac{1}{\lambda_R} + \lambda_R} \right)^2 \sigma_s^2 = \\
 &= \frac{1}{4} |h_{RD}|^2 |h_{SR}|^2 |g|^2 \sigma_s^2 \left(1 - \frac{2\cos(\rho_R)}{\frac{1}{\lambda_R} + \lambda_R} \right) \cdot \\
 &\quad \cdot \left(\left(1 + \frac{2\cos(\rho_R)}{\frac{1}{\lambda_R} + \lambda_R} \right) \frac{(g + g^*)^2}{|g|^2} + \left(1 - \frac{2\cos(\rho_R)}{\frac{1}{\lambda_R} + \lambda_R} \right) \right). \tag{3.124}
 \end{aligned}$$

Obviously, it depends on the current gain factor g . With

$$\begin{aligned}
 \frac{(g + g^*)^2}{|g|^2} &= \left(\frac{|g| e^{j\varphi_g} + |g| e^{-j\varphi_g}}{|g|} \right)^2 = \\
 &= 4\cos^2(\varphi_g), \tag{3.125}
 \end{aligned}$$

where $g = |g| \cdot e^{j\varphi_g}$, equation (3.124) can be rewritten as

$$\begin{aligned}
 P_i &= \frac{1}{4} |h_{RD}|^2 |h_{SR}|^2 |g|^2 \sigma_s^2 \left(1 - \frac{2\cos(\rho_R)}{\frac{1}{\lambda_R} + \lambda_R} \right) \cdot \\
 &\quad \cdot \left(\left(1 + \frac{2\cos(\rho_R)}{\frac{1}{\lambda_R} + \lambda_R} \right) 4\cos^2(\varphi_g) + \left(1 - \frac{2\cos(\rho_R)}{\frac{1}{\lambda_R} + \lambda_R} \right) \right). \tag{3.126}
 \end{aligned}$$

It is now possible to upper and lower bound the interference power with respect to the phase of the gain factor $\varphi_g \in (-\pi, \pi]$:

- **Upper bound:** For $\varphi_g \in \{-\pi, 0, \pi\}$ the interference power is maximized because $\cos^2(\varphi_g) = 1$ in this case:

$$\begin{aligned}
 P_{i,u} &= \frac{1}{4} |h_{RD}|^2 |h_{SR}|^2 |g|^2 \sigma_s^2 \left(1 - \frac{2\cos(\rho_R)}{\frac{1}{\lambda_R} + \lambda_R} \right) \cdot \\
 &\quad \cdot \left(\left(1 + \frac{2\cos(\rho_R)}{\frac{1}{\lambda_R} + \lambda_R} \right) 4 + \left(1 - \frac{2\cos(\rho_R)}{\frac{1}{\lambda_R} + \lambda_R} \right) \right) \tag{3.127}
 \end{aligned}$$

- **Lower bound:** For $\varphi_g \in \{-\frac{\pi}{2}, \frac{\pi}{2}\}$ the interference power is minimized because

$\cos^2(\varphi_g) = 0$ in this case:

$$P_{i,l} = \frac{1}{4} |h_{RD}|^2 |h_{SR}|^2 |g|^2 \sigma_s^2 \left(1 - \frac{2\cos(\rho_R)}{\frac{1}{\lambda_R} + \lambda_R} \right)^2 \quad (3.128)$$

- **Mean:** If the phase of the gain factor is a random variable that is uniformly distributed between $-\pi$ and π , i.e. $\varphi_g \sim \mathcal{U}(-\pi, \pi)$, the expected interference power is

$$\begin{aligned} P_{i,\text{mean}} &= \mathbb{E}_{\varphi_g} [P_i] = \\ &= \frac{1}{4} |h_{RD}|^2 |h_{SR}|^2 |g|^2 \sigma_s^2 \left(1 - \frac{2\cos(\rho_R)}{\frac{1}{\lambda_R} + \lambda_R} \right) \cdot \\ &\quad \cdot \left(\left(1 + \frac{2\cos(\rho_R)}{\frac{1}{\lambda_R} + \lambda_R} \right) 2 + \left(1 - \frac{2\cos(\rho_R)}{\frac{1}{\lambda_R} + \lambda_R} \right) \right) \end{aligned} \quad (3.129)$$

because $\mathbb{E}_{\varphi_g} [\cos^2(\varphi_g)] = \frac{1}{2}$ in this case.

In analogy to Section 3.3.4.1 the impact of amplitude and phase uncertainty is investigated separately:

1. **Amplitude uncertainty:** In order to extract the impact of an amplitude mismatch between the in-phase and quadrature branches, the phase mismatch is neglected, i.e., $\rho_R = 0$. The respective terms depending on λ_R for the upper bound, lower bound, and expected value of the interference power are given by

$$\Lambda_{i,u} = \left(1 - \frac{2}{\frac{1}{\lambda_R} + \lambda_R} \right) \left(\left(1 + \frac{2}{\frac{1}{\lambda_R} + \lambda_R} \right) 4 + \left(1 - \frac{2}{\frac{1}{\lambda_R} + \lambda_R} \right) \right) \quad (3.130)$$

$$\Lambda_{i,l} = \left(1 - \frac{2}{\frac{1}{\lambda_R} + \lambda_R} \right)^2 \quad (3.131)$$

$$\Lambda_{i,\text{mean}} = \left(1 - \frac{2}{\frac{1}{\lambda_R} + \lambda_R} \right) \left(\left(1 + \frac{2}{\frac{1}{\lambda_R} + \lambda_R} \right) 2 + \left(1 - \frac{2}{\frac{1}{\lambda_R} + \lambda_R} \right) \right) \quad (3.132)$$

In Fig. 3.18 $\Lambda_{i,u}$, $\Lambda_{i,l}$, and $\Lambda_{i,\text{mean}}$ are plotted versus the amplitude mismatch λ_R . At $\lambda_R = 1$ the interference completely vanishes, i.e. $\Lambda_{i,u} = \Lambda_{i,l} = \Lambda_{i,\text{mean}} = 0$, and thus $P_i = 0$.

2. **Phase uncertainty:** Now, the amplitude mismatch is assumed to be negligible, i.e. $\lambda_R = 1$. The respective terms depending on ρ_R for the upper bound, lower bound, and

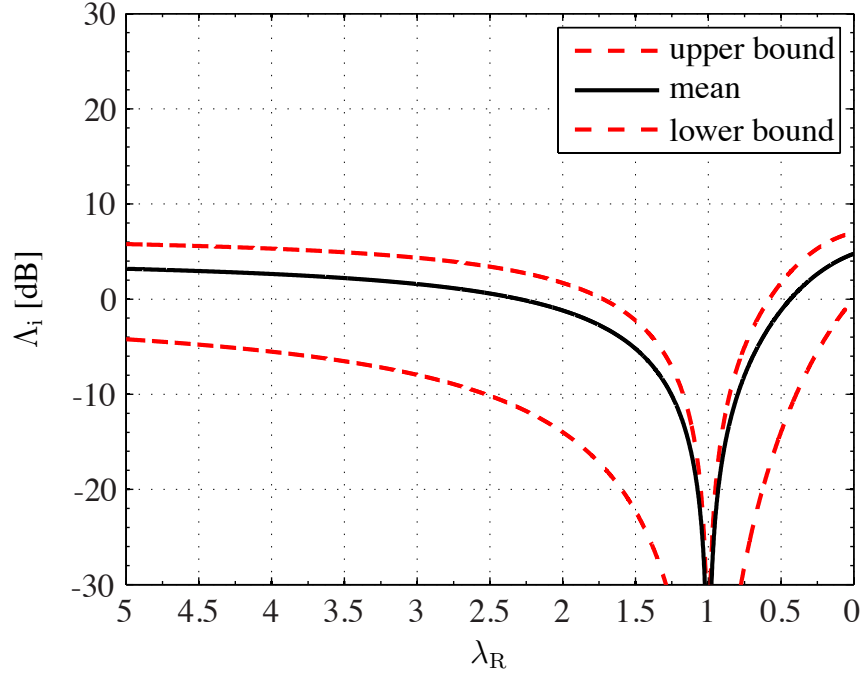


Fig. 3.18: Dependence of the interference power on the amplitude mismatch λ_R .

expected value of the interference power are given by

$$\Omega_{i,u} = (1 - \cos(\rho_R)) ((1 + \cos(\rho_R)) 4 + (1 - \cos(\rho_R))) \quad (3.133)$$

$$\Omega_{i,l} = (1 - \cos(\rho_R))^2 \quad (3.134)$$

$$\Omega_{i,\text{mean}} = (1 - \cos(\rho_R)) ((1 + \cos(\rho_R)) 2 + (1 - \cos(\rho_R))) \quad (3.135)$$

In Fig. 3.19 $\Omega_{i,u}$, $\Omega_{i,l}$, and $\Omega_{i,\text{mean}}$ are plotted versus the phase mismatch ρ_R . At $\rho_R = 0$ the interference completely vanishes, i.e. $\Omega_{i,u} = \Omega_{i,l} = \Omega_{i,\text{mean}} = 0$, and thus $P_i = 0$.

3.3.4.3 Noise Power

The noise part of the signal at the destination is given in (3.106) as

$$\begin{aligned} n_D[n] = & h_{RD} h_{SR} \eta_R^{(\text{tx})} \left(g \eta_R^{(\text{rx})} k_{R,1}^{(\text{rx})} k_{R,1}^{(\text{tx})} + g^* \eta_R^{(\text{rx}),*} k_{R,2}^{(\text{rx}),*} k_{R,2}^{(\text{tx})} \right) w_R[n] + \\ & + h_{RD} h_{SR}^* \eta_R^{(\text{tx})} \left(g \eta_R^{(\text{rx})} k_{R,2}^{(\text{rx})} k_{R,1}^{(\text{tx})} + g^* \eta_R^{(\text{rx}),*} k_{R,1}^{(\text{rx}),*} k_{R,2}^{(\text{tx})} \right) w_R^*[n] + \\ & + w_D[n]. \end{aligned} \quad (3.136)$$

There are two noise sources:

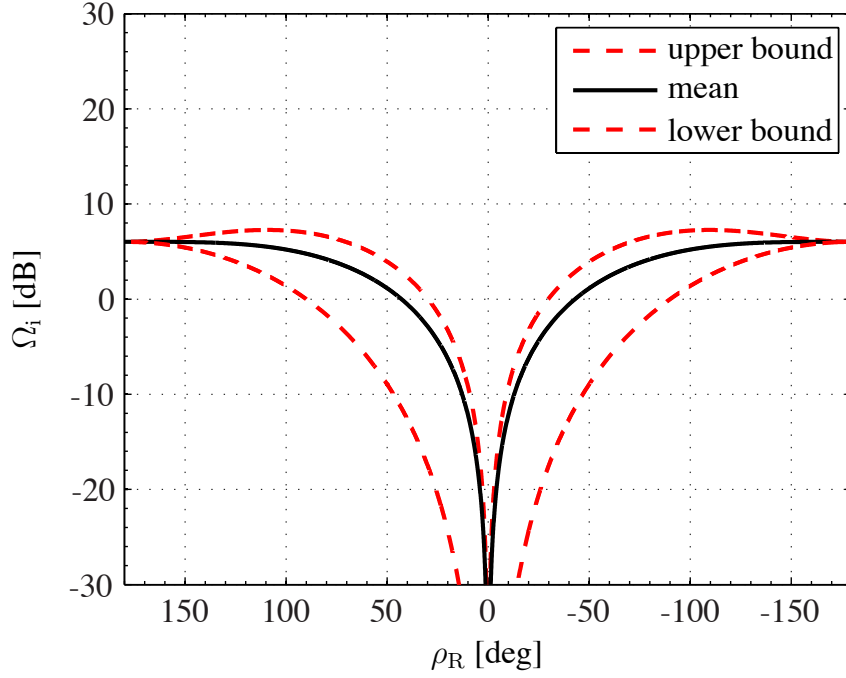


Fig. 3.19: Dependence of the interference power on the phase mismatch ρ_R .

1. AWGN at the relay denoted by $w_R[n] \sim \mathcal{CN}(0, \sigma_n^2)$.
2. AWGN at the destination denoted by $w_D[n] \sim \mathcal{CN}(0, \sigma_n^2)$.

Since they are mutually independent, the total noise power can be written as

$$P_n = \text{E} [|n_D[n]|^2] = P_{w_R} + P_{w_D}, \quad (3.137)$$

where

$$P_{w_R} = \left| h_{RD} \eta_R^{(tx)} \eta_R^{(rx)} \left(g k_{R,1}^{(tx)} k_{R,1}^{(rx)} + g^* k_{R,2}^{(tx)} k_{R,2}^{(rx),*} \right) \right|^2 \sigma_n^2 + \left| h_{RD} \eta_R^{(tx)} \eta_R^{(rx)} \left(g k_{R,1}^{(tx)} k_{R,2}^{(rx)} + g^* k_{R,2}^{(tx)} k_{R,1}^{(rx),*} \right) \right|^2 \sigma_n^2 \quad (3.138)$$

$$P_{w_D} = \sigma_n^2. \quad (3.139)$$

Assuming again that $\lambda_{\text{R}}^{(\text{rx})} = \lambda_{\text{R}}^{(\text{tx})} := \lambda_{\text{R}}$ and $\rho_{\text{R}}^{(\text{rx})} = \rho_{\text{R}}^{(\text{tx})} := \rho_{\text{R}}$ (as in Section 3.3.4.1), the first summand of (3.138) becomes

$$\begin{aligned}
 & \left| h_{\text{RD}} \eta_{\text{R}}^{(\text{tx})} \eta_{\text{R}}^{(\text{rx})} \left(g k_{\text{R},1}^{(\text{tx})} k_{\text{R},1}^{(\text{rx})} + g^* k_{\text{R},2}^{(\text{tx})} k_{\text{R},2}^{(\text{rx}),*} \right) \right|^2 \sigma_{\text{n}}^2 = \\
 & = |h_{\text{RD}}|^2 \frac{2}{1 + \lambda_{\text{R}}^2} \frac{2}{1 + \lambda_{\text{R}}^2} \cdot \\
 & \quad \cdot \left| g \cdot \frac{1 + \lambda_{\text{R}} e^{j\rho_{\text{R}}}}{2} \frac{1 + \lambda_{\text{R}} e^{-j\rho_{\text{R}}}}{2} + g^* \cdot \frac{1 - \lambda_{\text{R}} e^{j\rho_{\text{R}}}}{2} \frac{1 - \lambda_{\text{R}} e^{-j\rho_{\text{R}}}}{2} \right|^2 \sigma_{\text{n}}^2 = \\
 & = \frac{1}{4} |h_{\text{RD}}|^2 \frac{1}{1 + \lambda_{\text{R}}^2} \frac{1}{1 + \lambda_{\text{R}}^2} \cdot \\
 & \quad \cdot \left| g \cdot (1 + \lambda_{\text{R}} e^{j\rho_{\text{R}}}) (1 + \lambda_{\text{R}} e^{-j\rho_{\text{R}}}) + g^* \cdot (1 - \lambda_{\text{R}} e^{j\rho_{\text{R}}}) (1 - \lambda_{\text{R}} e^{-j\rho_{\text{R}}}) \right|^2 \sigma_{\text{n}}^2 = \\
 & = \frac{1}{4} |h_{\text{RD}}|^2 \left| g \left(1 + \frac{\lambda_{\text{R}} 2 \cos(\rho_{\text{R}})}{1 + \lambda_{\text{R}}^2} \right) + g^* \left(1 - \frac{\lambda_{\text{R}} 2 \cos(\rho_{\text{R}})}{1 + \lambda_{\text{R}}^2} \right) \right|^2 \sigma_{\text{n}}^2. \tag{3.140}
 \end{aligned}$$

Substituting $\alpha := \frac{\lambda_{\text{R}} 2 \cos(\rho_{\text{R}})}{1 + \lambda_{\text{R}}^2} = \frac{2 \cos(\rho_{\text{R}})}{\frac{1}{\lambda_{\text{R}}} + \lambda_{\text{R}}} \in \mathbb{R}$, equation (3.140) can be written as

$$\begin{aligned}
 & \left| h_{\text{RD}} \eta_{\text{R}}^{(\text{tx})} \eta_{\text{R}}^{(\text{rx})} \left(g k_{\text{R},1}^{(\text{tx})} k_{\text{R},1}^{(\text{rx})} + g^* k_{\text{R},2}^{(\text{tx})} k_{\text{R},2}^{(\text{rx}),*} \right) \right|^2 \sigma_{\text{n}}^2 = \\
 & = \frac{1}{4} |h_{\text{RD}}|^2 |g(1 + \alpha) + g^*(1 - \alpha)|^2 \sigma_{\text{n}}^2 = \\
 & = \frac{1}{4} |h_{\text{RD}}|^2 (|g|^2 (1 + \alpha)^2 + g^2 (1 - \alpha^2) + g^{*,2} (1 - \alpha^2) + |g|^2 (1 - \alpha)^2) \sigma_{\text{n}}^2 = \\
 & = \frac{1}{4} |h_{\text{RD}}|^2 |g|^2 \left(2(1 + \alpha^2) + \frac{(g^2 + g^{*,2})}{|g|^2} (1 - \alpha^2) \right) \sigma_{\text{n}}^2 \tag{3.141}
 \end{aligned}$$

It can easily be verified that $-1 \leq \alpha \leq 1$. With

$$\begin{aligned}
 \frac{g^2 + g^{*,2}}{|g|^2} & = \frac{|g|^2 e^{2j\varphi_{\text{g}}} + |g|^2 e^{-2j\varphi_{\text{g}}}}{|g|^2} = \\
 & = e^{2j\varphi_{\text{g}}} + e^{-2j\varphi_{\text{g}}} = \\
 & = 2 \cos(2\varphi_{\text{g}}), \tag{3.142}
 \end{aligned}$$

equation (3.141) can finally be written as

$$\begin{aligned}
 & \left| h_{\text{RD}} \eta_{\text{R}}^{(\text{tx})} \eta_{\text{R}}^{(\text{rx})} \left(g k_{\text{R},1}^{(\text{tx})} k_{\text{R},1}^{(\text{rx})} + g^* k_{\text{R},2}^{(\text{tx})} k_{\text{R},2}^{(\text{rx}),*} \right) \right|^2 \sigma_{\text{n}}^2 = \\
 & = \frac{1}{4} |h_{\text{RD}}|^2 |g|^2 (2(1 + \alpha^2) + 2 \cos(2\varphi_{\text{g}}) (1 - \alpha^2)) \sigma_{\text{n}}^2. \tag{3.143}
 \end{aligned}$$

The second summand in (3.138) is

$$\begin{aligned}
 & \left| h_{\text{RD}} \eta_{\text{R}}^{(\text{tx})} \eta_{\text{R}}^{(\text{rx})} \left(g k_{\text{R},1}^{(\text{tx})} k_{\text{R},2}^{(\text{rx})} + g^* k_{\text{R},2}^{(\text{tx})} k_{\text{R},1}^{(\text{rx},*)} \right) \right|^2 \sigma_{\text{n}}^2 = \\
 & = |h_{\text{RD}}|^2 \frac{2}{1 + \lambda_{\text{R}}^2} \frac{2}{1 + \lambda_{\text{R}}^2} \cdot \\
 & \quad \cdot \left| g \cdot \frac{1 + \lambda_{\text{R}} e^{j\rho_{\text{R}}}}{2} \cdot \frac{1 - \lambda_{\text{R}} e^{j\rho_{\text{R}}}}{2} + g^* \cdot \frac{1 - \lambda_{\text{R}} e^{j\rho_{\text{R}}}}{2} \cdot \frac{1 + \lambda_{\text{R}} e^{j\rho_{\text{R}}}}{2} \right|^2 \sigma_{\text{n}}^2 = \\
 & = \frac{1}{4} |h_{\text{RD}}|^2 \left(\frac{1}{1 + \lambda_{\text{R}}^2} \right)^2 \cdot |(g + g^*) \cdot (1 + \lambda_{\text{R}} e^{j\rho_{\text{R}}}) (1 - \lambda_{\text{R}} e^{j\rho_{\text{R}}})|^2 \sigma_{\text{n}}^2 = \\
 & = \frac{1}{4} |h_{\text{RD}}|^2 \left(\frac{1}{1 + \lambda_{\text{R}}^2} \right)^2 |g|^2 \frac{|g + g^*|^2}{|g|^2} \cdot \\
 & \quad \cdot (1 + \lambda_{\text{R}}^2 + \lambda_{\text{R}} (e^{j\rho_{\text{R}}} + e^{-j\rho_{\text{R}}})) \cdot (1 + \lambda_{\text{R}}^2 - \lambda_{\text{R}} (e^{j\rho_{\text{R}}} + e^{-j\rho_{\text{R}}})) \sigma_{\text{n}}^2 = \\
 & = \frac{1}{4} |h_{\text{RD}}|^2 |g|^2 \frac{|g + g^*|^2}{|g|^2} \left(1 + \frac{\lambda_{\text{R}} 2 \cos(\rho_{\text{R}})}{1 + \lambda_{\text{R}}^2} \right) \left(1 - \frac{\lambda_{\text{R}} 2 \cos(\rho_{\text{R}})}{1 + \lambda_{\text{R}}^2} \right) \sigma_{\text{n}}^2. \quad (3.144)
 \end{aligned}$$

Substituting $\alpha := \frac{\lambda_{\text{R}} 2 \cos(\rho_{\text{R}})}{1 + \lambda_{\text{R}}^2} = \frac{2 \cos(\rho_{\text{R}})}{\frac{1}{\lambda_{\text{R}}} + \lambda_{\text{R}}} \in \mathbb{R}$, equation (3.144) can be written as

$$\begin{aligned}
 & \left| h_{\text{RD}} \eta_{\text{R}}^{(\text{tx})} \eta_{\text{R}}^{(\text{rx})} \left(g k_{\text{R},1}^{(\text{tx})} k_{\text{R},2}^{(\text{rx})} + g^* k_{\text{R},2}^{(\text{tx})} k_{\text{R},1}^{(\text{rx},*)} \right) \right|^2 \sigma_{\text{n}}^2 = \\
 & = \frac{1}{4} |h_{\text{RD}}|^2 |g|^2 \frac{|g + g^*|^2}{|g|^2} (1 + \alpha) (1 - \alpha) \sigma_{\text{n}}^2. \quad (3.145)
 \end{aligned}$$

With

$$\begin{aligned}
 \frac{|g + g^*|^2}{|g|^2} & = \frac{(|g| e^{j\varphi_{\text{g}}} + |g| e^{-j\varphi_{\text{g}}})^2}{|g|^2} = \\
 & = (e^{j\varphi_{\text{g}}} + e^{-j\varphi_{\text{g}}})^2 = \\
 & = 4 \cos^2(\varphi_{\text{g}}), \quad (3.146)
 \end{aligned}$$

equation (3.145) becomes

$$\begin{aligned}
 & \left| h_{\text{RD}} \eta_{\text{R}}^{(\text{tx})} \eta_{\text{R}}^{(\text{rx})} \left(g k_{\text{R},1}^{(\text{tx})} k_{\text{R},2}^{(\text{rx})} + g^* k_{\text{R},2}^{(\text{tx})} k_{\text{R},1}^{(\text{rx},*)} \right) \right|^2 \sigma_{\text{n}}^2 = \\
 & = \frac{1}{4} |h_{\text{RD}}|^2 |g|^2 4 \cos^2(\varphi_{\text{g}}) (1 - \alpha^2) \sigma_{\text{n}}^2. \quad (3.147)
 \end{aligned}$$

Finally, the sum of (3.143) and (3.147) yields the power of the noise contribution due to AWGN at the relay, i.e. P_{w_R} . It is given by

$$\begin{aligned} P_{w_R} &= \frac{1}{4} |h_{RD}|^2 |g|^2 (2(1 + \alpha^2) + 2\cos(2\varphi_g)(1 - \alpha^2)) \sigma_n^2 + \\ &\quad + \frac{1}{4} |h_{RD}|^2 |g|^2 4\cos^2(\varphi_g)(1 - \alpha^2) \sigma_n^2 = \\ &= |h_{RD}|^2 |g|^2 \sigma_n^2 (1 + (1 - \alpha^2) \cos(2\varphi_g)). \end{aligned} \quad (3.148)$$

The total noise power at the destination is thus

$$\begin{aligned} P_n &= P_{w_R} + P_{w_D} = \\ &= |h_{RD}|^2 |g|^2 \sigma_n^2 (1 + (1 - \alpha^2) \cos(2\varphi_g)) + \sigma_n^2, \end{aligned} \quad (3.149)$$

where $\alpha = \frac{2\cos(\rho_R)}{\frac{1}{\lambda_R} + \lambda_R}$. An upper and lower bound on the noise power can now be derived with respect to the phase $\varphi_g \in (-\pi, \pi]$ of the gain factor.

- **Upper bound:** Since $-1 \leq \alpha \leq 1$ and thus $0 \leq (1 - \alpha^2) \leq 1$, the noise power is maximized if $\cos(2\varphi_g) = 1$:

$$P_{n,u} = |h_{RD}|^2 |g|^2 \sigma_n^2 (2 - \alpha^2) + \sigma_n^2 \quad (3.150)$$

- **Lower bound:** For $\cos(2\varphi_g) = -1$, the noise power is minimized:

$$P_{n,l} = |h_{RD}|^2 |g|^2 \sigma_n^2 \alpha^2 + \sigma_n^2 \quad (3.151)$$

- **Mean:** The expected noise power for the case that the phase of the gain factor is uniformly distributed, i.e. $\varphi_g \sim \mathcal{U}(-\pi, \pi)$, is

$$P_{n,\text{mean}} = E_{\varphi_g} [P_n] = |h_{RD}|^2 |g|^2 \sigma_n^2 + \sigma_n^2, \quad (3.152)$$

where $E_{\varphi_g} [\cos(2\varphi_g)] = 0$.

As for the signal power in Section 3.3.4.1 and the interference power in Section 3.3.4.2, the impact of amplitude and phase uncertainty are investigated separately:

1. **Amplitude uncertainty:** The phase mismatch is neglected ($\varphi_R = 0$) in order to extract the impact of the amplitude mismatch. The respective terms depending on λ_R for the

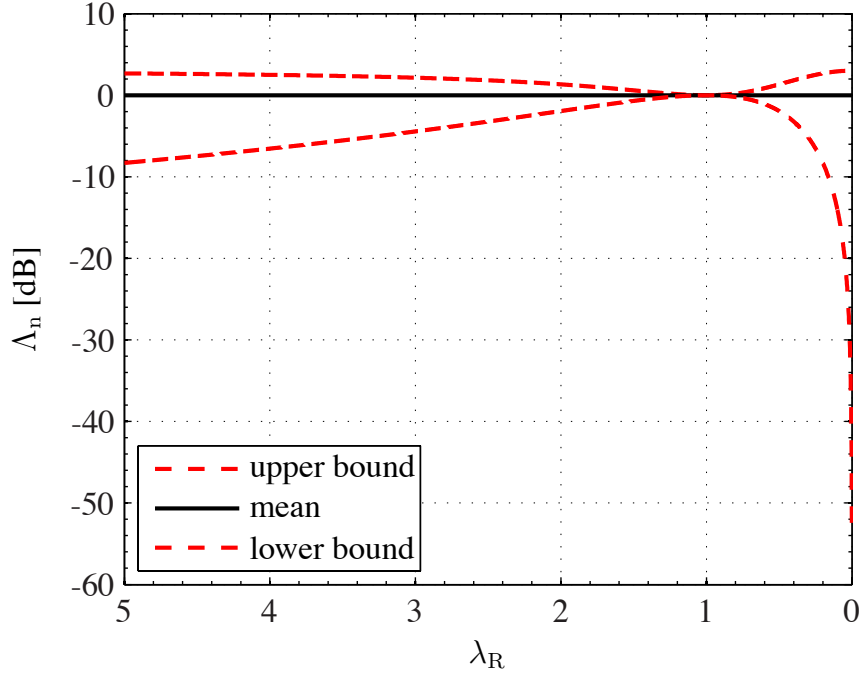


Fig. 3.20: Dependence of the noise power on the amplitude mismatch λ_R .

upper bound, lower bound, and mean value of the noise power are given by

$$\Lambda_{n,u} = 2 - \left(\frac{2}{\frac{1}{\lambda_R} + \lambda_R} \right)^2 \quad (3.153)$$

$$\Lambda_{n,l} = \left(\frac{2}{\frac{1}{\lambda_R} + \lambda_R} \right)^2 \quad (3.154)$$

$$\Lambda_{n,\text{mean}} = 1 \quad (3.155)$$

In Fig. 3.20, $\Lambda_{n,u}$, $\Lambda_{n,l}$, and $\Lambda_{n,\text{mean}}$ are plotted versus the amplitude uncertainty Λ_R .

2. **Phase uncertainty:** If the amplitude uncertainty is neglected, i.e. $\lambda_R = 1$, the influence of the phase uncertainty on the noise power is isolated. The respective terms depending on ρ_R for the upper bound, lower bound, and mean value of the noise power are given by

$$\Omega_{n,u} = 2 - \cos^2(\rho_R) \quad (3.156)$$

$$\Omega_{n,l} = \cos^2(\rho_R) \quad (3.157)$$

$$\Omega_{n,\text{mean}} = 1 \quad (3.158)$$

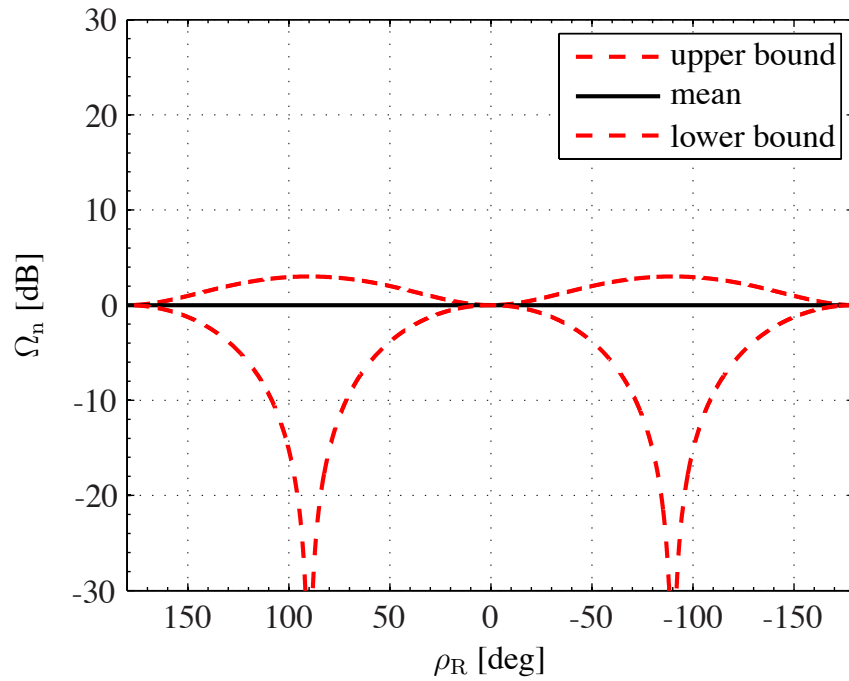


Fig. 3.21: Dependence of the noise power on the phase mismatch ρ_R .

In Fig. 3.21, $\Omega_{n,u}$, $\Omega_{n,l}$, and $\Omega_{n,\text{mean}}$ are plotted versus the phase mismatch ρ_R .

Obviously, the average noise power is not affected by I/Q imbalance because both $\Omega_{n,\text{mean}}$ and $\Omega_{n,\text{mean}}$ are independent of λ_R and ρ_R .

Chapter 4

Channel Estimation

For any coherent forwarding scheme, the relays require a certain amount of channel knowledge if they are to calculate their gain factors locally. In particular, every relay needs to have full channel knowledge for the gain allocation schemes that will be discussed in Chapter 6. This means that every relay needs to have estimates of $\tilde{\mathbf{H}}_{SR}$, $\tilde{\mathbf{H}}_{RD}$, and, if the direct link is used¹, also of $\tilde{\mathbf{H}}_{SD}$. In order to provide this information, all channel coefficients have to be estimated and then disseminated to the relays. This essentially requires two phases:

1. *Channel estimation phase*
2. *Dissemination phase*

In Section 4.1 it will be shown that the direction in which the channels are measured has an impact on the estimates (even if they are noiseless). Based on this observation, it turns out in Section 4.2 that in some cases a global phase reference is required for a certain set of nodes in order to allow for coherent forwarding. The following question is answered: *Which nodes in a two-hop relaying network require a global phase reference so that coherent distributed beamforming is possible?* To this end, a framework is derived to determine the phase synchronization requirements. They will be shown to depend on the direction (relative to the data transmission) in which the point-to-point channels are estimated. All possible combinations for the direction in which the channel matrices can be measured are therefore investigated. In multi-hop relaying networks there are different reasons to estimate the single-hop channels in one direction or the other. For example, the number of required channel uses depends on the direction the channels are measured if the number of transmitters and receivers is different. Furthermore, consider a network where the assignment of the nodes (sources, relays, and destinations) is dynamic. Reorganizing the network, e.g. sources becoming destinations and vice versa, automatically changes the direction of the current

¹The direct link is used in traffic patterns II – IV, which were introduced in Section 2.4

channel estimates relative to the data transmission direction. A specification of the phase synchronization requirements is a valuable tool to organize such networks or to compare the effort required for phase synchronization with the benefits of different directions of channel measurement. In general, the gain factors are computed correctly if the anticipated objective function for which they are optimized (e.g. the signal-to-interference-and-noise ratio (SINR) at the destinations) is the same as the actual one for the data transmission. Since the relays only have knowledge of the estimated channel coefficients and not the actual ones, this may not always be the case. If the anticipated and the actual objective function are not the same, the relay gain factors are optimized for the wrong situation. This leads to a performance degradation. All four traffic patterns I – IV, that were introduced in Section 2.4, are investigated regarding this issue for the case that the single-hop channels are estimated in different directions.

Thoughts on the channel update rate are presented in **Section 4.3**. In **Section 4.4**, four protocols to measure all single-hop channel coefficients in a two-hop wireless network are identified and compared. They differ in the direction in which the channels are estimated. As a consequence, also the number of channel uses required to estimate all coefficients is different. Two of them require the relays to possess a global phase reference, which requires additional overhead. Thus a tradeoff exists between the number of channel uses necessary to estimate the channel coefficients and the need for global phase reference at the relays. Finally, the impact of additive signal noise and phase noise on the quality of the channel estimates is investigated. Two important representatives of the protocols identified in Section 4.4 are compared based on the quality of the channel estimates they deliver.

To simplify matters in this chapter, all nodes employ a single antenna only, i.e. $M_S = M_D = N_{SD}$ and $M_R = N_R$. The extension to multi-antenna nodes is, however, straightforward. Until otherwise stated, it is furthermore assumed that all channel estimates are noiseless.

4.1 Channel Estimation and Dissemination

A point-to-point channel between any two nodes A and B can be estimated in two directions: Either from node A to node B or from node B to node A. Although the wireless propagation channel between the two nodes is reciprocal, the equivalent baseband channel is generally not when A and B are not phase synchronous. In (2.2), the equivalent channel between A

and B is given by

$$\tilde{h}_{AB} = h_{AB}e^{j(\varphi_A - \varphi_B)}, \quad (4.1)$$

where φ_A and φ_B denote their respective LO phase offsets. Consequently, the equivalent channel between node B and A is

$$\begin{aligned} \tilde{h}_{BA} &= h_{BA}e^{j(\varphi_B - \varphi_A)} = \\ &= \tilde{h}_{AB}e^{2j(\varphi_B - \varphi_A)}, \end{aligned} \quad (4.2)$$

where the reciprocity of the propagation channel, i.e. $h_{AB} = h_{BA}$, was used. The equivalent channel is only reciprocal if A and B possess a joint phase reference, i.e. $\varphi_A = \varphi_B$. The direction in which the channel is measured has obviously an impact on the estimate because of the LO phase offsets. There is no way of learning \tilde{h}_{AB} from \tilde{h}_{BA} or \tilde{h}_{BA} from \tilde{h}_{AB} when φ_A and φ_B are unknown.

Consider the two-hop network in Fig. 2.1. Each channel coefficient can be estimated either in 'forward direction', i.e., in the same direction as the data transmission², or in 'backward direction'. The noiseless channel estimates in forward direction, i.e., from source k to destination m , from source k to relay l , and from relay l to destination m are, respectively, given by

$$\hat{h}_{S_k D_m} = \tilde{h}_{S_k D_m}, \quad (4.3)$$

$$\hat{h}_{S_k R_l} = \tilde{h}_{S_k R_l}, \quad (4.4)$$

$$\hat{h}_{R_l D_m} = \tilde{h}_{R_l D_m}. \quad (4.5)$$

The corresponding estimated channel matrices are³

$$\hat{\mathbf{H}}_{SD} = \tilde{\mathbf{H}}_{SD}, \quad (4.6)$$

$$\hat{\mathbf{H}}_{SR} = \tilde{\mathbf{H}}_{SR}, \quad (4.7)$$

$$\hat{\mathbf{H}}_{RD} = \tilde{\mathbf{H}}_{RD}. \quad (4.8)$$

²The forward direction of each matrix channel is indicated by the arrows in Fig. 2.1.

³Please recall that the channel estimates are assumed to be noiseless.

Measuring the channel coefficients in backward direction yields (in accordance with (4.2))

$$\hat{h}_{D_m S_k} = \tilde{h}_{S_k D_m} e^{2j(\varphi_{D_m} - \varphi_{S_k})}, \quad (4.9)$$

$$\hat{h}_{R_l S_k} = \tilde{h}_{S_k R_l} e^{2j(\varphi_{R_l} - \varphi_{S_k})}, \quad (4.10)$$

$$\hat{h}_{D_m R_l} = \tilde{h}_{R_l D_m} e^{2j(\varphi_{D_m} - \varphi_{R_l})}. \quad (4.11)$$

If $\hat{h}_{D_m S_k}$, $\hat{h}_{R_l S_k}$, and $\hat{h}_{D_m R_l}$ are used as estimates for the forward direction, i.e., as estimates for $\tilde{h}_{S_k D_m}$, $\tilde{h}_{S_k R_l}$, and $\tilde{h}_{R_l D_m}$, a phase error is introduced. The estimated channel matrices are in this case given by

$$\hat{\mathbf{H}}_{SD} = \hat{\mathbf{H}}_{DS}^T = \mathbf{\Phi}_D \mathbf{\Phi}_D \cdot \tilde{\mathbf{H}}_{SD} \cdot \mathbf{\Phi}_S^H \mathbf{\Phi}_S^H, \quad (4.12)$$

$$\hat{\mathbf{H}}_{SR} = \hat{\mathbf{H}}_{RS}^T = \mathbf{\Phi}_R \mathbf{\Phi}_R \cdot \tilde{\mathbf{H}}_{SR} \cdot \mathbf{\Phi}_S^H \mathbf{\Phi}_S^H, \quad (4.13)$$

$$\hat{\mathbf{H}}_{RD} = \hat{\mathbf{H}}_{DR}^T = \mathbf{\Phi}_D \mathbf{\Phi}_D \cdot \tilde{\mathbf{H}}_{RD} \cdot \mathbf{\Phi}_R^H \mathbf{\Phi}_R^H. \quad (4.14)$$

Once all channel coefficients are measured, they have to be disseminated to the relays so that they can locally compute their gain factors. The number of channel uses required to disseminate all channel coefficients to the relays is equal to the number of channel coefficients, i.e. $2N_{SD}N_R + N_{SD}^2$. This will be called the *dissemination overhead*. In order to broadcast a channel coefficient, the respective node has to transmit the signal at a rate that all relays are able to decode. In large networks this will generate quite some amount of overhead. Every time the propagation channels change, channel knowledge has to be updated at the relays. In the worst case, the whole estimation and dissemination procedure has to be repeated. Global channel state information at the relays is therefore only feasible if the propagation environment changes slowly. If the nodes are close to each other, a secondary system (e.g. Bluetooth or ultra wideband (UWB)) might be used to disseminate the channel estimates. In this case no system resources of the primary communication system would be used.

4.2 Coherent Distributed Beamforming

The work in this section was triggered by the fact that in the presence of unknown and random LO phases, the direction in which wireless point-to-point (single-hop) channels are measured has an impact on the estimates (in the form of a phase rotation). Although the propagation channels are reciprocal, the equivalent baseband channels are generally not if the nodes are not phase synchronous (cf. Section 4.1). Since the gain factors are computed

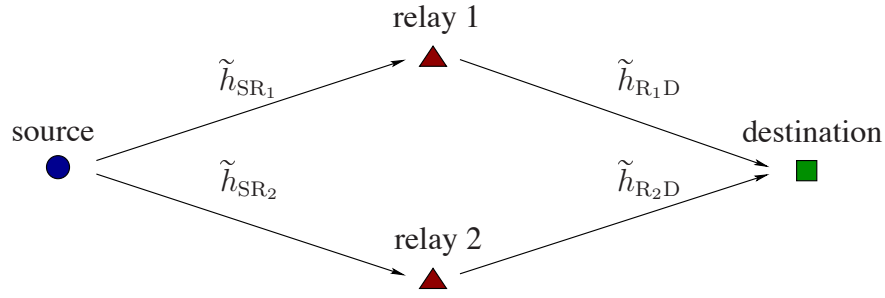


Fig. 4.1: Simple two-hop relaying scenario.

from channel estimates, an unknown and random phase shift is in some cases introduced to the forwarded signals at the relays. This phase shift depends on the direction in which the point-to-point channels have been estimated. If no global phase reference is present, it may destroy coherency.

It is often assumed that 'coherent beamforming' requires perfect CSI. In the context of distributed AF relaying networks, this definition has to be adapted. Phase errors in the channel estimates that are the result of the measurement direction have in some cases no impact on the system performance. It makes sense to call those cases 'coherent', even if perfect CSI is not available. In this section, a formal condition for coherent distributed beamforming is provided that captures this issue. In order to get an intuition for the reasoning that is behind this (adapted) condition, a simple single-user scenario is first considered. It will be found that if (4.20) is fulfilled, coherent beamforming is possible. Afterwards, this condition is extended to the multiuser case. Equation (4.27) is an extension of (4.20) that takes multiple users and the resulting inter-user interference into account.

4.2.1 Single-User System

Consider the simple scenario with a single source-destination pair and two AF relays shown in Fig. 4.1. The received signal at the destination is

$$d = \left(\sum_{l=1}^2 \tilde{h}_{R_lD} g_l \tilde{h}_{SR_l} \right) s := \tilde{h}_{SRD} \cdot s, \quad (4.15)$$

where $s \sim \mathcal{CN}(0, \sigma_s^2)$ is the source transmit symbol, $g_l, l \in \{1, 2\}$, are the relay gain factors, and

$$\tilde{h}_{SRD} = \sum_{l=1}^2 \tilde{h}_{R_lD} g_l \tilde{h}_{SR_l} \quad (4.16)$$

is called the 'compound channel coefficient'. The power of the received signal at the destination is $P_R = E_s[|d|^2]$. It is bounded by

$$0 \leq P_R \leq \left(\sum_{l=1}^2 |\tilde{h}_{R_lD} g_l \tilde{h}_{SR_l}| \right)^2 \sigma_s^2. \quad (4.17)$$

If perfect CSI is available, the received signal power can be adjusted explicitly by choosing the gain factors accordingly. But what if the gain factors have to be computed from channel estimates rather than the actual coefficients? Let \hat{h}_{SR_l} and \hat{h}_{R_lD} denote the estimates of \tilde{h}_{SR_l} and \tilde{h}_{R_lD} , respectively, based on which the relay gains have to be computed. Then, the *anticipated* received signal power is $\hat{P}_R = E_s[|\hat{d}|^2]$, where

$$\hat{d} = \left(\sum_{l=1}^2 \hat{h}_{R_lD} g_l \hat{h}_{SR_l} \right) s := \hat{h}_{SRD} \cdot s. \quad (4.18)$$

It is bounded by

$$0 \leq \hat{P}_R \leq \left(\sum_{l=1}^2 |\hat{h}_{R_lD} g_l \hat{h}_{SR_l}| \right)^2 \sigma_s^2. \quad (4.19)$$

The gain factors can adjust the received signal power explicitly within its bounds if P_R is a linear function of \hat{P}_R , i.e., $E_s[|\hat{d}|^2] = E_s[|cd|^2]$, where $c \in \mathbb{C}$. This corresponds to requiring

$$\hat{h}_{SRD} = c \cdot \tilde{h}_{SRD}. \quad (4.20)$$

The anticipated receive power \hat{P}_R is equal to the actual one P_R if $|c|^2 = 1$. The anticipated receive SNR is in this case equal to the actual one.

Proposition 4.2.1. *In general, coherent distributed beamforming is possible if the anticipated objective function, based on which the relay gains are computed (e.g. receive SNR), is a linear function of the actual one.*

If in the current example the objective function is the receive SNR, it suffices to check whether (4.20) is fulfilled with $|c|^2 = 1$ to find out if coherent beamforming is possible⁴. The following example demonstrates that this may be the case even with imperfect CSI.

⁴This is because the gain factors can adjust the received signal power but not the noise power at the destination. Equation (4.20) has therefore to be fulfilled with $|c|^2 = 1$ in order for the estimated SNR to be a linear function of the actual one.

Example: Let

$$\hat{h}_{\text{SR}_l} = \tilde{h}_{\text{SR}_l} e^{2j(\varphi_{\text{R}_l} - \varphi_{\text{S}})} \quad (4.21)$$

$$\hat{h}_{\text{R}_l\text{D}} = \tilde{h}_{\text{R}_l\text{D}} e^{2j(\varphi_{\text{D}} - \varphi_{\text{R}_l})} \quad (4.22)$$

denote the estimates of the first-hop and second-hop channels, respectively. They are obtained by estimating all channels in backward direction (cf. (4.10) and (4.11)). Since in this case $\hat{P}_{\text{R}} = P_{\text{R}}$ it is possible to explicitly adjust the receive SNR with gain factors that are computed from imperfect CSI.

4.2.2 Multi-User System

The refined definition of coherency for distributed beamforming in the single-user case can be extended to multi-user networks. In analogy to the compound channel coefficient in (4.16) a 'compound channel matrix' has to be defined for the multiuser scenario. This is done based on the input/output relations for traffic patterns I – IV derived in Section 2.4. The most demanding requirements for phase synchronization are imposed on the network if the signals from all possible paths (direct link in the first time slot as well as direct and two-hop link in the second time slot) have to combine coherently at the destinations. For traffic pattern I, this is the case if both of the following assumptions hold:

- The sources transmit a scaled version of $\mathbf{s}^{(1)}$ in the second time slot, i.e. $\mathbf{s}^{(2)} = \mathbf{\Gamma}_{\text{S}}\mathbf{s}^{(1)}$, where the matrix $\mathbf{\Gamma}_{\text{S}}$ is diagonal with complex-valued entries $\gamma_{\text{S}_k} \in \mathbb{C}$, for $k \in \{1, \dots, N_{\text{SD}}\}$.
- The destinations compute

$$\mathbf{d}_{\text{I}} = \mathbf{\Gamma}_{\text{D}}\mathbf{d}^{(1)} + \mathbf{d}^{(2)}, \quad (4.23)$$

prior to decoding, where $\mathbf{\Gamma}_{\text{D}}$ is a diagonal matrix of scaling factors γ_{D_m} , $m \in \{1, \dots, N_{\text{SD}}\}$ at the destinations.

Relaxing any of the two assumptions relaxes the phase synchronization requirements for traffic pattern I:

- If the symbols in $\mathbf{s}^{(1)}$ and $\mathbf{s}^{(2)}$ are mutually independent, they need not combine coherently at the destination. In this case, the phase synchronization requirements are the same as for traffic pattern II, where the source is silent in the second time slot.

- If the vectors $\mathbf{d}^{(1)}$ and $\mathbf{d}^{(2)}$ are not required to combine coherently, the phase synchronization requirements are the same as for traffic pattern III, where the destinations do not listen in the first time slot.
- If both assumptions are dropped, the phase synchronization requirements are the same as for traffic pattern IV.

Equation (4.23) can be written as

$$\mathbf{d}_I = \tilde{\mathbf{H}}_I \mathbf{s} + \tilde{\mathbf{n}}_I, \quad (4.24)$$

where

$$\tilde{\mathbf{H}}_I = \Gamma_D \tilde{\mathbf{H}}_{SD} + \tilde{\mathbf{H}}_{RD} \mathbf{G} \tilde{\mathbf{H}}_{SR} + \tilde{\mathbf{H}}_{SD} \Gamma_S \quad (4.25)$$

$$\text{and } \tilde{\mathbf{n}}_I = \Gamma_D \mathbf{n}_D^{(1)} + \tilde{\mathbf{H}}_{RD} \mathbf{G} \mathbf{n}_R + \mathbf{n}_D^{(2)} \quad (4.26)$$

are called the 'compound channel matrix' and the 'compound noise vector', respectively. The compound channel matrices for traffic patterns II – IV are readily obtained from (4.25) by setting either Γ_D or Γ_S or both to zero.

Remark 4.2.1. *It turns out that $\tilde{\mathbf{H}}_I$ is independent of the LO phases of the relays (cf. Section 2.4)). Consequently, the gain matrix \mathbf{G} as well as the scaling matrices Γ_D and Γ_S only have to be updated when the propagation channels change. Once they are computed, the LO phases of the nodes have no impact on the receive SINR.*

The next step is to identify the requirements that have to be fulfilled so that the estimated compound channel coefficient from source k to destination m is a linear function of the actual one. This means that the conditions for

$$\hat{\mathbf{H}}_X[m, k] = c_{m,k} \cdot \tilde{\mathbf{H}}_X[m, k], \quad X \in \{I, II, III, IV\}, \quad (4.27)$$

where $c_{m,k} \in \mathbb{C}$, have to be found. The following propositions can be identified:

Proposition 4.2.2. *If (4.27) holds with $|c_{m,k}| = |c_m|$ for all k , the anticipated receive SIR at destination m is equal to the actual one.*

Proposition 4.2.3. *If Proposition 4.2.2 holds and furthermore $|c_{m,k}|^2 = 1$ for all k , the anticipated and the actual SINR at destination m are equal.*

Both propositions follow immediately from the fact that the received signal and interference power at destination m are

$$P_m^{(s)} = \left| \tilde{\mathbf{H}}_I[m, m] \right|^2 \sigma_s^2 \quad (4.28)$$

$$P_m^{(i)} = \sum_{\substack{k=1 \\ k \neq m}}^{N_{SD}} \left| \tilde{\mathbf{H}}_I[m, k] \right|^2 \sigma_s^2. \quad (4.29)$$

If the phase synchronization requirements that are necessary to fulfill (4.27) are found, it is straightforward to find the phase synchronization requirements for any coherent gain allocation scheme by investigating its objective function: Equation (4.27) has to hold for m and k if the gain factors are a function of the signal power from source k at destination m .

Example: For MUZF relaying [25], equation (4.27) has to hold for all $m \neq k$ and for MMSE relaying [73], special case 2) has to be fulfilled for all m .

In Sections 4.2.3 – 4.2.10 the phase synchronization requirements for all eight possible combinations of directions in which the single-hop channel matrices can be estimated are derived. The case that the channel matrix $\tilde{\mathbf{H}}_{AB}$ between nodes A and B is measured in forward direction (from A to B) will be denoted by $A \rightarrow B$. Likewise, the case where $\tilde{\mathbf{H}}_{AB}$ is measured in backward direction (from B to A) will be denoted by $A \leftarrow B$. For each of the combinations, all four traffic patterns are discussed. Each section starts with traffic pattern I. The requirements for traffic patterns II – IV can then be easily derived from the discussion of traffic pattern I. Table 4.1 in Section 4.2.11 finally summarizes all results.

The knowledge of the measured channel matrices $\hat{\mathbf{H}}_{SD}$, $\hat{\mathbf{H}}_{SR}$, and $\hat{\mathbf{H}}_{RD}$, is assumed to be available for the computation of the gain matrix. Furthermore, it is assumed that each destination m has measured its local compound channel coefficient $\tilde{\mathbf{H}}_X[m, m]$ with the help of a preamble during data transmission. This knowledge is necessary to decode the data. Furthermore, it will in some cases be used to allow for coherent combining of the received signals from both time slots at the destinations.

4.2.3 Required Phase Synchronization for $\mathbf{S} \rightarrow \mathbf{D} / \mathbf{S} \rightarrow \mathbf{R} / \mathbf{R} \rightarrow \mathbf{D}$

All channel matrices are estimated in forward direction. This means that the estimates

$$\hat{\mathbf{H}}_{\text{SD}} = \tilde{\mathbf{H}}_{\text{SD}}, \quad (4.30)$$

$$\hat{\mathbf{H}}_{\text{SR}} = \tilde{\mathbf{H}}_{\text{SR}}, \quad (4.31)$$

$$\hat{\mathbf{H}}_{\text{RD}} = \tilde{\mathbf{H}}_{\text{RD}} \quad (4.32)$$

are available in the network. For traffic pattern I, the compound channel matrix $\tilde{\mathbf{H}}_{\text{I}}$ is given in (4.25). At the relays, its estimate is computed from the single-hop channel estimates (4.30) – (4.32):

$$\begin{aligned} \hat{\mathbf{H}}_{\text{I}} &= \hat{\Gamma}_{\text{D}} \hat{\mathbf{H}}_{\text{SD}} + \hat{\mathbf{H}}_{\text{RD}} \mathbf{G} \hat{\mathbf{H}}_{\text{SR}} + \hat{\mathbf{H}}_{\text{SD}} \hat{\Gamma}_{\text{S}} = \\ &= \hat{\Gamma}_{\text{D}} \tilde{\mathbf{H}}_{\text{SD}} + \tilde{\mathbf{H}}_{\text{RD}} \mathbf{G} \tilde{\mathbf{H}}_{\text{SR}} + \tilde{\mathbf{H}}_{\text{SD}} \hat{\Gamma}_{\text{S}}, \end{aligned} \quad (4.33)$$

where $\hat{\Gamma}_{\text{S}}$ and $\hat{\Gamma}_{\text{D}}$ are estimates of the scaling matrices Γ_{S} and Γ_{D} that have to be generated locally. It has to be checked whether (4.27) is fulfilled for $\hat{\mathbf{H}}_{\text{I}}$ given in (4.33) and $\tilde{\mathbf{H}}_{\text{I}}$ given in (4.25). Obviously, $\hat{\mathbf{H}}_{\text{I}} = \tilde{\mathbf{H}}_{\text{I}}$ if $\hat{\Gamma}_{\text{S}} = \tilde{\Gamma}_{\text{S}}$ and $\hat{\Gamma}_{\text{D}} = \tilde{\Gamma}_{\text{D}}$. A particularly simple and valid choice would be $\hat{\Gamma}_{\text{S}} = \tilde{\Gamma}_{\text{S}} = \hat{\Gamma}_{\text{D}} = \tilde{\Gamma}_{\text{D}} = \mathbf{I}_{N_{\text{SD}}}$. In this case, (4.27) holds for all m and k and all traffic patterns. Since (4.27) is fulfilled for $c_{m,k} = 1$, the anticipated SINR at all destinations is equal to the actual one.

4.2.4 Required Phase Synchronization for $\mathbf{S} \rightarrow \mathbf{D} / \mathbf{S} \leftarrow \mathbf{R} / \mathbf{R} \leftarrow \mathbf{D}$

The direct link is measured in forward direction while both the first-hop and the second-hop link are measured in backward direction. This means that the estimates

$$\hat{\mathbf{H}}_{\text{SD}} = \tilde{\mathbf{H}}_{\text{SD}}, \quad (4.34)$$

$$\hat{\mathbf{H}}_{\text{SR}} = \Phi_{\text{R}} \Phi_{\text{R}}^H \cdot \tilde{\mathbf{H}}_{\text{SR}} \cdot \Phi_{\text{S}}^H \Phi_{\text{S}}^H, \quad (4.35)$$

$$\hat{\mathbf{H}}_{\text{RD}} = \Phi_{\text{D}} \Phi_{\text{D}}^H \cdot \tilde{\mathbf{H}}_{\text{RD}} \cdot \Phi_{\text{R}}^H \Phi_{\text{R}}^H \quad (4.36)$$

are available in the network. For traffic pattern I, the compound channel matrix $\tilde{\mathbf{H}}_{\text{I}}$ is given in (4.25). At the relays, its estimate is computed from the single-hop channel estimates given

in (4.34) – (4.36):

$$\begin{aligned}\hat{\mathbf{H}}_I &= \hat{\Gamma}_D \hat{\mathbf{H}}_{SD} + \hat{\mathbf{H}}_{RD} \mathbf{G} \hat{\mathbf{H}}_{SR} + \hat{\mathbf{H}}_{SD} \hat{\Gamma}_S = \\ &= \hat{\Gamma}_D \tilde{\mathbf{H}}_{SD} + \Phi_D \Phi_D \tilde{\mathbf{H}}_{RD} \mathbf{G} \tilde{\mathbf{H}}_{SR} \Phi_S^H \Phi_S^H + \tilde{\mathbf{H}}_{SD} \hat{\Gamma}_S,\end{aligned}\quad (4.37)$$

where $\hat{\Gamma}_S$ and $\hat{\Gamma}_D$ are estimates of the scaling matrices Γ_S and Γ_D that have to be generated locally. It has to be checked whether (4.27) is fulfilled for $\hat{\mathbf{H}}_I$ given in (4.37) and $\tilde{\mathbf{H}}_I$ given in (4.25). Since (4.27) has to hold for all channel realizations including the case where any of the channel coefficients is zero, two conditions are obtained:

1. For $\tilde{\mathbf{H}}_{SR} = \mathbf{0}$ or $\tilde{\mathbf{H}}_{RD} = \mathbf{0}$, equation (4.27) becomes

$$\hat{\gamma}_{D_m} + \hat{\gamma}_{S_k} = c_{m,k} \cdot (\gamma_{D_m} + \gamma_{S_k}). \quad (4.38)$$

2. For $\tilde{\mathbf{H}}_{SD} = \mathbf{0}$, equation (4.27) becomes

$$e^{2j(\varphi_{D_m} - \varphi_{S_k})} \cdot \tilde{h}_{S_k R D_m} = c_{m,k} \cdot \tilde{h}_{S_k R D_m}, \quad (4.39)$$

where

$$\tilde{h}_{S_k R D_m} = \sum_{l=1}^{N_R} \left(\tilde{h}_{R_l D_m} g_l \tilde{h}_{S_k R_l} \right). \quad (4.40)$$

Consequently,

$$e^{2j(\varphi_{D_m} - \varphi_{S_k})} = c_{m,k}. \quad (4.41)$$

It follows from (4.41) that in this section $|c_{m,k}| = 1$ for all traffic patterns.

Inserting (4.41) in (4.38) yields

$$\hat{\gamma}_{D_m} + \hat{\gamma}_{S_k} = e^{2j(\varphi_{D_m} - \varphi_{S_k})} \cdot (\gamma_{D_m} + \gamma_{S_k}). \quad (4.42)$$

The phase synchronization requirements for all four traffic patterns can now be derived from (4.42):

Traffic Pattern I: For traffic pattern I, (4.27) is fulfilled if (4.42) holds. With the CSI available in the network, there is, however, no way to compute $\hat{\gamma}_{S_k}$, γ_{S_k} , $\hat{\gamma}_{D_m}$, and γ_{D_m} , unequal to zero such that (4.42) is fulfilled. Consequently, source k and destination m are required to possess a common LO phase reference, i.e. $\varphi_{S_k} = \varphi_{D_m}$. In this case, $c_{m,k} = 1$

and (4.42) is fulfilled by $\hat{\gamma}_{S_k} = \gamma_{S_k}$ and $\hat{\gamma}_{D_m} = \gamma_{D_m}$. A particularly simple and valid choice is $\hat{\gamma}_{S_k} = \gamma_{S_k} = \hat{\gamma}_{D_m} = \gamma_{D_m} = 1$. The anticipated received power from source k at destination m is then equal to the actual one.

Traffic Pattern II: With $\hat{\gamma}_S = \gamma_S = 0$, equation (4.42) becomes

$$\hat{\gamma}_{D_m} = e^{2j(\varphi_{D_m} - \varphi_{S_k})} \cdot \gamma_{D_m}. \quad (4.43)$$

If destination m chooses

$$\gamma_{D_m} = \tilde{h}_{S_m R D_m} \quad (4.44)$$

and the relays use their respective estimates

$$\begin{aligned} \hat{\gamma}_{D_m} &= \hat{h}_{S_m R D_m} = \\ &= e^{2j(\varphi_{D_m} - \varphi_{S_m})} \cdot \tilde{h}_{S_m R D_m}, \end{aligned} \quad (4.45)$$

equation (4.43) is fulfilled for source m , i.e.

$$\hat{\mathbf{H}}_{\text{II}}[m, m] = c_{m,m} \cdot \tilde{\mathbf{H}}_{\text{II}}[m, m], \quad (4.46)$$

for all $m \in (1, \dots, N_{\text{SD}})$. Only if source k and source m possess a common phase reference, i.e. $\varphi_{S_k} = \varphi_{S_m}$, is equation (4.43) fulfilled for source $k \neq m$.

Traffic Pattern III: With $\hat{\gamma}_D = \gamma_D = 0$, equation (4.42) becomes

$$\hat{\gamma}_{S_k} = e^{2j(\varphi_{D_m} - \varphi_{S_k})} \cdot \gamma_{S_k}. \quad (4.47)$$

With the channel knowledge available in the network, there is no way to compute $\hat{\gamma}_{S_k}$ and γ_{S_k} such that (4.47) is fulfilled. Consequently, source k and destination m are required to possess the same LO phase, i.e. $\varphi_{S_k} = \varphi_{D_m}$. In this case, $c_{m,k} = 1$ and (4.47) can be fulfilled by choosing $\hat{\gamma}_{S_k} = \gamma_{S_k}$. A particularly simple and valid choice is $\hat{\gamma}_{S_k} = \gamma_{S_k} = 1$.

Traffic Pattern IV: With $\hat{\gamma}_S = \gamma_S = \hat{\gamma}_D = \gamma_D = 0$, equation (4.42) is always fulfilled. In this case, (4.27) holds for $c_{m,k} = 1$. Thus, the anticipated and the actual SINR at all destinations are the same.

4.2.5 Required Phase Synchronization for $\mathbf{S} \rightarrow \mathbf{D} / \mathbf{S} \rightarrow \mathbf{R} / \mathbf{R} \leftarrow \mathbf{D}$

The first-hop link and the direct link are estimated in forward direction and the second-hop link is estimated in backward direction. This means that the estimates

$$\hat{\mathbf{H}}_{\text{SD}} = \tilde{\mathbf{H}}_{\text{SD}}, \quad (4.48)$$

$$\hat{\mathbf{H}}_{\text{SR}} = \tilde{\mathbf{H}}_{\text{SR}}, \quad (4.49)$$

$$\hat{\mathbf{H}}_{\text{RD}} = \Phi_{\text{D}} \Phi_{\text{D}}^H \cdot \tilde{\mathbf{H}}_{\text{RD}} \cdot \Phi_{\text{R}}^H \Phi_{\text{R}}^H \quad (4.50)$$

are available in the network. For traffic pattern I, the compound channel matrix $\tilde{\mathbf{H}}_{\text{I}}$ is given in (4.25). At the relays, its estimate is computed from the single-hop channel estimates given in (4.48) – (4.50):

$$\begin{aligned} \hat{\mathbf{H}}_{\text{I}} &= \hat{\Gamma}_{\text{D}} \hat{\mathbf{H}}_{\text{SD}} + \hat{\mathbf{H}}_{\text{RD}} \mathbf{G} \hat{\mathbf{H}}_{\text{SR}} + \hat{\mathbf{H}}_{\text{SD}} \hat{\Gamma}_{\text{S}} = \\ &= \hat{\Gamma}_{\text{D}} \tilde{\mathbf{H}}_{\text{SD}} + \Phi_{\text{D}} \Phi_{\text{D}}^H \tilde{\mathbf{H}}_{\text{RD}} \Phi_{\text{R}}^H \Phi_{\text{R}}^H \mathbf{G} \tilde{\mathbf{H}}_{\text{SR}} + \tilde{\mathbf{H}}_{\text{SD}} \hat{\Gamma}_{\text{S}}, \end{aligned} \quad (4.51)$$

where $\hat{\Gamma}_{\text{S}}$ and $\hat{\Gamma}_{\text{D}}$ are estimates of the scaling matrices Γ_{S} and Γ_{D} that have to be generated locally. It has to be checked whether (4.27) is fulfilled for $\hat{\mathbf{H}}_{\text{I}}$ given in (4.51) and $\tilde{\mathbf{H}}_{\text{I}}$ given in (4.25). Since (4.27) has to hold for all channel realizations including the case where any of the channel coefficients is zero, two conditions are obtained:

1. For $\tilde{\mathbf{H}}_{\text{SR}} = \mathbf{0}$ or $\tilde{\mathbf{H}}_{\text{RD}} = \mathbf{0}$, equation (4.27) becomes

$$\hat{\gamma}_{\text{D}_m} + \hat{\gamma}_{\text{S}_k} = c_{m,k} \cdot (\gamma_{\text{D}_m} + \gamma_{\text{S}_k}). \quad (4.52)$$

2. For $\tilde{\mathbf{H}}_{\text{SD}} = \mathbf{0}$, equation (4.27) becomes

$$e^{2j\varphi_{\text{D}_m}} \cdot \sum_{l=1}^{N_{\text{R}}} \left(e^{-2j\varphi_{\text{R}_l}} \cdot \tilde{h}_{\text{R}_l \text{D}_m} g_l \tilde{h}_{\text{S}_k \text{R}_l} \right) = c_{m,k} \cdot \tilde{h}_{\text{S}_k \text{RD}_m}, \quad (4.53)$$

where

$$\tilde{h}_{\text{S}_k \text{RD}_m} = \sum_{l=1}^{N_{\text{R}}} \left(\tilde{h}_{\text{R}_l \text{D}_m} g_l \tilde{h}_{\text{S}_k \text{R}_l} \right). \quad (4.54)$$

Equation (4.53) can only hold for all channel realizations if the LO phases of all relays are equal, i.e.

$$\varphi_{R_l} = \phi, \quad \forall l \in \{1, \dots, N_R\}. \quad (4.55)$$

This means that they have to possess a common phase reference. The phase offset ϕ may be unknown and random but has to be the same for all relays. With (4.55), equation (4.53) implies

$$e^{2j(\varphi_{D_m} - \phi)} = c_{m,k}. \quad (4.56)$$

Inserting (4.56) into (4.52) finally yields

$$\hat{\gamma}_{D_m} + \hat{\gamma}_{S_k} = e^{2j(\varphi_{D_m} - \phi)} \cdot (\gamma_{D_m} + \gamma_{S_k}). \quad (4.57)$$

The phase synchronization requirements for all four traffic patterns can now be derived from (4.57):

Traffic Pattern I: For traffic pattern I, (4.27) is fulfilled if (4.57) holds. With the CSI available in the network, there is, however, no way to compute $\hat{\gamma}_{S_k}$, γ_{S_k} , $\hat{\gamma}_{D_m}$, and γ_{D_m} , unequal to zero, such that (4.57) is fulfilled. In this case, destination m is required to possess the same LO phase as the relays, i.e. $\varphi_{D_m} = \phi$. Equation (4.57) can then be fulfilled for all k by choosing $\hat{\gamma}_{S_k} = \gamma_{S_k}$ and $\hat{\gamma}_{D_m} = \gamma_{D_m}$. A particular simple and valid choice is $\hat{\gamma}_{S_k} = \gamma_{S_k} = \hat{\gamma}_{D_m} = \gamma_{D_m} = 1$. Since in this case $c_{m,k} = 1$, the anticipated SINR at destination m is equal to the actual one.

Traffic Pattern II: With $\hat{\gamma}_S = \gamma_S = 0$, equation (4.57) becomes

$$\hat{\gamma}_{D_m} = e^{2j(\varphi_{D_m} - \phi)} \cdot \gamma_{D_m}. \quad (4.58)$$

For traffic pattern II, destination m can estimate $\tilde{h}_{S_kRD_m}$ using a preamble during data transmission. If it chooses

$$\gamma_{D_m} = \tilde{h}_{S_kRD_m} \quad (4.59)$$

and the relays compute

$$\begin{aligned} \hat{\gamma}_{D_m} &= \hat{h}_{S_kRD_m} = \\ &= e^{2j(\varphi_{D_m} - \phi)} \cdot \tilde{h}_{S_kRD_m} \end{aligned} \quad (4.60)$$

from their channel estimates, equation (4.58) is fulfilled for all k . The anticipated SINR at destination m is then equal to the actual one because $|c_{m,k}|^2 = 1$ for all k .

Traffic Pattern III: With $\hat{\gamma}_D = \gamma_D = 0$, equation (4.57) becomes

$$\hat{\gamma}_{S_k} = e^{2j(\varphi_{D_m} - \phi)} \cdot \gamma_{S_k}. \quad (4.61)$$

From the available channel knowledge, it is not possible to compute $\hat{\gamma}_{S_k}$ and γ_{S_k} , unequal to zero, so that (4.61) is fulfilled. Consequently, destination m has to have the same LO phase as the relays, i.e., destination m and the relays require a joint global phase reference. In this case, $\varphi_{D_m} = \phi$ and (4.61) can be fulfilled by choosing $\hat{\gamma}_{S_k} = \gamma_{S_k}$. Since (4.27) then holds for $c_{m,k} = 1$, the anticipated and the actual SINR at destination m are equal.

Traffic Pattern IV: With $\hat{\gamma}_S = \gamma_S = \hat{\gamma}_D = \gamma_D = 0$, equation (4.57) is always fulfilled. In this case, (4.27) holds for $c_{m,k} = 1$. Thus, the anticipated and the actual SINR at all destinations are the same.

4.2.6 Required Phase Synchronization for $\mathbf{S} \rightarrow \mathbf{D} / \mathbf{S} \leftarrow \mathbf{R} / \mathbf{R} \rightarrow \mathbf{D}$

The direct link and the second-hop link are estimated in forward direction and the first-hop link is estimated in backward direction. This means that the estimates

$$\hat{\mathbf{H}}_{SD} = \tilde{\mathbf{H}}_{SD}, \quad (4.62)$$

$$\hat{\mathbf{H}}_{SR} = \hat{\mathbf{H}}_{RS}^T = \mathbf{\Phi}_R \mathbf{\Phi}_R \cdot \tilde{\mathbf{H}}_{SR} \cdot \mathbf{\Phi}_S^H \mathbf{\Phi}_S^H, \quad (4.63)$$

$$\hat{\mathbf{H}}_{RD} = \tilde{\mathbf{H}}_{RD} \quad (4.64)$$

are available in the network. For traffic pattern I, the compound channel matrix $\tilde{\mathbf{H}}_I$ is given in (4.25). At the relays, its estimate is computed from the single-hop channel estimates given in (4.62) – (4.64):

$$\begin{aligned} \hat{\mathbf{H}}_I &= \hat{\Gamma}_D \hat{\mathbf{H}}_{SD} + \hat{\mathbf{H}}_{RD} \mathbf{G} \hat{\mathbf{H}}_{SR} + \hat{\mathbf{H}}_{SD} \hat{\Gamma}_S = \\ &= \hat{\Gamma}_D \tilde{\mathbf{H}}_{SD} + \tilde{\mathbf{H}}_{RD} \mathbf{G} \mathbf{\Phi}_R \mathbf{\Phi}_R \tilde{\mathbf{H}}_{SR} \mathbf{\Phi}_S^H \mathbf{\Phi}_S^H + \tilde{\mathbf{H}}_{SD} \hat{\Gamma}_S, \end{aligned} \quad (4.65)$$

where $\hat{\Gamma}_S$ and $\hat{\Gamma}_D$ are estimates of the scaling matrices Γ_S and Γ_D that have to be generated locally. It has to be checked whether (4.27) is fulfilled for $\hat{\mathbf{H}}_I$ given in (4.65) and $\tilde{\mathbf{H}}_I$ given in (4.25). Since (4.27) has to hold for all channel realizations including the case where any of the channel coefficients is zero, two conditions are obtained:

1. For $\tilde{\mathbf{H}}_{\text{SR}} = \mathbf{0}$ or $\tilde{\mathbf{H}}_{\text{RD}} = \mathbf{0}$, equation (4.27) becomes

$$\hat{\gamma}_{\text{D}_m} + \hat{\gamma}_{\text{S}_k} = c_{m,k} \cdot (\gamma_{\text{D}_m} + \gamma_{\text{S}_k}). \quad (4.66)$$

2. For $\tilde{\mathbf{H}}_{\text{SD}} = \mathbf{0}$, equation (4.27) becomes

$$e^{-2j\varphi_{\text{S}_k}} \cdot \sum_{l=1}^{N_{\text{R}}} \left(e^{2j\varphi_{\text{R}_l}} \cdot \tilde{h}_{\text{R}_l\text{D}_m} g_l \tilde{h}_{\text{S}_k\text{R}_l} \right) = c_{m,k} \cdot \tilde{h}_{\text{S}_k\text{RD}_m}, \quad (4.67)$$

where

$$\tilde{h}_{\text{S}_k\text{RD}_m} = \sum_{l=1}^{N_{\text{R}}} \left(\tilde{h}_{\text{R}_l\text{D}_m} g_l \tilde{h}_{\text{S}_k\text{R}_l} \right). \quad (4.68)$$

Equation (4.67) can only hold for all channel realizations if the LO phases of all relays are equal, i.e.

$$\varphi_{\text{R}_l} = \phi, \quad \forall l \in \{1, \dots, N_{\text{R}}\}. \quad (4.69)$$

This means that they have to possess a common phase reference. The phase offset ϕ may be unknown and random but has to be the same for all relays. With (4.69), equation (4.67) implies

$$e^{2j(\phi - \varphi_{\text{S}_k})} = c_{m,k}. \quad (4.70)$$

Inserting (4.70) into (4.66) finally yields

$$\hat{\gamma}_{\text{D}_m} + \hat{\gamma}_{\text{S}_k} = e^{2j(\phi - \varphi_{\text{S}_k})} \cdot (\gamma_{\text{D}_m} + \gamma_{\text{S}_k}). \quad (4.71)$$

The phase synchronization requirements for all four traffic patterns can now be derived from (4.71):

Traffic Pattern I: For traffic pattern I, (4.27) is fulfilled if (4.71) holds. With the CSI available in the network, there is, however, no way to compute $\hat{\gamma}_{\text{S}_k}$, γ_{S_k} , $\hat{\gamma}_{\text{D}_m}$, and γ_{D_m} , unequal to zero, such that (4.71) is fulfilled. In this case, source k is required to possess the same LO phase reference as the relays, i.e. $\varphi_{\text{S}_k} = \phi$. Equation (4.71) can then be fulfilled for all m by choosing $\hat{\gamma}_{\text{S}_k} = \gamma_{\text{S}_k}$ and $\hat{\gamma}_{\text{D}_m} = \gamma_{\text{D}_m}$. Since in this case $c_{m,k} = 1$, the anticipated received power from source k at destination m is equal to the actual one. A particular simple and valid choice for the scaling factors is $\hat{\gamma}_{\text{S}_k} = \gamma_{\text{S}_k} = \hat{\gamma}_{\text{D}_m} = \gamma_{\text{D}_m} = 1$.

Traffic Pattern II: With $\hat{\gamma}_S = \gamma_S = 0$, equation (4.71) becomes

$$\hat{\gamma}_{D_m} = e^{2j(\phi - \varphi_{S_k})} \cdot \gamma_{D_m}. \quad (4.72)$$

With the channel knowledge available in the network, there is no nontrivial way to compute $\hat{\gamma}_{D_m}$ and γ_{D_m} such that (4.72) is fulfilled. Consequently, source k is required to possess the same LO phase as the relays, i.e. $\varphi_{S_k} = \phi$. In this case, $c_{m,k} = 1$ and (4.72) can be fulfilled by choosing $\hat{\gamma}_{D_m} = \gamma_{D_m}$. A particular simple and valid choice is $\hat{\gamma}_{D_m} = \gamma_{D_m} = 1$. The anticipated and the actual received power from source k at destination m is in this case equal.

Traffic Pattern III: With $\hat{\gamma}_D = \gamma_D = 0$, equation (4.71) becomes

$$\hat{\gamma}_{S_k} = e^{2j(\phi - \varphi_{S_k})} \cdot \gamma_{S_k}. \quad (4.73)$$

From the available channel knowledge, it is not possible to compute $\hat{\gamma}_{S_k}$ and γ_{S_k} , unequal to zero, so that (4.73) is fulfilled. Consequently, source k has to have the same LO phase as the relays, i.e., source k and the relays require a joint global phase reference. In this case, $\varphi_{S_k} = \phi$ and (4.73) can be fulfilled by choosing $\hat{\gamma}_{S_k} = \gamma_{S_k}$. Since (4.27) then holds with $c_{m,k} = 1$ for all m , the anticipated and the actual received power from source k at all destinations are equal.

Traffic Pattern IV: With $\hat{\gamma}_S = \gamma_S = \hat{\gamma}_D = \gamma_D = 0$, equation (4.71) is always fulfilled. In this case, (4.27) holds for $c_{m,k} = 1$. Thus, the anticipated and the actual SINR at all destinations are the same.

4.2.7 Required Phase Synchronization for $\mathbf{S} \leftarrow \mathbf{D} / \mathbf{S} \rightarrow \mathbf{R} / \mathbf{R} \rightarrow \mathbf{D}$

The direct link is measured in backward direction while both the first-hop and the second-hop link are measured in forward direction. This means that the estimates

$$\hat{\mathbf{H}}_{SD} = \mathbf{\Phi}_D \mathbf{\Phi}_D^H \cdot \tilde{\mathbf{H}}_{SD} \cdot \mathbf{\Phi}_S^H \mathbf{\Phi}_S^H, \quad (4.74)$$

$$\hat{\mathbf{H}}_{SR} = \tilde{\mathbf{H}}_{SR}, \quad (4.75)$$

$$\hat{\mathbf{H}}_{RD} = \tilde{\mathbf{H}}_{RD} \quad (4.76)$$

are available in the network. For traffic pattern I, the compound channel matrix $\tilde{\mathbf{H}}_I$ is given in (4.25). At the relays, its estimate is computed from the single-hop channel estimates given

in (4.74) – (4.76):

$$\begin{aligned}\hat{\mathbf{H}}_I &= \hat{\Gamma}_D \hat{\mathbf{H}}_{SD} + \hat{\mathbf{H}}_{RD} \mathbf{G} \hat{\mathbf{H}}_{SR} + \hat{\mathbf{H}}_{SD} \hat{\Gamma}_S = \\ &= \hat{\Gamma}_D \Phi_D \Phi_D \tilde{\mathbf{H}}_{SD} \Phi_S^H \Phi_S^H + \tilde{\mathbf{H}}_{RD} \mathbf{G} \tilde{\mathbf{H}}_{SR} + \Phi_D \Phi_D \tilde{\mathbf{H}}_{SD} \Phi_S^H \Phi_S^H \hat{\Gamma}_S,\end{aligned}\quad (4.77)$$

where $\hat{\Gamma}_S$ and $\hat{\Gamma}_D$ are estimates of the scaling matrices Γ_S and Γ_D that have to be generated locally. It has to be checked whether (4.27) is fulfilled for $\hat{\mathbf{H}}_I$ given in (4.77) and $\tilde{\mathbf{H}}_I$ given in (4.25). Since (4.27) has to hold for all channel realizations including the case where any of the channel coefficients is zero, two conditions are obtained:

1. For $\tilde{\mathbf{H}}_{SR} = \mathbf{0}$ or $\tilde{\mathbf{H}}_{RD} = \mathbf{0}$, equation (4.27) becomes

$$e^{2j(\varphi_{D_m} - \varphi_{S_k})} \cdot (\hat{\gamma}_{D_m} + \hat{\gamma}_{S_k}) = c_{m,k} \cdot (\gamma_{D_m} + \gamma_{S_k}). \quad (4.78)$$

2. For $\tilde{\mathbf{H}}_{SD} = \mathbf{0}$, equation (4.27) becomes

$$\tilde{h}_{S_k R D_m} = c_{m,k} \cdot \tilde{h}_{S_k R D_m}, \quad (4.79)$$

where

$$\tilde{h}_{S_k R D_m} = \sum_{l=1}^{N_R} \left(\tilde{h}_{R_l D_m} g_l \tilde{h}_{S_k R_l} \right). \quad (4.80)$$

It follows from (4.79) that (4.27) can only be fulfilled for $c_{m,k} = 1$ in this section.

Inserting $c_{m,k} = 1$ in (4.78) yields

$$e^{2j(\varphi_{D_m} - \varphi_{S_k})} \cdot (\hat{\gamma}_{D_m} + \hat{\gamma}_{S_k}) = \gamma_{D_m} + \gamma_{S_k}. \quad (4.81)$$

The phase synchronization requirements for all four traffic patterns can now be derived from (4.81):

Traffic Pattern I: For traffic pattern I, (4.27) is fulfilled if (4.81) holds. With the CSI available in the network, there is, however, no way to compute $\hat{\gamma}_{S_k}$, γ_{S_k} , $\hat{\gamma}_{D_m}$, and γ_{D_m} , unequal to zero, such that (4.81) is fulfilled. Consequently, source k and destination m are required to possess the same LO phase, i.e., $\varphi_{S_k} = \varphi_{D_m}$. Equation (4.81) can then be fulfilled by choosing $\hat{\gamma}_{S_k} = \gamma_{S_k}$ and $\hat{\gamma}_{D_m} = \gamma_{D_m}$. A particularly simple and valid choice is $\hat{\gamma}_{S_k} = \gamma_{S_k} = \hat{\gamma}_{D_m} = \gamma_{D_m} = 1$. The anticipated received power from source k at destination m is then equal to the actual one.

Traffic Pattern II: With $\hat{\gamma}_S = \gamma_S = 0$, equation (4.81) becomes

$$e^{2j(\varphi_{D_m} - \varphi_{S_k})} \cdot \hat{\gamma}_{D_m} = \gamma_{D_m}. \quad (4.82)$$

If destination m chooses

$$\gamma_{D_m} = \tilde{h}_{S_m D_m} \quad (4.83)$$

and the relays compute

$$\begin{aligned} \hat{\gamma}_{D_m} &= \hat{h}_{S_m D_m} = \\ &= e^{2j(\varphi_{D_m} - \varphi_{S_m})} \cdot \tilde{h}_{S_m D_m}, \end{aligned} \quad (4.84)$$

from their channel estimates, equation (4.82) is fulfilled for source m , i.e.,

$$\hat{\mathbf{H}}_{\text{II}}[m, m] = c_{m,m} \cdot \tilde{\mathbf{H}}_{\text{II}}[m, m] \quad (4.85)$$

for all m . Only if source k and source m possess a common global phase reference, i.e. $\varphi_{S_k} = \varphi_{S_m}$, is equation (4.82) fulfilled for source $k \neq m$.

Traffic Pattern III: With $\hat{\gamma}_D = \gamma_D = 0$, equation (4.81) becomes

$$e^{2j(\varphi_{D_m} - \varphi_{S_k})} \hat{\gamma}_{S_k} = \gamma_{S_k}. \quad (4.86)$$

With the channel knowledge available in the network, there is no way to compute $\hat{\gamma}_{S_k}$ and γ_{S_k} , unequal to zero, such that (4.86) is fulfilled. Consequently, source k and destination m are required to possess the same LO phase, i.e. $\varphi_{S_k} = \varphi_{D_m}$. Equation (4.86) can then be fulfilled by choosing $\hat{\gamma}_{S_k} = \gamma_{S_k}$. A particularly simple and valid choice is $\hat{\gamma}_{S_k} = \gamma_{S_k} = 1$.

Traffic Pattern IV: With $\hat{\gamma}_S = \gamma_S = \hat{\gamma}_D = \gamma_D = 0$, equation (4.81) is always fulfilled. Since $c_{m,k} = 1$, the anticipated and the actual SINR at all destinations are the same.

4.2.8 Required Phase Synchronization for $\mathbf{S} \leftarrow \mathbf{D} / \mathbf{S} \leftarrow \mathbf{R} / \mathbf{R} \leftarrow \mathbf{D}$

All channel matrices are estimated in backward direction. This means that the estimates

$$\hat{\mathbf{H}}_{\text{SD}} = \Phi_{\text{D}} \Phi_{\text{D}} \cdot \tilde{\mathbf{H}}_{\text{SD}} \cdot \Phi_{\text{S}}^{\text{H}} \Phi_{\text{S}}^{\text{H}}, \quad (4.87)$$

$$\hat{\mathbf{H}}_{\text{SR}} = \Phi_{\text{R}} \Phi_{\text{R}} \cdot \tilde{\mathbf{H}}_{\text{SR}} \cdot \Phi_{\text{S}}^{\text{H}} \Phi_{\text{S}}^{\text{H}}, \quad (4.88)$$

$$\text{and } \hat{\mathbf{H}}_{\text{RD}} = \Phi_{\text{D}} \Phi_{\text{D}} \cdot \tilde{\mathbf{H}}_{\text{RD}} \cdot \Phi_{\text{R}}^{\text{H}} \Phi_{\text{R}}^{\text{H}} \quad (4.89)$$

are available in the network. For traffic pattern I, the compound channel matrix $\tilde{\mathbf{H}}_{\text{I}}$ is given in (4.25). At the relays, its estimate is computed from the single-hop channel estimates given in (4.87) – (4.89):

$$\begin{aligned} \hat{\mathbf{H}}_{\text{I}} &= \hat{\Gamma}_{\text{D}} \hat{\mathbf{H}}_{\text{SD}} + \hat{\mathbf{H}}_{\text{RD}} \mathbf{G} \hat{\mathbf{H}}_{\text{SR}} + \hat{\mathbf{H}}_{\text{SD}} \hat{\Gamma}_{\text{S}} = \\ &= \Phi_{\text{D}} \Phi_{\text{D}} \left(\hat{\Gamma}_{\text{D}} \tilde{\mathbf{H}}_{\text{SD}} + \tilde{\mathbf{H}}_{\text{RD}} \mathbf{G} \tilde{\mathbf{H}}_{\text{SR}} + \tilde{\mathbf{H}}_{\text{SD}} \hat{\Gamma}_{\text{S}} \right) \Phi_{\text{S}}^{\text{H}} \Phi_{\text{S}}^{\text{H}}, \end{aligned} \quad (4.90)$$

where $\hat{\Gamma}_{\text{S}}$ and $\hat{\Gamma}_{\text{D}}$ are estimates of the scaling matrices Γ_{S} and Γ_{D} that have to be generated locally. It has to be checked whether (4.27) is fulfilled for $\hat{\mathbf{H}}_{\text{I}}$ given in (4.90) and $\tilde{\mathbf{H}}_{\text{I}}$ given in (4.25). For $\hat{\Gamma}_{\text{S}} = \tilde{\Gamma}_{\text{S}}$ and $\hat{\Gamma}_{\text{D}} = \tilde{\Gamma}_{\text{D}}$, the anticipated compound channel coefficient between source k and destination m is

$$\hat{\mathbf{H}}_{\text{I}}[m, k] = e^{2j(\varphi_{\text{D}m} - \varphi_{\text{S}k})} \cdot \tilde{\mathbf{H}}_{\text{I}}[m, k]. \quad (4.91)$$

Consequently, (4.27) is fulfilled for all traffic patterns with $c_{m,k} = e^{2j(\varphi_{\text{D}m} - \varphi_{\text{S}k})}$. Since $|c_{m,k}| = 1$, the anticipated SINR at all destinations is equal to the actual one.

4.2.9 Required Phase Synchronization for $\mathbf{S} \leftarrow \mathbf{D} / \mathbf{S} \rightarrow \mathbf{R} / \mathbf{R} \leftarrow \mathbf{D}$

The direct link and the second-hop link are estimated in backward direction and the first-hop link is estimated in forward direction. This means that the estimates

$$\hat{\mathbf{H}}_{\text{SD}} = \hat{\mathbf{H}}_{\text{DS}}^{\text{T}} = \Phi_{\text{D}} \Phi_{\text{D}} \cdot \tilde{\mathbf{H}}_{\text{SD}} \cdot \Phi_{\text{S}}^{\text{H}} \Phi_{\text{S}}^{\text{H}}, \quad (4.92)$$

$$\hat{\mathbf{H}}_{\text{SR}} = \tilde{\mathbf{H}}_{\text{SR}}, \quad (4.93)$$

$$\hat{\mathbf{H}}_{\text{RD}} = \hat{\mathbf{H}}_{\text{DR}}^{\text{T}} = \Phi_{\text{D}} \Phi_{\text{D}} \cdot \tilde{\mathbf{H}}_{\text{RD}} \cdot \Phi_{\text{R}}^{\text{H}} \Phi_{\text{R}}^{\text{H}} \quad (4.94)$$

are available in the network. For traffic pattern I, the compound channel matrix $\tilde{\mathbf{H}}_{\text{I}}$ is given in (4.25). At the relays, its estimate is computed from the single-hop channel estimates given

in (4.92) – (4.94):

$$\begin{aligned}\hat{\mathbf{H}}_I &= \hat{\Gamma}_D \hat{\mathbf{H}}_{SD} + \hat{\mathbf{H}}_{RD} \mathbf{G} \hat{\mathbf{H}}_{SR} + \hat{\mathbf{H}}_{SD} \hat{\Gamma}_S = \\ &= \hat{\Gamma}_D \Phi_D \Phi_D \tilde{\mathbf{H}}_{SD} \Phi_S^H \Phi_S^H + \Phi_D \Phi_D \tilde{\mathbf{H}}_{RD} \Phi_R^H \Phi_R^H \mathbf{G} \tilde{\mathbf{H}}_{SR} + \Phi_D \Phi_D \tilde{\mathbf{H}}_{SD} \Phi_S^H \Phi_S^H \hat{\Gamma}_S,\end{aligned}\quad (4.95)$$

where $\hat{\Gamma}_S$ and $\hat{\Gamma}_D$ are estimates of the scaling matrices Γ_S and Γ_D that have to be generated locally. It has to be checked whether (4.27) is fulfilled for $\hat{\mathbf{H}}_I$ given in (4.95) and $\tilde{\mathbf{H}}_I$ given in (4.25). Since (4.27) has to hold for all channel realizations including the case where any of the channel coefficients is zero, two conditions are obtained:

1. For $\tilde{\mathbf{H}}_{SR} = \mathbf{0}$ or $\tilde{\mathbf{H}}_{RD} = \mathbf{0}$, equation (4.27) becomes

$$e^{2j(\varphi_{D_m} - \varphi_{S_k})} (\hat{\gamma}_{D_m} + \hat{\gamma}_{S_k}) = c_{m,k} \cdot (\gamma_{D_m} + \gamma_{S_k}). \quad (4.96)$$

2. For $\tilde{\mathbf{H}}_{SD} = \mathbf{0}$, equation (4.27) becomes

$$e^{2j\varphi_{D_m}} \cdot \sum_{l=1}^{N_R} \left(e^{-2j\varphi_{R_l}} \cdot \tilde{h}_{R_l D_m} g_l \tilde{h}_{S_k R_l} \right) = c_{m,k} \cdot \tilde{h}_{S_k R D_m}, \quad (4.97)$$

where

$$\tilde{h}_{S_k R D_m} = \sum_{l=1}^{N_R} \left(\tilde{h}_{R_l D_m} g_l \tilde{h}_{S_k R_l} \right). \quad (4.98)$$

Equation (4.97) can only hold for all channel realizations if the LO phases of all relays are equal, i.e.

$$\varphi_{R_l} = \phi, \quad \forall l \in \{1, \dots, N_R\}. \quad (4.99)$$

This means that they have to possess a common phase reference. The phase offset ϕ may be unknown and random but has to be the same for all relays. With (4.99), equation (4.97) implies

$$e^{2j(\varphi_{D_m} - \phi)} = c_{m,k}. \quad (4.100)$$

It follows from (4.100) that (4.27) can only be fulfilled for $|c_{m,k}| = 1$ in this section. Inserting (4.100) into (4.96) finally yields

$$e^{2j(\varphi_{D_m} - \varphi_{S_k})} (\hat{\gamma}_{D_m} + \hat{\gamma}_{S_k}) = e^{2j(\varphi_{D_m} - \phi)} (\gamma_{D_m} + \gamma_{S_k}). \quad (4.101)$$

The phase synchronization requirements for all four traffic patterns can now be derived from (4.101):

Traffic Pattern I: For traffic pattern I, (4.27) is fulfilled if (4.101) holds. With the CSI available in the network, there is, however, no way to compute $\hat{\gamma}_{S_k}$, γ_{S_k} , $\hat{\gamma}_{D_m}$, and γ_{D_m} , unequal to zero, such that (4.101) is fulfilled. In this case, source k is required to possess the same LO phase reference as the relays, i.e. $\varphi_{S_k} = \phi$. Equation (4.101) can then be fulfilled by choosing $\hat{\gamma}_{S_k} = \gamma_{S_k}$ and $\hat{\gamma}_{D_m} = \gamma_{D_m}$. Since in this case $c_{m,k} = 1$, the anticipated received power from source k at destination m is equal to the actual one. A particular simple and valid choice for the scaling factors is $\hat{\gamma}_{S_k} = \gamma_{S_k} = \hat{\gamma}_{D_m} = \gamma_{D_m} = 1$.

Traffic Pattern II: With $\hat{\gamma}_S = \gamma_S = 0$, equation (4.101) becomes

$$e^{2j(\varphi_{D_m} - \varphi_{S_k})} \hat{\gamma}_{D_m} = e^{2j(\varphi_{D_m} - \phi)} \gamma_{D_m}. \quad (4.102)$$

With the channel knowledge available in the network, there is no way to compute $\hat{\gamma}_{D_m}$ and γ_{D_m} , unequal to zero, such that (4.102) is fulfilled. Consequently, source k is required to possess the same LO phase as the relays, i.e. $\varphi_{S_k} = \phi$. Equation (4.102) can be fulfilled by choosing $\hat{\gamma}_{D_m} = \gamma_{D_m}$. A particular simple and valid choice is $\hat{\gamma}_{D_m} = \gamma_{D_m} = 1$. The anticipated and the actual received power from source k at destination m are in this case equal.

Traffic Pattern III: With $\hat{\gamma}_D = \gamma_D = 0$, equation (4.101) becomes

$$e^{2j(\varphi_{D_m} - \varphi_{S_k})} \hat{\gamma}_{S_k} = e^{2j(\varphi_{D_m} - \phi)} \gamma_{S_k}. \quad (4.103)$$

From the available channel knowledge, it is not possible to compute $\hat{\gamma}_{S_k}$ and γ_{S_k} , unequal to zero, so that (4.103) is fulfilled. Consequently, source k has to have the same LO phase as the relays, i.e., source k and the relays require a joint phase reference. In this case, $\varphi_{S_k} = \phi$ and (4.103) can be fulfilled by choosing $\hat{\gamma}_{S_k} = \gamma_{S_k}$.

Traffic Pattern IV: With $\hat{\gamma}_S = \gamma_S = \hat{\gamma}_D = \gamma_D = 0$, equation (4.101) is always fulfilled. In this case, (4.27) holds for $|c_{m,k}| = 1$. Thus, the anticipated and the actual SINR at all destinations are the same.

4.2.10 Required Phase Synchronization for $\mathbf{S} \leftarrow \mathbf{D} / \mathbf{S} \leftarrow \mathbf{R} / \mathbf{R} \rightarrow \mathbf{D}$

The direct link and the first-hop link are estimated in backward direction while the second-hop link is estimated in forward direction. This means that the estimates

$$\hat{\mathbf{H}}_{\text{SD}} = \hat{\mathbf{H}}_{\text{DS}}^{\text{T}} = \Phi_{\text{D}} \Phi_{\text{D}} \cdot \tilde{\mathbf{H}}_{\text{SD}} \cdot \Phi_{\text{S}}^{\text{H}} \Phi_{\text{S}}^{\text{H}}, \quad (4.104)$$

$$\hat{\mathbf{H}}_{\text{SR}} = \hat{\mathbf{H}}_{\text{RS}}^{\text{T}} = \Phi_{\text{R}} \Phi_{\text{R}} \cdot \tilde{\mathbf{H}}_{\text{SR}} \cdot \Phi_{\text{S}}^{\text{H}} \Phi_{\text{S}}^{\text{H}}, \quad (4.105)$$

$$\hat{\mathbf{H}}_{\text{RD}} = \tilde{\mathbf{H}}_{\text{RD}} \quad (4.106)$$

are available in the network. For traffic pattern I, the compound channel matrix $\tilde{\mathbf{H}}_{\text{I}}$ is given in (4.25). At the relays, its estimate is computed from the single-hop channel estimates given in (4.104) – (4.106):

$$\begin{aligned} \hat{\mathbf{H}}_{\text{I}} &= \hat{\Gamma}_{\text{D}} \hat{\mathbf{H}}_{\text{SD}} + \hat{\mathbf{H}}_{\text{RD}} \mathbf{G} \hat{\mathbf{H}}_{\text{SR}} + \hat{\mathbf{H}}_{\text{SD}} \hat{\Gamma}_{\text{S}} = \\ &= \hat{\Gamma}_{\text{D}} \Phi_{\text{D}} \Phi_{\text{D}} \tilde{\mathbf{H}}_{\text{SD}} \Phi_{\text{S}}^{\text{H}} \Phi_{\text{S}}^{\text{H}} + \tilde{\mathbf{H}}_{\text{RD}} \mathbf{G} \Phi_{\text{R}} \Phi_{\text{R}} \tilde{\mathbf{H}}_{\text{SR}} \Phi_{\text{S}}^{\text{H}} \Phi_{\text{S}}^{\text{H}} + \Phi_{\text{D}} \Phi_{\text{D}} \tilde{\mathbf{H}}_{\text{SD}} \Phi_{\text{S}}^{\text{H}} \Phi_{\text{S}}^{\text{H}} \hat{\Gamma}_{\text{S}}, \end{aligned} \quad (4.107)$$

where $\hat{\Gamma}_{\text{S}}$ and $\hat{\Gamma}_{\text{D}}$ are estimates of the scaling matrices Γ_{S} and Γ_{D} that have to be generated locally. It has to be checked whether (4.27) is fulfilled for $\hat{\mathbf{H}}_{\text{I}}$ given in (4.107) and $\tilde{\mathbf{H}}_{\text{I}}$ given in (4.25). Since (4.27) has to hold for all channel realizations including the case where any of the channel coefficients is zero, two conditions are obtained:

1. For $\tilde{\mathbf{H}}_{\text{SR}} = \mathbf{0}$ or $\tilde{\mathbf{H}}_{\text{RD}} = \mathbf{0}$, equation (4.27) becomes

$$e^{2j(\varphi_{\text{D}_m} - \varphi_{\text{S}_k})} (\hat{\gamma}_{\text{D}_m} + \hat{\gamma}_{\text{S}_k}) = c_{m,k} (\gamma_{\text{D}_m} + \gamma_{\text{S}_k}). \quad (4.108)$$

2. For $\tilde{\mathbf{H}}_{\text{SD}} = \mathbf{0}$, equation (4.27) becomes

$$e^{-2j\varphi_{\text{S}_k}} \cdot \sum_{l=1}^{N_{\text{R}}} \left(e^{2j\varphi_{\text{R}_l}} \cdot \tilde{h}_{\text{R}_l \text{D}_m} g_l \tilde{h}_{\text{S}_k \text{R}_l} \right) = c_{m,k} \cdot \tilde{h}_{\text{S}_k \text{RD}_m}, \quad (4.109)$$

where

$$\tilde{h}_{\text{S}_k \text{RD}_m} = \sum_{l=1}^{N_{\text{R}}} \left(\tilde{h}_{\text{R}_l \text{D}_m} g_l \tilde{h}_{\text{S}_k \text{R}_l} \right). \quad (4.110)$$

Equation (4.109) can only hold for all channel realizations if the LO phases of all relays are equal, i.e.

$$\varphi_{R_l} = \phi, \quad \forall l \in \{1, \dots, N_R\}. \quad (4.111)$$

This means that they have to possess a common phase reference. The phase offset ϕ may be unknown and random but has to be the same for all relays. With (4.111), equation (4.109) implies

$$e^{2j(\phi - \varphi_{S_k})} = c_{m,k}. \quad (4.112)$$

It follows from (4.112) that (4.27) can only be fulfilled for $|c_{m,k}| = 1$ in this section. Inserting (4.112) into (4.108) finally yields

$$e^{2j(\varphi_{D_m} - \varphi_{S_k})} (\hat{\gamma}_{D_m} + \hat{\gamma}_{S_k}) = e^{2j(\phi - \varphi_{S_k})} (\gamma_{D_m} + \gamma_{S_k}). \quad (4.113)$$

The phase synchronization requirements for all four traffic patterns can now be derived from (4.113):

Traffic Pattern I: For traffic pattern I, (4.27) is fulfilled if (4.113) holds. With the CSI available in the network, there is, however, no way to compute $\hat{\gamma}_{S_k}$, γ_{S_k} , $\hat{\gamma}_{D_m}$, and γ_{D_m} , unequal to zero, such that (4.113) is fulfilled. In this case, destination m is required to possess the same LO phase as the relays, i.e. $\varphi_{D_m} = \phi$. Equation (4.113) can then be fulfilled for all k by choosing $\hat{\gamma}_{S_k} = \gamma_{S_k}$ and $\hat{\gamma}_{D_m} = \gamma_{D_m}$. A particular simple and valid choice is $\hat{\gamma}_{S_k} = \gamma_{S_k} = \hat{\gamma}_{D_m} = \gamma_{D_m} = 1$.

Traffic Pattern II: With $\hat{\gamma}_S = \gamma_S = 0$, equation (4.113) becomes

$$e^{2j(\varphi_{D_m} - \varphi_{S_k})} \hat{\gamma}_{D_m} = e^{2j(\phi - \varphi_{S_k})} \gamma_{D_m}. \quad (4.114)$$

With the channel knowledge available in the network, there is no way to compute $\hat{\gamma}_{D_m}$ and γ_{D_m} , unequal to zero, such that (4.114) is fulfilled. Consequently, the destination m is required to possess the same LO phase as the relays, i.e. $\varphi_{D_m} = \phi$. Equation (4.114) can then be fulfilled by choosing $\hat{\gamma}_{D_m} = \gamma_{D_m}$. A particular simple and valid choice is $\hat{\gamma}_{D_m} = \gamma_{D_m} = 1$.

Traffic Pattern III: With $\hat{\gamma}_D = \gamma_D = 0$, equation (4.113) becomes

$$e^{2j(\varphi_{D_m} - \varphi_{S_k})} \hat{\gamma}_{S_k} = e^{2j(\phi - \varphi_{S_k})} \gamma_{S_k}. \quad (4.115)$$

$\hat{\mathbf{H}}_{SD} / \hat{\mathbf{H}}_{SR} / \hat{\mathbf{H}}_{RD}$	Tr. Pattern I	Tr. Pattern II	Tr. Pattern III	Tr. Pattern IV
S → D / S → R / R → D	-	-	-	-
S → D / S ← R / R ← D	S _k & D _m	S _k & S _m	S _k & D _m	-
S → D / S → R / R ← D	R & D _m	R	R & D _m	R
S → D / S ← R / R → D	R & S _k	R & S _k	R & S _k	R
S ← D / S → R / R → D	S _k & D _m	S _k & S _m	S _k & D _m	-
S ← D / S ← R / R ← D	-	-	-	-
S ← D / S → R / R ← D	R & S _k	R & S _k	R & S _k	R
S ← D / S ← R / R → D	R & D _m	R & D _m	R & D _m	R

Table 4.1: Summary of phase synchronization requirements; S: sources, R: relays, D: destinations; A → B indicates that the respective channel matrix is estimated from nodes A to B.

From the available channel knowledge, it is not possible to compute $\hat{\gamma}_{S_k}$ and γ_{S_k} , unequal to zero, so that (4.115) is fulfilled. Consequently, destination m has to have the same LO phase as the relays, i.e., destination m and the relays require a common phase reference. In this case, $\varphi_{D_m} = \phi$ and (4.115) can be fulfilled by choosing $\hat{\gamma}_{S_k} = \gamma_{S_k}$.

Traffic Pattern IV: With $\hat{\gamma}_S = \gamma_S = \hat{\gamma}_D = \gamma_D = 0$, equation (4.113) is always fulfilled. In this case, (4.27) holds for $c_{m,k} = 1$. Thus, the anticipated and the actual SINR at all destinations are the same.

4.2.11 Summary of Results

Table 4.1 summarizes the phase synchronization requirements for each traffic pattern and all combinations of directions in which the first-hop, second-hop, and direct link channel matrices can be measured. Equation (4.27) is only fulfilled if the respective phase synchronization is available in the network. The meaning of the entries is as follows:

- ‘-’: No global phase reference is required.
- ‘R’: A common phase reference is required at all relays.
- ‘R & S_k’: All relays and source k require a common phase reference.
- ‘R & D_m’: All relays and destination m require a common phase reference.
- ‘S_k & D_m’: Source k and destination m require a common phase reference.
- ‘S_k & S_m’: Equation (4.27) holds for $k = m$ without global phase reference. However, a common phase reference between source k and m is required for $k \neq m$.

Given that the required global phase reference is available in the network, equation (4.27) can in all cases be fulfilled with $|c_{m,k}|^2 = 1$. This means that the anticipated received power from source k at destination m is equal to the actual one.

Final Remark: The investigations in this section cover the case that all coefficients in a channel matrix are measured in the same direction. Note, however, that the presented framework is also applicable for the case that individual channel coefficients within a channel matrix are measured in different directions.

4.3 Channel Update Rate

In Section 4.2 it was found that the relay phases do not have an impact on the computation of the gain matrix (given the phase reference is provided if necessary). This means that the gain factors do not have to be adapted if the LO phases of any of the nodes in the network change. Hence, the coherence time of the propagation channel and not LO phase noise determines the time until the channel estimates become outdated. This is good news because in a slow fading environment, the propagation channel coefficients are much more stable than the LO phases (that are subject to phase noise). Thus, the channel estimates have to be updated only if the propagation environment changes. Note that like in an ordinary point-to-point communication system, the destinations have to regularly estimate their respective source-destination channels to be able to decode the data.

In order to give a rough estimate of the required channel update rate, it is assumed that the propagation channel is constant up to a distance of $\alpha\lambda$ from the antenna, where λ is the carrier wavelength. Typically, α is between $\frac{1}{2}$ and $\frac{1}{10}$. For a signal with carrier frequency $f_c = 5$ GHz and wavelength $\lambda_c = 0.06$ m the coherence distance $\alpha\lambda_c$ is then 0.03 m for $\alpha = 0.5$ and 0.006 m for $\alpha = 0.1$. At pedestrian speed, i.e. at about $v = 1 \frac{\text{m}}{\text{s}}$, the coherence time T_α would then be between $T_{0.1} = \frac{\lambda_c}{10v} = 6$ ms and $T_{0.5} = \frac{\lambda_c}{2v} = 30$ ms.

4.4 Channel Estimation Protocols

In Section 4.1 it was shown that the direction in which the channel coefficients are measured has an impact on their estimates. Based on this observation it was found in Section 4.2 that a global phase reference may be required at a certain set of nodes in order to allow for coherent distributed beamforming. In this section, different channel estimation protocols that measure all single-hop channel coefficients in a distributed two-hop network are investigated. They

are compared based on the accuracy of the gain factors that are computed from the resulting channel estimates.

Note that coherent distributed beamforming requires channel knowledge at the relays to compute the gain factors and at the destinations to combine different signal observations and to decode the received data. Obtaining CSI at the destinations in a cooperative network has been treated e.g. in [184, 185]. Both papers focus on measuring the compound source-destination channels. In contrast to that, the protocols that are discussed here obtain global CSI, i.e., they measure all single-hop channels in the network. This is important for coherent gain allocation schemes where the relays cannot compute their gain factors from the compound channels (e.g. MUZF or MMSE relaying, c.f. Chapter 6). The accuracy of the channel estimates determines the precision with which the gain factors can be computed. This in turn affects how the signals add up at the destination antennas and thus is crucial for the overall system performance.

The authors of [186] consider this problem for a simple special case. They investigate the accuracy of a channel estimation protocol (that corresponds to protocol B1 in this work) for a distributed network with a single source-destination pair and multiple AF relays. The gain factors are to be computed such that all signals combine coherently at the destination antenna (distributed equal gain combining). There is no phase noise and a perfect carrier phase synchronization between all relays and the destination is implicitly assumed. In comparison to [186], this work generalizes the number of source-destination pairs, takes phase noise into account, and drops the assumption of perfect phase synchronization. In those cases where the relays require a global phase reference, the additional error that is introduced by imperfect phase synchronization is also taken into account here.

There are altogether four different combinations of directions in which the first-hop and second-hop channel matrices can be measured. Four protocols to measure these channel matrices that correspond to the four combinations are in the following identified. They will be compared based on

1. the effort required to estimate all channel coefficients,
2. the need for global phase reference at the relays, and
3. the quality of the channel estimates in the presence of additive noise and relay phase noise.

Since the direct link is independent of the LO phases of the relays, the quality of its estimate is the same for all four protocols. Furthermore, the number of channel uses required to estimate all direct-link channel coefficients does not depend on the direction in which they

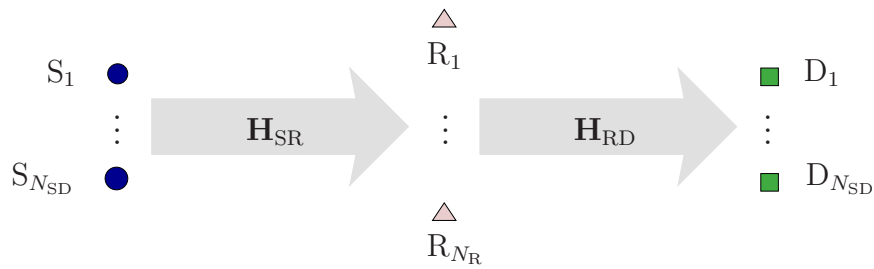


Fig. 4.2: Two-hop system configuration without direct link.

are measured. For these reasons, only traffic pattern IV (where the direct link is not used) is considered. The corresponding system configuration is shown in Fig. 4.2. Without going further into detail, it is assumed that all nodes in the network are synchronized on a time slot basis.

In Section 4.2.2 it was shown that the phase error introduced to the signal when it is received by the relays is compensated when it is retransmitted again. Consequently, the compound channel between any source k and destination m is independent of the LO phases of the relays. However, this only holds if the relay phases stay constant during that time. The same reasoning applies to the channel estimates:

- If both the first-hop and the second-hop channel matrices are measured in the same direction, the impact of the relay phases on the estimated first-hop channel matrix compensates the impact on the estimated second-hop channel matrix. Consequently, the estimated compound channel matrix is independent of the LO phases of the relays. In the presence of relay phase noise, this is no longer the case. If the relay phases change during the channel measurement procedure, their impact on the estimated compound channel matrix does not completely compensate.
- For the case that the first-hop and second-hop channel matrices are measured in different directions, the impact of the LO phases of the relays on the compound channel matrix can be compensated by a phase correction term that is the result of the phase synchronization scheme (cf. Chapter 5). In the presence of relay phase noise, the LO phases of the relays change during the time between channel estimation and the phase synchronization. The phase correction term can thus not completely compensate the impact of the LO phases of the relays on the estimated compound channel matrix.

The estimated compound channel matrix depends to some degree on the relay phases if their impact on the measured single-hop channels does not completely compensate. Since the relay gains are computed from instantaneous CSI for any coherent forwarding scheme, they will in this case also depend on the LO phases of the relays. The gain matrix thus becomes

outdated as soon as the relay phases change. This leads to a performance degradation of the whole network that depends on the phase noise severity. The impact of the relay phases that remains in the estimated compound channel matrix is consequently one indicator for the quality of the channel estimates delivered by the protocols. For the Wiener phase noise model, the phase noise severity is a linear function of time. Hence, the quality of the channel estimates delivered by the four protocols is influenced by their number of required channel uses.

Section 4.4.1 motivates the usage of the MSE of the estimated compound channels to judge the quality of the channel estimates. The four previously mentioned protocols are then derived in Section 4.4.2. As predicted in Section 4.2, it turns out that two of them require the relays to have a global phase reference in order to allow for efficient coherent forwarding. Section 4.4.3 discusses the impact of additive noise and relay phase noise on the quality of the channel estimates delivered by the protocols. The estimated first-hop and second-hop channel coefficients for two of the protocols are then derived in Sections 4.4.3.2 and 4.4.3.3. Since the squared estimation error of the compound two-hop channels cannot be averaged over the noise without knowing the explicit dependence of the gain factors on the channel estimates, two approximations are introduced. The first one fixes the channel estimates and thus the (unknown) gain factors and averages the squared channel estimation error over all channel realizations that might have led to the estimates (Section 4.4.3.4). The resulting MSEs are in this case a function of the gain factors. Their gradients can be used to design a gain allocation scheme that is robust to channel estimation errors. The second approximation only takes the second-hop channels into account because the quality of the first-hop estimates turns out to be the same for all protocols (Section 4.4.3.5). The results are thus independent of the gain factors. In order to provide a reference for the performance comparison, the application example introduced in Section 4.4.3.6. It is the same system configuration as considered in [186]: The network comprises a single source-destination pair and the relays perform distributed MRC. Since the gain factors are known explicitly, the MSEs of the compound channel estimates can in this case be computed in closed-form by averaging the squared estimation error over all channel and noise realizations. Finally, the quality of the channel estimates produced by the protocols and the accuracy with which the two approximations judge their performance are compared in Section 4.4.4. The results reveal which protocol performs best for which set of parameters (number of nodes in the network, estimation SNR, and phase noise severity) in the application example. This allows to decide which channel estimation protocol delivers the most accurate channel estimates.

Since noise is assumed to be complex Gaussian (and therefore possesses a circularly sym-

metric pdf), the SINR at destination m is independent of its current LO phase φ_{D_m} . If the sources transmit mutually independent symbols, it is furthermore independent of the LO phases of the sources (denoted by φ_{S_k} for $k \in \{1, \dots, N_{SD}\}$). For the sake of a simpler notation, the LO phases of all sources and destinations are set to zero, i.e. $\varphi_{S_k} = \varphi_{D_m} = 0$, for the rest of this chapter because they do not have an impact on the system performance. This means that

$$\tilde{h}_{S_k R_l} = h_{S_k R_l} e^{-j\varphi_{R_l}} \quad (4.116)$$

$$\tilde{h}_{R_l D_m} = h_{R_l D_m} e^{j\varphi_{R_l}}. \quad (4.117)$$

The compound channel coefficient between any source k and destinations m is then

$$\tilde{h}_{S_k R D_m} = \sum_{l=1}^{N_R} \left(\tilde{h}_{R_l D_m} g_l \tilde{h}_{S_k R_l} \right) = \sum_{l=1}^{N_R} \left(h_{R_l D_m} g_l h_{S_k R_l} \right) = h_{S_k R D_m}. \quad (4.118)$$

4.4.1 Performance Measure

Coherent gain allocation schemes compute the gain factors in a way that the signals from all relays combine coherently at the destinations. Consider for example MUZF relaying [25]. There, the objective is to compute the gain factors such that all inter-user interference is cancelled, i.e., $h_{S_k R D_m} = 0$ for all $m \neq k$. In any practical network, only estimates $\hat{h}_{S_k R_l}$ and $\hat{h}_{R_l D_m}$ of the actual equivalent channels $\tilde{h}_{S_k R_l}$ and $\tilde{h}_{R_l D_m}$ are available. Consequently, the relay gains are computed for the *anticipated* compound channels $\hat{h}_{S_k R D_m}$ rather than for $h_{S_k R D_m}$. This makes $\hat{h}_{S_k R D_m}$ the *desired* case in contrast to the *actual* compound channels $h_{S_k R D_m}$. In the presence of channel estimation errors it can be written as

$$h_{S_k R D_m} = \hat{h}_{S_k R D_m} + \delta_{S_k R D_m}, \quad (4.119)$$

where the estimation error $\delta_{S_k R D_m}$ directly translates into an SINR loss at destination m . A sensible performance measure for the channel estimation protocols is consequently how well the anticipated compound channels match the actual ones. This is well-reflected by the MSE

$$\text{MSE}_{m,k} = \text{E} \left[\left| \delta_{S_k R D_m} \right|^2 \right], \quad (4.120)$$

which will be used as a figure of merit.

4.4.2 Compound Channel Estimates and Required Number of Channel Uses

In this section, the anticipated compound channel coefficients are derived for four different channel estimation protocols. They differ in the direction in which the single-hop channels $\tilde{h}_{S_k R_l}$ and $\tilde{h}_{R_l D_m}$ are measured and can be compared based on two observations:

1. **Number of required channel uses:** The effort required to estimate all first-hop and second-hop channel coefficients depends on the direction in which they are measured. In the following, it is assumed that it takes one channel use to estimate one channel coefficient.
2. **Need for global phase reference:** As predicted in Section 4.2, it will turn out for two of the protocols that the gain factors can only be computed correctly if the relays possess a common phase reference.

The channel coefficients in the two-hop network shown in Fig. 4.2 can be estimated either in *forward direction*, i.e. from sources/relays to relays/destinations, or in *backward direction*, i.e. from relays/destinations to sources/relays. In order to highlight the impact of the LO phases of the relays, estimation noise is neglected throughout this section. If the first-hop and second-hop channels are measured in forward direction, their estimates are

$$\hat{h}_{S_k R_l} = \tilde{h}_{S_k R_l} \quad (4.121)$$

$$\hat{h}_{R_l D_m} = \tilde{h}_{R_l D_m}. \quad (4.122)$$

Measuring the channels in backward direction delivers the estimates (cf. (4.2))

$$\hat{h}_{R_l S_k} = \tilde{h}_{S_k R_l} e^{2j\varphi_{R_l}} \quad (4.123)$$

$$\hat{h}_{D_m R_l} = \tilde{h}_{R_l D_m} e^{-2j\varphi_{R_l}}. \quad (4.124)$$

Fig. 4.3 shows the four combinations of directions in which the first-hop and second-hop channel matrices can be measured. The four corresponding protocols are:

- **Protocol A1:** All channels are measured in forward direction. The resulting estimates are given in (4.121) and (4.122). Consequently, the anticipated compound channel between source k and destination m is

$$\hat{h}_{S_k R D_m}^{(A1)} = \sum_{l=1}^{N_R} \left(\tilde{h}_{D_m R_l} g_l \tilde{h}_{S_k R_l} \right) = h_{S_k R D_m}. \quad (4.125)$$

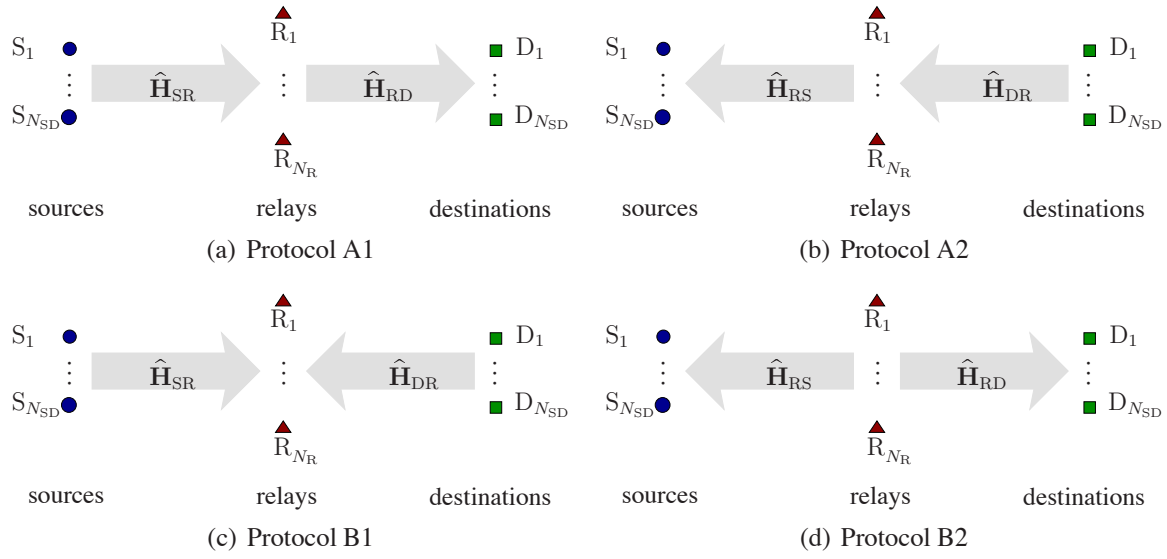


Fig. 4.3: Channel estimation protocols corresponding to the different directions in which the single-hop channels are measured.

- **Protocol A2:** All channels are measured in backward direction. The resulting estimates are now given in (4.123) and (4.124). The anticipated compound channel between source k and destination m is

$$\hat{h}_{S_kRD_m}^{(A2)} = \sum_{l=1}^{N_R} \left(\tilde{h}_{D_mR_l} e^{-2j\varphi_{R_l}} \cdot g_l \cdot \tilde{h}_{S_kR_l} e^{2j\varphi_{R_l}} \right) = h_{S_kRD_m}, \quad (4.126)$$

which is the same as for protocol A1.

- **Protocol B1:** For protocol B1, all channel coefficients are measured at the relays. Consequently, the estimates are given in (4.121) and (4.124). The anticipated compound channel between source k and destination m is

$$\hat{h}_{S_kRD_m}^{(B1)} = \sum_{l=1}^{N_R} \left(\hat{h}_{D_mR_l} g_l \hat{h}_{S_kR_l} \right) = \sum_{l=1}^{N_R} \left(e^{-2j\varphi_{R_l}} \cdot h_{R_lD_m} g_l h_{S_kR_l} \right). \quad (4.127)$$

In general, $\hat{h}_{S_kRD_m}^{(B1)} \neq h_{S_kRD_m}$ if the LO phases of the relays are unknown and random (cf. Section 4.2). The gain factors can in this case not be computed correctly based on the estimates (even if they are noiseless). Hence, the relays require a common phase reference. This means that their LO phases have to be equal, i.e. $\varphi_{R_l} = \phi$, for all

	First-hop channel	Second-hop channel	Required channel uses
Protocol A1	forward direction	forward direction	$N_{SD} + N_R$
Protocol A2	backward direction	backward direction	$N_{SD} + N_R$
Protocol B1	forward direction	backward direction	$2N_{SD}$
Protocol B2	backward direction	forward direction	N_R

Table 4.2: Direction of measurement and required number of channel uses to estimate all first-hop and second-hop channel coefficients.

$l \in \{1, \dots, N_R\}$. Equation (4.127) then becomes

$$\hat{h}_{S_kRD_m}^{(B1)} = e^{-2j\phi} h_{S_kRD_m}. \quad (4.128)$$

The phase ϕ that still enters $\hat{h}_{S_kRD_m}^{(B1)}$ may be random and unknown. As long as it is the same for all relays, it has no impact on the way the signals add up at the destination antennas. Since $|e^{-2j\phi}|^2 = 1$, equation (4.128) implies that the anticipated SINR at destination m (which is based on $\hat{h}_{S_kRD_m}^{(B1)}$) is equal to the actual one.

- **Protocol B2:** For protocol B2 all channels are measured at the sources and destinations. The estimates are thus given in (4.122) and (4.123). In this case, the anticipated compound channel between source k and destination m is

$$\hat{h}_{S_kRD_m}^{(B2)} = \sum_{l=1}^{N_R} \left(\hat{h}_{R_lD_m} g_l \hat{h}_{R_lS_k} \right) = \sum_{l=1}^{N_R} \left(e^{2j\phi_{R_l}} \cdot h_{R_lD_m} g_l h_{S_kR_l} \right). \quad (4.129)$$

Again, the relays require a common phase reference. Otherwise the gain factors cannot be computed correctly (cf. Protocol B1). Equation (4.129) becomes

$$\hat{h}_{S_kRD_m}^{(B2)} = e^{2j\phi} h_{S_kRD_m}. \quad (4.130)$$

The relays have been found to require a common phase reference if the channels are estimated with protocols B1 and B2. This means that an additional effort is necessary compared to A1 and A2. However, it turns out that protocols A1 and A2 require more channel uses to estimate all first-hop and second-hop channel coefficients than B1 and B2 if $N_R > N_{SD}$. Table 4.2 provides a summary of the number of channel uses each protocol requires to estimate all single-hop channels. The total effort in a two-hop network depends on the number

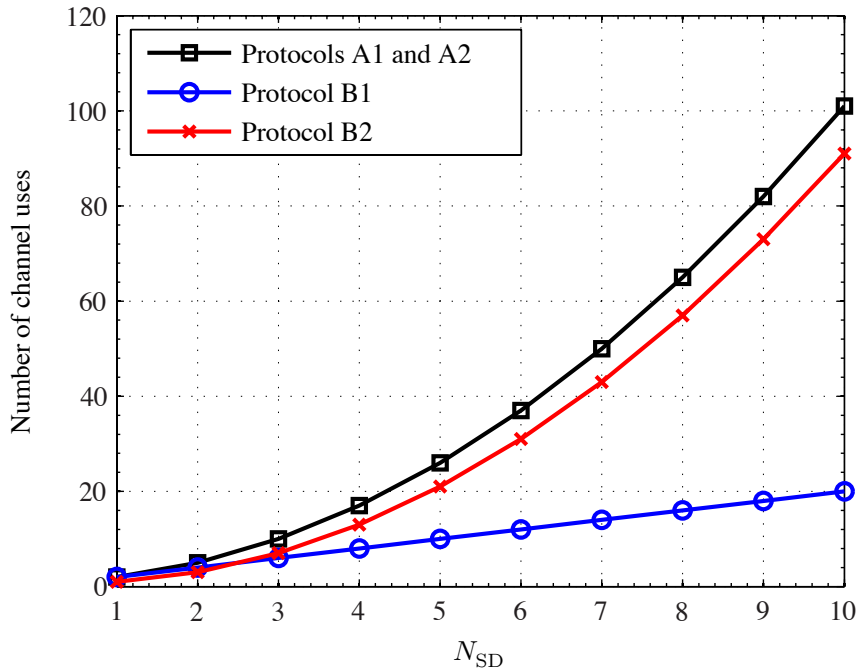


Fig. 4.4: Number of channel uses required to estimate all channel coefficients for the four protocols if $N_R = N_{SD}^2 - N_{SD} + 1$.

of sources, relays, and destinations. Fig. 4.4 shows the required number of channel uses for all four protocols versus the number of source-destination pairs for $N_R = N_{SD}^2 - N_{SD} + 1$. In Section 6.2, this will be shown to be the minimum number of relays that can orthogonalize N_{SD} source-destination pairs. All values in the plot can take only integer numbers. The connecting lines between the points are simply for the sake of a better visualization. It can be seen that protocols B1 and B2 require less channel uses than protocols A1 and A2. In particular, the effort for B1 is by far the least of all protocols if the number of relays is large.

Apart from the effort to measure all channel coefficients, the four protocols differ in the quality of the channel estimates they deliver in the presence of noise. In Section 4.4.3, the impact of additive noise and relay phase noise on the quality of the channel estimates will be discussed. Since the estimated compound channel is the same for protocol A1 and A2 (cf. (4.125) and (4.126)), it suffices to consider only one of them. Furthermore, equations (4.128) and (4.130) reveal that $|\hat{h}_{S_kRD_m}^{(B1)}|^2 = |\hat{h}_{S_kRD_m}^{(B2)}|^2$. Consequently, the MSE of the estimated compound channels is the same for both protocols. The following considerations are thus confined to the discussion of protocols A1 and B1. The results then also hold for A2 and B2.

Once all channel coefficients are measured, they have to be disseminated to the relays so that they can locally compute their gain factors. The effort in number of channel uses is the

same for all protocols because it only depends on the number of coefficients that have to be disseminated.

4.4.3 Impact of Noise

Up to now, phase noise and additive noise perturbing the channel estimates have been neglected. Both will, however, degrade the quality of the channel estimates and therefore the performance of any coherent gain allocation scheme. While the impact of additive noise on all protocols identified in Section 4.4.2 turns out to be the same, the impact of phase noise is not. In this section, the impact of relay phase noise and additive noise on the quality of the channel estimates produced by protocols A1 and B1 is investigated. The result is a comparison stating which protocol delivers more accurate channel estimates under which circumstances.

All relays are assumed to employ free running LOs. Wiener phase noise is in this case an appropriate model that describes the LO phase fluctuations as sampled Wiener process (e.g. [172]). The severity of the unknown and random phase changes is then a linear function of time (cf. Chapter 3). Consequently, the protocols requiring more channel uses to estimate all coefficients suffer more from phase noise than those requiring less channel uses. In order to assess the impact of relay phase noise on the quality of the channel estimates, the notion of 'block phase noise' is introduced: the LO phases of the relays stay constant for a single channel use and change randomly afterwards (similar to a block fading channel model). In the Wiener phase noise model, the phase changes are mutually independent, zero-mean Gaussian random variables. Their variance is in the following denoted by σ_{pn}^2 . It is assumed to be the same for all relays.

In addition to phase noise, additive signal noise perturbs the measurement signal and thus has a degrading effect on the estimates. Let

$$\hat{h} = c(h + n) \quad (4.131)$$

denote the MMSE estimate of a channel coefficient $h \sim \mathcal{CN}(0, \sigma_h^2)$, where $n \sim \mathcal{CN}(0, \sigma_n^2)$ is additive noise and $c \in \mathbb{R}^+$ a scaling factor. The estimation error is given by $e = h - \hat{h}$. By the property of the MMSE estimation, \hat{h} and e are uncorrelated and $e \sim \mathcal{CN}(0, \sigma_e^2)$, where $\sigma_e^2 = \text{E}[|h|^2] - \text{E}[|\hat{h}|^2]$ (e.g. [187]). If σ_h^2 and σ_n^2 are known to the receiver, it can choose

$$c = \sqrt{\frac{\sigma_h^2}{\sigma_h^2 + \sigma_n^2}}. \quad (4.132)$$

The estimate \hat{h} has then the same variance as h and thus $\sigma_e^2 = 0$. For a given estimation SNR (denoted by SNR_{est}), the noise variance is given by

$$\sigma_n^2 = \frac{\sigma_h^2}{\text{SNR}_{\text{est}}}. \quad (4.133)$$

In the following, expressions are derived for the perturbed single-hop channel estimates obtained by protocols A1 and B1. These are then used as basis for the subsequent performance comparison of both protocols.

4.4.3.1 Distributed Phase Synchronization Scheme

In Section 4.4.2 it has been shown that the gain factors can only be computed correctly from channel estimates obtained with protocols B1 or B2 if the relays are phase synchronous. A simple scheme to provide multiple relay nodes with a global phase reference is presented in Chapter 5. Since it is required for the discussion in Section 4.4.3.3 it will be shortly introduced here. Chapter 5 then provides a more detailed discussion.

A single node in the network is assigned 'master' M while all relays are 'slaves'. Each relay transmits a training sequence to the master node, which in turn retransmits conjugate-complex and time-inverted versions of its received sequences back to the relays. From their received signals, the relays can compute an estimate $\hat{\varphi}_{R_l M}$ of

$$\varphi_{R_l M} = -2\varphi_{R_l} + 2\varphi_M, \quad (4.134)$$

where φ_{R_l} and φ_M are the current LO phases of relay l and the master node, respectively. Each relay thus estimates two times the phase difference between its own LO and the LO of the master node. The phase error introduced to $\hat{h}_{S_k R D_m}^{(B1)}$ by the LO phases of the relays can be compensated with knowledge of $\varphi_{R_l M}$. Instead of $\hat{h}_{D_m R_l}$, each relay l disseminates

$$\hat{h}_{R_l D_m} = e^{-j\hat{\varphi}_{R_l M}} \cdot \hat{h}_{D_m R_l}, \quad m = 1, \dots, N_{SD} \quad (4.135)$$

to all other relays. Together with $\hat{h}_{S_k R_l}$ the anticipated compound channel (4.127) becomes

$$\hat{h}_{S_k R D_m}^{(B1)} = \sum_{l=1}^{N_R} (e^{-2j\varphi_M} \cdot h_{R_l D_m} g_l h_{S_k R_l}) = e^{-2j\varphi_M} h_{S_k R D_m}. \quad (4.136)$$

It has the same form as (4.128), where $\phi = \varphi_M$, and is independent of the LO phases of the relays. Note that knowledge of $\varphi_{R_l M}$ is used to compensate the phase error introduced to

$\hat{h}_{S_k R_{D_m}}^{(B1)}$ by the channel estimates. This means that the phase synchronization scheme only has to be performed when the channel estimates are updated (and $\varphi_{R_l M}$ has become outdated due to phase noise).

4.4.3.2 Single-Hop Channel Estimates: Protocol A1

Channel estimation protocol A1 starts with the sources transmitting training sequences sequentially so that the relays can estimate their local first-hop channels. Afterwards, the relays sequentially transmit training sequences so that the destinations can estimate their local second-hop channels. The time slots at which the nodes transmit their training sequences are:

Time slot	1	...	N_{SD}	$N_{SD} + 1$...	$N_{SD} + N_R$
Transmitting node	S_1	...	$S_{N_{SD}}$	R_1	...	R_{N_R}

After all channel coefficients are measured, the relays and destinations disseminate their local estimates to all relays so that they can locally compute their respective gain factors. In the following, expressions for the channel estimates are derived as function of the actual channels and the perturbing noise (additive estimation noise and phase noise).

First-Hop Channels: Let φ_{R_l} denote the phase offset of relay l in time slot 1. Furthermore, the phase change between time slots $k - 1$ and k is denoted by $\Delta\psi_{S_k R_l}$, for $2 \leq k \leq N_{SD}$. Consequently, the phase offset of relay l in time slot k , i.e., while source k is transmitting its training sequence, is given by

$$\phi_{S_k R_l} = \varphi_{R_l} + \sum_{p=1}^k \Delta\psi_{S_p R_l} := \varphi_{R_l} + \psi_{S_k R_l}, \quad (4.137)$$

where $\Delta\psi_{S_1 R_l} = 0$. Since all $\Delta\psi_{S_p R_l}$ are mutually independent⁵, their sum is zero-mean Gaussian with variance $(k - 1) \sigma_{pn}^2$. The estimated channel coefficient between source k and relay l is then given by

$$\hat{h}_{S_k R_l} = c \left(\tilde{h}_{S_k R_l} e^{-j\psi_{S_k R_l}} + n_{S_k R_l} \right), \quad (4.138)$$

where c is given in (4.132) and $n_{S_k, R_l} \sim \mathcal{N}(0, \sigma_n^2)$ is AWGN (cf. (4.131)).

Second-Hop Channels: The relays transmit training sequences to the destinations from time

⁵This is a property of the Wiener phase noise model.

slot $N_{\text{SD}} + 1$ until time slot $N_{\text{SD}} + N_{\text{R}}$. Let $\psi_{S_{N_{\text{SD}}}\text{R}_l}$ be defined as in (4.137) for $k = N_{\text{SD}}$. Then the estimated channel coefficients are

$$\hat{h}_{\text{R}_l\text{D}_m} = c \left(\tilde{h}_{\text{R}_l\text{D}_m} e^{j\psi_{\text{R}_l\text{D}_m}} + n_{\text{R}_l\text{D}_m} \right), \quad (4.139)$$

where $n_{\text{R}_l\text{D}_m} \sim \mathcal{N}(0, \sigma_n^2)$ is AWGN and

$$\psi_{\text{R}_l\text{D}_m} = \psi_{S_{N_{\text{SD}}}\text{R}_l} + \Delta\psi_{\text{R}_l\text{D}_m}. \quad (4.140)$$

The phase changes $\Delta\psi_{\text{R}_l\text{D}_m}$ are zero-mean Gaussian with variance $l\sigma_{\text{pn}}^2$. Furthermore, the scaling factor c is assumed to be the same as for the estimation of the first-hop channel coefficients because the channel coefficients and noise samples have the same statistics.

4.4.3.3 Single-Hop Channel Estimates: Protocol B1

Protocol B1 starts in the same way as A1. The sources sequentially transmit training sequences so that the relays can estimate their local first-hop channels. Afterwards, phase synchronization as described in Section 5.2.1 is performed to provide the required phase reference at the relays. This scheme is assumed to require τ time slots (where $1 \leq \tau \leq N_{\text{R}}$) for the transmission of all training sequences to the master node and again τ time slots for the retransmission from the master node to all relays. For the phase synchronization scheme each relay is required to estimate a single coefficient. In a broadband communication system, the relays may thus be orthogonalized either in frequency or in time. If all relays are orthogonalized in frequency, the phase synchronization scheme requires a total of two time slots, i.e. $\tau = 1$. For the case that the relays are orthogonalized in time, a total of $2\tau = 2N_{\text{R}}$ time slots is required. Finally, the destinations sequentially transmit training sequences so that the relays can estimate the local second-hop channels in backward direction. The time slots at which the nodes transmit their training sequences are:

Time slot	1	...	N_{SD}	$N_{\text{SD}} + 1$	$N_{\text{SD}} + \tau + 1$	$N_{\text{SD}} + 2\tau + 1$...	$2N_{\text{SD}} + 2\tau$
Transmitting node	S_1	...	$S_{N_{\text{SD}}}$	R_l	M	D_1	...	$\text{D}_{N_{\text{SD}}}$

For the phase synchronization, all relays transmit their training sequences in time slots $N_{\text{SD}} + 1$ to $N_{\text{SD}} + \tau$. The master node M then transmits in time slots $N_{\text{SD}} + \tau + 1$ until $N_{\text{SD}} + 2\tau$.

First-Hop Channels: The estimated first-hop channel coefficients are the same as for protocol A1. They are given in (4.138).

Phase Synchronization: At time slot $N_{\text{SD}} + 1$ the relays start to transmit their training symbols s_l on orthogonal channels to the master node M. The phase offset of relay l at this time is denoted by

$$\varphi_{R_l}^{(\text{tx})} = \phi_{S_{N_{\text{SD}} R_l}} + \Delta\varphi_{R_l}^{(\text{tx})}, \quad (4.141)$$

where $\phi_{S_{N_{\text{SD}} R_l}}$ is the phase offset at time slot N_{SD} (cf. (4.137) for $k = N_{\text{SD}}$) and

$$\Delta\varphi_{R_l}^{(\text{tx})} \sim \mathcal{N}(0, \sigma_{\text{pn}}^2) \quad (4.142)$$

is the phase change between time slots N_{SD} and $N_{\text{SD}} + 1$ due to phase noise. For the phase synchronization scheme it is assumed that the average accuracy is equal for all relays. This is realized by the assumption the relay phases stay constant not only for a single channel use, but for τ channel uses. Thus, they remain unchanged for the time it takes all relays to transmit their training sequences to M. Afterwards the phases change and remain unchanged again for the time the master node retransmits to the relays. The signal that is received at M from relay l can then be written as

$$r_{M,l}^{(\text{rx})} = h_{R_l M} s_l \cdot e^{j(\varphi_{R_l}^{(\text{tx})} - \varphi_M)} + n_{M,l}, \quad (4.143)$$

where $h_{R_l M}$ is the respective channel coefficient and $n_{M,l}$ additive noise at the master node. The transmission from relays to the master node takes τ time slots. At time slot $N_{\text{SD}} + \tau + 1$, the master node starts retransmitting

$$r_{M,l}^{(\text{tx})} = h_{R_l M}^* s_l^* \cdot e^{-j(\varphi_{R_l}^{(\text{tx})} - \varphi_M)} + n_{M,l}^*, \quad (4.144)$$

which is the conjugate complex of its received symbol $r_{M,l}^{(\text{rx})}$. At this time, the LO phase offset of relay l is $\varphi_{R_l}^{(\text{rx})} = \varphi_{R_l}^{(\text{tx})} + \Delta\varphi_{R_l}^{(\text{rx})}$, where

$$\Delta\varphi_{R_l}^{(\text{rx})} \sim \mathcal{N}(0, \tau\sigma_{\text{pn}}^2) \quad (4.145)$$

is the phase change due to phase noise. Consequently, relay l receives

$$r_{R_l}^{(\text{rx})} = |h_{R_l M}|^2 s_l^* \cdot e^{j(2\varphi_M - \varphi_{R_l}^{(\text{tx})} - \varphi_{R_l}^{(\text{rx})})} + h_{R_l M} n_{M,l}^* \cdot e^{j(\varphi_M - \varphi_{R_l}^{(\text{rx})})} + n_{R_l}. \quad (4.146)$$

Multiplication with s and phase estimation yields

$$\hat{\varphi}_{R_l M} = 2\varphi_M - \varphi_{R_l}^{(\text{tx})} - \varphi_{R_l}^{(\text{rx})} - \psi_{R_l M}^{(\text{sn})} := \varphi_{R_l M} - \psi_{R_l M}, \quad (4.147)$$

where

$$\varphi_{R_l M} = 2\varphi_M - 2\varphi_{R_l} \quad (4.148)$$

$$\psi_{R_l M} = \psi_{R_l M}^{(\text{pn})} + \psi_{R_l M}^{(\text{sn})}. \quad (4.149)$$

The phase offset

$$\psi_{R_l M}^{(\text{pn})} = 2\psi_{S_{N_{\text{SD}}} R_l} + 2\Delta\varphi_{R_l}^{(\text{tx})} + \Delta\varphi_{R_l}^{(\text{rx})} \quad (4.150)$$

is due to phase noise and $\psi_{R_l M}^{(\text{sn})}$ due to the additive noise components in (4.146). In Chapter 5 it will be shown that for large SNR, $\psi_{R_l M}^{(\text{sn})}$ is approximately Gaussian. For the following considerations, this assumption is made and thus

$$\psi_{R_l M}^{(\text{pn})} \sim \mathcal{N}(0, (2N_{\text{SD}} + 1)\sigma_{\text{pn}}^2) \quad (4.151)$$

$$\psi_{R_l M}^{(\text{sn})} \sim \mathcal{N}(0, \sigma_{\text{sn}}^2). \quad (4.152)$$

Second-Hop Channels: For the estimation of the second-hop channel coefficients the relay phases stay constant for a single channel use and change independently afterwards. In contrast to protocol A1, the second-hop channels are now estimated in backward direction. This means that the channel coefficients are measured at the relays. Their estimates are given by

$$\hat{h}_{D_m R_l} = c \left(\tilde{h}_{D_m R_l} e^{-j\psi_{D_m R_l}} + n_{D_m R_l} \right). \quad (4.153)$$

The respective relay phases $\psi_{D_m R_l}$ are

$$\psi_{D_m R_l} = \psi_{S_{N_{\text{SD}}} R_l} + \Delta\varphi_{R_l}^{(\text{tx})} + \Delta\varphi_{R_l}^{(\text{rx})} + \sum_{q=1}^m \Delta\psi_{D_q R_l}, \quad (4.154)$$

where the phase changes $\Delta\varphi_{R_l}^{(\text{tx})}$ and $\Delta\varphi_{R_l}^{(\text{rx})}$ are given in (4.142) and (4.145), respectively. Furthermore,

$$\Delta\psi_{D_1 R_l} \sim \mathcal{N}(0, \tau\sigma_{\text{pn}}^2), \quad (4.155)$$

$$\Delta\psi_{D_q R_l} \sim \mathcal{N}(0, \sigma_{\text{pn}}^2), \quad \text{for } q \geq 2. \quad (4.156)$$

The variance of $\Delta\psi_{D_1R_l}$ is larger than the variance of $\Delta\psi_{D_qR_l}$ for $q \geq 2$ because it took the master τ time slots to transmit to all relays during the phase synchronization procedure.

Disseminated Channel Coefficients: After the first-hop and second-hop channel coefficients have been measured, the estimates have to be disseminated to all relays. The disseminated first-hop and second-hop channel estimates are $\hat{h}_{S_kR_l}$ as given in (4.138) and

$$\hat{h}_{R_lD_m} = \hat{h}_{D_mR_l} e^{-j\hat{\varphi}_{R_lM}}, \quad (4.157)$$

respectively (cf. (4.135)). The phase correction term $\hat{\varphi}_{R_lM}$ is given in (4.147). It is the result of the phase synchronization scheme. In this way the estimates of the first-hop channel are the same for both protocols.

4.4.3.4 Channel Estimation Error: Equivalent Two-Hop Channels

A sensible performance measure for the channel estimation schemes was found to be how well the anticipated equivalent-two hop channels match the actual ones. In this section, $\text{MSE}_{m,k}$ defined in (4.120) is derived for protocols A1 and B1, respectively. The main results are (4.163) and (4.173).

Protocol A1: For channel estimation protocol A1, the estimates of the first-hop and second-hop channel coefficients are given in (4.138) and (4.139), respectively. The anticipated and the actual equivalent two-hop channel coefficients between source k and destination m are in this case

$$\hat{h}_{S_kRD_m} = \sum_{l=1}^{N_R} \hat{h}_{R_lD_m} g_l \hat{h}_{S_kR_l} \quad (4.158)$$

$$h_{S_kRD_m} = \sum_{l=1}^{N_R} \tilde{h}_{R_lD_m} g_l \tilde{h}_{S_kR_l}. \quad (4.159)$$

Note that the gain factors g_l in (4.158) and (4.159) are the same. The channel estimation error

$$\delta_{S_kRD_m} = h_{S_kRD_m} - \hat{h}_{S_kRD_m} \quad (4.160)$$

is defined in (4.119). Since the relay gains are computed from the channel estimates (and thus depend on the estimation errors), it is not possible to average $|\delta_{S_kRD_m}|^2$ over the perturbing noise for fixed gain factors. Instead, the channel estimates (and therefore also g_l) are fixed.

The squared estimation error is then averaged over all channel realizations that might have led to this estimates. Let

$$\tilde{\mathcal{H}} = \left\{ \tilde{h}_{S_k R_1}, \dots, \tilde{h}_{S_k R_{N_R}}, \tilde{h}_{R_1 D_m}, \dots, \tilde{h}_{R_{N_R} D_m} \right\} \quad (4.161)$$

denote the sets of actual channel coefficients between source k and all relays and between all relays and destination m . Then, the MSE of the estimated equivalent two-hop channels is then given by

$$e_{S_k R D_m}^{(A1)} = E_{\tilde{\mathcal{H}}} \left[\left| \delta_{S_k R D_m} \right|^2 \right]. \quad (4.162)$$

It is shown in Appendix A.1 that

$$\begin{aligned} e_{S_k R D_m}^{(A1)} &= \\ &= \sum_{l=1}^{N_R} \left(|g_l|^2 \left(\sigma_n^2 + \frac{1}{c^2} \left| \hat{h}_{R_l D_m} \right|^2 \right) \left(\sigma_n^2 + \frac{1}{c^2} \left| \hat{h}_{S_k R_l} \right|^2 \right) + \right. \\ &\quad \left. + \left(1 - \frac{2}{c^2} e^{-\frac{1}{2}(N_{SD}-k+l)\sigma_{pn}^2} \right) \left| \hat{h}_{S_k R_l D_m} \right|^2 \right) + \\ &\quad + \sum_{p=1}^{N_R} \sum_{\substack{q=1 \\ q \neq p}}^{N_R} \left(\left(\frac{1}{c^2} e^{-\frac{1}{2}(N_{SD}-k+p)\sigma_{pn}^2} - 1 \right) \hat{h}_{S_k R_p D_m} \cdot \right. \\ &\quad \left. \cdot \left(\frac{1}{c^2} e^{-\frac{1}{2}(N_{SD}-k+q)\sigma_{pn}^2} - 1 \right) \hat{h}_{S_k R_q D_m}^* \right), \end{aligned} \quad (4.163)$$

where $\hat{h}_{S_k R_l D_m} = \hat{h}_{R_l D_m} g_l \hat{h}_{S_k R_l}$.

The gradient of the MSE with respect to the gain factors is $\frac{\partial}{\partial \mathbf{g}^*} e_{S_k R D_m}^{(A1)}$, where \mathbf{g} is the vector comprising all gain factors g_l . It is useful for a gradient-based gain allocation that optimizes the relay gains for robustness against channel estimation errors. Using *Wirtinger Calculus*, which provides simple rules for the derivation with respect to a complex variable (e.g. Appendix A in [188]), the partial derivative $\frac{\partial}{\partial g_i^*} e_{S_k R D_m}^{(A1)}$ is easily obtained from (4.163).

It is given by

$$\begin{aligned}
 \frac{\partial}{\partial g_i^*} e_{S_k R D_m}^{(A1)} &= \frac{\partial}{\partial g_i^*} \sum_{l=1}^{N_R} \left(|g_l|^2 \left(\sigma_n^2 + \frac{1}{c^2} |\hat{h}_{R_l D_m}|^2 \right) \left(\sigma_n^2 + \frac{1}{c^2} |\hat{h}_{S_k R_l}|^2 \right) + \right. \\
 &\quad \left. + \left(1 - \frac{2}{c^2} e^{-\frac{1}{2}(N_{SD}-k+l)\sigma_{pn}^2} \right) |\hat{h}_{R_l D_m}|^2 |g_l|^2 |\hat{h}_{S_k R_l}|^2 \right) + \\
 &\quad + \frac{\partial}{\partial g_i^*} \sum_{p=1}^{N_R} \sum_{\substack{q=1 \\ q \neq p}}^{N_R} \left(\left(\frac{1}{c^2} e^{-\frac{1}{2}(N_{SD}-k+p)\sigma_{pn}^2} - 1 \right) \hat{h}_{R_p D_m} g_p \hat{h}_{S_k R_p} \cdot \right. \\
 &\quad \left. \cdot \left(\frac{1}{c^2} e^{-\frac{1}{2}(N_{SD}-k+q)\sigma_{pn}^2} - 1 \right) \hat{h}_{R_q D_m}^* g_q^* \hat{h}_{S_k R_q}^* \right) = \\
 &= g_i \left(\left(\sigma_n^2 + \frac{1}{c^2} |\hat{h}_{R_i D_m}|^2 \right) \left(\sigma_n^2 + \frac{1}{c^2} |\hat{h}_{S_k R_i}|^2 \right) + \right. \\
 &\quad \left. + \left(1 - \frac{2}{c^2} e^{-\frac{1}{2}(N_{SD}-k+i)\sigma_{pn}^2} \right) |\hat{h}_{R_i D_m}|^2 |\hat{h}_{S_k R_i}|^2 \right) + \\
 &\quad + \sum_{\substack{p=1 \\ p \neq i}}^{N_R} g_p \left(\left(\frac{1}{c^2} e^{-\frac{1}{2}(N_{SD}-k+p)\sigma_{pn}^2} - 1 \right) \hat{h}_{R_p D_m} \hat{h}_{S_k R_p} \cdot \right. \\
 &\quad \left. \cdot \left(\frac{1}{c^2} e^{-\frac{1}{2}(N_{SD}-k+i)\sigma_{pn}^2} - 1 \right) \hat{h}_{R_i D_m}^* \hat{h}_{S_k R_i}^* \right). \tag{4.164}
 \end{aligned}$$

Protocol B1: For channel estimation protocol B1, the estimates of the first-hop and second-hop channel coefficients are given in (4.138) and (4.157), respectively. They can be written as

$$\hat{h}_{S_k R_l} = c \left(\tilde{h}_{S_k R_l} e^{-j\psi_{S_k R_l}} + n_{S_k R_l} \right) \tag{4.165}$$

$$\hat{h}_{R_l D_m} = c \left(\tilde{h}_{R_l D_m} e^{j(\psi_{R_l M} - \psi_{D_m R_l})} + n'_{D_m R_l} \right) e^{-2j\varphi_M}. \tag{4.166}$$

For (4.166) equations (4.157), (4.147), (4.153), and $\tilde{h}_{D_m R_l} = \tilde{h}_{R_l D_m} e^{-2j\varphi_{R_l}}$ (cf. (4.2)) have been used. Furthermore, $n'_{D_m R_l} = e^{2j\varphi_{R_l}} \cdot n_{D_m R_l}$ has the same statistics as $n_{D_m R_l}$. The anticipated and the actual compound channel coefficients between source k and destination

m are

$$\hat{h}_{S_kRD_m} = \sum_{l=1}^{N_R} \hat{h}_{R_lD_m} g_l \hat{h}_{S_kR_l} \quad (4.167)$$

$$h_{S_kRD_m} = \sum_{l=1}^{N_R} \tilde{h}_{R_lD_m} g_l \tilde{h}_{S_kR_l}. \quad (4.168)$$

Note that the gain factors g_l in (4.167) and (4.168) are the same. For a noiseless estimation, i.e. $\hat{h}_{S_kR_l} = \tilde{h}_{S_kR_l}$ and $\hat{h}_{R_lD_m} = \tilde{h}_{D_mR_l} e^{-j\varphi_{R_lM}}$ (cf. (4.157)), equation (4.167) becomes

$$\hat{h}_{S_kRD_m} = e^{-2j\varphi_M} \sum_{l=1}^{N_R} \tilde{h}_{R_lD_m} g_l \tilde{h}_{S_kR_l}. \quad (4.169)$$

Again, the channel estimates (and therefore also g_l) are fixed and the channel estimation error $\delta_{S_kRD_m}$ is averaged over all channel realizations that might have led to these estimates. The phase offset $-2\varphi_M$ between (4.168) and (4.169) has to be taken into account when computing $\delta_{S_kRD_m}$. It is in this case given by

$$\begin{aligned} \delta_{S_kRD_m} &= \tilde{h}_{S_kRD_m} - \hat{h}_{S_kRD_m} e^{2j\varphi_M} = \\ &= \tilde{h}_{S_kRD_m} - \hat{h}'_{S_kRD_m}, \end{aligned} \quad (4.170)$$

where

$$\begin{aligned} \hat{h}'_{S_kRD_m} &= \sum_{l=1}^{N_R} c \left(\tilde{h}_{R_lD_m} e^{j(\psi_{R_lM} - \psi_{D_mR_l})} + n'_{D_mR_l} \right) g_l \hat{h}_{S_kR_l} = \\ &= \sum_{l=1}^{N_R} \hat{h}'_{R_lD_m} g_l \hat{h}_{S_kR_l}. \end{aligned} \quad (4.171)$$

Comparing (4.171) with (4.167) and (4.170) with (4.119), it can be seen that the MSE of the estimated equivalent two-hop channel coefficients for protocol B1 can easily be derived from (4.163). Since

$$\psi_{R_lM} - \psi_{D_mR_l} \sim \mathcal{N} \left(0, (N_{SD} + \tau + m - 1) \sigma_{pn}^2 + \sigma_{sn}^2 \right), \quad (4.172)$$

the resulting MSE is found by replacing $(N_{SD} - 1 + l) \sigma_{pn}^2$ in (4.163) by

$(N_{\text{SD}} + \tau + m - 1) \sigma_{\text{pn}}^2 + \sigma_{\text{sn}}^2$. Consequently,

$$\begin{aligned}
 e_{\text{S}_k\text{RD}_m}^{(\text{B1})} &= \sum_{l=1}^{N_{\text{R}}} \left(|g_l|^2 \left(\sigma_{\text{n}}^2 + \frac{1}{c^2} |\hat{h}_{\text{R}_l\text{D}_m}|^2 \right) \left(\sigma_{\text{n}}^2 + \frac{1}{c^2} |\hat{h}_{\text{S}_k\text{R}_l}|^2 \right) + \right. \\
 &\quad \left. + \left(1 - \frac{2}{c^2} e^{-\frac{1}{2}((N_{\text{SD}}-k+\tau+m)\sigma_{\text{pn}}^2+\sigma_{\text{sn}}^2)} \right) |\hat{h}_{\text{S}_k\text{R}_l\text{D}_m}|^2 \right) + \\
 &\quad + \left(\frac{1}{c^2} e^{-\frac{1}{2}((N_{\text{SD}}-k+\tau+m)\sigma_{\text{pn}}^2+\sigma_{\text{sn}}^2)} - 1 \right)^2 \cdot \sum_{p=1}^{N_{\text{R}}} \sum_{\substack{q=1 \\ q \neq p}}^{N_{\text{R}}} \left(\hat{h}_{\text{S}_k\text{R}_p\text{D}_m} \cdot \hat{h}_{\text{S}_k\text{R}_q\text{D}_m}^* \right),
 \end{aligned} \tag{4.173}$$

where $\hat{h}_{\text{S}_k\text{R}_l\text{D}_m}$ is defined in (4.167). The gradient $\frac{\partial}{\partial \mathbf{g}^*} e_{\text{S}_k\text{RD}_m}^{(\text{B1})}$ can easily be computed from (4.173). The partial derivative of $e_{\text{S}_k\text{RD}_m}^{(\text{B1})}$ with respect to g_i^* is

$$\begin{aligned}
 \frac{\partial}{\partial g_i^*} e_{\text{S}_k\text{RD}_m}^{(\text{B1})} &= \\
 &= \frac{\partial}{\partial g_i^*} \sum_{l=1}^{N_{\text{R}}} \left(|g_l|^2 \left(\sigma_{\text{n}}^2 + \frac{1}{c^2} |\hat{h}_{\text{R}_l\text{D}_m}|^2 \right) \left(\sigma_{\text{n}}^2 + \frac{1}{c^2} |\hat{h}_{\text{S}_k\text{R}_l}|^2 \right) + \right. \\
 &\quad \left. + \left(1 - \frac{2}{c^2} e^{-\frac{1}{2}((N_{\text{SD}}-k+\tau+m)\sigma_{\text{pn}}^2+\sigma_{\text{sn}}^2)} \right) |\hat{h}_{\text{R}_l\text{D}_m}|^2 |g_l|^2 |\hat{h}_{\text{S}_k\text{R}_l}|^2 \right) + \\
 &\quad + \frac{\partial}{\partial g_i^*} \left(\frac{1}{c^2} e^{-\frac{1}{2}((N_{\text{SD}}-k+\tau+m)\sigma_{\text{pn}}^2+\sigma_{\text{sn}}^2)} - 1 \right)^2 \sum_{p=1}^{N_{\text{R}}} \sum_{\substack{q=1 \\ q \neq p}}^{N_{\text{R}}} \left(\hat{h}_{\text{R}_p\text{D}_m} g_p \hat{h}_{\text{S}_k\text{R}_p} \cdot \hat{h}_{\text{R}_q\text{D}_m}^* g_q^* \hat{h}_{\text{S}_k\text{R}_q}^* \right) = \\
 &= g_i \left(\left(\sigma_{\text{n}}^2 + \frac{1}{c^2} |\hat{h}_{\text{R}_i\text{D}_m}|^2 \right) \left(\sigma_{\text{n}}^2 + \frac{1}{c^2} |\hat{h}_{\text{S}_k\text{R}_i}|^2 \right) + \right. \\
 &\quad \left. + \left(1 - \frac{2}{c^2} e^{-\frac{1}{2}((N_{\text{SD}}-k+\tau+m)\sigma_{\text{pn}}^2+\sigma_{\text{sn}}^2)} \right) |\hat{h}_{\text{R}_i\text{D}_m}|^2 |\hat{h}_{\text{S}_k\text{R}_i}|^2 \right) + \\
 &\quad + \left(\frac{1}{c^2} e^{-\frac{1}{2}((N_{\text{SD}}-k+\tau+m)\sigma_{\text{pn}}^2+\sigma_{\text{sn}}^2)} - 1 \right)^2 \sum_{\substack{p=1 \\ p \neq i}}^{N_{\text{R}}} g_p \left(\hat{h}_{\text{R}_p\text{D}_m} \hat{h}_{\text{S}_k\text{R}_p} \cdot \hat{h}_{\text{R}_i\text{D}_m}^* \hat{h}_{\text{S}_k\text{R}_i}^* \right).
 \end{aligned} \tag{4.174}$$

4.4.3.5 Channel Estimation Error: Single-Hop Channels

Instead of averaging over all channel and noise realizations, the MSEs in the previous section have been computed for fixed channel estimates. It is not clear how well the actual quality of the estimates is reflected in this measure. In this section, an alternative measure that is

very simple is investigated. Since both protocols deliver the same estimates for the first-hop channels, they can be compared solely on the quality of the second-hop channel estimates.

For protocol A1, the estimated channel coefficient between relay l and destination m is given in (4.139). The MSE of the second-hop channel estimate is then

$$\begin{aligned} e_{R_l D_m}^{(A1)} &= \mathbb{E}_{h, \psi, n} \left[\left| \tilde{h}_{R_l D_m} - \hat{h}_{R_l D_m} \right|^2 \right] = \\ &= \sigma_h^2 \cdot \left(1 - 2c \cdot e^{-\frac{1}{2}(N_{SD}-1+l)\sigma_{pn}^2} + c^2 \right) + c^2 \sigma_n^2. \end{aligned} \quad (4.175)$$

For protocol B1, the estimate of the second hop channel between relay l and destination m is given in (4.157). The MSE with respect to the noiseless case is thus

$$e_{R_l D_m}^{(B1)} = \mathbb{E}_{h, \psi, n} \left[\left| e^{-j\varphi_{R_l M}} \tilde{h}_{D_m R_l} - e^{-j\hat{\varphi}_{R_l M}} \hat{h}_{D_m R_l} \right|^2 \right], \quad (4.176)$$

where $\hat{h}_{D_m R_l}$ is given in (4.153) and $\hat{\varphi}_{R_l M}$ in (4.147). Equation (4.176) can be written as

$$\begin{aligned} e_{R_l D_m}^{(B1)} &= \mathbb{E}_h \left[\left| \tilde{h}_{D_m R_l} \right|^2 \right] \cdot \mathbb{E}_\psi \left[\left| 1 - c e^{-j(\psi_{D_m R_l} - \psi_{R_l M})} \right|^2 \right] + \mathbb{E}_n \left[\left| c n_{D_m R_l} \right|^2 \right] = \\ &= \sigma_h^2 \cdot \mathbb{E}_\psi \left[\left(1 - 2c \cdot \cos(\psi_{D_m R_l} - \psi_{R_l M}) + c^2 \right) \right] + c^2 \sigma_n^2, \end{aligned} \quad (4.177)$$

where $\psi_{R_l M}$ and $\psi_{D_m R_l}$ are given in (4.149) and (4.154), respectively. Taking their mutual dependency into account, the MSE finally becomes

$$e_{R_l D_m}^{(B1)} = \sigma_h^2 \cdot \left(1 - 2c \cdot e^{-\frac{1}{2}((N_{SD} + \tau + m - 1)\sigma_{pn}^2 + \sigma_{sn}^2)} + c^2 \right) + c^2 \sigma_n^2 := e_{RD_m}^{(B1)}. \quad (4.178)$$

Note that $e_{R_l D_m}^{(B1)} = e_{RD_m}^{(B1)}$ is independent of l .

4.4.3.6 Application Example

In Section 4.4.3.4 it was established that it is not possible to average the squared estimation error of the compound channel coefficients (i.e. $|\delta_{S_k R D_m}|^2$) over the perturbing noise (additive noise and phase noise) if the gain factors are not specified. Instead, two alternative performance measures for the channel estimation protocols have been introduced:

- **Section 4.4.3.4:** Instead of fixing the channel realization and averaging the squared estimation error over the noise, the channel estimates (and therefore also the gain factors) are fixed. The averaging is then performed over all channel realizations that might

have led to the respective estimates.

- **Section 4.4.3.5:** The first-hop channel estimates of A1 and B1 are found to be equal. Therefore, the performance of the protocols can be compared based on the quality of the second-hop channel estimates.

It is, however, not clear to which degree these measures reflect the actual quality of the compound channel estimates. In the following, an application example is therefore discussed, where the gain factors are explicitly known: distributed MRC. It is in this case possible to compute the MSE between the anticipated and the actual compound channels by averaging over the perturbing noise. The result serves as an indicator of the accuracy with which the performance of channel estimation protocols A1 and B1 can be approximated by the alternative measures of Sections 4.4.3.4 and 4.4.3.5.

Consider a two-hop relaying network as shown in Fig. 4.2 with a single source-destination pair and N_R relays. The gain factors are computed from local CSI at each relay. They are to be chosen such that, under an average transmit power constraint, the signals from all relays combine coherently at the destination. The gain factor at relay l is thus

$$\hat{g}_l = \gamma \cdot \hat{h}_{R_l D}^* \hat{h}_{SR_l}^*, \quad (4.179)$$

where the scaling factor γ is a function of σ_s^2 , σ_h^2 , σ_n^2 and the desired average transmit power per relay ensuring that the power constraint is met. It is assumed to be the same for all relays. The actual and the anticipated equivalent two-hop channels are in this case given by

$$\tilde{h}_{SRD} = \sum_{l=1}^{N_R} \tilde{h}_{R_l D} g_l \tilde{h}_{SR_l} = \gamma \sum_{l=1}^{N_R} \tilde{h}_{R_l D} \cdot \hat{h}_{R_l D}^* \hat{h}_{SR_l}^* \cdot \tilde{h}_{SR_l} \quad (4.180)$$

$$\hat{h}_{SRD} = \sum_{l=1}^{N_R} \hat{h}_{R_l D} g_l \hat{h}_{SR_l} = \gamma \sum_{l=1}^{N_R} \left| \hat{h}_{R_l D} \right|^2 \left| \hat{h}_{SR_l} \right|^2. \quad (4.181)$$

Protocol A1: For channel estimation protocol A1, all channels are measured in forward direction. The equivalent first-hop and second-hop channel coefficients are \tilde{h}_{SR_l} and $\tilde{h}_{R_l D}$, respectively. Their respective estimates \hat{h}_{SR_l} and $\hat{h}_{R_l D}$ are given in (4.138) and (4.139). Consequently, the MSE of the estimated compound channel is

$$e_{SRD}^{(A1)} = \gamma^2 \mathbb{E}_{h,n,\psi} \left[\left| \sum_{l=1}^{N_R} \tilde{h}_{R_l D} \hat{h}_{R_l D}^* \hat{h}_{SR_l}^* \tilde{h}_{SR_l} - \left| \hat{h}_{R_l D} \right|^2 \left| \hat{h}_{SR_l} \right|^2 \right|^2 \right]. \quad (4.182)$$

Equation (4.182) can be rewritten as

$$\begin{aligned}
 e_{\text{SRD}}^{(\text{A1})} &= \gamma^2 \sum_{l=1}^{N_{\text{R}}} \mathbb{E}_{h,n,\psi} \left[\left| \tilde{h}_{\text{R}_l\text{D}} \hat{h}_{\text{R}_l\text{D}}^* \hat{h}_{\text{SR}_l}^* \tilde{h}_{\text{SR}_l} - \left| \hat{h}_{\text{R}_l\text{D}} \right|^2 \left| \hat{h}_{\text{SR}_l} \right|^2 \right|^2 \right] + \\
 &+ \gamma^2 \sum_{p=1}^{N_{\text{R}}} \sum_{\substack{q=1 \\ q \neq p}}^{N_{\text{R}}} \mathbb{E}_{h,n,\psi} \left[\left(\tilde{h}_{\text{R}_p\text{D}} \hat{h}_{\text{R}_p\text{D}}^* \hat{h}_{\text{SR}_p}^* \tilde{h}_{\text{SR}_p} - \left| \hat{h}_{\text{R}_p\text{D}} \right|^2 \left| \hat{h}_{\text{SR}_p} \right|^2 \right) \right. \\
 &\cdot \left. \mathbb{E}_{h,n,\psi} \left[\left(\tilde{h}_{\text{R}_q\text{D}} \hat{h}_{\text{R}_q\text{D}}^* \hat{h}_{\text{SR}_q}^* \tilde{h}_{\text{SR}_q} - \left| \hat{h}_{\text{R}_q\text{D}} \right|^2 \left| \hat{h}_{\text{SR}_q} \right|^2 \right)^* \right] \right], \tag{4.183}
 \end{aligned}$$

where the three expectations in (4.183) can be computed independently of each other. The MSE of the equivalent two-hop channel is given by

$$\begin{aligned}
 e_{\text{SRD}}^{(\text{A1})} &= \gamma^2 \sum_{l=1}^{N_{\text{R}}} \left(-8c^2 \sigma_{\text{h}}^8 e^{-\frac{1}{2}l\sigma_{\text{pn}}^2} + 4\sigma_{\text{h}}^8 + 4c^2 \sigma_{\text{h}}^8 + c^4 \sigma_{\text{h}}^4 \sigma_{\text{n}}^4 \right) + \\
 &+ \gamma^2 \sum_{p=1}^{N_{\text{R}}} \sum_{\substack{q=1 \\ q \neq p}}^{N_{\text{R}}} \left(-c^2 \sigma_{\text{h}}^4 e^{-\frac{1}{2}p\sigma_{\text{pn}}^2} + \sigma_{\text{h}}^4 \right) \left(-c^2 \sigma_{\text{h}}^4 e^{-\frac{1}{2}q\sigma_{\text{pn}}^2} + \sigma_{\text{h}}^4 \right). \tag{4.184}
 \end{aligned}$$

The MSE of the compound channel derived in Section 4.4.3.4 depends in the gain factors and the current realizations of the single-hop channel estimates. In order to compare (4.163) with (4.184), $e_{\text{S}_1\text{RD}_1}^{(\text{A1})}$ from (4.163) has to be average over all channel estimates for the case that the gain factors are given in (4.179):

$$\begin{aligned}
 \mathbb{E}_{\hat{h}} \left[e_{\text{S}_1\text{RD}_1}^{(\text{A1})} \right] &= \mathbb{E}_{\hat{h}} \left[\sum_{l=1}^{N_{\text{R}}} \left(\gamma^2 \left| \hat{h}_{\text{R}_l\text{D}} \right|^2 \left| \hat{h}_{\text{SR}_l} \right|^2 \left(\sigma_{\text{n}}^2 + \frac{1}{c^2} \left| \hat{h}_{\text{R}_l\text{D}} \right|^2 \right) \left(\sigma_{\text{n}}^2 + \frac{1}{c^2} \left| \hat{h}_{\text{SR}_l} \right|^2 \right) + \right. \right. \\
 &+ \left. \left(1 - \frac{2}{c^2} e^{-\frac{1}{2}l\sigma_{\text{pn}}^2} \right) \gamma^2 \left| \hat{h}_{\text{R}_l\text{D}} \right|^4 \left| \hat{h}_{\text{SR}_l} \right|^4 \right) + \\
 &+ \sum_{p=1}^{N_{\text{R}}} \sum_{\substack{q=1 \\ q \neq p}}^{N_{\text{R}}} \left(\left(\frac{1}{c^2} e^{-\frac{1}{2}p\sigma_{\text{pn}}^2} - 1 \right) \gamma \left| \hat{h}_{\text{R}_p\text{D}} \right|^2 \left| \hat{h}_{\text{SR}_p} \right|^2 \cdot \right. \\
 &\cdot \left. \left. \left(\frac{1}{c^2} e^{-\frac{1}{2}q\sigma_{\text{pn}}^2} - 1 \right) \gamma \left| \hat{h}_{\text{R}_q\text{D}} \right|^2 \left| \hat{h}_{\text{SR}_q} \right|^2 \right) \right]. \tag{4.185}
 \end{aligned}$$

The expectation of the summands in (4.185) can be computed separately. Recall that the scaling factor c has been chosen such that $\hat{h}_{\text{R}_l\text{D}}$ and \hat{h}_{SR_l} are zero-mean Gaussian with variance σ_{h}^2 (cf. (4.131) and (4.132)).

$$\begin{aligned}
 & \bullet \\
 & \mathbb{E}_{\hat{\mathcal{H}}} \left[\gamma^2 \left| \hat{h}_{\text{R}_i\text{D}} \right|^2 \left| \hat{h}_{\text{S}_i\text{R}_i} \right|^2 \left(\sigma_n^2 + \frac{1}{c^2} \left| \hat{h}_{\text{R}_i\text{D}} \right|^2 \right) \left(\sigma_n^2 + \frac{1}{c^2} \left| \hat{h}_{\text{S}_i\text{R}_i} \right|^2 \right) \right] = \\
 & = \mathbb{E}_{\hat{\mathcal{H}}} \left[\gamma^2 \sigma_n^4 \left| \hat{h}_{\text{R}_i\text{D}} \right|^2 \left| \hat{h}_{\text{S}_i\text{R}_i} \right|^2 \right] + \mathbb{E}_{\hat{\mathcal{H}}} \left[\frac{1}{c^2} \gamma^2 \sigma_n^2 \left| \hat{h}_{\text{R}_i\text{D}} \right|^2 \left| \hat{h}_{\text{S}_i\text{R}_i} \right|^4 \right] + \\
 & \quad + \mathbb{E}_{\hat{\mathcal{H}}} \left[\frac{1}{c^2} \gamma^2 \sigma_n^2 \left| \hat{h}_{\text{R}_i\text{D}} \right|^4 \left| \hat{h}_{\text{S}_i\text{R}_i} \right|^2 \right] + \mathbb{E}_{\hat{\mathcal{H}}} \left[\frac{\gamma^2}{c^4} \left| \hat{h}_{\text{R}_i\text{D}} \right|^4 \left| \hat{h}_{\text{S}_i\text{R}_i} \right|^4 \right] = \\
 & = \gamma^2 \sigma_n^4 \sigma_h^4 + \frac{4}{c^2} \gamma^2 \sigma_n^2 \sigma_h^6 + \frac{4\gamma^2}{c^4} \sigma_h^8 \tag{4.186}
 \end{aligned}$$

$$\bullet \\
 \mathbb{E}_{\hat{\mathcal{H}}} \left[\left(1 - \frac{2}{c^2} e^{-\frac{1}{2} l \sigma_{\text{pn}}^2} \right) \gamma^2 \left| \hat{h}_{\text{R}_i\text{D}} \right|^4 \left| \hat{h}_{\text{S}_i\text{R}_i} \right|^4 \right] = \left(1 - \frac{2}{c^2} e^{-\frac{1}{2} l \sigma_{\text{pn}}^2} \right) \gamma^2 \cdot 4\sigma_h^8 \tag{4.187}$$

$$\bullet \\
 \mathbb{E}_{\hat{\mathcal{H}}} \left[\left(\frac{1}{c^2} e^{-\frac{1}{2} l \sigma_{\text{pn}}^2} - 1 \right) \gamma \left| \hat{h}_{\text{R}_i\text{D}} \right|^2 \left| \hat{h}_{\text{S}_i\text{R}_i} \right|^2 \right] = \left(\frac{1}{c^2} e^{-\frac{1}{2} l \sigma_{\text{pn}}^2} - 1 \right) \gamma \sigma_h^4 \tag{4.188}$$

With (4.186) – (4.188), equation (4.185) becomes

$$\begin{aligned}
 \mathbb{E}_{\hat{\mathcal{H}}} \left[e_{\text{S}_1\text{RD}_1}^{(\text{A1})} \right] & = \sum_{l=1}^{N_{\text{R}}} \left(\gamma^2 \sigma_n^4 \sigma_h^4 + \frac{4}{c^2} \gamma^2 \sigma_n^2 \sigma_h^6 + \frac{4\gamma^2}{c^4} \sigma_h^8 + \left(1 - \frac{2}{c^2} e^{-\frac{1}{2} l \sigma_{\text{pn}}^2} \right) \gamma^2 \cdot 4\sigma_h^8 \right) + \\
 & \quad + \sum_{p=1}^{N_{\text{R}}} \sum_{\substack{q=1 \\ q \neq p}}^{N_{\text{R}}} \left(\frac{1}{c^2} e^{-\frac{1}{2} p \sigma_{\text{pn}}^2} - 1 \right) \left(\frac{1}{c^2} e^{-\frac{1}{2} q \sigma_{\text{pn}}^2} - 1 \right) \gamma^2 \sigma_h^8 = \\
 & = \gamma^2 \sum_{l=1}^{N_{\text{R}}} \left(\sigma_n^4 \sigma_h^4 + \frac{4}{c^2} \sigma_n^2 \sigma_h^6 + \frac{4}{c^4} \sigma_h^8 + 4\sigma_h^8 - \frac{8}{c^2} \sigma_h^8 e^{-\frac{1}{2} l \sigma_{\text{pn}}^2} \right) + \\
 & \quad + \gamma^2 \sigma_h^8 \sum_{p=1}^{N_{\text{R}}} \sum_{\substack{q=1 \\ q \neq p}}^{N_{\text{R}}} \left(\frac{1}{c^2} e^{-\frac{1}{2} p \sigma_{\text{pn}}^2} - 1 \right) \left(\frac{1}{c^2} e^{-\frac{1}{2} q \sigma_{\text{pn}}^2} - 1 \right) = \\
 & = \gamma^2 \left(N_{\text{R}} \left(4\sigma_h^8 + \frac{4}{c^4} \sigma_h^8 + \sigma_n^4 \sigma_h^4 + \frac{4}{c^2} \sigma_n^2 \sigma_h^6 \right) - \frac{8}{c^2} \sigma_h^8 \sum_{l=1}^{N_{\text{R}}} e^{-\frac{1}{2} l \sigma_{\text{pn}}^2} \right) + \\
 & \quad + \gamma^2 \sigma_h^8 \sum_{p=1}^{N_{\text{R}}} \sum_{\substack{q=1 \\ q \neq p}}^{N_{\text{R}}} \left(\frac{1}{c^2} e^{-\frac{1}{2} p \sigma_{\text{pn}}^2} - 1 \right) \left(\frac{1}{c^2} e^{-\frac{1}{2} q \sigma_{\text{pn}}^2} - 1 \right). \tag{4.189}
 \end{aligned}$$

Protocol B1: For channel estimation protocol B1, the second-hop channel is measured in backward direction. The respective estimates \hat{h}_{SR_l} and \hat{h}_{DR_l} are given in (4.138) and (4.153). In Section 4.4.2 it was found that a global phase reference is required at the relays in order to allow for coherent forwarding. The phase synchronization scheme presented in Section 5.2.1 is again used to provide that reference. Then,

$$\hat{h}_{\text{R}_l\text{D}} = \hat{h}_{\text{DR}_l} e^{-j\hat{\varphi}_{\text{R}_l\text{M}}} \quad (4.190)$$

is the estimate for the second-hop channel coefficient (cf. (4.157)). The phase estimate $\hat{\varphi}_{\text{R}_l\text{M}} = \varphi_{\text{R}_l\text{M}} - \psi_{\text{R}_l\text{M}}$ is given in (4.147). Since all gain factors are computed from local CSI, the relays do not have to disseminate any coefficients. The gain factor at relay l is

$$g_l = \gamma \cdot e^{j\hat{\varphi}_{\text{R}_l\text{M}}} \hat{h}_{\text{DR}_l}^* \cdot \hat{h}_{\text{SR}_l}^*. \quad (4.191)$$

With (4.191), the actual compound channel (4.180) becomes

$$\tilde{h}_{\text{SRD}} = \gamma \sum_{l=1}^{N_{\text{R}}} \tilde{h}_{\text{R}_l\text{D}} \cdot e^{j\hat{\varphi}_{\text{R}_l\text{M}}} \hat{h}_{\text{DR}_l}^* \hat{h}_{\text{SR}_l}^* \cdot \tilde{h}_{\text{SR}_l} \quad (4.192)$$

and the anticipated one is

$$\hat{h}_{\text{SRD}} = \gamma \sum_{l=1}^{N_{\text{R}}} \left| \hat{h}_{\text{R}_l\text{D}} \right|^2 \left| \hat{h}_{\text{SR}_l} \right|^2. \quad (4.193)$$

Note that for a noiseless gain factor, (4.192) would be

$$\tilde{h}_{\text{SRD}} = \gamma e^{2j\varphi_{\text{M}}} \sum_{l=1}^{N_{\text{R}}} \left| \tilde{h}_{\text{R}_l\text{D}} \right|^2 \left| \tilde{h}_{\text{SR}_l} \right|^2, \quad (4.194)$$

where $\varphi_{\text{R}_l\text{M}} = 2\varphi_{\text{M}} - 2\varphi_{\text{R}_l}$ from (4.148) and

$$\tilde{h}_{\text{DR}_l} = \tilde{h}_{\text{R}_l\text{D}} e^{-2j\varphi_{\text{R}_l}} \quad (4.195)$$

was used. The phase offset $2\varphi_{\text{M}}$ between (4.194) and a noiseless version of (4.193), that is due to the phase synchronization scheme, has to be taken into account when the channel estimation error is computed. The MSE of the anticipated compound channel is therefore

given by

$$e_{\text{SRD}}^{(\text{B1})} = \mathbb{E}_{h,n,\psi} \left[\left| e^{-j(2\varphi_{\text{M}} - 2\varphi_{\text{D}})} \tilde{h}_{\text{SRD}} - \hat{h}_{\text{SRD}} \right|^2 \right]. \quad (4.196)$$

Equation (4.196) can be written as

$$\begin{aligned} e_{\text{SRD}}^{(\text{B1})} &= \gamma^2 \sum_{l=1}^{N_{\text{R}}} \mathbb{E}_{h,n,\psi} \left[\left| \tilde{h}_{\text{DR}_l} \hat{h}_{\text{DR}_l}^* \hat{h}_{\text{SR}_l}^* \tilde{h}_{\text{SR}_l} e^{-j\psi_{\text{R}_l \text{M}}} - \left| \hat{h}_{\text{DR}_l} \right|^2 \left| \hat{h}_{\text{SR}_l} \right|^2 \right|^2 \right] + \\ &+ \gamma^2 \sum_{p=1}^{N_{\text{R}}} \sum_{\substack{q=1 \\ q \neq p}}^{N_{\text{R}}} \mathbb{E}_{h,n,\psi} \left[\left(\tilde{h}_{\text{DR}_p} \hat{h}_{\text{DR}_p}^* \hat{h}_{\text{SR}_p}^* \tilde{h}_{\text{SR}_p} e^{-j\psi_{\text{R}_p \text{M}}} - \left| \hat{h}_{\text{DR}_p} \right|^2 \left| \hat{h}_{\text{SR}_p} \right|^2 \right) \right. \\ &\cdot \mathbb{E}_{h,n,\psi} \left[\left(\tilde{h}_{\text{DR}_q} \hat{h}_{\text{DR}_q}^* \hat{h}_{\text{SR}_q}^* \tilde{h}_{\text{SR}_q} e^{-j\psi_{\text{R}_q \text{M}}} - \left| \hat{h}_{\text{DR}_q} \right|^2 \left| \hat{h}_{\text{SR}_q} \right|^2 \right)^* \right]. \end{aligned} \quad (4.197)$$

The three expectations in (4.197) can be computed independently from each other. The MSE of the equivalent two-hop channel is then given by

$$\begin{aligned} e_{\text{SRD}}^{(\text{B1})} &= \gamma^2 N_{\text{R}} \left(-8c^2 \sigma_{\text{h}}^8 e^{-\frac{1}{2}((1+\tau)\sigma_{\text{pn}}^2 + \sigma_{\text{sn}}^2)} + 4\sigma_{\text{h}}^8 + 4c^2 \sigma_{\text{h}}^8 + c^4 \sigma_{\text{h}}^4 \sigma_{\text{n}}^4 \right) + \\ &+ \gamma^2 (N_{\text{R}}^2 - N_{\text{R}}) \left(c^2 \sigma_{\text{h}}^4 e^{-\frac{1}{2}((1+\tau)\sigma_{\text{pn}}^2 + \sigma_{\text{sn}}^2)} - \sigma_{\text{h}}^4 \right)^2. \end{aligned} \quad (4.198)$$

In order to compare (4.173) with (4.198), $e_{\text{S}_1\text{RD}_1}^{(\text{B1})}$ from (4.173) has to be average over all channel estimates for the case that the gain factors are given in (4.179). The result is easily obtained by replacing $(N_{\text{SD}} - 1 + l) \sigma_{\text{pn}}^2$ in (4.189) by $(N_{\text{SD}} + \tau + m - 1) \sigma_{\text{pn}}^2 + \sigma_{\text{sn}}^2$. For $m = N_{\text{SD}} = 1$ this corresponds to replacing $l \sigma_{\text{pn}}^2$ by $(\tau + 1) \sigma_{\text{pn}}^2 + \sigma_{\text{sn}}^2$. This yields

$$\begin{aligned} \mathbb{E}_{\mathcal{H}} \left[e_{\text{S}_1\text{RD}_1}^{(\text{B1})} \right] &= \\ &= \gamma^2 \left(N_{\text{R}} \left(4\sigma_{\text{h}}^8 + \frac{4}{c^4} \sigma_{\text{h}}^8 + \sigma_{\text{n}}^4 \sigma_{\text{h}}^4 + \frac{4}{c^2} \sigma_{\text{n}}^2 \sigma_{\text{h}}^6 \right) - \frac{8}{c^2} \sigma_{\text{h}}^8 \sum_{l=1}^{N_{\text{R}}} e^{-\frac{1}{2}((\tau+1)\sigma_{\text{pn}}^2 + \sigma_{\text{sn}}^2)} \right) + \\ &+ \gamma^2 \sigma_{\text{h}}^8 \sum_{p=1}^{N_{\text{R}}} \sum_{\substack{q=1 \\ q \neq p}}^{N_{\text{R}}} \left(\frac{1}{c^2} e^{-\frac{1}{2}((\tau+1)\sigma_{\text{pn}}^2 + \sigma_{\text{sn}}^2)} - 1 \right) \left(\frac{1}{c^2} e^{-\frac{1}{2}((\tau+1)\sigma_{\text{pn}}^2 + \sigma_{\text{sn}}^2)} - 1 \right) = \\ &= \gamma^2 N_{\text{R}} \left(4\sigma_{\text{h}}^8 + \frac{4}{c^4} \sigma_{\text{h}}^8 + \sigma_{\text{n}}^4 \sigma_{\text{h}}^4 + \frac{4}{c^2} \sigma_{\text{n}}^2 \sigma_{\text{h}}^6 - \frac{8}{c^2} \sigma_{\text{h}}^8 e^{-\frac{1}{2}((\tau+1)\sigma_{\text{pn}}^2 + \sigma_{\text{sn}}^2)} \right) + \\ &+ \gamma^2 \sigma_{\text{h}}^8 (N_{\text{R}}^2 - N_{\text{R}}) \left(\frac{1}{c^2} e^{-\frac{1}{2}((\tau+1)\sigma_{\text{pn}}^2 + \sigma_{\text{sn}}^2)} - 1 \right)^2. \end{aligned} \quad (4.199)$$

4.4.4 Performance Comparison

This section finally quantitatively compares the quality of the channel estimates produced by protocols A1 and B1 and the accuracy with which the approximations in Sections 4.4.3.4 and 4.4.3.5 judge the performance of the protocols. Note that the results of Sections 4.4.3.4 depend on the gain factors while the results of 4.4.3.5 are independent of the gain allocation scheme. In order to provide quantitative results, the application example presented in Section 4.4.3.6 is considered as example. It comprises a single source-destination pair and N_R relays and the gain factors realize distributed MRC. The results derived in Sections 4.4.3.4 and 4.4.3.5 are used as follows:

- **Section 4.4.3.4:** The quality of the estimates produced by A1 and B1 is compared based on (4.189) and (4.199). The ratio $E_{\hat{\mathcal{H}}} \left[e_{S_1RD_1}^{(A1)} \right] / E_{\hat{\mathcal{H}}} \left[e_{S_1RD_1}^{(B1)} \right]$ is used as figure of merit. It is denoted by 'Fixed estimate MSE'.
- **Section 4.4.3.5:** Since (4.175) depends on the order in which the relays transmit their training sequences, an averaging is performed over all relays:

$$\bar{e}_{RD_1}^{(A1)} = \frac{1}{N_R} \sum_{l=1}^{N_R} e_{R_lD_1}^{(A1)} \quad (4.200)$$

The MSE ratio $\bar{e}_{RD_1}^{(A1)} / e_{RD_1}^{(B1)}$ is then denoted by 'Second-hop MSE', where $e_{R_lD_1}^{(A1)}$ and $e_{RD_1}^{(B1)}$ are given in (4.175) and (4.178), respectively.

As reference, the ratio $e_{SRD}^{(A1)} / e_{SRD}^{(B1)}$ is plotted for the case that $e_{SRD}^{(A1)}$ and $e_{SRD}^{(B1)}$ are given in (4.184) and (4.198), respectively. This case is denoted by 'Two-hop MSE'.

The quality of the channel estimates produced by protocols A1 and B1 can be easily compared by examining the ratio of MSEs. A value larger than one means that the estimates produced by B1 are better than those produced by A1 (they exhibit a smaller MSE with respect to the actual channels). Figs. 4.5 – 4.8 can thus be used to derive a specification which protocol produces better channel estimates (based on the MSE of the estimates) for the application example and a certain set of parameters. The dashed, horizontal line in all plots indicates the points where the performance of protocols A1 and B1 is equal. The estimation SNR is defined in (4.133), where $\sigma_h^2 = 1$. It is assumed to be the same for both the first-hop and the second-hop channel estimates.

In Fig. 4.5 the MSE ratios are plotted versus the number of relays N_R for $\tau = 1$. For small number of relays, Protocol A1 delivers the more accurate channel estimates. Protocol B1 outperforms A1 in terms of estimation accuracy for large N_R because the number of channel

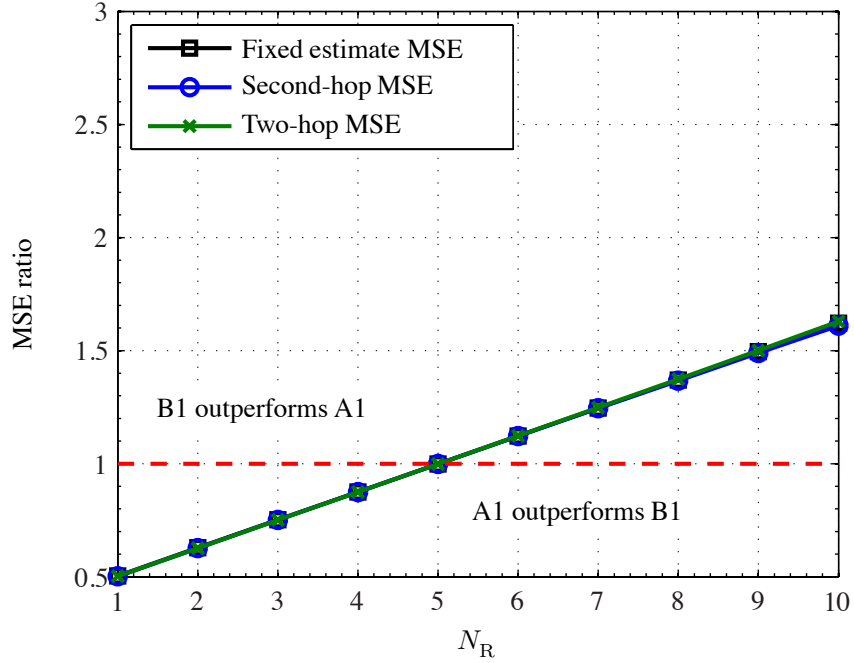


Fig. 4.5: MSE ratios versus N_R for $\tau = 1$, $\text{SNR}_{\text{est}} = 20$ dB, and $\sigma_{\text{pn}}^2 = 10^{-2}$.

uses required by A1 to estimate all coefficients increases with N_R whereas B1 is unaffected (see Table 4.2).

Fig. 4.6 shows the MSE ratios versus τ . Increasing the number of time slots required by the phase synchronization scheme leads to a decreasing quality of the channel estimates obtained by protocol B1. Since protocol A1 does not require phase synchronization, its performance is unaffected.

In Fig. 4.7 the MSE ratio versus the phase noise variance σ_{pn}^2 is depicted. Obviously, phase noise degrades the estimates produced by protocol A1 more than those obtained by B1. The reason for this behavior is that in the present configuration A1 requires more channel uses to estimate all channel coefficients than B1. For large σ_{pn}^2 the performance of both protocols converges because the phases of the channel estimates will asymptotically be uniformly distributed. Furthermore, it can be observed that the comparison based on the results from Section 4.4.3.5 slightly overestimates the performance of protocol A1 for large phase noise variance σ_{pn}^2 .

The MSE ratios versus the estimation SNR are shown in Fig. 4.8. The quality of the estimates produced by protocol B1 suffers more from decreasing SNR_{est} than A1. The reason for this behavior is that, apart from the channel coefficients, the phase values have to be estimated for the phase synchronization scheme. This is an additional source of error that

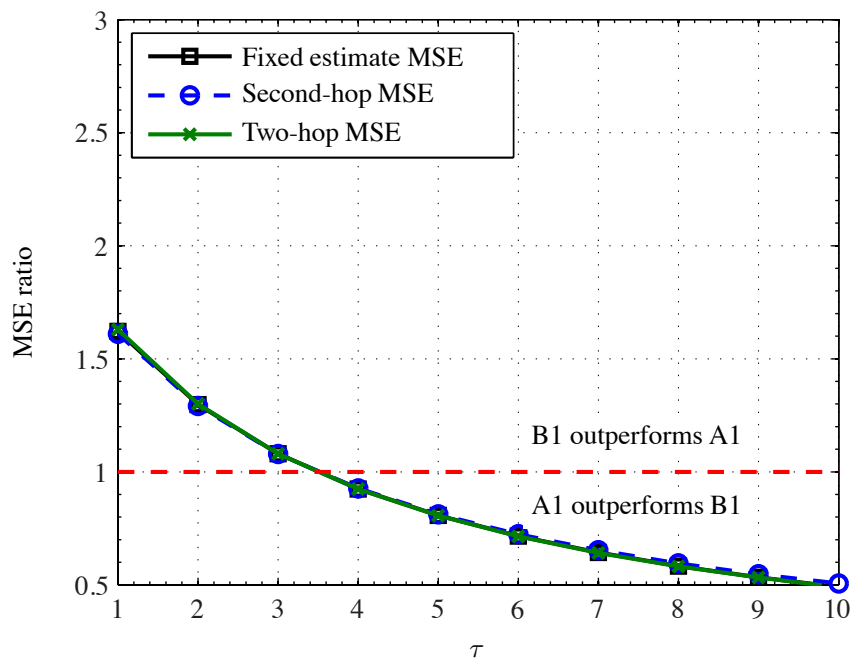


Fig. 4.6: MSE ratios versus τ for $N_R = 10$, $\text{SNR}_{\text{est}} = 20$ dB, and $\sigma_{\text{pn}}^2 = 10^{-2}$.

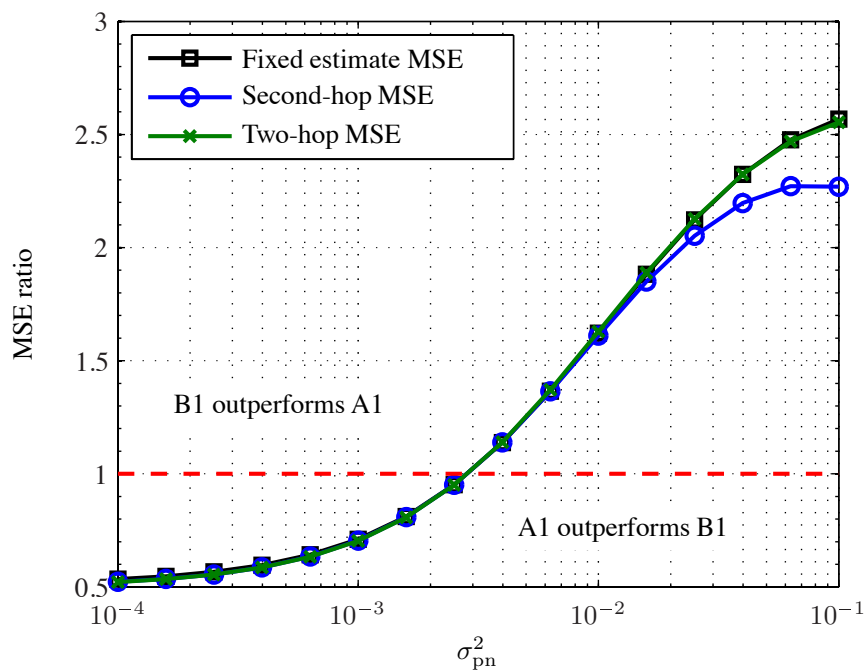


Fig. 4.7: MSE ratios versus σ_{pn}^2 for $N_R = 10$, $\tau = 1$, and $\text{SNR}_{\text{est}} = 20$ dB.

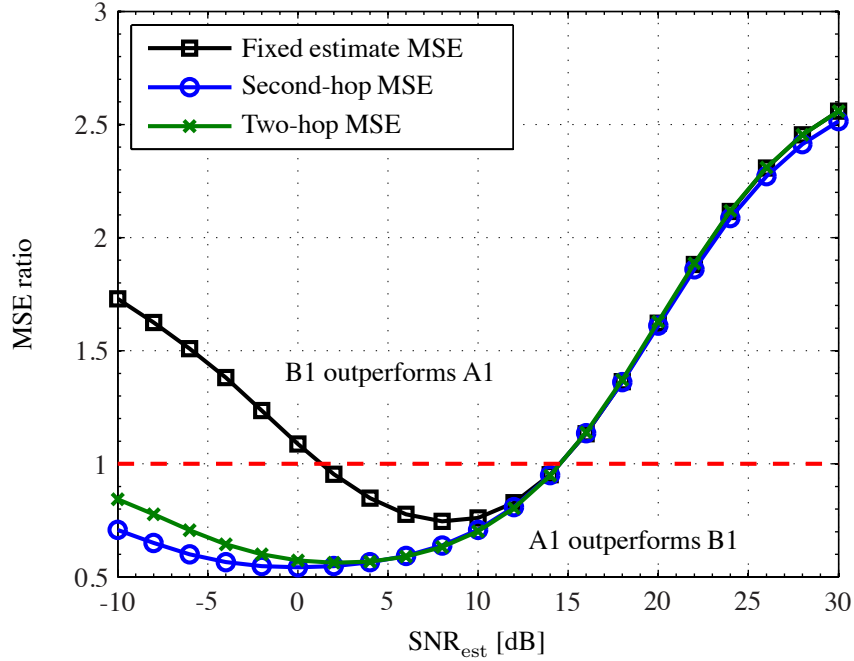


Fig. 4.8: MSE ratios versus SNR_{est} for $N_R = 10$, $\tau = 1$, and $\sigma_{\text{pn}}^2 = 10^{-2}$.

degrades performance. However, for large SNR_{est} the impact of additive noise becomes negligible and the fact that protocol A1 suffers more from phase noise than B1 dominates. Protocol B1 thus outperforms A1 at high SNR_{est} . For low estimation SNR the comparison based on Section 4.4.3.4 extremely overestimates the performance of protocol B1.

Comparing the curves to the respective references ('Two-hop MSE') shows that the measure in Section 4.4.3.4 ('Fixed estimate MSE') is very accurate for high estimation SNR (from about 15 dB). Furthermore, the measure in Section 4.4.3.5 ('Second-hop MSE') is very accurate for medium estimation SNR ($5 \text{ dB} \leq \text{SNR}_{\text{est}} \leq 20 \text{ dB}$) and low phase noise ($\sigma_{\text{pn}}^2 \leq 10^{-2}$). In the respective range of parameters both measures are able to judge the performance of both channel estimation protocols very well.

Chapter 5

Distributed Phase Synchronization

This chapter is divided into two parts that discuss different aspects of distributed phase synchronization. The first (smaller) part given in **Section 5.1** shows how a common beacon signal can alleviate the degrading effect of relay phase noise on the performance of traffic pattern IV. The beacon does not, however, provide a global phase reference because individual propagation distances from the beacon terminal, i.e., the terminal transmitting the beacon signal, to each relay introduce unknown phase shifts.

The second part given in **Section 5.2** disregards phase noise and discusses schemes to provide a global phase reference at a set of relay nodes. In Section 4.2 it was shown that, depending on the direction of channel measurement, distributed coherent beamforming requires a certain set of nodes to have a common phase reference. This means that the LO phases of the respective nodes have to be equal. They may exhibit an unknown and random phase offset, but it has to be the same for all of them. In **Section 5.2.1** a simple scheme to provide this global phase reference for multiple relays is presented. It is based on a master-slave architecture where one node is assigned master, all others are slaves. A broadband training sequence is used to estimate a scalar phase compensation value locally at each slave. Frequency diversity and antenna diversity can both be exploited by the scheme. This makes it very robust to deep fades on single subchannels. The achieved coding gain helps to further enhance the estimation accuracy.

A slightly different approach that has been presented by other authors in [161] is shortly revisited in **Section 5.2.2**. It is also based on a master-slave architecture but has the disadvantage that neither frequency nor antenna diversity can be exploited. Based on a simple example with a single source, multiple relays and a remote destination, the performance of both schemes is finally compared in **Section 5.2.3**.

5.1 Relay Phase Noise

In Section 4.2.2 the compound channel matrices of a system with multiple sources, relays, and destination were

$$\tilde{\mathbf{H}}_{\text{I}} = \Gamma_{\text{D}} \tilde{\mathbf{H}}_{\text{SD}} + \tilde{\mathbf{H}}_{\text{RD}} \mathbf{G} \tilde{\mathbf{H}}_{\text{SR}} + \tilde{\mathbf{H}}_{\text{SD}} \Gamma_{\text{S}}, \quad (5.1)$$

$$\tilde{\mathbf{H}}_{\text{II}} = \Gamma_{\text{D}} \tilde{\mathbf{H}}_{\text{SD}} + \tilde{\mathbf{H}}_{\text{RD}} \mathbf{G} \tilde{\mathbf{H}}_{\text{SR}}, \quad (5.2)$$

$$\tilde{\mathbf{H}}_{\text{III}} = \tilde{\mathbf{H}}_{\text{RD}} \mathbf{G} \tilde{\mathbf{H}}_{\text{SR}} + \tilde{\mathbf{H}}_{\text{SD}} \Gamma_{\text{S}}, \quad (5.3)$$

$$\text{and } \tilde{\mathbf{H}}_{\text{IV}} = \tilde{\mathbf{H}}_{\text{RD}} \mathbf{G} \tilde{\mathbf{H}}_{\text{SR}} \quad (5.4)$$

for traffic patterns I – IV, respectively (cf. (4.25)). If the relay phases do not change during the time between reception and retransmission, they are independent of Φ_{R} . In this case, the unknown and random LO phases of the relays do not have an impact on the received signals at the destinations. In the presence of relay phase noise, a phase error θ_{R_l} is introduced to the signal at each relay l . The compound channel matrices become

$$\tilde{\mathbf{H}}_{\text{I}} = \Gamma_{\text{D}} \tilde{\mathbf{H}}_{\text{SD}} + \tilde{\mathbf{H}}_{\text{RD}} \Theta_{\text{R}} \mathbf{G} \tilde{\mathbf{H}}_{\text{SR}} + \tilde{\mathbf{H}}_{\text{SD}} \Gamma_{\text{S}}, \quad (5.5)$$

$$\tilde{\mathbf{H}}_{\text{II}} = \Gamma_{\text{D}} \tilde{\mathbf{H}}_{\text{SD}} + \tilde{\mathbf{H}}_{\text{RD}} \Theta_{\text{R}} \mathbf{G} \tilde{\mathbf{H}}_{\text{SR}}, \quad (5.6)$$

$$\tilde{\mathbf{H}}_{\text{III}} = \tilde{\mathbf{H}}_{\text{RD}} \Theta_{\text{R}} \mathbf{G} \tilde{\mathbf{H}}_{\text{SR}} + \tilde{\mathbf{H}}_{\text{SD}} \Gamma_{\text{S}}, \quad (5.7)$$

$$\tilde{\mathbf{H}}_{\text{IV}} = \tilde{\mathbf{H}}_{\text{RD}} \Theta_{\text{R}} \mathbf{G} \tilde{\mathbf{H}}_{\text{SR}}, \quad (5.8)$$

where Θ_{R} is a diagonal matrix defined as

$$\Theta_{\text{R}} = \begin{bmatrix} e^{j\theta_{\text{R}_1}} & & & \\ & \ddots & & \\ & & \ddots & \\ & & & e^{j\theta_{\text{R}_{N_{\text{R}}}}} \end{bmatrix}. \quad (5.9)$$

It comprises the phase errors that are introduced at the relays due to phase noise. Coherency is clearly destroyed by Θ_{R} because the signal paths no longer combine as desired by the gain allocation. In the following section it will be shown that coherency can be preserved for traffic pattern IV if the relays synchronize their LO phases to a simple beacon signal even if the beacon is subject to phase noise.

5.1.1 Phase Beacon at the Relays

Assume that all relays synchronize their LOs to a common phase beacon. The individual propagation distances from the beacon terminal, i.e., the terminal transmitting the beacon signal, to each relay introduces unknown phase shifts. The LOs of the relays will thus exhibit different phase offsets with respect to a global reference even if their PLLs can follow the beacon phase perfectly. Let φ_b denote the unknown phase of the beacon signal at the time the relays receive the signals from the sources. It is assumed to remain constant for one signal burst. The phase reference at relay node l at this time is then

$$\varphi_{R_l} = \varphi_{h,l} + \varphi_b, \quad (5.10)$$

where $\varphi_{h,l}$ is the phase shift due to propagation delay between the beacon terminal and relay l . If all relays adjust their phases perfectly to the beacon signal the phase matrix Φ_R becomes

$$\Phi_R = \text{diag} \left(e^{j\varphi_{h1}}, \dots, e^{j\varphi_{hN_R}} \right) \cdot e^{j\varphi_b}. \quad (5.11)$$

Obviously, the relays are not provided with a global phase reference because their LO phases are still different. The LO of the beacon node is subject to phase noise as is the case for all other nodes. Assume that the beacon phase is $\varphi_b + \psi_b$ when the relays retransmit their signals to the destinations, where ψ_b is the phase change due to phase noise. As long as the propagation channels (and thus φ_{h_l}) stay constant, the phase differences between the LOs of the relays are constant because they are subject to the same phase noise process. The phase noise matrix is in this case given by

$$\Theta_R = e^{j\psi_b} \mathbf{I}_{N_R}. \quad (5.12)$$

Inserting (5.12) into (5.5) – (5.8) delivers the compound channel matrices

$$\tilde{\mathbf{H}}_I = \Gamma_D \tilde{\mathbf{H}}_{SD} + e^{j\psi_b} \tilde{\mathbf{H}}_{RD} \mathbf{G} \tilde{\mathbf{H}}_{SR} + \tilde{\mathbf{H}}_{SD} \Gamma_S, \quad (5.13)$$

$$\tilde{\mathbf{H}}_{II} = \Gamma_D \tilde{\mathbf{H}}_{SD} + e^{j\psi_b} \tilde{\mathbf{H}}_{RD} \mathbf{G} \tilde{\mathbf{H}}_{SR}, \quad (5.14)$$

$$\tilde{\mathbf{H}}_{III} = e^{j\psi_b} \tilde{\mathbf{H}}_{RD} \mathbf{G} \tilde{\mathbf{H}}_{SR} + \tilde{\mathbf{H}}_{SD} \Gamma_S, \quad (5.15)$$

$$\text{and } \tilde{\mathbf{H}}_{IV} = e^{j\psi_b} \tilde{\mathbf{H}}_{RD} \mathbf{G} \tilde{\mathbf{H}}_{SR}. \quad (5.16)$$

The multiplication with the scalar $e^{j\psi_b}$ in $\tilde{\mathbf{H}}_{IV}$ corresponds to a random rotation of the whole signal space. This means that although $\tilde{\mathbf{H}}_{IV}$ changes with the phase of the beacon node, the

SINR at the destinations is not influenced. Cheap terminals with unstable LOs can consequently be used as relays if they synchronize their LO phases to a simple beacon signal.

For $\tilde{\mathbf{H}}_{\text{I}} - \tilde{\mathbf{H}}_{\text{III}}$ coherency¹ is destroyed by the multiplication with $e^{j\psi_b}$. However, if the beacon node exhibits less phase noise than the relays, system performance can still be enhanced compared to the case where the LOs of the relays run freely. This performance gain is bought at the cost of a higher system complexity.

5.1.2 Phase Error

The assumption that the PLLs of the relays can follow the beacon signal perfectly is not true in practical systems. In reality there will be noise and the beacon channel is subject to fading. Its quality will thus be different for each relay. When an unmodulated carrier is broadcasted from a terminal for the purpose of providing synchronization to all relays, the PLL in each relay will be tracking a sinusoidal signal of the form (e.g. [163])

$$b(t) = A_c \cos(2\pi f_c t + \varphi(t)). \quad (5.17)$$

This signal is corrupted by additive narrowband noise

$$n(t) = x(t)\cos(2\pi f_c t) - y(t)\sin(2\pi f_c t). \quad (5.18)$$

The in-phase and quadrature components of the noise are assumed to be statistically independent, stationary Gaussian noise processes with (two-sided) power spectral density $\frac{1}{2}N_0$ W/Hz. The output of the VCO in the PLL is $\hat{\varphi}$ which is an estimate of the actual phase value φ . For a first-order loop the pdf of the phase error $\Delta\varphi = \hat{\varphi} - \varphi$ has the form [163]

$$P(\Delta\varphi) = \frac{\exp(\rho \cdot \cos(\Delta\varphi))}{2\pi I_0(\rho)}, \quad (5.19)$$

where $I_0(\cdot)$ is the modified Bessel function of order zero. ρ is the SNR within the closed-loop bandwidth and is defined as

$$\rho = \frac{A_c^2}{N_0 B_c}, \quad (5.20)$$

where B_c is the (one-sided) noise equivalent bandwidth of the loop. The pdf in (5.19) corresponds to *von Mises distribution* $\mathcal{VM}(0, \kappa)$ for $\kappa = \rho$. Much of the statistical theory

¹Coherency means in this case the coherent addition of all signals at the destinations.

associated with this distribution is analytically intractable. The problem of efficient generation of a pseudo-random observation from $\mathcal{VM}(0, \kappa)$ has been investigated in [189]. For the simulations in Section 5.2.3.2, the algorithm was implemented using the wrapped Cauchy distribution (section 4 in [189]) to generate random variables $\Delta\varphi \sim \mathcal{VM}(0, \rho)$.

5.2 Distributed Phase Synchronization Schemes

Synchronizing a set of distributed wireless terminals with a single narrow-band beacon signal in a fading environment may lead to inaccurate results. If one or more beacon channels are in a deep fade, the phase and frequency synchronization at the respective nodes is very bad. Since the resulting phase error has a strong impact on the system performance, a practical system may want to exploit frequency diversity. In Section 5.2.1 a simple scheme is presented that achieves carrier phase synchronization of a set of distributed relay nodes. Broadband training sequences are used to estimate a scalar phase compensation value locally at each relay. Frequency diversity can be exploited because of the broadband nature of the sequences. This makes the scheme very robust to deep fades on single subchannels. The achieved coding gain helps to further enhance the estimation accuracy.

The introduced phase synchronization scheme is based on a master-slave architecture: A single node in the network is assigned 'master' M. The set of nodes that are to be synchronized, i.e. the relays, are called 'slaves'. The scheme will be referred to as 'slave-based (SB)' because the computational load is distributed equally among all slave nodes. For the moment, additive signal noise is omitted. Furthermore, reciprocity of the propagation channels is assumed.

In order to have a performance reference for the scheme, Section 5.2.2 shortly introduces a scheme for global phase synchronization that has been presented in [161] and is treated also in [190, 191]. It is based on a master providing the clock for distributed slave nodes using a beacon signal. The unknown phase changes due to propagation delay between master and slaves are estimated by the master up to an uncertainty of π using a bounce-back scheme. This scheme will be referred to as 'master-based (MB)' because the computational load is mainly with the master node. It disseminates its phase estimate to each slave which in turn uses the information to adjust a local PLL to tune to the beacon of the master.

5.2.1 Slave-Based Scheme

This section starts by giving a short summary of the idea behind the SB scheme. A more detailed discussion follows. Consider a generic distributed wireless network where N terminals require a common LO phase reference. The nodes that are to be synchronized become the slaves S_i , $i \in \{1, \dots, N\}$ for which a master M provides the phase reference. Let φ_{S_i} and φ_M denote the current LO phases of slave i and the master node, respectively. All slaves transmit a sequence $p_i[n]$ to the master node which retransmits the conjugate complex of its received signal. From its own received signal, each slave can then locally generate an estimate of $-2\varphi_{S_i} + 2\varphi_M$ which is two times the difference between the respective LO phases. When all slaves transmit their sequence $p_i[n]$ *concurrently* to the master, the whole scheme uses two time slots, independent of the number of participating nodes N . However, the slaves cause interference to each other which degrades the quality of the phase estimation. No interference occurs when the slaves use orthogonal channels to transmit their sequences to the master node. The phase estimation thus improves, but $2N$ channel uses are required to synchronize a network of N slaves.

Cyclically shifted m-sequences can be used when synchronizing the carrier phase of all slaves at the same time. Let $m[n]$ denote an m-sequence of length T_m . Slave i uses the sequence $p_i[n] = m_i[n]$, where $m_i[n]$ is obtained by shifting $m[n]$ cyclically by $\lfloor (i-1) \frac{T_m}{N} \rfloor$ samples. The correlation properties of the m-sequence yield

$$\sum_{n=0}^{T_m-1} p_i[n] p_j^*[n] = \begin{cases} T_m & \text{for } i = j \\ -1 & \text{for } i \neq j \end{cases} \quad (5.21)$$

Thus, the interference generated by all other slaves $S_{j, j \neq i}$ to S_i can be made small when T_m is large. m-sequences have, apart from the small dc component, a flat frequency spectrum. This means that they exhibit the same power in all frequency bins and the scheme benefits from frequency diversity. The impulse response of the channel from slave S_i to the master node M is modeled as a tapped delay line. It is denoted by $h_{S_i M}[n]$ and has a length of T_h taps. It is assumed that all nodes are perfectly frequency matched. The details for the case that all training sequences are transmitted on the same physical channel (concurrent synchronization strategy) are as follows:

- 0) Initially, every slave S_i is assigned one sequence $p_i[n]$ that is generated as described above.
- 1) All slaves transmit their respective baseband signals $s_i^{(\text{tx})}[n] = p_i[n]$ simultaneously to the master node.

2) The baseband received sequence of the master node is then given by

$$d^{(\text{rx})}[n] = e^{-j\varphi_M} \sum_{i=1}^N \left(p_i[n] \circledast h_{S_iM}[n] \cdot e^{j\varphi_{S_i}} \right) + n_M[n], \quad (5.22)$$

where $n_M[n]$ comprises the AWGN samples at the master node.

3) The master calculates

$$d^{(\text{tx})}[n] = \left(d^{(\text{rx})}[-n + T_{h,m}] \right)^* \quad (5.23)$$

and broadcasts this signal to all slaves. The time shift by $T_{h,m} := T_m + T_h - 1$ is used to make the transmit signal causal.

4) Slave i receives the baseband signal

$$s_i^{(\text{rx})}[n] = d^{(\text{tx})}[n] \circledast h_{S_iM}[n] \cdot e^{j(-\varphi_{S_i} + \varphi_M)}. \quad (5.24)$$

5) Knowing all used phase estimation sequences $p_i[n]$, each slave computes

$$c_i[n] = p_i[n] \circledast s_i^{(\text{rx})}[n] := c_i^{(S)}[n] + c_i^{(I)}[n] + c_i^{(N)}[n], \quad (5.25)$$

where $c_i^{(S)}[n]$, $c_i^{(I)}[n]$, and $c_i^{(N)}[n]$ are the signal, interference, and noise components of $c_i[n]$, respectively. The signal part $c_i^{(S)}[n]$ is given by

$$c_i^{(S)}[n] = p_i[n] \circledast p_i^*[-n + T_{h,m}] \circledast h_{S_iM}^*[-n + T_{h,m}] \circledast h_{S_iM}[n] \cdot e^{j(-2\varphi_{S_i} + 2\varphi_M)}, \quad (5.26)$$

the interference part by

$$c_i^{(I)}[n] = \sum_{\substack{j=1 \\ j \neq i}}^N p_i[n] \circledast p_j^*[-n + T_{h,m}] \circledast h_{S_jM}^*[-n + T_{h,m}] \circledast h_{S_iM}[n] \cdot e^{j(-\varphi_{S_i} - \varphi_{S_j} + 2\varphi_M)}, \quad (5.27)$$

and the noise part by

$$c_i^{(N)}[n] = p_i[n] \circledast h_{S_iM}[n] \circledast n_M^*[-n + T_{h,m}] \cdot e^{j(-\varphi_{S_i} + \varphi_M)} + n_{S_i}[n], \quad (5.28)$$

where $n_{S_i}[n]$ comprises the AWGN samples at slave i . Equation (5.26) can be written

as

$$c_i^{(S)}[n] = c_{p_i}^{(S)}[n] \circledast c_{h_i}^{(S)}[n] \cdot e^{j(-2\varphi_{S_i} + 2\varphi_M)}, \quad (5.29)$$

where

$$c_{p_i}^{(S)}[n] = p_i[n] \circledast p_i^*[-n + T_{h,m}] \quad (5.30)$$

$$c_{h_i}^{(S)}[n] = h_{S_i,M}^*[-n + T_{h,m}] \circledast h_{S_i,M}[n]. \quad (5.31)$$

Since $c_{p_i}^{(S)}[T_m] = T_m$ due to the correlation properties of the m-sequences and $\angle \{c_{h_i}^{(S)}[T_h]\} = 0$, it is not difficult to see that

$$\angle \{c_i^{(S)}[T_m + T_h - 1]\} = -2\varphi_{S_i} + 2\varphi_M := \varphi_{S_i,M}. \quad (5.32)$$

Assuming that the interference and noise components are small, each slave S_i finally has an estimate $\hat{\varphi}_{S_i,M} = \angle \{c_i[T_{h,m}]\}$ of $\varphi_{S_i,M}$ with phase estimation error

$$\Delta\varphi_{S_i}^{(SB)} = \hat{\varphi}_{S_i,M} - \varphi_{S_i,M}. \quad (5.33)$$

Note that for the sequential synchronization strategy the interference term (5.27) is zero.

In those cases where a global LO phase reference at the relays is required (e.g., if both the first-hop and the second-hop channels are estimated at the relays; cf. Table 4.1 in Section 4.2.11), knowing $\varphi_{S_i,M}$ enables relay S_i to compensate the unwanted impact of its LO phase on the signal. It is sufficient for each relay to know two times the phase difference between its own LO phase and the LO phase of the master node because effectively, the phase error of the product channel has to be compensated (cf. Section 5.2.3.1 for an application example).

5.2.2 Master-Based Scheme

A different approach to provide multiple distributed nodes with a common LO phase reference has been proposed for example in [161, 190]. It is also based on a master-slave architecture. Only now, the master node broadcasts a sinusoidal reference signal. It arrives at each slave S_i with a phase offset of $\varphi_i = \varphi_M - \varphi_{S_i} + \varphi_{h_i}$, where φ_M is the current LO phase of the master, φ_{S_i} the current LO phase of the respective slave, and φ_{h_i} a phase offset due to

the propagation delay between master and slave S_i . Having received the reference signal, the slaves sequentially retransmit it back to the master. When their LO phases stay constant for this time, the master receives a signal from which it can measure $2\varphi_{h_i}$. Denoting the estimation error by $\Delta\varphi_{S_i}^{(\text{MB})} = 2\Delta\varphi_{h_i}$, the estimate can be written as $\widehat{2\varphi_{h_i}} = 2\varphi_{h_i} + 2\Delta\varphi_{h_i}$ (please note specifically that the 'hat' is above $2\varphi_{h_i}$ and not only above φ_{h_i} because the master can only estimate two times the channel phase). The master node then computes

$$\frac{1}{2} \left(\widehat{2\varphi_{h_i}} \right) = \begin{cases} \varphi_{h_i} + \Delta\varphi_{h_i} & \text{for } \varphi_{h_i} < \pi \\ \varphi_{h_i} + \Delta\varphi_{h_i} - \pi & \text{for } \varphi_{h_i} \geq \pi \end{cases} \quad (5.34)$$

and feeds this information back to each respective slave. The π -ambiguity in (5.34) comes from the modulo nature of the phase. The slaves use the knowledge of $\frac{1}{2} \left(\widehat{2\varphi_{h_i}} \right)$ together with the received reference signal to generate a phase synchronized oscillator signal. Assuming they can perfectly track the beacon signal of the master node, their LO phase offset is

$$\begin{aligned} \varphi_{S_i} &= \varphi_M + \varphi_{h_i} - \frac{1}{2} \left(\widehat{2\varphi_{h_i}} \right) = \\ &= \begin{cases} \varphi_M - \Delta\varphi_{h_i} & \text{for } \varphi_{h_i} < \pi \\ \varphi_M - \Delta\varphi_{h_i} + \pi & \text{for } \varphi_{h_i} \geq \pi \end{cases} \end{aligned} \quad (5.35)$$

Obviously, the π -ambiguity is still in the LO phases of the relays even if the estimate is perfect. In those cases where a global phase reference at the relays is required (e.g., if both the first-hop and the second-hop channels are estimated at the relays; cf. Table 4.1 in Section 4.2.11), this uncertainty affects both the estimates of the first-hop and the second-hop channels in the same way. Consequently, in the estimated product channel coefficients, being the product of the first-hop and second-hop channel estimates, the ambiguity becomes 2π and thus vanishes (cf. Section 5.2.3.1 for an application example).

5.2.3 Comparison

Comparing the SB and MB schemes, the following observations can be made:

Slave-based scheme (SB):

- Due to the broadband nature of the phase estimation sequences, frequency diversity (being present in a frequency selective channel) can be exploited.
- Multiple slave antennas provide a diversity gain by simple antenna selection if the LO phase offset is the same for all employed antennas.

- As the computational load is distributed equally among the network, any simple AF node can act as master.
- By dynamically adjusting the sequence length T_m , estimation accuracy (T_m large) can be easily traded for system resources (T_m small).

Master-based scheme (MB):

- In a frequency selective environment the master reference signal might be in a deep fade for some of the nodes. As a consequence, the phase synchronization will be very imprecise in this case.
- The scheme does not benefit from multiple antennas at the slaves because the estimate of $2\varphi_{h_i}$ has to be calculated for each slave antenna individually.
- The master node has to perform much more calculations than the slaves. This means that the computational load is not distributed equally among the network. As a consequence, there are systems where not every node is suited to act as master. Restricting the set of potential master nodes is surely disadvantageous.
- In a mobile environment the overhead to synchronize a large number of nodes might be prohibitive as the slaves have to be synchronized sequentially. Note that multiple slaves could be synchronized concurrently if the master used several beacon signals at different frequencies. However, the slaves would have to be equipped with different hardware in this case because their PLLs need to be designed for the respective beacon frequency. In ad-hoc networks this does not seem to be practical.

In order to quantify the implications of the above statements, a simple application scenario is considered. The performance of the two phase synchronization schemes is then assessed in MATLAB[®].

5.2.3.1 Application Example

Consider a scenario with a cluster of $N_R + 1$ wireless sensor nodes employing a single antenna each. One of the nodes (in the following referred to as source S) wants to transmit data to a remote destination D. Due to its small size and limited power supply, a single node out of the cluster is not able to reach the destination on its own. However, when they cooperate to form a distributed array, the sensor nodes are able to cover a much larger distance using distributed MRC. In Section 5.2.1 the SB phase synchronization scheme was developed considering frequency-selective channels. Now, the impact of the phase synchronization error on the performance of the present scenario is investigated. Therefore, it suffices to consider

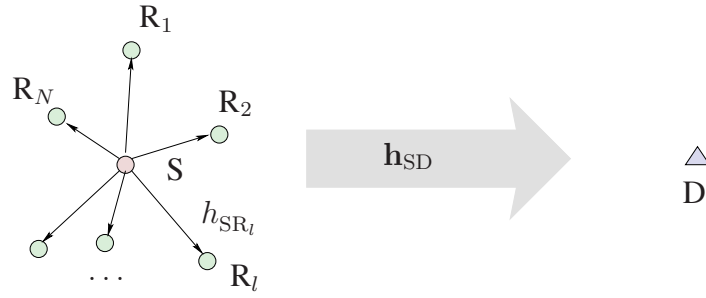


Fig. 5.1: Distributed beamforming scenario

frequency-flat Rayleigh fading channels. All channel coefficients are assumed to be independent, identically distributed (iid), complex normal random variables with zero mean and variance σ_h^2 . Since it wouldn't have an impact on the results of the comparison, all channel estimates are furthermore assumed to be noiseless.

In order to achieve a coherent addition of all signal at the destination, all nodes have to transmit the same information but with a different precompensation factor g_l to compensate for their individual propagation channel to the destination and their LO phase offset. The question arises how the transmit data can be shared among the nodes. One approach that certainly suggests itself is to distribute this information over the air. The source node therefore broadcasts its data to all other nodes that act as AF relays R_l , $l \in \{1, \dots, N\}$. In Fig. 5.1 the above mentioned scenario is depicted. Note that this is the same scenario as considered in [161]. Assume that every relay has a noiseless estimate of its local equivalent first-hop channel \tilde{h}_{SR_l} in forward direction and of its local equivalent second-hop channel \tilde{h}_{R_lD} in backward direction. In order to forward their data coherently, the relays require a global phase reference (cf. Section 4.2). The schemes presented in Sections 5.2.1 and 5.2.2 are subsequently used to provide that reference. One node out of the whole set of sensors is assigned *master* while all other sensor nodes are *slaves*. The master has to provide a global phase reference to the *slaves*. In the following it is assumed that the source acts as master while all relays are slaves.

SB scheme: Every relay R_l obtains an estimate $\hat{\varphi}_{R_lM}$ of φ_{R_lM} as described in Section 5.2.1.

It then multiplies its estimated product channel

$$\hat{h}_{SR_lD} = h_{R_lD} h_{SR_l} e^{j(\varphi_S - 2\varphi_{R_l} + \varphi_D)} \quad (5.36)$$

with $e^{-j\hat{\varphi}_{R_lM}}$. In case the phase estimation is perfect, i.e. $\hat{\varphi}_{R_lM} = \varphi_{R_lM}$, it can compute

$$\hat{h}_{\text{SR}_i\text{D}} \cdot e^{-j\hat{\varphi}_{\text{R}_i\text{M}}} = h_{\text{R}_i\text{D}} h_{\text{SR}_i} e^{j(\varphi_{\text{S}} - 2\varphi_{\text{M}} + \varphi_{\text{D}})}, \quad (5.37)$$

which does not depend on the relay phases and thus allows the signals from all relays to add up coherently at the destination antenna.

MB scheme: All relays have, apart from a π -ambiguity the same LO phase reference. Their estimated product channel coefficient then is

$$\hat{h}_{\text{SR}_i\text{D}} = h_{\text{R}_i\text{D}} h_{\text{SR}_i} e^{j(\varphi_{\text{S}} - 2\varphi_{\text{M}} + \varphi_{\text{D}})}, \quad (5.38)$$

which is the same as (5.37).

The phase values φ_{S} , φ_{M} , and φ_{D} in (5.37) and (5.38) are the LO phases at the time the phase synchronization is performed. Assume that the source S wants to transmit the complex baseband data symbol s to the remote destination D. All relays form a distributed antenna array to assist the communication. Knowing either (5.37) or (5.38) the relays choose their gain factors as

$$\begin{aligned} g_l &= \gamma_l \cdot \tilde{g}_l = \\ &= \gamma_l \cdot h_{\text{R}_i\text{D}}^* h_{\text{SR}_i}^* e^{j(-\varphi_{\text{S}} + 2\varphi_{\text{M}} - \varphi_{\text{D}})} \end{aligned} \quad (5.39)$$

in order to achieve distributed maximum ratio combining at the destination antenna. The real-valued scalar

$$\gamma_l = \sqrt{\frac{P_{\text{R}}}{|\tilde{g}_l|^2 (\sigma_{\text{s}}^2 \sigma_{\text{h}}^2 + \sigma_{n_{\text{R}_i}}^2)}} \quad (5.40)$$

ensures that the average relay sum transmit power is equal to a specified value P_{R} . Transmission from source to destination follows a two-hop traffic pattern consuming two time slots. The destination receives

$$d = e^{j\varphi_{\text{signal}}} \cdot \sum_{l=1}^{N_{\text{R}}} \gamma_l |h_{\text{SR}_l}|^2 |h_{\text{R}_l\text{D}}|^2 s + e^{j\varphi_{\text{noise}}} \cdot \sum_{l=1}^N \gamma_l h_{\text{SR}_l}^* |h_{\text{R}_l\text{D}}|^2 n_{\text{R}_l} + n_{\text{D}}, \quad (5.41)$$

where φ_{signal} and φ_{noise} are real-valued random variables that depend on φ_{M} and the LO

phases of the source and destination node. Equation (5.41) can be split into a signal part

$$d_{\text{signal}} = e^{j\varphi_{\text{signal}}} \cdot \sum_{l=1}^{N_R} \gamma_l |h_{\text{SR}_l}|^2 |h_{\text{R}_l\text{D}}|^2 s \quad (5.42)$$

and a noise part

$$d_{\text{noise}} = e^{j\varphi_{\text{noise}}} \cdot \sum_{l=1}^N \gamma_l h_{\text{SR}_l}^* |h_{\text{R}_l\text{D}}|^2 n_{\text{R}_l} + n_{\text{D}}. \quad (5.43)$$

Obviously, the signals of all relays add up constructively at the destination antenna yielding maximum receive SNR. In order to decode the signal, the destination has to estimate and compensate the phase φ_{signal} of the equivalent two-hop (source-relays-destination) channel. Once the gain factors are computed this can be done using a training sequence that is transmitted by the source.

5.2.3.2 Simulation Results

Consider the application example in Section 5.2.3.1. Monte-Carlo simulations were performed to compare the performance of the SB and MB carrier phase synchronization schemes in this scenario. For the SB scheme a distinction between sequential and concurrent phase estimation is made (cf. Section 5.2.1). Sequential phase estimation occupies $2N_R$ channel uses but there is no interference. In contrast to that, it only takes two channel uses to concurrently synchronize all slaves but interference will decrease the performance. First, the estimation errors of the two schemes are investigated. Then the impact of phase estimation errors on the performance of the distributed beamforming scheme from section 5.2.3.1 is investigated.

The propagation channels between master node M and all N_R slaves are modeled to exhibit frequency-selective Rayleigh fading with impulse responses $h_{\text{R}_l\text{M}}[n]$, where $l \in \{1, \dots, N_R\}$ and $n \in \{0, \dots, T_h - 1\}$. The average path strengths are chosen according to the Hiperlan channel model A [178] with a bandwidth of 100 MHz and an average rms delay spread of 50 ns. It corresponds to a typical office environment. The channel impulse responses are normalized such that their average total power is equal to one. In Figs. 5.2 and 5.3 the average power delay profile and a typical transfer function of a Hiperlan A channel are plotted, respectively. The tapped delay line model of the Hiperlan A model consists of 40 relevant taps with a resolution of 10 ns. The transfer function is quite frequency-selective, but the fades are not very deep. For the simulations a block fading environment is

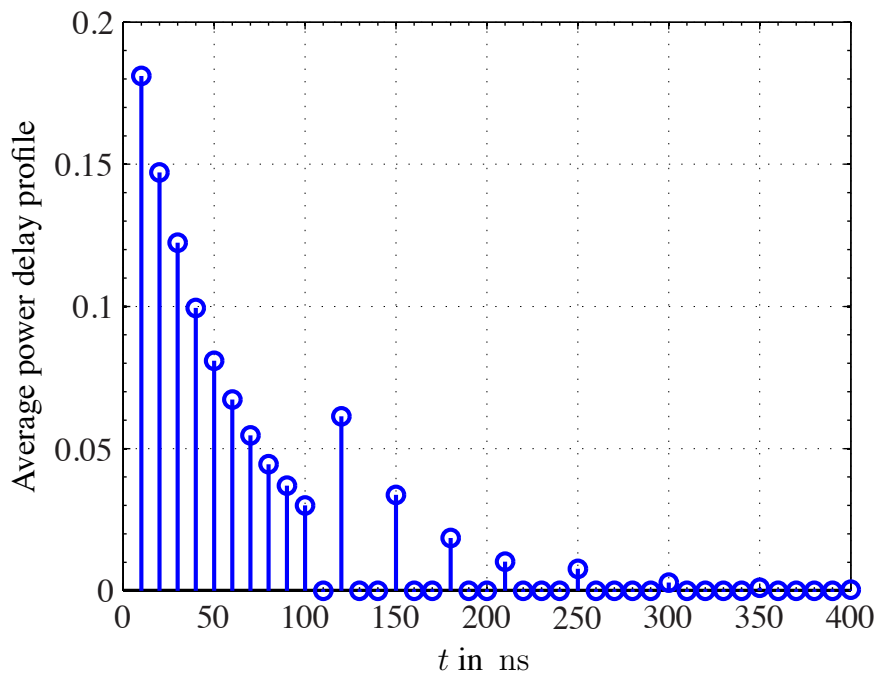


Fig. 5.2: Average power delay profile of the Hiperlan A channel model.

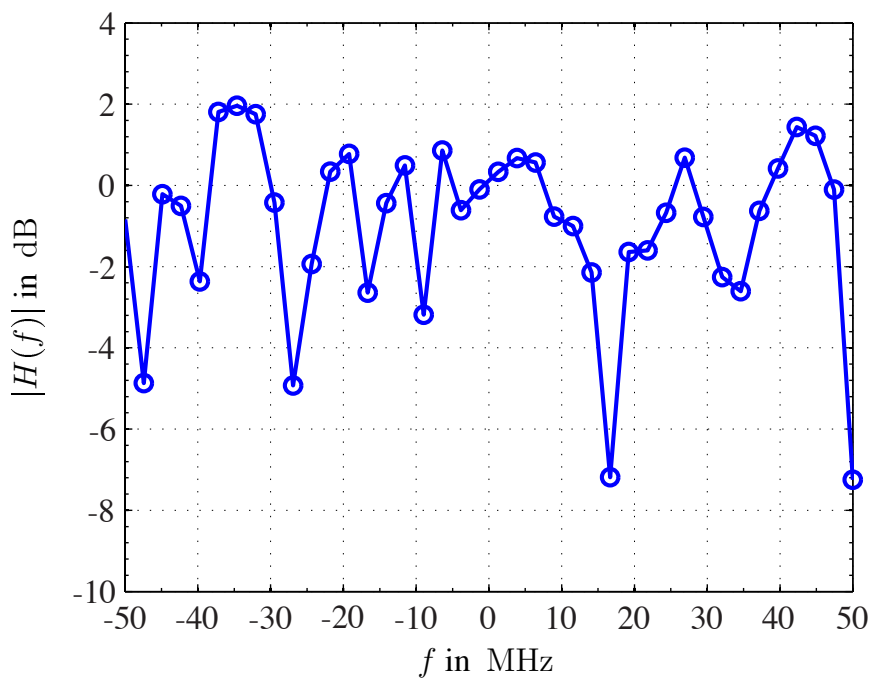


Fig. 5.3: Typical channel transfer function for the Hiperlan A channel model.

assumed, i.e., the channel coefficients stay constant during one transmission cycle. Different channel realizations are temporally uncorrelated. The LO phase offsets φ_{R_l} are modeled as iid random variables with uniform pdf, i.e. $\varphi_{R_l} \sim \mathcal{U}(-\pi, \pi]$. They are assumed to remain constant during one transmission cycle and change independently afterwards. The phase estimation sequences $p_l[n]$ are chosen such that they use the whole channel bandwidth of 100 MHz. The SNR for the phase estimation at slave node l is defined as

$$\text{SNR}_{\text{phase}}^{(l)} = \frac{E_s}{N_0} \cdot E_h \left[\sum_{n=0}^{T_h-1} |h_{R_l M}[n]|^2 \right], \quad (5.44)$$

where E_s is energy per symbol, N_0 the noise power spectral density and $E_h \left[\sum_{n=0}^{T_h-1} |h_{R_l M}[n]|^2 \right]$ average total channel power.

First, the accuracy of the respective phase estimates $\hat{\varphi}_{R_l M}$ and $\widehat{2\varphi_{h_l}}$ for the SB and MB scheme is investigated. The impact of the estimation errors $\Delta\varphi_{R_l}^{(\text{SB})}$ and $\Delta\varphi_{R_l}^{(\text{MB})}$ on the system performance is the same for both schemes because they have the same impact on the estimated product channel (cf. (5.37) and (5.38)). For this reason, they can be directly compared. Considering a single master-slave pair, the length T_m of the phase estimation sequences is varied. Fig. 5.4 shows the rms of the phase estimation errors versus the phase estimation SNR for the SB and the MB scheme. The belonging cumulative density function (cdf) in Fig. 5.5 is calculated at $\text{SNR}_{\text{phase}} = -10$ dB. As expected, the quality of the phase estimation increases with increasing T_m . It can be observed that the SB approach performs better than the MB approach. Furthermore, it can be seen that the cdfs for the SB approach are steeper at the zero-error point and flatten out much later compared to the MB approach. This hints at the frequency diversity the scheme can exploit. The chance of a serious misdetection is thus much smaller.

Next, more slaves are taken into account and the impact of interference on the SB scheme is investigated when the synchronization is performed concurrently. Although the phase synchronization in the MB scheme has to be done sequentially, it is used as a reference. $2N_R$ time slots are required to synchronize N_R slaves for the MB scheme and only two time slots for the SB scheme, regardless of the number of slaves. In Fig. 5.6, the rms of the phase estimation errors is plotted versus the phase estimation SNR with the number of slaves as a parameter. The corresponding cdf for $\text{SNR}_{\text{phase}} = -10$ dB is shown in Fig. 5.7.

Synchronizing multiple slaves concurrently decreases the performance but only requires two time slots. The performance is in this case interference limited so that increasing the estimation SNR does not gain additional accuracy from a certain point on.

The achievable gain in terms of estimation accuracy of a simple antenna selection scheme

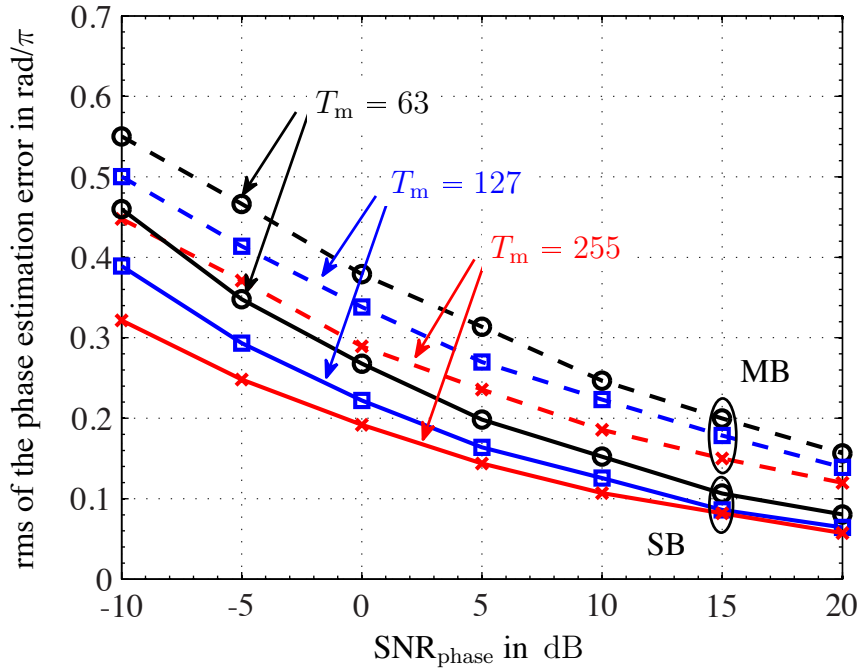


Fig. 5.4: rms of the phase estimation errors $\Delta\varphi_{R_l}^{(SB)}$, $\Delta\varphi_{R_l}^{(MB)}$ in rad/π for a single master-slave pair with one antenna at each terminal.

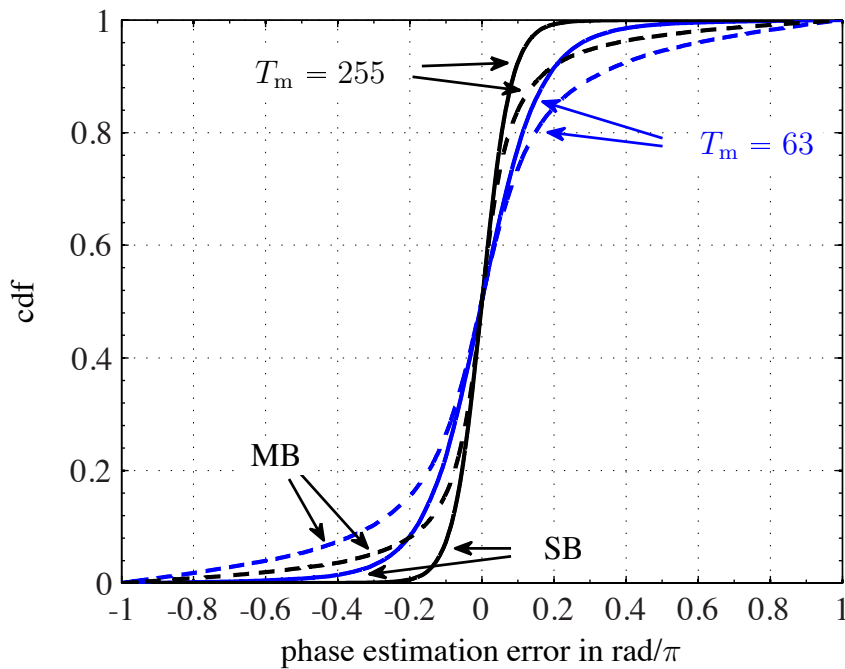


Fig. 5.5: cdf of the phase estimation errors $\Delta\varphi_{R_l}^{(SB)}$, $\Delta\varphi_{R_l}^{(MB)}$ in rad/π for $\text{SNR}_{\text{phase}} = -10$ dB, one master-slave pair with a single antenna at each terminal.

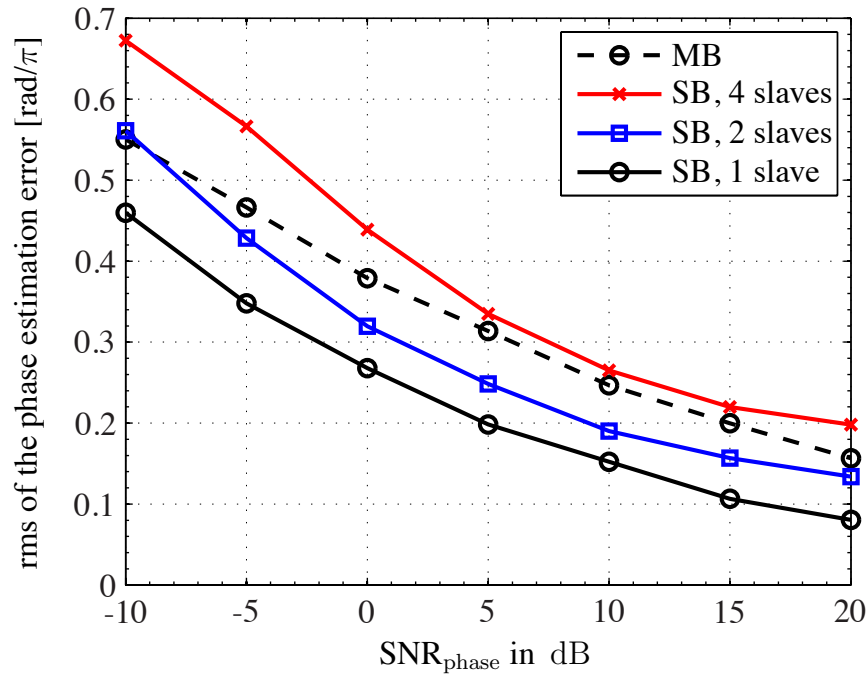


Fig. 5.6: rms of the phase estimation errors $\Delta\varphi_{R_l}^{(SB)}$, $\Delta\varphi_{R_l}^{(MB)}$ in rad/π when concurrently synchronizing different number of slaves with 1 antenna each.

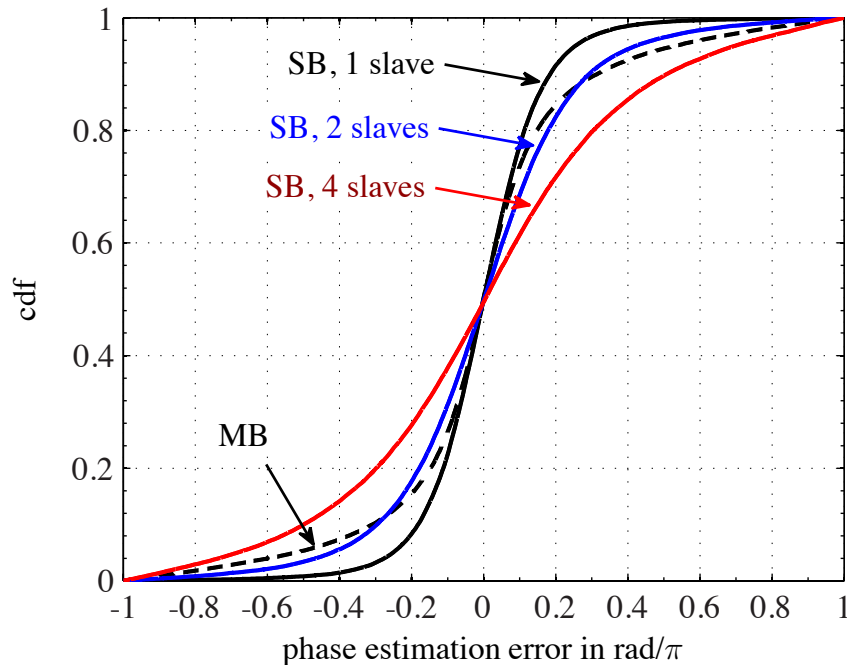


Fig. 5.7: cdf of the phase estimation errors $\Delta\varphi_{R_l}^{(SB)}$, $\Delta\varphi_{R_l}^{(MB)}$ in rad/π for $\text{SNR}_{\text{phase}} = -10\text{dB}$ when concurrently synchronizing different number of slaves with 1 antenna each.

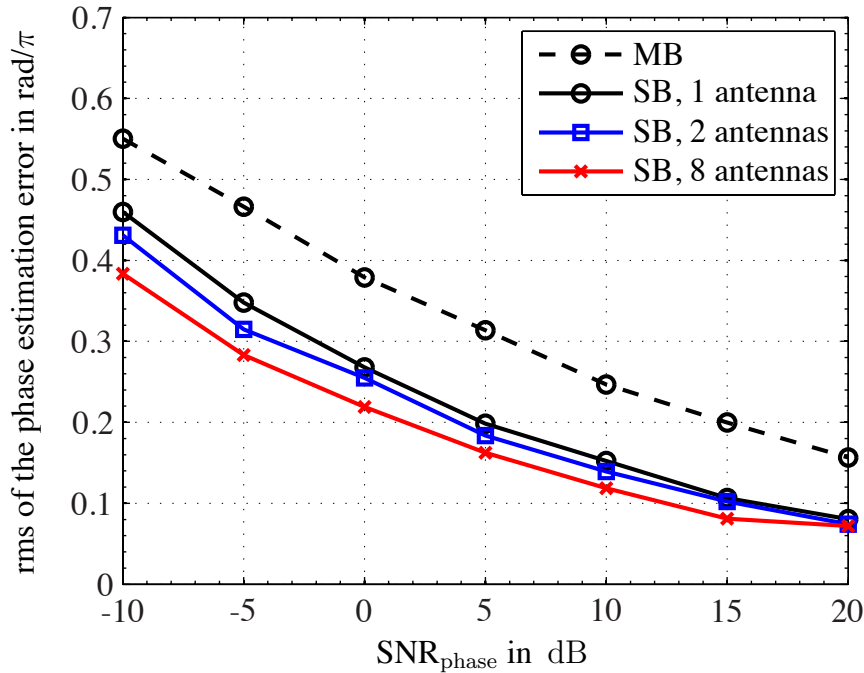


Fig. 5.8: rms of the phase estimation errors $\Delta\varphi_{R_l}^{(SB)}$, $\Delta\varphi_{R_l}^{(MB)}$ in rad/π when synchronizing a slave with different number of antennas using a simple antenna selection scheme.

at the slaves is investigated in Fig. 5.8. The belonging cdfs for $\text{SNR}_{\text{phase}} = -10$ dB are shown in Fig. 5.9. While the SB approach benefits from a simple antenna selection scheme, the MB approach does not, because the phase estimation has to be performed for every slave antenna separately. The additional diversity gain provided by the antenna selection seems to gain only a little accuracy. The reason for this behavior is that the Hiperlan A channel model represents a quite frequency selective environment that already provides a lot of frequency diversity. If the channel model was less frequency selective the additional diversity provided by an antenna selection scheme would have more impact on the performance.

Finally, the impact of phase estimation errors on the receive SNR at the destination is investigated. $N = 8$ relays forward the signal from the source using the channel matched gain factors g_l as in (5.39). The transmit sequence length is $T_m = 63$ and every slave has a single antenna only. In Fig. 5.10, the average receive SNR loss with respect to perfect phase synchronization is plotted versus the SNR of the phase estimation, i.e. $\text{SNR}_{\text{phase}}$. As reference the receive SNR loss of a system with random LO phases at the relays is shown (denoted by 'random relay phases'). The SB approach with sequential synchronization (denoted by 'SB sequential') performs very good even for low phase estimation SNR. The concurrent synchronization (denoted by 'SB concurrent') at low SNR leads

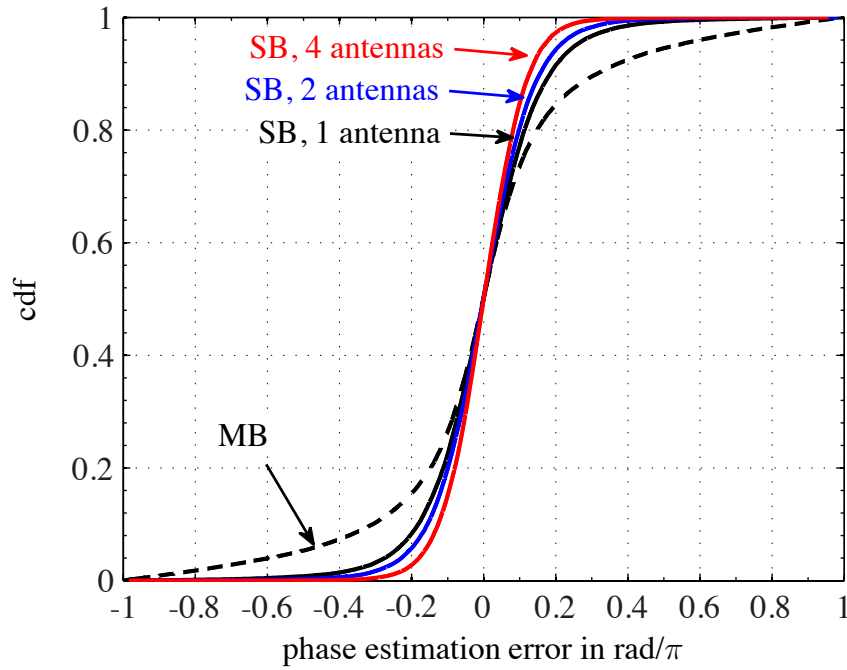


Fig. 5.9: cdf of the phase estimation errors $\Delta\varphi_{R_l}^{(SB)}$, $\Delta\varphi_{R_l}^{(MB)}$ in rad/ π for $\text{SNR}_{\text{phase}} = -10\text{dB}$ when synchronizing a slave with different number of antennas using a simple antenna selection scheme.

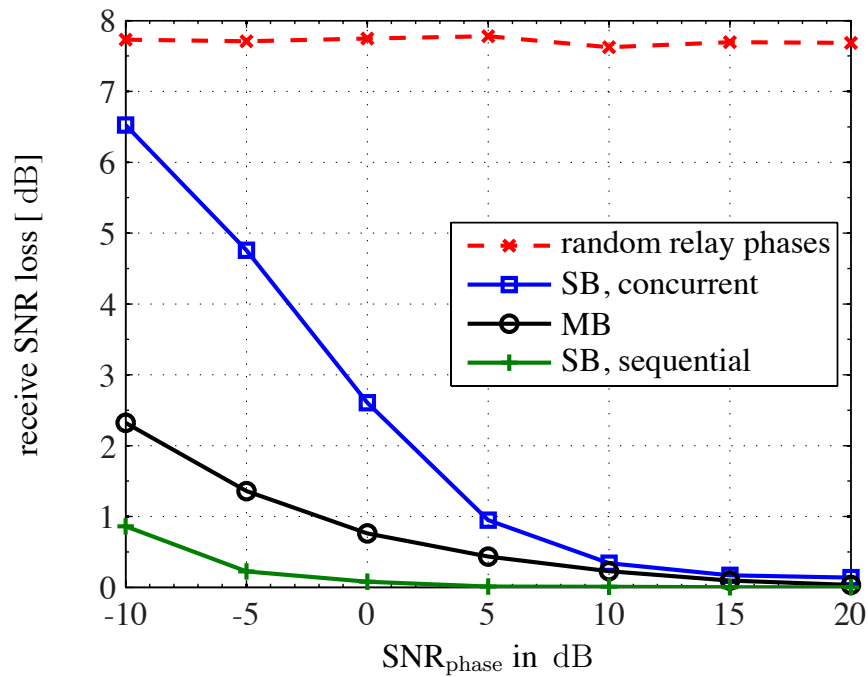


Fig. 5.10: Receive SNR loss due to inaccurate phase estimation.

to a substantial loss compared to the MB approach. However, only two channel uses are required to synchronize all nodes. From about $\text{SNR}_{\text{phase}} = 10$ dB there is only a very small performance loss compared to the MB approach.

5.2.4 Phase Error

Consider a wireless ad hoc network in a slowly fading environment with multiple source-destination pairs and several relay terminals. All relays synchronize their LO phases at time t_0 using the SB scheme with sequential synchronization. Each relay with current LO phase $\varphi_{R_l}(t_0)$ consequently estimates $\varphi_{R_l M}(t_0) = -2\varphi_{R_l}(t_0) + 2\varphi_M(t_0)$, where $\varphi_M(t_0)$ is the LO phase of the master node at time t_0 , in order to compensate the impact of its unknown LO phase offset on the estimated product channel coefficient $\hat{h}_{S_k R_l D_m}$. Assume that the LO phases stay constant during the whole phase estimation procedure. At time $t = t_0 + \Delta t$, the first-hop and second-hop channel coefficient $h_{S_k R_l}$ and $h_{R_l D_m}$ are measured using channel estimation scheme B1 introduced in Section 4.4. For the sake of simplicity it is assumed that all channel estimates are noiseless. In this case, the product of the estimated single-hop channel coefficients between source k and relay l and between relay l and destination m is

$$\hat{h}_{S_k R_l D_m}(t) = h_{R_l D_m} h_{S_k R_l} \cdot e^{j(\varphi_{S_k}(t) - 2\varphi_{R_l}(t) + \varphi_{D_m}(t))}. \quad (5.45)$$

The dependency of $h_{S_k R_l}$ and $h_{R_l D_m}$ on the time t has been omitted because it is assumed that they change much slower than the LO phases² in a slow fading environment. The impact of the LO phase offsets of the relays on $\hat{h}_{S_k R_l D_m}(t)$ can be perfectly compensated if

1. the phase estimate at time t_0 was perfect, i.e. $\hat{\varphi}_{R_l M}(t_0) = \varphi_{R_l M}(t_0)$ and
2. the relay phases have not changed in the time Δt between phase estimation at t_0 and channel estimation at time t , i.e. $\varphi_{R_l}(t) = \varphi_{R_l}(t_0)$.

Multiplying (5.45) with $e^{-j\hat{\varphi}_{R_l M}(t_0)}$ delivers

$$\hat{h}_{S_k R_l D_m}(t) \cdot e^{-j\hat{\varphi}_{R_l M}(t_0)} = h_{R_l D_m} h_{S_k R_l} \cdot e^{j(\varphi_{S_k}(t) - 2\varphi_{R_l}(t) - \hat{\varphi}_{R_l M}(t_0) + \varphi_{D_m}(t))}. \quad (5.46)$$

²The LOs are assumed to suffer from phase noise.

Using the definition of the phase estimation error $\Delta\varphi_{R_l}^{(\text{SB})} = \hat{\varphi}_{R_lM} - \varphi_{R_lM} := \Delta\varphi_{R_l}$ given in (5.33) yields

$$\begin{aligned} -2\varphi_{R_l}(t) - \hat{\varphi}_{R_lM}(t_0) &= -2\varphi_{R_l}(t) - \Delta\varphi_{R_l}(t_0) - \varphi_{R_lM}(t_0) = \\ &= -2\varphi_{R_l}(t) - \Delta\varphi_{R_l}(t_0) + 2\varphi_{R_l}(t_0) - 2\varphi_M(t_0) = \\ &= \phi_{R_l}(t, t_0) - 2\varphi_M(t_0), \end{aligned} \quad (5.47)$$

where the remaining phase error is $\phi_{R_l}(t, t_0) = -2\varphi_{R_l}(t) + 2\varphi_{R_l}(t_0) - \Delta\varphi_{R_l}(t_0)$. There are two independent sources of error that appear explicitly in $\phi_{R_l}(t, t_0)$:

- Phase error due to estimation noise (AWGN): The term $\Delta\varphi_{R_l}(t_0)$ relates to the accuracy of the phase estimation at time t_0 . It disappears when the phase estimation was perfect, i.e., estimation noise is negligible.
- Phase error due to outdated phase information (phase noise): The term $-2\varphi_{R_l}(t) + 2\varphi_{R_l}(t_0)$ represents the change of the LO phase offset due to phase noise during the time between phase synchronization and channel estimation.

Using the definition of $\phi_{R_l}(t, t_0)$, equation (5.46) can be rewritten as

$$\hat{h}_{S_kR_lD_m}(t) \cdot e^{-j\hat{\varphi}_{R_lM}(t_0)} = h_{R_lD_m} h_{S_kR_l} \cdot e^{j(\varphi_{S_k}(t) + \phi_{R_l}(t, t_0) - 2\varphi_M(t_0) + \varphi_{D_m}(t))}, \quad (5.48)$$

where the impact of the LO phase offset of the relay disappears if $\phi_{R_l}(t, t_0) = 0$. In the following, the phase errors due to estimation noise and phase noise are investigated separately because they are independent of each other. Having done that, the phase error $\phi_{R_l}(t, t_0)$ is characterized. Finally, it is shown that for high SNR, it can be approximated by a Gaussian random variable. For the sake of a simpler notation, the LO phases of all sources and destinations are assumed to be zero, i.e., $\varphi_{S_k}(t) = \varphi_{D_m}(t) = 0$ for $k, m, \in \{1, \dots, N_{\text{SD}}\}$. And finally, the relay index l is omitted for the rest of this section because the mechanisms are the same for all relays. This means that $\varphi_{R_l} := \varphi_R$ and $\Delta\varphi_{R_l} := \Delta\varphi_R$.

5.2.4.1 Phase Error Due to Estimation Noise

In Section 5.2.3.2 the accuracy of the phase estimation and its impact on a simple, distributed, coherent forwarding scheme has been investigated. Now, the phase estimation error due to estimation noise, i.e. $\Delta\varphi_R$, is characterized as a random variable. Recall that for the SB theme each relay computes

$$\hat{\varphi}_{RM} = \angle \{c[T_{h,m}]\}, \quad (5.49)$$

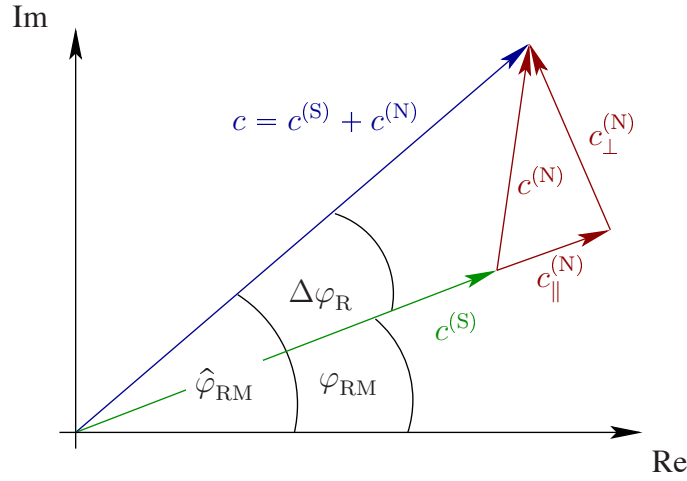


Fig. 5.11: Noisy phase estimation. Note that $c[n]$ is sampled at $T_{h,m}$ and explicit time dependence is omitted to simplify notation.

where $c[n] = c^{(S)}[n] + c^{(I)}[n] + c^{(N)}[n]$ as defined in (5.25) with signal, interference, and noise components $c^{(S)}[n]$, $c^{(I)}[n]$, and $c^{(N)}[n]$, respectively. In order to simplify notation, the explicit time dependence of $c[n]$ at sampling time $T_{h,m}$ is omitted:

$$c[T_{h,m}] := c \quad (5.50)$$

$$c^{(S)}[T_{h,m}] := c^{(S)} \quad (5.51)$$

$$c^{(I)}[T_{h,m}] := c^{(I)} \quad (5.52)$$

$$c^{(N)}[T_{h,m}] := c^{(N)} \quad (5.53)$$

The interference part $c^{(I)}$ is zero because the synchronization is performed sequentially. Furthermore, the noise contribution $c^{(N)}$ is a weighted sum of iid, zero-mean, complex Gaussian random variables (cf. (5.28)). Therefore, it is also zero-mean complex Gaussian with variance denoted by σ_N^2 . Fig. 5.11 shows how $c^{(N)}$ can be split into $c_{\parallel}^{(N)}$, which is parallel to $c^{(S)}$, and $c_{\perp}^{(N)}$, which is perpendicular to $c^{(S)}$. The real-valued scalars α and β are defined such that

$$c_{\parallel}^{(N)} = \alpha \cdot \frac{c^{(S)}}{\|c^{(S)}\|_2} \quad \text{and} \quad c_{\perp}^{(N)} = \beta \cdot \frac{c^{(S)}}{\|c^{(S)}\|_2} e^{j\frac{\pi}{2}}. \quad (5.54)$$

Clearly,

$$\alpha \sim \mathcal{N}\left(0, \frac{1}{2}\sigma_N^2\right) \quad \text{and} \quad \beta \sim \mathcal{N}\left(0, \frac{1}{2}\sigma_N^2\right) \quad (5.55)$$

because $c^{(N)}$ is complex Gaussian with variance σ_N^2 . The value of $\|c^{(S)}\|_2$ is related to a specific instantaneous receive SNR since it represents the received signal strength. It is therefore treated as a constant in the following. The phase estimation error given a fixed $\delta := \|c^{(S)}\|_2$ can then be written as

$$\begin{aligned}\Delta\varphi_R &= \tan^{-1}\left(\frac{\beta}{\delta + \alpha}\right) := \\ &:= \tan^{-1}\left(\frac{\beta}{\gamma}\right),\end{aligned}\tag{5.56}$$

where $\gamma = \delta + \alpha$ with $\gamma \sim \mathcal{N}\left(\delta, \frac{1}{2}\sigma_N^2\right)$. Furthermore, let $\xi := \frac{\beta}{\gamma}$ and thus

$$\Delta\varphi_R = \tan^{-1}(\xi).\tag{5.57}$$

The pdf of $\Delta\varphi_R$ given δ is then

$$f_{\Delta\varphi_R|\delta} = \frac{f_\xi}{\left|\frac{\partial}{\partial\xi}g(\xi)\right|},\tag{5.58}$$

where $g(\xi) = \tan^{-1}(\xi)$. Details are provided in Appendix A.2. In the following, the numerator and denominator of (5.58) are computed separately to obtain an explicit expression for $f_{\Delta\varphi_R|\delta}$.

- **Calculation of f_ξ :** Using Appendix A.3, the pdf of ξ is

$$\begin{aligned}f_\xi &= \int_{-\infty}^{\infty} |\gamma| f_\beta(\xi\gamma) f_\gamma(\gamma) d\gamma = \\ &= \int_{-\infty}^{\infty} \frac{|\gamma|}{\pi\sigma_N^2} \cdot e^{-\frac{\xi^2\gamma^2 + (\gamma-\delta)^2}{\sigma_N^2}} d\gamma = \\ &= \frac{e^{-\frac{\delta^2}{\sigma_N^2}}}{\pi(1+\xi^2)^{\frac{3}{2}}\sigma_N} \left(\sigma_N\sqrt{1+\xi^2} + \sqrt{\pi}\delta e^{\frac{\delta^2}{(1+\xi^2)\sigma_N^2}} \operatorname{erf}\left(\frac{\delta}{\sigma_N\sqrt{1+\xi^2}}\right) \right),\end{aligned}\tag{5.59}$$

where the pdfs

$$f_\beta = \frac{1}{\sqrt{\pi\sigma_N^2}} \cdot e^{-\frac{\beta^2}{\sigma_N^2}} \quad \text{and} \quad f_\gamma = \frac{1}{\sqrt{\pi\sigma_N^2}} \cdot e^{-\frac{(\gamma-\delta)^2}{\sigma_N^2}}\tag{5.60}$$

are known.

- **Calculation of $\frac{\partial}{\partial \xi} g(\xi)$:** The denominator of (5.58) is easily calculated:

$$\begin{aligned} \frac{\partial}{\partial \xi} g(\xi) &= \frac{\partial}{\partial \xi} \tan^{-1}(\xi) = \\ &= \frac{1}{1 + \xi^2} \end{aligned} \quad (5.61)$$

Inserting (5.59) and (5.61) into (5.58) and replacing ξ by $\tan(\Delta\varphi_R)$ (cf. (5.57)) yields

$$\begin{aligned} f_{\Delta\varphi_R|\delta} &= f_{\xi}(1 + \xi^2) = \\ &= \frac{e^{-\frac{\delta^2}{\sigma_N^2}}}{\pi\sigma_N} \left(\sigma_N + \sqrt{\pi}\delta \cos(\Delta\varphi_R) e^{\frac{\delta^2 \cos^2(\Delta\varphi_R)}{\sigma_N^2}} \operatorname{erf}\left(\frac{\delta \cos(\Delta\varphi_R)}{\sigma_N}\right) \right). \end{aligned} \quad (5.62)$$

For large SNR a simple approximation for $f_{\Delta\varphi_R|\delta}$ can be derived by assuming $|\delta| \gg |\alpha|$ and $|\delta| \gg |\beta|$. These assumptions state that the length of the vector $c^{(S)}$, which represents the signal part of $c[T_{h,m}]$, is much larger than the noise parts $c_{\parallel}^{(N)}$ and $c_{\perp}^{(N)}$. Consequently,

1. $\delta + \alpha \approx \delta$ and thus

$$\Delta\varphi_R \approx \tan^{-1}\left(\frac{\beta}{\delta}\right) \quad (5.63)$$

2. $\Delta\varphi_R$ is small so that

$$\tan(\Delta\varphi_R) \approx \Delta\varphi_R \quad (5.64)$$

With (5.63) and (5.64) it follows that

$$\Delta\varphi_R \approx \frac{\beta}{\delta} \quad (5.65)$$

and the approximated pdf of $\Delta\varphi_R$ given δ can be directly written as

$$f_{\Delta\varphi_R|\delta} \approx \frac{1}{\sqrt{\pi \frac{\sigma_N^2}{\delta^2}}} \cdot e^{-\frac{\beta^2 \delta^2}{\sigma_N^2}}, \quad (5.66)$$

i.e. $\Delta\varphi_R \sim \mathcal{N}\left(0, \frac{\sigma_N^2}{2\delta^2}\right)$, because the pdf of β is known (cf. (5.60)).

Monte-Carlo simulations were performed in order to assess how well (5.66) approximates (5.62) for high instantaneous SNR. In Figs. 5.12 and 5.13 the simulated pdfs are compared with the analytical ones and their high SNR approximations. They are normalized such that

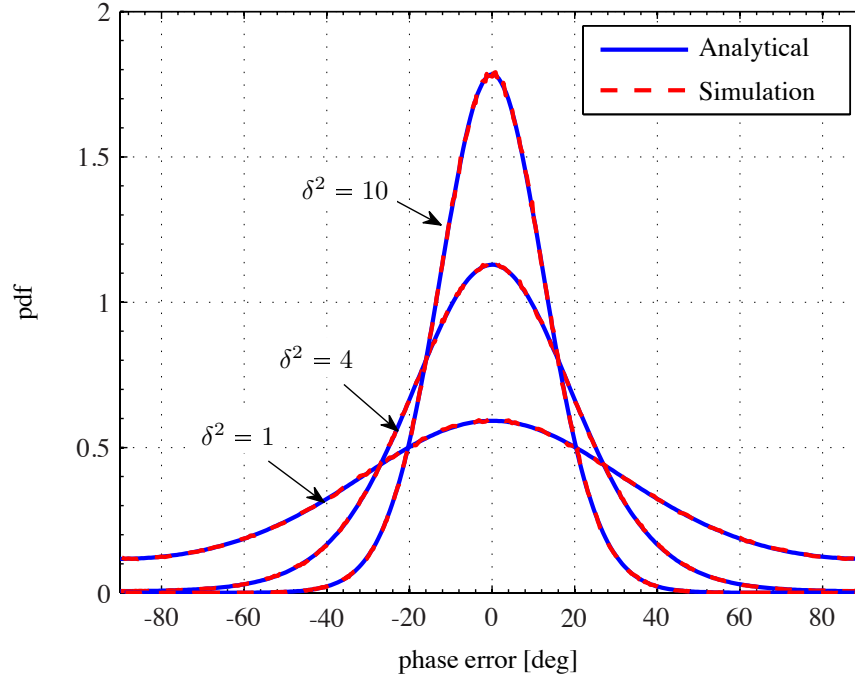


Fig. 5.12: Comparison of analytical (5.62) and simulated pdfs for different values of δ^2 and $\sigma_N^2 = 1$.

the area beneath the curves equals one. The noise variance is fixed at $\sigma_N^2 = 1$ and δ , which is the strength of the signal part $c^{(S)}$ of the estimation vector c , is varied. The instantaneous receive SNR during the phase estimation is defined as $\text{SNR}_R^{(\Delta\varphi)} = \frac{\delta}{\sigma_N^2}$. Fig. 5.12 shows that the analytical solution (5.62) fits the simulation very well. Furthermore, it can be seen in Fig. 5.13 that the approximation models the simulation reasonably well starting from $\delta^2 \approx 10$. This means that the Gaussian approximation holds very well in the SNR range where a phase estimation achieves a sensible accuracy.

5.2.4.2 Phase Error Due to Phase Noise

The error due to phase noise is defined as (cf. (5.47) and Fig. 5.14)

$$\psi_R(t) := -2\varphi_R(t) + 2\varphi_R(t_0). \quad (5.67)$$

It corresponds to the phase change during the time between phase estimation (at t_0) and the time the channel coefficients are estimates (at $t = t_0 + \Delta t$). For Wiener phase noise (cf. Chapter 3) the LO phases are modeled as independent Wiener processes. Thus, $\psi_R(t)$

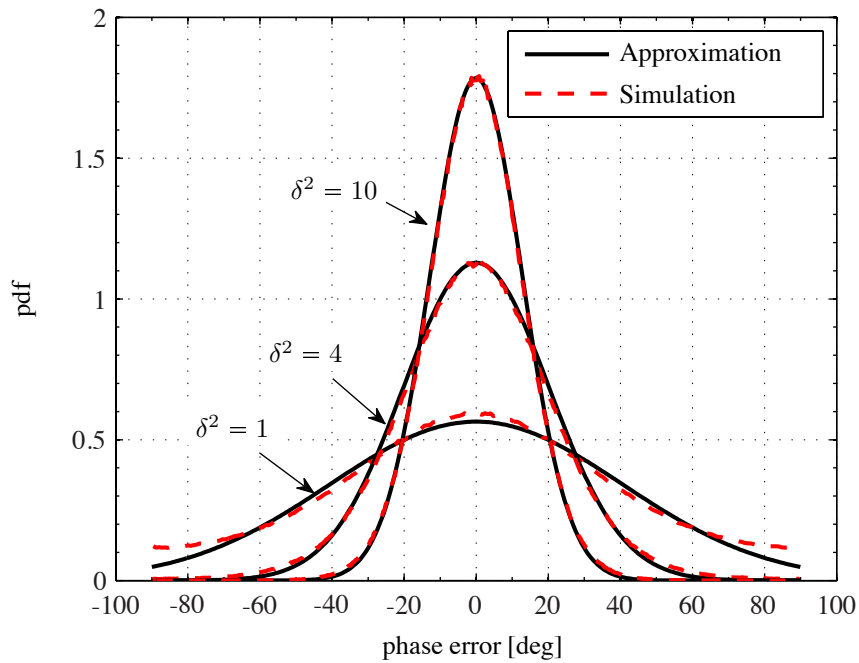


Fig. 5.13: Comparison of approximated (5.66) and simulated pdfs for different values of δ^2 and $\sigma_N^2 = 1$.

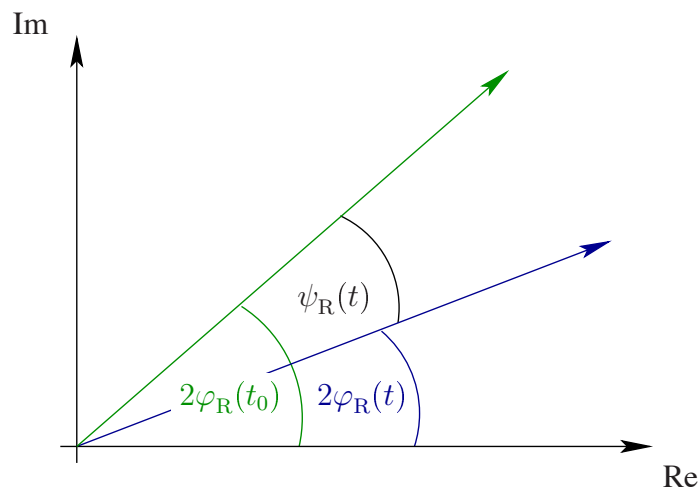


Fig. 5.14: Estimation error due to phase noise.

is a zero-mean Gaussian random variable with variance $\sigma_{\text{pn}}^2 \Delta t$, where the scalar σ_{pn}^2 is a constant hardware parameter. For $t_0 = 0$, it is distributed as $\psi_{\text{R}}(t) \sim \mathcal{N}(0, 4\sigma_{\text{pn}}^2 t)$. Its pdf is consequently given by

$$f_{\psi_{\text{R}}(t)} = \frac{1}{\sqrt{8\pi\sigma_{\text{pn}}^2 t}} \cdot e^{-\frac{\psi_{\text{R}}^2(t)}{8\sigma_{\text{pn}}^2 t}}. \quad (5.68)$$

5.2.4.3 Joint Phase Error

In order to model the joint phase error $\phi_{\text{R}}(t, t_0)$ as defined in (5.47), the Gaussian approximation (5.66) is used for the phase error due to estimation noise. The joint phase error is then the sum of two independent Gaussian random variables $\Delta\varphi_{\text{R}} \sim \mathcal{N}\left(0, \frac{\sigma_{\text{N}}^2}{2\delta^2}\right)$ and $\psi_{\text{R}}(t) \sim \mathcal{N}(0, 4\sigma_{\text{pn}}^2 t)$ with pdf (conditioned on δ)

$$f_{\phi_{\text{R}}(t, t_0)|\delta} = \frac{1}{\sqrt{2\pi\left(\frac{\sigma_{\text{N}}^2}{2\delta^2} + 4\sigma_{\text{pn}}^2 t\right)}} \cdot e^{-\frac{\beta^2}{2\left(\frac{\sigma_{\text{N}}^2}{2\delta^2} + 4\sigma_{\text{pn}}^2 t\right)}}, \quad (5.69)$$

and thus $\phi_{\text{R}}(t, t_0) \sim \mathcal{N}\left(0, \frac{\sigma_{\text{N}}^2}{2\delta^2} + 4\sigma_{\text{pn}}^2 t\right)$.

Chapter 6

Gain Allocation Schemes

A distributed spatial multiplexing gain is obtained if multiple source-destination pairs in a wireless network communicate concurrently on the same physical channel. To this end, inter-user interference has to be suppressed. This can be achieved if the signals from all paths add up coherently, i.e. with the same carrier phase, at the destinations. In this chapter two gain allocation schemes for a two-hop AF relay network are discussed that exhibit a distributed spatial multiplexing gain. They are called MUZF relaying and multiuser MMSE relaying and were first presented in [25] and [73], respectively. Instantaneous global channel knowledge is required in both cases to generate the gain matrix, i.e., the equivalent first-hop as well as the equivalent second-hop channel matrix have to be known. It is assumed that all channel coefficients are disseminated to all relays on a perfect, i.e. error and delay-free, feedback channel after they have been estimated.

MUZF relaying: One way to allow multiple source-destination pairs to communicate concurrently on the same physical channel is to choose the gain factors at the relays such that inter-user interference is completely suppressed. The approach where the relays orthogonalize all source-destination pairs in space is called MUZF relaying [25]. The resulting compound channel matrix between sources and destinations is in this case block diagonal (for the special case of single-antenna sources and destinations it is diagonal). It turns out that a minimum number of relays, that depends on the number of source-destination pairs, is required to achieve this. A system configuration employing exactly this number of relays will be called 'minimum relay configuration'. The gain factors are then, apart from a common scaling factor, uniquely determined. No diversity gain is achievable in this case.

The impact of noisy channel state information on the performance of MUZF relaying was investigated in [68]. The case where arbitrary relay antennas are able to exchange

receive data is called 'partial relay cooperation' [69]. While the gain matrix is always block diagonal for multi-antenna relays that do not exchange received signals, partial relay cooperation essentially means that arbitrary entries of the gain matrix may be nonzero. For multi-antenna relays it is sensible to assume that the data exchange capability between all antennas belonging to the same relay is bi-directional. This means that all antennas of a single relays can retransmit a linear combinations of all received signals of that relay.

In previous works discussing MUZF relaying, the unknown and random LO phases of the nodes in the network have not been taken into account. Furthermore, the direct link has also been neglected so far. Both are considered in this work. Each node in the network is assumed to employ its own, independent LO with unknown and random phase offset. The performance of traffic pattern III, where the direct link is used in the second time slot, and traffic pattern IV, where the direct link is not used, is compared in this chapter. Furthermore, the impact of channel estimation protocols A1 and B1 (introduced in Section 4.4) on the system performance is investigated for both traffic patterns.

Multiuser MMSE relaying: The second gain allocation scheme being discussed in this chapter is called multiuser MMSE relaying. The gain factors are computed to minimize the MMSE of the received signals at the destinations. Interference is suppressed, but not completely. Some interference is admitted in order not to suffer from the noise enhancement that is characteristic for ZF-based approaches. Two cases will be distinguished:

1. All source-destination links are weighted equally. This is a very fair scheme because the gain factors are computed such that the average SINR at all destinations is equal. However, in the presence of shadowing or very weak subchannels, the overall system performance suffers greatly because most of the available relay transmit power will be directed into the bad links.
2. Each source-destination link is weighted individually so that the total MMSE of the received signals at all destinations is minimized. The sum rate of this system is higher than for the equal link weighting. However, since the source-destination pairs with good channels get most of the relay transmit power, it is not a very fair scheme. Good links are rewarded while bad ones are punished.

It turns out that there is no minimum required relay number (such as the minimum relay configuration for ZF relaying) for MMSE relaying. Instead, a smooth degradation of system performance can be observed for decreasing number of relays.

Let N_{coop} denote the number of relay cooperations, i.e., the number of nonzero entries of \mathbf{G} . Two extreme cases, namely linear relaying (LinRel) and linear distributed antenna system (LDAS), are furthermore distinguished in this work:

- **LinRel:** All relays employ a single antenna only, i.e. $M_{\text{R}} = N_{\text{R}}$. No inter-relay cooperation is possible in this case, i.e. $N_{\text{coop}} = N_{\text{R}}$. Since the relays employ a single antenna each and do not share any received data, the gain matrix is diagonal.
- **LDAS:** There is only a single multi-antenna relay, i.e. $N_{\text{R}} = 1$. Full relay cooperation is possible, i.e. $N_{\text{coop}} = N_{\text{R}}^2$. All relay antennas completely share their received data. The gain matrix then has normally no zero entries.

For the derivation of the gain allocation schemes, there is assumed to be no phase noise. This means that the LO phases of all nodes in the network are constant for at least one transmission cycle.

6.1 Transmit Power Constraint

In order to investigate the performance of different gain allocation schemes, it is necessary to impose a transmit power constraint on the network: The total instantaneous transmit power of all nodes is in each time slot equal to P_{S} . The total transmit power per transmission cycle (comprising two time slots) is then $2P_{\text{S}}$. A scaling of the gain matrix \mathbf{G} and, in case of traffic patterns I and III, a scaling of the source transmit symbols in the second time slot is necessary to meet this constraint.

- **Traffic patterns II and IV:** In time slot 1 the sources transmit with total power P_{S} satisfying the constraint by definition. In the second time slot, the source nodes are silent while the relays transmit with power

$$P_{\text{R}} = \text{tr} \left(\mathbf{G} \left(\sigma_{\text{s}}^2 \tilde{\mathbf{H}}_{\text{SR}} \tilde{\mathbf{H}}_{\text{SR}}^{\text{H}} + \sigma_{\text{nR}}^2 \mathbf{I}_{N_{\text{R}}} \right) \mathbf{G}^{\text{H}} \right). \quad (6.1)$$

In general $P_{\text{R}} \neq P_{\text{S}}$. The gain matrix \mathbf{G} has to be scaled with

$$\gamma_{\text{II}} = \gamma_{\text{IV}} = \sqrt{\frac{P_{\text{S}}}{P_{\text{R}}}} \quad (6.2)$$

for both traffic patterns so that the total relay transmit power is equal to P_{S} .

- **Traffic patterns I and III:** The transmit power constraint in the first time slot is again met by definition. The sources and the relays transmit in the second time slot. Once

the gain factors are calculated, the source and relay transmit powers have to be scaled with the same factor in order not to lose the properties of the gain allocation. The transmit power constraint can be formulated as

$$\gamma_I^2 (P_S + P_R) \stackrel{!}{=} P_S \quad \text{and} \quad \gamma_{III}^2 (P_S + P_R) \stackrel{!}{=} P_S \quad (6.3)$$

for traffic patterns I and III, respectively. This results in

$$\gamma_I = \gamma_{III} = \sqrt{\frac{P_S}{P_S + P_R}}, \quad (6.4)$$

where P_R is given in (6.1). Scaling the source transmit symbols in the second time slot requires a feedback link.

6.2 Multiuser Zero-Forcing Relaying

In this section the gain factors for MUZF relaying are computed for traffic patterns III and IV. Their respective input/output relations are given in Section 2.4. They are

$$\mathbf{d}_{III}^{(1)} = \mathbf{0} \quad (6.5)$$

$$\mathbf{d}_{III}^{(2)} = \tilde{\mathbf{H}}_{RD} \mathbf{G} \left(\tilde{\mathbf{H}}_{SR} \mathbf{s}^{(1)} + \mathbf{n}_R^{(1)} \right) + \tilde{\mathbf{H}}_{SD} \mathbf{s}^{(2)} + \mathbf{n}_D^{(2)} \quad (6.6)$$

for traffic pattern III and

$$\mathbf{d}_{IV}^{(1)} = \mathbf{0} \quad (6.7)$$

$$\mathbf{d}_{IV}^{(2)} = \tilde{\mathbf{H}}_{RD} \mathbf{G} \left(\tilde{\mathbf{H}}_{SR} \mathbf{s}^{(1)} + \mathbf{n}_R^{(1)} \right) + \mathbf{n}_D^{(2)} \quad (6.8)$$

for traffic pattern IV. For traffic pattern III it is assumed that the sources transmit scaled versions of the same transmit symbols in both time slots, i.e. $\mathbf{s}^{(2)} = \gamma_{III} \mathbf{s}^{(1)}$, where $\gamma_{III} \in \mathbb{R}$ is given in (6.4). The signals from sources and relays thus have to combine coherently at the destination antennas so that the compound channel becomes block diagonal and inter-user interference is suppressed. Since the received signal at the destinations in the first time slot is in both cases equal to zero the superscripts indicating the time slot number are in the following omitted for the sake of a simpler notation. Equations (6.6) and (6.8) can be

rewritten as

$$\mathbf{d}_{\text{III}} = \tilde{\mathbf{H}}_{\text{III}}\mathbf{s} + \mathbf{n}_{\text{III}} \quad (6.9)$$

$$\text{and } \mathbf{d}_{\text{IV}} = \tilde{\mathbf{H}}_{\text{IV}}\mathbf{s} + \mathbf{n}_{\text{IV}}, \quad (6.10)$$

where

$$\tilde{\mathbf{H}}_{\text{III}} = \tilde{\mathbf{H}}_{\text{SRD}} + \gamma_{\text{III}}\tilde{\mathbf{H}}_{\text{SD}} \quad (6.11)$$

$$\tilde{\mathbf{H}}_{\text{IV}} = \tilde{\mathbf{H}}_{\text{SRD}} \quad (6.12)$$

are the 'compound channel matrices' comprising all 'compound channel coefficients'. The vectors

$$\mathbf{n}_{\text{III}} = \mathbf{n}_{\text{IV}} = \tilde{\mathbf{H}}_{\text{RD}}\mathbf{G}\mathbf{n}_{\text{R}} + \mathbf{n}_{\text{D}} \quad (6.13)$$

are the 'compound noise vectors'. Furthermore, the matrix

$$\tilde{\mathbf{H}}_{\text{SRD}} = \tilde{\mathbf{H}}_{\text{RD}}\mathbf{G}\tilde{\mathbf{H}}_{\text{SR}} \quad (6.14)$$

is the 'equivalent two-hop channel' matrix because it comprises the concatenation of first-hop channel matrix, gain matrix, and second-hop channel matrix.

In the following, the computation of the gain factors from channel estimates obtained by estimation protocols A1 and B1 (introduced in Section 4.4) is discussed for each of the traffic patterns. Recall that the relays require a global carrier phase reference in order to coherently forward their signals if the gain factors are computed from channel estimates obtained by protocol B1. It is assumed that the SB scheme introduced in Section 5.2.1 is used to achieve this. Section 6.2.3 then treats the impact of a phase estimation error on the interference suppression capability of MUZF relaying. Finally, Section 6.2.4 contains simulation results comparing the performance of both traffic patterns in combination with the two channel estimation protocols. Imperfect phase synchronization and phase noise at the relays are also taken into account.

6.2.1 Traffic Pattern III

For traffic pattern III, the compound channel matrix is given in (6.11):

$$\begin{aligned}\tilde{\mathbf{H}}_{\text{III}} &= \tilde{\mathbf{H}}_{\text{SRD}} + \gamma_{\text{III}} \tilde{\mathbf{H}}_{\text{SD}} = \\ &= \Phi_{\text{D}}^{\text{H}} \mathbf{H}_{\text{RD}} \mathbf{G} \mathbf{H}_{\text{SR}} \Phi_{\text{S}} + \gamma_{\text{III}} \Phi_{\text{D}}^{\text{H}} \mathbf{H}_{\text{SD}} \Phi_{\text{S}}.\end{aligned}\quad (6.15)$$

Recall that the scaling factor γ_{III} ensures that the sum transmit power of all nodes is in each time slot equal to P_{S} . The aim of this section is to find \mathbf{G} such that $\tilde{\mathbf{H}}_{\text{III}}$ becomes block diagonal. Using the simple matrix equalities (e.g. [192])

$$\text{vec}(\mathbf{ABC}) = (\mathbf{C}^{\text{T}} \otimes \mathbf{A}) \text{vec}(\mathbf{B}) \quad (6.16)$$

$$\text{and } (\mathbf{AB} \otimes \mathbf{CD}) = (\mathbf{A} \otimes \mathbf{C})(\mathbf{B} \otimes \mathbf{D}) \quad (6.17)$$

delivers

$$\begin{aligned}\tilde{\mathbf{h}}_{\text{III}} &:= \text{vec}(\tilde{\mathbf{H}}_{\text{III}}) = \\ &= \text{vec}(\Phi_{\text{D}}^{\text{H}} \mathbf{H}_{\text{RD}} \mathbf{G} \mathbf{H}_{\text{SR}} \Phi_{\text{S}}) + \text{vec}(\gamma_{\text{III}} \Phi_{\text{D}}^{\text{H}} \mathbf{H}_{\text{SD}} \Phi_{\text{S}}) = \\ &= (\Phi_{\text{S}}^{\text{T}} \otimes \Phi_{\text{D}}^{\text{H}}) (\mathbf{H}_{\text{SR}}^{\text{T}} \otimes \mathbf{H}_{\text{RD}}) \cdot \text{vec}(\mathbf{G}) + \gamma_{\text{III}} (\Phi_{\text{S}}^{\text{T}} \otimes \Phi_{\text{D}}^{\text{H}}) \cdot \text{vec}(\mathbf{H}_{\text{SD}}) := \\ &:= \Theta \Lambda \cdot \mathbf{g} + \gamma_{\text{III}} \Theta \mathbf{h}_{\text{SD}},\end{aligned}\quad (6.18)$$

where

$$\Theta := \Phi_{\text{S}}^{\text{T}} \otimes \Phi_{\text{D}}^{\text{H}}, \quad (6.19)$$

$$\Lambda := \mathbf{H}_{\text{SR}}^{\text{T}} \otimes \mathbf{H}_{\text{RD}}, \quad (6.20)$$

$$\text{and } \mathbf{g} := \text{vec}(\mathbf{G}). \quad (6.21)$$

The vector $\tilde{\mathbf{h}}_{\text{III}} \in \mathbb{C}^{M_{\text{S}}M_{\text{D}}}$ is called 'compound channel vector' because it comprises all compound channel coefficients. Note that the gain matrix contains zeros where there is no cooperation between the relay antennas. The zero elements of the compound gain vector \mathbf{g} and the corresponding columns of Λ may simply be dropped for a given relay cooperation pattern¹. The emanating vector and matrix are denoted by $\bar{\mathbf{g}}$ and $\bar{\Lambda}$, respectively:

$$\mathbf{g} \in \mathbb{C}^{M_{\text{R}}^2} \rightarrow \bar{\mathbf{g}} \in \mathbb{C}^{N_{\text{coop}}} \quad \text{and} \quad \Lambda \in \mathbb{C}^{M_{\text{S}}M_{\text{D}} \times M_{\text{R}}^2} \rightarrow \bar{\Lambda} \in \mathbb{C}^{M_{\text{S}}M_{\text{D}} \times N_{\text{coop}}}. \quad (6.22)$$

¹The relay cooperation pattern indicates which relay antennas exchange received signals. This essentially corresponds to a specific pattern of nonzero elements in the gain matrix \mathbf{G} .

The parameter N_{coop} denotes the number of nonzero elements of \mathbf{G} , i.e., the number of cooperations among the relays. With (6.22), the compound channel vector can be written as

$$\tilde{\mathbf{h}}_{\text{III}} = \Theta \bar{\Lambda} \cdot \bar{\mathbf{g}} + \gamma_{\text{III}} \Theta \mathbf{h}_{\text{SD}}. \quad (6.23)$$

It can be divided into $N_{\text{signal}} = \sum_{i=1}^{N_{\text{SD}}} M_{S_i} M_{D_i}$ coefficients over which signal power arrives at the destinations and $N_{\text{int}} = M_S M_D - N_{\text{signal}}$ coefficient over which interference is generated. Let $\tilde{\mathbf{h}}_{\text{III},s} \in \mathbb{C}^{N_{\text{signal}}}$ and $\tilde{\mathbf{h}}_{\text{III},i} \in \mathbb{C}^{N_{\text{int}}}$ denote the vector of signal channel coefficients and the vector of interference channel coefficients, respectively. Together they constitute $\tilde{\mathbf{h}}_{\text{III}}$. The 'compound signal channel matrix' $\bar{\Lambda}_s \in \mathbb{C}^{N_{\text{signal}} \times N_{\text{coop}}}$ and the 'compound interference channel matrix' $\bar{\Lambda}_i \in \mathbb{C}^{N_{\text{int}} \times N_{\text{coop}}}$ as well as the corresponding matrices Θ_s and Θ_i are defined such that

$$\tilde{\mathbf{h}}_{\text{III},s} = \Theta_s \bar{\Lambda}_s \cdot \bar{\mathbf{g}} + \gamma_{\text{III}} \Theta_s \mathbf{h}_{\text{SD},s} \quad \text{and} \quad \tilde{\mathbf{h}}_{\text{III},i} = \Theta_i \bar{\Lambda}_i \cdot \bar{\mathbf{g}} + \gamma_{\text{III}} \Theta_i \mathbf{h}_{\text{SD},i}. \quad (6.24)$$

The matrix $\bar{\Lambda}_s$ is obtained from $\bar{\Lambda}$ by taking the rows that correspond to source-destination pairs and $\bar{\Lambda}_i$ by taking the rows corresponding to non-belonging sources and destinations. The vectors $\mathbf{h}_{\text{SD},s}$ and $\mathbf{h}_{\text{SD},i}$ comprise the direct link channel coefficients contributing signal and interference power at the destinations, respectively. The matrices Θ_s and Θ_i are again diagonal. Please refer to Appendix A.4 for a simple example. In order to block-orthogonalize all source-destination pairs, i.e., cancel all inter-user interference, it is required that

$$\tilde{\mathbf{h}}_{\text{III},i} \stackrel{!}{=} \mathbf{0}. \quad (6.25)$$

Equation (6.25) is called the 'ZF condition'. Inserting (6.24) into (6.25) yields

$$\Theta_i \bar{\Lambda}_i \cdot \frac{1}{\gamma_{\text{III}}} \bar{\mathbf{g}} + \Theta_i \mathbf{h}_{\text{SD},i} \stackrel{!}{=} \mathbf{0}. \quad (6.26)$$

A vector $\bar{\mathbf{g}}_{\text{ZF}}$ fulfilling the ZF condition can be found by solving (6.26) for $\bar{\mathbf{g}}$. Consequently,

$$\begin{aligned} \bar{\mathbf{g}}_{\text{ZF}} &= \gamma_{\text{III}} \cdot \bar{\mathbf{g}}'_{\text{ZF}} = \\ &= -\gamma_{\text{III}} \cdot \bar{\Lambda}_i^H \Theta_i^H (\Theta_i \bar{\Lambda}_i \bar{\Lambda}_i^H \Theta_i^H)^{-1} \Theta_i \mathbf{h}_{\text{SD},i} = \\ &= -\gamma_{\text{III}} \cdot \bar{\Lambda}_i^H (\bar{\Lambda}_i \bar{\Lambda}_i^H)^{-1} \mathbf{h}_{\text{SD},i}. \end{aligned} \quad (6.27)$$

Note that the ZF gain vector does not depend on the LO phase offsets. Finding $\bar{\mathbf{g}}_{\text{ZF}}$ according to (6.27) fulfills the ZF condition (6.25) as long as the propagation channel coefficients stay

constant. The inverse in (6.27) exists when $\bar{\Lambda}_i \bar{\Lambda}_i^H$ has full rank N_{int} . It is well-known that

$$\text{rank}(\bar{\Lambda}_i \bar{\Lambda}_i^H) \leq \min\{N_{\text{int}}, N_{\text{coop}}\}. \quad (6.28)$$

Consequently, a necessary but not sufficient condition for $\bar{\mathbf{g}}_{\text{ZF}}$ to exist is $N_{\text{coop}} \geq N_{\text{int}}$. The case that $N_{\text{coop}} = N_{\text{int}}$ is referred to as 'minimum cooperation configuration'.

In order to calculate $\bar{\mathbf{g}}_{\text{ZF}}$, the relays need to know $\Theta_i \bar{\Lambda}_i$ and $\Theta_i \mathbf{h}_{\text{SD},i}$, where the LO phases in Θ_i may have arbitrary values, or $\bar{\Lambda}_i$ and $\mathbf{h}_{\text{SD},i}$. In the following, it is shown how the relays can compute their ZF gain factors if the channels have been measured with schemes A1 and B1. It is assumed that all channel estimates are noiseless and there is no phase noise, i.e., the relay phases stay constant for at least one transmission cycle.

6.2.1.1 Channel Estimation Protocol A1

For channel estimation protocol A1, the relays possess the channel estimates

$$\hat{\mathbf{H}}_{\text{SD}} = \tilde{\mathbf{H}}_{\text{SD}}, \quad \hat{\mathbf{H}}_{\text{SR}} = \tilde{\mathbf{H}}_{\text{SR}}, \quad \text{and} \quad \hat{\mathbf{H}}_{\text{RD}} = \tilde{\mathbf{H}}_{\text{RD}}. \quad (6.29)$$

They have to learn $\Theta_i \bar{\Lambda}_i$ and $\Theta_i \mathbf{h}_{\text{SD},i}$ in order to be able to compute the ZF gain vector $\bar{\mathbf{g}}_{\text{ZF}}$ from (6.27). The procedure is as follows:

- Calculation of $\Theta_i \bar{\Lambda}_i$:

First, the relays have to compute

$$\begin{aligned} \hat{\mathbf{H}}_{\text{SR}}^T \otimes \hat{\mathbf{H}}_{\text{RD}} &= (\Phi_{\text{S}}^T \otimes \Phi_{\text{D}}^H) (\mathbf{H}_{\text{SR}}^T \Phi_{\text{R}}^* \otimes \mathbf{H}_{\text{RD}} \Phi_{\text{R}}) := \\ &:= \Theta \hat{\Lambda}, \end{aligned} \quad (6.30)$$

where Θ is the same as in (6.19). Assume that all cooperating relay antennas exhibit the same LO phase offset, i.e., $\Phi_{\text{R}}[i, i] = \Phi_{\text{R}}[j, j]$ for the case that antenna i and j belong to the same relay. Then, $\Theta \bar{\Lambda}$ as in (6.23) can be obtained from $\Theta \hat{\Lambda}$ by omitting all columns corresponding to non-cooperating relay antennas. The LO phase offsets of the relays cancel because $\hat{\Lambda}$ depends on the two-hop product channels only.

From there the relays can easily generate $\Theta_i \bar{\Lambda}_i$ and $\Theta_s \bar{\Lambda}_s$ in the same way that was described above. As long as the LO phase offsets of the relays remain constant for a single transmission cycle, they do not have an impact on the gain allocation.

- Calculation of $\Theta_i \mathbf{h}_{\text{SD},i}$:

Utilizing the matrix equality $\text{vec}(\mathbf{ABC}) = (\mathbf{C}^T \otimes \mathbf{A}) \text{vec}(\mathbf{B})$ readily delivers

$$\begin{aligned} \text{vec}(\hat{\mathbf{H}}_{\text{SD}}) &= (\Phi_{\text{S}}^T \otimes \Phi_{\text{D}}^H) \text{vec}(\mathbf{H}_{\text{SD}}) = \\ &= \Theta \mathbf{h}_{\text{SD}}. \end{aligned} \quad (6.31)$$

From (6.31) the relays get $\Theta_i \mathbf{h}_{\text{SD},i}$ by omitting all rows corresponding to antennas of belonging source-destination pairs.

The relays can thus compute \mathbf{g}_{ZF} according to (6.27) when having estimates $\hat{\mathbf{H}}_{\text{SR}}$, $\hat{\mathbf{H}}_{\text{RD}}$, and $\hat{\mathbf{H}}_{\text{SD}}$ of the channels. As long as the propagation channel coefficients remain unchanged, there is no inter-user interference even if the source and destination LO phase offsets change.

6.2.1.2 Channel Estimation Protocol B1

If the channel coefficients are measured using scheme B1, the relays possess the estimates

$$\hat{\mathbf{H}}_{\text{SD}} = \tilde{\mathbf{H}}_{\text{SD}}, \quad \hat{\mathbf{H}}_{\text{SR}} = \tilde{\mathbf{H}}_{\text{SR}}, \quad \text{and} \quad \hat{\mathbf{H}}_{\text{RD}} = \hat{\mathbf{H}}_{\text{DR}}^T = \Phi_{\text{D}} \Phi_{\text{D}} \tilde{\mathbf{H}}_{\text{RD}} \Phi_{\text{R}}^H \Phi_{\text{R}}^H \quad (6.32)$$

as given in (4.6), (4.7), and (4.14). The LO phases of the relays do not cancel in $\hat{\mathbf{H}}_{\text{SR}}^T \otimes \hat{\mathbf{H}}_{\text{RD}}$ as they do in (6.30). A gain matrix that is calculated in this way depends on Φ_{R} and has to be updated every time the LO phases of the relays change. In a practical system where the LOs of the nodes are subject to phase noise, this is not feasible. The relays are thus required to compensate the impact of their LO phase offsets on the channel estimates. This can be done by providing a common phase reference to all relay terminals (cf. Chapter 5).

In Section 5.2.1, a very simple scheme was introduced that allows each relay R_l to obtain an estimate $\hat{\varphi}_{R_l M}$ of

$$\varphi_{R_l M} = -2\varphi_{R_l} + 2\varphi_M, \quad (6.33)$$

as defined in (5.32). For channel estimation scheme B1, every relay R_l locally estimates its $M_{R_l} M_{\text{S}}$ first-hop and $M_{R_l} M_{\text{D}}$ second-hop channel coefficients. Let $h_{S_k R_{l,i}}$ denote the channel coefficient from source antenna k to antenna i of relay l and, likewise, $h_{D_m R_{l,i}}$ the channel coefficient from destination antenna m to antenna i of the relay. The channel estimates available at relay l are in this case

$$\hat{h}_{S_k R_{l,i}} = h_{S_k R_{l,i}} e^{j(\varphi_{S_k} - \varphi_{R_l})} \quad (6.34)$$

$$\hat{h}_{D_m R_{l,i}} = h_{D_m R_{l,i}} e^{j(\varphi_{D_m} - \varphi_{R_l})}, \quad (6.35)$$

where $k \in \{1, \dots, M_S\}$, $m \in \{1, \dots, M_D\}$, and $i \in \{1, \dots, M_{R_l}\}$. The matrices $\hat{\mathbf{H}}_{\text{SR}}$ and $\hat{\mathbf{H}}_{\text{DR}}$ are estimates of the matrices $\tilde{\mathbf{H}}_{\text{SR}} = \Phi_{\text{R}}^{\text{H}} \mathbf{H}_{\text{SR}} \Phi_{\text{S}}$ and $\tilde{\mathbf{H}}_{\text{DR}} = \Phi_{\text{R}}^{\text{H}} \mathbf{H}_{\text{DR}} \Phi_{\text{D}}$ and comprise the measured channel coefficients from sources to relays and from destinations to relays, respectively. Using its respective phase estimate $\hat{\varphi}_{R_l M}$, relay l then computes

$$\check{h}_{S_k R_l, i} = \hat{h}_{S_k R_l, i} \cdot e^{-j \frac{1}{2} \hat{\varphi}_{R_l M}} \quad (6.36)$$

$$\check{h}_{D_m R_l, i} = \hat{h}_{D_m R_l, i} \cdot e^{-j \frac{1}{2} \hat{\varphi}_{R_l M}}, \quad (6.37)$$

for $i \in \{1, \dots, M_{R_l}\}$, and disseminates this information instead of $\hat{h}_{S_k R_l, i}$ and $\hat{h}_{D_m R_l, i}$ to all other relays. Every relay can then locally generate the matrices

$$\check{\mathbf{H}}_{\text{SR}} = \begin{bmatrix} e^{-j \frac{1}{2} \hat{\varphi}_{R_1 M}} & & \\ & \ddots & \\ & & e^{-j \frac{1}{2} \hat{\varphi}_{R_{N_R} M}} \end{bmatrix} \cdot \hat{\mathbf{H}}_{\text{SR}} := \hat{\Phi}_{\text{RM}}^{\frac{1}{2}} \hat{\mathbf{H}}_{\text{SR}} \quad (6.38)$$

and

$$\check{\mathbf{H}}_{\text{DR}} = \begin{bmatrix} e^{-j \frac{1}{2} \hat{\varphi}_{R_1 M}} & & \\ & \ddots & \\ & & e^{-j \frac{1}{2} \hat{\varphi}_{R_{N_R} M}} \end{bmatrix} \cdot \hat{\mathbf{H}}_{\text{DR}} := \hat{\Phi}_{\text{RM}}^{\frac{1}{2}} \hat{\mathbf{H}}_{\text{DR}}. \quad (6.39)$$

Calculating $\check{\mathbf{H}}_{\text{SR}}^{\text{T}} \otimes \check{\mathbf{H}}_{\text{RD}}$, where $\check{\mathbf{H}}_{\text{RD}} = \check{\mathbf{H}}_{\text{DR}}^{\text{T}}$, results in

$$\begin{aligned} \check{\mathbf{H}}_{\text{SR}}^{\text{T}} \otimes \check{\mathbf{H}}_{\text{RD}} &= \left(\hat{\mathbf{H}}_{\text{SR}}^{\text{T}} \hat{\Phi}_{\text{RM}}^{\frac{1}{2}} \otimes \hat{\mathbf{H}}_{\text{RD}} \hat{\Phi}_{\text{RM}}^{\frac{1}{2}} \right) = \\ &= \left(\Phi_{\text{S}}^{\text{T}} \mathbf{H}_{\text{SR}}^{\text{T}} \Phi_{\text{R}}^* \hat{\Phi}_{\text{RM}}^{\frac{1}{2}} \otimes \Phi_{\text{D}} \mathbf{H}_{\text{RD}} \Phi_{\text{R}}^{\text{H}} \hat{\Phi}_{\text{RM}}^{\frac{1}{2}} \right). \end{aligned} \quad (6.40)$$

Again, the simple matrix equality $(\mathbf{A}\mathbf{B} \otimes \mathbf{C}\mathbf{D}) = (\mathbf{A} \otimes \mathbf{C})(\mathbf{B} \otimes \mathbf{D})$ is used to get

$$\begin{aligned} \check{\mathbf{H}}_{\text{SR}}^{\text{T}} \otimes \check{\mathbf{H}}_{\text{RD}} &= (\Phi_{\text{S}}^{\text{T}} \otimes \Phi_{\text{D}}^{\text{T}}) \left(\mathbf{H}_{\text{SR}}^{\text{T}} \Phi_{\text{R}}^{\text{H}} \hat{\Phi}_{\text{RM}}^{\frac{1}{2}} \otimes \mathbf{H}_{\text{RD}} \Phi_{\text{R}}^{\text{H}} \hat{\Phi}_{\text{RM}}^{\frac{1}{2}} \right) := \\ &:= \Theta' \check{\mathbf{\Lambda}}, \end{aligned} \quad (6.41)$$

where $\Theta' := (\Phi_{\text{S}}^{\text{T}} \otimes \Phi_{\text{D}}^{\text{T}})$ and $\check{\mathbf{\Lambda}} := \left(\mathbf{H}_{\text{SR}}^{\text{T}} \Phi_{\text{R}}^{\text{H}} \hat{\Phi}_{\text{RM}}^{\frac{1}{2}} \otimes \mathbf{H}_{\text{RD}} \Phi_{\text{R}}^{\text{H}} \hat{\Phi}_{\text{RM}}^{\frac{1}{2}} \right)$. Assume that all cooperating relay antennas exhibit the same LO phase offset. Then, $e^{-j2\varphi_M} \Theta' \bar{\mathbf{\Lambda}}$ (with $\bar{\mathbf{\Lambda}}$ as in (6.23)) can be obtained from $\check{\mathbf{\Lambda}}$ by omitting the columns that correspond to non-cooperating relay antennas. From there, the relays get $e^{-j2\varphi_M} \Theta'_i \bar{\mathbf{\Lambda}}_i$ by omitting the rows corresponding to belonging source-destination pairs. Furthermore, they know $\Theta \mathbf{h}_{\text{SD}}$ using

the estimated direct link channel matrix $\hat{\mathbf{H}}_{SD}$ (see (6.31)). Note that $\Theta = (\Phi_S^T \otimes \Phi_D^H) \neq \Theta'$. The ZF condition (6.26) is

$$\Theta_i \bar{\Lambda}_i \cdot \frac{1}{\gamma_{III}} \bar{\mathbf{g}}_{ZF} + \Theta_i \mathbf{h}_{SD,i} \stackrel{!}{=} \mathbf{0}. \quad (6.42)$$

With knowledge of $\Theta_i' \bar{\Lambda}_i$ and $\Theta_i \mathbf{h}_{SD,i}$, there is no way the relays can compute $\bar{\mathbf{g}}_{ZF}$ fulfilling (6.42). In particular,

$$\bar{\mathbf{g}}'_{ZF} = -\gamma_{III} \cdot \bar{\Lambda}_i^H \Theta_i'^H \left(\Theta_i' \bar{\Lambda}_i \bar{\Lambda}_i^H \Theta_i'^H \right)^{-1} \Theta_i \mathbf{h}_{SD,i}. \quad (6.43)$$

does not fulfill (6.42) if the LO phases of the destinations are random and unknown.

Only if the relays and destinations possess a common global phase reference (as predicted in Section 4.2), can the relays compute the gain factors correctly. Assume that the LOs of all relays and destinations exhibit a phase denoted by ϕ . Then, $\hat{\mathbf{H}}_{RD} = \tilde{\mathbf{H}}_{RD}$ and the gain factors can be computed as for channel estimation protocol A1 in Section 6.2.1.1.

6.2.2 Traffic Pattern IV

For traffic pattern IV, the relays have to orthogonalize the two-hop link, i.e. the equivalent two-hop channel matrix $\tilde{\mathbf{H}}_{IV} = \tilde{\mathbf{H}}_{SRD}$ (cf. (6.12)) has to become block diagonal. Using the simple matrix equalities (6.16) and (6.17) delivers the compound channel vector

$$\begin{aligned} \tilde{\mathbf{h}}_{IV} &= \text{vec} \left(\tilde{\mathbf{H}}_{IV} \right) = \\ &= (\Phi_S^T \otimes \Phi_D^H) (\mathbf{H}_{SR}^T \otimes \mathbf{H}_{RD}) \cdot \text{vec}(\mathbf{G}) := \\ &:= \Theta \Lambda \cdot \mathbf{g}, \end{aligned} \quad (6.44)$$

where

$$\Theta := \Phi_S^T \otimes \Phi_D^H, \quad (6.45)$$

$$\Lambda := \mathbf{H}_{SR}^T \otimes \mathbf{H}_{RD}, \quad (6.46)$$

$$\text{and } \mathbf{g} := \text{vec}(\mathbf{G}). \quad (6.47)$$

The gain matrix contains zeros where there is no cooperation between the relay antennas. The zero elements of the compound gain vector \mathbf{g} and the corresponding columns of Λ can

simply be dropped for a given relay cooperation pattern. Consequently,

$$\mathbf{g} \in \mathbb{C}^{M_R^2} \rightarrow \bar{\mathbf{g}} \in \mathbb{C}^{N_{\text{coop}}} \quad \text{and} \quad \mathbf{\Lambda} \in \mathbb{C}^{M_S M_D \times M_R^2} \rightarrow \bar{\mathbf{\Lambda}} \in \mathbb{C}^{M_S M_D \times N_{\text{coop}}}. \quad (6.48)$$

The compound channel vector can then be written as

$$\tilde{\mathbf{h}}_{\text{IV}} = \mathbf{\Theta} \bar{\mathbf{\Lambda}} \cdot \bar{\mathbf{g}}. \quad (6.49)$$

The compound channel coefficients can be divided into $N_{\text{signal}} = \sum_{i=1}^{N_{\text{SD}}} M_{S_i} M_{D_i}$ coefficients over which signal power arrives at the destinations and $N_{\text{int}} = M_S M_D - N_{\text{signal}}$ coefficient over which interference is generated. Let $\tilde{\mathbf{h}}_{\text{IV},s} \in \mathbb{C}^{N_{\text{signal}}}$ and $\tilde{\mathbf{h}}_{\text{IV},i} \in \mathbb{C}^{N_{\text{int}}}$ denote the vector of signal channel coefficients and the vector of interference channel coefficients, respectively. Together they constitute $\tilde{\mathbf{h}}_{\text{IV}}$. The 'compound signal channel matrix' $\bar{\mathbf{\Lambda}}_s \in \mathbb{C}^{N_{\text{signal}} \times N_{\text{coop}}}$ and the 'compound interference channel matrix' $\bar{\mathbf{\Lambda}}_i \in \mathbb{C}^{N_{\text{int}} \times N_{\text{coop}}}$ as well as the corresponding matrices $\mathbf{\Theta}_s$ and $\mathbf{\Theta}_i$ are defined such that

$$\tilde{\mathbf{h}}_{\text{IV},s} = \mathbf{\Theta}_s \bar{\mathbf{\Lambda}}_s \cdot \bar{\mathbf{g}} \quad \text{and} \quad \tilde{\mathbf{h}}_{\text{IV},i} = \mathbf{\Theta}_i \bar{\mathbf{\Lambda}}_i \cdot \bar{\mathbf{g}}. \quad (6.50)$$

The matrix $\bar{\mathbf{\Lambda}}_s$ is obtained from $\bar{\mathbf{\Lambda}}$ by taking the rows that correspond to antennas belonging to a source-destination pair and $\bar{\mathbf{\Lambda}}_i$ is obtained by taking the rows corresponding to antennas of non-belonging sources and destinations. The matrices $\mathbf{\Theta}_s$ and $\mathbf{\Theta}_i$ are then again diagonal. In order to block-orthogonalize all source-destination pairs, i.e. cancel all inter-user interference, it is required that

$$\tilde{\mathbf{h}}_{\text{IV},i} = \mathbf{0}. \quad (6.51)$$

Equation (6.51) is called the 'ZF condition'. The SVD of $\bar{\mathbf{\Lambda}}_i^H \mathbf{\Theta}_i^H$ is given by

$$\mathbf{U} \mathbf{S} \mathbf{V}^H = \bar{\mathbf{\Lambda}}_i^H \mathbf{\Theta}_i^H, \quad (6.52)$$

where the matrices \mathbf{U} and \mathbf{V} are unitary and \mathbf{S} is diagonal (comprising the ordered singular values). The nullspace of $\mathbf{\Theta}_i \bar{\mathbf{\Lambda}}_i$ is denoted by

$$\mathbf{Z}_{\text{IV}} = \text{Null}(\mathbf{\Theta}_i \bar{\mathbf{\Lambda}}_i). \quad (6.53)$$

If it is nonempty and has rank N_0 , it is spanned by the last N_0 columns of \mathbf{U} . Any vector $\bar{\mathbf{g}}_{\text{ZF}}$ lying in this nullspace fulfills

$$\Theta_i \bar{\Lambda}_i \cdot \bar{\mathbf{g}}_{\text{ZF}} = \mathbf{0} \quad (6.54)$$

and thus the ZF condition (6.51). Choosing $\bar{\mathbf{g}}_{\text{ZF}}$ as the last column of \mathbf{U} fulfills the ZF condition if $N_0 > 0$. And in the case that the nullspace is empty, i.e. $N_0 = 0$, inter-user interference is projected onto the weakest subchannel, thus keeping it small.

For the case that $N_0 > 1$, the gain factors can be further optimized (e.g. [70]). A particularly simple way of doing this is to choose a smart initial gain vector and project it onto the nullspace \mathbf{Z}_{IV} of $\Theta_i \bar{\Lambda}_i$. In [25] and [90] the authors find that performing a simple channel matched receive and transmit filtering at each relay orthogonalizes all source-destination pairs if the number of relay antennas goes to infinity. Following this notion, the initial gain vector is chosen as

$$\mathbf{g}_{\text{init}} = \bar{\Lambda}_s^H \Theta_s^H \cdot \mathbf{1}_{N_{\text{signal}}}, \quad (6.55)$$

where $\mathbf{1}_{N_{\text{signal}}}$ is a vector of size $N_{\text{signal}} \times 1$ comprising all ones. Each component of \mathbf{g}_{init} is now matched to the sum of all two-hop channel coefficients contributing signal energy at the destinations.

Example: In a system with single antenna nodes, the N_{R} entries of \mathbf{g}_{init} would be

$$\mathbf{g}_{\text{init}}[l] = \sum_{i=1}^{N_{\text{SD}}} h_{\text{R}_l \text{D}_i}^* h_{\text{S}_i \text{R}_l}^*, \quad \text{for } l \in \{1, \dots, N_{\text{R}}\}. \quad (6.56)$$

In this way, the gain factors are weighted with the strength of the first-hop and second-hop channel coefficients contributing signal power at the destinations. In order to get $\bar{\mathbf{g}}_{\text{ZF}}$, the vector \mathbf{g}_{init} has to be projected onto the nullspace \mathbf{Z}_{IV} :

$$\bar{\mathbf{g}}_{\text{ZF}} = \mathbf{Z}_{\text{IV}} \mathbf{Z}_{\text{IV}}^H \cdot \mathbf{g}_{\text{init}}. \quad (6.57)$$

A necessary but not sufficient condition for the nullspace of $\Theta_i \bar{\Lambda}_i$ to be nonempty is $N_{\text{coop}} > N_{\text{int}}$. The case that $N_{\text{coop}} = N_{\text{int}} + 1$ is referred to as 'minimum cooperation configuration'. The nullspace of $\Theta_i \bar{\Lambda}_i$ has then dimension one. Note that this is one dimension more than required for traffic pattern III. In order to achieve the full spatial multiplexing gain $N_{\text{SM}} =$

$\sum_{i=1}^{N_{SD}} \min \{M_{S_i}, M_{D_i}\}$, the compound channel matrix has to have rank N_{SM} . Since

$$\text{rank} \left(\tilde{\mathbf{H}}_{RD} \mathbf{G} \tilde{\mathbf{H}}_{SR} \right) \leq \min \left\{ \text{rank} \left(\tilde{\mathbf{H}}_{RD} \right), \text{rank} (\mathbf{G}), \text{rank} \left(\tilde{\mathbf{H}}_{SR} \right) \right\}, \quad (6.58)$$

the gain matrix \mathbf{G} has to have at least rank N_{SM} . For the computation of $\bar{\mathbf{g}}_{ZF}$ according to (6.57), each relay needs to know $\Theta_i \bar{\Lambda}_i$ and $\Theta_s \bar{\Lambda}_s$. Two issues arise:

1. The LO phase offsets of all sources and destinations (contained in Φ_S and Φ_D , respectively) enter the calculation of $\bar{\mathbf{g}}_{ZF}$ via the matrix Θ . Due to phase noise, its entries will change over time. Given a quasi-static propagation environment, the channel coefficients (and therefore also $\bar{\Lambda}_i$ and $\bar{\Lambda}_s$) are assumed to stay constant for a couple of transmission cycles. However, Θ is likely to change more rapidly in the presence of phase noise. Luckily, this does not impede the calculation of a gain vector fulfilling the ZF condition (6.51), since any $\bar{\mathbf{g}}_{ZF}$ fulfilling $\Theta_i \bar{\Lambda}_i \cdot \bar{\mathbf{g}}_{ZF} = \mathbf{0}$ will do so for any invertible matrix Θ_i .
2. The channel estimates from which the gain vector is computed depend on the LO phase offsets of the relays (contained in Φ_R). However, they appear neither in Θ nor in Λ . The following Sections 6.2.2.1 and 6.2.2.2 show how the relays can still compute their ZF gain factors based on channel estimates obtained by channel estimation protocols A1 and B1 introduced in Section 4.4.

It is again assumed that all channel estimates are noiseless and that the LO phases of all relays remain constant for at least one transmission cycle.

6.2.2.1 Channel Estimation Protocol A1

Assume that the channel coefficients have been measured using protocol A1 and then disseminated to all relays. Each relay then possesses the estimates

$$\hat{\mathbf{H}}_{SR} = \tilde{\mathbf{H}}_{SR} \quad \text{and} \quad \hat{\mathbf{H}}_{RD} = \tilde{\mathbf{H}}_{RD}. \quad (6.59)$$

The relays have to calculate

$$\begin{aligned} \hat{\mathbf{H}}_{SR}^T \otimes \hat{\mathbf{H}}_{RD} &= (\Phi_S^T \otimes \Phi_D^H) (\mathbf{H}_{SR}^T \Phi_R^* \otimes \mathbf{H}_{RD} \Phi_R) := \\ &:= \Theta \hat{\Lambda}, \end{aligned} \quad (6.60)$$

where Θ is the same as in (6.49). Assume that all cooperating relay antennas exhibit the same LO phase offset, i.e., $\Phi_R[i, i] = \Phi_R[j, j]$ for the case that antenna i and j belong to

the same relay. Then, $\Theta\bar{\Lambda}$ (as in (6.49)) can be obtained from $\Theta\hat{\Lambda}$ by omitting all columns corresponding to non-cooperating relay antennas. The LO phase offsets of the relays cancel because $\hat{\Lambda}$ depends on the two-hop product channels only.

From there they can easily generate $\bar{\Lambda}_i$, $\bar{\Lambda}_s$ and thus the gain factors in the same way that was described in Section 6.2.1.1. As long as the LO phase offsets of the relays remain constant for a single transmission cycle, they do not have an impact on the gain allocation.

6.2.2.2 Channel Estimation Protocol B1

If channel estimation protocol B1 is used to estimate all channel coefficients, the relays possess the estimates

$$\hat{\mathbf{H}}_{\text{SR}} = \tilde{\mathbf{H}}_{\text{SR}}, \quad \text{and} \quad \hat{\mathbf{H}}_{\text{RD}} = \hat{\mathbf{H}}_{\text{DR}}^T = \Phi_{\text{D}} \Phi_{\text{D}} \tilde{\mathbf{H}}_{\text{RD}} \Phi_{\text{R}}^H \Phi_{\text{R}}^H \quad (6.61)$$

The gain factors depend on the current LO phases of the relays if they are computed from $\hat{\mathbf{H}}_{\text{SR}}$ and $\hat{\mathbf{H}}_{\text{RD}}$. This means that the gain matrix becomes outdated as soon as the relay phases change. Assume instead that the same procedure as described in Section 6.2.1.2 is followed. The relays can then calculate $e^{-j2\varphi_{\text{M}}}\Theta'\bar{\Lambda}$, where $\Theta' = (\Phi_{\text{S}}^T \otimes \Phi_{\text{D}}^T) \neq \Theta$ and $\bar{\Lambda}$ as in (6.49). Next, they compute the nullspace

$$\mathbf{Z}_{\text{IV}} = \text{Null} \left(e^{-j2\varphi_{\text{M}}}\Theta'_i \bar{\Lambda}_i \right), \quad (6.62)$$

where $e^{-j2\varphi_{\text{M}}}\Theta'_i \bar{\Lambda}_i$ is obtained from $e^{-j2\varphi_{\text{M}}}\Theta'\bar{\Lambda}$ in the same $\Theta'_i \bar{\Lambda}_i$ is obtained from $\Theta\bar{\Lambda}$ in (6.50). Any vector $\bar{\mathbf{g}}_{\text{ZF}}$ that lies in the vector space spanned by the columns of \mathbf{Z}_{IV} fulfills

$$e^{-j2\varphi_{\text{M}}}\Theta'_i \bar{\Lambda}_i \cdot \bar{\mathbf{g}}_{\text{ZF}} = \mathbf{0}. \quad (6.63)$$

Since Θ'_i is invertible and $e^{-j2\varphi_{\text{M}}}$ a scalar, $\bar{\mathbf{g}}_{\text{ZF}}$ also meets the ZF constraint (6.51).

6.2.3 Impact of Phase Estimation Error

Consider a wireless ad hoc network using traffic pattern IV in combination with channel estimation protocol B1. Phase synchronization is achieved with the SB scheme introduced in Section 5.2.1. The aim of this section is to assess the impact of phase estimation errors $\Delta\varphi_{\text{R}_i}^{(\text{SB})}$ on the performance of the ZF gain allocation. For the sake of a simpler notation, all nodes in the network are assumed to employ a single antenna only. The gain matrix \mathbf{G} is then diagonal. Extending the considerations to multi-antenna nodes is straightforward.

All relays estimate φ_{R_iM} according to the SB phase estimation scheme with sequential synchronization. The LO phase offsets of all nodes are assumed to stay constant during a whole transmission cycle. The compound channel matrix is then given by

$$\tilde{\mathbf{H}}_{IV} = \mathbf{\Phi}_D^H \mathbf{H}_{RD} \mathbf{G} \mathbf{H}_{SR} \mathbf{\Phi}_S. \quad (6.64)$$

The vector \mathbf{h}_{S_kR} is defined such that it comprises the channel coefficients from source k to all relays and \mathbf{h}_{RD_m} is defined such that it comprises the coefficients from all relays to destination m . They correspond to the k th and m th column of \mathbf{H}_{SR} and \mathbf{H}_{RD}^T , respectively. The compound channel coefficient from source k to destination m can then be written as

$$\tilde{\mathbf{H}}_{IV}[m, k] = \mathbf{g}^T (\mathbf{h}_{S_kR} \odot \mathbf{h}_{RD_m}) e^{j(\varphi_{S_k} - \varphi_{D_m})}, \quad (6.65)$$

where $\mathbf{g} = \text{diag}(\mathbf{G})$. For channel estimation protocol B1, the relays know

$$\check{\mathbf{H}}_{SR} = \hat{\mathbf{\Phi}}_{RM}^{\frac{1}{2}} \hat{\mathbf{H}}_{SR} \quad \text{and} \quad \check{\mathbf{H}}_{DR} = \hat{\mathbf{\Phi}}_{RM}^{\frac{1}{2}} \hat{\mathbf{H}}_{DR} \quad (6.66)$$

as defined in (6.38) and (6.39), rather than $\tilde{\mathbf{H}}_{SR}$ and $\tilde{\mathbf{H}}_{RD}$. The compound channel matrix anticipated by the relays is

$$\begin{aligned} \check{\mathbf{H}}_{IV} &= \check{\mathbf{H}}_{DR}^T \mathbf{G} \check{\mathbf{H}}_{SR} = \\ &= \left(\hat{\mathbf{\Phi}}_{RM}^{\frac{1}{2}} \mathbf{\Phi}_R^H \mathbf{H}_{DR} \mathbf{\Phi}_D \right)^T \cdot \mathbf{G} \cdot \hat{\mathbf{\Phi}}_{RM}^{\frac{1}{2}} \mathbf{\Phi}_R^H \mathbf{H}_{SR} \mathbf{\Phi}_S = \\ &= \mathbf{\Phi}_D^H \mathbf{H}_{RD} \hat{\mathbf{\Phi}}_{RM} \mathbf{\Phi}_R^H \mathbf{\Phi}_R^H \mathbf{G} \mathbf{H}_{SR} \mathbf{\Phi}_S, \end{aligned} \quad (6.67)$$

where the fact that $\mathbf{\Phi}_R$, $\mathbf{\Phi}_D$, and $\hat{\mathbf{\Phi}}_{RM}^{\frac{1}{2}}$ are diagonal was used. Furthermore, it was assumed that all antennas belonging to one relay exhibit the same LO phase offset. With (6.65), the anticipated compound channel coefficient from source k to destination m is

$$\begin{aligned} \check{\mathbf{H}}_{IV}[m, k] &= \mathbf{g}^T \left(\check{\mathbf{h}}_{S_kR} \odot \check{\mathbf{h}}_{RD_m} \right) e^{j(\varphi_{S_k} - \varphi_{D_m})} = \\ &= \mathbf{g}^T \hat{\mathbf{\Phi}}_{RM} \mathbf{\Phi}_R^H \mathbf{\Phi}_R^H (\mathbf{h}_{S_kR} \odot \mathbf{h}_{RD_m}) e^{j(\varphi_{S_k} - \varphi_{D_m})}. \end{aligned} \quad (6.68)$$

The matrix $\check{\mathbf{Z}}_{IV}$ is defined such that its columns span the vector space out of which any vector $\check{\mathbf{g}}_{ZF}$ satisfies

$$\check{\mathbf{H}}_{IV}[m, k] = \check{\mathbf{g}}_{ZF}^T (\mathbf{h}_{S_kR} \odot \mathbf{h}_{RD_m}) e^{j(\varphi_{S_k} - \varphi_{D_m})} = 0, \quad (6.69)$$

for all $m \neq k$. Furthermore, the matrix $\check{\mathbf{Z}}_{IV}$ is defined such that its columns span the vector space out of which any vector $\check{\mathbf{g}}_{ZF}$ satisfies

$$\check{\mathbf{H}}_{IV}[m, k] = \check{\mathbf{g}}_{ZF}^T \hat{\Phi}_{RM} \Phi_R^H \Phi_R^H (\mathbf{h}_{S_kR} \odot \mathbf{h}_{RD_m}) e^{j(\varphi_{S_k} - \varphi_{D_m})} = 0, \quad (6.70)$$

for all $m \neq k$. If the phase estimation is perfect, i.e. $\hat{\varphi}_{R_lM} = \varphi_{R_lM} = -2\varphi_{R_l} + 2\varphi_{R_M}$, then $\hat{\Phi}_{RM} \Phi_R^H \Phi_R^H = e^{-2j\varphi_M} \mathbf{I}_{N_R}$. In the presence of a phase error, i.e. $\Delta\hat{\varphi}_{R_l} = \hat{\varphi}_{R_lM} - \varphi_{R_lM} \neq 0$, we get

$$\hat{\Phi}_{RM} \Phi_R^H \Phi_R^H = e^{-2j\varphi_M} \Theta_R, \quad (6.71)$$

where

$$\Theta_R = \begin{bmatrix} e^{j\theta_{R_1}} & & & \\ & \ddots & & \\ & & \ddots & \\ & & & e^{j\theta_{R_{N_R}}} \end{bmatrix}. \quad (6.72)$$

The phase errors $\theta_{R_l} = -\hat{\varphi}_{R_lM} - 2\varphi_{R_l} + 2\varphi_M$ in Θ_R are the difference between φ_{R_lM} defined in (6.33) and its estimate $\hat{\varphi}_{R_lM}$. From and (6.69) and (6.70) it follows that there exists a vector $\check{\mathbf{g}}_{ZF}$ such that

$$\check{\mathbf{g}}_{ZF}^T = \check{\mathbf{g}}_{ZF}^T \Theta_R. \quad (6.73)$$

Knowing $\check{\mathbf{H}}_{IV}$, the relays can compute $\check{\mathbf{g}}_{ZF}$ such that it satisfies (6.70). With (6.73), it can be written as

$$\check{\mathbf{g}}_{ZF}^T = \check{\mathbf{g}}_{ZF}^T \Theta_R^H. \quad (6.74)$$

Inserting $\check{\mathbf{g}}_{ZF}^T$ from (6.74) into (6.65) yields

$$\begin{aligned} \check{\mathbf{H}}_{IV}[m, k] &= \check{\mathbf{g}}_{ZF}^T (\mathbf{h}_{S_kR} \odot \mathbf{h}_{RD_m}) e^{j(\varphi_{S_k} - \varphi_{D_m})} = \\ &= \check{\mathbf{g}}_{ZF}^T \Theta_R^H (\mathbf{h}_{S_kR} \odot \mathbf{h}_{RD_m}) e^{j(\varphi_{S_k} - \varphi_{D_m})} = \\ &= \Theta_R^H (\check{\mathbf{g}}_{ZF} \odot \mathbf{h}_{S_kR} \odot \mathbf{h}_{RD_m}) e^{j(\varphi_{S_k} - \varphi_{D_m})} := \\ &:= \Theta_R^H \tilde{\mathbf{h}}_{S_kRD_m}, \end{aligned} \quad (6.75)$$

where $\boldsymbol{\theta}_R = \text{diag}(\boldsymbol{\Theta}_R)$. Furthermore, the vector

$$\tilde{\mathbf{h}}_{S_k R D_m} := (\tilde{\mathbf{g}}_{ZF} \odot \mathbf{h}_{S_k R} \odot \mathbf{h}_{R D_m}) e^{j(\varphi_{S_k} - \varphi_{D_m})} \quad (6.76)$$

comprises the compound channel coefficient from source k via all relays to destination m . For perfect phase estimates, i.e. $\boldsymbol{\Theta}_R = \mathbf{I}_{N_R}$, all inter-user interference is suppressed because in this case $\tilde{\mathbf{H}}_{IV}[m, k] = 0$ for $m \neq k$ (cf. (6.69)). If the phase estimates are noisy, inter-user interference will not be cancelled completely. For a given channel realization, the expected signal and interference power at the destinations in the presence of phase estimation error is

$$\begin{aligned} E_{\theta_R} \left[\left| \tilde{\mathbf{H}}_{IV}[m, k] \right|^2 \right] &= E_{\theta_R} \left[\tilde{\mathbf{h}}_{S_k R D_m}^H \boldsymbol{\theta}_R \boldsymbol{\theta}_R^H \tilde{\mathbf{h}}_{S_k R D_m} \right] = \\ &= \tilde{\mathbf{h}}_{S_k R D_m}^H \cdot E_{\theta_R} \left[\boldsymbol{\theta}_R \boldsymbol{\theta}_R^H \right] \cdot \tilde{\mathbf{h}}_{S_k R D_m} := \\ &:= \tilde{\mathbf{h}}_{S_k R D_m}^H \cdot \mathbf{R}_{\theta_R \theta_R} \cdot \tilde{\mathbf{h}}_{S_k R D_m}, \end{aligned} \quad (6.77)$$

where $\mathbf{R}_{\theta_R \theta_R} := E_{\theta_R} \left[\boldsymbol{\theta}_R \boldsymbol{\theta}_R^H \right]$. The phase errors at different relays are uncorrelated. In Section 5.2.4.3 it was stated that the phase errors are approximately normally distributed. Using this assumption yields $\theta_{R_i} - \theta_{R_j} \sim \mathcal{N} \left(0, \sigma_{\theta_{R_i}}^2 + \sigma_{\theta_{R_j}}^2 \right)$ for $i \neq j$. The variance of the phase error of each relay node is given in (5.69). The entries of the covariance matrix are then

$$\mathbf{R}_{\theta_R \theta_R}[i, j] = E_{\theta_R} \left[e^{j(\theta_{R_i} - \theta_{R_j})} \right] = \begin{cases} 1, & i = j \\ e^{-\frac{1}{2}(\sigma_{\theta_{R_i}}^2 + \sigma_{\theta_{R_j}}^2)}, & i \neq j \end{cases}, \quad (6.78)$$

where the expectation for $i \neq j$ follows directly from the characteristic function of a Gaussian random variable. Obviously, the interference power is bounded with respect to the variance of the phase error:

- If $\sigma_{\theta_{R_l}}^2 \rightarrow 0$, for all relays $l \in \{1, \dots, N_R\}$, then $\tilde{\mathbf{H}}_{IV}[m, k] = 0$ for $k \neq m$.
- If $\sigma_{\theta_{R_l}}^2 \rightarrow \infty$, for all relays $l \in \{1, \dots, N_R\}$, then $\mathbf{R}_{\theta_R \theta_R} \rightarrow \mathbf{I}_{N_R}$. In this case, the expected power of the compound channel coefficient simplifies to

$$E_{\theta_R} \left[\left| \tilde{\mathbf{H}}_{IV}[m, k] \right|^2 \right] = \mathbf{h}_{S_k R D_m}^H \mathbf{h}_{S_k R D_m}. \quad (6.79)$$

6.2.4 Simulation Results

This section presents the results of Monte-Carlo simulations that have been performed in MATLAB[®]. Consider the system introduced in Chapter 2 with N_{SD} source-destination pairs and N_{R} relays. Although the relays may have an arbitrary number of antennas, the focus lies on the two special cases LinRel and LDAS. Furthermore, all source and destination nodes are assumed to be equipped with a single antenna only.

The SNR is defined by means of the reference system introduced in Section 2.5. An instantaneous sum transmit power constraint as described in Section 6.1 is used for all nodes. The channel model described in Section 2.2 is slightly adapted for the simulation results in this section. The channel coefficients are

$$\mathbf{H}_{\text{SR}}[l, k] \sim \mathcal{CN}(0, \sigma_h^2), \quad k \in \{1, \dots, M_{\text{S}}\}, l \in \{1, \dots, M_{\text{R}}\} \quad (6.80)$$

$$\mathbf{H}_{\text{RD}}[m, l] \sim \mathcal{CN}(0, \sigma_h^2), \quad l \in \{1, \dots, M_{\text{R}}\}, m \in \{1, \dots, M_{\text{D}}\} \quad (6.81)$$

$$\mathbf{H}_{\text{SD}}[m, k] \sim \mathcal{CN}(0, \alpha \sigma_h^2), \quad k \in \{1, \dots, M_{\text{S}}\}, m \in \{1, \dots, M_{\text{D}}\} \quad (6.82)$$

for the first-hop, second-hop and direct link, respectively. The factor α , with $0 \leq \alpha \leq 1$, indicates the relative strength of the direct link compared to each of the single-hop links. Until otherwise stated, it is assumed that the LO phase offsets of all nodes stay constant for at least two time slots, i.e. one transmission cycle. In the following, the performance of MUZF for traffic patterns III and IV is compared. The reference curve in the plots represents the reference scenario introduced in Section 2.5. It comprises N_{SD} single-antenna source-destination pairs communicating without relays in a TDD manner.

In Figs. 6.1 and 6.2, the average sum rate of the network is plotted versus the number of relay antennas for the two special cases LinRel and LDAS. There are $N_{\text{SD}} = 4$ single-antenna source-destination pairs and the SNR is 20 dB. On average, all channel coefficients are equally strong, i.e. $\alpha = 1$. For *traffic pattern IV* two gain allocation schemes are distinguished:

- 'traffic pattern IV, U': The gain vector is chosen to be the last column of the unitary matrix \mathbf{U} obtained by singular value decomposition of $\bar{\mathbf{\Lambda}}_1^{\text{H}} \mathbf{\Theta}_1^{\text{H}}$ (cf. (6.52)).
- 'traffic pattern IV, Z': In order to obtain the ZF gain vector, the initial gain vector \mathbf{g}_{init} as defined in (6.55) is projected onto the nullspace \mathbf{Z}_{IV} of $\mathbf{\Theta}_1 \bar{\mathbf{\Lambda}}_1$ (cf. (6.57)).

For the case that the number of relay cooperations is less than the 'minimum cooperation configuration', the nullspace \mathbf{Z}_{IV} is empty. Therefore, the curve labeled 'traffic pattern IV, Z' starts only at $N_{\text{R}} = 13$ and $M_{\text{R}} = 4$ in Figs. 6.1 and 6.2, respectively. However, choosing

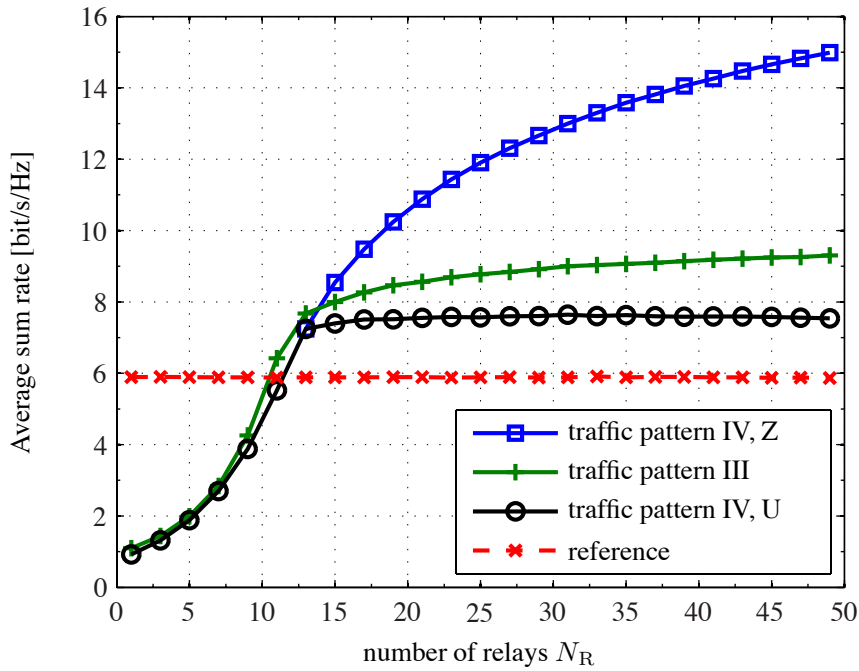


Fig. 6.1: Average sum rate versus N_R for LinRel (single-antenna relays) with 4 single-antenna source-destination pairs, SNR = 20 dB, and $\alpha = 1$.

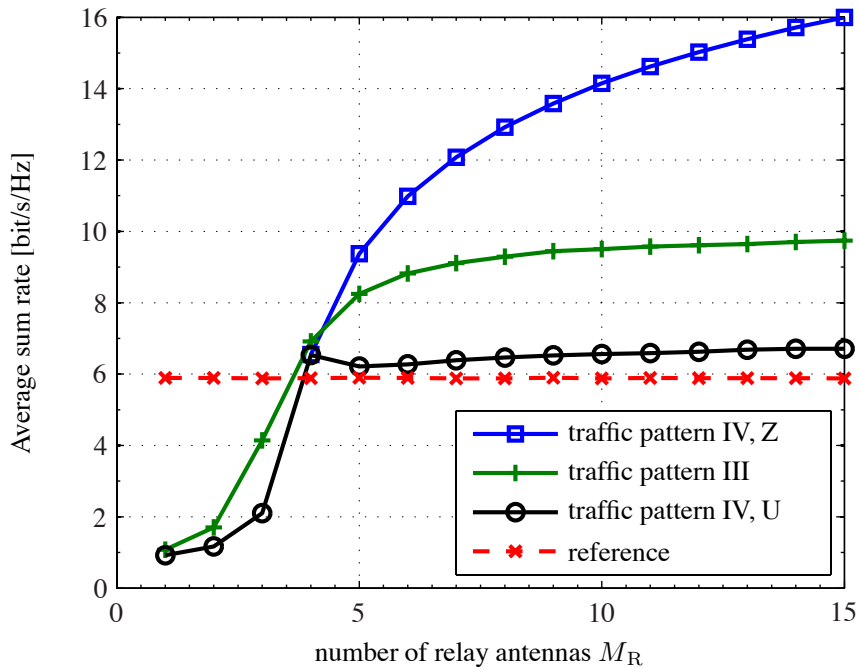


Fig. 6.2: Average sum rate versus M_R for LDAS (single multi-antenna relay) with 4 single-antenna source-destination pairs, SNR = 20 dB, and $\alpha = 1$.

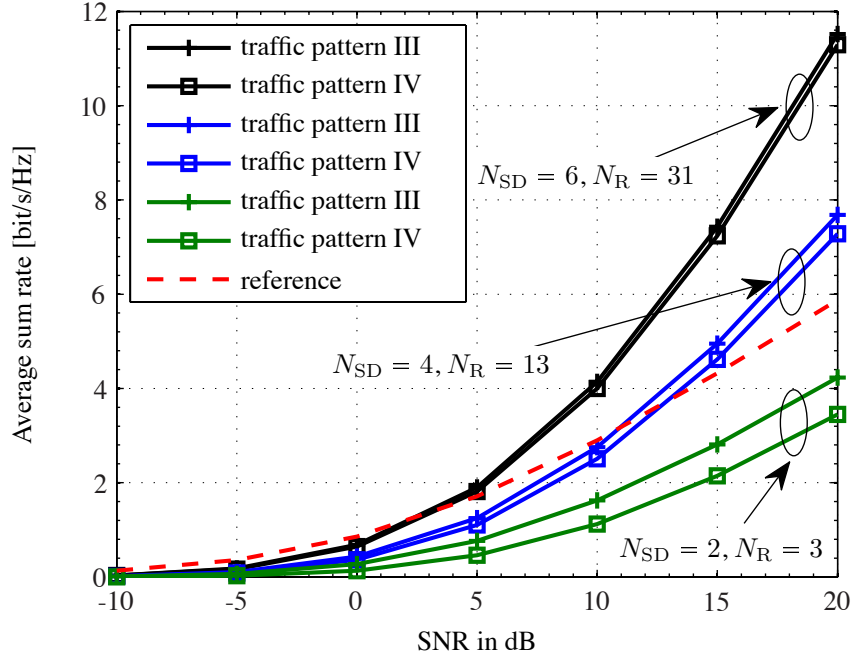


Fig. 6.3: Average sum rate versus SNR for LinRel (single-antenna relays) and $\alpha = 1$.

the last column of \mathbf{U} as gain vector results in a more or less smooth performance degradation for small number of relays. For 'traffic pattern III', the pseudo inverse in (6.27) is used for the cases where the number of relay cooperations is below the minimum cooperation configuration. Inter-user interference is responsible for a low average sum rate in this case. Above the minimum cooperation configuration it can be observed that 'traffic pattern III' gains from excess number of cooperations while the average sum rate remains fairly constant for 'traffic pattern IV, U'. However, 'traffic pattern IV, Z' gains even more substantially from excess number of relays. In the end the curves saturate because the sum transmit power of all relays is constrained. For the minimum cooperation configuration, e.g. $N_R = 13$ for LinRel, both schemes designed for traffic pattern IV exhibit exactly the same performance. The reason for this behavior is that the nullspace has rank one in this case and the two strategies lead to the same gain vector. For the rest of this section, it is assumed that the nullspace \mathbf{Z}_{IV} has at least dimension one. Furthermore, 'traffic pattern IV, U' will be omitted in the following results because it performs worse than 'traffic pattern IV, Z' in this case. The curves for 'traffic pattern IV, Z' will be denoted by 'traffic pattern IV'.

Figs. 6.3 and 6.4 show the average sum rate versus SNR. Again it is assumed that $\alpha = 1$. This represents a worst case scenario for multi-hop relaying since the network cannot benefit from the range-extension capabilities of the relays compared to classical point-to-point

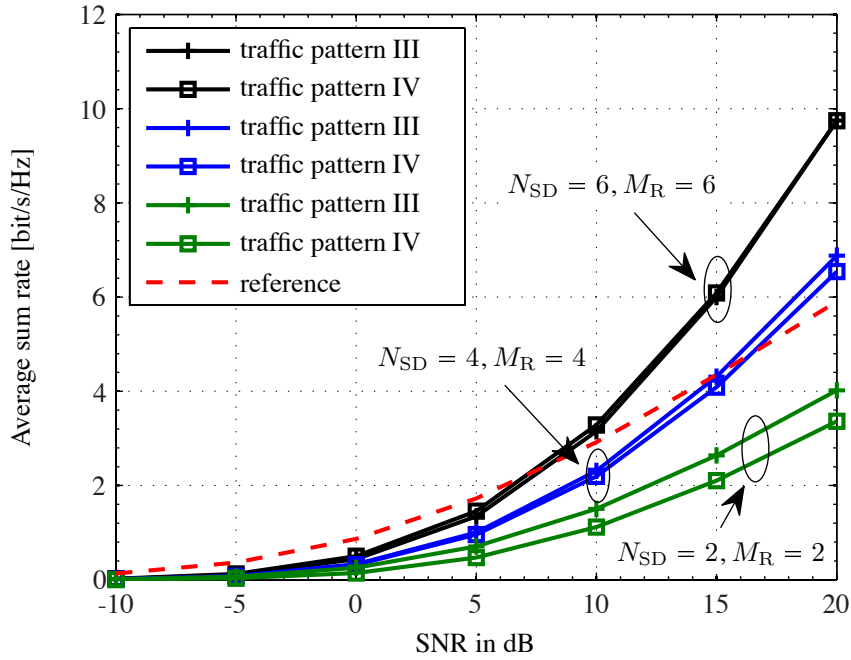


Fig. 6.4: Average sum rate versus SNR for LDAS (single multi-antenna relay) and $\alpha = 1$.

communication. The slope of the curves for both traffic patterns increases with the number of source-destination pairs at high SNR. This shows that the system exhibits a distributed spatial multiplexing gain in the order of source-destination antennas. In Fig. 6.3, the number of cooperations is equal to the minimum cooperation configuration for all curves. Note that for $N_{SD} = 2$, the relaying schemes can never be better than the reference system because of the half-duplex constraint and the fact that $\alpha = 1$.

The average sum rate for different values of α is shown in Figs. 6.5 and 6.6. There are four single-antenna source-destination pairs and the SNR is 20 dB. A smaller value of α corresponds to a weaker direct link compared to the first-hop and second-hop link. The performance of traffic pattern IV is not influenced by α because the direct link is not used. For $\alpha = \frac{1}{4}$ the relays are half-way between sources and destinations when assuming free space propagation with path loss exponent two. For $\alpha = 1$ all channel coefficients have the same variance. Obviously, the two-hop relaying schemes are most beneficial if the direct link is weak.

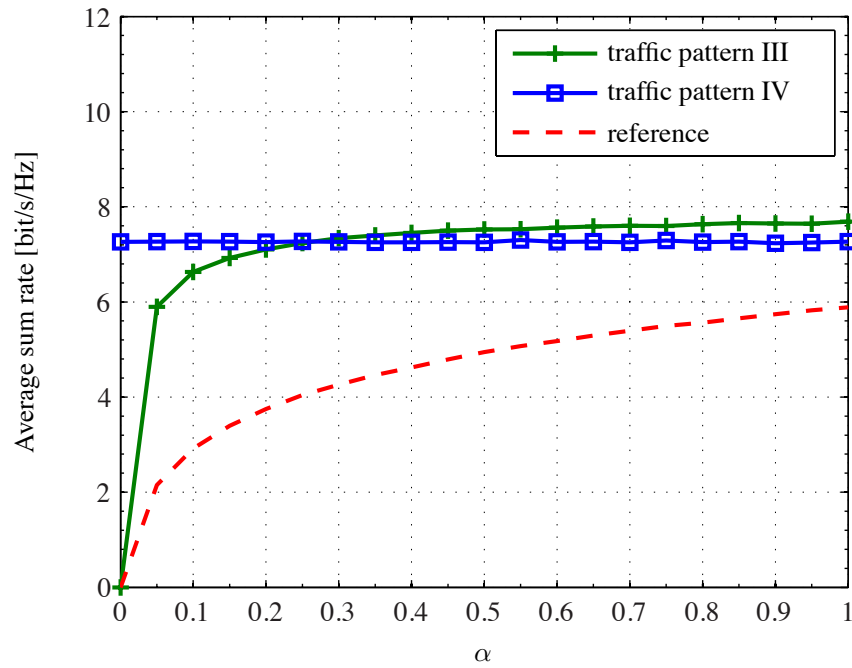


Fig. 6.5: Average sum rate versus α for LinRel (single-antenna relays), 4 single-antenna source-destination pairs and SNR = 20 dB.

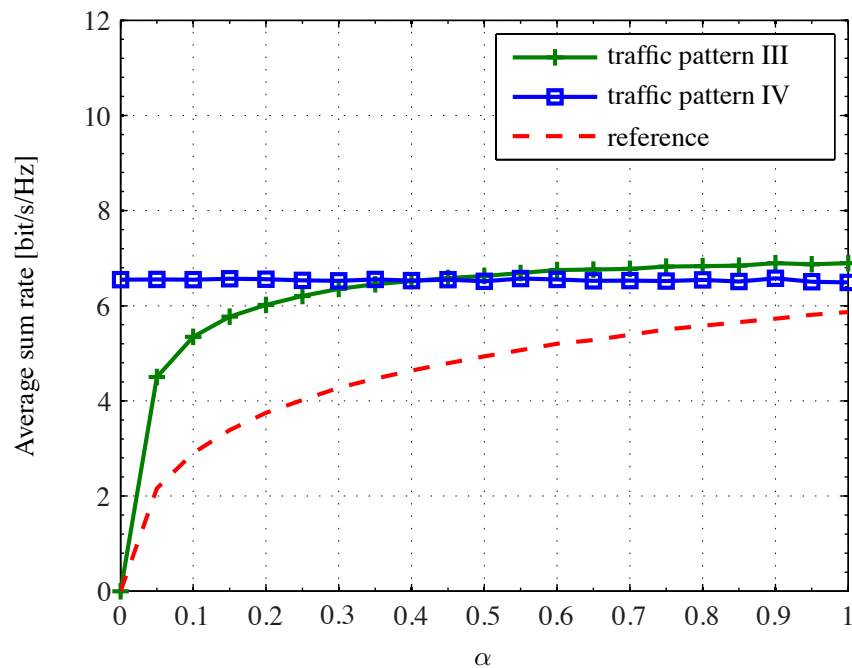


Fig. 6.6: Average sum rate versus α for LDAS (single multi-antenna relay), 4 single-antenna source-destination pairs and SNR = 20 dB.

6.3 Multiuser MMSE Relaying

In this section, an MMSE criterion is used to find the relay gain matrix. In contrast to MUZF relaying, inter-user interference is not completely suppressed. The investigations are restricted to traffic pattern IV introduced in Section 2.4 and the two extreme cases LinRel and LDAS. The superscripts indicating the time slot numbers will be omitted throughout the derivation because the direct link is not used and there is no need to explicitly distinguish between first and second time slot. It is furthermore assumed that all sources and destinations are single-antenna terminals. The constrained optimization problem that has to be solved in order to find the gain matrix \mathbf{G}_{MMSE} can be formulated as follows:

$$\mathbf{G}_{\text{MMSE}} = \arg \min_{\mathbf{G}, \mathbf{\Gamma}} E_{\mathbf{s}, \mathbf{n}_R, \mathbf{n}_D} [\|\mathbf{s} - \mathbf{\Gamma} \mathbf{d}_{\text{IV}}\|_2^2] \quad (6.83)$$

subject to the instantaneous relay transmit power constraint

$$E_{\mathbf{s}, \mathbf{n}_R} [\|\mathbf{G} \mathbf{r}\|_2^2] = P_S. \quad (6.84)$$

The vectors \mathbf{s} ,

$$\mathbf{r} = \tilde{\mathbf{H}}_{\text{SR}} \mathbf{s} + \mathbf{n}_R, \quad (6.85)$$

$$\text{and } \mathbf{d}_{\text{IV}} = \tilde{\mathbf{H}}_{\text{RD}} \mathbf{G} \tilde{\mathbf{H}}_{\text{SR}} \mathbf{s} + \tilde{\mathbf{H}}_{\text{RD}} \mathbf{G} \mathbf{n}_R + \mathbf{n}_D \quad (6.86)$$

comprise the source transmit symbols, the receive symbols at the relays, and the symbols received by the destinations, respectively. The matrix $\mathbf{\Gamma}$ is diagonal and contains scaling factors $\gamma_k \in \mathbb{C}$, $k \in \{1, \dots, N_{\text{SD}}\}$ allowing for received signals that are a scaled and rotated version of the transmitted symbols. The off-diagonal elements of $\mathbf{\Gamma}$ have to be zero because the destinations do not exchange received symbols. For the remainder of this section, all expectations $E[\cdot]$ are taken with respect to transmit symbols $s[k]$ and noise samples $\mathbf{n}_R[l]$ and $\mathbf{n}_D[m]$. In order to solve the constrained optimization problem in equations (6.83) and (6.84), the method of Lagrangian Multipliers (e.g. [193]) is used. The Lagrangian function

L is in the present case a function of \mathbf{G} , $\mathbf{\Gamma}$, and λ :

$$\begin{aligned}
 L(\mathbf{G}, \mathbf{\Gamma}, \lambda) &= \mathbb{E} \left[\|\mathbf{s} - \mathbf{\Gamma} \mathbf{d}_{\text{IV}}\|_2^2 \right] + \lambda \left(\mathbb{E} \left[\|\mathbf{G} \mathbf{r}\|_2^2 \right] - P_S \right) = \\
 &= \mathbb{E} \left[\left\| \mathbf{s} - \mathbf{\Gamma} \tilde{\mathbf{H}}_{\text{RD}} \mathbf{G} \tilde{\mathbf{H}}_{\text{SR}} \mathbf{s} - \mathbf{\Gamma} \tilde{\mathbf{H}}_{\text{RD}} \mathbf{G} \mathbf{n}_{\text{R}} - \mathbf{\Gamma} \mathbf{n}_{\text{D}} \right\|_2^2 \right] + \\
 &\quad + \lambda \left(\mathbb{E} \left[\|\mathbf{G} \mathbf{r}\|_2^2 \right] - P_S \right) = \\
 &= \text{tr}(\mathbf{R}_{\text{s}}) - \\
 &\quad - \text{tr} \left(\mathbf{R}_{\text{s}} \tilde{\mathbf{H}}_{\text{SR}}^{\text{H}} \mathbf{G}^{\text{H}} \tilde{\mathbf{H}}_{\text{RD}}^{\text{H}} \mathbf{\Gamma}^{\text{H}} \right) - \\
 &\quad - \text{tr} \left(\mathbf{\Gamma} \tilde{\mathbf{H}}_{\text{RD}} \mathbf{G} \tilde{\mathbf{H}}_{\text{SR}} \mathbf{R}_{\text{s}} \right) + \\
 &\quad + \text{tr} \left(\mathbf{\Gamma} \tilde{\mathbf{H}}_{\text{RD}} \mathbf{G} \tilde{\mathbf{H}}_{\text{SR}} \mathbf{R}_{\text{s}} \tilde{\mathbf{H}}_{\text{SR}}^{\text{H}} \mathbf{G}^{\text{H}} \tilde{\mathbf{H}}_{\text{RD}}^{\text{H}} \mathbf{\Gamma}^{\text{H}} \right) + \\
 &\quad + \text{tr} \left(\mathbf{\Gamma} \tilde{\mathbf{H}}_{\text{RD}} \mathbf{G} \mathbf{R}_{\text{n}_{\text{R}}} \mathbf{G}^{\text{H}} \tilde{\mathbf{H}}_{\text{RD}}^{\text{H}} \mathbf{\Gamma}^{\text{H}} \right) + \\
 &\quad + \text{tr} \left(\mathbf{\Gamma} \mathbf{R}_{\text{n}_{\text{D}}} \mathbf{\Gamma}^{\text{H}} \right) \\
 &\quad + \lambda \left(\text{tr} \left(\mathbf{G} \tilde{\mathbf{H}}_{\text{SR}} \mathbf{R}_{\text{s}} \tilde{\mathbf{H}}_{\text{SR}}^{\text{H}} \mathbf{G}^{\text{H}} \right) + \text{tr} \left(\mathbf{G} \mathbf{R}_{\text{n}_{\text{R}}} \mathbf{G}^{\text{H}} \right) - P_S \right), \tag{6.87}
 \end{aligned}$$

where $\mathbf{R}_{\text{s}} = \mathbb{E}_{\text{s}} [\mathbf{s} \mathbf{s}^{\text{H}}]$, $\mathbf{R}_{\text{n}_{\text{R}}} = \mathbb{E}_{\text{n}_{\text{R}}} [\mathbf{n}_{\text{R}} \mathbf{n}_{\text{R}}^{\text{H}}]$, and $\mathbf{R}_{\text{n}_{\text{D}}} = \mathbb{E}_{\text{n}_{\text{D}}} [\mathbf{n}_{\text{D}} \mathbf{n}_{\text{D}}^{\text{H}}]$ are the covariance matrices of the source transmit symbols, the relay noise symbols, and the destination noise symbols, respectively. In order to find \mathbf{G} , $\mathbf{\Gamma}$, and λ such that they are a solution to the optimization problem, the following three conditions have to be fulfilled:

$$\frac{\partial}{\partial \mathbf{G}} L(\mathbf{G}, \mathbf{\Gamma}, \lambda) \stackrel{!}{=} \mathbf{0} \tag{6.88}$$

$$\frac{\partial}{\partial \mathbf{\Gamma}} L(\mathbf{G}, \mathbf{\Gamma}, \lambda) \stackrel{!}{=} \mathbf{0} \tag{6.89}$$

$$\frac{\partial}{\partial \lambda} L(\mathbf{G}, \mathbf{\Gamma}, \lambda) \stackrel{!}{=} 0 \tag{6.90}$$

It is possible to find $\mathbf{\Gamma} = f(\lambda)$ and λ such that the power constraint (6.84) is always fulfilled by solving (6.88) and (6.90). The constrained optimization problem can then be reduced to an unconstrained one. At this point, a 'generic' and a 'special' case are distinguished:

Generic case The diagonal weighting matrix $\mathbf{\Gamma}$ may have arbitrary entries (but is still a diagonal matrix). The optimization problem is in this case non-convex and can only be solved by numerical means.

Special case The matrix $\mathbf{\Gamma}$ is reduced to a weighted identity matrix, i.e. $\mathbf{\Gamma} = \gamma^{-1} \mathbf{I}$, $\gamma \in \mathbb{R}$ (the inverse γ^{-1} is used for convenience of notation). The gain matrix can be computed in closed-form for this case.

In the following, the LinRel and LDAS scenarios are treated separately because they lead to gain matrices with different structures.

6.3.1 Linear Relaying, Generic Case

For the LinRel system configuration, the gain matrix \mathbf{G} is diagonal. Equation (6.88) states that the partial derivative of $L(\mathbf{G}, \Gamma, \lambda)$ with respect to \mathbf{G} has to vanish. It can be calculated using Appendix A.5.1, equation (A.71) and is given by

$$\begin{aligned}
 \frac{\partial}{\partial \mathbf{G}} L(\mathbf{G}, \Gamma, \lambda) &= -\tilde{\mathbf{H}}_{\text{RD}}^{\text{T}} \Gamma^{\text{T}} \mathbf{R}_{\text{s}}^{\text{T}} \tilde{\mathbf{H}}_{\text{SR}}^{\text{T}} \odot \mathbf{I} + \\
 &\quad + \tilde{\mathbf{H}}_{\text{RD}}^{\text{T}} \Gamma^{\text{T}} \Gamma^* \tilde{\mathbf{H}}_{\text{RD}}^* \mathbf{G}^* \tilde{\mathbf{H}}_{\text{SR}}^* \mathbf{R}_{\text{s}}^{\text{T}} \tilde{\mathbf{H}}_{\text{SR}}^{\text{T}} \odot \mathbf{I} + \\
 &\quad + \tilde{\mathbf{H}}_{\text{RD}}^{\text{T}} \Gamma^{\text{T}} \Gamma^* \tilde{\mathbf{H}}_{\text{RD}}^* \mathbf{G}^* \mathbf{R}_{\text{nr}}^{\text{T}} \odot \mathbf{I} + \\
 &\quad + \lambda \mathbf{G}^* \tilde{\mathbf{H}}_{\text{SR}}^* \mathbf{R}_{\text{s}}^{\text{T}} \tilde{\mathbf{H}}_{\text{SR}}^{\text{T}} \odot \mathbf{I} + \\
 &\quad + \lambda \mathbf{G}^* \mathbf{R}_{\text{nr}}^{\text{T}} \odot \mathbf{I} = \\
 &= -\tilde{\mathbf{H}}_{\text{RD}}^{\text{T}} \Gamma^{\text{T}} \mathbf{R}_{\text{s}}^{\text{T}} \tilde{\mathbf{H}}_{\text{SR}}^{\text{T}} \odot \mathbf{I} + \\
 &\quad + \tilde{\mathbf{H}}_{\text{RD}}^{\text{T}} \Gamma^{\text{T}} \Gamma^* \tilde{\mathbf{H}}_{\text{RD}}^* \mathbf{G}^* \underbrace{\left(\tilde{\mathbf{H}}_{\text{SR}}^* \mathbf{R}_{\text{s}}^{\text{T}} \tilde{\mathbf{H}}_{\text{SR}}^{\text{T}} + \mathbf{R}_{\text{nr}}^{\text{T}} \right)}_{:= \tilde{\mathbf{A}}^{\text{T}}} \odot \mathbf{I} + \\
 &\quad + \lambda \mathbf{G}^* \underbrace{\left(\tilde{\mathbf{H}}_{\text{SR}}^* \mathbf{R}_{\text{s}}^{\text{T}} \tilde{\mathbf{H}}_{\text{SR}}^{\text{T}} + \mathbf{R}_{\text{nr}}^{\text{T}} \right)}_{:= \tilde{\mathbf{A}}^{\text{T}}} \odot \mathbf{I} \stackrel{!}{=} \\
 &\stackrel{!}{=} \mathbf{0}, \tag{6.91}
 \end{aligned}$$

Furthermore, the partial derivative of $L(\mathbf{G}, \Gamma, \lambda)$ with respect to λ also has to vanish (cf. (6.90)). This requirement corresponds to the constraint on the sum transmit power of the relays (6.84). The matrix equivalency given in Appendix A.6, (A.74) leads to

$$\begin{aligned}
 \frac{\partial}{\partial \lambda} L(\mathbf{G}, \Gamma, \lambda) &= \text{tr} \left(\mathbf{G} \tilde{\mathbf{H}}_{\text{SR}} \mathbf{R}_{\text{s}} \tilde{\mathbf{H}}_{\text{SR}}^{\text{H}} \mathbf{G}^{\text{H}} \right) + \text{tr} \left(\mathbf{G} \mathbf{R}_{\text{nr}} \mathbf{G}^{\text{H}} \right) - P_{\text{S}} = \\
 &= \text{tr} \left(\mathbf{G} \tilde{\mathbf{A}} \mathbf{G}^{\text{H}} \right) - P_{\text{S}} = \\
 &= \mathbf{g}^{\text{H}} \left(\tilde{\mathbf{A}} \odot \mathbf{I} \right) \mathbf{g} - P_{\text{S}} \stackrel{!}{=} 0, \tag{6.92}
 \end{aligned}$$

where $\tilde{\mathbf{A}}$ is defined as in (6.91). Next, equation (6.91) has to be solved for \mathbf{G} in order to write the gain matrix as a function of

- the equivalent channel matrices $\tilde{\mathbf{H}}_{\text{SR}}$ and $\tilde{\mathbf{H}}_{\text{RD}}$,

- the covariance matrices \mathbf{R}_s and \mathbf{R}_{n_R} of the signal vector \mathbf{s} and the relay noise vector \mathbf{n}_R ,
- the Lagrangian multiplier λ , and
- the diagonal weighting matrix $\mathbf{\Gamma}$.

From (6.91) it follows that

$$\begin{aligned}
 \tilde{\mathbf{H}}_{RD}^T \mathbf{\Gamma}^T \mathbf{R}_s^T \tilde{\mathbf{H}}_{SR}^T \odot \mathbf{I} &= \tilde{\mathbf{H}}_{RD}^T \mathbf{\Gamma}^T \mathbf{\Gamma}^* \tilde{\mathbf{H}}_{RD}^* \mathbf{G}^* \tilde{\mathbf{A}}^T \odot \mathbf{I} + \lambda \cdot \mathbf{G}^* \tilde{\mathbf{A}}^T \odot \mathbf{I} \\
 \tilde{\mathbf{H}}_{RD}^T \mathbf{\Gamma}^T \mathbf{R}_s^T \tilde{\mathbf{H}}_{SR}^T \odot \mathbf{I} &= \left(\tilde{\mathbf{H}}_{RD}^T \mathbf{\Gamma}^T \mathbf{\Gamma}^* \tilde{\mathbf{H}}_{RD}^* + \lambda \cdot \mathbf{I} \right) \mathbf{G}^* \tilde{\mathbf{A}}^T \odot \mathbf{I} \quad / \cdot \lambda^{-1} \\
 \lambda^{-\frac{1}{2}} \cdot \tilde{\mathbf{H}}_{RD}^T \underbrace{\left(\lambda^{-\frac{1}{2}} \mathbf{\Gamma}^T \right)}_{:= \mathbf{\Upsilon}^T} \mathbf{R}_s^T \tilde{\mathbf{H}}_{SR}^T \odot \mathbf{I} &= \left(\tilde{\mathbf{H}}_{RD}^T \underbrace{\left(\lambda^{-1} \mathbf{\Gamma}^T \mathbf{\Gamma}^* \right)}_{:= \mathbf{\Upsilon}^T \mathbf{\Upsilon}^*} \tilde{\mathbf{H}}_{RD}^* + \mathbf{I} \right) \mathbf{G}^* \tilde{\mathbf{A}}^T \odot \mathbf{I}
 \end{aligned} \tag{6.93}$$

Defining $\mathbf{\Upsilon} := \lambda^{-\frac{1}{2}} \mathbf{\Gamma}$ is a trick that allows to find a λ such that the power constraint (6.84) is fulfilled for any \mathbf{G} . This can be done without loss of generality because $\mathbf{\Gamma}$ can always be chosen accordingly. With the matrix equivalency (A.77) in Appendix A.6, equation (6.93) can be solved for $\mathbf{g} = \text{diag}(\mathbf{G})$:

$$\begin{aligned}
 \mathbf{g} &= \lambda^{-\frac{1}{2}} \left(\left(\tilde{\mathbf{H}}_{RD}^H \mathbf{\Upsilon}^H \mathbf{\Upsilon} \tilde{\mathbf{H}}_{RD} + \mathbf{I} \right) \odot \tilde{\mathbf{A}}^* \right)^{-1} \cdot \text{diag} \left(\tilde{\mathbf{H}}_{RD}^H \mathbf{\Upsilon}^H \mathbf{R}_s^H \tilde{\mathbf{H}}_{SR}^H \right) = \\
 &= \lambda^{-\frac{1}{2}} \left(\tilde{\mathbf{B}} \odot \tilde{\mathbf{A}}^* \right)^{-1} \text{diag} \left(\tilde{\mathbf{C}}^H \right) := \\
 &:= \lambda^{-\frac{1}{2}} \tilde{\mathbf{g}}.
 \end{aligned} \tag{6.94}$$

The following substitutions have been used:

$$\tilde{\mathbf{A}} := \tilde{\mathbf{H}}_{SR} \mathbf{R}_s \tilde{\mathbf{H}}_{SR}^H + \mathbf{R}_{n_R} = \tilde{\mathbf{A}}^H \tag{6.95}$$

$$\tilde{\mathbf{B}} := \tilde{\mathbf{H}}_{RD}^H \mathbf{\Upsilon}^H \mathbf{\Upsilon} \tilde{\mathbf{H}}_{RD} + \mathbf{I} = \tilde{\mathbf{B}}^H \tag{6.96}$$

$$\tilde{\mathbf{C}} := \tilde{\mathbf{H}}_{SR} \mathbf{R}_s \mathbf{\Upsilon} \tilde{\mathbf{H}}_{RD} \tag{6.97}$$

Equation (6.94) shows the structure of the gain vector \mathbf{g} . The scaling factor λ can now be chosen such that the power constraint (6.84) is fulfilled for any $\tilde{\mathbf{g}}$. The Lagrangian function $L(\mathbf{G}, \mathbf{\Gamma}, \lambda)$ then becomes

$$L(\mathbf{G}, \mathbf{\Gamma}, \lambda) = E \left[\|\mathbf{s} - \mathbf{\Gamma} \mathbf{d}_{IV}\|_2^2 \right] = L(\mathbf{G}, \mathbf{\Gamma}), \tag{6.98}$$

in which case the constrained optimization problem reduces to an unconstrained one. In order to find λ , the gain vector $\mathbf{g} = \lambda^{-\frac{1}{2}} \tilde{\mathbf{g}}$ has to be inserted into (6.92):

$$\lambda = \frac{\tilde{\mathbf{g}}^H (\tilde{\mathbf{A}} \odot \mathbf{I}) \tilde{\mathbf{g}}}{P_S} \quad (6.99)$$

If the gain vector is chosen as

$$\begin{aligned} \mathbf{g} &= \lambda^{-\frac{1}{2}} \left(\tilde{\mathbf{B}} \odot \tilde{\mathbf{A}}^* \right)^{-1} \text{diag} \left(\tilde{\mathbf{C}}^H \right) = \\ &= \sqrt{\frac{P_S}{\tilde{\mathbf{g}}^H (\tilde{\mathbf{A}} \odot \mathbf{I}) \tilde{\mathbf{g}}}} \left(\tilde{\mathbf{B}} \odot \tilde{\mathbf{A}}^* \right)^{-1} \text{diag} \left(\tilde{\mathbf{C}}^H \right), \end{aligned} \quad (6.100)$$

the power constraint is always fulfilled. This essentially means that the domain of the gain matrix is adapted according to the power constraint. Consequently, the number of equations is reduced from $N_{SD} + N_R + 1$ to N_{SD} . The cost function $\epsilon := E [\|\mathbf{s} - \Gamma \mathbf{d}_{IV}\|_2^2]$ can be written as

$$\begin{aligned} \epsilon &= E \left[\left\| \mathbf{s} - \Gamma \tilde{\mathbf{H}}_{RD} \mathbf{G} \tilde{\mathbf{H}}_{SR} \mathbf{s} - \Gamma \tilde{\mathbf{H}}_{RD} \mathbf{G} \mathbf{n}_R - \Gamma \mathbf{n}_D \right\|_2^2 \right] = \\ &= E \left[\left\| \mathbf{s} - \lambda^{-\frac{1}{2}} \Gamma \tilde{\mathbf{H}}_{RD} \tilde{\mathbf{G}} \tilde{\mathbf{H}}_{SR} \mathbf{s} - \lambda^{-\frac{1}{2}} \Gamma \tilde{\mathbf{H}}_{RD} \tilde{\mathbf{G}} \mathbf{n}_R - \lambda^{\frac{1}{2}} \Upsilon \mathbf{n}_D \right\|_2^2 \right] = \\ &= E \left[\left\| \mathbf{s} - \Upsilon \tilde{\mathbf{H}}_{RD} \tilde{\mathbf{G}} \tilde{\mathbf{H}}_{SR} \mathbf{s} - \Upsilon \tilde{\mathbf{H}}_{RD} \tilde{\mathbf{G}} \mathbf{n}_R - \lambda^{\frac{1}{2}} \Upsilon \mathbf{n}_D \right\|_2^2 \right], \end{aligned} \quad (6.101)$$

where $\Upsilon = \lambda^{-\frac{1}{2}} \Gamma$. Note that ϵ - which is the MMSE - no longer depends on Γ but only on Υ . The gain vector solving the original constrained optimization problem can finally be found by calculating

$$\mathbf{g}_{\text{MMSE}} = \lambda^{-\frac{1}{2}} \cdot \tilde{\mathbf{g}}(\Upsilon_{\text{MMSE}}), \quad (6.102)$$

where Υ_{MMSE} is the solution of the unconstrained optimization problem

$$\Upsilon_{\text{MMSE}} = \arg \min_{\Upsilon} \epsilon(\Upsilon). \quad (6.103)$$

Unfortunately, this is not a convex problem that has to be solved numerically. However, the special case $\Gamma = \gamma^{-1} \mathbf{I}$ is analytically tractable. It will be treated in the next section.

6.3.2 Linear Relaying, Special Case

Assume that the diagonal weighting matrix Γ reduces to a weighted identity matrix $\gamma^{-1}\mathbf{I}$, where $\gamma \in \mathbb{R}$. The optimization problem then is

$$\mathbf{G}_{\text{MMSE}} = \arg \min_{\mathbf{G}} \mathbb{E} \left[\|\mathbf{s} - \gamma^{-1} \mathbf{d}_{\text{IV}}\|_2^2 \right] \quad (6.104)$$

subject to

$$\mathbb{E} [\|\mathbf{G}\mathbf{r}\|_2^2] = P_S. \quad (6.105)$$

The same derivation that results in the first row of (6.93) can be used here, too. Starting from there we have

$$\begin{aligned} \tilde{\mathbf{H}}_{\text{RD}}^T \Gamma^T \mathbf{R}_s^T \tilde{\mathbf{H}}_{\text{SR}}^T \odot \mathbf{I} &= \left(\tilde{\mathbf{H}}_{\text{RD}}^T \Gamma^T \Gamma^* \tilde{\mathbf{H}}_{\text{RD}}^* + \lambda \cdot \mathbf{I} \right) \mathbf{G}^* \tilde{\mathbf{A}}^T \odot \mathbf{I} \quad / \Gamma = \gamma^{-1} \mathbf{I} \\ \rightarrow \gamma^{-1} \tilde{\mathbf{H}}_{\text{RD}}^T \mathbf{R}_s^T \tilde{\mathbf{H}}_{\text{SR}}^T \odot \mathbf{I} &= \left(\gamma^{-2} \tilde{\mathbf{H}}_{\text{RD}}^T \tilde{\mathbf{H}}_{\text{RD}}^* + \lambda \cdot \mathbf{I} \right) \mathbf{G}^* \tilde{\mathbf{A}}^T \odot \mathbf{I} \quad / \cdot \gamma^2 \\ \rightarrow \gamma \tilde{\mathbf{H}}_{\text{RD}}^T \mathbf{R}_s^T \tilde{\mathbf{H}}_{\text{SR}}^T \odot \mathbf{I} &= \left(\tilde{\mathbf{H}}_{\text{RD}}^T \tilde{\mathbf{H}}_{\text{RD}}^* + \underbrace{\gamma^2 \lambda}_{:=\mu} \cdot \mathbf{I} \right) \mathbf{G}^* \tilde{\mathbf{A}}^T \odot \mathbf{I} \end{aligned} \quad (6.106)$$

In the generic case $\lambda^{-\frac{1}{2}}\Gamma$ was substituted by Υ because the scaling matrix Γ could be chosen arbitrarily. Now, let $\mu := \gamma^2 \lambda$ with the same argument. Equation (6.106) can be solved for the gain vector $\mathbf{g} = \text{diag}(\mathbf{G})$ using the matrix equivalency (A.77) in Appendix A.6:

$$\begin{aligned} \mathbf{g} &= \gamma \left(\left(\tilde{\mathbf{H}}_{\text{RD}}^H \tilde{\mathbf{H}}_{\text{RD}} + \mu \mathbf{I} \right) \odot \tilde{\mathbf{A}}^* \right)^{-1} \cdot \text{diag} \left(\tilde{\mathbf{H}}_{\text{RD}}^H \mathbf{R}_s^H \tilde{\mathbf{H}}_{\text{SR}}^H \right) = \\ &= \gamma \left(\tilde{\mathbf{B}} \odot \tilde{\mathbf{A}}^* \right)^{-1} \text{diag} \left(\tilde{\mathbf{C}}^H \right) := \\ &:= \gamma \tilde{\mathbf{g}}, \end{aligned} \quad (6.107)$$

where now $\tilde{\mathbf{A}}$, $\tilde{\mathbf{B}}$, and $\tilde{\mathbf{C}}$ are defined as

$$\tilde{\mathbf{A}} := \tilde{\mathbf{H}}_{\text{SR}} \mathbf{R}_s \tilde{\mathbf{H}}_{\text{SR}}^H + \mathbf{R}_{\text{nr}} = \tilde{\mathbf{A}}^H \quad (6.108)$$

$$\tilde{\mathbf{B}} := \tilde{\mathbf{H}}_{\text{RD}}^H \tilde{\mathbf{H}}_{\text{RD}} + \mu \mathbf{I} = \tilde{\mathbf{B}}^H \quad (6.109)$$

$$\tilde{\mathbf{C}} := \tilde{\mathbf{H}}_{\text{SR}} \mathbf{R}_s \tilde{\mathbf{H}}_{\text{RD}}. \quad (6.110)$$

Choosing γ such that the power constraint (6.105) is always fulfilled delivers

$$\gamma = \sqrt{\frac{P_S}{\tilde{\mathbf{g}}^H (\tilde{\mathbf{A}} \odot \mathbf{I}) \tilde{\mathbf{g}}}} \quad (6.111)$$

in the same way λ was obtained in (6.99) for the generic case. The gain vector then is

$$\mathbf{g} = \sqrt{\frac{P_S}{\tilde{\mathbf{g}}^H (\tilde{\mathbf{A}} \odot \mathbf{I}) \tilde{\mathbf{g}}}} (\tilde{\mathbf{B}} \odot \tilde{\mathbf{A}}^*)^{-1} \text{diag}(\tilde{\mathbf{C}}^H). \quad (6.112)$$

Consequently, the Lagrangian function becomes

$$L(\mathbf{G}, \gamma, \lambda) = \underbrace{\mathbb{E} \left[\|\mathbf{s} - \gamma^{-1} \mathbf{d}_{\text{IV}}\|_2^2 \right]}_{:=\epsilon} + \lambda \underbrace{\left(\mathbb{E} [\|\mathbf{G}\mathbf{r}\|_2^2] - P_S \right)}_{=0} = L(\mathbf{G}, \gamma), \quad (6.113)$$

where the cost function ϵ can be written as

$$\begin{aligned} \epsilon &= \mathbb{E} \left[\|\mathbf{s} - \gamma^{-1} \mathbf{d}_{\text{IV}}\|_2^2 \right] = \\ &= \mathbb{E} \left[\left\| \mathbf{s} - \gamma^{-1} \tilde{\mathbf{H}}_{\text{RD}} \mathbf{G} \tilde{\mathbf{H}}_{\text{SR}} \mathbf{s} - \gamma^{-1} \tilde{\mathbf{H}}_{\text{RD}} \mathbf{G} \mathbf{n}_{\text{R}} - \gamma^{-1} \mathbf{n}_{\text{D}} \right\|_2^2 \right] = \\ &= \mathbb{E} \left[\left\| \mathbf{s} - \tilde{\mathbf{H}}_{\text{RD}} \tilde{\mathbf{G}} \tilde{\mathbf{H}}_{\text{SR}} \mathbf{s} - \tilde{\mathbf{H}}_{\text{RD}} \tilde{\mathbf{G}} \mathbf{n}_{\text{R}} - \gamma^{-1} \mathbf{n}_{\text{D}} \right\|_2^2 \right] \end{aligned} \quad (6.114)$$

and $\tilde{\mathbf{G}} = \text{diag}(\tilde{\mathbf{g}})$. The only variable left in ϵ that is subject to optimization, is μ . It is hidden in $\tilde{\mathbf{B}}$, which is contained in $\tilde{\mathbf{g}}$. The gain vector solving the constrained optimization problem (6.104), (6.105) can be found by computing

$$\mathbf{g}_{\text{MMSE}} = \gamma \cdot \tilde{\mathbf{g}}(\mu_{\text{MMSE}}), \quad (6.115)$$

where μ_{MMSE} is the solution of the unconstrained optimization problem

$$\mu_{\text{MMSE}} = \arg \min_{\mu} \epsilon(\mu). \quad (6.116)$$

In order to find μ_{MMSE} , the derivative of ϵ with respect to μ has to be computed. To this end, the gain matrix $\tilde{\mathbf{G}}$ is first written as a linear function of $\tilde{\mathbf{g}}$:

$$\tilde{\mathbf{G}} = \sum_{i=1}^{N_{\text{R}}} \mathbf{E}_i \tilde{\mathbf{g}} \mathbf{e}_i^T, \quad (6.117)$$

where \mathbf{E}_i and \mathbf{e}_i are defined in Appendix A.7, (A.78). The cost function ϵ is then

$$\begin{aligned}
 \epsilon &= \mathbb{E} \left[\left\| \mathbf{s} - \tilde{\mathbf{H}}_{\text{RD}} \left(\sum_{i=1}^{N_{\text{R}}} \mathbf{E}_i \tilde{\mathbf{g}} \mathbf{e}_i^{\text{T}} \right) \tilde{\mathbf{H}}_{\text{SR}} \mathbf{s} - \tilde{\mathbf{H}}_{\text{RD}} \left(\sum_{i=1}^{N_{\text{R}}} \mathbf{E}_i \tilde{\mathbf{g}} \mathbf{e}_i^{\text{T}} \right) \mathbf{n}_{\text{R}} - \gamma^{-1} \mathbf{n}_{\text{D}} \right\|_2^2 \right] = \\
 &= \text{tr}(\mathbf{R}_{\text{s}}) - \\
 &\quad - \text{tr} \left(\sum_{i=1}^{N_{\text{R}}} \left(\mathbf{R}_{\text{s}} \tilde{\mathbf{H}}_{\text{SR}}^{\text{H}} \mathbf{e}_i \tilde{\mathbf{g}}^{\text{H}} \mathbf{E}_i^{\text{T}} \tilde{\mathbf{H}}_{\text{RD}}^{\text{H}} \right) \right) - \\
 &\quad - \text{tr} \left(\sum_{i=1}^{N_{\text{R}}} \left(\tilde{\mathbf{H}}_{\text{RD}} \mathbf{E}_i \tilde{\mathbf{g}} \mathbf{e}_i^{\text{T}} \tilde{\mathbf{H}}_{\text{SR}} \mathbf{R}_{\text{s}} \right) \right) + \\
 &\quad + \text{tr} \left(\tilde{\mathbf{H}}_{\text{RD}} \left(\sum_{i=1}^{N_{\text{R}}} \mathbf{E}_i \tilde{\mathbf{g}} \mathbf{e}_i^{\text{T}} \right) \tilde{\mathbf{A}} \left(\sum_{i=1}^{N_{\text{R}}} \mathbf{e}_i \tilde{\mathbf{g}}^{\text{H}} \mathbf{E}_i^{\text{T}} \right) \tilde{\mathbf{H}}_{\text{RD}}^{\text{H}} \right) + \\
 &\quad + \frac{\text{tr}(\mathbf{R}_{\text{nD}})}{P_{\text{S}}} \tilde{\mathbf{g}}^{\text{H}} \left(\tilde{\mathbf{A}} \odot \mathbf{I} \right) \tilde{\mathbf{g}}, \tag{6.118}
 \end{aligned}$$

where the definition of γ in (6.111) was used together with the fact that

$$\sum_i \text{tr}(\mathbf{A} \mathbf{B}_i \mathbf{C}) = \text{tr} \left(\sum_i \mathbf{A} \mathbf{B}_i \mathbf{C} \right) = \text{tr} \left(\mathbf{A} \left(\sum_i \mathbf{B}_i \right) \mathbf{C} \right) \tag{6.119}$$

for any matrices \mathbf{A} , \mathbf{B}_i , and \mathbf{C} . In order to find the μ that minimizes ϵ , the partial derivative of (6.118) with respect to μ is computed:

$$\begin{aligned}
 \frac{\partial \epsilon}{\partial \mu} &= -\tilde{\mathbf{g}}^{\text{H}} \left(\tilde{\mathbf{A}}^{\text{T}} \odot \mu \mathbf{I} \right) \frac{\partial \tilde{\mathbf{g}}}{\partial \mu} - \frac{\partial \tilde{\mathbf{g}}^{\text{H}}}{\partial \mu} \left(\tilde{\mathbf{A}}^{\text{T}} \odot \mu \mathbf{I} \right) \tilde{\mathbf{g}} + \\
 &\quad + \tilde{\mathbf{g}}^{\text{H}} \left(\tilde{\mathbf{A}} \odot \frac{\text{tr}(\mathbf{R}_{\text{nD}})}{P_{\text{S}}} \mathbf{I} \right) \frac{\partial \tilde{\mathbf{g}}}{\partial \mu} + \frac{\partial \tilde{\mathbf{g}}^{\text{H}}}{\partial \mu} \left(\tilde{\mathbf{A}} \odot \frac{\text{tr}(\mathbf{R}_{\text{nD}})}{P_{\text{S}}} \mathbf{I} \right) \tilde{\mathbf{g}} \tag{6.120}
 \end{aligned}$$

Details about the derivation are given in Appendix A.8. Choosing

$$\mu_{\text{MMSE}} = \frac{\text{tr}(\mathbf{R}_{\text{nD}})}{P_{\text{S}}} \tag{6.121}$$

fulfills $\frac{\partial \epsilon}{\partial \mu} = 0$ and minimizes the MMSE cost function ϵ .

Summary of results:

The gain vector \mathbf{g}_{MMSE} is

$$\begin{aligned}\mathbf{g}_{\text{MMSE}} &= \gamma \cdot \tilde{\mathbf{g}}_{\text{MMSE}} \\ &= \gamma \cdot \left(\tilde{\mathbf{B}} \odot \tilde{\mathbf{A}}^* \right)^{-1} \text{diag} \left(\tilde{\mathbf{C}}^{\text{H}} \right),\end{aligned}\tag{6.122}$$

where

$$\tilde{\mathbf{g}}_{\text{MMSE}} = \left(\tilde{\mathbf{B}} \odot \tilde{\mathbf{A}}^* \right)^{-1} \text{diag} \left(\tilde{\mathbf{C}}^{\text{H}} \right),\tag{6.123}$$

$$\gamma = \sqrt{\frac{P_s}{\tilde{\mathbf{g}}_{\text{MMSE}}^{\text{H}} \left(\tilde{\mathbf{A}} \odot \mathbf{I} \right) \tilde{\mathbf{g}}_{\text{MMSE}}}},\tag{6.124}$$

and

$$\tilde{\mathbf{A}} := \tilde{\mathbf{H}}_{\text{SR}} \mathbf{R}_s \tilde{\mathbf{H}}_{\text{SR}}^{\text{H}} + \mathbf{R}_{\text{nr}},\tag{6.125}$$

$$\tilde{\mathbf{B}} := \tilde{\mathbf{H}}_{\text{RD}}^{\text{H}} \tilde{\mathbf{H}}_{\text{RD}} + \frac{\text{tr}(\mathbf{R}_{\text{nd}})}{P_s} \mathbf{I},\tag{6.126}$$

$$\tilde{\mathbf{C}} := \tilde{\mathbf{H}}_{\text{SR}} \mathbf{R}_s \tilde{\mathbf{H}}_{\text{RD}}.\tag{6.127}$$

6.3.3 Linear Distributed Antenna System, Generic Case

This section considers the situation where there is only a single relay with multiple antennas (LDAS), i.e., the gain matrix does normally not contain any zeros. The discussion starts from the Lagrangian function $L(\mathbf{G}, \mathbf{\Gamma}, \lambda)$ defined in (6.87) and the three conditions (6.88) – (6.90). The partial derivative of $L(\mathbf{G}, \mathbf{\Gamma}, \lambda)$ with respect to the gain matrix \mathbf{G} is now

$$\begin{aligned}
 \frac{\partial}{\partial \mathbf{G}} L(\mathbf{G}, \mathbf{\Gamma}, \lambda) &= -\tilde{\mathbf{H}}_{\text{RD}}^{\text{T}} \mathbf{\Gamma}^{\text{T}} \mathbf{R}_{\text{s}}^{\text{T}} \tilde{\mathbf{H}}_{\text{SR}}^{\text{T}} + \\
 &\quad + \tilde{\mathbf{H}}_{\text{RD}}^{\text{T}} \mathbf{\Gamma}^{\text{T}} \mathbf{\Gamma}^* \tilde{\mathbf{H}}_{\text{RD}}^* \mathbf{G}^* \tilde{\mathbf{H}}_{\text{SR}}^* \mathbf{R}_{\text{s}}^{\text{T}} \tilde{\mathbf{H}}_{\text{SR}}^{\text{T}} + \\
 &\quad + \tilde{\mathbf{H}}_{\text{RD}}^{\text{T}} \mathbf{\Gamma}^{\text{T}} \mathbf{\Gamma}^* \tilde{\mathbf{H}}_{\text{RD}}^* \mathbf{G}^* \mathbf{R}_{\text{nr}}^{\text{T}} + \\
 &\quad + \lambda \mathbf{G}^* \tilde{\mathbf{H}}_{\text{SR}}^* \mathbf{R}_{\text{s}}^{\text{T}} \tilde{\mathbf{H}}_{\text{SR}}^{\text{T}} + \lambda \mathbf{G}^* \mathbf{R}_{\text{nr}}^{\text{T}} = \\
 &= -\tilde{\mathbf{H}}_{\text{RD}}^{\text{T}} \mathbf{\Gamma}^{\text{T}} \mathbf{R}_{\text{s}}^{\text{T}} \tilde{\mathbf{H}}_{\text{SR}}^{\text{T}} + \\
 &\quad + \tilde{\mathbf{H}}_{\text{RD}}^{\text{T}} \mathbf{\Gamma}^{\text{T}} \mathbf{\Gamma}^* \tilde{\mathbf{H}}_{\text{RD}}^* \mathbf{G}^* \underbrace{\left(\mathbf{H}_{\text{SR}}^* \mathbf{R}_{\text{s}}^{\text{T}} \tilde{\mathbf{H}}_{\text{SR}}^{\text{T}} + \mathbf{R}_{\text{nr}}^{\text{T}} \right)}_{:= \tilde{\mathbf{A}}^{\text{T}}} + \\
 &\quad + \lambda \mathbf{G}^* \underbrace{\left(\tilde{\mathbf{H}}_{\text{SR}}^* \mathbf{R}_{\text{s}}^{\text{T}} \tilde{\mathbf{H}}_{\text{SR}}^{\text{T}} + \mathbf{R}_{\text{nr}}^{\text{T}} \right)}_{:= \tilde{\mathbf{A}}^{\text{T}}} \stackrel{!}{=} \\
 &\stackrel{!}{=} \mathbf{0}, \tag{6.128}
 \end{aligned}$$

where Appendix A.5.1, equation (A.70) was used. The partial derivative of $L(\mathbf{G}, \mathbf{\Gamma}, \lambda)$ with respect to λ also has to vanish:

$$\begin{aligned}
 \frac{\partial}{\partial \lambda} L(\mathbf{G}, \mathbf{\Gamma}, \lambda) &= \text{tr} \left(\mathbf{G} \tilde{\mathbf{H}}_{\text{SR}} \mathbf{R}_{\text{s}} \tilde{\mathbf{H}}_{\text{SR}}^{\text{H}} \mathbf{G}^{\text{H}} \right) + \text{tr} \left(\mathbf{G} \mathbf{R}_{\text{nr}} \mathbf{G}^{\text{H}} \right) - P_{\text{S}} = \\
 &= \text{tr} \left(\mathbf{G} \tilde{\mathbf{A}} \mathbf{G}^{\text{H}} \right) - P_{\text{S}} \stackrel{!}{=} \\
 &\stackrel{!}{=} 0 \tag{6.129}
 \end{aligned}$$

In order to be able to solve for \mathbf{G} , equation (6.128) is rewritten as follows:

$$\begin{aligned}
 \tilde{\mathbf{H}}_{\text{RD}}^{\text{T}} \mathbf{\Gamma}^{\text{T}} \mathbf{R}_{\text{s}}^{\text{T}} \tilde{\mathbf{H}}_{\text{SR}}^{\text{T}} &= \tilde{\mathbf{H}}_{\text{RD}}^{\text{T}} \mathbf{\Gamma}^{\text{T}} \mathbf{\Gamma}^* \tilde{\mathbf{H}}_{\text{RD}}^* \mathbf{G}^* \tilde{\mathbf{A}}^{\text{T}} + \lambda \cdot \mathbf{G}^* \tilde{\mathbf{A}}^{\text{T}} \\
 \tilde{\mathbf{H}}_{\text{RD}}^{\text{T}} \mathbf{\Gamma}^{\text{T}} \mathbf{R}_{\text{s}}^{\text{T}} \tilde{\mathbf{H}}_{\text{SR}}^{\text{T}} &= \left(\tilde{\mathbf{H}}_{\text{RD}}^{\text{T}} \mathbf{\Gamma}^{\text{T}} \mathbf{\Gamma}^* \tilde{\mathbf{H}}_{\text{RD}}^* + \lambda \cdot \mathbf{I} \right) \mathbf{G}^* \tilde{\mathbf{A}}^{\text{T}} \quad / \cdot \lambda^{-1} \\
 \lambda^{-\frac{1}{2}} \cdot \tilde{\mathbf{H}}_{\text{RD}}^{\text{T}} \underbrace{\left(\lambda^{-\frac{1}{2}} \mathbf{\Gamma}^{\text{T}} \right)}_{:= \mathbf{\Upsilon}^{\text{T}}} \mathbf{R}_{\text{s}}^{\text{T}} \tilde{\mathbf{H}}_{\text{SR}}^{\text{T}} &= \left(\tilde{\mathbf{H}}_{\text{RD}}^{\text{T}} \underbrace{\left(\lambda^{-1} \mathbf{\Gamma}^{\text{T}} \mathbf{\Gamma}^* \right)}_{:= \mathbf{\Upsilon}^{\text{T}} \mathbf{\Upsilon}^*} \tilde{\mathbf{H}}_{\text{RD}}^* + \lambda \cdot \mathbf{I} \right) \mathbf{G}^* \tilde{\mathbf{A}}^{\text{T}} \tag{6.130}
 \end{aligned}$$

The definition $\Upsilon := \lambda^{-\frac{1}{2}}\Gamma$ is used to find λ such that the relay transmit power constraint is fulfilled for any \mathbf{G} . The same trick has been used in Section 6.3.1. Solving (6.130) for \mathbf{G} yields

$$\begin{aligned}\mathbf{G} &= \lambda^{-\frac{1}{2}} \cdot \left(\tilde{\mathbf{H}}_{\text{RD}}^{\text{H}} \Upsilon^{\text{H}} \Upsilon \tilde{\mathbf{H}}_{\text{RD}} + \mathbf{I} \right)^{-1} \tilde{\mathbf{H}}_{\text{RD}}^{\text{H}} \Upsilon^{\text{H}} \mathbf{R}_s^{\text{H}} \tilde{\mathbf{H}}_{\text{SR}}^{\text{H}} \tilde{\mathbf{A}}^{-\text{H}} = \\ &= \lambda^{-\frac{1}{2}} \cdot \tilde{\mathbf{B}}^{-1} \tilde{\mathbf{C}}^{\text{H}} \tilde{\mathbf{A}}^{-\text{H}} := \\ &:= \lambda^{-\frac{1}{2}} \cdot \tilde{\mathbf{G}},\end{aligned}\tag{6.131}$$

where the substitutions

$$\tilde{\mathbf{A}} := \tilde{\mathbf{H}}_{\text{SR}} \mathbf{R}_s \tilde{\mathbf{H}}_{\text{SR}}^{\text{H}} + \mathbf{R}_{\text{nR}} = \tilde{\mathbf{A}}^{\text{H}}\tag{6.132}$$

$$\tilde{\mathbf{B}} := \tilde{\mathbf{H}}_{\text{RD}}^{\text{H}} \Upsilon^{\text{H}} \Upsilon \tilde{\mathbf{H}}_{\text{RD}} + \mathbf{I} = \tilde{\mathbf{B}}^{\text{H}}\tag{6.133}$$

$$\tilde{\mathbf{C}} := \tilde{\mathbf{H}}_{\text{SR}} \mathbf{R}_s \Upsilon \tilde{\mathbf{H}}_{\text{RD}}\tag{6.134}$$

are the same as in Section 6.3.1. Equation (6.129) represents the relay transmit power constraint. Solving for λ delivers

$$\lambda = \frac{\text{tr}(\tilde{\mathbf{G}} \tilde{\mathbf{A}} \tilde{\mathbf{G}}^{\text{H}})}{P_s}.\tag{6.135}$$

The relay transmit power constraint is consequently always fulfilled if the gain matrix is chosen as

$$\begin{aligned}\mathbf{G} &= \lambda^{-\frac{1}{2}} \cdot \tilde{\mathbf{B}}^{-1} \tilde{\mathbf{C}}^{\text{H}} \tilde{\mathbf{A}}^{-\text{H}} = \\ &= \sqrt{\frac{P_s}{\text{tr}(\tilde{\mathbf{G}} \tilde{\mathbf{A}} \tilde{\mathbf{G}}^{\text{H}})}} \tilde{\mathbf{B}}^{-1} \tilde{\mathbf{C}}^{\text{H}} \tilde{\mathbf{A}}^{-\text{H}}.\end{aligned}\tag{6.136}$$

The constrained optimization then reduces to an unconstrained one and the Lagrangian function becomes

$$L(\mathbf{G}, \Gamma, \lambda) = \text{E}[\|\mathbf{s} - \Gamma \mathbf{d}_{\text{IV}}\|_2^2] = L(\mathbf{G}, \Gamma).\tag{6.137}$$

The cost function $\epsilon = \text{E}[\|\mathbf{s} - \Gamma \mathbf{d}_{\text{IV}}\|_2^2]$ is now no longer a function of Γ but of Υ (cf. (6.101)). Consequently, the MMSE gain matrix is

$$\mathbf{G}_{\text{MMSE}} = \lambda^{-\frac{1}{2}} \cdot \tilde{\mathbf{G}}(\Upsilon_{\text{MMSE}}),\tag{6.138}$$

where Υ_{MMSE} is the solution of the unconstrained optimization problem

$$\Upsilon_{\text{MMSE}} = \arg \min_{\Upsilon} \epsilon(\Upsilon). \quad (6.139)$$

Unfortunately, this is not a convex problem and has to be solved numerically. For the special case that $\Gamma = \gamma^{-1}\mathbf{I}$, $\gamma \in \mathbb{R}$, a closed-form solution is found in the next section.

6.3.4 Linear Distributed Antenna System, Special Case

For the case that the weighting matrix Γ reduces to a weighted identity matrix $\gamma^{-1}\mathbf{I}$, $\gamma \in \mathbb{R}$, the optimization problem becomes

$$\mathbf{G}_{\text{MMSE}} = \arg \min_{\mathbf{G}} E_{\mathbf{s}, \mathbf{n}_R, \mathbf{n}_D} \left[\|\mathbf{s} - \gamma^{-1} \mathbf{d}_{\text{IV}}\|_2^2 \right] \quad (6.140)$$

subject to

$$E_{\mathbf{s}, \mathbf{n}_R} [\|\mathbf{G}\mathbf{r}\|_2^2] = P_S. \quad (6.141)$$

For the generic case, the structure of the gain matrix (6.131) was computed from (6.130). With $\Gamma = \gamma^{-1}\mathbf{I}$, equation (6.130) becomes

$$\begin{aligned} \tilde{\mathbf{H}}_{\text{RD}}^T \Gamma^T \mathbf{R}_s^T \tilde{\mathbf{H}}_{\text{SR}}^T &= \tilde{\mathbf{H}}_{\text{RD}}^T \Gamma^T \Gamma^* \tilde{\mathbf{H}}_{\text{RD}}^* \mathbf{G}^* \tilde{\mathbf{A}}^T + \lambda \cdot \mathbf{G}^* \tilde{\mathbf{A}}^T \\ \gamma^{-1} \tilde{\mathbf{H}}_{\text{RD}}^T \mathbf{R}_s^T \tilde{\mathbf{H}}_{\text{SR}}^T &= \left(\gamma^{-2} \tilde{\mathbf{H}}_{\text{RD}}^T \tilde{\mathbf{H}}_{\text{RD}}^* + \lambda \cdot \mathbf{I} \right) \mathbf{G}^* \tilde{\mathbf{A}}^T \quad / \cdot \gamma^2 \\ \gamma \tilde{\mathbf{H}}_{\text{RD}}^T \mathbf{R}_s^T \tilde{\mathbf{H}}_{\text{SR}}^T &= \left(\tilde{\mathbf{H}}_{\text{RD}}^T \tilde{\mathbf{H}}_{\text{RD}}^* + \gamma^2 \lambda \cdot \mathbf{I} \right) \mathbf{G}^* \tilde{\mathbf{A}}^T \end{aligned} \quad (6.142)$$

Solving (6.142) for \mathbf{G} delivers

$$\begin{aligned} \mathbf{G} &= \gamma \cdot \left(\tilde{\mathbf{H}}_{\text{RD}}^H \tilde{\mathbf{H}}_{\text{RD}} + \gamma^2 \lambda \mathbf{I} \right)^{-1} \cdot \tilde{\mathbf{H}}_{\text{RD}}^H \mathbf{R}_s^H \tilde{\mathbf{H}}_{\text{SR}}^H \cdot \tilde{\mathbf{A}}^{-H} := \\ &:= \gamma \cdot \tilde{\mathbf{G}}. \end{aligned} \quad (6.143)$$

If the scaling factor γ is chosen in analogy to (6.135) as

$$\gamma = \sqrt{\frac{P_S}{\text{tr}(\tilde{\mathbf{G}} \tilde{\mathbf{A}} \tilde{\mathbf{G}}^H)}}, \quad (6.144)$$

the relay transmit power constraint is always fulfilled and λ can take on any value. Defining a new variable $\mu := \gamma^2 \lambda$ yields

$$\begin{aligned}\tilde{\mathbf{G}} &= \left(\tilde{\mathbf{H}}_{\text{RD}}^{\text{H}} \tilde{\mathbf{H}}_{\text{RD}} + \mu \mathbf{I} \right)^{-1} \cdot \tilde{\mathbf{H}}_{\text{RD}}^{\text{H}} \mathbf{R}_s^{\text{H}} \tilde{\mathbf{H}}_{\text{SR}}^{\text{H}} \cdot \tilde{\mathbf{A}}^{-\text{H}} = \\ &= \tilde{\mathbf{B}}^{-1} \tilde{\mathbf{C}}^{\text{H}} \tilde{\mathbf{A}}^{-\text{H}},\end{aligned}\quad (6.145)$$

where the substitutions

$$\tilde{\mathbf{A}} := \tilde{\mathbf{H}}_{\text{SR}} \mathbf{R}_s \tilde{\mathbf{H}}_{\text{SR}}^{\text{H}} + \mathbf{R}_{\text{nR}} = \tilde{\mathbf{A}}^{\text{H}} \quad (6.146)$$

$$\tilde{\mathbf{B}} := \tilde{\mathbf{H}}_{\text{RD}}^{\text{H}} \tilde{\mathbf{H}}_{\text{RD}} + \mu \mathbf{I} = \tilde{\mathbf{B}}^{\text{H}} \quad (6.147)$$

$$\tilde{\mathbf{C}} := \tilde{\mathbf{H}}_{\text{SR}} \mathbf{R}_s \tilde{\mathbf{H}}_{\text{RD}}. \quad (6.148)$$

were used. Since the transmit power constraint is now no longer active (because it is always met), the original constrained optimization problem with respect to \mathbf{G} reduces to an unconstrained one with respect to μ . Consequently, the parameter μ has to minimize the cost function

$$\begin{aligned}\epsilon &= \text{E} \left[\|\mathbf{s} - \gamma^{-1} \mathbf{d}_{\text{IV}}\|_2^2 \right] = \\ &= \text{E} \left[\left\| \mathbf{s} - \gamma^{-1} \tilde{\mathbf{H}}_{\text{RD}} \mathbf{G} \tilde{\mathbf{H}}_{\text{SR}} \mathbf{s} - \gamma^{-1} \tilde{\mathbf{H}}_{\text{RD}} \mathbf{G} \mathbf{n}_{\text{R}} - \gamma^{-1} \mathbf{n}_{\text{D}} \right\|_2^2 \right] = \\ &= \text{E} \left[\left\| \mathbf{s} - \tilde{\mathbf{H}}_{\text{RD}} \tilde{\mathbf{G}} \tilde{\mathbf{H}}_{\text{SR}} \mathbf{s} - \tilde{\mathbf{H}}_{\text{RD}} \tilde{\mathbf{G}} \mathbf{n}_{\text{R}} - \gamma^{-1} \mathbf{n}_{\text{D}} \right\|_2^2 \right].\end{aligned}\quad (6.149)$$

The gain matrix

$$\mathbf{G}_{\text{MMSE}} = \gamma \cdot \tilde{\mathbf{G}}(\mu_{\text{MMSE}}) \quad (6.150)$$

is then found by solving the unconstrained optimization problem

$$\mu_{\text{MMSE}} = \arg \min_{\mu} \epsilon(\mu). \quad (6.151)$$

In order to get μ_{MMSE} , the derivative of ϵ with respect to μ has to be set to zero. It is given by

$$\frac{\partial \epsilon}{\partial \mu} = 2 \text{tr} \left(\tilde{\mathbf{B}}^{-3} \left(\tilde{\mathbf{B}} - \tilde{\mathbf{H}}_{\text{RD}}^{\text{H}} \tilde{\mathbf{H}}_{\text{RD}} - \frac{\text{tr}(\mathbf{R}_{\text{nD}})}{P_s} \mathbf{I} \right) \tilde{\mathbf{C}}^{\text{H}} \tilde{\mathbf{A}}^{-1} \tilde{\mathbf{C}} \right). \quad (6.152)$$

Details about the derivation of (6.152) are given in Appendix A.9. The derivative vanishes if the inner term is equal to zero. Using the definition of the substitution for $\tilde{\mathbf{B}}$ yields

$$\begin{aligned} & \tilde{\mathbf{B}} - \tilde{\mathbf{H}}_{\text{RD}}^{\text{H}} \tilde{\mathbf{H}}_{\text{RD}} - \frac{\text{tr}(\mathbf{R}_{\text{nD}})}{P_{\text{S}}} \mathbf{I} \stackrel{!}{=} 0 \\ \rightarrow & \tilde{\mathbf{H}}_{\text{RD}}^{\text{H}} \tilde{\mathbf{H}}_{\text{RD}} + \mu \mathbf{I} - \tilde{\mathbf{H}}_{\text{RD}}^{\text{H}} \tilde{\mathbf{H}}_{\text{RD}} - \frac{\text{tr}(\mathbf{R}_{\text{nD}})}{P_{\text{S}}} \mathbf{I} \stackrel{!}{=} 0 \end{aligned} \quad (6.153)$$

From (6.153) it follows directly that

$$\mu_{\text{MMSE}} = \frac{\text{tr}(\mathbf{R}_{\text{nD}})}{P_{\text{S}}}. \quad (6.154)$$

Summary of results:

The gain matrix \mathbf{G}_{MMSE} is

$$\begin{aligned} \mathbf{G}_{\text{MMSE}} &= \gamma \cdot \tilde{\mathbf{G}}_{\text{MMSE}} \\ &= \gamma \cdot \tilde{\mathbf{B}}^{-1} \tilde{\mathbf{C}}^{\text{H}} \tilde{\mathbf{A}}^{-\text{H}}, \end{aligned} \quad (6.155)$$

where

$$\tilde{\mathbf{G}}_{\text{MMSE}} = \tilde{\mathbf{B}}^{-1} \tilde{\mathbf{C}}^{\text{H}} \tilde{\mathbf{A}}^{-\text{H}} \quad (6.156)$$

$$\gamma = \sqrt{\frac{P_{\text{S}}}{\text{tr}(\tilde{\mathbf{G}}_{\text{MMSE}} \tilde{\mathbf{A}} \tilde{\mathbf{G}}_{\text{MMSE}}^{\text{H}})}} \quad (6.157)$$

and

$$\tilde{\mathbf{A}} := \tilde{\mathbf{H}}_{\text{SR}} \mathbf{R}_{\text{s}} \tilde{\mathbf{H}}_{\text{SR}}^{\text{H}} + \mathbf{R}_{\text{nR}} \quad (6.158)$$

$$\tilde{\mathbf{B}} := \tilde{\mathbf{H}}_{\text{RD}}^{\text{H}} \tilde{\mathbf{H}}_{\text{RD}} + \frac{\text{tr}(\mathbf{R}_{\text{nD}})}{P_{\text{S}}} \mathbf{I} \quad (6.159)$$

$$\tilde{\mathbf{C}} := \tilde{\mathbf{H}}_{\text{SR}} \mathbf{R}_{\text{s}} \tilde{\mathbf{H}}_{\text{RD}}. \quad (6.160)$$

6.3.5 Impact of Phase Noise

In this section we investigate what happens to the MMSE of the received signals if the LO phases of all nodes change randomly during the time between channel estimation and data transmission (e.g. due to phase noise). To this end it is assumed that the LO phases of all terminals are zero at the time the channels are measured, i.e. $\Phi_{\text{S}} = \Phi_{\text{R}} = \Phi_{\text{D}} = \mathbf{I}$. Assume

that the channel estimates are noiseless in which case the gain matrix \mathbf{G} and the weighting matrix $\mathbf{\Gamma}$ are computed from $\tilde{\mathbf{H}}_{\text{SR}} = \mathbf{H}_{\text{SR}}$ and $\tilde{\mathbf{H}}_{\text{RD}} = \mathbf{H}_{\text{RD}}$. During data transmission the LO phases then take on arbitrary values, i.e. $\Phi_{\text{S}} \neq \mathbf{I}$, $\Phi_{\text{R}} \neq \mathbf{I}$, and $\Phi_{\text{D}} \neq \mathbf{I}$. The equivalent channel matrices are in this case given by $\tilde{\mathbf{H}}_{\text{SR}} = \Phi_{\text{R}}^{\text{H}} \mathbf{H}_{\text{SR}} \Phi_{\text{S}}$ and $\tilde{\mathbf{H}}_{\text{RD}} = \Phi_{\text{D}}^{\text{H}} \mathbf{H}_{\text{RD}} \Phi_{\text{R}}$. For the generic cases treated in Sections 6.3.1 and 6.3.3, the MSE of the received signals for fixed \mathbf{G} and $\mathbf{\Gamma}$ is given by

$$\begin{aligned}
 \epsilon &= \text{E} \left[\|\mathbf{s} - \mathbf{\Gamma} \mathbf{d}_{\text{IV}}\|_2^2 \right] = \\
 &= \text{E} \left[\left\| \mathbf{s} - \mathbf{\Gamma} \tilde{\mathbf{H}}_{\text{RD}} \mathbf{G} \tilde{\mathbf{H}}_{\text{SR}} \mathbf{s} - \mathbf{\Gamma} \tilde{\mathbf{H}}_{\text{RD}} \mathbf{G} \mathbf{n}_{\text{R}} - \mathbf{\Gamma} \mathbf{n}_{\text{D}} \right\|_2^2 \right] = \\
 &= \text{tr}(\mathbf{R}_{\text{s}}) - \\
 &\quad - \text{tr} \left(\mathbf{R}_{\text{s}} \tilde{\mathbf{H}}_{\text{SR}}^{\text{H}} \mathbf{G}^{\text{H}} \tilde{\mathbf{H}}_{\text{RD}}^{\text{H}} \mathbf{\Gamma}^{\text{H}} \right) - \text{tr} \left(\mathbf{\Gamma} \tilde{\mathbf{H}}_{\text{RD}} \mathbf{G} \tilde{\mathbf{H}}_{\text{SR}} \mathbf{R}_{\text{s}} \right) + \\
 &\quad + \text{tr} \left(\mathbf{\Gamma} \tilde{\mathbf{H}}_{\text{RD}} \mathbf{G} \tilde{\mathbf{H}}_{\text{SR}} \mathbf{R}_{\text{s}} \tilde{\mathbf{H}}_{\text{SR}}^{\text{H}} \mathbf{G}^{\text{H}} \tilde{\mathbf{H}}_{\text{RD}}^{\text{H}} \mathbf{\Gamma}^{\text{H}} \right) + \\
 &\quad + \text{tr} \left(\mathbf{\Gamma} \tilde{\mathbf{H}}_{\text{RD}} \mathbf{G} \mathbf{R}_{\text{nR}} \mathbf{G}^{\text{H}} \tilde{\mathbf{H}}_{\text{RD}}^{\text{H}} \mathbf{\Gamma}^{\text{H}} \right) + \\
 &\quad + \text{tr} \left(\mathbf{\Gamma} \mathbf{R}_{\text{nD}} \mathbf{\Gamma}^{\text{H}} \right). \tag{6.161}
 \end{aligned}$$

Equation (6.161) will be investigated line by line to see what happens:

- The first summand is the trace of the covariance matrix of the transmit symbol vector \mathbf{s} . It is not affected by the LO phase offsets of any of the terminals.
- The second and third summand are

$$\begin{aligned}
 &\text{tr} \left(\mathbf{R}_{\text{s}} \tilde{\mathbf{H}}_{\text{SR}}^{\text{H}} \mathbf{G}^{\text{H}} \tilde{\mathbf{H}}_{\text{RD}}^{\text{H}} \mathbf{\Gamma}^{\text{H}} \right) + \text{tr} \left(\mathbf{\Gamma} \tilde{\mathbf{H}}_{\text{RD}} \mathbf{G} \tilde{\mathbf{H}}_{\text{SR}} \mathbf{R}_{\text{s}} \right) = \\
 &= \text{tr} \left(\mathbf{R}_{\text{s}} \Phi_{\text{S}}^{\text{H}} \mathbf{H}_{\text{SR}}^{\text{H}} \mathbf{G}^{\text{H}} \mathbf{H}_{\text{RD}}^{\text{H}} \Phi_{\text{D}} \mathbf{\Gamma}^{\text{H}} + \mathbf{\Gamma} \Phi_{\text{D}}^{\text{H}} \mathbf{H}_{\text{RD}} \mathbf{G} \mathbf{H}_{\text{SR}} \Phi_{\text{S}} \mathbf{R}_{\text{s}} \right) = \\
 &= \text{tr} \left(\mathbf{R}_{\text{s}} \mathbf{H}_{\text{SR}}^{\text{H}} \mathbf{G}^{\text{H}} \mathbf{H}_{\text{RD}}^{\text{H}} \Phi_{\text{D}} \mathbf{\Gamma}^{\text{H}} \Phi_{\text{S}} + \Phi_{\text{S}} \mathbf{\Gamma} \Phi_{\text{D}}^{\text{H}} \mathbf{H}_{\text{RD}} \mathbf{G} \mathbf{H}_{\text{SR}} \mathbf{R}_{\text{s}} \right). \tag{6.162}
 \end{aligned}$$

The LO phase offsets of sources and destinations obviously do have an impact on (6.162).

- The fourth summand is given by

$$\begin{aligned}
 &\text{tr} \left(\mathbf{\Gamma} \tilde{\mathbf{H}}_{\text{RD}} \mathbf{G} \tilde{\mathbf{H}}_{\text{SR}} \mathbf{R}_{\text{s}} \tilde{\mathbf{H}}_{\text{SR}}^{\text{H}} \mathbf{G}^{\text{H}} \tilde{\mathbf{H}}_{\text{RD}}^{\text{H}} \mathbf{\Gamma}^{\text{H}} \right) = \\
 &= \text{tr} \left(\mathbf{\Gamma} \Phi_{\text{D}}^{\text{H}} \mathbf{H}_{\text{RD}} \mathbf{G} \mathbf{H}_{\text{SR}} \Phi_{\text{S}} \mathbf{R}_{\text{s}} \Phi_{\text{S}}^{\text{H}} \mathbf{H}_{\text{SR}}^{\text{H}} \mathbf{G}^{\text{H}} \mathbf{H}_{\text{RD}}^{\text{H}} \Phi_{\text{D}} \mathbf{\Gamma}^{\text{H}} \right) = \\
 &= \text{tr} \left(\mathbf{\Gamma} \mathbf{H}_{\text{RD}} \mathbf{G} \mathbf{H}_{\text{SR}} \mathbf{R}_{\text{s}} \mathbf{H}_{\text{SR}}^{\text{H}} \mathbf{G}^{\text{H}} \mathbf{H}_{\text{RD}}^{\text{H}} \mathbf{\Gamma}^{\text{H}} \right), \tag{6.163}
 \end{aligned}$$

which is independent of the LO phases of the nodes.

- The fifth summand is

$$\begin{aligned}
 & \text{tr} \left(\tilde{\Gamma} \tilde{\mathbf{H}}_{\text{RD}} \mathbf{G} \mathbf{R}_{\text{nR}} \mathbf{G}^{\text{H}} \tilde{\mathbf{H}}_{\text{RD}}^{\text{H}} \tilde{\Gamma}^{\text{H}} \right) = \\
 & = \text{tr} \left(\tilde{\Gamma} \Phi_{\text{D}}^{\text{H}} \mathbf{H}_{\text{RD}} \mathbf{G} \mathbf{R}_{\text{nR}} \mathbf{G}^{\text{H}} \mathbf{H}_{\text{RD}}^{\text{H}} \Phi_{\text{D}} \tilde{\Gamma}^{\text{H}} \right) = \\
 & = \text{tr} \left(\tilde{\Gamma} \mathbf{H}_{\text{RD}} \mathbf{G} \mathbf{R}_{\text{nR}} \mathbf{G}^{\text{H}} \mathbf{H}_{\text{RD}}^{\text{H}} \tilde{\Gamma}^{\text{H}} \right). \tag{6.164}
 \end{aligned}$$

It is also independent of the LO phase offsets.

- Finally, the last summand of (6.161), i.e. $\text{tr} \left(\tilde{\Gamma} \mathbf{R}_{\text{nD}} \tilde{\Gamma}^{\text{H}} \right)$, is also not affected by the LO phase offsets of the terminals.

The LO phase offsets of the relays obviously do not have an impact on ϵ and therefore on the performance of the system. Furthermore, weighting the receive signal vector \mathbf{d}_{IV} with $\tilde{\Gamma} = \Phi_{\text{S}}^{\text{H}} \tilde{\Gamma} \Phi_{\text{D}}$ instead of $\tilde{\Gamma}$ (while leaving \mathbf{G} unchanged), removes the dependency of ϵ on Φ_{S} and Φ_{D} . This means that the MMSE is also independent of the LO phases of sources and destinations. The cost function becomes

$$\begin{aligned}
 & \text{E} \left[\left\| \mathbf{s} - \tilde{\Gamma} \tilde{\mathbf{H}}_{\text{RD}} \mathbf{G} \tilde{\mathbf{H}}_{\text{SR}} \mathbf{s} - \tilde{\Gamma} \tilde{\mathbf{H}}_{\text{RD}} \mathbf{G} \mathbf{n}_{\text{R}} - \tilde{\Gamma} \mathbf{n}_{\text{D}} \right\|_2^2 \right] = \\
 & = \text{E} \left[\left\| \mathbf{s} - \tilde{\Gamma} \mathbf{H}_{\text{RD}} \mathbf{G} \mathbf{H}_{\text{SR}} \mathbf{s} - \tilde{\Gamma} \mathbf{H}_{\text{RD}} \mathbf{G} \mathbf{n}_{\text{R}} - \tilde{\Gamma} \mathbf{n}_{\text{D}} \right\|_2^2 \right], \tag{6.165}
 \end{aligned}$$

which is independent of the current realization of Φ_{S} , Φ_{R} , and Φ_{D} . This holds for the generic case and thus also for the special case that $\tilde{\Gamma} = \gamma^{-1} \mathbf{I}$.

6.3.6 Simulation Results

In this section the results of Monte-Carlo simulations are presented. Consider a system as introduced in Chapter 2 with N_{SD} single antenna source-destination pairs. Since the direct link is not taken into account in the context of MMSE relaying, only traffic pattern IV is considered in the simulation results. The average sum rate as defined in Section 2.6 is used as figure of merit. The relay gain factors are chosen as described in Sections 6.3.1 to 6.3.4. For each of the two special cases LinRel and LDAS, simulation results for both the generic and the special case are presented.

The scenario described in Section 2.5, where N_{SD} single-antenna source-destination pairs communicate in a TDD manner, is used as reference for the system performance. 'reference 1' denotes the case where the first-hop and second-hop channel coefficients of the two-hop scenario exhibit a variance of $\sigma_{\text{h}}^2 = 1$ while the direct link channel coefficients of the reference scenario have a variance of $\frac{1}{4} \sigma_{\text{h}}^2 = \frac{1}{4}$. For free-space propagation and path loss exponent

two this corresponds to a system topology where the relays are half-way between sources and destinations. In contrast to that, 'reference 2' refers to the case where all channel coefficients have variance $\sigma_h^2 = 1$. In a sense, this represents a worst-case scenario for a two-hop relaying protocol because it cannot benefit from the range-extension capabilities of the relays.

In order to have an additional reference, the performance of MUZF relaying presented in Section 6.2 is also plotted. For all cases where the number of relay cooperations is below the minimum cooperation configuration, the gain vector of MUZF relaying is chosen as the last column of \mathbf{U} in (6.52). In the simulation results presented in Section 6.2.4 this case was denoted by 'traffic pattern IV, U'. If, however, the number of relay cooperations is equal to or higher than the minimum cooperation configuration, the gain factors are chosen according to (6.57). This case is denoted by 'traffic pattern I, Z' in Section 6.2.4. In the following, MMSE relaying with individual and equal scaling factors at the destinations (generic and special case) are denoted by 'MMSE, generic' and 'MMSE special', respectively. Finally, MUZF relaying is denoted by 'MUZF'.

6.3.6.1 Linear Relaying (LinRel)

In Figs. 6.7 and 6.8, the average sum rate is plotted versus the SNR (as defined in Section 2.5) for $N_{SD} = 2$ and $N_{SD} = 4$ source-destination pairs with $N_R = 3$ and $N_R = 13$ single-antenna relays, respectively. Both configurations represent the minimum cooperation configuration for their respective number of source-destination pairs. For $N_{SD} = 2$, the maximum spatial multiplexing gain for two-hop relaying with half-duplex relays is one. This is due to the pre-log factor of $\frac{1}{2}$ in the mutual information. 'reference 1' thus represents a strict upper bound for the two-hop sum rate at high SNR. In both plots, the curves representing 'MMSE special' exhibit a lower slope than 'MMSE generic' and 'MUZF' at high SNR. This indicates a smaller spatial multiplexing gain compared to the other schemes. The reason for this behavior is that 'MMSE special' tries to make the equivalent two-hop channel matrix a weighted identity. It is a very fair scheme because it aims at providing all destinations with the same signal strength. This happens at the cost of sum rate, though.

The average sum rate versus the number of relays N_R for $N_{SD} = 2$ and $N_{SD} = 4$ source-destination pairs and SNR = 20 dB is shown in Figs. 6.9 and 6.10, respectively. For increasing number of relays, the performance of all three two-hop gain allocation schemes increases. They outperform both reference scenarios for large N_R because they are able to exploit a distributed array gain. This essentially means that they are able to provide a receive power gain due to coherent combining of the signals at the destinations. The instantaneous

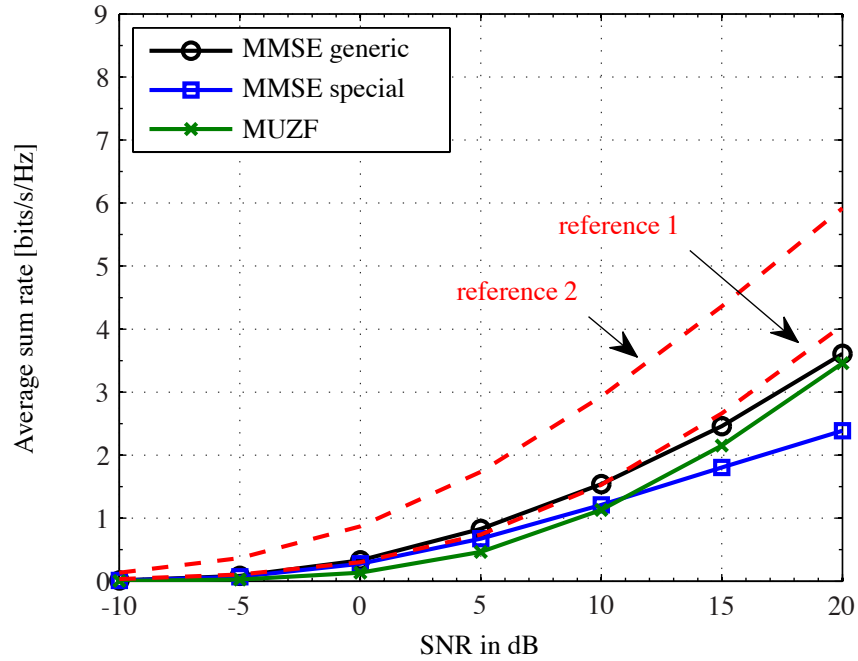


Fig. 6.7: Average sum rate versus SNR for $N_{SD} = 2$ single-antenna source-destination pairs and $N_R = 3$ relays.

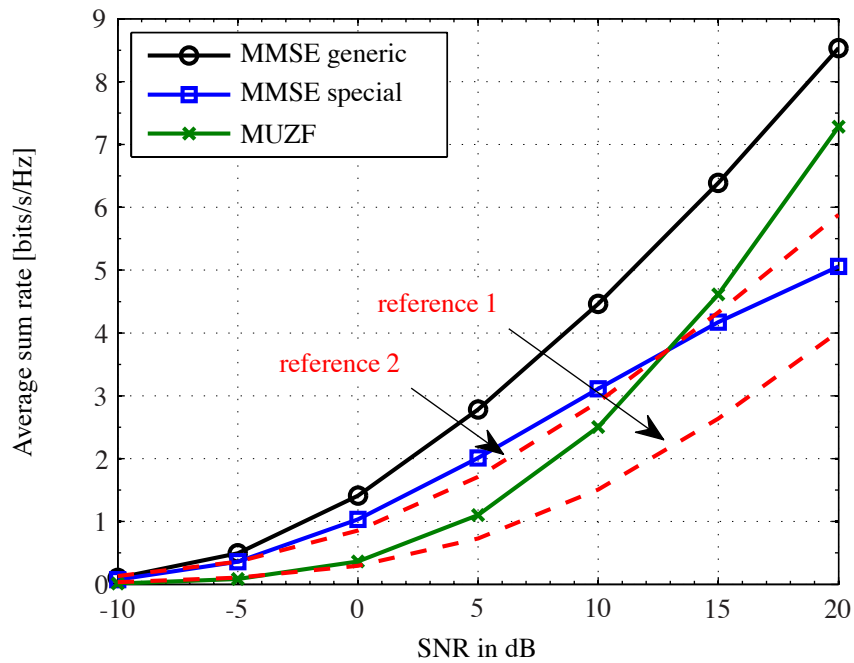


Fig. 6.8: Average sum rate versus SNR for $N_{SD} = 4$ single-antenna source-destination pairs and $N_R = 13$ relays.

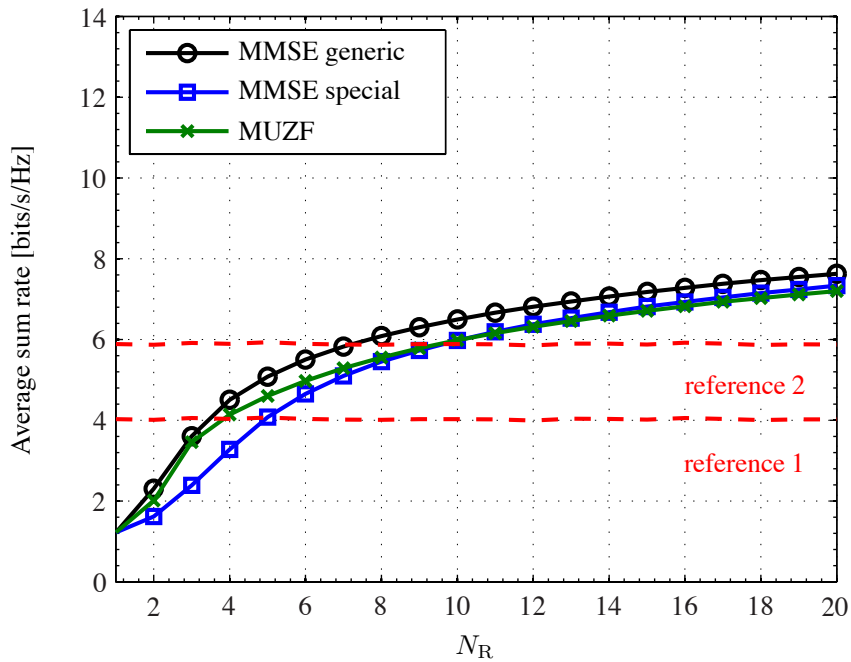


Fig. 6.9: Average sum rate versus N_R for $N_{SD} = 2$ single-antenna source-destination pairs and SNR = 20 dB.

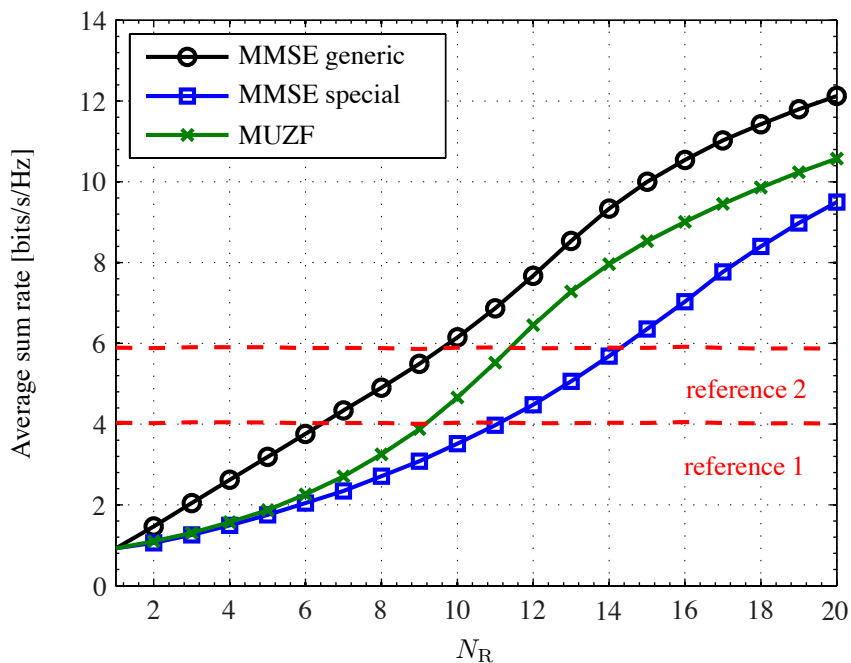


Fig. 6.10: Average sum rate versus N_R for $N_{SD} = 4$ single-antenna source-destination pairs and SNR = 20 dB.

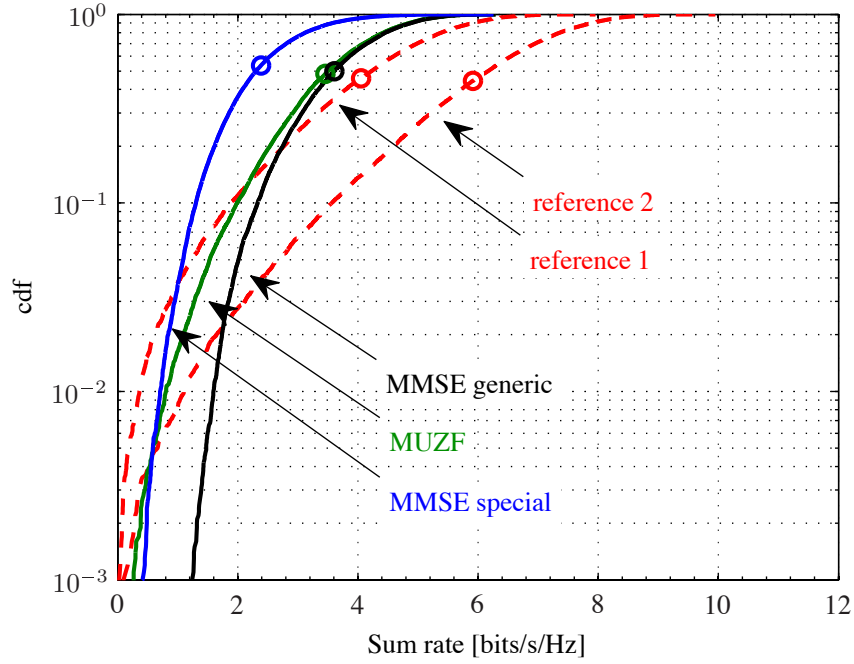


Fig. 6.11: Empirical cdf of the sum rate for $N_{SD} = 2$ single-antenna source-destination pairs and $N_R = 3$ relays at $\text{SNR} = 20$ dB.

transmit power constraint of the relays leads to a saturation of the curves for large N_R . Note also that the larger the number of relays, the better the relaying schemes are able to orthogonalize the equivalent channels. This shows itself in the fact that the average sum rate for $N_{SD} = 2$ is larger than for $N_{SD} = 4$ when the number of relays is small (compare Figs. 6.9 and 6.10 for example for $N_R = 4$).

Finally, Figs. 6.11 and 6.12 show empirical cdfs of the sum rate for $N_{SD} = 2$ and $N_{SD} = 4$ source-destination pairs with $N_R = 3$ and $N_R = 13$ relays, respectively, at $\text{SNR} = 20$ dB. The circles indicate the mean value for each curve. Compared to the two reference systems and MUZF relaying a substantial diversity gain can be observed for both MMSE relaying schemes.

6.3.6.2 Linear Relaying (LDAS)

Figs. 6.13 and 6.14 show the average sum rate versus SNR for $N_{SD} = 2$ and $N_{SD} = 4$ source-destination pairs with a single relay employing $M_R = 2$ and $M_R = 4$ antennas, respectively.

For $N_{SD} = 2$ and $M_R = 2$ the number of relay cooperations is equal to the minimum cooperation configuration. In this case, 'reference 1' represents a strict upper bound for the

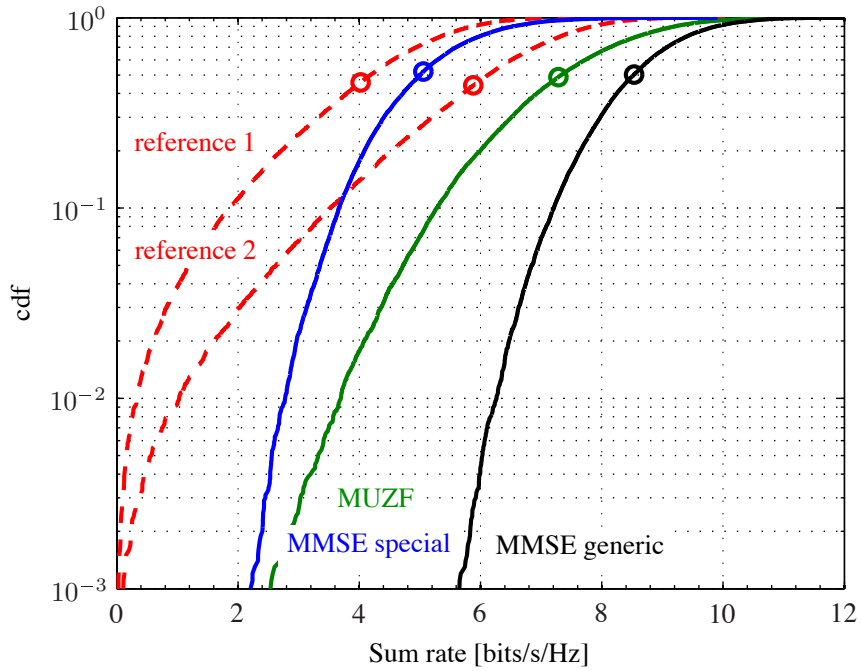


Fig. 6.12: Empirical cdf of the sum rate for $N_{SD} = 4$ single-antenna source-destination pairs and $N_R = 13$ relays at SNR = 20 dB.

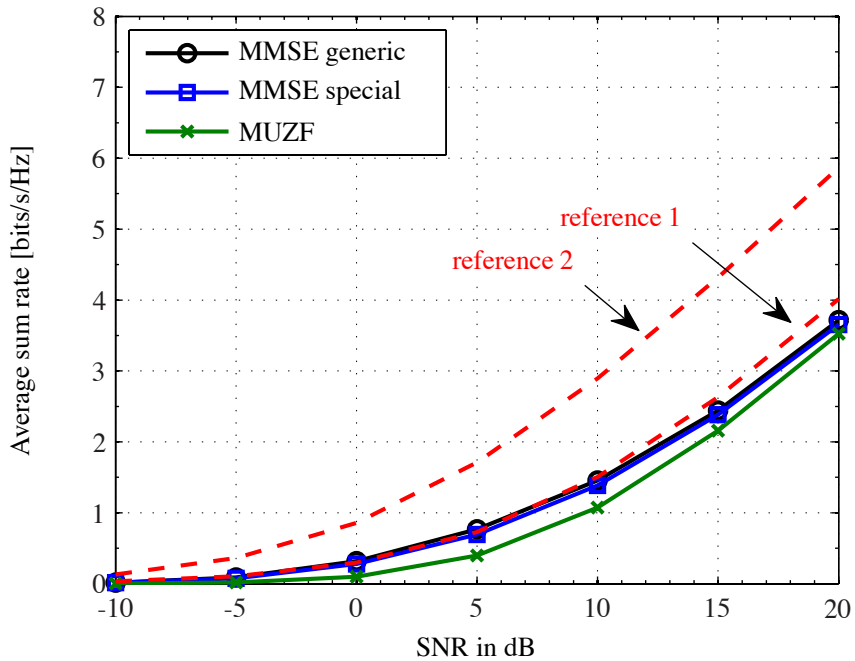


Fig. 6.13: Average sum rate versus SNR for $N_{SD} = 2$ single-antenna source-destination pairs and $M_R = 2$ relay antennas.

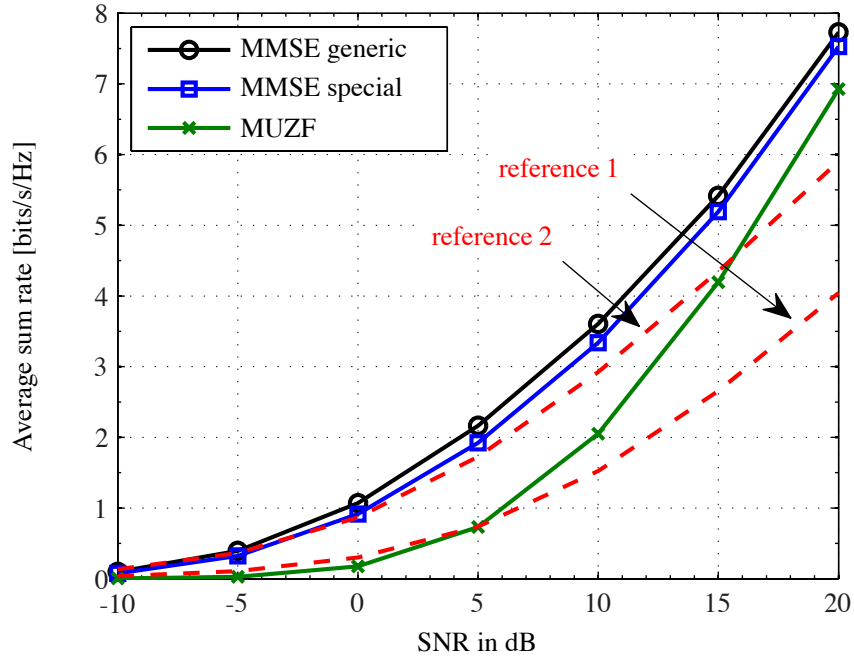


Fig. 6.14: Average sum rate versus SNR for $N_{SD} = 4$ single-antenna source-destination pairs and $M_R = 4$ relay antennas.

two-hop sum rates for high SNR. We can furthermore observe that the average sum rate for both MMSE relaying schemes is nearly the same if all channel coefficients exhibit the same variance. They both outperform MUZF relaying, especially for low SNR. For high SNR, the performance of all three two-hop relaying schemes will converge because the gain matrices will be identical.

In Figs. 6.15 and 6.16 the average sum rate is plotted versus the number of relay antennas M_R for $N_{SD} = 2$ and $N_{SD} = 4$ source-destination pairs, respectively, at SNR = 20 dB. The performance is virtually the same for all three two-hop relaying schemes if the number of cooperations is at least equal to the minimum cooperation configuration. Increasing the number of relay antennas increases the average sum rate because the additional degrees of freedom allow to shape the equivalent source-destination channels more accurately. The performance of 'reference 2' is exceeded even for $N_{SD} = 2$ if the number of cooperations is sufficiently large. Note that the instantaneous sum power constraint results in a saturation of the average sum rate for large number of relay antennas.

Finally, in Figs. 6.17 and 6.18, the cdfs of the sum rates are plotted for $N_{SD} = 2$ and $N_{SD} = 4$ source-destination pairs with a relay employing $M_R = 2$ and $M_R = 4$ antennas, respectively, at SNR = 20dB. The circles indicate the mean value for each curve. Compared

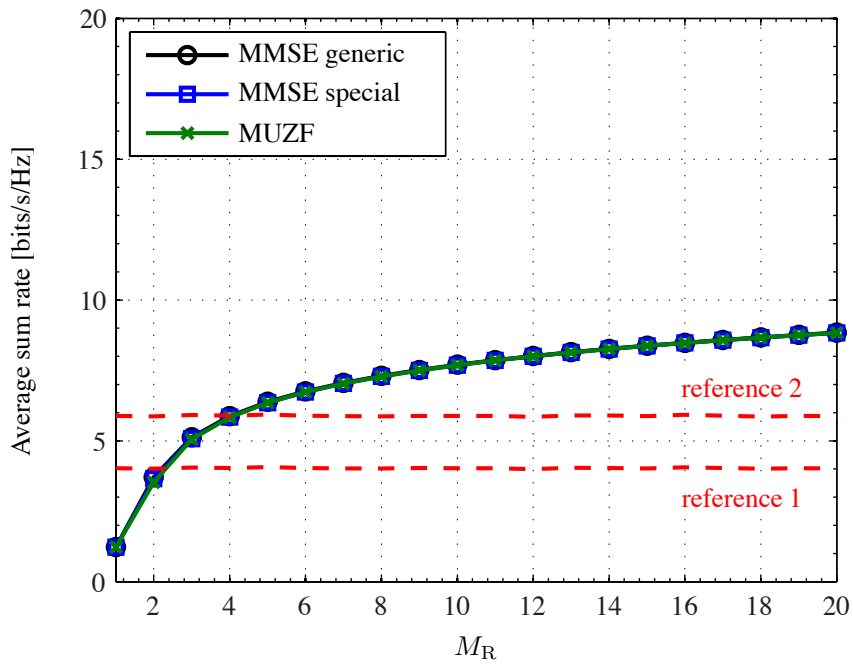


Fig. 6.15: Average sum rate versus M_R for $N_{SD} = 2$ single-antenna source-destination pairs and $SNR = 20$ dB.

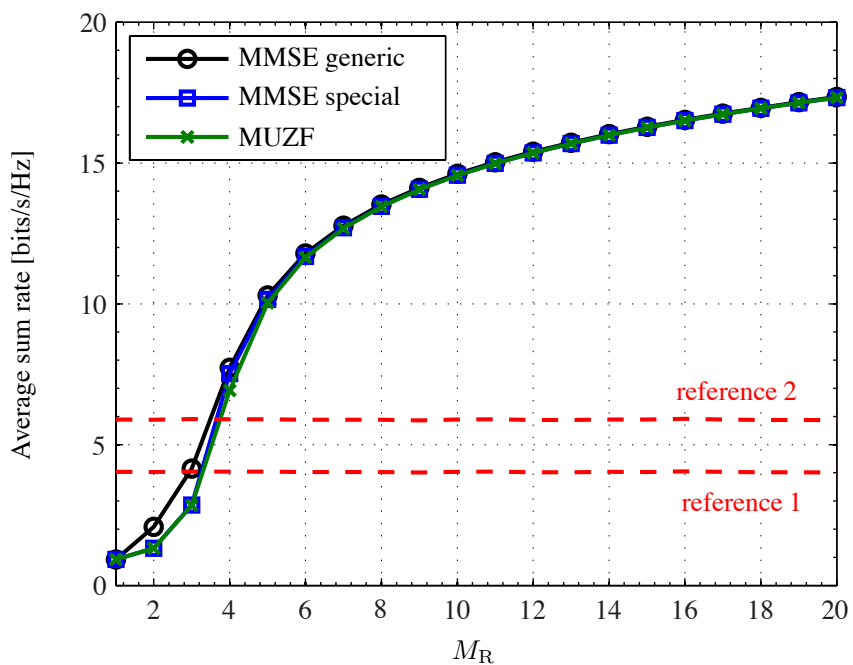


Fig. 6.16: Average sum rate versus M_R for $N_{SD} = 4$ single-antenna source-destination pairs and $SNR = 20$ dB.

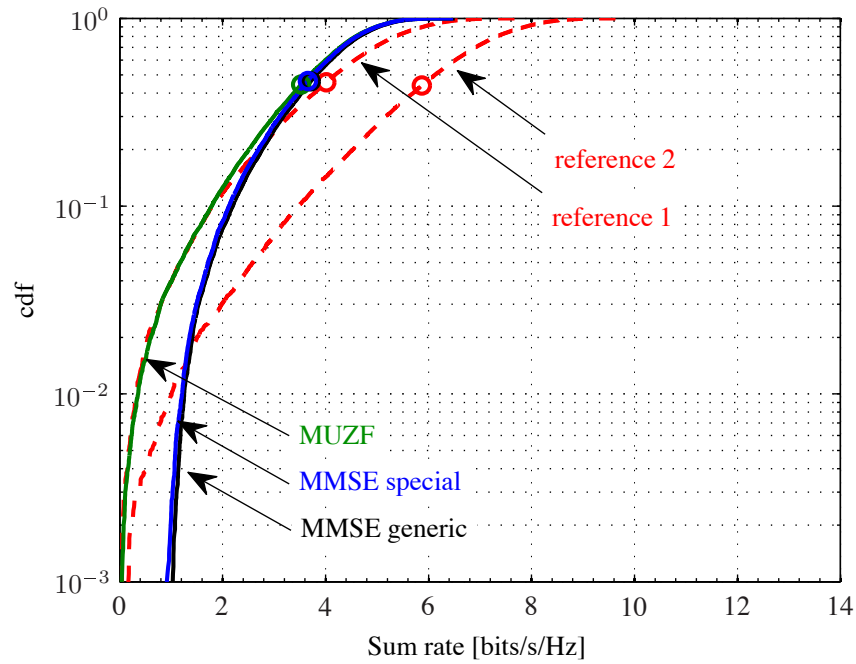


Fig. 6.17: cdf of the sum rate for $N_{SD} = 2$ single-antenna source-destination pairs and $M_R = 2$ relay antennas at $SNR = 20$ dB.

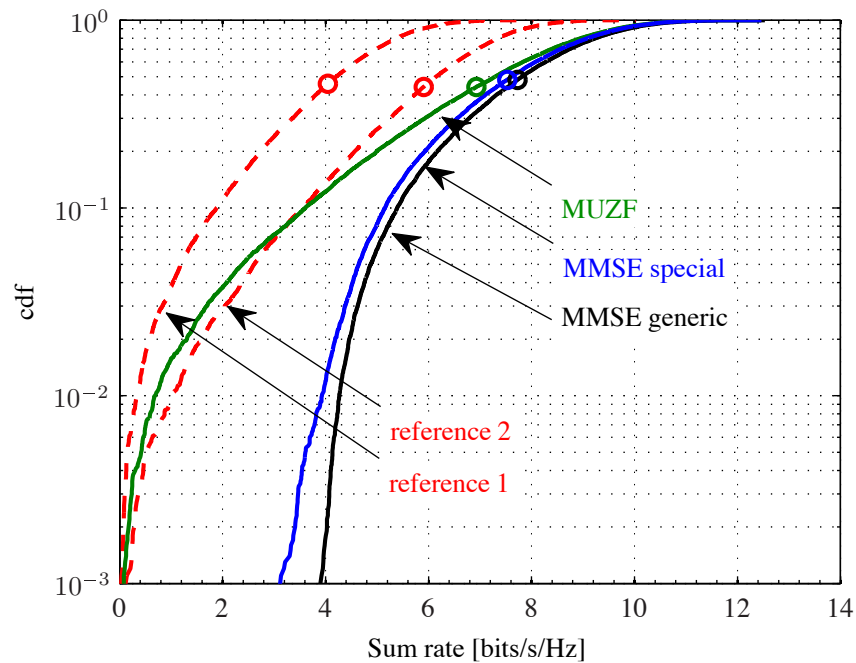


Fig. 6.18: cdf of the sum rate for $N_{SD} = 4$ single-antenna source-destination pairs and $M_R = 4$ relay antennas at $SNR = 20$ dB.

to the two reference systems a substantial diversity gain can be observed for both MMSE relaying schemes. They also exhibit a higher diversity than MUZF relaying.

6.4 Impact of Relay Imperfections

The performance results in the previous sections did not consider any relay imperfections apart from AWGN during the data transmission phase. In this section, the impact of imperfections at the relays on the performance of MUZF and MMSE relaying is investigated based on Monte-Carlo simulations performed in MATLAB[®]. In particular, the following aspects are considered:

- *Noisy CSI*: The gain matrix cannot be computed correctly if the channel estimates are noisy. This basically means that the relay gains are optimized for an erroneous assumption about the channel situation. The signals from the relays will in this case not add up in the desired fashion at the destination antennas. As a consequence, the receive SINR and hence the system performance decreases.
- *Phase noise at the relays*: If the LO phases of the relays change during the time between reception and retransmission the signals from the relays no longer add up coherently at the destination antennas. This leads to increased inter-user interference which in turn decreases the overall system performance.
- *Phase synchronization errors* for the cases that the relays require a common phase reference: In the presence of phase synchronization errors (due to noisy estimates and phase noise) the impact of the relay phases on the channel estimates (and therefore on the gain factors) cannot be compensated completely. This reduces the accuracy with which the gain matrix can shape the equivalent source-destination channels.

In order to be able to judge the performance quantitatively, reference curves are included in the plots. They represent the following cases:

'reference 1': This denotes the situation where N_{SD} source-destination pairs communicate in a TDD scheme. It is the same reference that was used for the simulation results in Section 6.3.6. The total transmit power of all sources is scaled such that a transmission cycle for the reference scenario uses the same amount of total transmit power in N_{SD} time slots as the two-hop relaying system requires in two time slots. For 'reference 1' it is furthermore assumed that the direct link channel coefficients have a variance of $\frac{1}{4}\sigma_h^2 = \frac{1}{4}$ whereas the first-hop and second-hop channel coefficients in the two-hop

scenario exhibit a variance of $\sigma_h^2 = 1$. For free-space propagation and path loss exponent two this corresponds to a configuration where the relays are half-way between sources and destinations.

'reference 2': This is the same situation as for 'reference 1' except for the fact that all channel coefficients have variance $\sigma_h^2 = 1$. In a sense, this represents a worst-case scenario for the two-hop relaying protocols because they cannot benefit from the range-extension capabilities of the relays.

'Max sumrate': This reference represents a two-hop relaying network where the gain factors are computed with a gradient search algorithm that tries to maximize the network sum rate while meeting the sum transmit power constraint at the relays [194]. It turned out during the simulations, that the result highly depends on the starting vector. This hints at a nonconvex problem formulation because the gradient algorithm seems to get stuck in local minima. The best results have been obtained by using the gain matrix from the generic MMSE gain allocation (cf. Sections 6.3.1 and 6.3.3) as starting point for the optimization.

The average receive SNR is defined in Section 2.5 as

$$\text{SNR} = \frac{2\sigma_h^2\sigma_s^2}{\sigma_n^2}, \quad (6.166)$$

where σ_s^2 and σ_n^2 are the signal power and the noise variance, respectively.

6.4.1 Noisy CSI

The gain factors of any coherent gain allocation scheme are computed from instantaneous channel knowledge. If perfect CSI is available, the signals from all relays add up in the desired fashion at the destination antennas. However, if the channel estimates are inaccurate, i.e., they differ from the actual channels, the gain factors cannot be computed correctly. This basically means that the gain matrix is optimized for a channel situation that is different from the actual one. Consequently, the signals from the relays will not add up coherently at the destination antennas.

In this section, the impact of noisy channel estimates on the overall system performance is investigated. The matrices $\tilde{\mathbf{H}}_{\text{SR}}$ and $\tilde{\mathbf{H}}_{\text{RD}}$ denote the equivalent first-hop and second-hop channel matrices of a two-hop network. It is assumed that the channel estimates $\hat{\mathbf{H}}_{\text{SR}}$ and $\hat{\mathbf{H}}_{\text{RD}}$, from which the gain matrix is computed, are perturbed by AWGN. They can be written

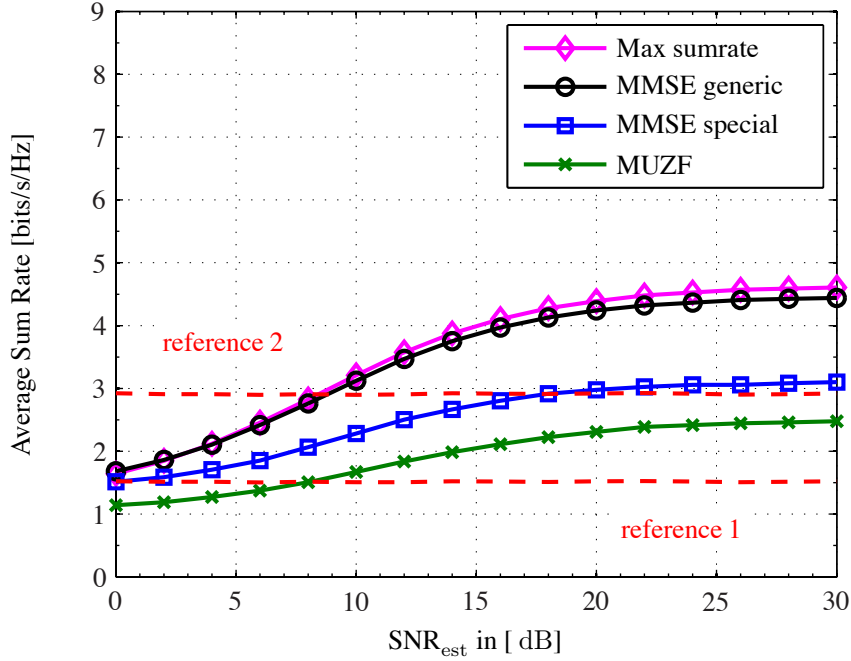


Fig. 6.19: Average sum rate versus estimation SNR for LinRel (single-antenna relays), 4 single-antenna source-destination pairs, 13 relays, and SNR = 10 dB.

as

$$\hat{\mathbf{H}}_{\text{SR}} = \tilde{\mathbf{H}}_{\text{SR}} + \Delta\tilde{\mathbf{H}}_{\text{SR}} \quad (6.167)$$

$$\hat{\mathbf{H}}_{\text{RD}} = \tilde{\mathbf{H}}_{\text{RD}} + \Delta\tilde{\mathbf{H}}_{\text{RD}}, \quad (6.168)$$

where $\Delta\tilde{\mathbf{H}}_{\text{SR}} \in \mathbb{C}^{N_{\text{R}} \times N_{\text{SD}}}$ and $\Delta\tilde{\mathbf{H}}_{\text{RD}} \in \mathbb{C}^{N_{\text{SD}} \times N_{\text{R}}}$ comprise AWGN samples. They are iid, zero-mean, complex Gaussian random variables with variance σ_e^2 . The estimation SNR is then defined as

$$\text{SNR}_{\text{est}} = \frac{\sigma_{\text{h}}^2}{\sigma_e^2}. \quad (6.169)$$

Fig. 6.19 and 6.20 show the average sum rate versus the estimation SNR for a 'LinRel' system configuration comprising four source-destination pairs and 13 single-antenna relays. Note that this corresponds to the minimum relay configuration for MUZF relaying. The average receive SNR is 10 dB and 20 dB, respectively. The reference cases ('reference 1' and 'reference 2') are independent of the channel estimation error because they represent point-to-point communication without relays. It can generally be observed that the average sum

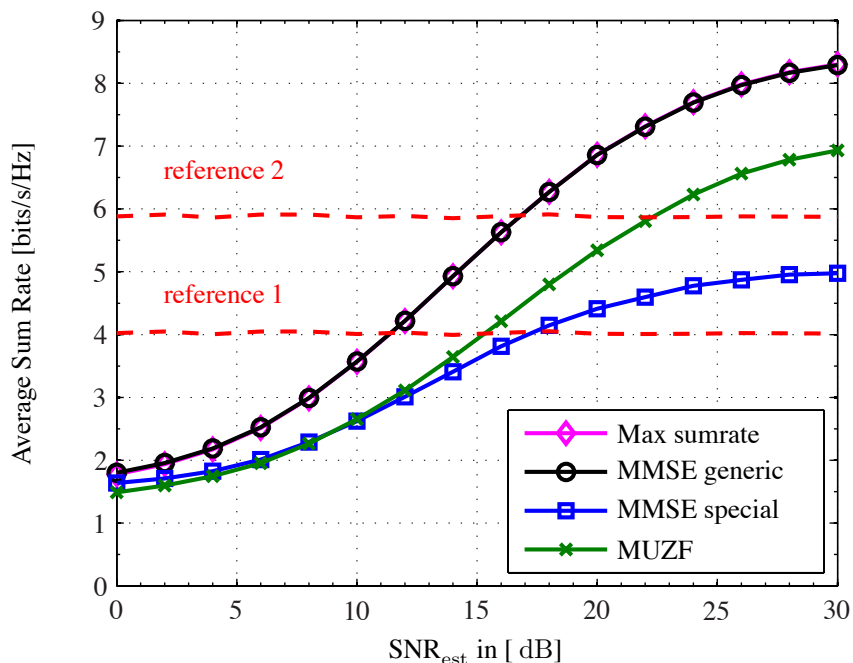


Fig. 6.20: Average sum rate versus estimation SNR for LinRel (single-antenna relays), 4 single-antenna source-destination pairs, 13 relays, and $\text{SNR} = 20$ dB.

rate saturates earlier for lower receive SNR. The plots also show that the larger the number of relays the higher the estimation SNR that is required to outperform the reference scenarios. Furthermore, the performance of the 'Max sumrate' scheme is similar to 'MMSE generic'. This means that 'MMSE generic' maximizes the sum rate of the system for high SNR. The fact that 'MMSE generic' always outperforms 'MUZF' relaying finally shows that the MMSE-based gain allocation is more robust with respect to noisy CSI than the zero-forcing-based gain allocation.

An LDAS system configuration with four source-destination pairs and a relay with four antennas is considered in Figs. 6.21 and 6.22. The average receive SNR is 10 dB and 20 dB, respectively. In general the impact of noisy CSI on the performance of the LDAS system is very similar to its impact on a LinRel system. The average sum rate saturates earlier for lower receive SNR. For $\text{SNR} = 10$ dB the maximum average sum rate is achieved already for an estimation SNR of about 20 dB. In contrast to that, the average sum rate saturates much later for $\text{SNR} = 20$ dB. There, an increase in the average sum rate can be observed even for $\text{SNR}_{\text{est}} = 30$ dB. The plots show furthermore that the larger the number of relay antennas the higher the estimation SNR that is required to outperform the reference scenarios. It can finally be observed that, in contrast to LinRel, the performance of both MMSE-based

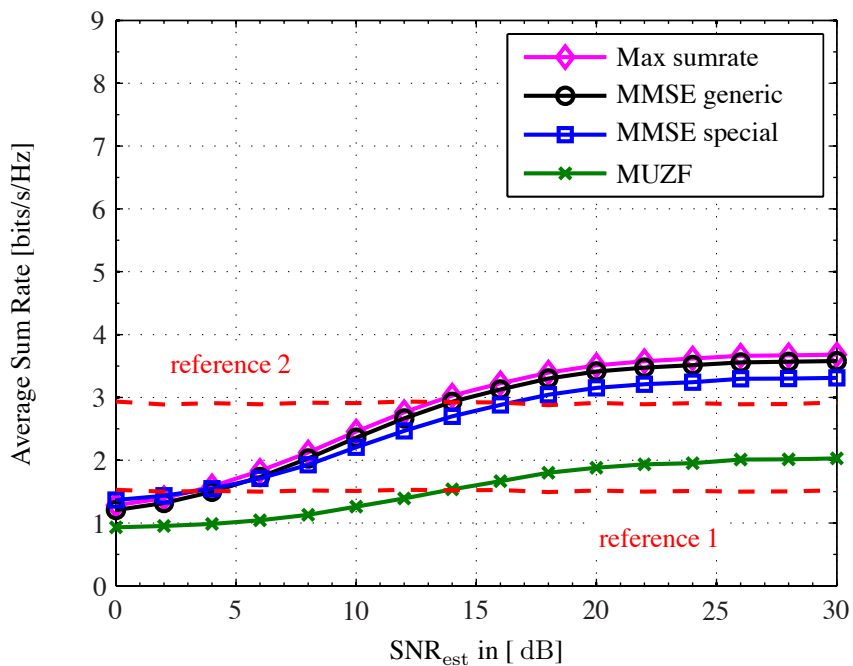


Fig. 6.21: Average sum rate versus estimation SNR for LDAS (single multi-antenna relay), 4 single-antenna source-destination pairs, 4 relay antennas, SNR = 10 dB.

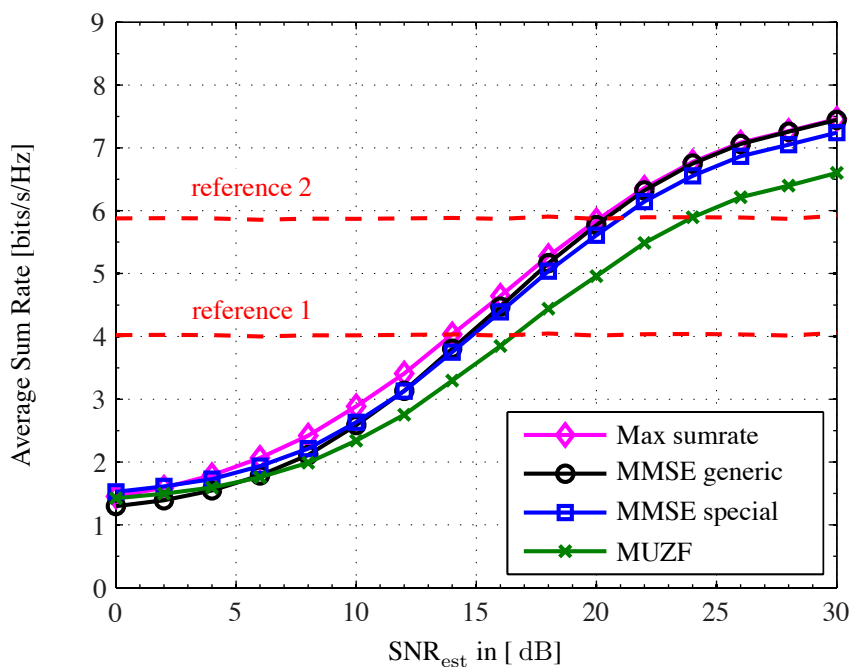


Fig. 6.22: Average sum rate versus estimation SNR for LDAS (single multi-antenna relay), 4 single-antenna source-destination pairs, 4 relay antennas, SNR = 20 dB.

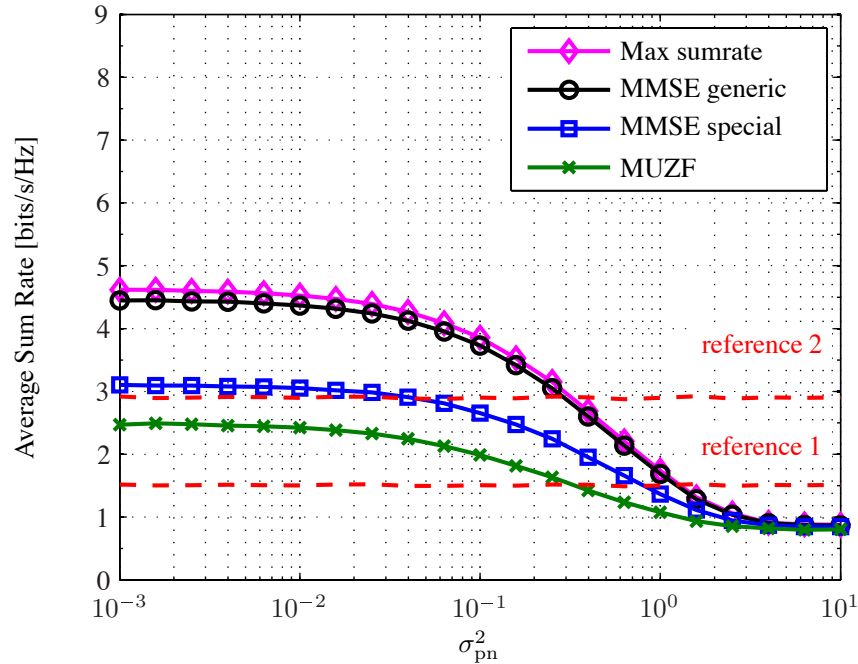


Fig. 6.23: Average sum rate versus phase noise variance for LinRel (single-antenna relays), 4 single-antenna source-destination pairs, 13 relays, and SNR = 10 dB.

gain allocation schemes is close to 'Max sumrate' for an LDAS system configuration (the performance of 'MMSE special' was worse than 'MMSE generic' and 'Max sumrate' for the LinRel system).

6.4.2 Phase Noise

In Chapter 5 it was stated that if the LO phases of the relays remain constant for at least one transmission cycle they have no impact on the received signals at the destinations. However, in case they change during the time between reception and retransmission an unknown and random phase offset is introduced at each relay. Consequently, the signals from the relays do not combine coherently at the destination antennas anymore.

Figs. 6.23 and 6.24 show the average sum rate for a 'LinRel' system configuration with 4 source-destination pairs and 13 relays versus the phase noise severity. For a Wiener phase noise model (cf. Chapter 3), the change of the LO phase at each relay is a zero-mean Gaussian random variable with variance σ_{pn}^2 . The system SNR is 10 dB and 20 dB, respectively. It can be observed that networks operating at a low SNR are generally more robust against relay phase noise than networks operating at high SNR. In Fig. 6.23 the average sum rate

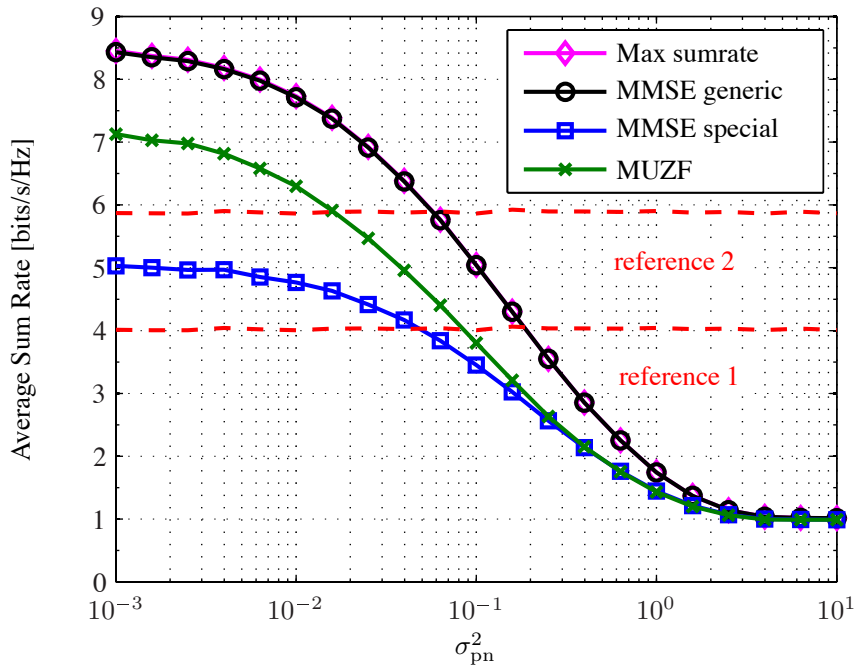


Fig. 6.24: Average sum rate versus phase noise variance for LinRel (single-antenna relays), 4 single-antenna source-destination pairs, 13 relays, and SNR = 20 dB.

remains more or less unchanged up until $\sigma_{\text{pn}}^2 \approx 10^{-2}$ for SNR = 10 dB. Performance degrades quickly for more severe phase noise. In contrast to that, Fig. 6.24 shows that a severe performance degradation can already be observed from $\sigma_{\text{pn}}^2 \approx 10^{-3}$ on for SNR = 20 dB.

In Figs. 6.25 and 6.26 the average sum rate is depicted versus σ_{pn}^2 for an LDAS system configuration with 4 source-destination pairs and a single relay with 4 antennas. The system SNR is again 10 dB and 20 dB, respectively. Relay phase noise has no impact on the average sum rate because all relay antennas are connected to the same LO. The reason for this behavior is that the unknown and random phase offset affects the transmit signals from all relay antennas in the same way. Consequently, the signals from the relays still combine coherently at the destination antennas. However, in order to decode the data, the destinations have to frequently estimate the equivalent two-hop channel from their respective source terminal.

6.4.3 Phase Synchronization Error

For a two-hop relaying network where communication takes place according to traffic pattern IV, there are four combinations of directions in which the single-hop channel matrices can be measured. The corresponding channel estimation protocols have been introduced and

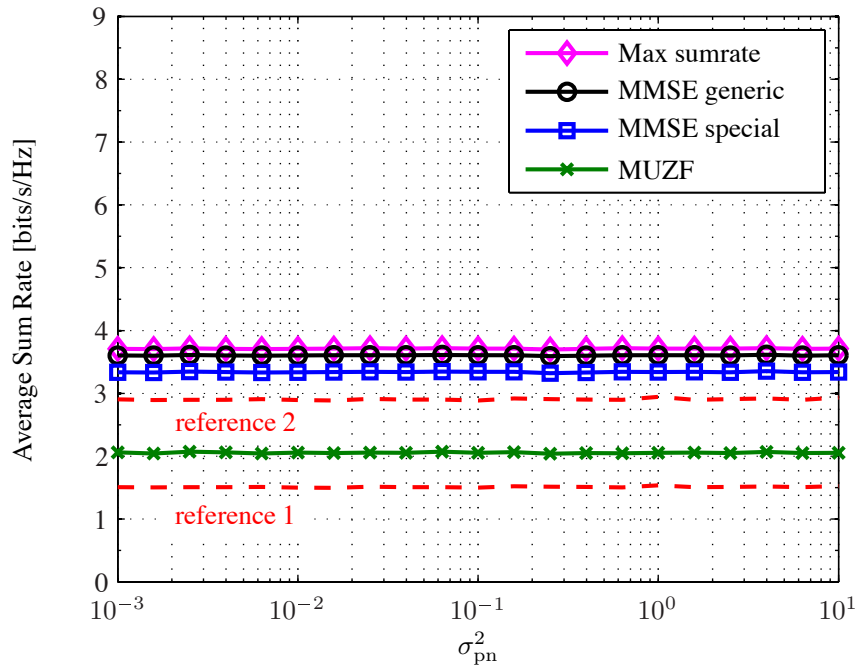


Fig. 6.25: Average sum rate versus phase noise variance for LDAS (single multi-antenna relay), 4 single-antenna source-destination pairs, 4 relay antennas, SNR = 10 dB.

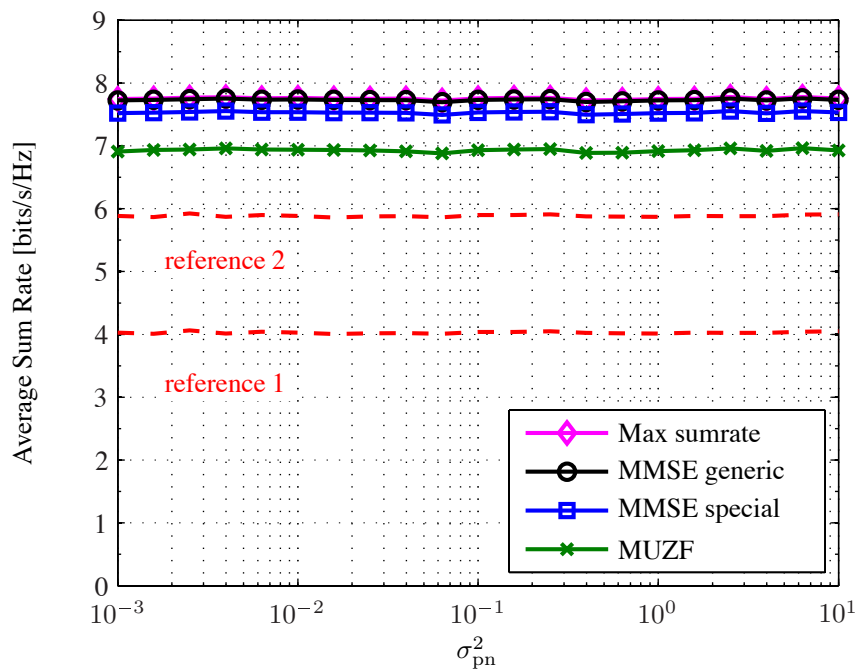


Fig. 6.26: Average sum rate versus phase noise variance for LDAS (single multi-antenna relay), 4 single-antenna source-destination pairs, 4 relay antennas, SNR = 20 dB.

discussed in Chapter 4. It turned out that two of them (namely protocols B1 and B2) require the relays to possess a common carrier phase reference in order to allow for efficient coherent forwarding. This section discusses the impact of inaccurate relay phase synchronization on the average sum rate of MUZF and multiuser MMSE relaying. Since the MSE of the estimated compound channels for protocols B1 and B2 are equal, the results obtained in this section hold for both of them (cf. Section 4.4). Chapter 5 introduced a very simple scheme with which such a phase reference can be established among the relays. To this end, the relays have to multiply their local channel estimates with a phase correction term prior to disseminating them to the other relays. These phase correction terms have to compensate the phase errors due to the LO phases at the relays that are introduced to the local channel estimates (cf. Chapter 5). The total phase synchronization error was found to have two sources: estimation noise (AWGN) and phase noise. Both will be investigated separately in this section.

A system configuration with $N_{SD} = 4$ source-destination pairs and $N_R = 13$ relays forms the basis of the simulation results. All nodes in the network employ a single antenna. This corresponds to a LinRel system with minimum relay configuration. Figs. 6.27 and 6.28 show the average sum rate for the case that there is no phase noise. This means that the phase synchronization error is solely the result of estimation noise. Two cases are depicted in the plots:

- **Solid:** The solid curves represent the case where the phase error is the result of *additive signal noise* leading to an estimation error.
- **Dashed:** For the dashed curves, the *Gaussian approximation* (5.66) was used to directly generate the resulting phase errors.

The SNR in Figs. 6.27 and 6.28 is 10 dB and 20 dB, respectively. It can be observed that all curves saturate quite slowly. Furthermore, the Gaussian model tends to overestimate the phase error due to estimation noise. However, for low and high estimation SNR or low system SNR, the model fits the simulation very well.

Figs. 6.29 and 6.30 finally depict the average sum rate for the case that the phase synchronization error is solely the result of phase noise. The phase error is modeled as a zero-mean Gaussian random variable (cf. (5.68)). The SNR in the figures is 10 dB and 20 dB, respectively. It can be observed that phase noise during data transmission (i.e. the LO phases change during the time between reception and retransmission, cf. (6.23), (6.24)) has a similar effect on the average sum rate as phase noise during phase synchronization (i.e. the LO phases change during the time between phase synchronization and channel estimation²).

²In this case 'channel estimation' refers to the channel estimates that are used to compute the gain factors.

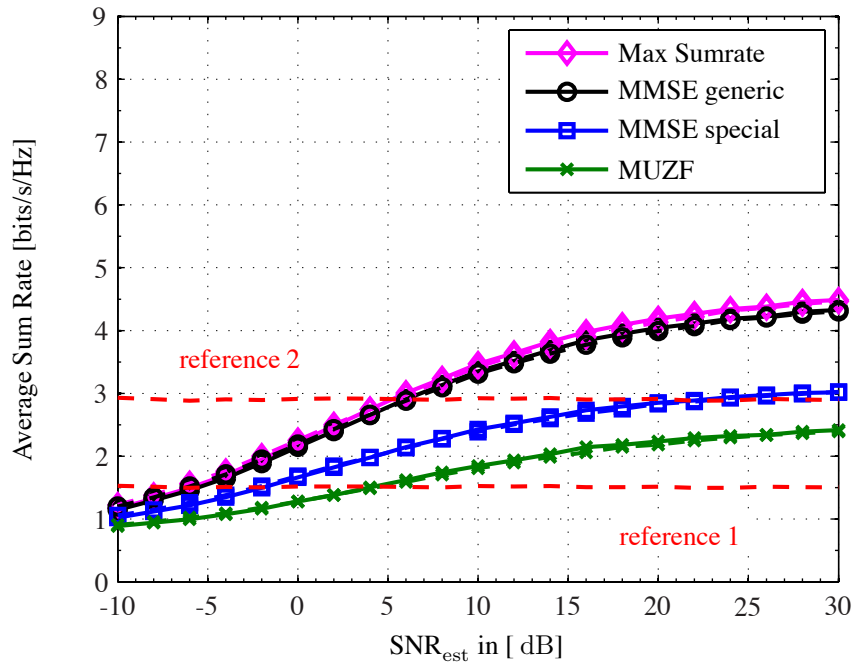


Fig. 6.27: Average sum rate versus estimation SNR for LinRel (single-antenna relays), 4 single-antenna source-destination pairs, 13 relays, and $\text{SNR} = 10$ dB.

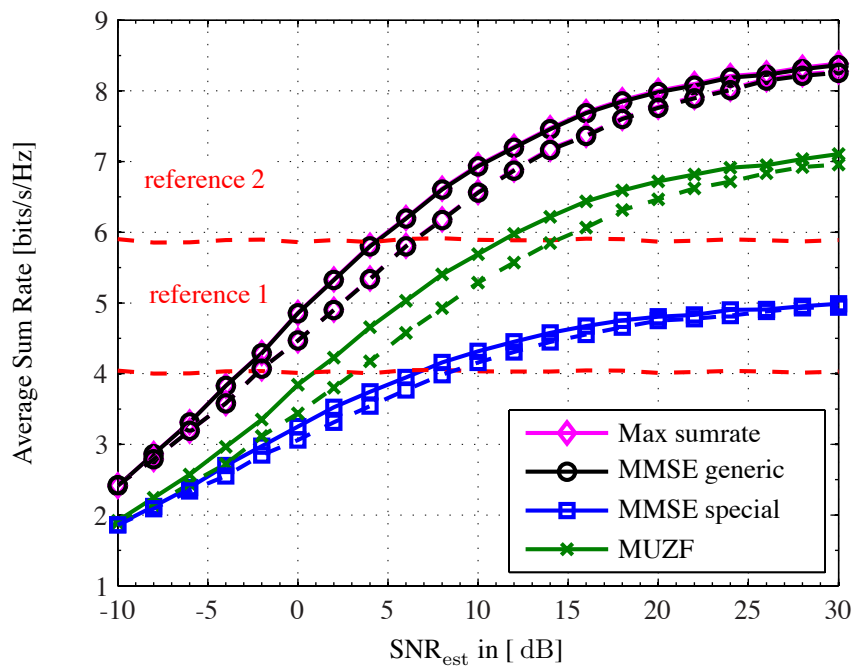


Fig. 6.28: Average sum rate versus estimation SNR for LinRel (single-antenna relays), 4 single-antenna source-destination pairs, 13 relays, and $\text{SNR} = 20$ dB.

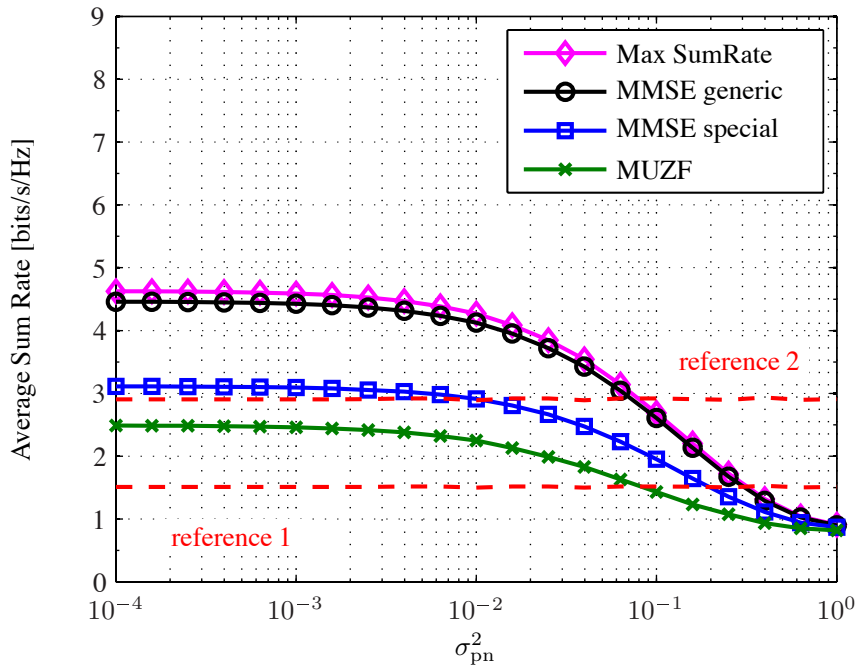


Fig. 6.29: Average sum rate versus phase noise variance for LinRel (single-antenna relays), 4 single-antenna source-destination pairs, 13 relays, and SNR = 10 dB.

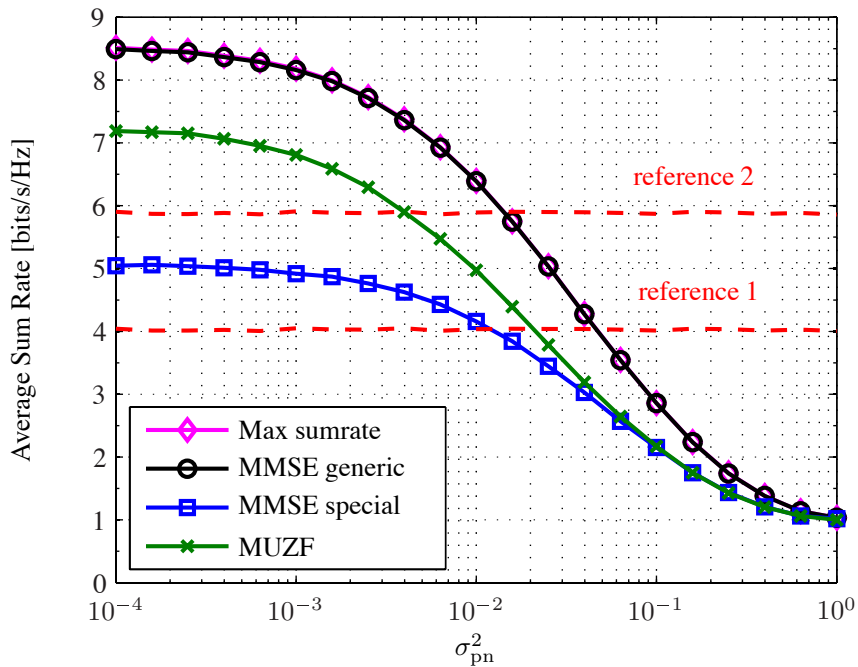


Fig. 6.30: Average sum rate versus phase noise variance for LinRel (single-antenna relays), 4 single-antenna source-destination pairs, 13 relays, and SNR = 20 dB.

Chapter 7

The RACooN Lab

The previous chapters investigated gain allocation schemes, phase synchronization and channel estimation protocols as well as the impact of certain hardware imperfections on the performance of two-hop relaying networks. Simplifying assumptions had to be made for example about the propagation channels and hardware components to make the discussed problems tractable. In order to justify the simplifications and to validate the results some of the theoretical findings have been tested on a practical demonstrator in a real-world scenario.

In this chapter, the results of experiments performed with the 'RACooN Lab', which is a demonstrator for distributed wireless communication networks available at the Wireless Communications Group at ETH Zurich, are presented. It has been used to verify that in some cases - depending on the direction in which the single-hop channels are measured - coherent distributed beamforming is possible without a common phase reference at the relays. This issue was investigated theoretically in Section 4.2, where it was shown that in the absence of phase noise the unknown and random LO phases of the relays do not have an impact on the SINR at the destinations. MUZF relaying was implemented on the RACooN Lab for a network configuration with 2 source-destination pairs and 3 relays. Under idealized assumptions, this gain allocation scheme exhibits a distributed spatial multiplexing gain (cf. Section 6.2). By investigating its interference rejections capabilities on the RACooN Lab it was shown to allow multiple source-destination pairs to communicate concurrently on the same physical channel under real-world conditions and without requiring the relays to possess a common carrier phase reference.

The remainder of this chapter is organized as follows: **Section 7.1** starts with a general description of the RACooN Lab. It explains the basic functionality of the equipment and gives an overview over important system characteristics. Some basics about system operation and features are also provided. In **Section 7.2** some selected system characteristics are explained

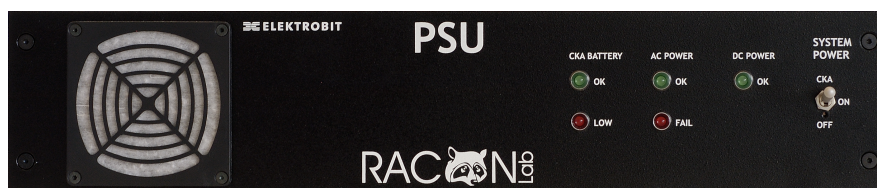


Fig. 7.1: Power supply unit (PSU) front-panel.

in more detail. The system transmit power and a switchable analog power gain are highlighted in **Sections 7.2.1** and **7.2.2**. **Section 7.2.3** discusses the implications of a selection of hardware imperfections on the system operation. The focus lies on an inherent system delay and LO phase noise. Both effects have to be taken into account in order to produce reliable measurement results. **Section 7.3** then presents the result of a channel measurement campaign that has been conducted in a typical laboratory environment. The RACooN Lab is able to measure 'real' MIMO channels, i.e., no antenna switching or time duplexing is necessary. The scenario consisted of 4 receivers and 4 transmitters and represented a network with 2 source-destination pairs (transmitters) and 4 relays (receivers), where all channels are estimated at the relays. Concatenating two point-to-point channels then results in the compound source-destination channel. From the estimated two-hop channel transfer functions, the rms delay spread and coherence bandwidth are computed. This knowledge is then used in **Section 7.4**, where the implementation of MUZF relaying on the RACooN Lab is described. The results show the interference rejection capabilities of MUZF relaying on a real-world demonstrator (i.e., in the presence of hardware imperfections) without a global carrier phase reference.

7.1 General Description

RACooN stands for *Radio Access with Cooperating Nodes* and is a custom-built radio testbed at the Communication Technology Laboratory at ETH Zurich. The RACooN Lab comprises 10 identical single-antenna nodes (RACooN nodes) that consist of three units each:

- **Power Supply Unit:** The power supply unit (PSU) is responsible for the power supply of a single RACooN node. It can be powered either by 230 V AC or 24 V DC. Fig. 7.1 shows a picture of the front-panel of a PSU.
- **Storage Unit:** The storage unit (STU) is responsible for the baseband data processing and operation control. Basically, this is a computer running Linux that controls the operation of a single node. It can be accessed either via Ethernet or directly by plugging

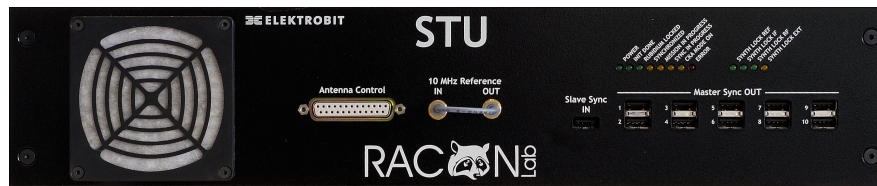


Fig. 7.2: Storage unit (STU) front-panel.



Fig. 7.3: Storage unit (RFU) front-panel.

in a keyboard and monitor. The DACs and ADCs are also located here. Fig. 7.2 shows a picture of the front-panel of a STU.

- **Radio Frequency Unit:** All RF processing is done at the radio frequency unit (RFU). The DACs and ADCs of the STU are directly connected to the RFU. Fig. 7.3 shows a picture of the front-panel of a RFU.

The units can transmit or receive at a carrier frequency of 5.1 GHz to 5.9 GHz with a maximum output power of 25 dBm at 1 dB compression. Individual Rubidium normals running at 10 MHz provide the clock for each unit. All frequencies generated in a RACoon node are derived from this clock. As a consequence, each LO exhibits an individual and unknown phase offset that changes due to phase noise. However, the output of a single clock can be used to supply a reference to all other units. In this way, all LOs can become frequency and phase synchronous.

The baseband sampling rate is 80 MHz leading to a symbol duration of 12.5 ns. The nodes possess a user bandwidth of 34 MHz (30 MHz with equalized phase response). Time slot synchronization has to be performed prior to operation using USB cables of a defined length of 4 m. A set of real-time features furthermore allows for limited signal processing without delay. In this way, every terminal can act as source, relay, or destination node in a distributed wireless network.

Each RACoon node possesses an internal 20GB hard disk memory and a random access memory (RAM) that is able to hold $256 \cdot 2^{13}$ samples in 14 bit resolution. The units are placed on carts to provide mobility (see Fig. 7.4). Self-made short dipole antennas are used during all experiments that will be presented in this work. They have been designed for the required



Fig. 7.4: RACooN nodes on carts for mobility.

frequency range and are mounted on poles at a height of about 1.5 m. Table 7.1 summarizes important characteristics of the RACooN nodes. Further details can be found in the system specification [195,196] or in the documentation [197] with its appendices [198–200]. In the following, *Courier* font will be used to indicate RACooN-specific termini. Table 7.2 gives an overview of the frequently-used expressions.

Item	Value
Operational band	5.1 GHz – 5.9 GHz
Center frequency spacing	1 MHz
Signal bandwidth (baseband)	34 MHz, 30 MHz with equalized phase response
Baseband sampling rate	80 MHz
Burst memory size	$256 \cdot 2^{13} \approx 2 \cdot 10^6$ samples
Receiver noise figure	< 7 dB, includes antenna switch loss
ADC/DAC dynamic range	14 bit
Max. output power	25 dBm (≈ 316 mW) at 1 dB compression
Power supply	230 V AC or 24 V DC

Table 7.1: RACooN characteristics.

Item	Value
Mission	Sum of operation commands for all nodes
Buffer	Block of 2^{13} samples in the RAM
Command	Operation mode of a single node during the execution of a mission; can be transmit, receive, process, or idle.
Time slot	Duration of a single command

Table 7.2: Frequently-used RACooN-specific termini.

7.1.1 Baseband Processing

Baseband processing is done in MATLAB[®]. This comprises the generation of transmit symbols as well as data pre- and post processing. Arbitrary complex-valued samples can be generated that have to be mapped onto 16 bit signed integers in the 2's complement format. By default, the valid baseband amplitude range is from -1 to 1. Since the DACs and ADCs only have 14 bit resolution, an internal conversion between the two formats is performed: All ADC samples are multiplied by a factor of 4. Thus the two least significant bits are always zero. The transmit samples are rounded to 14 bit, so the two least significant bits are used for rounding only.

The system RAM is divided into 255 block (so-called buffers) of 2^{13} samples each. Only bursts of samples that corresponds to an integer number of buffers can be transmitted by the RACooN nodes. The vector of transmit or receive samples thus always has to have a length that is an integer multiple of 2^{13} .

7.1.2 System Operation

Operation of the RACooN Lab is mission-based. A mission basically comprises a chain of commands (specifying for each participating unit what to do and when to do it) and a set of operation parameters. Dedicated .xml files, that need to have a special structure, comprise the complete mission configuration (c.f. [198]). There are altogether six commands:

Transmit: The `transmit` command instructs a node to transmit the samples contained in certain buffers of its RAM.

Load: This command loads a specified file of data samples from the internal hard disk to the RAM.

Receive: A node in receive mode generates complex baseband samples from the current RF input and writes them to a certain range of buffers in the RAM.

Store: The `Store` command copies a specified range of `buffers` from the RAM to the internal hard disk.

Idle: During the `idle` command, the unit waits for a specified time until the next command is executed.

Process: The `process` command is in fact a chain of `Store`, `Idle`, and `Load` commands. A specified range of `buffers` is first stored from the RAM to the internal hard disk. Then a remote MATLAB[®] process is called (via remote procedure call (RPC)) that executes an `m-file` with arbitrary code. The previously stored baseband samples can thus be processed in MATLAB[®] before they are written back to a specified range of `buffers` in the RAM.

The most important parameters defined in the `.xml` files are

- the length of the transmit/receive burst,
- the carrier frequency,
- the analog transmit and receive gain settings (LOW or HIGH, cf. Section 7.2.2),
- how often the `mission` is executed (number of repetitions), and
- the utilization of the real-time features (cf. Section 7.1.3).

An individual `.xml` file is copied to each RACooN node participating in the mission prior to operation. For details on the system operation, see [197,198].

7.1.3 Real-Time Features

The RACooN Lab provides a set of real-time features, that can be utilized without time delay:

(Adaptive) Digital gain control: The current input signal strength can be measured at any point during the execution of a `mission`. A pre-defined table maps the current radio signal strength indicator (RSSI) value to a 16 bit digital gain value within the range of ± 100 . This feature can be used to adapt the signal amplification to the current signal strength or to apply a previously defined gain factor to the signal.

Phase rotation: A sequence of previously defined phase rotations can be applied to the samples prior to transmission.

Add AWGN: White Gaussian noise can be added to the digital baseband data. The noise level is within a range of 0 – 15.9 dB.

The RACooN documentation [197,198] gives a detailed description about the characteristics and usage of the real-time features.

7.2 System Characteristics

In the following, some system characteristics of the RACooN nodes are introduced in detail. Characterizing them was important to understand their impact on the operation of the RACooN Lab. This in turn was crucial for the implementation of MUZF relaying. This section covers the transmit power, the analog gain control (including analog transmit and receive gain), the inherent signal delay, and the LO phase noise and frequency offset.

7.2.1 Transmit Power

The RACooN nodes are specified to have a maximum transmit power of 25 dBm (≈ 316 mW) at 1 dB compression [195]. The output power is determined by the amplitude of the baseband signal (`level`) and the 'analog transmit gain', which is in fact an optional 20 dB attenuator that can be activated in the transmit path of the RFU. The analog transmit gain is said to be `LOW` if the attenuator is switched on (20 dB attenuation) and `HIGH` if it is switched off (no attenuation). In order to measure the transmit power of the nodes for different baseband amplitudes, the output of a RACooN node was connected via a Huber & Suhner Sucoflex¹ cable of length 1.6 m to a power meter. A real-valued sine wave with an amplitude equal to `level` was then transmitted at a carrier frequency of 5.5 GHz.

Analog transmit gain LOW: The first set of measurements was performed for analog transmit gain set to `LOW`, i.e., the 20 dB attenuator is activated. Table 7.3 gives an overview of the measurement configurations and shows the measurement results, i.e., the measured output power, of RACooN nodes 3 and 4 as representatives. The attenuation of the cable of approximately 1 dB is already taken out for the results.

Analog transmit gain HIGH: For the next set of measurements, the analog transmit gain is set to `HIGH`, i.e., the 20 dB attenuator is removed from the analog transmit path. In order to protect the measurement device, an additional external 20 dB attenuator was plugged in-between the RACooN transmit output and the power meter input. Table 7.4 shows the measurement results for all configurations, where the external attenuator and cable attenuation have been taken into account.

Comparison: The measurement results are compared by plotting the values from Tables 7.3 and 7.4 together in Fig. 7.5. Obviously, the maximum transmit power is about 24.2 dBm. In Fig. 7.6, the difference between analog transmit gain `LOW` and `HIGH` is depicted. The

¹Huber & Suhner, Sucoflex 104: Attenuation $\approx 0.6 \frac{\text{dB}}{\text{m}}$ at 5.0 – 6.0 GHz and 25°C.

level1	RACooN 3	RACooN 4	level1	RACooN 3	RACooN 4
0.01	-26, 20 dBm	-25, 25 dBm	0.2	-6, 09 dBm	-5, 56 dBm
0.02	-23, 95 dBm	-22, 89 dBm	0.3	-2, 60 dBm	-2, 09 dBm
0.03	-21, 46 dBm	-20, 62 dBm	0.4	-0, 12 dBm	0.38 dBm
0.04	-19, 40 dBm	-18, 68 dBm	0.5	1, 80 dBm	2, 28 dBm
0.05	-17, 69 dBm	-17, 04 dBm	0.6	3, 35 dBm	3, 83 dBm
0.06	-16, 24 dBm	-15, 62 dBm	0.7	4, 67 dBm	5, 13 dBm
0.07	-14, 99 dBm	-14, 39 dBm	0.8	5, 79 dBm	6, 25 dBm
0.08	-13, 88 dBm	-13, 31 dBm	0.9	6, 78 dBm	7, 23 dBm
0.09	-12, 90 dBm	-12, 34 dBm	1.0	7, 66 dBm	8, 10 dBm
0.1	-12, 01 dBm	-11, 47 dBm			

Table 7.3: Measured output power for analog transmit gain set to LOW.

level1	RACooN 3	RACooN 4	level1	RACooN 3	RACooN 4
0.01	-6, 51 dBm	-5, 30 dBm	0.2	14, 01 dBm	14, 75 dBm
0.02	-3, 76 dBm	-2, 77 dBm	0.3	17, 39 dBm	18, 01 dBm
0.03	-1, 27 dBm	-0, 39 dBm	0.4	19, 64 dBm	20, 12 dBm
0.04	0, 76 dBm	1, 59 dBm	0.5	21, 25 dBm	21, 62 dBm
0.05	2, 48 dBm	3, 22 dBm	0.6	22, 44 dBm	22, 73 dBm
0.06	3, 92 dBm	4, 65 dBm	0.7	23, 38 dBm	23, 58 dBm
0.07	5, 17 dBm	5, 88 dBm	0.8	24, 12 dBm	24, 24 dBm
0.08	6, 27 dBm	6, 96 dBm	0.9	24, 72 dBm	24, 76 dBm
0.09	7, 25 dBm	7, 94 dBm	1.0	25, 19 dBm	25, 18 dBm
0.1	8, 13 dBm	8, 82 dBm			

Table 7.4: Measured output power for analog transmit gain set to HIGH.

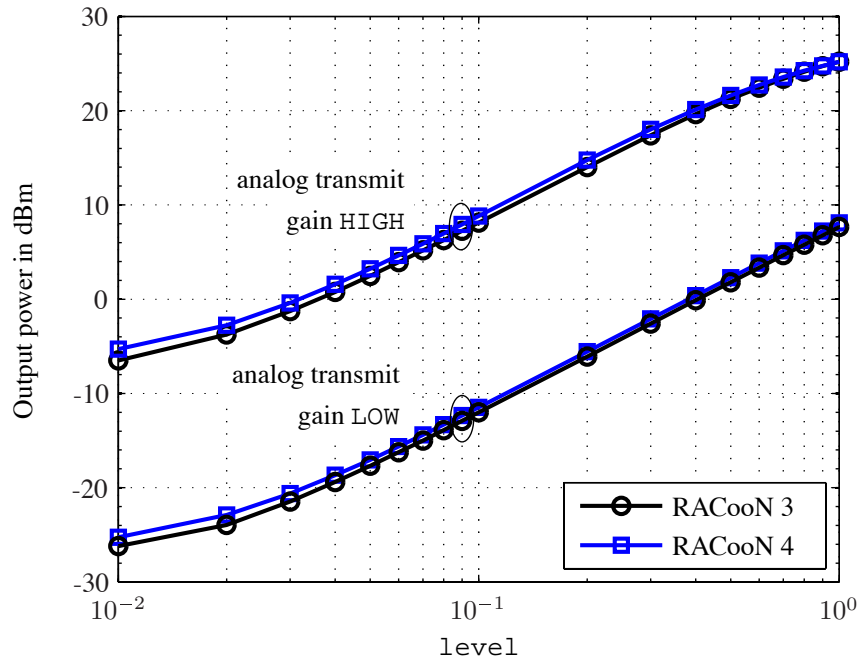


Fig. 7.5: Comparison of the output power for analog transmit gain LOW and HIGH.

	Analog receive gain LOW	Analog receive gain HIGH
Analog transmit gain LOW	30dB	50dB
Analog transmit gain HIGH	50dB	70dB

Table 7.5: Overall analog signal gain.

effective attenuation is about 20 dB for low levels but for values starting from about 0.3 it becomes less.

7.2.2 Analog Gain Control

According to the STU manual [196] the analog signal gains are as follows:

- Analog transmit gain: 0 dB or 20 dB
- Analog receive gain: 30 dB or 50 dB

The absolute gain accuracy is ± 2 dB. In Table 7.5, the overall analog signal gain is shown for the four possible combinations of the analog gain settings.

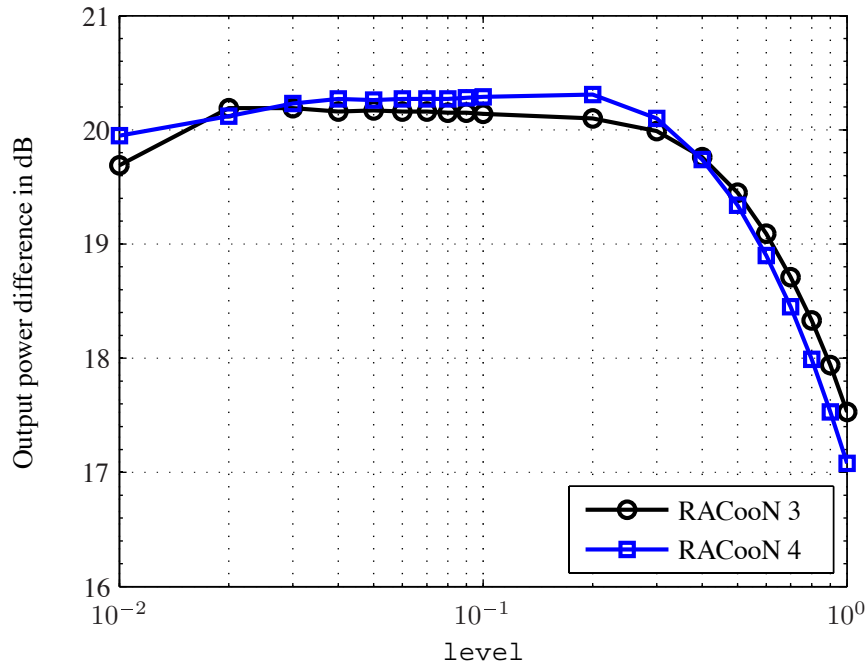


Fig. 7.6: Difference of the output power for analog transmit gain LOW and HIGH.

7.2.3 Imperfections

All practical hardware components exhibit imperfections that have an impact on the system performance. Two of them had to be studied carefully in order to successfully implement the distributed beamforming scheme (MUZF relaying) on the RACooN Lab. They are namely the inherent system delay, i.e., the delay experienced by the signal in the transmit and receive chains of each node, and the LO phase noise. Both of them have to be taken into account when designing the mission that controls the system operation and when analyzing the results.

7.2.3.1 Inherent Delay

The RF transmit and receive chains of the RACooN nodes exhibit an inherent delay. As a result, the first N_{delay} samples of any received symbol vector only contain noise. This fact has to be taken into account when working with the RACooN Lab because inherent system delay is not related to propagation distance. In order to identify N_{delay} , the RF output/input plugs of two RACooN nodes have been connected by two concatenated cables² of length 1 m

²Huber & Suhner, Sucoflex 104: Attenuation $\approx 0.6 \frac{\text{dB}}{\text{m}}$ at 5.0 – 6.0 GHz and 25°C. These cables are the same that are used to connect the antennas to the RF input/output in normal operation mode.

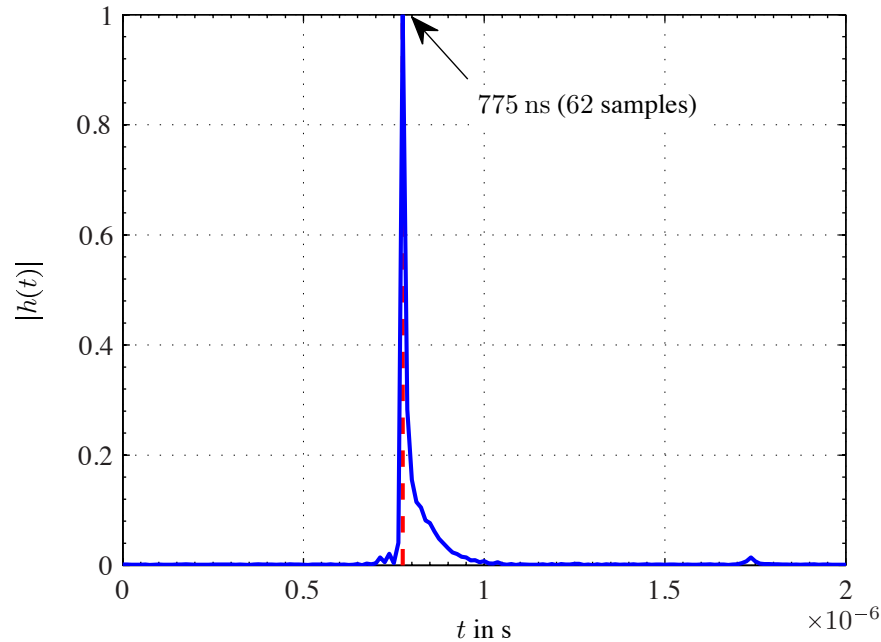


Fig. 7.7: Absolute value of the baseband-to-baseband channel impulse response between RACooN nodes 2 and 8.

each. The setup comprised two cables because in the normal operation mode each RACooN node is connected to its antenna by one cable of length 1 m. The inherent delay can then be determined by measuring the resulting equivalent baseband channel. An additional external 20 dB attenuator is used to protect the hardware of the receiving node.

The source node transmits a concatenation of m-sequences of length 1023 samples each. Periodic correlation at the destination allows to estimate the impulse response of the equivalent baseband channel. Fig. 7.7 shows the normalized result of a measurement between RACooN 2 (acting as source) and RACooN 8 (acting as destination). The position of the main peak corresponds to the joint delay of the RACooN nodes plus two antenna cables. The red dashed line indicates the peak position at 775 ns, which corresponds to a shift of 62 baseband samples. This value has been confirmed by measurements between other RACooN pairs.

Although the delay induced by hardware imperfections can be assumed to be more or less stable, a mismatch in time slot synchronization has an impact on the position of the peak. Since the clocks of the units drift apart with time, this eventually becomes an issue when operating the units without frequent resynchronization. According to the RACooN specification [197], the clocks drift apart by less than eight samples per hour. This corresponds to a

	RACooN 3	RACooN 6
Time slot 1	transmit	receive

Table 7.6: Calibration mission command setup.

time difference of 100 ns. When performing a measurement campaign, the time slot synchronization thus has to be repeated periodically in order to prevent errors. Furthermore, when performing channel measurements, the absolute delay of the paths is obviously error-prone and results have to be analyzed with great care.

7.2.3.2 LO Phase Noise and Frequency Offset

The LOs of all RACooN nodes exhibit a frequency offset and phase noise. As a result, they oscillate at different frequencies and their phases change randomly over time. In order to assess the phase noise severity and the frequency difference, the changes between the LO phases of two nodes are monitored by transmitting a known training sequence and observing the phase difference at the receiver. A constant frequency difference between the LOs leads to a drift of the observed phase difference while phase noise occurs as random fluctuation. In order to measure the phase difference between the LOs of two RACooN nodes, their antenna input/output is connected via a Huber & Suhner Sucoflex³ cable to provide a static propagation channel. An additional external 30 dB attenuator is used to protect the hardware of the receiving unit.

Calibration measurement: First, a calibration measurement is performed to identify the characteristics of background interference and hardware effects. To this end, the destination node is in receive mode while the source is silent. The very simple `mission` setup is shown in Table 7.6. Exemplarily, RACooN nodes 3 and 6 are used. However, similar results have been observed for other nodes. In Fig. 7.8, the magnitude of the frequency spectrum $R(f)$ of the received complex baseband signal $r(t)$ is plotted. Obviously, the signal contains a large direct current (DC) component (which is actually cut off in the plot; $|R(0)| = 2740$) and several peaks at integer multiples of about 246 kHz which are hardware effects.

Phase and frequency offset measurement: In order to observe the frequency and phase difference, the complex baseband signal

$$s(t) = \sin(2\pi f_s t) + j \cdot \cos(2\pi f_s t) \quad (7.1)$$

³Huber & Suhner, Sucoflex 104: Attenuation $\approx 0.6 \frac{\text{dB}}{\text{m}}$ at 5.0 – 6.0 GHz and 25°C.

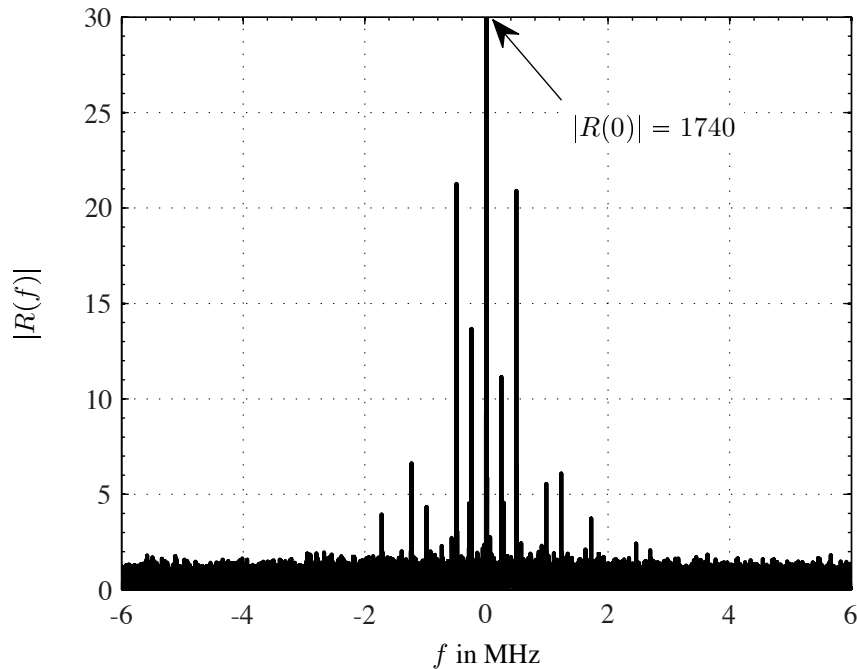


Fig. 7.8: Magnitude of the frequency spectrum $R(f)$ of the received signal $r(t)$ when the source is idle.

	RACooN 3	RACooN 6
Time slot 1	transmit	receive
Time slot 2	transmit	receive

Table 7.7: Measurement mission command setup.

is transmitted, where $f_s = 5$ MHz. In this way, the distorting effects present at lower frequencies can be filtered out (cf. Fig. 7.8). Table 7.7 shows the mission setup. RACooN 3 transmits in both time slots while RACooN 6 receives. For the time being, the received data of the first time slot is ignored. It will be shown later that a characteristic phase response, which is due to the RACooN hardware, dominates and thus perturbs this data. In Fig. 7.9, the spectrum of the received signal is plotted in order to investigate the frequency offset of the units and the phase processes due to phase noise. As reference, the spectrum of the transmitted signal is also displayed.

Frequency offset: A close zoom at $f = -5$ MHz is displayed in Fig. 7.10. The sequence that has been used to produce the results is a complex-valued sine-wave of 100 buffers length, corresponding to 819 200 samples or 10.2ms. Consequently, the frequency resolution is $\frac{1}{10.2 \text{ ms}} = 97.66 \text{ Hz}$. Since the peak of the received signal is still clearly at $f = -5$ MHz, the

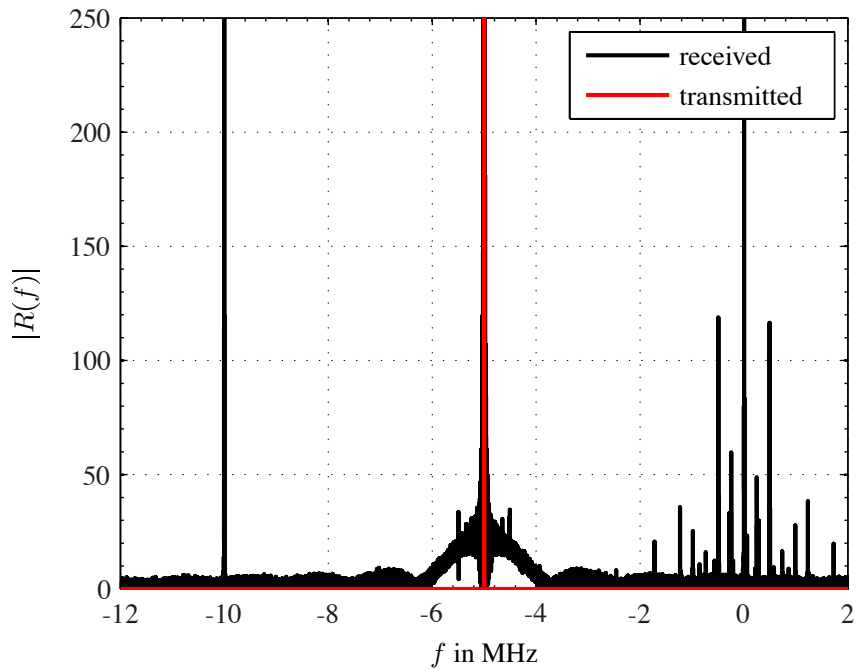


Fig. 7.9: Magnitude of the frequency spectrum of the received signal $r(t)$.

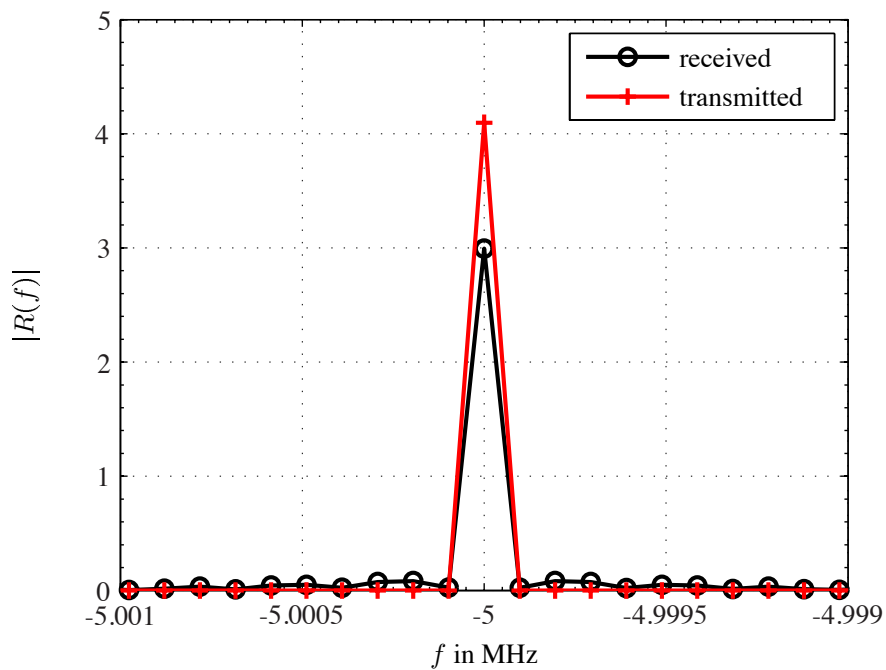


Fig. 7.10: Close zoom of the received and transmitted signal spectrum at $f = -5$ MHz.

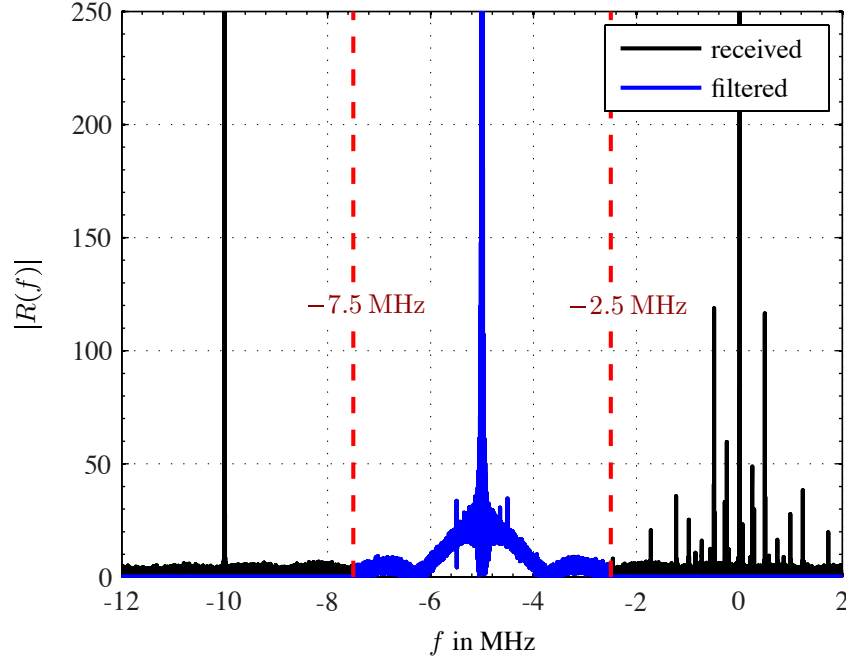


Fig. 7.11: Spectrum of the received signal.

frequency offset between the two nodes must be much less than the resolution of 97.66 Hz. During the time of one `buffer`, i.e. $102.4 \mu\text{s}$, the phase rotation of an oscillation with a frequency of 97.66 Hz is $\Delta\phi_z = 2\pi \cdot 97.66 \text{ Hz} \cdot 102.4 \mu\text{s} = 0.0628 \text{ rad} \hat{=} 3.6^\circ$. Later, it can be seen by analyzing measured realizations of the phase fluctuations that the impact of a frequency offset Δf is very small compared to the impact of phase noise.

Phase noise: In order to isolate the components of the received signal that are due to phase noise, it has to be filtered. Since the baseband samples are available in MATLAB[®], an arbitrary digital filter can be realized to get rid of the harmonics, the DC component, and all components due to hardware effects, e.g., the peaks at integer multiples of 246 kHz. In the present case, an ideal discrete-time rectangular filter $g(f)$ was used, where

$$g(f) = \begin{cases} 1 & , \quad -7500 \text{ kHz} \leq f \leq -2500 \text{ kHz} \\ 0 & , \quad \text{else} \end{cases} \quad (7.2)$$

The filtered signal is shown in Fig. 7.11. In Fig. 7.12, a realization of the unfiltered and filtered phase process is plotted for the length of 10 `buffers`. Finally, Fig. 7.13 depicts several realizations of the phase process that have been measured a couple of second apart from each other. It can be seen that the LO phase difference between the LOs of both nodes

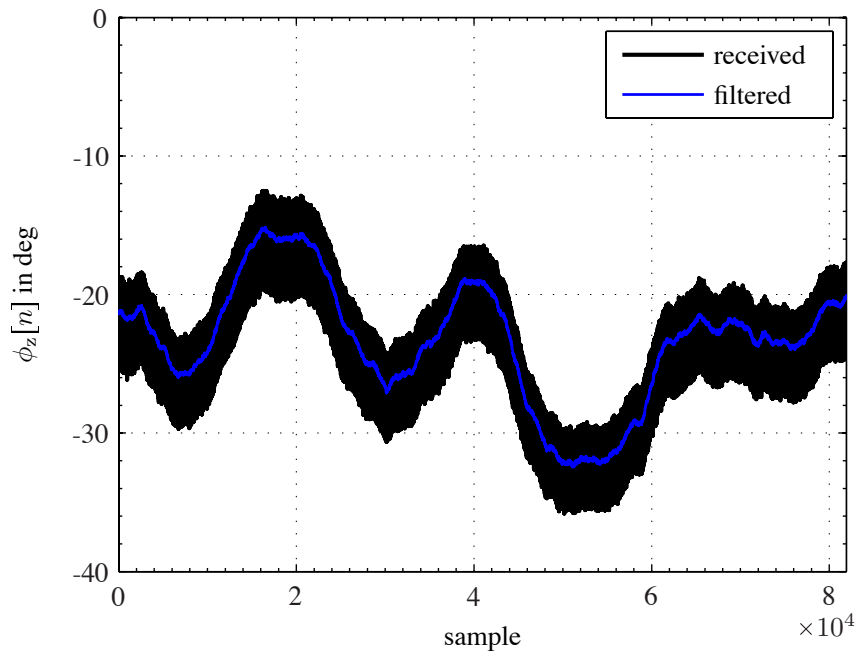


Fig. 7.12: Unfiltered and filtered phase process.

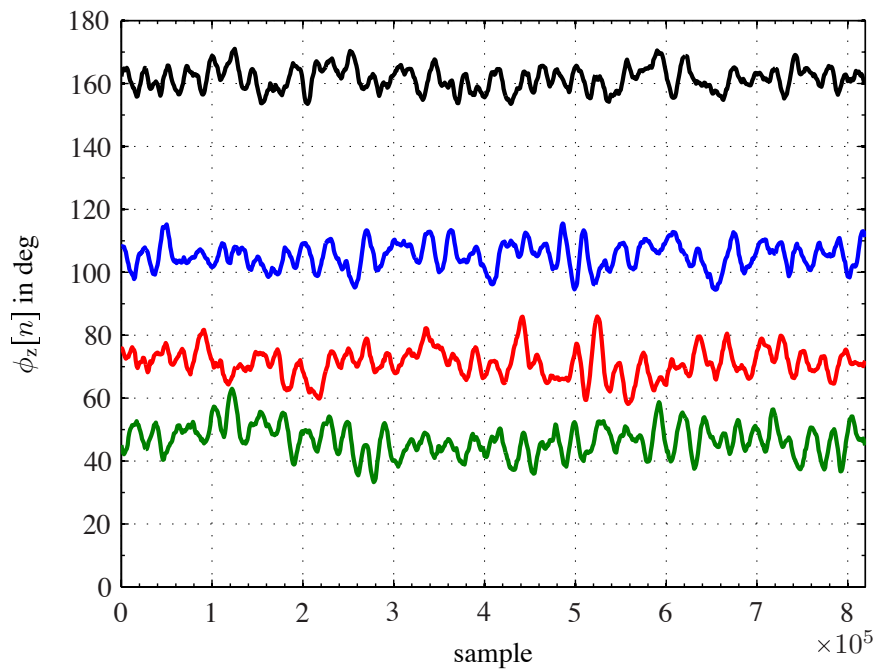


Fig. 7.13: Filtered phase processes for transmission of 100 buffers.

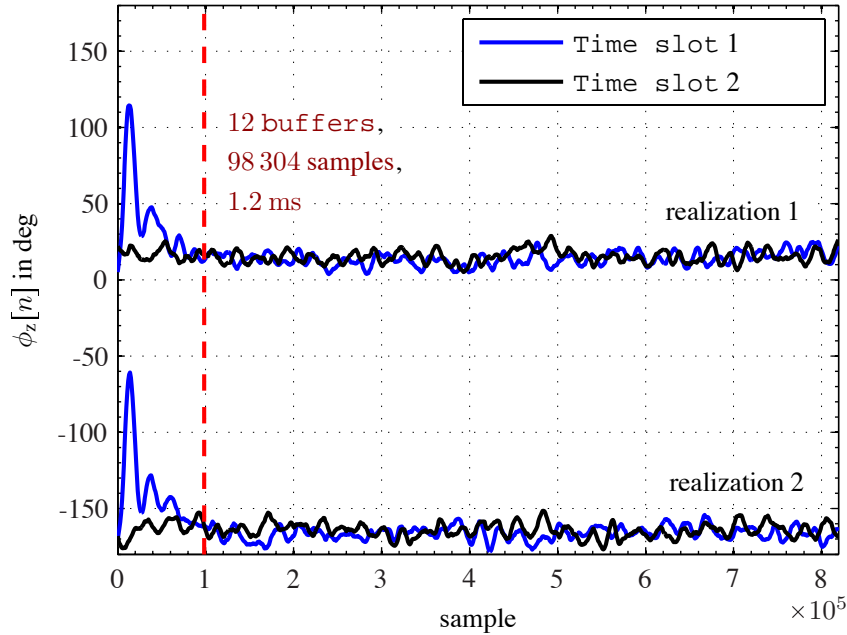


Fig. 7.14: Two realizations of the filtered phase process for transmission of 100 buffers observed in time slots 1 and 2.

varies around a mean value that is approximately constant for each of the realizations. A drift due to frequency offset Δf is not observable in the depicted time interval.

The simple mission setup that was used to investigate frequency offset and phase noise characteristics of the RACooN nodes was shown in Table 7.7. For the analysis in Section 7.2.3.2, the data that was received in the first time slot was omitted because it exhibits a characteristic phase response due to switching between transmit and receive mode. This phase response is discussed in the following. Using the same procedure as described before, the time-varying LO phase difference between RACooN nodes 3 and 6 is extracted. Both units switch from receive mode into transmit mode (rx/tx switching) and from transmit mode into receive mode (tx/rx switching), respectively, at the start of each measurement.

Fig. 7.14 shows two realizations of the phase process observed in the first and second time slot, respectively. Obviously, the phase process in the time slot following the switching from receive/transmit to transmit/receive command exhibits a characteristic phase response for the first symbols. The influence of the switching has died out after about 12 buffers, which corresponds to a time of 1.2 ms. This behavior has been confirmed in several measurements for different RACooN pairs. For future work with

the RACooN Lab this means that after switching between `receive` and `transmit` mode (and actually also after an `idle` command), the first 12 buffers of data are affected by the characteristic phase response of the nodes.

7.3 Channel Measurements

The RACooN Lab has been used to perform channel measurements at a carrier frequency of $f_c = 5.25$ GHz in two typical office environments. The goal was to characterize the rms delay spread and coherence bandwidth of the propagation environment for a two-hop ad hoc network. These characteristic values will be used in Section 7.4 to determine the required guard interval for a demonstrator using OFDM modulation. Eight RACooN nodes were positioned to represent a scenario with two source-destination pairs and four relays. In order to estimate all channels simultaneously, four nodes transmitted training sequences to the other four nodes. The training sequences were orthogonalized by a small shift in frequency. In this way, the source-relay and destination-relay channels could be estimated at the same time. Note, however, that they have been sampled at slightly different frequency bins. It was important to estimate the channels at the same time to prevent LO phase noise from introducing artificial channel rank [201].

7.3.1 Measurement Scenario

The measurements have been performed in a large laboratory room⁴ at ETH, where two different topologies represented two typical scenarios:

- **Open office:** The open office scenario describes a situation where the source-destination pairs are a couple of meters apart, e.g., in different working spaces (see Fig. 7.15).
- **Meeting room:** For the meeting room scenario all source-destination pairs are close to each other, e.g., on the same table (see Fig. 7.16).

The nodes transmitting the training sequences represented the source-destination pairs (RACooN nodes 5, 6, 7, and 8 in the middle of the room), while the receiving nodes represented the relays (RACooN nodes 1, 2, 3, and 4 in the four corners of the room). The room where the measurements have been performed is an electronic laboratory with lots of metallic equipment on long tables (long, light gray rectangles in Figs. 7.15 and 7.16), chairs

⁴room ETZ D61

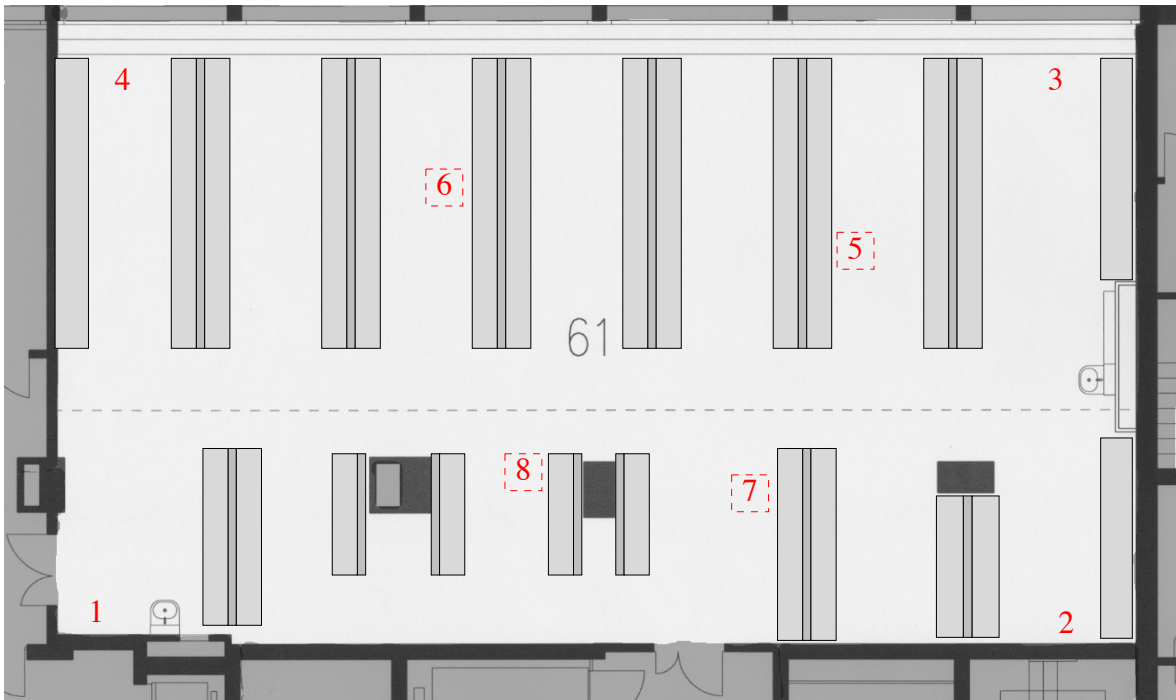


Fig. 7.15: Open office scenario.

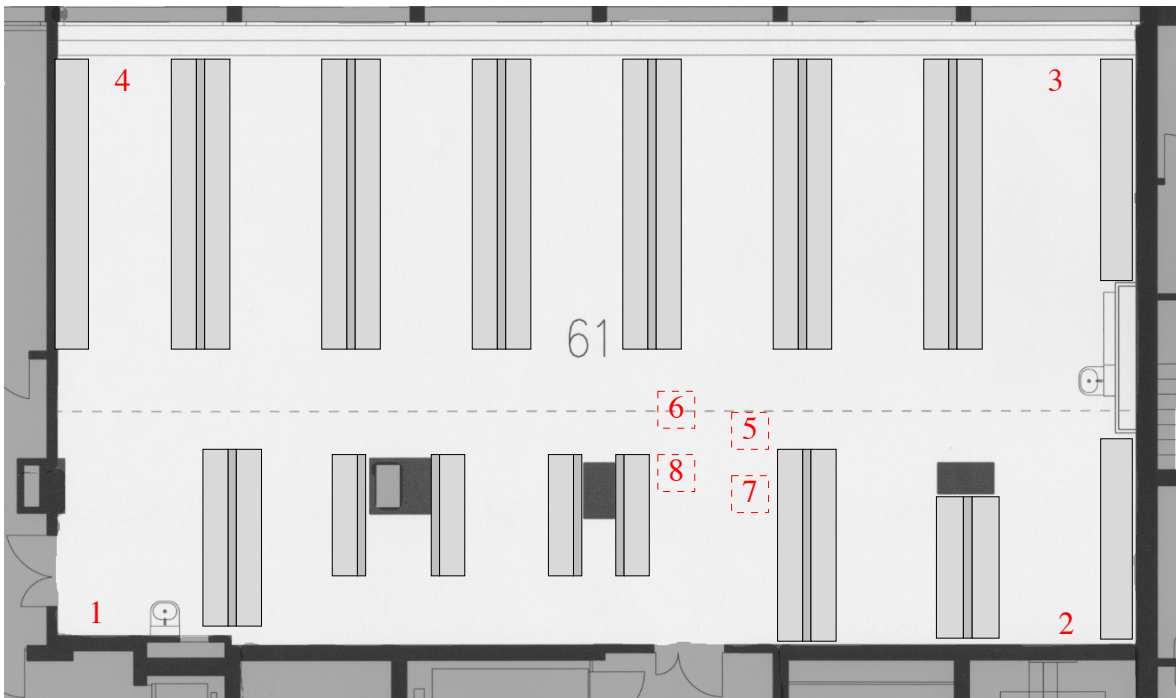


Fig. 7.16: Meeting room scenario.

and cupboards (dark rectangles) that acted as scatterers. It has a size of 12.3 m × 22.3 m. One side of the room has large windows ('upper side'), the other sides consist of concrete. The RACooN nodes were placed on carts for mobility and their antennas were mounted at a height of about 1.5 m. The training sequences were transmitted about every second, delivering snapshots of the channels. During the whole measurement of 1000 snapshots, the antennas of the transmitting nodes were moved at a slow speed and in an arbitrary fashion within a square of size 0.6 m × 0.6 m (indicated by the dashed squares in Figs. 7.15 and 7.16).

7.3.2 RACooN Setup

In order to prevent phase noise from introducing artificial rank to the channel [201], all coefficients have to be measured simultaneously. Let $p[n]$ denote an m-sequence of length $2^N - 1$, where $N \in \mathbb{N}^+$. To estimate the channels, each transmitting node used a training sequence based on $p[n]$ that has been made mutually orthogonal to all other sequences by a shift in frequency domain. The training sequence used by node k , $k \in \{1, \dots, K\}$ was a concatenation of M times the sequence

$$s_k[n] = p[n] \cdot \exp\left(j2\pi(k-1)\left\lfloor\frac{M}{K}\right\rfloor n\right), \quad n \in \{1, \dots, 2^N - 1\}, \quad (7.3)$$

where K is the number of transmitting nodes and $M \geq K$. For the measurements, four transmitters and a concatenation of 128 times $s_k[n]$ of length 127 have been used. The baseband frequency spectrum of the training sequences is shown up to a frequency of 2 MHz in Fig. 7.17. The spectrum of $s_1[n]$, $s_2[n]$, $s_3[n]$, and $s_4[n]$ are plotted in black, blue, red, and green, respectively. Since all $s_k[n]$ have a length of $T = 127 \cdot 12.5 \text{ ns} = 1.5875 \mu\text{s}$, the spacing between adjacent frequency bins is 0.63 MHz. The sequences were shifted in frequency by $\frac{1}{4} \cdot 0.63 \text{ MHz} = 0.16 \text{ MHz}$ in order to make them orthogonal.

At each receiving node (RACooN nodes 1–4), the channel coefficients have been estimated by extracting the respective frequency bins from the received sequence. The baseband frequency spectrum of a received sequence at RACooN node 1 is plotted as an example in Fig. 7.18. The spectrum of the transmit sequences is shown as reference in the background of the figure. There is a large DC component in the received signal, which has also been observed in the measurements of Section 7.2.3.2. The estimated channel coefficients from all four transmitting nodes can be obtained by extracting the respective frequency bins. Since the amplitude of the first frequency bin of all transmitted m-sequences (at 0 MHz, 0.16 MHz, 0.32 MHz, and 0.48 MHz) is only 128 compared to $128\sqrt{128}$ for all other frequency bins,

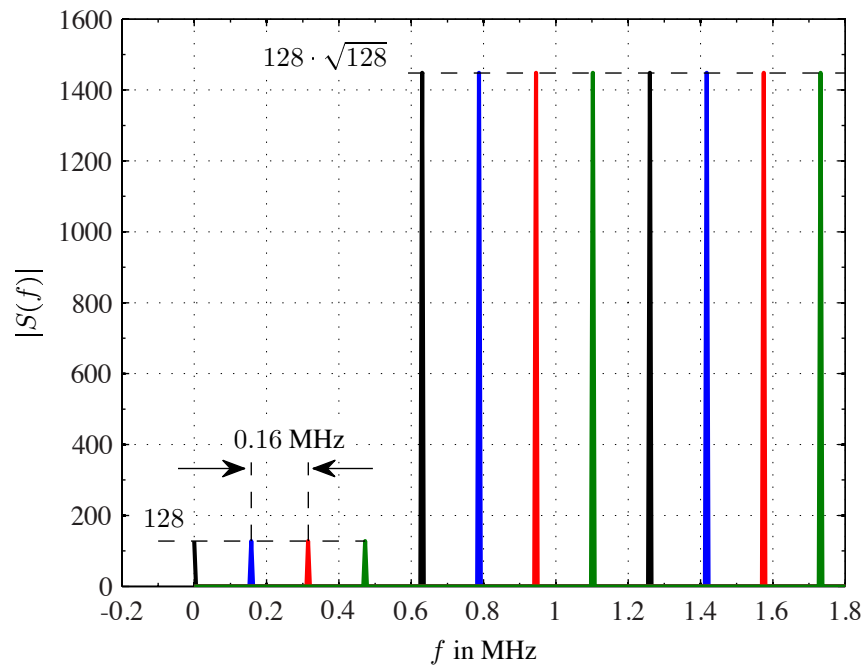


Fig. 7.17: Baseband frequency spectrum of the four training sequences.

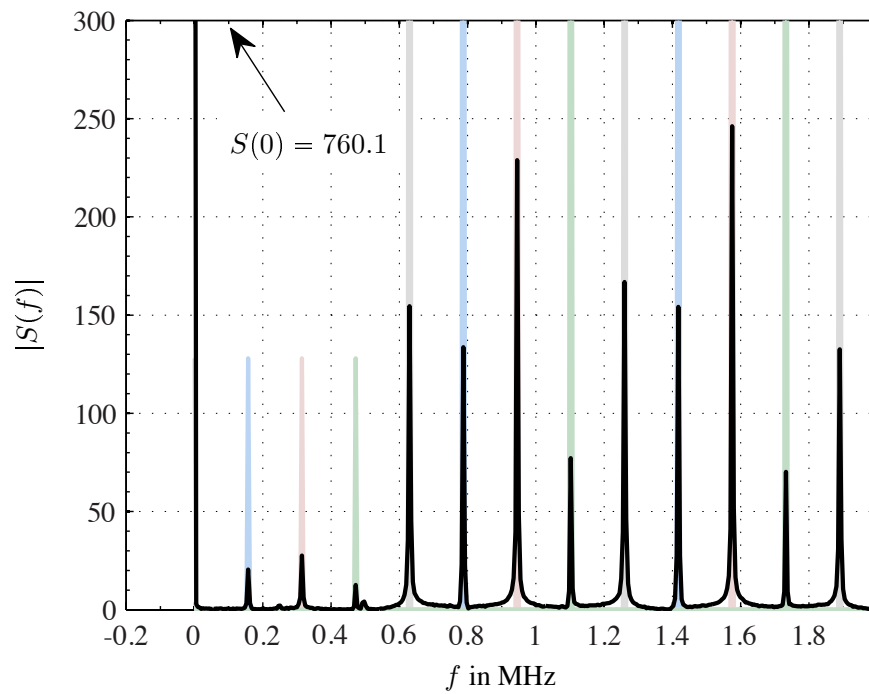


Fig. 7.18: Baseband frequency spectrum of the received signal at RACoon 1.

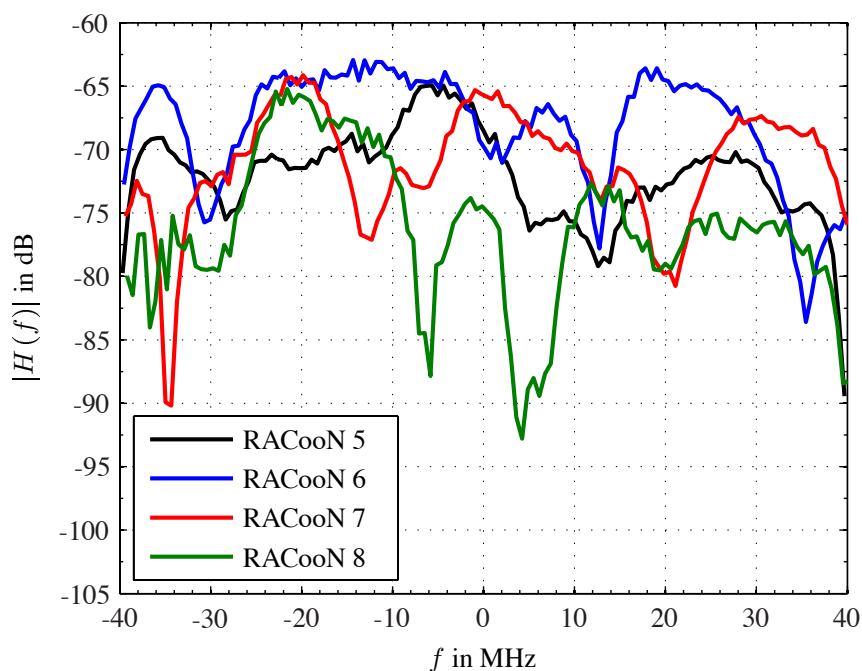


Fig. 7.19: Example of estimated transfer functions from RACooN nodes 5–8 at RACooN 1 in the open office scenario.

the estimation is much less reliable there. The respective estimates are therefore dropped and replaced by the average between the second and last estimated channel coefficient. This makes sense because the sampled channel transfer function is periodic in frequency.

7.3.3 Measurement Results

In this section, the results of the channel measurement campaign are presented. Fig. 7.19 shows an example of the estimated channel transfer functions from all transmitting nodes, i.e., RACooNs 5–8, to RACooN 1 in the open office scenario. In the following, the rms delay spread and coherence bandwidth are estimated from the measurement results. They characterize the time dispersion and frequency selectivity, respectively, of the propagation environment [202]:

- **rms delay spread:** The rms delay spread is a parameter that characterizes the time dispersive behavior of the propagation environment only if the channel is at least wide-sense stationary (WSS). This means that the autocorrelation function of the channel impulse response merely depends on the time difference and not on the absolute time.
- **Coherence bandwidth:** The coherence bandwidth is defined as the frequency sep-

aration at which the frequency correlation function has dropped to a certain value K . This definition only makes sense if the correlation depends merely on the frequency separation and not the absolute frequency itself. This is the case if scattering components arriving with different propagation delays are uncorrelated (uncorrelated scattering (US)).

Stochastic time-variant linear channel models with wide-sense stationary impulse responses and uncorrelated scattering components are called wide-sense stationary uncorrelated scattering (WSSUS) channel models [203]. A comprehensive treatment of the WSSUS channel models can be found for example in [202,204]).

In Section 7.3.3.1 the *rms delay spread* is estimated from the measured channel impulse responses assuming that they are wide-sense stationary. In order to get an estimate of the rms delay spread of two-hop relaying channels, it is assumed that RACooN nodes 5–8 represent sources and destinations and RACooN nodes 1–4 relays in a two-hop relaying configuration. The first-hop and second-hop channels are then concatenated to compute the rms delay spread for the two-hop scenario.

The *coherence bandwidth* of the single-hop and two-hop channels is investigated in Section 7.3.3.2. Since the correlation between the channel taps is unknown, a coherence bandwidth is computed for every frequency bin from its respective frequency correlation function. The smallest coherence bandwidth of all subchannels within the specified RACooN user bandwidth is then defined as the coherence bandwidth of that channel.

7.3.3.1 rms Delay Spread

The *average delay* D_{avg} and the *rms delay spread* D_{spread} are two important characteristic quantities that describe the time-dispersive behavior of a propagation channel. For the sake of completeness, they are shortly revisited in this section (see e.g. [204]). Let $h(\tau, t)$ denote the response of the time-variant channel at time t to a delta impulse that was transmitted at $t - \tau$ (channel impulse response). The average delay is the first central moment of the *delay power spectral density* $S_{\tau\tau}(\tau)$ (also known as *power delay profile*). It determines the average power of scattering components arriving at propagation delay τ and is given by

$$D_{\text{avg}} = \frac{\int_{-\infty}^{\infty} \tau S_{\tau\tau}(\tau) d\tau}{\int_{-\infty}^{\infty} S_{\tau\tau}(\tau) d\tau}, \quad (7.4)$$

where the delay power spectral density $S_{\tau\tau}(\tau)$ is

$$S_{\tau\tau}(\tau) = E_t [h^*(\tau, t)h(\tau, t)]. \quad (7.5)$$

The rms delay spread is defined as the square root of the second central moment of $S_{\tau\tau}(\tau)$, i.e.,

$$D_{\text{spread}} = \sqrt{\frac{\int_{-\infty}^{\infty} (\tau - D_{\text{avg}})^2 S_{\tau\tau}(\tau) d\tau}{\int_{-\infty}^{\infty} S_{\tau\tau}(\tau) d\tau}}. \quad (7.6)$$

For channels that are not stationary at least in the wide sense, the delay power spectral density changes over time t . The average delay and rms delay spread thus also become time-dependent. It is, however, assumed that this is not the case for the present measurements.

In order to estimate D_{avg} and D_{spread} for all links, the delay power spectral density has to be computed from the measured channel impulse responses $\hat{h}_q(\tau)$. It is then given by

$$\hat{S}_{\tau\tau}(\tau) = \frac{1}{Q} \sum_{q=1}^Q \hat{h}_q^*(\tau) \hat{h}_q(\tau), \quad (7.7)$$

where $Q = 1000$ is the number of channel estimates and $\hat{h}_q(\tau)$ the q th estimated channel impulse response. Fig. 7.20 shows a typical measured delay power spectral density $\hat{S}_{\tau\tau}(\tau)$ for the channel between RACooN nodes 5 and 3 in the open office scenario. Further examples can be found in Appendix A.10.1, Fig. A.2. The absolute delay τ depends on the propagation delay, the inherent system delay (see Section 7.2.3.1), and an unknown error that results from a time slot synchronization mismatch. Consequently, the absolute delays of the paths are not reliably estimated. However, this has no impact on the rms delay spread because it does not depend on the absolute delays. For the computation of the delay power spectral density from the channel estimates it was assumed that the clock synchronization mismatch remains constant during a measurement cycle of 1000 channel impulse responses.

There are characteristic peaks that appear more or less dominant in the noise floors of Figs. A.2(a) and A.2(b). This leads to the assumption that some hardware effects are responsible for them. To verify this claim, the average power delay profiles for different links are investigated. Fig. 7.21 shows several measured power delay profiles for the links between all transmitter-receiver pairs. The peaks in each figure are aligned by a cyclic shift to better visualize the characteristic shape of the noise floor. Since the transmitting node is the same for all curves in a figure, it is sensible to assume that the observed characteristic peaks are

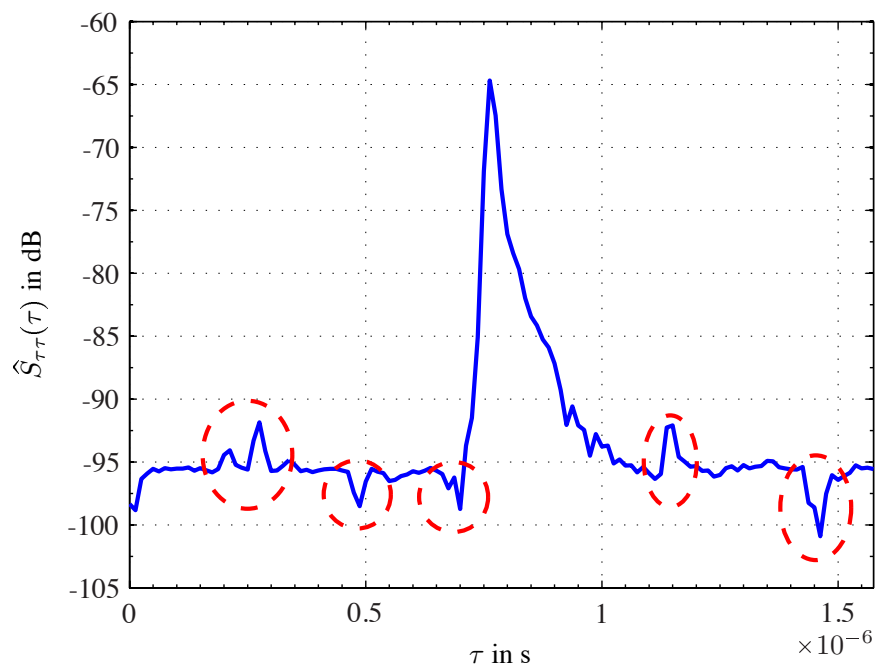


Fig. 7.20: Measured delay power spectral density for the channel between RACooN 5 and 3 in the open office scenario. The noise floor exhibits a characteristic shape (indicated by the red, dashed circles).

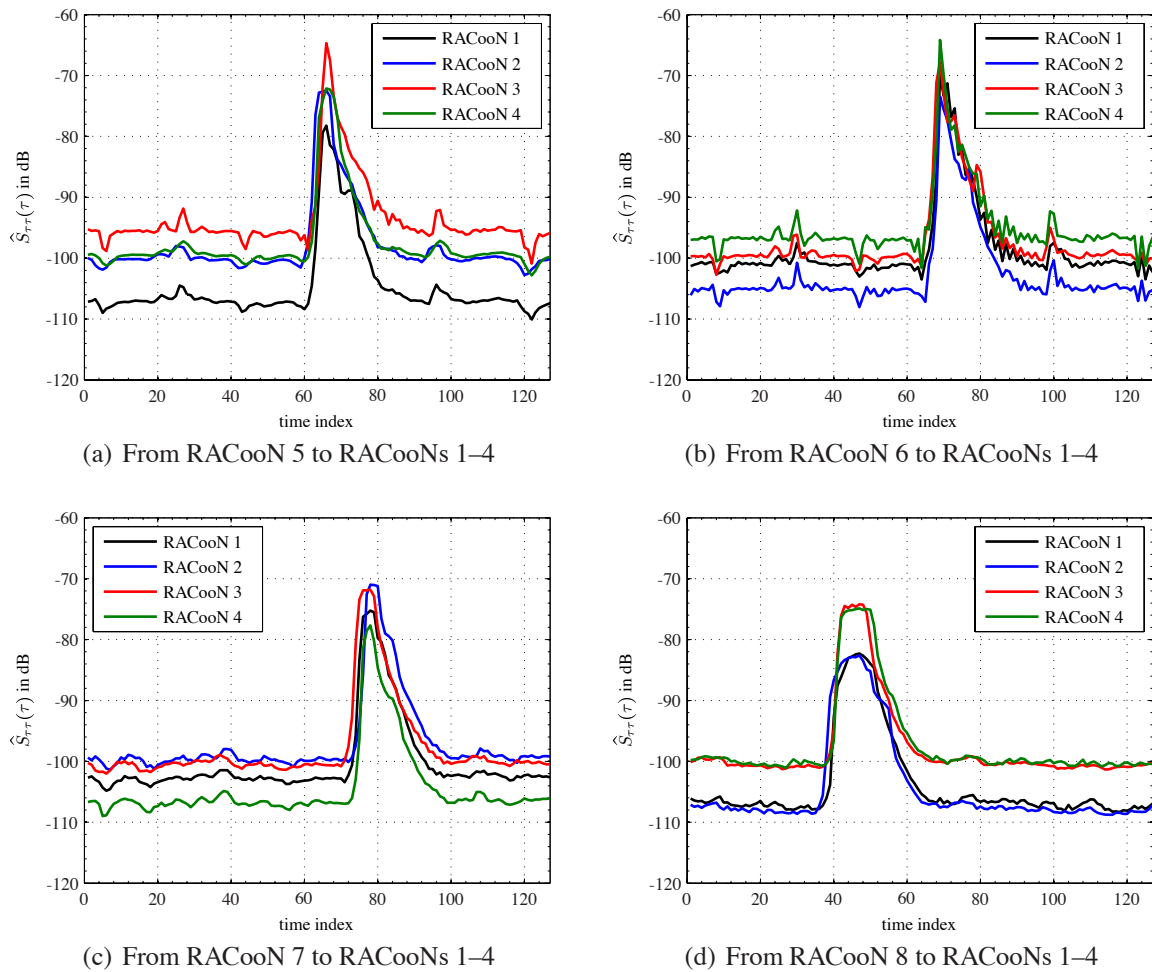


Fig. 7.21: Measured delay power spectral densities in the open office scenario. The peaks of the impulse responses are aligned by a cyclic shift in each figure.

due to a hardware effect in the transmit chain of the RACooN nodes.

In order to estimate D_{spread} , all relevant paths in the measured impulse responses have to be identified. To this end a threshold, below which all samples are regarded as noise, is defined. A simple, heuristic approach is used to find this threshold:

1. The estimated absolute delay is partially due to the inherent system delay and the synchronization mismatch between the nodes. This means that the first couple of samples in $\hat{S}_{\tau\tau}(\tau)$ consist only of noise.
2. The position of the main peak in the measured impulse responses is different for each link. The number of noise samples before the main peak is consequently not known beforehand. In order not to accidentally consider relevant signal paths as noise, all samples only up to half the delay of the highest peak are considered as noise.
3. The threshold is then defined as 25% above the maximum squared magnitude of the noise samples in each impulse response. This is a heuristic value that has no physical meaning but it turns out to deliver good results. In fact, the estimated delay spread is quite insensitive to changes of the noise threshold.

Fig. 7.22 depicts the same measured delay power spectral density as in Fig. 7.20. The calculated noise threshold is shown by the dashed, red line and the identified relevant taps are indicated in blue. Again, more examples can be found in Appendix A.10.1, Fig. A.3. The channel taps not corresponding to a relevant path, i.e., all samples below the noise threshold, are set to zero before the average delay and rms delay spread are computed. Table 7.8 shows the results for the single-hop links between RACooN nodes 5–8 and 1–4 in the open office and the meeting room scenario, respectively. A simple color-coding visualizes the results. 'The more blue' the number, the smaller the value, and 'the more red', the larger it is. The results seem to be quite reasonable when compared to literature. Measurements around 5 GHz in a similar environment have shown estimated rms delay spreads of about 10 ns to 50 ns (e.g., [205] locations C and D, [206], [207] business properties, and [208]).

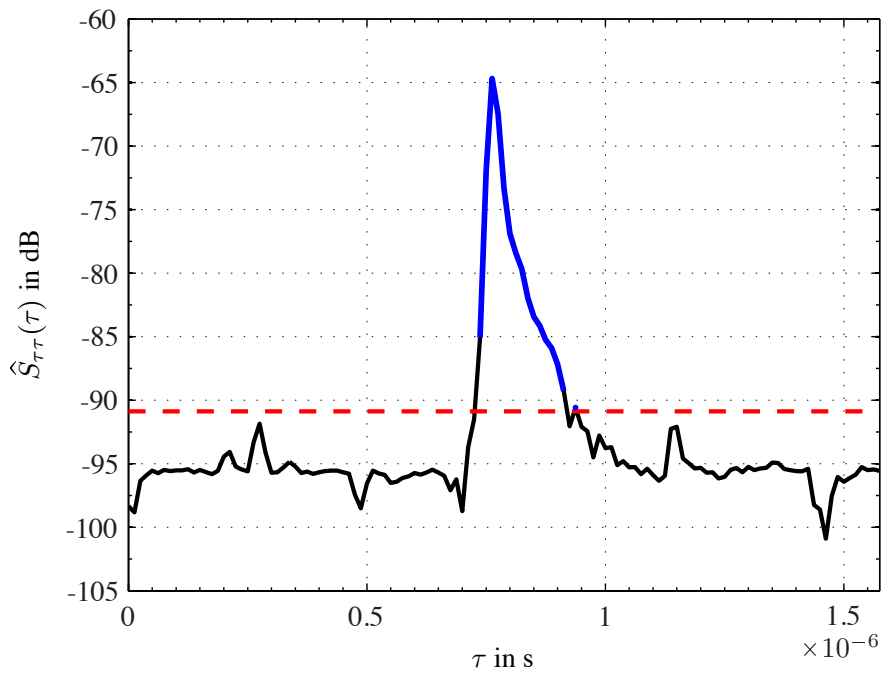


Fig. 7.22: Measured delay power spectral density for the channel between RACooN 5 and 3 in the open office scenario. All samples below the threshold indicated by the red dashed line are regarded as noise.

Open office scenario

RACooN #	5	6	7	8
1	30.0 ns	25.1 ns	30.4 ns	43.2 ns
2	26.5 ns	28.5 ns	28.6 ns	48.0 ns
3	23.2 ns	31.4 ns	27.9 ns	35.3 ns
4	23.7 ns	21.4 ns	29.6 ns	40.4 ns

Meeting room scenario

RACooN #	5	6	7	8
1	29.4 ns	30.6 ns	31.0 ns	46.3 ns
2	26.4 ns	23.8 ns	28.2 ns	43.5 ns
3	20.6 ns	25.1 ns	26.5 ns	38.7 ns
4	21.7 ns	22.2 ns	30.2 ns	43.4 ns

Table 7.8: Estimated rms delay spread for all single-hop links in the open office and meeting room scenario.

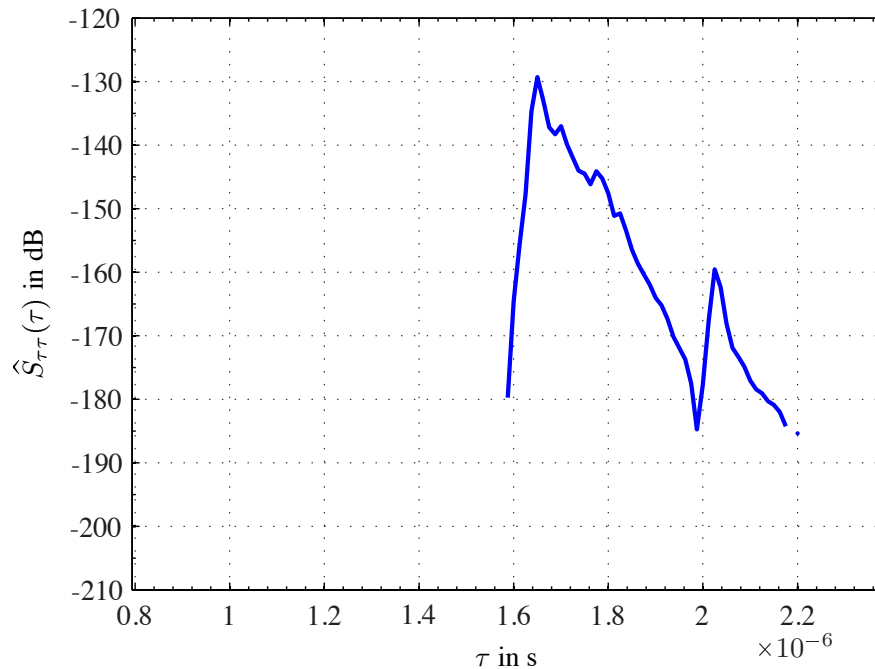


Fig. 7.23: Measured delay power spectral densities for the two-hop channel from RACooN 5 to 6 via 3 in the open office scenario. Only the relevant paths identified in the single-hop impulse responses are taken into account.

Now, a two-hop relaying scenario is considered. RACooN nodes 5–8 represent the sources and destinations and RACooN nodes 1–4 the relays. The equivalent source–destination channels are generated from the respective estimated single-hop impulse responses as follows:

1. Having already identified the relevant paths for all 16 single-hop links from the estimated delay power spectral densities, all taps not belonging to a relevant path are set to zero in every estimated channel.
2. To obtain the impulse response of a two-hop link, the relevant taps of the measured impulse responses of two single-hop links are convolved.
3. Averaging over all realizations delivers the estimated delay power spectral density of the equivalent two-hop channels.

Fig. 7.23 shows a typical example of the resulting estimated delay power spectral density of a two-hop link in the open office scenario. More examples can be found in Appendix A.10.1, Fig. A.4. Since only the previously identified relevant paths of the single-hop links have been considered, no noise floor exists in the plots. The range of time on the abscissa in Fig. 7.23 is the same as in Fig. 7.22, namely $127 \cdot 12.5 \text{ ns} \approx 1.6 \mu\text{s}$. This makes it possible to compare the delay power spectral densities by inspection. In Table 7.9, the computed rms delay spreads

Open office scenario				
RACooN #	5	6	7	8
5 → 3 →	34.0 ns	38.2 ns	33.6 ns	44.3 ns
6 → 4 →	31.6 ns	31.1 ns	35.2 ns	45.8 ns
7 → 2 →	35.6 ns	40.8 ns	46.0 ns	47.3 ns
8 → 1 →	56.0 ns	47.2 ns	44.3 ns	75.5 ns

Meeting room scenario				
RACooN #	5	6	7	8
5 → 3 →	29.9 ns	30.8 ns	30.7 ns	46.1 ns
6 → 4 →	30.4 ns	32.5 ns	36.3 ns	48.7 ns
7 → 2 →	35.4 ns	37.1 ns	45.0 ns	41.6 ns
8 → 1 →	59.0 ns	54.1 ns	46.4 ns	81.4 ns

Table 7.9: rms delay spread estimated for two-hop links in the open office and meeting room scenario. The rms delay spread for the channel from source k to destination m via relay l is given in row $\mathbf{k} \rightarrow \mathbf{l} \rightarrow$ and column \mathbf{m} .

for some of the possible two-hop links are given. The same color-coding as in Table 7.8 indicates large values in red and small values in blue. As expected, the values are generally larger, especially for the non-line-of-sight (NLoS) links.

7.3.3.2 Coherence Bandwidth

Multipath propagation leads to frequency-selective fading. Consequently, the rms delay spread, being a measure of the number and strength of multiple paths, is directly linked to the correlation of the frequency bins. If all scattering components with different propagation delays are uncorrelated (uncorrelated scattering, US), the *frequency correlation function* $r_{\tau\tau}(\Delta f)$ and *delay power spectral density* $S_{\tau\tau}(\tau)$ form a Fourier transformation pair [202]:

$$r_{\tau\tau}(\Delta f) = \int_{-\infty}^{\infty} S_{\tau\tau}(\tau) e^{-j2\pi\Delta f\tau} d\tau \quad (7.8)$$

The frequency correlation function characterizes the similarity of the time-variant transfer functions as a function of the frequency separation Δf . The coherence bandwidth B_K is defined as the frequency separation $|\Delta f|$ at which the frequency correlation function $|r_{\tau\tau}(\Delta f)|$ has reduced to a certain value K . Frequently-used values for K are 0.9, 0.7 or 0.5 (e.g. [202, 204, 209]).

If the scattering components are correlated (which they are for the two-hop channels), the frequency correlation function not only depends on the frequency separation, but also on the absolute frequency. The coherence bandwidth is in this case not readily defined. Figs. 7.24 and 7.25 show typical examples of estimated frequency correlation functions at $f = -20.32$ MHz of a single-hop and two-hop link, respectively. The points where the correlation has dropped to 0.9, i.e. $|r_{\tau\tau}(\Delta f)| = 0.9$, are indicated by the small red circle in each figure. More examples can be found in Appendix A.10.2, Figs. A.5 and A.6. Linear interpolation between adjacent samples was used to increase the frequency resolution.

Figs. 7.26 and 7.27 show the coherence bandwidths for $K = 0.9$ for each subchannel of the same links as in Figs. 7.24 and 7.25. More examples can be found in Appendix A.10.2, Figs. A.7 and A.8. In order to avoid border effects as far as possible, positive frequency shifts, i.e., $\Delta f \geq 0$, were considered for $f \leq 0$ and negative frequency shifts, i.e. $\Delta f \leq 0$, for $f > 0$. It can be seen that the points around $f = 0$ and the borders of the frequency range still exhibit some characteristic shape. Avoiding these, the overall (wideband) coherence bandwidth is chosen to be the minimum coherence bandwidth in the band from -30 MHz to -10 MHz and 10 MHz to 30 MHz. Tables 7.10 and 7.11 summarize the results for the single-hop and two-hop links, respectively. Small coherence bandwidths are colored red and large ones blue.

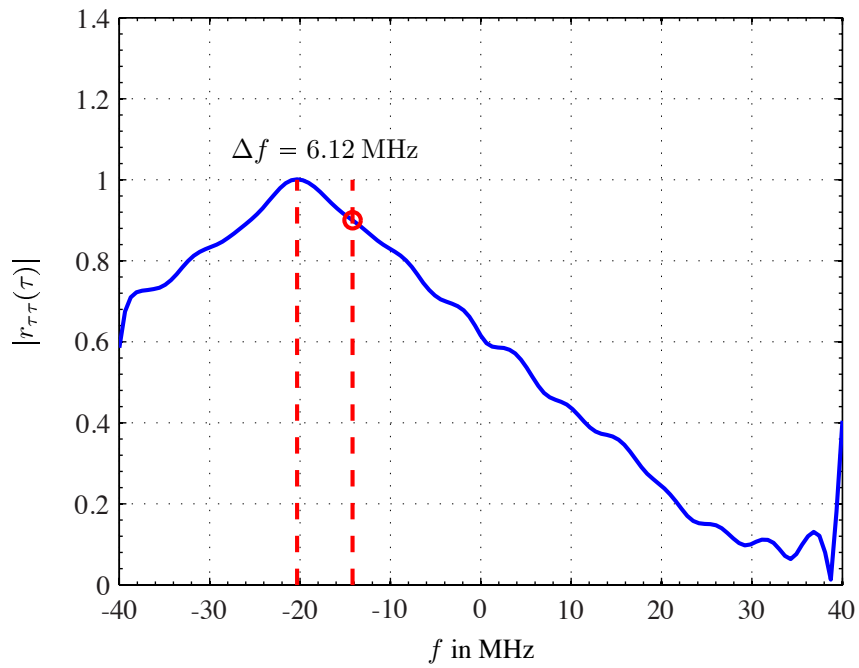


Fig. 7.24: Estimated frequency correlation function at $f = -20.32$ MHz in the open office scenario for the single-hop link between RACooN 5 and 3.

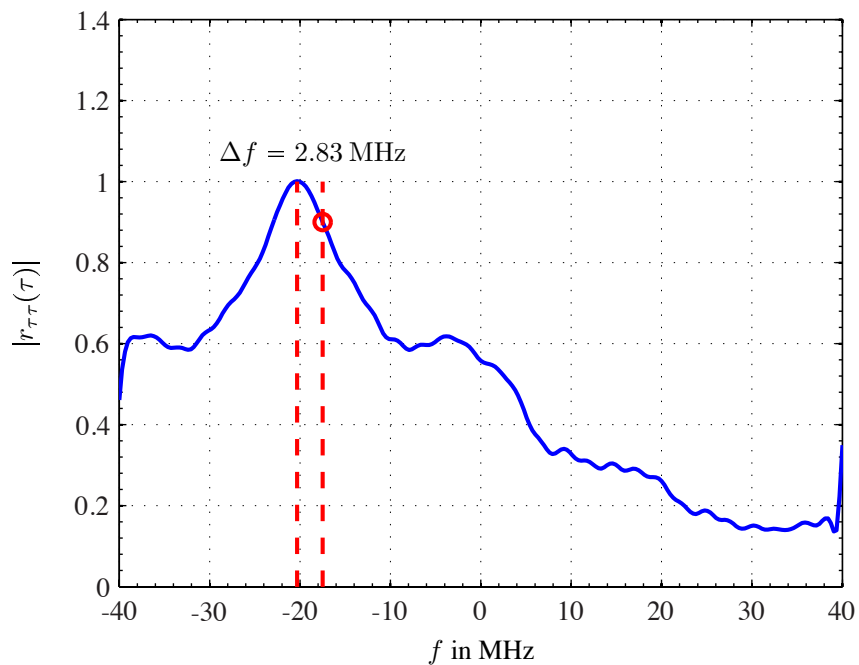


Fig. 7.25: Estimated frequency correlation function at $f = -20.32$ MHz in the open office scenario for the two-hop link from RACooN 5 to 6 via 3.

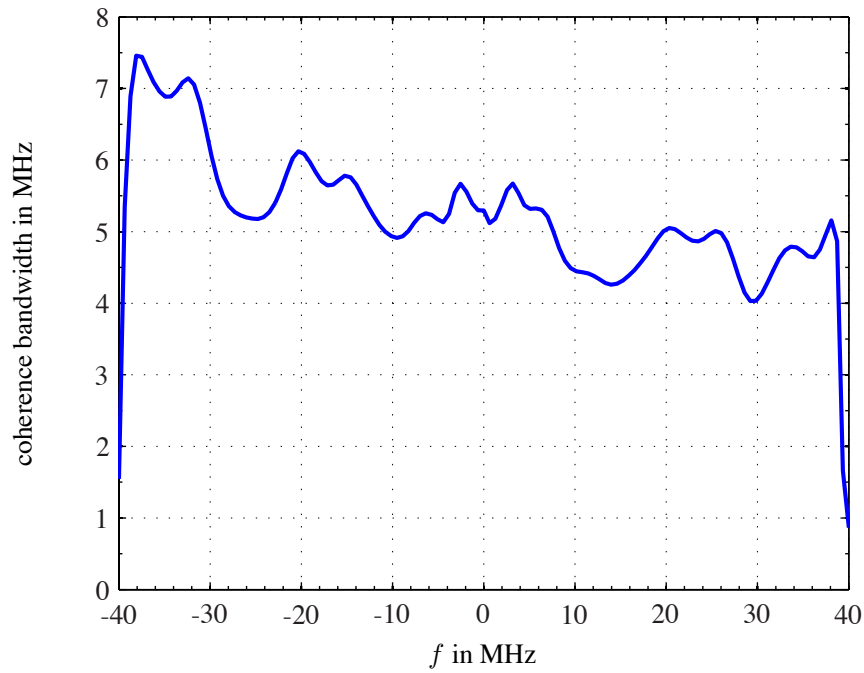


Fig. 7.26: Estimated coherence bandwidth for each subchannel of the single-hop link between RACoon 5 and 3 and $K = 0.9$ in the open office scenario.

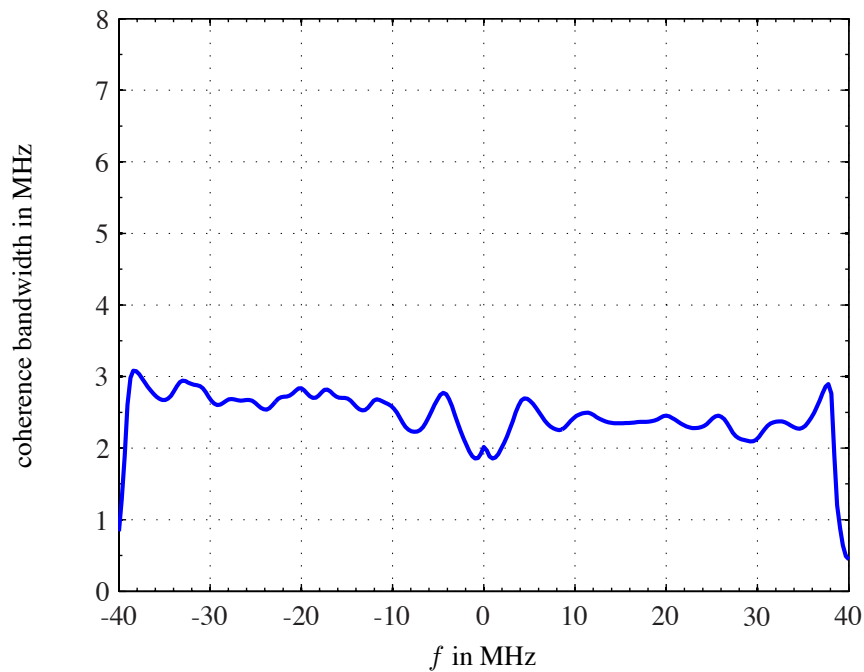


Fig. 7.27: Estimated coherence bandwidth for each subchannel of the two-hop link from RACoon 5 to 6 via 3 and $K = 0.9$ in the open office scenario.

Open office scenario

RACooN #	5	6	7	8
1	2.50 MHz	3.29 MHz	2.44 MHz	1.71 MHz
2	3.15 MHz	2.88 MHz	2.92 MHz	1.47 MHz
3	4.03 MHz	2.77 MHz	3.20 MHz	2.10 MHz
4	3.41 MHz	4.24 MHz	2.50 MHz	1.84 MHz

Meeting room scenario

RACooN #	5	6	7	8
1	2.55 MHz	2.50 MHz	2.37 MHz	1.54 MHz
2	3.00 MHz	3.30 MHz	3.09 MHz	1.72 MHz
3	4.66 MHz	3.49 MHz	2.34 MHz	1.93 MHz
4	3.81 MHz	4.43 MHz	2.54 MHz	1.70 MHz

Table 7.10: Estimated wideband coherence bandwidth for single-hop links with $K = 0.9$ in the open office and meeting room scenario.

Open office scenario

RACooN #	5	6	7	8
5 → 3 →	2.36 MHz	2.09 MHz	2.70 MHz	1.73 MHz
6 → 4 →	2.47 MHz	2.38 MHz	2.00 MHz	1.63 MHz
7 → 2 →	2.35 MHz	1.95 MHz	1.60 MHz	1.58 MHz
8 → 1 →	2.35 MHz	1.95 MHz	1.60 MHz	1.58 MHz

Meeting room scenario

RACooN #	5	6	7	8
5 → 3 →	1.34 MHz	1.63 MHz	1.73 MHz	0.94 MHz
6 → 4 →	2.69 MHz	2.69 MHz	3.11 MHz	1.61 MHz
7 → 2 →	2.63 MHz	2.46 MHz	2.20 MHz	1.55 MHz
8 → 1 →	1.25 MHz	1.35 MHz	1.72 MHz	0.85 MHz

Table 7.11: Estimated wideband coherence bandwidth for two-hop links with $K = 0.9$ in the open office and meeting room scenario. The coherence bandwidth for the channel from source k to destination m via relay l is given in row $\mathbf{k} \rightarrow \mathbf{l} \rightarrow$ and column \mathbf{m} .

7.4 RACooN Demonstrator

The RACooN Lab was used as a demonstrator for coherent MUZF relaying as described in Sections 6.2. A LinRel system configuration with single-antenna nodes, where the relays do not share their received data, was built. The real-time features `digital gain control` and `phase rotation` are used to realize a complex scalar relay gain factor for AF relaying. A global phase reference is not required, so all LOs run independently.

7.4.1 System Setup

The demonstrator comprises two source-destination pairs and three relays. This corresponds to the minimum relay configuration for MUZF relaying with single-antenna relays. Altogether, seven of the ten available RACooN nodes are used. The measurements have been performed in a laboratory room⁵ located in the basement of a university building at ETH Zurich. Fig. 7.28 shows a map of the room and the measurement topology. The walls consist of concrete and a row of windows is located in the 'lower' wall of the figure. Electronic equipment is placed on the tables. During the measurements no one was in the room to guarantee a static propagation environment. This was necessary because a single measurement cycle took a couple of seconds during which the estimated channel had to be constant. Each RACooN node is placed on its own cart, except for nodes 3 and 6. They are stacked on top of each other on the same cart. RACooN nodes 4, 5, and 7 acted as relays during all measurements. The other nodes acted either as source or destination, altogether forming two source-destination pairs.

7.4.2 Transmission Cycle

The `mission` that was used to demonstrate the relaying schemes comprised two phases:

1. *Training phase*: All relevant channel coefficients are measured in the training phase using `m`-sequences. The estimates are generated from the raw received data on a local desktop computer. Therefore, global CSI is available at all nodes without having to disseminate it. The gain matrix is then computed from the channel estimates and inserted into the `mission` configuration files.
2. *Evaluation phase*: The performance of the gain allocation scheme on the demonstrator is evaluated.

⁵room ETF A105

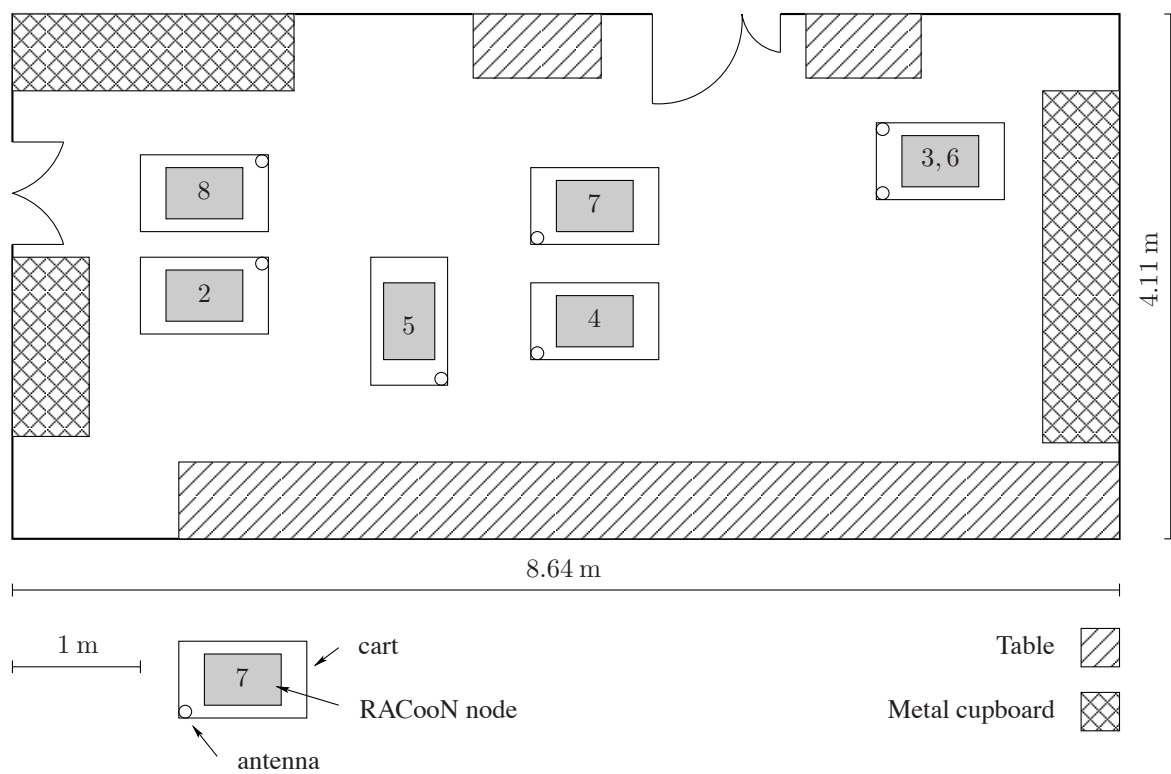


Fig. 7.28: Measurement environment and topology. The numbers 3–8 indicate the numbering of the RACooN nodes. RACooNs 3 and 6 are stacked on top of each other on the same cart.

In the following, both phases are described in detail:

Training phase: The training phase comprises all steps necessary to compute the relay gain matrix.

1. Both source nodes transmit mutually orthogonal training sequences to all relay nodes. Afterwards, all relay nodes transmit mutually orthogonal training sequences to all destination nodes. Knowing the transmitted training sequences, relays and destinations can estimate the first-hop and second-hop channels, respectively. The gain matrix has to be computed for a single frequency-flat subchannel out of the whole 80 MHz bandwidth because the real-time features of the RACooN nodes (phase rotation and amplification) can only realize a scalar gain factor.
2. The smallest coherence bandwidth for the environment considered in Section 7.3.3.2 was about 0.85 MHz for $K = 0.9$ (see Table 7.11). In order to operate on a subchannel that is approximately frequency-flat, the subchannel bandwidth is chosen to be $\frac{80 \text{ MHz}}{511} \approx 0.16 \text{ MHz}$. This corresponds to roughly 20 percent of the 0.9 correlation coherence bandwidth. The length of the m-sequences used for channel estimation has in this case to be equal to 511 samples.
3. Cyclically shifted m-sequences with a length of 511 samples are used as training sequences. A shift of 255 samples means that the maximum observable path delay can be $255 \cdot 12.5 \text{ ns} = 3.1875 \mu\text{s}$. This corresponds to a propagation distance of about $3.1875 \mu\text{s} \cdot 3 \cdot 10^8 \text{ m/s} = 956.25 \text{ m}$. In the present indoor scenario, no relevant paths should arrive after this time.
4. A desktop computer acts as central processor. It computes the gain matrix from the estimated first and second-hop channel coefficients. Afterwards, the complex-valued gain factors are disseminated to the respective RACooN nodes. They are able to apply an amplitude scaling and phase rotation to their transmit signals in realtime. Once these values have been adjusted according to their gain factors, RACooN nodes 4, 5, and 7 can act as AF relays.

Evaluation phase: In the evaluation phase the performance of the gain allocation scheme is assessed. The gain factors in MUZF relaying are computed to completely suppress all inter-user interference. Hence, the SIR on the respective subchannels is a sensible performance indicator.

1. The source nodes transmit mutually orthogonal training sequences with equal transmit power to all relays.

2. The RACooN nodes acting as relays apply their previously calculated amplitude scaling and phase rotation to all samples when retransmitting them to the destinations. In Section 7.2.3.2, a characteristic phase response was observed in the first 1.2 ms of the signal after switching between receive and transmit mode. The time between reception and retransmission at the relay consequently has to be at least 1.2 ms so that the signal is not perturbed. During that time the LO phases will, however, have changed because of phase noise. The gain factors no longer diagonalize the equivalent channel matrix even if the propagation environment remains constant. As a result, inter-user interference can be observed at the destination nodes due to nonzero off-diagonal elements of the compound channel matrix $\tilde{\mathbf{H}}_{\text{SRD}}$.
3. The estimate $\hat{\mathbf{H}}_{\text{SRD}}$ of the equivalent two-hop channel matrix is computed from the received signals at both destinations. The measured SIR at destination node m is then defined as

$$\widehat{\text{SIR}}_m = \frac{\left| \hat{\mathbf{H}}_{\text{SRD}}[m, m] \right|^2}{\left| \hat{\mathbf{H}}_{\text{SRD}}[m, k] \right|^2}, \quad k \neq m. \quad (7.9)$$

The mission configuration of the RACooN nodes is done via .xml files, its operation is controlled by MATLAB[®] .m files [197–200]. In the following, a list of files that have been used for the MUZF relaying demonstrator is given.

- Overview of .xml files (RACooN configuration):
 1. mission files used for channel estimation
 - mission_Source_channel_estimation.m
 - mission_Relay_channel_estimation.m
 - mission_Destination_channel_estimation.m
 2. mission files used for evaluation
 - mission_Source_data_transmission.m
 - mission_Relay_data_transmission_original.m
 - mission_Destination_data_transmission.m
- Overview of .m files (RACooN operation):
 1. ExecuteMission.m: Definition of parameters. All the following files are subsequently called.

2. `Initialize_RACooN.m`: Initialization of the RACooN Lab.
3. `Generate_transmit_sequences.m`: The transmit bursts of both source nodes are generated.
4. `Copy_transmit_sequences.m`: Both transmit sequences are copied to the RACooN nodes acting as sources.
5. `Synchronize.m`: Time slot synchronization is performed via USB cables.
6. `Run_mission_channel_estimation.m`: Transmission and reception of the training sequences so that all single-hop channels can be estimated.
7. `Calculate_CIRs.m`: All single-hop channels are estimated.
8. `Calculate_gain_factors.m`: The gain factors for all relays are computed from the channel estimates.
9. `manipulate_xml.m`: The .xml files controlling the RACooN operation are modified. Each gain factor is realized by an amplitude scaling and phase rotation.
10. `Run_mission_data_transmission.m`: Transmission of training sequences from sources via relays to destinations so that the compound channel can be estimated at each destination.
11. `Calculate_compound_CIRs.m`: The compound channel matrix is computed.
12. `Calculate_compound_channel_power.m`: The signal and interference power at each destination is computed and plotted.

7.4.3 Results

This section presents the measurement results obtained by the demonstrator. Ideally, the gain matrix is computed such that all inter-user interference is suppressed. However, noisy channel estimates, phase noise, and other hardware imperfections degrade the interference rejection capabilities of the gain allocation scheme. The demonstration comprises a system with $N_S = N_D = 2$ source-destination pairs and $N_R = 3$ relays. The LOs of all relays run independently of each other. The assignment of source-destination pairs is as follows:

- Source 1: RACooN 2, destination 1: RACooN 6
- Source 2: RACooN 3, destination 2: RACooN 8

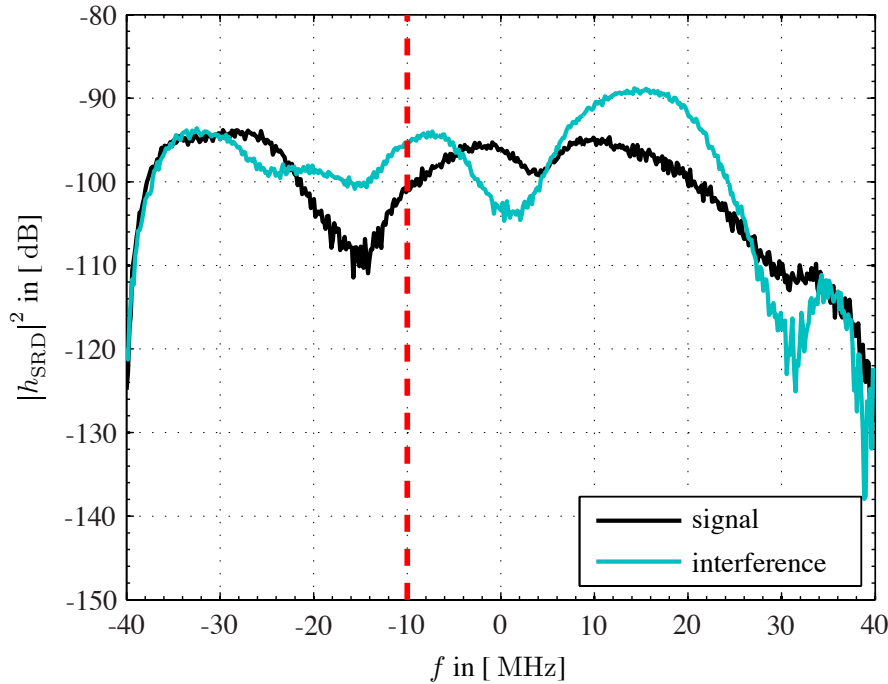


Fig. 7.29: Equivalent two-hop channels at RACooN 6 for noncoherent forwarding.

RACooN nodes 4, 5, and 7 act as relays. Figs. 7.29 and 7.30 show a single realization of the equivalent two-hop channels observed at destination nodes 6 and 8 for the case that $\mathbf{G} = \gamma \cdot \mathbf{I}_{N_R}$, where $\gamma \in \mathbb{C}$ is chosen such that the transmit power constraint at the relays is met. This specific choice of the gain matrix is in the following called 'noncoherent forwarding' because the relays simply forward their received signals without requiring channel knowledge. The plots show the squared magnitude of the compound channel coefficients versus the frequency. The bandwidth of the channel is 80 MHz around the carrier frequency $f_c = 5.5$ GHz. Please note that both 10 MHz bands at the border of the 80 MHz band, i.e., from -40 MHz to -30 MHz and from 30 MHz to 40 MHz are strongly influenced by the frequency response of the RACooN hardware. The curves labeled as 'signal' correspond to the channels from the belonging sources whereas the curves labeled as 'interference' correspond to the channels from the nonbelonging, i.e. interfering, sources. For the frequency bin at $f = -10$ MHz, indicated by the dashed vertical line in the plots, the SIR is -5.0 dB and -3.0 dB at RACooN 6 and RACooN 8, respectively.

In Figs. 7.31 and 7.32, a single realization of the compound channels is plotted for the case that the gain matrix is chosen according to MUZF relaying. Since the RACooN hardware restricts the AF gains to be scalar, the interference suppression is restricted to a single (frequency-flat) channel bin. The chosen frequency bin is located at $f_{ZF} = -10$ MHz and

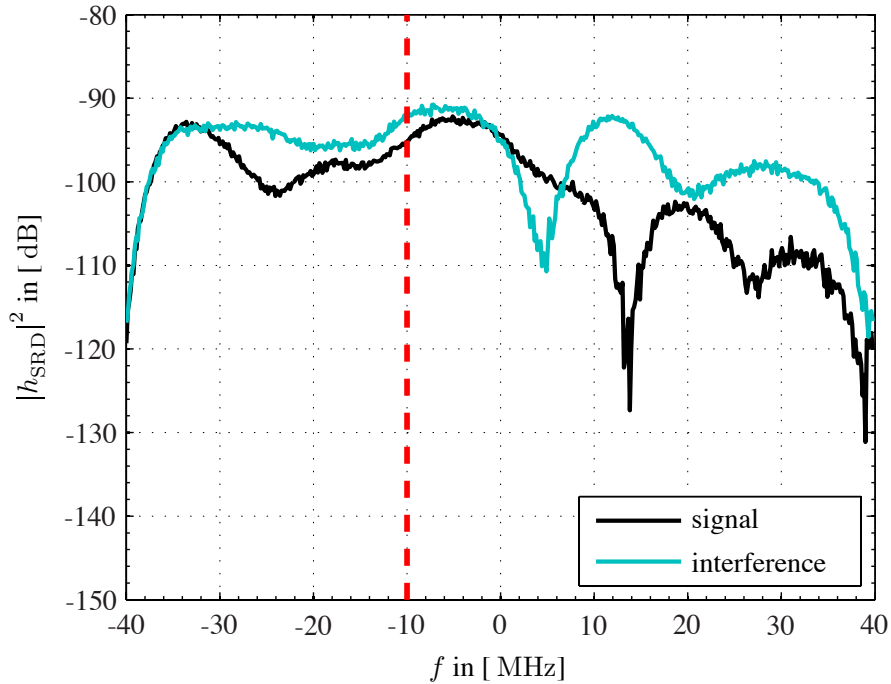


Fig. 7.30: Equivalent two-hop channels at RACooN 8 for noncoherent forwarding.

the gain factors are calculated based on the estimated channel coefficients at this frequency. The propagation environment is static, i.e., it is the same as for Figs. 7.29 and 7.30.

In a perfect world all inter-user interference would be cancelled at f_{ZF} . Indeed a reduction of the interference power at both destinations can be observed. At RACooN 6 the gain allocation places a deep notch at approximately f_{ZF} resulting in an SIR of 23.9dB (Fig. 7.31). This is a gain of 28.9 dB compared to Fig. 7.29. For RACooN 8, the SIR increases from -3.0 dB in Fig. 7.30 to 18.65 dB in Fig. 7.32. However, two deeper notches are placed near but not exactly at f_{ZF} . The reason for this observation is that due to LO phase noise at the relays, the gain allocation does not completely suppress the interference at f_{ZF} . As the channel bins are correlated across frequency, interference is instead suppressed more efficiently at a frequency bin in the vicinity of f_{ZF} . This can then be observed as a shift of the notch in frequency. The two notches in Fig. 7.32 indicate that the frequency bins around -13 MHz and -9 MHz are highly correlated.

In order to get some statistically relevant data, 1000 measurements were performed in a static propagation environment for $f_{ZF} = -10$ MHz. For each realization the SIR was calculated for the noncoherent case as well as the MUZF gain allocation. Figs. 7.33 and 7.34 show the cdfs of the SIR as defined in (7.9). The outage SIR improvements at 0.1, 0.5, and 0.9 outage probabilities are indicated in the figures. Furthermore, the numbers in the boxes

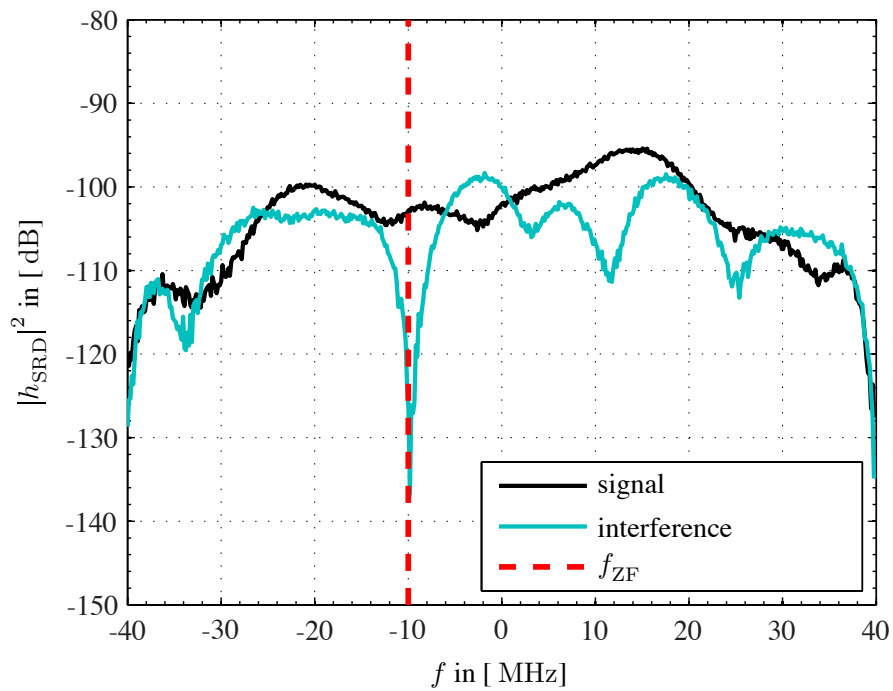


Fig. 7.31: Equivalent two-hop channels at RACooN 6 for MUZF relaying.

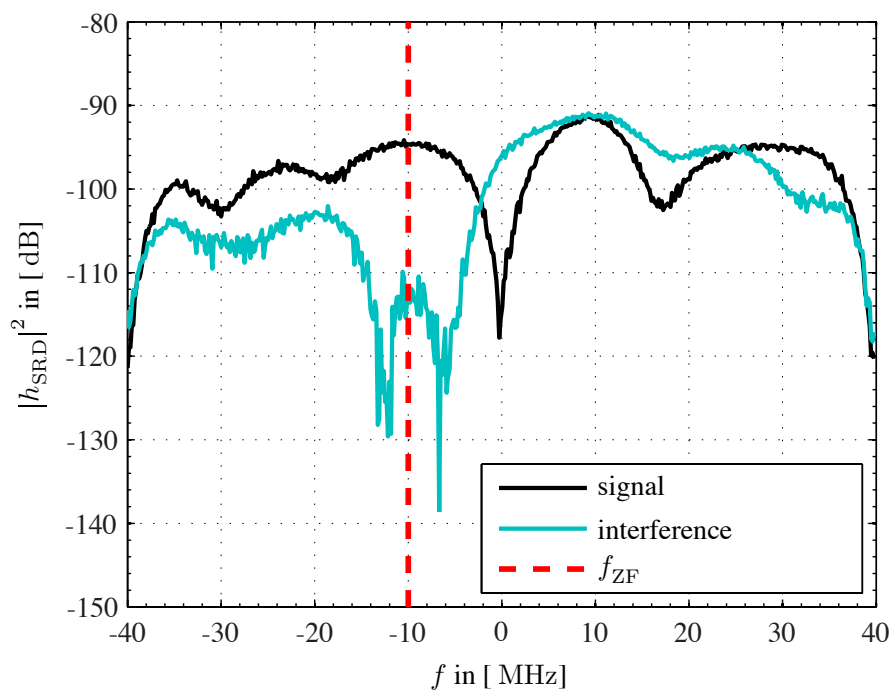


Fig. 7.32: Equivalent two-hop channels at RACooN 8 for MUZF relaying.

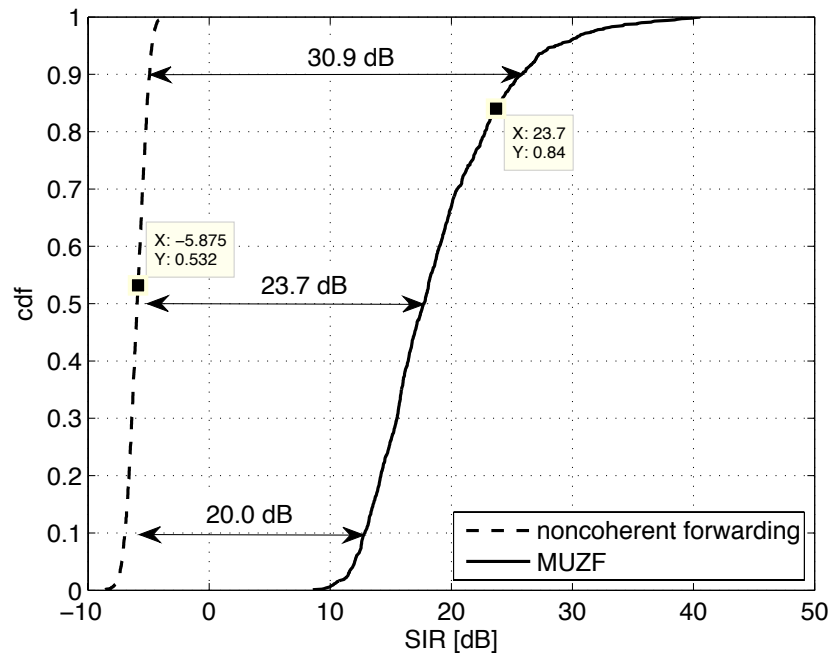


Fig. 7.33: cdf of the SIR at RACooN node 6 for noncoherent forwarding and MUZF.

indicate the respective mean values of all realizations. At RACooN 8 (Fig. 7.34), the SIR gain is 16 dB in 90% of the cases and at RACooN 6 (Fig. 7.33) the SIR gain is even 20 dB in 90% of the cases. This is a motivating result as the phase uncertainty is in the range of $\pm 10^\circ$ at each relay node (see Section 7.2.3.2). A system designed for a shorter processing time (that suffers less from phase noise) could easily perform even better.

Finally, the measurements were performed consecutively for all frequency bins in order to investigate the SIR gain over the whole bandwidth. For 30 subchannels (each of 0.16 MHz bandwidth) in the range of $f = -30$ MHz to $f = 30$ MHz, the mean SIR is plotted for 'noncoherent forwarding' as well as 'MUZF' relaying. Figs. 7.35 and 7.36 show the results for the case that all relays employed their own, independent LOs (as was the case for the previous considerations). In order to quantify the impact of LO phase noise on the performance, Figs. 7.37 and 7.38 show the same situation but with a common LO phase reference at the relays. It can be observed that the SIR gain for 'MUZF' relaying over 'noncoherent forwarding' is in the same order of magnitude for both cases. This hints at the fact that inaccurate channel estimates and not LO phase noise are the performance bottleneck for this demonstrator.

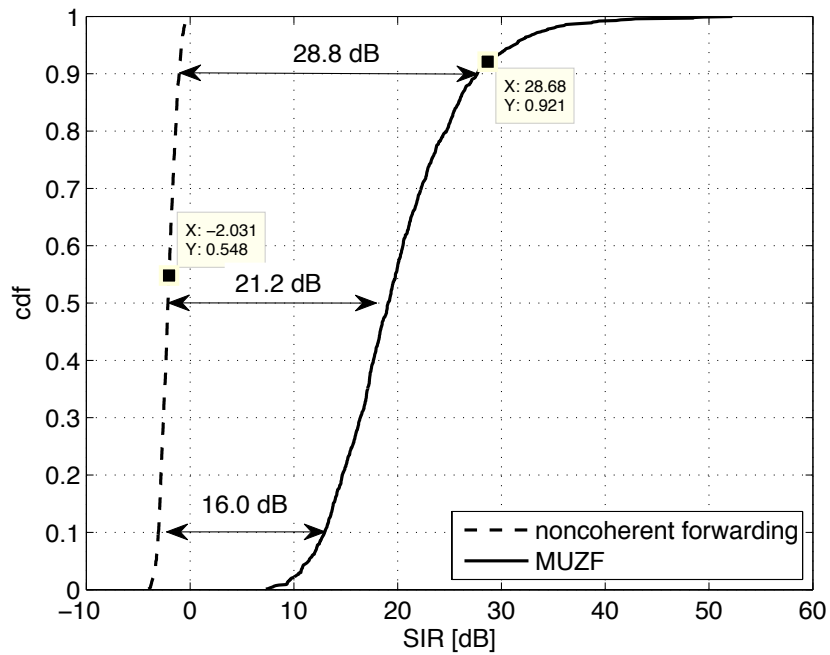


Fig. 7.34: cdf of the SIR at RACooN node 8 for noncoherent forwarding and MUZF.

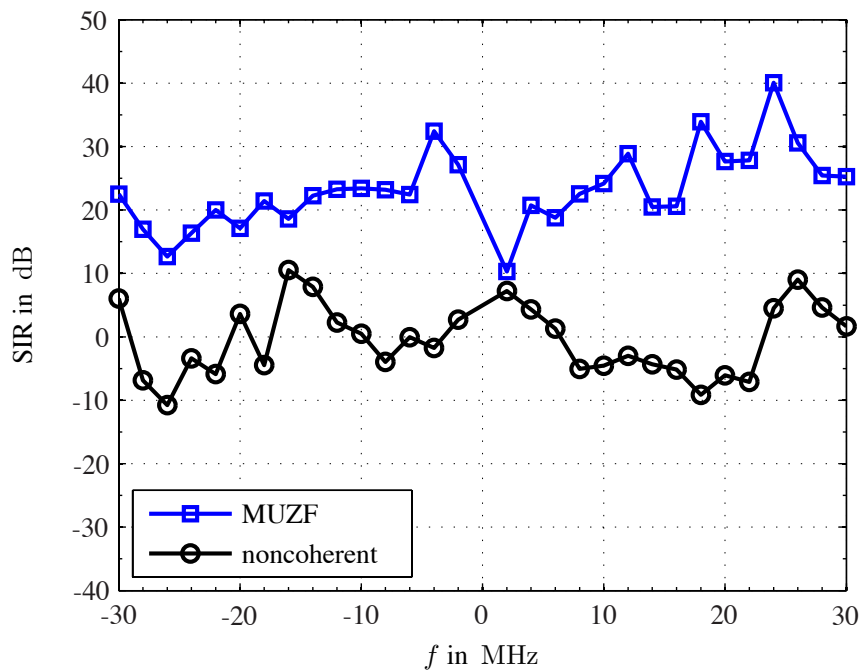


Fig. 7.35: Mean SIR at RACooN 3 for noncoherent forwarding and MUZF. Sources: 2, 6; Destinations: 3, 8. No global phase reference.

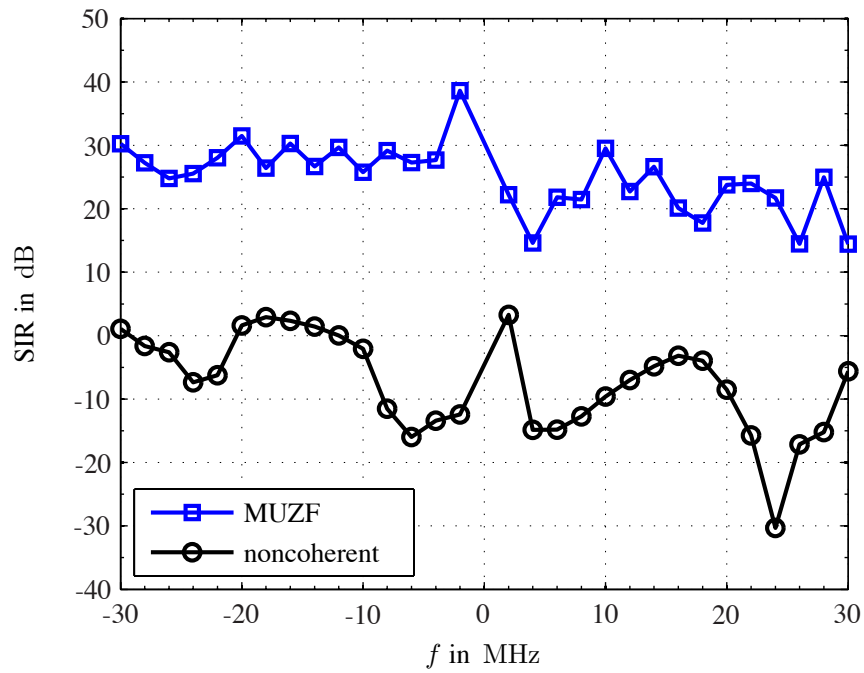


Fig. 7.36: Mean SIR at RACooN 8 for noncoherent forwarding and MUZF. Sources: 2, 6; Destinations: 3, 8. No global phase reference.

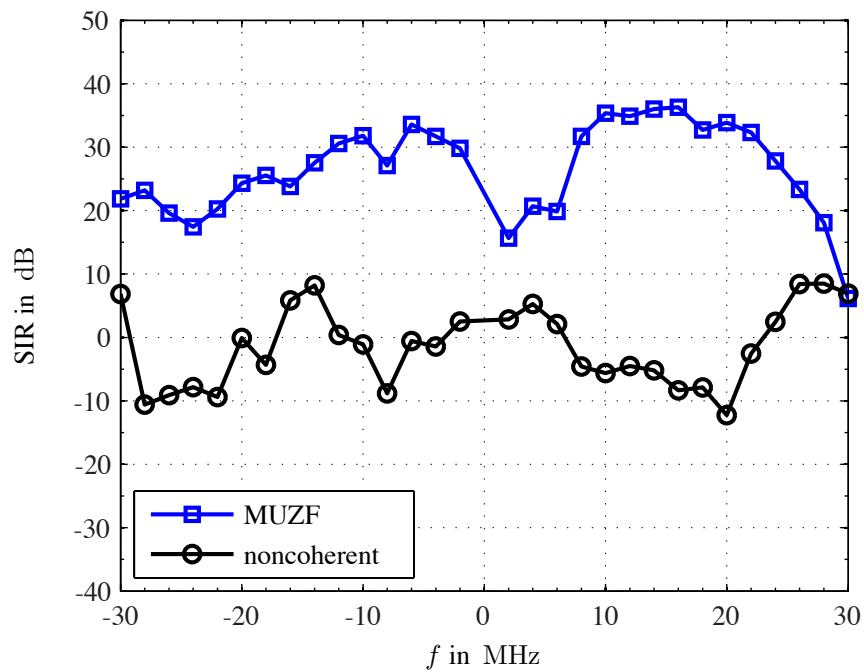


Fig. 7.37: Mean SIR at RACooN 3 for noncoherent forwarding and MUZF. Sources: 2, 6; Destinations: 3, 8. Global phase reference.

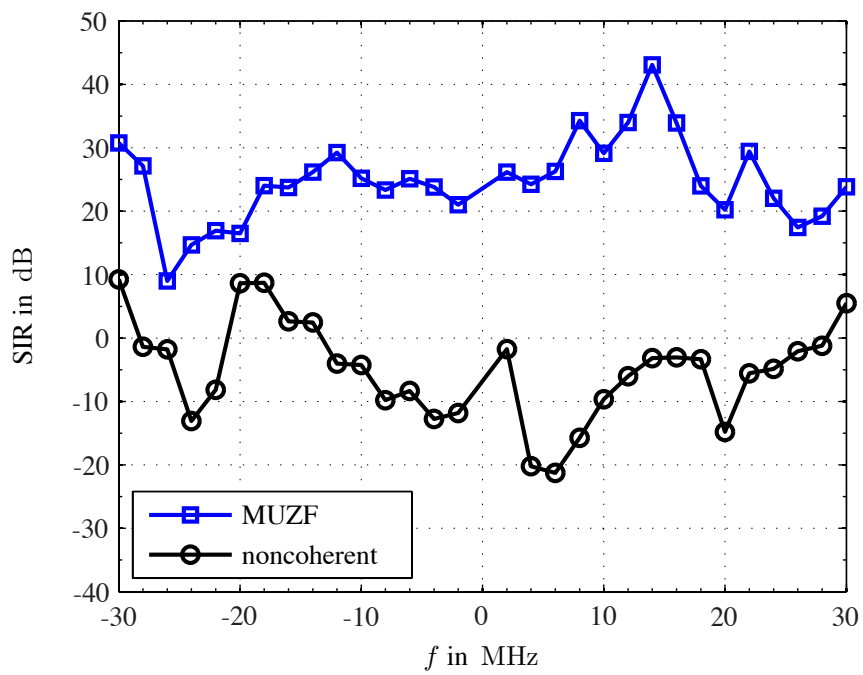


Fig. 7.38: Mean SIR at RACooN 8 for noncoherent forwarding and MUZF. Sources: 2, 6; Destinations: 3, 8. Global phase reference.

Chapter 8

Conclusions and Outlook

The density of wireless terminals that communicate on the same physical channel, i.e., at the same time, on the same frequency, and at the same place, is likely to increase drastically in the near future. The catchphrase is 'ubiquitous wireless access'. Channel resources, in particular the frequency bands available for communication, are, however, very limited. Interference avoidance will therefore be an ineffective strategy for future communication systems. It will be beneficial to rather 'use' the interference for the benefit of all present users. Following this concept, the key is to build the systems for cooperation rather than for mere coexistence. Cooperative networks promise to exhibit huge performance gains compared to traditional point-to-point communication systems, in particular in the presence of many users. This has triggered a lot of research lately. In particular, AF relaying is a promising candidate technology for future wireless multiuser networks. It is transparent to modulation and coding and the relay terminals can be very simple. Even single-antenna AF relays have been shown to be able to orthogonalize several source-destination pairs in space, allowing them to communicate concurrently on the same physical channel (e.g. [25]).

In this work several important aspects of two-hop AF relaying networks have been investigated. The focus was on coherent two-hop relaying, where the signals from the relays are required to add up coherently at the destination antennas. Understanding the implication of hardware imperfections for the signaling and thus the overall network performance is an important step towards building practical systems. *LO frequency offsets*, *LO phase noise* and *I/Q imbalance* have been investigated regarding their impact on coherent relaying. In particular, the impact of the considered LO imperfections on FDD and TDD relays has been compared in detail.

Channel estimation in distributed networks exhibits a peculiarity with respect to point-to-point links. It has been found that in some cases a common phase reference is required

at a certain set of nodes to allow for coherent forwarding. A solution to this problem has been presented in this work. A distributed phase synchronization scheme was introduced that provides multiple relays with a common global phase reference. Its performance has been analyzed in the presence of additive noise and phase noise, i.e., perturbances that are typically encountered in real-world systems. Another interesting aspect that has been investigated is the gain allocation, i.e., how to choose the relay gain factors. Two gain allocation schemes, namely MUZF and multiuser MMSE relaying, have been discussed. They both offer a *distributed spatial multiplexing gain*, allowing multiple users to communicate concurrently on the same physical channel. MMSE relaying has furthermore been found to additionally offer a *distributed diversity gain*. This allows for even higher communication rates for each individual user than in classical point-to-point systems.

MUZF relaying was finally implemented on the RACooN Lab, which is a demonstrator available at the Wireless Communications Group at ETH. The results indicated that inter-user interference can be efficiently suppressed in a real-world environment. This proves some of the theoretical concepts that have been presented previously and shows that the devised schemes work on practical hardware.

Although some interesting and very promising results have been obtained, there are still many issues that have not received much attention yet. An inherent disadvantage of one-way relaying, i.e. the type of networks discussed in this work, is that it takes four channel uses to exchange two messages between two users. Two-way relaying promises to offer considerable performance gains over one-way relaying in this case because only two channel uses are required to exchange two messages. An overview of recent advances in two-hop relaying is given in [210].

Open issues in cooperative communication that have yet to be addressed are for example two-way relaying schemes in the presence of multiple distributed relays or gain allocation schemes for broadband systems. The latter will lead to gain filters instead of scalar gain factors which are sufficient for frequency-flat channels. The assignment of sources, relays, and destinations from a set of nodes in a dynamic network is another very interesting problem. Physical layer as well as network layer concepts ('cross-layer optimization') have to be taken into account in order to find smart solutions. Efficient strategies to cope with mobile nodes entering or leaving the system have also yet to be found. Gain allocation schemes for cooperative communication systems that are practical and at the same time robust with respect to system imperfections like noisy or outdated CSI, timing errors, phase noise and other hardware imperfections will be a big step towards implementation. One of the biggest challenges for coherent cooperative communication systems will, however, be the exchange

of channel information and other feedback data to compute the relay gain factors. For large number of nodes, this overhead is likely to be prohibitive. Smart solution have to be found that either do not require this kind of feedback or can handle it efficiently. Secondary communication systems like Bluetooth or UWB might be the key to handle this problem. And finally, fundamental performance bounds of distributed communication protocols remain yet to be found.

A Appendix

A.1 Proof of (4.163)

Let

$$\tilde{\mathcal{H}} = \left\{ \tilde{h}_{S_k R_1}, \dots, \tilde{h}_{S_k R_{N_R}}, \tilde{h}_{R_1 D_m}, \dots, \tilde{h}_{R_{N_R} D_m} \right\} \quad (\text{A.1})$$

$$\hat{\mathcal{H}} = \left\{ \hat{h}_{S_k R_1}, \dots, \hat{h}_{S_k R_{N_R}}, \hat{h}_{R_1 D_m}, \dots, \hat{h}_{R_{N_R} D_m} \right\} \quad (\text{A.2})$$

denote the sets of actual and estimated channel coefficients between source k and all relays and between all relays and destination m . It will furthermore be useful to define the subset

$$\tilde{\mathcal{H}}_l = \left\{ \tilde{h}_{S_k R_l}, \tilde{h}_{R_l D_m} \right\}. \quad (\text{A.3})$$

The MSE of the estimated compound channels is given by

$$\begin{aligned} e_{S_k R D_m}^{(A1)} &= \mathbb{E}_{\tilde{\mathcal{H}}} \left[\left| \delta_{S_k R D_m} \right|^2 \right] = \\ &= \int_{\tilde{\mathcal{H}}} \left| \delta_{S_k R D_m} \right|^2 p \left(\tilde{\mathcal{H}} | \hat{\mathcal{H}} \right) d\tilde{\mathcal{H}}, \end{aligned} \quad (\text{A.4})$$

where $p \left(\tilde{\mathcal{H}} | \hat{\mathcal{H}} \right)$ is pdf of $\tilde{\mathcal{H}}$ given $\hat{\mathcal{H}}$. In order to find $e_{S_k R D_m}^{(A1)}$, the squared channel estimation error is first written as

$$\begin{aligned} \left| \delta_{S_k R D_m} \right|^2 &= \left| \sum_{l=1}^{N_R} \delta_{S_k R_l D_m} \right|^2 = \\ &= \sum_{p=1}^{N_R} \sum_{q=1}^{N_R} \delta_{S_k R_p D_m} \delta_{S_k R_q D_m}^*, \end{aligned} \quad (\text{A.5})$$

where

$$\delta_{S_k R_l D_m} := h_{S_k R_l D_m} - \hat{h}_{S_k R_l D_m} \quad (\text{A.6})$$

is the channel estimation error of the two-hop channel coefficient from source k via relay l to destination m . With (A.5), equation (A.4) becomes

$$e_{S_k R D_m}^{(\text{A1})} = \int_{\tilde{\mathcal{H}}} \sum_{p=1}^{N_R} \sum_{q=1}^{N_R} \left(\delta_{S_k R_p D_m} \delta_{S_k R_q D_m}^* \right) \cdot p \left(\tilde{\mathcal{H}} | \hat{\mathcal{H}} \right) d\tilde{\mathcal{H}}. \quad (\text{A.7})$$

Next, the conditional pdf $p \left(\tilde{\mathcal{H}} | \hat{\mathcal{H}} \right)$ has to be found. Since the propagation channels are mutually independent, it can be written as

$$p \left(\tilde{\mathcal{H}} | \hat{\mathcal{H}} \right) = \prod_{l=1}^{N_R} p \left(\tilde{h}_{S_k R_l} | \hat{\mathcal{H}} \right) \cdot p \left(\tilde{h}_{R_l D_m} | \hat{\mathcal{H}} \right). \quad (\text{A.8})$$

Let $\tilde{h} \in \tilde{\mathcal{H}}$ be an arbitrary element of $\tilde{\mathcal{H}}$ and $\hat{h} \in \hat{\mathcal{H}}$ the corresponding estimate in $\hat{\mathcal{H}}$. With the channel estimates

$$\hat{h}_{S_k R_l} = c \left(\tilde{h}_{S_k R_l} e^{-j\psi_{S_k R_l}} + n_{S_k R_l} \right) \quad (\text{A.9})$$

$$\hat{h}_{R_l D_m} = c \left(\tilde{h}_{R_l D_m} e^{j\psi_{R_l D_m}} + n_{R_l D_m} \right) \quad (\text{A.10})$$

given in (4.138) and (4.139), \hat{h} can be written in the form

$$\hat{h} = c \left(\tilde{h} e^{j\psi} + n \right), \quad (\text{A.11})$$

where $\tilde{h} \sim \mathcal{CN} (0, \sigma_h^2)$, $n \sim \mathcal{CN} (0, \sigma_n^2)$, and $\psi \sim \mathcal{N} (0, \sigma_\psi^2)$. The conditional pdf $p \left(\tilde{h} | \hat{\mathcal{H}} \right)$ can thus be written as

$$\begin{aligned} p \left(\tilde{h} | \hat{\mathcal{H}} \right) &= \int_{\psi} p \left(\tilde{h}, \psi | \hat{\mathcal{H}} \right) d\psi = \\ &= \int_{\psi} p \left(\tilde{h} | \psi, \hat{\mathcal{H}} \right) p \left(\psi | \hat{\mathcal{H}} \right) d\psi. \end{aligned} \quad (\text{A.12})$$

In order to compute $p \left(\tilde{h} | \hat{\mathcal{H}} \right)$, the conditional pdfs $p \left(\tilde{h} | \psi, \hat{\mathcal{H}} \right)$ and $p \left(\psi | \hat{\mathcal{H}} \right)$ have to be found:

- Finding $p(\tilde{h}|\psi, \hat{\mathcal{H}})$: Solving (A.11) for \tilde{h} delivers

$$\tilde{h} = \frac{1}{c} \hat{h} e^{-j\psi} - n', \quad (\text{A.13})$$

where $n' = n \cdot e^{-j\psi}$ has the same statistics as n . Obviously, $p(\tilde{h}|\psi, \hat{\mathcal{H}}) = p(\tilde{h}|\psi, \hat{h})$ and

$$p(\tilde{h}|\psi, \hat{h}) = \frac{1}{\pi\sigma_n^2} \cdot \exp\left(-\frac{1}{\sigma_n^2} \left| \tilde{h} - \frac{1}{c} \hat{h} e^{-j\psi} \right|^2\right). \quad (\text{A.14})$$

Equation (A.14) is the pdf of a complex Gaussian random variable with mean $\frac{1}{c} \hat{h} e^{-j\psi}$ and variance σ_n^2 .

- Finding $p(\psi|\hat{\mathcal{H}})$: Bayes' Theorem yields

$$p(\psi|\hat{\mathcal{H}}) = \frac{p(\hat{\mathcal{H}}|\psi) p(\psi)}{p(\hat{\mathcal{H}})} = p(\psi), \quad (\text{A.15})$$

where $p(\hat{\mathcal{H}}|\psi) = p(\hat{\mathcal{H}})$ because ψ and \tilde{h} are independent and \tilde{h} is circular symmetric. Intuitively, this means that knowledge of ψ does not give any information about the elements of $\hat{\mathcal{H}}$. Since ψ is real-valued, equation (A.15) becomes

$$p(\psi|\hat{\mathcal{H}}) = \frac{1}{\sqrt{2\pi\sigma_\psi^2}} \cdot \exp\left(-\frac{\psi^2}{2\sigma_\psi^2}\right). \quad (\text{A.16})$$

With (A.14) and (A.16), the pdf $p(\tilde{h}|\hat{\mathcal{H}})$ in (A.12) is

$$\begin{aligned} p(\tilde{h}|\hat{\mathcal{H}}) &= \int_{\psi} p(\tilde{h}|\psi, \hat{\mathcal{H}}) p(\psi|\hat{\mathcal{H}}) d\psi = \\ &= \int_{\psi} \frac{1}{\pi\sigma_n^2} \cdot \exp\left(-\frac{1}{\sigma_n^2} \left| \tilde{h} - \frac{1}{c} \hat{h} e^{-j\psi} \right|^2\right) \cdot \frac{1}{\sqrt{2\pi\sigma_\psi^2}} \cdot \exp\left(-\frac{\psi^2}{2\sigma_\psi^2}\right) d\psi = \\ &= \frac{1}{\pi\sigma_n^2 \sqrt{2\pi\sigma_\psi^2}} \cdot \int_{\psi} \exp\left(-\frac{1}{\sigma_n^2} \left| \tilde{h} - \frac{1}{c} \hat{h} e^{-j\psi} \right|^2 - \frac{\psi^2}{2\sigma_\psi^2}\right) d\psi = \\ &= p(\tilde{h}|\hat{h}). \end{aligned} \quad (\text{A.17})$$

The conditional pdfs of the actual first-hop channels given their estimates, i.e. $p\left(\tilde{h}_{S_k R_l} | \hat{\mathcal{H}}\right) = p\left(\tilde{h}_{S_k R_l} | \hat{h}_{S_k R_l}\right)$, are easily found by replacing $\psi = -\psi$ and inserting $\sigma_\psi^2 = (k-1)\sigma_{\text{pn}}^2$ into (A.17). Consequently,

$$p\left(\tilde{h}_{S_k R_l} | \hat{h}_{S_k R_l}\right) = \frac{1}{\pi \sigma_n^2 \sqrt{2\pi (k-1) \sigma_{\text{pn}}^2}} \cdot \int_{\psi} \exp\left(-\frac{1}{\sigma_n^2} \left| \tilde{h}_{S_k R_l} - \frac{1}{c} \hat{h}_{S_k R_l} e^{j\psi} \right|^2 - \frac{\psi^2}{2(k-1)\sigma_{\text{pn}}^2}\right) d\psi. \quad (\text{A.18})$$

Likewise, the pdfs of the actual second-hop channels given their estimates, i.e. $p\left(\tilde{h}_{R_l D_m} | \hat{h}_{R_l D_m}\right)$, are found by inserting $\sigma_\psi^2 = (N_{\text{SD}} - 1 + l)\sigma_{\text{pn}}^2$ into (A.17). Hence,

$$p\left(\tilde{h}_{R_l D_m} | \hat{h}_{R_l D_m}\right) = \frac{1}{\pi \sigma_n^2 \sqrt{2\pi (N_{\text{SD}} - 1 + l) \sigma_{\text{pn}}^2}} \cdot \int_{\psi} \exp\left(-\frac{1}{\sigma_n^2} \left| \tilde{h}_{R_l D_m} - \frac{1}{c} \hat{h}_{R_l D_m} e^{-j\psi} \right|^2 - \frac{\psi^2}{2(N_{\text{SD}} - 1 + l) \sigma_{\text{pn}}^2}\right) d\psi. \quad (\text{A.19})$$

The integrals in (A.18) and (A.19) have no closed-form solution. The following substitutions are used for the sake of a simpler notation:

$$f_{S_k R_l} := p\left(\tilde{h}_{S_k R_l} | \hat{h}_{S_k R_l}\right) \quad (\text{A.20})$$

$$f_{R_l D_m} := p\left(\tilde{h}_{R_l D_m} | \hat{h}_{R_l D_m}\right) \quad (\text{A.21})$$

With (A.20) and (A.21), the MSE in (A.7) can be written as

$$\begin{aligned} e_{S_k R D_m}^{(\text{A1})} &= \int_{\tilde{\mathcal{H}}} \sum_{p=1}^{N_R} \sum_{q=1}^{N_R} \left(\delta_{S_k R_p D_m} \delta_{S_k R_q D_m}^* \right) \cdot \prod_{l=1}^{N_R} f_{S_k R_l} f_{R_l D_m} d\tilde{\mathcal{H}} = \\ &= \sum_{p=1}^{N_R} \sum_{q=1}^{N_R} \left(\int_{\tilde{\mathcal{H}}} \delta_{S_k R_p D_m} \delta_{S_k R_q D_m}^* \cdot \prod_{l=1}^{N_R} f_{S_k R_l} f_{R_l D_m} d\tilde{\mathcal{H}} \right). \end{aligned} \quad (\text{A.22})$$

Since $f_{S_k R_l}$ and $f_{R_l D_m}$ are pdfs, it holds that

$$\int_{\tilde{h}_{S_k R_l}} f_{S_k R_l} d\tilde{h}_{S_k R_l} = \int_{\tilde{h}_{R_l D_m}} f_{R_l D_m} d\tilde{h}_{R_l D_m} = 1. \quad (\text{A.23})$$

Consequently, (A.22) reduces to

$$\begin{aligned}
e_{S_k R D_m}^{(A1)} &= \sum_{l=1}^{N_R} \int_{\tilde{\mathcal{H}}_l} |\delta_{S_k R_l D_m}|^2 f_{S_k R_l} f_{R_l D_m} d\tilde{\mathcal{H}}_l + \\
&\quad + \sum_{p=1}^{N_R} \sum_{\substack{q=1 \\ q \neq p}}^{N_R} \left(\int_{\tilde{\mathcal{H}}_p} \delta_{S_k R_p D_m} f_{S_k R_p} f_{R_p D_m} d\tilde{\mathcal{H}}_p \cdot \int_{\tilde{\mathcal{H}}_q} \delta_{S_k R_q D_m}^* f_{S_k R_q} f_{R_q D_m} d\tilde{\mathcal{H}}_q \right),
\end{aligned} \tag{A.24}$$

where the set $\tilde{\mathcal{H}}_l$ is defined in (A.3). In order to compute (A.24), the following two equalities will be used:

$$\begin{aligned}
&\int_{\tilde{h}} \tilde{h} \cdot p(\tilde{h}|\hat{h}) d\tilde{h} = \\
&= \int_{\tilde{h}} \frac{\tilde{h}}{\pi \sigma_n^2 \sqrt{2\pi\sigma_\psi^2}} \int_{\psi} \exp\left(-\frac{1}{\sigma_n^2} \left| \tilde{h} - \frac{1}{c} \hat{h} e^{-j\psi} \right|^2 - \frac{\psi^2}{2\sigma_\psi^2}\right) d\psi d\tilde{h} = \\
&= \frac{1}{\pi \sigma_n^2 \sqrt{2\pi\sigma_\psi^2}} \cdot \int_{\psi} e^{-\frac{\psi^2}{2\sigma_\psi^2}} \int_{\tilde{h}} \tilde{h} \cdot \exp\left(-\frac{1}{\sigma_n^2} \left| \tilde{h} - \frac{1}{c} \hat{h} e^{-j\psi} \right|^2\right) d\tilde{h} d\psi = \\
&= \frac{1}{\pi \sigma_n^2 \sqrt{2\pi\sigma_\psi^2}} \cdot \int_{\psi} e^{-\frac{\psi^2}{2\sigma_\psi^2}} \cdot \frac{\pi \sigma_n^2}{c} \hat{h} e^{-j\psi} d\psi = \\
&= \frac{\hat{h}}{c \sqrt{2\pi\sigma_\psi^2}} \cdot \int_{\psi} e^{-\frac{\psi^2}{2\sigma_\psi^2} - j\psi} d\psi = \\
&= \frac{\hat{h}}{c \sqrt{2\pi\sigma_\psi^2}} \cdot \sqrt{2\pi\sigma_\psi^2} e^{-\frac{1}{2}\sigma_\psi^2} = \\
&= \frac{1}{c} \hat{h} e^{-\frac{1}{2}\sigma_\psi^2}
\end{aligned} \tag{A.25}$$

and

$$\begin{aligned}
 & \int_{\tilde{h}} |\tilde{h}|^2 \cdot p(\tilde{h}|\hat{h}) d\tilde{h} = \\
 & = \int_{\tilde{h}} \frac{|\tilde{h}|^2}{\pi\sigma_n^2\sqrt{2\pi\sigma_\psi^2}} \int_{\psi} \exp\left(-\frac{1}{\sigma_n^2}\left|\tilde{h} - \frac{1}{c}\hat{h}e^{-j\psi}\right|^2 - \frac{\psi^2}{2\sigma_\psi^2}\right) d\psi d\tilde{h} = \\
 & = \frac{1}{\pi\sigma_n^2\sqrt{2\pi\sigma_\psi^2}} \cdot \int_{\psi} e^{-\frac{\psi^2}{2\sigma_\psi^2}} \int_{\tilde{h}} |\tilde{h}|^2 \cdot \exp\left(-\frac{1}{\sigma_n^2}\left|\tilde{h} - \frac{1}{c}\hat{h}e^{-j\psi}\right|^2\right) d\tilde{h} d\psi = \\
 & = \frac{1}{\pi\sigma_n^2\sqrt{2\pi\sigma_\psi^2}} \cdot \int_{\psi} e^{-\frac{\psi^2}{2\sigma_\psi^2}} \cdot \pi\sigma_n^2 \left(\sigma_n^2 + \frac{|\hat{h}|^2}{c^2}\right) d\psi = \\
 & = \frac{1}{\sqrt{2\pi\sigma_\psi^2}} \cdot \left(\sigma_n^2 + \frac{|\hat{h}|^2}{c^2}\right) \cdot \int_{\psi} e^{-\frac{\psi^2}{2\sigma_\psi^2}} d\psi = \\
 & = \frac{1}{\sqrt{2\pi\sigma_\psi^2}} \cdot \left(\sigma_n^2 + \frac{|\hat{h}|^2}{c^2}\right) \cdot \sqrt{2\pi\sigma_\psi^2} = \\
 & = \sigma_n^2 + \frac{|\hat{h}|^2}{c^2} \tag{A.26}
 \end{aligned}$$

For the first-hop channel estimates, \hat{h} has to be replaced by $\hat{h}_{S_k R_l}$ and σ_ψ^2 by $(k-1)\sigma_{\text{pn}}^2$. For the second-hop channel estimates, \hat{h} has to be replaced by $\hat{h}_{R_l D_m}$ and σ_ψ^2 by $(N_{\text{SD}} - 1 + l)\sigma_{\text{pn}}^2$. The MSE $e_{S_k R D_m}^{(A1)}$ is found by analyzing the sum and the double sum in (A.24) separately:

Sum: First, the squared channel estimation error in (A.24) can be written as (cf. (A.6))

$$\begin{aligned}
 |\delta_{S_k R_l D_m}|^2 & = \left|\tilde{h}_{S_k R_l D_m} - \hat{h}_{S_k R_l D_m}\right|^2 = \\
 & = \left|\tilde{h}_{R_l D_m}\right|^2 |g_l|^2 \left|\tilde{h}_{S_k R_l}\right|^2 + \left|\hat{h}_{R_l D_m}\right|^2 |g_l|^2 \left|\hat{h}_{S_k R_l}\right|^2 - \\
 & \quad - 2\text{Re}\left\{\tilde{h}_{R_l D_m} g_l \tilde{h}_{S_k R_l} \hat{h}_{R_l D_m}^* g_l^* \hat{h}_{S_k R_l}^*\right\}. \tag{A.27}
 \end{aligned}$$

Inserting (A.27) into the sum in (A.24) yields a sum of integrals:

$$\begin{aligned}
& \int_{\tilde{\mathcal{H}}_l} |\delta_{S_k R_l D_m}|^2 f_{S_k R_l} f_{R_l D_m} d\tilde{\mathcal{H}}_l = \\
& = |g_l|^2 \left(\int_{\tilde{\mathcal{H}}_l} |\tilde{h}_{R_l D_m}|^2 |\tilde{h}_{S_k R_l}|^2 f_{S_k R_l} f_{R_l D_m} d\tilde{\mathcal{H}}_l + \int_{\tilde{\mathcal{H}}_l} |\hat{h}_{R_l D_m}|^2 |\hat{h}_{S_k R_l}|^2 f_{S_k R_l} f_{R_l D_m} d\tilde{\mathcal{H}}_l - \right. \\
& \quad \left. - 2\text{Re} \left\{ \int_{\tilde{\mathcal{H}}_l} \tilde{h}_{R_l D_m} \tilde{h}_{S_k R_l} \hat{h}_{R_l D_m}^* \hat{h}_{S_k R_l}^* f_{S_k R_l} f_{R_l D_m} d\tilde{\mathcal{H}}_l \right\} \right) \quad (\text{A.28})
\end{aligned}$$

- The first summand in (A.28) can be solved using (A.26):

$$\begin{aligned}
& \int_{\tilde{\mathcal{H}}_l} |\tilde{h}_{R_l D_m}|^2 |\tilde{h}_{S_k R_l}|^2 f_{S_k R_l} f_{R_l D_m} d\tilde{\mathcal{H}}_l = \\
& = \int_{\tilde{h}_{R_l D_m}} |\tilde{h}_{R_l D_m}|^2 f_{R_l D_m} d\tilde{h}_{R_l D_m} \cdot \int_{\tilde{h}_{S_k R_l}} |\tilde{h}_{S_k R_l}|^2 f_{S_k R_l} d\tilde{h}_{S_k R_l} = \\
& = \left(\sigma_n^2 + \frac{1}{c^2} |\hat{h}_{R_l D_m}|^2 \right) \left(\sigma_n^2 + \frac{1}{c^2} |\hat{h}_{S_k R_l}|^2 \right). \quad (\text{A.29})
\end{aligned}$$

- The second summand in (A.28) is trivially solved:

$$\begin{aligned}
& \int_{\tilde{\mathcal{H}}_l} |\hat{h}_{R_l D_m}|^2 |\hat{h}_{S_k R_l}|^2 f_{S_k R_l} f_{R_l D_m} d\tilde{\mathcal{H}}_l = |\hat{h}_{R_l D_m}|^2 |\hat{h}_{S_k R_l}|^2 \int_{\tilde{\mathcal{H}}_l} f_{S_k R_l} f_{R_l D_m} d\tilde{\mathcal{H}}_l = \\
& = |\hat{h}_{R_l D_m}|^2 |\hat{h}_{S_k R_l}|^2. \quad (\text{A.30})
\end{aligned}$$

- Finally, the third summand in (A.28) can be solved using (A.25). The integral can be written as

$$\begin{aligned}
& \int_{\tilde{\mathcal{H}}_l} \tilde{h}_{R_l D_m} \tilde{h}_{S_k R_l} \hat{h}_{R_l D_m}^* \hat{h}_{S_k R_l}^* f_{S_k R_l} f_{R_l D_m} d\tilde{\mathcal{H}}_l = \\
& = \hat{h}_{R_l D_m}^* \hat{h}_{S_k R_l}^* \cdot \int_{\tilde{\mathcal{H}}_l} \tilde{h}_{R_l D_m} \tilde{h}_{S_k R_l} f_{R_l D_m} f_{S_k R_l} d\tilde{\mathcal{H}}_l. \quad (\text{A.31})
\end{aligned}$$

The equivalent channel coefficients $\tilde{h}_{S_k R_l}$ and $\tilde{h}_{R_l D_m}$ can be written as a function of

their respective estimates defined in (4.138) and (4.139). Their product is thus

$$\begin{aligned}
\tilde{h}_{R_l D_m} \tilde{h}_{S_k R_l} &= \\
&= \left(\frac{1}{c} \hat{h}_{R_l D_m} - n_{R_l D_m} \right) e^{-j\psi_{R_l D_m}} \cdot \left(\frac{1}{c} \hat{h}_{S_k R_l} - n_{S_k R_l} \right) e^{j\psi_{S_k R_l}} = \\
&= \left(\frac{1}{c} \hat{h}_{R_l D_m} e^{j(\psi_{S_k R_l} - \psi_{R_l D_m})} - n'_{R_l D_m} \right) \cdot \left(\frac{1}{c} \hat{h}_{S_k R_l} - n_{S_k R_l} \right), \tag{A.32}
\end{aligned}$$

where $n'_{R_l D_m} = n_{R_l D_m} e^{j(\psi_{S_k R_l} - \psi_{R_l D_m})}$ has the same statistics as $n_{R_l D_m}$. Let

$$\tilde{h}'_{S_k R_l} := \frac{1}{c} \hat{h}_{S_k R_l} - n_{S_k R_l} \tag{A.33}$$

$$\tilde{h}'_{R_l D_m} := \frac{1}{c} \hat{h}_{R_l D_m} e^{j(\psi_{S_k R_l} - \psi_{R_l D_m})} - n'_{R_l D_m}, \tag{A.34}$$

where the phases $\psi_{S_k R_l}$ and $\psi_{R_l D_m}$ are given by (cf. (4.137) and (4.140))

$$\psi_{S_k R_l} = \sum_{p=1}^k \Delta\psi_{S_p R_l} \tag{A.35}$$

$$\psi_{R_l D_m} = \psi_{N_{SD} R_l} + \Delta\psi_{R_l D_m}. \tag{A.36}$$

Recall that $\psi_{S_1 R_l} = 0$, $\Delta\psi_{S_p R_l} \sim \mathcal{N}(0, \sigma_{pn}^2)$ for $p = 2, \dots, k$, and $\Delta\psi_{R_l D_m} \sim \mathcal{N}(0, l\sigma_{pn}^2)$, where $\Delta\psi_{S_p R_l}$ and $\Delta\psi_{R_l D_m}$ are mutually independent. Consequently, the phase $\psi_{S_k R_l} - \psi_{R_l D_m}$ in (A.34) is distributed as follows:

$$\psi_{S_k R_l} - \psi_{R_l D_m} \sim \mathcal{N}(0, (N_{SD} - k + l)\sigma_{pn}^2). \tag{A.37}$$

With (A.32) – (A.34), equation (A.31) becomes

$$\begin{aligned}
\int_{\tilde{\mathcal{H}}_l} \tilde{h}_{R_l D_m} \tilde{h}_{S_k R_l} \hat{h}_{R_l D_m}^* \hat{h}_{S_k R_l}^* f_{S_k R_l} f_{R_l D_m} d\tilde{\mathcal{H}}_l &= \\
&= \hat{h}_{R_l D_m}^* \hat{h}_{S_k R_l}^* \cdot \int_{\tilde{h}'_{R_l D_m}} \tilde{h}'_{R_l D_m} f_{R_l D_m} d\tilde{h}'_{R_l D_m} \cdot \int_{\tilde{h}'_{S_k R_l}} \tilde{h}'_{S_k R_l} f_{S_k R_l} d\tilde{h}'_{S_k R_l}. \tag{A.38}
\end{aligned}$$

Inserting $\sigma_\psi^2 = (N_{\text{SD}} - k + l) \sigma_{\text{pn}}^2$ and $\sigma_\psi^2 = 0$, respectively, into (A.25) delivers

$$\int_{\tilde{h}'_{\text{R}_l \text{D}_m}} \tilde{h}'_{\text{R}_l \text{D}_m} f_{\text{R}_l \text{D}_m} d\tilde{h}'_{\text{R}_l \text{D}_m} = \frac{1}{c} \hat{h}_{\text{R}_l \text{D}_m} e^{-\frac{1}{2}(N_{\text{SD}} - k + l) \sigma_{\text{pn}}^2} \quad (\text{A.39})$$

$$\int_{\tilde{h}'_{\text{S}_k \text{R}_l}} \tilde{h}'_{\text{S}_k \text{R}_l} f_{\text{S}_k \text{R}_l} d\tilde{h}'_{\text{S}_k \text{R}_l} = \frac{1}{c} \hat{h}_{\text{S}_k \text{R}_l}. \quad (\text{A.40})$$

Equation (A.38) can now be computed by inserting (A.39) and (A.40):

$$\begin{aligned} \int_{\tilde{\mathcal{H}}_l} \tilde{h}_{\text{R}_l \text{D}_m} \tilde{h}_{\text{S}_k \text{R}_l} \hat{h}_{\text{R}_l \text{D}_m}^* \hat{h}_{\text{S}_k \text{R}_l}^* f_{\text{S}_k \text{R}_l} f_{\text{R}_l \text{D}_m} d\tilde{\mathcal{H}}_l &= \\ &= \hat{h}_{\text{R}_l \text{D}_m}^* \hat{h}_{\text{S}_k \text{R}_l}^* \cdot \frac{1}{c} \hat{h}_{\text{R}_l \text{D}_m} e^{-\frac{1}{2}(N_{\text{SD}} - k + l) \sigma_{\text{pn}}^2} \cdot \frac{1}{c} \hat{h}_{\text{S}_k \text{R}_l} = \\ &= \left| \hat{h}_{\text{R}_l \text{D}_m} \right|^2 \left| \hat{h}_{\text{S}_k \text{R}_l} \right|^2 \cdot \frac{1}{c^2} e^{-\frac{1}{2}(N_{\text{SD}} - k + l) \sigma_{\text{pn}}^2}. \end{aligned} \quad (\text{A.41})$$

The sum in (A.24) is thus given by

$$\begin{aligned} \sum_{l=1}^{N_{\text{R}}} \int_{\tilde{\mathcal{H}}_l} \left| \delta_{\text{S}_k \text{R}_l \text{D}_m} \right|^2 f_{\text{S}_k \text{R}_l} f_{\text{R}_l \text{D}_m} d\tilde{\mathcal{H}}_l &= \\ &= \sum_{l=1}^{N_{\text{R}}} \left(|g_l|^2 \left(\sigma_{\text{n}}^2 + \frac{1}{c^2} \left| \hat{h}_{\text{R}_l \text{D}_m} \right|^2 \right) \left(\sigma_{\text{n}}^2 + \frac{1}{c^2} \left| \hat{h}_{\text{S}_k \text{R}_l} \right|^2 \right) + \right. \\ &\quad \left. + \left(1 - \frac{2}{c^2} e^{-\frac{1}{2}(N_{\text{SD}} - k + l) \sigma_{\text{pn}}^2} \right) \left| \hat{h}_{\text{R}_l \text{D}_m} \right|^2 |g_l|^2 \left| \hat{h}_{\text{S}_k \text{R}_l} \right|^2 \right), \end{aligned} \quad (\text{A.42})$$

where (A.29), (A.30), and (A.41) were inserted into (A.28).

Double sum: The summands of the double sum in (A.24) can be written as

$$\begin{aligned}
& \int_{\tilde{\mathcal{H}}_p} \delta_{S_k R_p D_m} f_{S_k R_p} f_{R_p D_m} d\tilde{\mathcal{H}}_p \cdot \int_{\tilde{\mathcal{H}}_q} \delta_{S_k R_q D_m}^* f_{S_k R_q} f_{R_q D_m} d\tilde{\mathcal{H}}_q = \\
& = \int_{\tilde{\mathcal{H}}_p} \left(\tilde{h}_{R_p D_m} p_l \tilde{h}_{S_k R_p} - \hat{h}_{R_p D_m} g_p \hat{h}_{S_k R_p} \right) f_{S_k R_p} f_{R_p D_m} d\tilde{\mathcal{H}}_p \cdot \\
& \quad \cdot \int_{\tilde{\mathcal{H}}_q} \left(\tilde{h}_{R_q D_m} q_l \tilde{h}_{S_k R_q} - \hat{h}_{R_q D_m} g_q \hat{h}_{S_k R_q} \right)^* f_{S_k R_q} f_{R_q D_m} d\tilde{\mathcal{H}}_q = \\
& = g_p \left(\int_{\tilde{h}'_{R_p D_m}} \tilde{h}'_{R_p D_m} f_{R_p D_m} d\tilde{h}'_{R_p D_m} \cdot \int_{\tilde{h}'_{S_k R_p}} \tilde{h}'_{S_k R_p} f_{S_k R_p} d\tilde{h}'_{S_k R_p} - \hat{h}_{R_p D_m} \hat{h}_{S_k R_p} \right) \cdot \\
& \quad \cdot g_q^* \left(\int_{\tilde{h}'_{R_q D_m}} \tilde{h}'_{R_q D_m} f_{R_q D_m} d\tilde{h}'_{R_q D_m} \cdot \int_{\tilde{h}'_{S_k R_q}} \tilde{h}'_{S_k R_q} f_{S_k R_q} d\tilde{h}'_{S_k R_q} - \hat{h}_{R_q D_m}^* \hat{h}_{S_k R_q}^* \right), \tag{A.43}
\end{aligned}$$

where $\tilde{h}'_{S_k R_l}$ and $\tilde{h}'_{R_l D_m}$ are defined in (A.33) and (A.34), respectively. Using the results in (A.39) and (A.40) delivers

$$\begin{aligned}
& \int_{\tilde{\mathcal{H}}_p} \delta_{S_k R_p D_m} f_{S_k R_p} f_{R_p D_m} d\tilde{\mathcal{H}}_p \cdot \int_{\tilde{\mathcal{H}}_q} \delta_{S_k R_q D_m}^* f_{S_k R_q} f_{R_q D_m} d\tilde{\mathcal{H}}_q = \\
& = g_p \left(\frac{1}{c^2} \hat{h}_{R_p D_m} \hat{h}_{S_k R_p} e^{-\frac{1}{2}(N_{SD} - k + p)\sigma_{pn}^2} - \hat{h}_{R_p D_m} \hat{h}_{S_k R_p} \right) \cdot \\
& \quad \cdot g_q^* \left(\frac{1}{c^2} \hat{h}_{R_q D_m}^* \hat{h}_{S_k R_q}^* e^{-\frac{1}{2}(N_{SD} - k + q)\sigma_{pn}^2} - \hat{h}_{R_q D_m}^* \hat{h}_{S_k R_q}^* \right) = \\
& = \left(\frac{1}{c^2} e^{-\frac{1}{2}(N_{SD} - k + p)\sigma_{pn}^2} - 1 \right) \hat{h}_{R_p D_m} g_p \hat{h}_{S_k R_p} \cdot \\
& \quad \cdot \left(\frac{1}{c^2} e^{-\frac{1}{2}(N_{SD} - k + q)\sigma_{pn}^2} - 1 \right) \hat{h}_{R_q D_m}^* g_q^* \hat{h}_{S_k R_q}^*. \tag{A.44}
\end{aligned}$$

The double sum in (A.24) is thus given by

$$\begin{aligned}
& \sum_{p=1}^{N_R} \sum_{\substack{q=1 \\ q \neq p}}^{N_R} \left(\int_{\tilde{\mathcal{H}}_p} \delta_{S_k R_p D_m} f_{S_k R_p} f_{R_p D_m} d\tilde{\mathcal{H}}_p \cdot \int_{\tilde{\mathcal{H}}_q} \delta_{S_k R_q D_m}^* f_{S_k R_q} f_{R_q D_m} d\tilde{\mathcal{H}}_q \right) = \\
& = \sum_{p=1}^{N_R} \sum_{\substack{q=1 \\ q \neq p}}^{N_R} \left(\left(\frac{1}{c^2} e^{-\frac{1}{2}(N_{SD}-k+p)\sigma_{pn}^2} - 1 \right) \hat{h}_{R_p D_m} g_p \hat{h}_{S_k R_p} \cdot \right. \\
& \quad \left. \cdot \left(\frac{1}{c^2} e^{-\frac{1}{2}(N_{SD}-k+q)\sigma_{pn}^2} - 1 \right) \hat{h}_{R_q D_m}^* g_q^* \hat{h}_{S_k R_q}^* \right). \tag{A.45}
\end{aligned}$$

The MSE in (A.24) can finally be computed with (A.42) and (A.45)

$$\begin{aligned}
e_{S_k R D_m}^{(A1)} & = \sum_{l=1}^{N_R} \left(|g_l|^2 \left(\sigma_n^2 + \frac{1}{c^2} |\hat{h}_{R_l D_m}|^2 \right) \left(\sigma_n^2 + \frac{1}{c^2} |\hat{h}_{S_k R_l}|^2 \right) + \right. \\
& \quad \left. + \left(1 - \frac{2}{c^2} e^{-\frac{1}{2}(N_{SD}-k+l)\sigma_{pn}^2} \right) |\hat{h}_{R_l D_m}|^2 |g_l|^2 |\hat{h}_{S_k R_l}|^2 \right) + \\
& \quad + \sum_{p=1}^{N_R} \sum_{\substack{q=1 \\ q \neq p}}^{N_R} \left(\left(\frac{1}{c^2} e^{-\frac{1}{2}(N_{SD}-k+p)\sigma_{pn}^2} - 1 \right) \hat{h}_{R_p D_m} g_p \hat{h}_{S_k R_p} \cdot \right. \\
& \quad \left. \cdot \left(\frac{1}{c^2} e^{-\frac{1}{2}(N_{SD}-k+q)\sigma_{pn}^2} - 1 \right) \hat{h}_{R_q D_m}^* g_q^* \hat{h}_{S_k R_q}^* \right). \tag{A.46}
\end{aligned}$$

A.2 pdf of a Function of a Random Variable

Let X be a real-valued random variable with pdf $f_X(x)$. Furthermore, let Y with pdf $f_Y(y)$ be a function of X :

$$Y = g(X) \tag{A.47}$$

The goal is to express the pdf $f_Y(y)$ of Y in terms of the pdf $f_X(x)$ of X and the function $g(X)$. It can be found for example in [173] that in order to find $f_Y(y)$ for a specific y , all x_n where $y = g(x_n)$, $n \in \{1, \dots, N\}$ have to be found. Then,

$$f_Y(y) = \frac{f_X(x_1)}{|g'(x_1)|} + \dots + \frac{f_X(x_N)}{|g'(x_N)|}, \tag{A.48}$$

where $g'(x_i) = \frac{\partial}{\partial x_i} g(x_i)$ is the partial derivative of $g(x_i)$ with respect to x_i .

A.3 pdf of a Function of Two Random Variables

Let X and Y be real-valued random variables with pdfs $f_X(x)$ and $f_Y(y)$, respectively. Furthermore, let Z be a function of both X and Y :

$$Z = g(X, Y) \tag{A.49}$$

The goal is to express the statistics of Z in terms of the function $g(X, Y)$ and the joint statistics of X and Y . Given the region D_z of the xy -plane such that $g(x, y) \leq z$ the distribution function (cdf) of Z can be calculated as follows [173]:

$$F_Z(z) = \iint_{D_z} f_{X,Y}(x, y) dx dy. \tag{A.50}$$

The function $f_{X,Y}(x, y)$ is the joint density of X and Y with

$$f_{X,Y}(x, y) = \frac{\partial^2 F_{X,Y}(x, y)}{\partial x \partial y}. \tag{A.51}$$

Considering the region ΔD_z of the xy -plane where $z < g(x, y) < z + dz$, the joint density function

$$f_Z(z) dz = \iint_{\Delta D_z} f_{X,Y}(x, y) dx dy \tag{A.52}$$

can be calculated.

Example: Joint pdf of the division of two random variables. The joint pdf of

$$Z = \frac{X}{Y} \tag{A.53}$$

is given in (A.52). To illustrate the present situation, consider Fig. A.1. With $x = y \cdot z$ and $dx = |y| \cdot dz$ we have

$$f_Z(z) dz = \int_{-\infty}^{\infty} |y| f(zy, y) dy dz, \tag{A.54}$$

and thus

$$f_Z(z) = \int_{-\infty}^{\infty} |y| f(zy, y) dy. \tag{A.55}$$

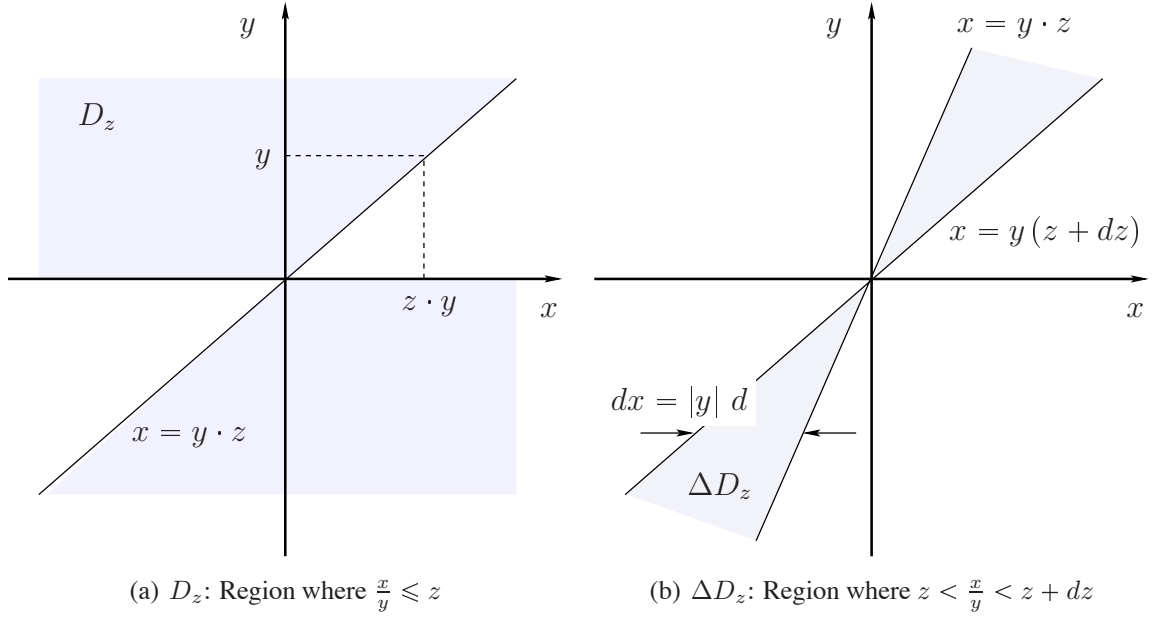


Fig. A.1: Region D_z and ΔD_z for the case of division of two random variables.

If the random variables X and Y are independent, then $f_{X,Y}(x, y) = f_X(x) \cdot f_Y(y)$. Using this property in (A.55) yields

$$f_Z(z) = \int_{-\infty}^{\infty} |y| f_X(z y) f_Y(y) dy, \quad (\text{A.56})$$

A.4 Multiuser Zero-Forcing Relaying Example

Consider the following simple example with 2 single-antenna source-destination pairs and 2 single-antenna relays¹. The first-hop and second-hop channel matrices are defined as

$$\mathbf{H}_{\text{SR}} = \begin{bmatrix} h_{S_1 R_1} & h_{S_2 R_1} \\ h_{S_1 R_2} & h_{S_2 R_2} \end{bmatrix} \quad \text{and} \quad \mathbf{H}_{\text{RD}} = \begin{bmatrix} h_{R_1 D_1} & h_{R_2 D_1} \\ h_{R_1 D_2} & h_{R_2 D_2} \end{bmatrix}, \quad (\text{A.57})$$

where $h_{S_k R_l}$ denotes the channel coefficient between source k and relay l and $h_{R_l D_m}$ the channel coefficient between relay l and destination m . Furthermore, the matrices

$$\Phi_S = \begin{bmatrix} e^{j\varphi_{S_1}} & 0 \\ 0 & e^{j\varphi_{S_2}} \end{bmatrix} \quad \text{and} \quad \Phi_D = \begin{bmatrix} e^{j\varphi_{D_1}} & 0 \\ 0 & e^{j\varphi_{D_2}} \end{bmatrix} \quad (\text{A.58})$$

¹Note that at least 3 relays are required to orthogonalize 2 source-destination pairs. However, 2 relays are sufficient for the purpose of explaining the notation.

comprise the LO phase offsets of the sources and destinations, respectively. The gain matrix is diagonal because the relays also employ a single antenna only. It can consequently be written as

$$\mathbf{G} = \begin{bmatrix} g_1 & 0 \\ 0 & g_2 \end{bmatrix}. \quad (\text{A.59})$$

Furthermore,

$$\mathbf{g} = \text{vec}(\mathbf{G}) = \begin{bmatrix} g_1 & 0 & 0 & g_2 \end{bmatrix}^T. \quad (\text{A.60})$$

Finally, the equivalent two-hop channel matrix for traffic pattern IV is

$$\tilde{\mathbf{H}}_{\text{IV}} = \begin{bmatrix} \tilde{h}_{\text{IV},11} & \tilde{h}_{\text{IV},12} \\ \tilde{h}_{\text{IV},21} & \tilde{h}_{\text{IV},22} \end{bmatrix} \quad (\text{A.61})$$

The coefficients $\tilde{h}_{\text{IV},11}$ and $\tilde{h}_{\text{IV},22}$ contribute signal power at the destinations, and the coefficients $\tilde{h}_{\text{IV},12}$ and $\tilde{h}_{\text{IV},21}$ interference power. The vector $\tilde{\mathbf{h}}_{\text{IV}}$ is obtained by stacking the columns of $\tilde{\mathbf{H}}_{\text{IV}}$ on top of each other. It can be calculated as

$$\begin{aligned} \tilde{\mathbf{h}}_{\text{IV}} &= \text{vec}(\tilde{\mathbf{H}}_{\text{I}}) = \\ &= (\Phi_{\text{S}}^T \otimes \Phi_{\text{D}}^H) (\mathbf{H}_{\text{SR}}^T \otimes \mathbf{H}_{\text{RD}}) \cdot \text{vec}(\mathbf{G}) := \\ &:= \Theta \Lambda \cdot \mathbf{g}, \end{aligned} \quad (\text{A.62})$$

where

$$\tilde{\mathbf{h}}_{\text{IV}} = \begin{bmatrix} \tilde{h}_{\text{IV},11} & \tilde{h}_{\text{IV},21} & \tilde{h}_{\text{IV},12} & \tilde{h}_{\text{IV},22} \end{bmatrix}^T \quad (\text{A.63})$$

$$\Theta = \begin{bmatrix} e^{j(\varphi_{\text{S}_1} - \varphi_{\text{D}_1})} & 0 & 0 & 0 \\ 0 & e^{j(\varphi_{\text{S}_1} - \varphi_{\text{D}_2})} & 0 & 0 \\ 0 & 0 & e^{j(\varphi_{\text{S}_2} - \varphi_{\text{D}_1})} & 0 \\ 0 & 0 & 0 & e^{j(\varphi_{\text{S}_2} - \varphi_{\text{D}_2})} \end{bmatrix} \quad (\text{A.64})$$

$$\Lambda = \begin{bmatrix} h_{\text{S}_1\text{R}_1} h_{\text{R}_1\text{D}_1} & h_{\text{S}_1\text{R}_1} h_{\text{R}_2\text{D}_1} & h_{\text{S}_2\text{R}_1} h_{\text{R}_1\text{D}_1} & h_{\text{S}_2\text{R}_1} h_{\text{R}_2\text{D}_1} \\ h_{\text{S}_1\text{R}_1} h_{\text{R}_1\text{D}_2} & h_{\text{S}_1\text{R}_1} h_{\text{R}_2\text{D}_2} & h_{\text{S}_2\text{R}_1} h_{\text{R}_1\text{D}_2} & h_{\text{S}_2\text{R}_1} h_{\text{R}_2\text{D}_2} \\ h_{\text{S}_1\text{R}_2} h_{\text{R}_1\text{D}_1} & h_{\text{S}_1\text{R}_2} h_{\text{R}_2\text{D}_1} & h_{\text{S}_2\text{R}_2} h_{\text{R}_1\text{D}_1} & h_{\text{S}_2\text{R}_2} h_{\text{R}_2\text{D}_1} \\ h_{\text{S}_1\text{R}_2} h_{\text{R}_1\text{D}_2} & h_{\text{S}_1\text{R}_2} h_{\text{R}_2\text{D}_2} & h_{\text{S}_2\text{R}_2} h_{\text{R}_1\text{D}_2} & h_{\text{S}_2\text{R}_2} h_{\text{R}_2\text{D}_2} \end{bmatrix}. \quad (\text{A.65})$$

If the zeros in \mathbf{g} are dropped, the corresponding columns of Λ can be omitted. This delivers

$$\bar{\mathbf{g}} = \begin{bmatrix} g_1 \\ g_2 \end{bmatrix} \quad \text{and} \quad \bar{\Lambda} = \begin{bmatrix} h_{S_1R_1}h_{R_1D_1} & h_{S_2R_1}h_{R_2D_1} \\ h_{S_1R_1}h_{R_1D_2} & h_{S_2R_1}h_{R_2D_2} \\ h_{S_1R_2}h_{R_1D_1} & h_{S_2R_2}h_{R_2D_1} \\ h_{S_1R_2}h_{R_1D_2} & h_{S_2R_2}h_{R_2D_2} \end{bmatrix}. \quad (\text{A.66})$$

$\bar{\Lambda}$ is obtained from Λ by omitting the second and the third column. The vector $\tilde{\mathbf{h}}_{\text{IV}}$ can then be written as

$$\tilde{\mathbf{h}}_{\text{IV}} = \Theta \bar{\Lambda} \cdot \bar{\mathbf{g}} \quad (\text{A.67})$$

Next, the vector $\tilde{\mathbf{h}}_{\text{IV},i}$ is obtained from $\tilde{\mathbf{h}}_{\text{IV}}$ by dropping the rows corresponding to channel coefficients that contribute signal power at the destinations. It is

$$\tilde{\mathbf{h}}_{\text{IV},i} = \Theta_i \bar{\Lambda}_i \cdot \bar{\mathbf{g}}, \quad (\text{A.68})$$

where $\tilde{\mathbf{h}}_{\text{IV},i} = [\tilde{h}_{\text{IV},21} \ \tilde{h}_{\text{IV},12}]^T$ and

$$\Theta_i = \begin{bmatrix} e^{j(\varphi_{S_1} - \varphi_{D_2})} & 0 \\ 0 & e^{j(\varphi_{S_2} - \varphi_{D_1})} \end{bmatrix}, \quad \bar{\Lambda}_i = \begin{bmatrix} h_{\text{SR},11}h_{\text{RD},21} & h_{\text{SR},21}h_{\text{RD},22} \\ h_{\text{SR},12}h_{\text{RD},11} & h_{\text{SR},22}h_{\text{RD},12} \end{bmatrix}. \quad (\text{A.69})$$

A.5 Matrix Derivatives

A.5.1 Derivatives of Traces

For any matrices $\mathbf{A}, \mathbf{B} \in \mathbb{C}^{n \times n}$ it holds that [211]

$$\frac{\partial}{\partial \mathbf{B}} \text{tr}(\mathbf{AB}) = \frac{\partial}{\partial \mathbf{B}} \text{tr}(\mathbf{BA}) = \mathbf{A}^T \quad (\text{A.70})$$

and for $\mathbf{A}, \mathbf{B} \in \mathbb{C}^{n \times n}$, \mathbf{B} diagonal

$$\frac{\partial}{\partial \mathbf{B}} \text{tr}(\mathbf{AB}) = \frac{\partial}{\partial \mathbf{B}} \text{tr}(\mathbf{BA}) = \mathbf{A}^T \odot \mathbf{I} = \mathbf{A} \odot \mathbf{I}. \quad (\text{A.71})$$

A.5.2 Derivatives of Matrix Inverses

For any matrix $\mathbf{A} \in \mathbb{C}^{n \times n}$ invertible, it holds that [211]

$$\frac{\partial \mathbf{A}^{-1}}{\partial \alpha} = -\mathbf{A}^{-1} \frac{\partial \mathbf{A}}{\partial \alpha} \mathbf{A}^{-1} \quad (\text{A.72})$$

and furthermore

$$\frac{\partial \mathbf{A}^{-2}}{\partial \alpha} = -\mathbf{A}^{-1} \left(\frac{\partial \mathbf{A}}{\partial \alpha} \mathbf{A}^{-1} + \mathbf{A}^{-1} \frac{\partial \mathbf{A}}{\partial \alpha} \right) \mathbf{A}^{-1}. \quad (\text{A.73})$$

A.6 Matrix Equivalencies

For any matrices $\mathbf{A}, \mathbf{B}, \mathbf{C} \in \mathbb{C}^{n \times n}$ and $\mathbf{D}_1 = \text{diag}(\mathbf{d}_1), \mathbf{D}_2 = \text{diag}(\mathbf{d}_2) \in \mathbb{C}^{n \times n}$, the following equivalencies hold [211]:

$$\text{tr}(\mathbf{D}_1 \mathbf{A} \mathbf{D}_1^H) = \mathbf{d}_1^T (\mathbf{A} \odot \mathbf{I}) \mathbf{d}_1^* = \mathbf{d}_1^H (\mathbf{A} \odot \mathbf{I}) \mathbf{d}_1 \quad (\text{A.74})$$

$$\text{tr}(\mathbf{D}_1 \mathbf{A} \mathbf{D}_2 \mathbf{B}) = \text{tr}(\mathbf{d}_1 \mathbf{d}_2^T \cdot (\mathbf{A}^T \odot \mathbf{B})) \quad (\text{A.75})$$

$$\text{tr}(\mathbf{x} \mathbf{y}^T \mathbf{A}) = \mathbf{x}^T \mathbf{A}^T \mathbf{y}, \quad (\text{A.76})$$

where $\mathbf{x}, \mathbf{y} \in \mathbb{C}^n$ are vectors. Furthermore from $\mathbf{A} \mathbf{D}_1 \mathbf{B} \odot \mathbf{I} = \mathbf{C} \odot \mathbf{I}$ it follows that

$$\mathbf{d}_1^T = \mathbf{c}^T (\mathbf{A}^T \odot \mathbf{B})^{-1} \quad \text{and} \quad \mathbf{d}_1 = (\mathbf{A} \odot \mathbf{B}^T)^{-1} \mathbf{c}, \quad (\text{A.77})$$

where $\mathbf{c} = \text{diag}(\mathbf{C})$.

A.7 Synthesis of a Diagonal Matrix

A diagonal matrix $\mathbf{D} \in \mathbb{C}^{n \times n}$ can be constructed from a vector $\mathbf{d} \in \mathbb{C}^n$ by

$$\mathbf{D} = \sum_{i=1}^n \mathbf{E}_i \mathbf{d} \mathbf{e}_i^T = \sum_{i=1}^n \mathbf{e}_i \mathbf{d}^T \mathbf{E}_i^T = \mathbf{D}^T \quad \text{and} \quad \mathbf{D}^H = \sum_{i=1}^n \mathbf{e}_i \mathbf{d}^H \mathbf{E}_i^T, \quad (\text{A.78})$$

where

$$\mathbf{E}_i[k, l] = \begin{cases} 1 & , \quad k, l = i \\ 0 & , \quad \text{else} \end{cases}, \quad \mathbf{e}_i[k] = \begin{cases} 1 & , \quad k = i \\ 0 & , \quad \text{else} \end{cases}. \quad (\text{A.79})$$

The matrices \mathbf{E}_i and the vectors \mathbf{e}_i are of size $n \times n$ and $n \times 1$, respectively:

$$\mathbf{E}_i = \underbrace{\begin{bmatrix} 0 & & \dots & & 0 \\ & \ddots & & & \\ & & 0 & & \\ \vdots & & & 1 & \vdots \\ & & & & 0 \\ 0 & & \dots & & 0 \end{bmatrix}}_{\text{ith column}} \leftarrow \text{ith row,} \quad \text{and} \quad \mathbf{e}_i = \begin{bmatrix} 0 \\ \vdots \\ 0 \\ 1 \\ 0 \\ \vdots \\ 0 \end{bmatrix} \leftarrow \text{ith row} \quad (\text{A.80})$$

A.8 Derivative Used in Linear Relaying Scenario

The cost function ϵ as given in (6.118) is

$$\begin{aligned} \epsilon = & \text{tr}(\mathbf{R}_s) - \\ & - \text{tr} \left(\sum_{i=1}^{N_R} \left(\mathbf{R}_s \tilde{\mathbf{H}}_{\text{SR}}^H \mathbf{e}_i \tilde{\mathbf{g}}^H \mathbf{E}_i^T \tilde{\mathbf{H}}_{\text{RD}}^H \right) \right) - \text{tr} \left(\sum_{i=1}^{N_R} \left(\tilde{\mathbf{H}}_{\text{RD}} \mathbf{E}_i \tilde{\mathbf{g}} \mathbf{e}_i^T \tilde{\mathbf{H}}_{\text{SR}} \mathbf{R}_s \right) \right) + \\ & + \text{tr} \left(\tilde{\mathbf{H}}_{\text{RD}} \left(\sum_{i=1}^{N_R} \mathbf{E}_i \tilde{\mathbf{g}} \mathbf{e}_i^T \right) \tilde{\mathbf{A}} \left(\sum_{i=1}^{N_R} \mathbf{e}_i \tilde{\mathbf{g}}^H \mathbf{E}_i^T \right) \tilde{\mathbf{H}}_{\text{RD}}^H \right) + \\ & + \frac{\text{tr}(\mathbf{R}_{n_D})}{P_S} \tilde{\mathbf{g}}^H (\tilde{\mathbf{A}} \odot \mathbf{I}) \tilde{\mathbf{g}}. \end{aligned} \quad (\text{A.81})$$

In order to compute the derivative $\frac{\partial}{\partial \mu} \epsilon$ the five summands in (A.81) are investigated separately.

A.8.1 Summand 1

It is obvious that

$$\frac{\partial}{\partial \mu} \text{tr}(\mathbf{R}_s) = 0. \quad (\text{A.82})$$

A.8.2 Summand 2 and 3

The following rules for matrix derivatives are used to compute the 2nd and 3rd summand of (A.81):

$$\frac{\partial}{\partial \alpha} \text{tr}(\tilde{\mathbf{A}}) = \text{tr}\left(\frac{\partial \tilde{\mathbf{A}}}{\partial \alpha}\right) \quad (\text{A.83})$$

$$\frac{\partial}{\partial \alpha} \sum_i \tilde{\mathbf{A}}_i = \sum_i \left(\frac{\partial \tilde{\mathbf{A}}_i}{\partial \alpha}\right) \quad (\text{A.84})$$

$$\frac{\partial}{\partial \alpha} \tilde{\mathbf{A}} \tilde{\mathbf{B}}(\alpha) \tilde{\mathbf{C}} = \tilde{\mathbf{A}} \frac{\partial \tilde{\mathbf{B}}(\alpha)}{\partial \alpha} \tilde{\mathbf{C}} \quad (\text{A.85})$$

Consequently,

$$\frac{\partial}{\partial \mu} \text{tr}\left(\sum_{i=1}^{N_R} \left(\mathbf{R}_s \tilde{\mathbf{H}}_{\text{SR}}^H \mathbf{e}_i \tilde{\mathbf{g}}^H \mathbf{E}_i^T \tilde{\mathbf{H}}_{\text{RD}}^H\right)\right) = \text{tr}\left(\sum_{i=1}^{N_R} \left(\mathbf{R}_s \tilde{\mathbf{H}}_{\text{SR}}^H \mathbf{e}_i \frac{\partial \tilde{\mathbf{g}}^H}{\partial \mu} \mathbf{E}_i^T \tilde{\mathbf{H}}_{\text{RD}}^H\right)\right) \quad (\text{A.86})$$

and

$$\frac{\partial}{\partial \mu} \text{tr}\left(\sum_{i=1}^{N_R} \left(\tilde{\mathbf{H}}_{\text{RD}} \mathbf{E}_i \tilde{\mathbf{g}} \mathbf{e}_i^T \tilde{\mathbf{H}}_{\text{SR}} \mathbf{R}_s\right)\right) = \text{tr}\left(\sum_{i=1}^{N_R} \left(\tilde{\mathbf{H}}_{\text{RD}} \mathbf{E}_i \frac{\partial \tilde{\mathbf{g}}}{\partial \mu} \mathbf{e}_i^T \tilde{\mathbf{H}}_{\text{SR}} \mathbf{R}_s\right)\right). \quad (\text{A.87})$$

A.8.3 Summand 4

The chain rule of matrix derivatives, i.e. [211]

$$\frac{\partial \tilde{\mathbf{A}} \tilde{\mathbf{B}}}{\partial \alpha} = \frac{\partial \tilde{\mathbf{A}}}{\partial \alpha} \tilde{\mathbf{B}} + \tilde{\mathbf{A}} \frac{\partial \tilde{\mathbf{B}}}{\partial \alpha}, \quad (\text{A.88})$$

is applied to the 4th summand:

$$\begin{aligned} & \frac{\partial}{\partial \mu} \text{tr}\left(\tilde{\mathbf{H}}_{\text{RD}} \left(\sum_{i=1}^{N_R} \mathbf{E}_i \tilde{\mathbf{g}} \mathbf{e}_i^T\right) \tilde{\mathbf{A}} \left(\sum_{i=1}^{N_R} \mathbf{e}_i \tilde{\mathbf{g}}^H \mathbf{E}_i^T\right) \tilde{\mathbf{H}}_{\text{RD}}^H\right) = \\ & = \text{tr}\left(\tilde{\mathbf{H}}_{\text{RD}} \left(\sum_{i=1}^{N_R} \mathbf{E}_i \frac{\partial \tilde{\mathbf{g}}}{\partial \mu} \mathbf{e}_i^T\right) \tilde{\mathbf{A}} \left(\sum_{i=1}^{N_R} \mathbf{e}_i \tilde{\mathbf{g}}^H \mathbf{E}_i^T\right) \tilde{\mathbf{H}}_{\text{RD}}^H\right) + \\ & + \text{tr}\left(\tilde{\mathbf{H}}_{\text{RD}} \left(\sum_{i=1}^{N_R} \mathbf{E}_i \tilde{\mathbf{g}} \mathbf{e}_i^T\right) \tilde{\mathbf{A}} \left(\sum_{i=1}^{N_R} \mathbf{e}_i \frac{\partial \tilde{\mathbf{g}}^H}{\partial \mu} \mathbf{E}_i^T\right) \tilde{\mathbf{H}}_{\text{RD}}^H\right) \end{aligned} \quad (\text{A.89})$$

A.8.4 Summand 5

Again the chain rule (A.88) is used to get

$$\begin{aligned} \frac{\partial}{\partial \mu} \left(\frac{\text{tr}(\mathbf{R}_{\mathbf{n}_D})}{P_S} \tilde{\mathbf{g}}^H (\tilde{\mathbf{A}} \odot \mathbf{I}) \tilde{\mathbf{g}} \right) &= \frac{\text{tr}(\mathbf{R}_{\mathbf{n}_D})}{P_S} \frac{\partial \tilde{\mathbf{g}}^H}{\partial \mu} (\tilde{\mathbf{A}} \odot \mathbf{I}) \tilde{\mathbf{g}} + \\ &+ \frac{\text{tr}(\mathbf{R}_{\mathbf{n}_D})}{P_S} \tilde{\mathbf{g}}^H (\tilde{\mathbf{A}} \odot \mathbf{I}) \frac{\partial \tilde{\mathbf{g}}}{\partial \mu} \end{aligned} \quad (\text{A.90})$$

from the 5th summand.

A.8.5 Derivative of $\tilde{\mathbf{g}}$ with respect to μ

In Appendix A.8.2 to A.8.4 the derivatives $\frac{\partial \tilde{\mathbf{g}}}{\partial \mu}$ and $\frac{\partial \tilde{\mathbf{g}}^H}{\partial \mu}$ have to be computed. To this end, the following rules for the derivatives of matrices are used.

$$\frac{\partial \mathbf{A}^{-1}}{\partial \alpha} = -\mathbf{A}^{-1} \frac{\partial \mathbf{A}}{\partial \alpha} \mathbf{A}^{-1} \quad (\text{A.91})$$

$$\frac{\partial}{\partial \alpha} (\mathbf{A} \odot \mathbf{B}) = \frac{\partial \mathbf{A}}{\partial \alpha} \odot \mathbf{B} + \mathbf{A} \odot \frac{\partial \mathbf{B}}{\partial \alpha} \quad (\text{A.92})$$

The derivative of the gain vectors $\tilde{\mathbf{g}}$ with respect to μ then is

$$\begin{aligned} \frac{\partial \tilde{\mathbf{g}}}{\partial \mu} &= \frac{\partial}{\partial \mu} \left((\tilde{\mathbf{B}} \odot \tilde{\mathbf{A}}^*)^{-1} \right) \cdot \text{diag}(\tilde{\mathbf{C}}^H) = \\ &= -(\tilde{\mathbf{B}} \odot \tilde{\mathbf{A}}^*)^{-1} \left(\underbrace{\frac{\partial}{\partial \mu} \tilde{\mathbf{B}} \odot \tilde{\mathbf{A}}^*}_{=\mathbf{I}} \right) (\tilde{\mathbf{B}} \odot \tilde{\mathbf{A}}^*)^{-1} \cdot \text{diag}(\tilde{\mathbf{C}}^H) = \\ &= -(\tilde{\mathbf{B}} \odot \tilde{\mathbf{A}}^*)^{-1} (\mathbf{I} \odot \tilde{\mathbf{A}}^*) \cdot \tilde{\mathbf{g}}. \end{aligned} \quad (\text{A.93})$$

Furthermore,

$$\begin{aligned} \frac{\partial \tilde{\mathbf{g}}^H}{\partial \mu} &= \text{diag}(\tilde{\mathbf{C}})^T \cdot \frac{\partial}{\partial \mu} \left((\tilde{\mathbf{B}} \odot \tilde{\mathbf{A}}^*)^{-1} \right) = \\ &= -\text{diag}(\tilde{\mathbf{C}})^T \cdot (\tilde{\mathbf{B}} \odot \tilde{\mathbf{A}}^*)^{-1} \left(\frac{\partial}{\partial \mu} \tilde{\mathbf{B}} \odot \tilde{\mathbf{A}}^* \right) (\tilde{\mathbf{B}} \odot \tilde{\mathbf{A}}^*)^{-1} = \\ &= -\tilde{\mathbf{g}}^H \cdot (\mathbf{I} \odot \tilde{\mathbf{A}}^*) (\tilde{\mathbf{B}} \odot \tilde{\mathbf{A}}^*)^{-1}. \end{aligned} \quad (\text{A.94})$$

A.8.6 Final Result

The derivative of ϵ with respect to μ is obtained by using the results of Appendix A.8.1 to A.8.4 as well as (A.93) and (A.94):

$$\begin{aligned}
\frac{\partial \epsilon}{\partial \mu} &= -\text{tr} \left(\sum_{i=1}^{N_R} \left(\mathbf{R}_s \tilde{\mathbf{H}}_{\text{SR}}^H \mathbf{e}_i \frac{\partial \tilde{\mathbf{g}}^H}{\partial \mu} \mathbf{E}_i^T \tilde{\mathbf{H}}_{\text{RD}}^H \right) \right) - \text{tr} \left(\sum_{i=1}^{N_R} \left(\tilde{\mathbf{H}}_{\text{RD}} \mathbf{E}_i \frac{\partial \tilde{\mathbf{g}}}{\partial \mu} \mathbf{e}_i^T \tilde{\mathbf{H}}_{\text{SR}} \mathbf{R}_s \right) \right) + \\
&+ \text{tr} \left(\tilde{\mathbf{H}}_{\text{RD}} \left(\sum_{i=1}^{N_R} \mathbf{E}_i \frac{\partial \tilde{\mathbf{g}}}{\partial \mu} \mathbf{e}_i^T \right) \tilde{\mathbf{A}} \left(\sum_{i=1}^{N_R} \mathbf{e}_i \tilde{\mathbf{g}}^H \mathbf{E}_i^T \right) \tilde{\mathbf{H}}_{\text{RD}}^H \right) + \\
&+ \text{tr} \left(\tilde{\mathbf{H}}_{\text{RD}} \left(\sum_{i=1}^{N_R} \mathbf{E}_i \tilde{\mathbf{g}} \mathbf{e}_i^T \right) \tilde{\mathbf{A}} \left(\sum_{i=1}^{N_R} \mathbf{e}_i \frac{\partial \tilde{\mathbf{g}}^H}{\partial \mu} \mathbf{E}_i^T \right) \tilde{\mathbf{H}}_{\text{RD}}^H \right) + \\
&+ \frac{\text{tr}(\mathbf{R}_{\text{n}_D})}{P_S} \frac{\partial \tilde{\mathbf{g}}^H}{\partial \mu} (\tilde{\mathbf{A}} \odot \mathbf{I}) \tilde{\mathbf{g}} + \frac{\text{tr}(\mathbf{R}_{\text{n}_D})}{P_S} \tilde{\mathbf{g}}^H (\tilde{\mathbf{A}} \odot \mathbf{I}) \frac{\partial \tilde{\mathbf{g}}}{\partial \mu}. \tag{A.95}
\end{aligned}$$

This expression can be simplified considerably:

Summand 1 and 2: Inserting (A.93) and (A.94) into the first two summands of (A.95) and using the matrix equivalency

$$\text{tr}(\mathbf{X}\mathbf{D}\mathbf{Y}) = \mathbf{d}^T \cdot \text{diag}(\mathbf{X}^T \mathbf{Y}^T), \tag{A.96}$$

where $\mathbf{X}, \mathbf{Y} \in \mathbb{C}^{n \times n}$ and $\mathbf{D} = \text{diag}(\mathbf{d}) \in \mathbb{C}^{n \times n}$, delivers

$$\begin{aligned}
& - \text{tr} \left(\sum_{i=1}^{N_R} \left(\mathbf{R}_s \tilde{\mathbf{H}}_{\text{SR}}^H \mathbf{e}_i \frac{\partial \tilde{\mathbf{g}}^H}{\partial \mu} \mathbf{E}_i^T \tilde{\mathbf{H}}_{\text{RD}}^H \right) \right) - \text{tr} \left(\sum_{i=1}^{N_R} \left(\tilde{\mathbf{H}}_{\text{RD}} \mathbf{E}_i \frac{\partial \tilde{\mathbf{g}}}{\partial \mu} \mathbf{e}_i^T \tilde{\mathbf{H}}_{\text{SR}} \mathbf{R}_s \right) \right) = \\
&= - \text{tr} \left(\mathbf{R}_s \tilde{\mathbf{H}}_{\text{SR}}^H \cdot \text{diag} \left(\frac{\partial \tilde{\mathbf{g}}^H}{\partial \mu} \right) \cdot \tilde{\mathbf{H}}_{\text{RD}}^H \right) - \text{tr} \left(\tilde{\mathbf{H}}_{\text{RD}} \cdot \text{diag} \left(\frac{\partial \tilde{\mathbf{g}}}{\partial \mu} \right) \cdot \tilde{\mathbf{H}}_{\text{SR}} \mathbf{R}_s \right) = \\
&= - \text{tr} \left(\mathbf{R}_s \tilde{\mathbf{H}}_{\text{SR}}^H \text{diag} \left(-\text{diag}(\tilde{\mathbf{C}})^T (\tilde{\mathbf{B}} \odot \tilde{\mathbf{A}}^*)^{-1} (\mathbf{I} \odot \tilde{\mathbf{A}}^*) (\tilde{\mathbf{B}} \odot \tilde{\mathbf{A}}^*)^{-1} \right) \tilde{\mathbf{H}}_{\text{RD}}^H \right) - \\
& - \text{tr} \left(\tilde{\mathbf{H}}_{\text{RD}} \text{diag} \left(-(\tilde{\mathbf{B}} \odot \tilde{\mathbf{A}}^*)^{-1} (\mathbf{I} \odot \tilde{\mathbf{A}}^*) (\tilde{\mathbf{B}} \odot \tilde{\mathbf{A}}^*)^{-1} \text{diag}(\tilde{\mathbf{C}}^H) \right) \tilde{\mathbf{H}}_{\text{SR}} \mathbf{R}_s \right) = \\
&= \text{diag}(\tilde{\mathbf{C}})^T (\tilde{\mathbf{B}} \odot \tilde{\mathbf{A}}^*)^{-1} (\mathbf{I} \odot \tilde{\mathbf{A}}^*) (\tilde{\mathbf{B}} \odot \tilde{\mathbf{A}}^*)^{-1} \text{diag}(\tilde{\mathbf{H}}_{\text{SR}}^* \mathbf{R}_s \tilde{\mathbf{H}}_{\text{RD}}^*) + \\
& + \text{diag}(\tilde{\mathbf{C}}^H)^T (\tilde{\mathbf{B}}^T \odot \tilde{\mathbf{A}}^H)^{-1} (\mathbf{I} \odot \tilde{\mathbf{A}}^H) (\tilde{\mathbf{B}}^T \odot \tilde{\mathbf{A}}^H)^{-1} \text{diag}(\tilde{\mathbf{H}}_{\text{RD}}^T \mathbf{R}_s \tilde{\mathbf{H}}_{\text{SR}}^T) = \\
&= 2 \cdot \text{diag}(\tilde{\mathbf{C}})^T (\tilde{\mathbf{B}} \odot \tilde{\mathbf{A}}^*)^{-1} \cdot (\mathbf{I} \odot \tilde{\mathbf{A}}^*) \cdot (\tilde{\mathbf{B}} \odot \tilde{\mathbf{A}}^*)^{-1} \text{diag}(\tilde{\mathbf{C}}^H) = \\
&= 2 \cdot \tilde{\mathbf{g}}^H (\mathbf{I} \odot \tilde{\mathbf{A}}^*) \tilde{\mathbf{g}}. \tag{A.97}
\end{aligned}$$

Summand 3 and 4: In order to simplify the 3rd and 4th summand of (A.95) the matrix equality

$$\text{tr}(\mathbf{D}_1 \mathbf{X} \mathbf{D}_2 \mathbf{Y}) = \text{tr}(\mathbf{d}_1 \mathbf{d}_2^T \cdot (\mathbf{X}^T \odot \mathbf{Y})) \quad (\text{A.98})$$

is used, where $\mathbf{X}, \mathbf{Y} \in \mathbb{C}^{n \times n}$, $\mathbf{D}_1 = \text{diag}(\mathbf{d}_1)$, $\mathbf{D}_2 = \text{diag}(\mathbf{d}_2) \in \mathbb{C}^{n \times n}$. Furthermore,

$$\text{tr}(\mathbf{u} \mathbf{v}^T \mathbf{X}) = \mathbf{u}^T \mathbf{X}^T \mathbf{v}. \quad (\text{A.99})$$

Consequently,

$$\begin{aligned} & \text{tr} \left(\tilde{\mathbf{H}}_{\text{RD}} \left(\sum_{i=1}^{N_{\text{R}}} \mathbf{E}_i \frac{\partial \tilde{\mathbf{g}}}{\partial \mu} \mathbf{e}_i^T \right) \tilde{\mathbf{A}} \left(\sum_{i=1}^{N_{\text{R}}} \mathbf{e}_i \tilde{\mathbf{g}}^H \mathbf{E}_i^T \right) \tilde{\mathbf{H}}_{\text{RD}}^H \right) = \\ &= \text{tr} \left(\tilde{\mathbf{H}}_{\text{RD}} \cdot \text{diag} \left(\frac{\partial \tilde{\mathbf{g}}}{\partial \mu} \right) \cdot \tilde{\mathbf{A}} \cdot \text{diag}(\tilde{\mathbf{g}}^H) \cdot \tilde{\mathbf{H}}_{\text{RD}}^H \right) = \\ &= \text{tr} \left(\text{diag} \left(\frac{\partial \tilde{\mathbf{g}}}{\partial \mu} \right) \cdot \tilde{\mathbf{A}} \cdot \text{diag}(\tilde{\mathbf{g}}^H) \cdot \tilde{\mathbf{H}}_{\text{RD}}^H \tilde{\mathbf{H}}_{\text{RD}} \right) = \\ &= \text{tr} \left(\frac{\partial \tilde{\mathbf{g}}}{\partial \mu} \cdot \tilde{\mathbf{g}}^H \cdot \left(\tilde{\mathbf{A}}^T \odot \tilde{\mathbf{H}}_{\text{RD}}^H \tilde{\mathbf{H}}_{\text{RD}} \right) \right) = \\ &= \text{tr} \left(- \left(\tilde{\mathbf{B}} \odot \tilde{\mathbf{A}}^* \right)^{-1} \left(\mathbf{I} \odot \tilde{\mathbf{A}}^* \right) \tilde{\mathbf{g}} \cdot \tilde{\mathbf{g}}^H \cdot \left(\tilde{\mathbf{A}}^T \odot \tilde{\mathbf{H}}_{\text{RD}}^H \tilde{\mathbf{H}}_{\text{RD}} \right) \right) = \\ &= - \text{tr} \left(\tilde{\mathbf{g}} \cdot \tilde{\mathbf{g}}^H \cdot \left(\tilde{\mathbf{A}}^T \odot \tilde{\mathbf{H}}_{\text{RD}}^H \tilde{\mathbf{H}}_{\text{RD}} \right) \left(\tilde{\mathbf{B}} \odot \tilde{\mathbf{A}}^* \right)^{-1} \left(\mathbf{I} \odot \tilde{\mathbf{A}}^* \right) \right) = \\ &= - \text{tr} \left(\tilde{\mathbf{g}} \cdot \tilde{\mathbf{g}}^H \cdot \left(\tilde{\mathbf{A}}^T \odot \left(\tilde{\mathbf{H}}_{\text{RD}}^H \tilde{\mathbf{H}}_{\text{RD}} + \mu \mathbf{I} - \mu \mathbf{I} \right) \right) \left(\tilde{\mathbf{B}} \odot \tilde{\mathbf{A}}^* \right)^{-1} \left(\mathbf{I} \odot \tilde{\mathbf{A}}^* \right) \right) = \\ &= - \text{tr} \left(\tilde{\mathbf{g}} \cdot \tilde{\mathbf{g}}^H \cdot \left(\underbrace{\left(\tilde{\mathbf{A}}^T \odot \tilde{\mathbf{B}} \right)}_{= (\tilde{\mathbf{B}} \odot \tilde{\mathbf{A}}^*)} - \left(\tilde{\mathbf{A}}^T \odot \mu \mathbf{I} \right) \right) \left(\tilde{\mathbf{B}} \odot \tilde{\mathbf{A}}^* \right)^{-1} \left(\mathbf{I} \odot \tilde{\mathbf{A}}^* \right) \right) = \\ &= - \text{tr} \left(\tilde{\mathbf{g}} \cdot \tilde{\mathbf{g}}^H \left(\mathbf{I} \odot \tilde{\mathbf{A}}^* \right) \right) + \text{tr} \left(\tilde{\mathbf{g}} \cdot \tilde{\mathbf{g}}^H \cdot \left(\tilde{\mathbf{A}}^T \odot \mu \mathbf{I} \right) \left(\tilde{\mathbf{B}} \odot \tilde{\mathbf{A}}^* \right)^{-1} \left(\mathbf{I} \odot \tilde{\mathbf{A}}^* \right) \right) = \\ &= - \tilde{\mathbf{g}}^T \left(\mathbf{I} \odot \tilde{\mathbf{A}}^H \right) \tilde{\mathbf{g}}^* + \tilde{\mathbf{g}}^T \left(\mathbf{I} \odot \tilde{\mathbf{A}}^H \right) \left(\tilde{\mathbf{B}}^T \odot \tilde{\mathbf{A}}^H \right)^{-1} \left(\tilde{\mathbf{A}} \odot \mu \mathbf{I} \right) \tilde{\mathbf{g}}^* = \\ &= - \tilde{\mathbf{g}}^H \left(\mathbf{I} \odot \tilde{\mathbf{A}}^* \right) \tilde{\mathbf{g}} + \tilde{\mathbf{g}}^H \left(\tilde{\mathbf{A}}^T \odot \mu \mathbf{I} \right) \left(\tilde{\mathbf{B}} \odot \tilde{\mathbf{A}}^* \right)^{-1} \left(\mathbf{I} \odot \tilde{\mathbf{A}}^* \right) \tilde{\mathbf{g}} = \\ &= - \tilde{\mathbf{g}}^H \left(\mathbf{I} \odot \tilde{\mathbf{A}}^* \right) \tilde{\mathbf{g}} - \tilde{\mathbf{g}}^H \left(\tilde{\mathbf{A}}^T \odot \mu \mathbf{I} \right) \frac{\partial \tilde{\mathbf{g}}}{\partial \mu}. \end{aligned} \quad (\text{A.100})$$

Summand 4 can be simplified in the same manner:

$$\begin{aligned} & \text{tr} \left(\tilde{\mathbf{H}}_{\text{RD}} \left(\sum_{i=1}^{N_{\text{R}}} \mathbf{E}_i \tilde{\mathbf{g}} \mathbf{e}_i^{\text{T}} \right) \tilde{\mathbf{A}} \left(\sum_{i=1}^{N_{\text{R}}} \mathbf{e}_i \frac{\partial \tilde{\mathbf{g}}^{\text{H}}}{\partial \mu} \mathbf{E}_i^{\text{T}} \right) \tilde{\mathbf{H}}_{\text{RD}}^{\text{H}} \right) = \\ & = -\tilde{\mathbf{g}}^{\text{H}} \left(\mathbf{I} \odot \tilde{\mathbf{A}}^* \right) \tilde{\mathbf{g}} - \frac{\partial \tilde{\mathbf{g}}^{\text{H}}}{\partial \mu} \left(\tilde{\mathbf{A}}^{\text{T}} \odot \mu \mathbf{I} \right) \tilde{\mathbf{g}}. \end{aligned} \quad (\text{A.101})$$

Inserting (A.97) – (A.101) into (A.95) finally yields

$$\begin{aligned} \frac{\partial \epsilon}{\partial \mu} &= 2\tilde{\mathbf{g}}^{\text{H}} \left(\mathbf{I} \odot \tilde{\mathbf{A}}^* \right) \tilde{\mathbf{g}} - \\ & - \tilde{\mathbf{g}}^{\text{H}} \left(\mathbf{I} \odot \tilde{\mathbf{A}}^* \right) \tilde{\mathbf{g}} - \tilde{\mathbf{g}}^{\text{H}} \left(\tilde{\mathbf{A}}^{\text{T}} \odot \mu \mathbf{I} \right) \frac{\partial \tilde{\mathbf{g}}}{\partial \mu} - \\ & - \tilde{\mathbf{g}}^{\text{H}} \left(\mathbf{I} \odot \tilde{\mathbf{A}}^* \right) \tilde{\mathbf{g}} - \frac{\partial \tilde{\mathbf{g}}^{\text{H}}}{\partial \mu} \left(\tilde{\mathbf{A}}^{\text{T}} \odot \mu \mathbf{I} \right) \tilde{\mathbf{g}} + \\ & + \frac{\text{tr}(\mathbf{R}_{\text{n}_D})}{P_{\text{S}}} \frac{\partial \tilde{\mathbf{g}}^{\text{H}}}{\partial \mu} \left(\tilde{\mathbf{A}} \odot \mathbf{I} \right) \tilde{\mathbf{g}} + \frac{\text{tr}(\mathbf{R}_{\text{n}_D})}{P_{\text{S}}} \tilde{\mathbf{g}}^{\text{H}} \left(\tilde{\mathbf{A}} \odot \mathbf{I} \right) \frac{\partial \tilde{\mathbf{g}}}{\partial \mu} = \\ & = -\tilde{\mathbf{g}}^{\text{H}} \left(\tilde{\mathbf{A}}^{\text{T}} \odot \mu \mathbf{I} \right) \frac{\partial \tilde{\mathbf{g}}}{\partial \mu} - \frac{\partial \tilde{\mathbf{g}}^{\text{H}}}{\partial \mu} \left(\tilde{\mathbf{A}}^{\text{T}} \odot \mu \mathbf{I} \right) \tilde{\mathbf{g}} + \\ & + \tilde{\mathbf{g}}^{\text{H}} \left(\tilde{\mathbf{A}} \odot \frac{\text{tr}(\mathbf{R}_{\text{n}_D})}{P_{\text{S}}} \mathbf{I} \right) \frac{\partial \tilde{\mathbf{g}}}{\partial \mu} + \frac{\partial \tilde{\mathbf{g}}^{\text{H}}}{\partial \mu} \left(\tilde{\mathbf{A}} \odot \frac{\text{tr}(\mathbf{R}_{\text{n}_D})}{P_{\text{S}}} \mathbf{I} \right) \tilde{\mathbf{g}}. \end{aligned} \quad (\text{A.102})$$

A.9 Derivative Used in LDAS Scenario

The cost function ϵ for the special case that $\mathbf{\Gamma} = \gamma^{-1} \mathbf{I}$ is given in (6.149). Using $\tilde{\mathbf{G}}$ from (6.145) delivers

$$\begin{aligned} \epsilon &= \text{E} \left[\left\| \mathbf{s} - \tilde{\mathbf{H}}_{\text{RD}} \tilde{\mathbf{G}} \tilde{\mathbf{H}}_{\text{SR}} \mathbf{s} - \tilde{\mathbf{H}}_{\text{RD}} \tilde{\mathbf{G}} \mathbf{n}_{\text{R}} - \gamma^{-1} \mathbf{n}_{\text{D}} \right\|_2^2 \right] = \\ &= \text{E} \left[\left\| \mathbf{s} - \tilde{\mathbf{H}}_{\text{RD}} \tilde{\mathbf{B}}^{-1} \tilde{\mathbf{C}}^{\text{H}} \tilde{\mathbf{A}}^{-\text{H}} \tilde{\mathbf{H}}_{\text{SR}} \mathbf{s} - \tilde{\mathbf{H}}_{\text{RD}} \tilde{\mathbf{B}}^{-1} \tilde{\mathbf{C}}^{\text{H}} \tilde{\mathbf{A}}^{-\text{H}} \mathbf{n}_{\text{R}} - \gamma^{-1} \mathbf{n}_{\text{D}} \right\|_2^2 \right]. \end{aligned} \quad (\text{A.103})$$

Expanding the norm and taking the expectation delivers

$$\begin{aligned}
\epsilon &= \text{tr}(\mathbf{R}_s) - \\
&\quad - \text{tr}\left(\mathbf{R}_s \tilde{\mathbf{H}}_{\text{SR}}^H \tilde{\mathbf{A}}^{-1} \tilde{\mathbf{C}} \tilde{\mathbf{B}}^{-H} \tilde{\mathbf{H}}_{\text{RD}}^H\right) - \text{tr}\left(\tilde{\mathbf{H}}_{\text{RD}} \tilde{\mathbf{B}}^{-1} \tilde{\mathbf{C}}^H \tilde{\mathbf{A}}^{-H} \tilde{\mathbf{H}}_{\text{SR}} \mathbf{R}_s\right) + \\
&\quad + \text{tr}\left(\tilde{\mathbf{H}}_{\text{RD}} \tilde{\mathbf{B}}^{-1} \tilde{\mathbf{C}}^H \tilde{\mathbf{A}}^{-H} \tilde{\mathbf{H}}_{\text{SR}} \mathbf{R}_s \tilde{\mathbf{H}}_{\text{SR}}^H \tilde{\mathbf{A}}^{-1} \tilde{\mathbf{C}} \tilde{\mathbf{B}}^{-H} \tilde{\mathbf{H}}_{\text{RD}}^H\right) + \\
&\quad + \text{tr}\left(\tilde{\mathbf{H}}_{\text{RD}} \tilde{\mathbf{B}}^{-1} \tilde{\mathbf{C}}^H \tilde{\mathbf{A}}^{-H} \mathbf{R}_{n_r} \tilde{\mathbf{A}}^{-1} \tilde{\mathbf{C}} \tilde{\mathbf{B}}^{-H} \tilde{\mathbf{H}}_{\text{RD}}^H\right) + \\
&\quad + \frac{\text{tr}(\mathbf{R}_{n_D})}{P_S} \text{tr}\left(\tilde{\mathbf{B}}^{-1} \tilde{\mathbf{C}}^H \tilde{\mathbf{A}}^{-H} \cdot \tilde{\mathbf{A}} \cdot \tilde{\mathbf{A}}^{-1} \tilde{\mathbf{C}} \tilde{\mathbf{B}}^{-H}\right) = \\
&= \text{tr}(\mathbf{R}_s) - \\
&\quad - \text{tr}\left(\tilde{\mathbf{B}}^{-1} \tilde{\mathbf{C}}^H \tilde{\mathbf{A}}^{-1} \tilde{\mathbf{C}}\right) - \text{tr}\left(\tilde{\mathbf{B}}^{-1} \tilde{\mathbf{C}}^H \tilde{\mathbf{A}}^{-H} \tilde{\mathbf{C}}\right) + \\
&\quad + \text{tr}\left(\tilde{\mathbf{H}}_{\text{RD}} \tilde{\mathbf{B}}^{-1} \tilde{\mathbf{C}}^H \tilde{\mathbf{A}}^{-H} \cdot \tilde{\mathbf{A}} \cdot \tilde{\mathbf{A}}^{-1} \tilde{\mathbf{C}} \tilde{\mathbf{B}}^{-H} \tilde{\mathbf{H}}_{\text{RD}}^H\right) + \\
&\quad + \frac{\text{tr}(\mathbf{R}_{n_D})}{P_S} \text{tr}\left(\tilde{\mathbf{B}}^{-2} \tilde{\mathbf{C}}^H \tilde{\mathbf{A}}^{-H} \tilde{\mathbf{C}}\right), \tag{A.104}
\end{aligned}$$

where $\tilde{\mathbf{B}} = \tilde{\mathbf{B}}^H$ and

$$\gamma^{-1} = \sqrt{\frac{\text{tr}\left(\tilde{\mathbf{G}} \tilde{\mathbf{A}} \tilde{\mathbf{G}}^H\right)}{P_S}}. \tag{A.105}$$

were used. The second last line of (A.104) can be rewritten by using (e.g. [211])

$$\mathbf{X} (\mathbf{X}^H \mathbf{X} + \xi \mathbf{I}_m)^{-1} = (\mathbf{X} \mathbf{X}^H + \xi \mathbf{I}_n)^{-1} \mathbf{X} \tag{A.106}$$

$$\mathbf{X}^H (\mathbf{X} \mathbf{X}^H + \xi \mathbf{I}_n)^{-1} = (\mathbf{X}^H \mathbf{X} + \xi \mathbf{I}_m)^{-1} \mathbf{X}^H, \tag{A.107}$$

where $\mathbf{X} \in \mathbb{C}^{n \times m}$. We get

$$\begin{aligned}
 & \text{tr} \left(\tilde{\mathbf{H}}_{\text{RD}} \tilde{\mathbf{B}}^{-1} \tilde{\mathbf{C}}^{\text{H}} \tilde{\mathbf{A}}^{-\text{H}} \tilde{\mathbf{C}} \tilde{\mathbf{B}}^{-\text{H}} \tilde{\mathbf{H}}_{\text{RD}}^{\text{H}} \right) = \\
 & = \text{tr} \left(\tilde{\mathbf{H}}_{\text{RD}} \left(\tilde{\mathbf{H}}_{\text{RD}}^{\text{H}} \tilde{\mathbf{H}}_{\text{RD}} + \mu \mathbf{I} \right)^{-1} \tilde{\mathbf{C}}^{\text{H}} \tilde{\mathbf{A}}^{-\text{H}} \tilde{\mathbf{C}} \left(\tilde{\mathbf{H}}_{\text{RD}}^{\text{H}} \tilde{\mathbf{H}}_{\text{RD}} + \mu \mathbf{I} \right)^{-1} \tilde{\mathbf{H}}_{\text{RD}}^{\text{H}} \right) = \\
 & = \text{tr} \left(\left(\tilde{\mathbf{H}}_{\text{RD}}^{\text{H}} \tilde{\mathbf{H}}_{\text{RD}} + \mu \mathbf{I} \right)^{-1} \tilde{\mathbf{H}}_{\text{RD}} \tilde{\mathbf{C}}^{\text{H}} \tilde{\mathbf{A}}^{-\text{H}} \tilde{\mathbf{C}} \left(\tilde{\mathbf{H}}_{\text{RD}}^{\text{H}} \tilde{\mathbf{H}}_{\text{RD}} + \mu \mathbf{I} \right)^{-1} \tilde{\mathbf{H}}_{\text{RD}}^{\text{H}} \right) = \\
 & = \text{tr} \left(\tilde{\mathbf{C}}^{\text{H}} \tilde{\mathbf{A}}^{-\text{H}} \tilde{\mathbf{C}} \left(\tilde{\mathbf{H}}_{\text{RD}}^{\text{H}} \tilde{\mathbf{H}}_{\text{RD}} + \mu \mathbf{I} \right)^{-1} \tilde{\mathbf{H}}_{\text{RD}}^{\text{H}} \left(\tilde{\mathbf{H}}_{\text{RD}}^{\text{H}} \tilde{\mathbf{H}}_{\text{RD}} + \mu \mathbf{I} \right)^{-1} \tilde{\mathbf{H}}_{\text{RD}} \right) = \\
 & = \text{tr} \left(\tilde{\mathbf{C}}^{\text{H}} \tilde{\mathbf{A}}^{-\text{H}} \tilde{\mathbf{C}} \left(\tilde{\mathbf{H}}_{\text{RD}}^{\text{H}} \tilde{\mathbf{H}}_{\text{RD}} + \mu \mathbf{I} \right)^{-1} \left(\tilde{\mathbf{H}}_{\text{RD}}^{\text{H}} \tilde{\mathbf{H}}_{\text{RD}} + \mu \mathbf{I} \right)^{-1} \tilde{\mathbf{H}}_{\text{RD}}^{\text{H}} \tilde{\mathbf{H}}_{\text{RD}} \right) = \\
 & = \text{tr} \left(\left(\tilde{\mathbf{H}}_{\text{RD}}^{\text{H}} \tilde{\mathbf{H}}_{\text{RD}} + \mu \mathbf{I} \right)^{-2} \tilde{\mathbf{H}}_{\text{RD}}^{\text{H}} \tilde{\mathbf{H}}_{\text{RD}} \tilde{\mathbf{C}}^{\text{H}} \tilde{\mathbf{A}}^{-\text{H}} \tilde{\mathbf{C}} \right). \tag{A.108}
 \end{aligned}$$

The cost function ϵ only depends on μ . Inserting (A.108) into (A.104) and taking the derivative with respect to μ delivers

$$\begin{aligned}
 \frac{\partial \epsilon}{\partial \mu} &= \frac{\partial}{\partial \mu} \left(\text{tr}(\mathbf{R}_{\text{s}}) - 2 \text{tr} \left(\tilde{\mathbf{B}}^{-1} \tilde{\mathbf{C}}^{\text{H}} \tilde{\mathbf{A}}^{-1} \tilde{\mathbf{C}} \right) + \right. \\
 & \quad \left. + \text{tr} \left(\tilde{\mathbf{B}}^{-2} \tilde{\mathbf{H}}_{\text{RD}}^{\text{H}} \tilde{\mathbf{H}}_{\text{RD}} \tilde{\mathbf{C}}^{\text{H}} \tilde{\mathbf{A}}^{-\text{H}} \tilde{\mathbf{C}} \right) + \frac{\text{tr}(\mathbf{R}_{\text{n}_D})}{P_{\text{S}}} \text{tr} \left(\tilde{\mathbf{B}}^{-2} \tilde{\mathbf{C}}^{\text{H}} \tilde{\mathbf{A}}^{-\text{H}} \tilde{\mathbf{C}} \right) \right) = \\
 & = 2 \text{tr} \left(\tilde{\mathbf{B}}^{-2} \tilde{\mathbf{C}}^{\text{H}} \tilde{\mathbf{A}}^{-1} \tilde{\mathbf{C}} \right) - 2 \text{tr} \left(\tilde{\mathbf{B}}^{-3} \tilde{\mathbf{H}}_{\text{RD}}^{\text{H}} \tilde{\mathbf{H}}_{\text{RD}} \tilde{\mathbf{C}}^{\text{H}} \tilde{\mathbf{A}}^{-\text{H}} \tilde{\mathbf{C}} \right) - \\
 & \quad - \frac{2 \text{tr}(\mathbf{R}_{\text{n}_D})}{P_{\text{S}}} \text{tr} \left(\tilde{\mathbf{B}}^{-3} \tilde{\mathbf{C}}^{\text{H}} \tilde{\mathbf{A}}^{-\text{H}} \tilde{\mathbf{C}} \right) = \\
 & = 2 \text{tr} \left(\tilde{\mathbf{B}}^{-3} \left(\tilde{\mathbf{B}} - \tilde{\mathbf{H}}_{\text{RD}}^{\text{H}} \tilde{\mathbf{H}}_{\text{RD}} - \frac{\text{tr}(\mathbf{R}_{\text{n}_D})}{P_{\text{S}}} \mathbf{I} \right) \tilde{\mathbf{C}}^{\text{H}} \tilde{\mathbf{A}}^{-1} \tilde{\mathbf{C}} \right), \tag{A.109}
 \end{aligned}$$

where

$$\begin{aligned}
 \frac{\partial}{\partial \mu} \tilde{\mathbf{B}}^{-1} &= \frac{\partial}{\partial \mu} \left(\tilde{\mathbf{H}}_{\text{RD}}^{\text{H}} \tilde{\mathbf{H}}_{\text{RD}} + \mu \mathbf{I} \right)^{-1} = \\
 &= - \left(\tilde{\mathbf{H}}_{\text{RD}}^{\text{H}} \tilde{\mathbf{H}}_{\text{RD}} + \mu \mathbf{I} \right)^{-2} \tag{A.110}
 \end{aligned}$$

and

$$\begin{aligned} \frac{\partial}{\partial \mu} \tilde{\mathbf{B}}^{-2} &= \frac{\partial}{\partial \mu} \left(\tilde{\mathbf{H}}_{\text{RD}}^{\text{H}} \tilde{\mathbf{H}}_{\text{RD}} + \mu \mathbf{I} \right)^{-2} = \\ &= -2 \left(\tilde{\mathbf{H}}_{\text{RD}}^{\text{H}} \tilde{\mathbf{H}}_{\text{RD}} + \mu \mathbf{I} \right)^{-3} \end{aligned} \quad (\text{A.111})$$

were used.

A.10 RACooN Channel Measurements

A.10.1 rms Delay Spread

Some typical examples of estimated delay power spectral densities in the open office environment are depicted in Fig. A.2. In Fig. A.3 the estimated noise floors and identified relevant paths are plotted for the same transmitter-receiver pairs as in Fig. A.2. Fig. A.4 depicts typical examples of the delay power spectral density of two-hop links in the open office scenario. Only the previously identified relevant paths are considered.

A.10.2 Coherence Bandwidth

In Fig. A.5 and A.6 the frequency correlation functions $|r_{\tau\tau}(\tau)|$ of some of the single-hop and two-hop channels in the open office scenario are depicted. The considered frequency bin is located at $f = -20.32$ MHz for all figures. The coherence bandwidth can be computed for every frequency f from the frequency correlation functions. In Fig. A.7 and A.8 the computed coherence bandwidths over the whole frequency range of 80 MHz are shown for $K = 0.9$. Some typical single-hop and two-hop links in the open office scenario have been considered.

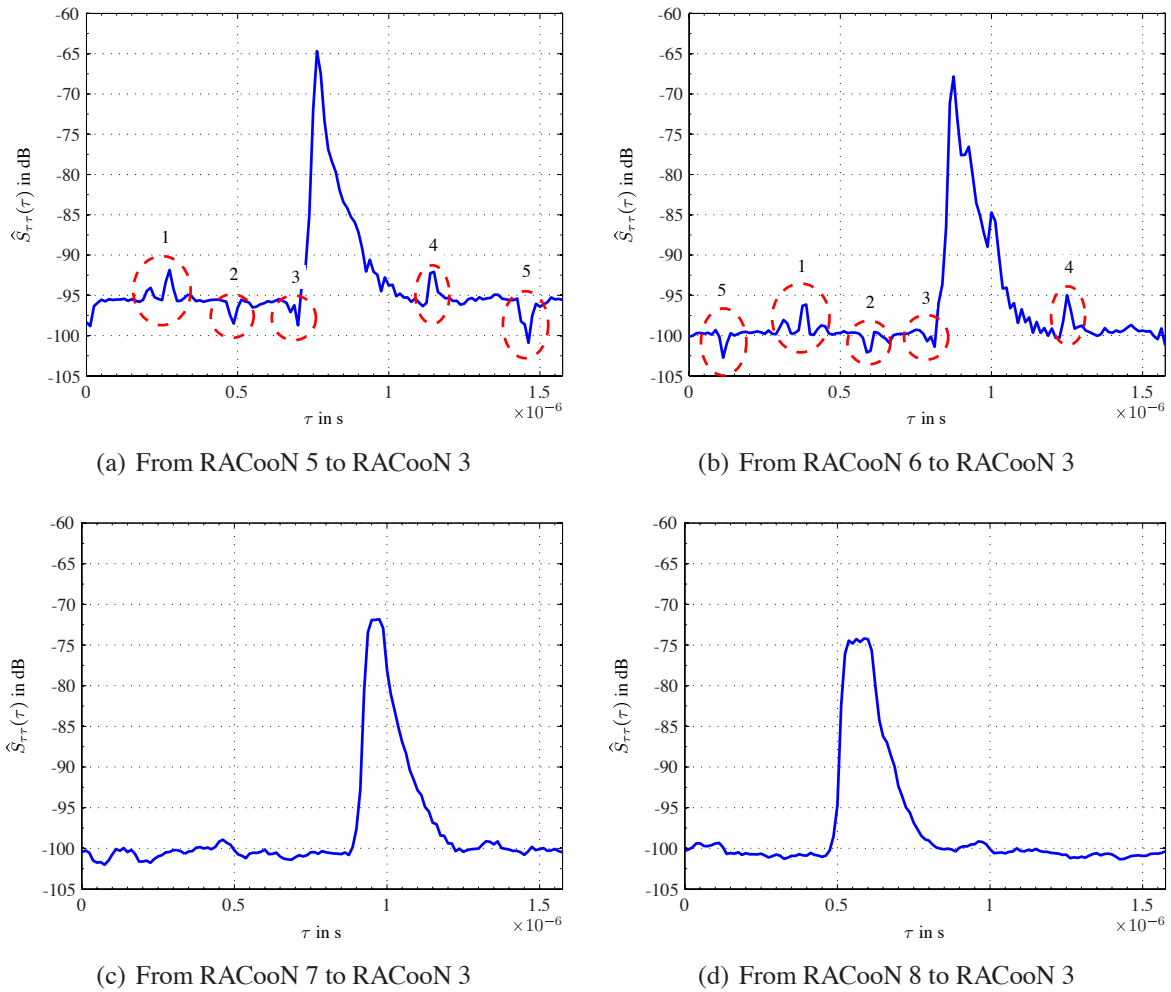


Fig. A.2: Measured delay power spectral densities in the open office scenario. A characteristic shape of the noise floor can be observed (indicated by the dashed circles in (a) and (b)).

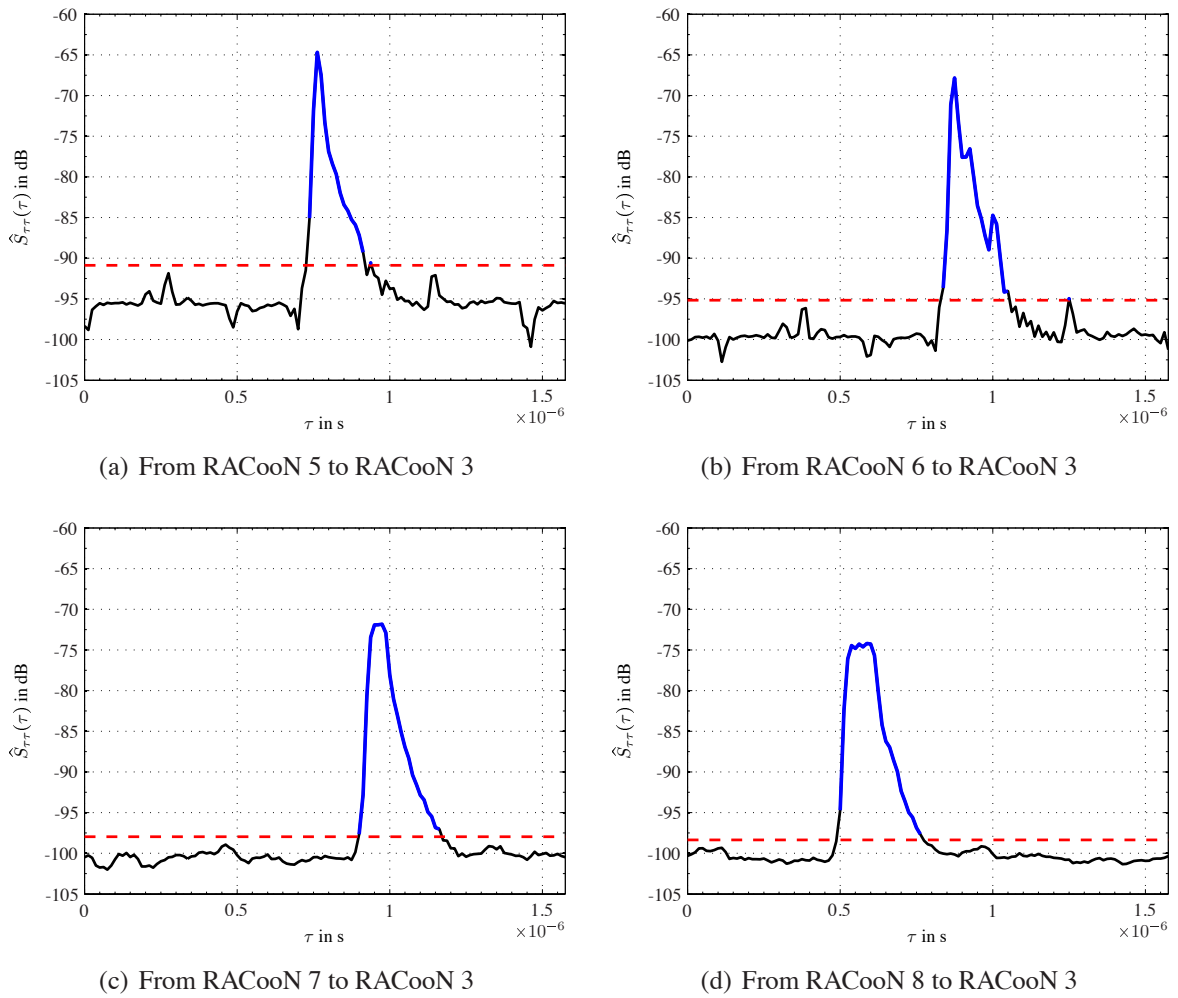
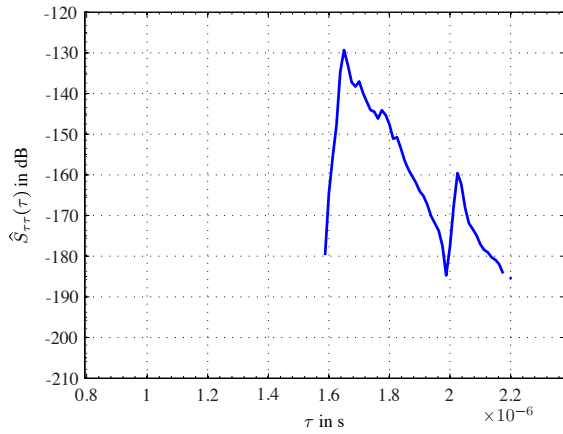
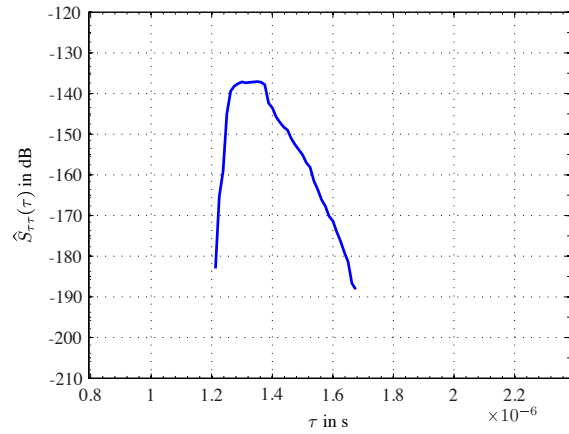


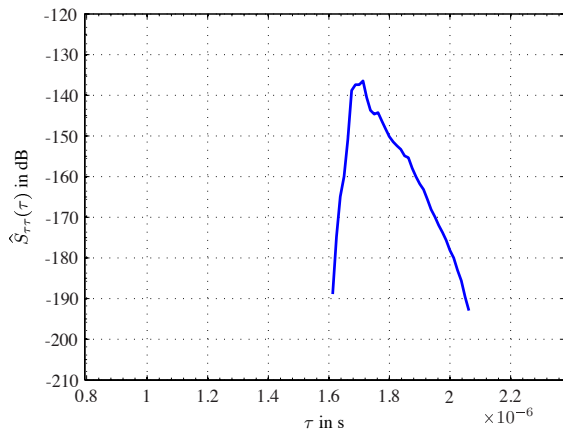
Fig. A.3: Measured delay power spectral densities with noise floor (dashed, red line) and identified relevant paths (drawn in blue) in the open office scenario.



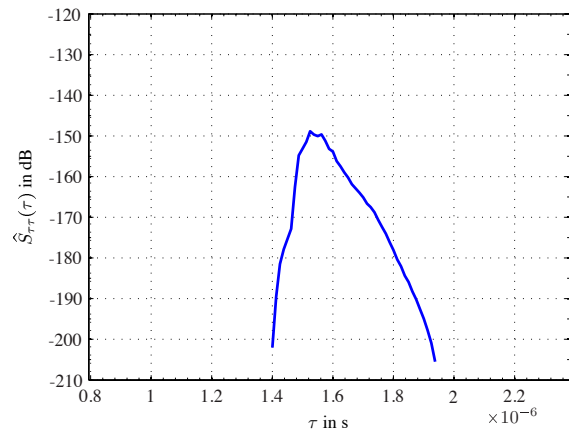
(a) From RACooN 5 via RACooN 3 to RACooN 6



(b) From RACooN 6 via RACooN 4 to RACooN 8



(c) From RACooN 7 via RACooN 2 to RACooN 5



(d) From RACooN 8 via RACooN 1 to RACooN 7

Fig. A.4: Measured delay power spectral densities for some two-hop channels in the open office scenario.

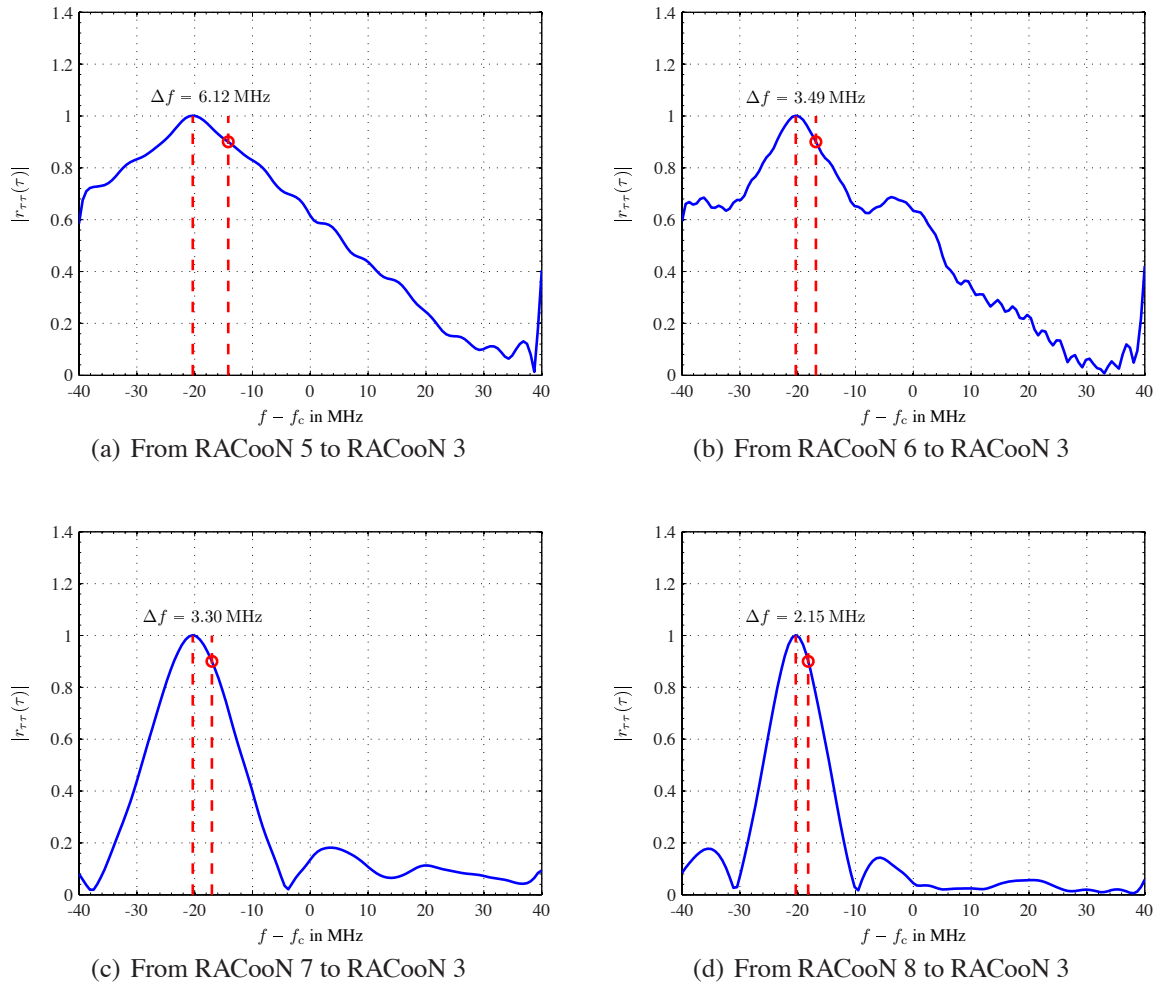
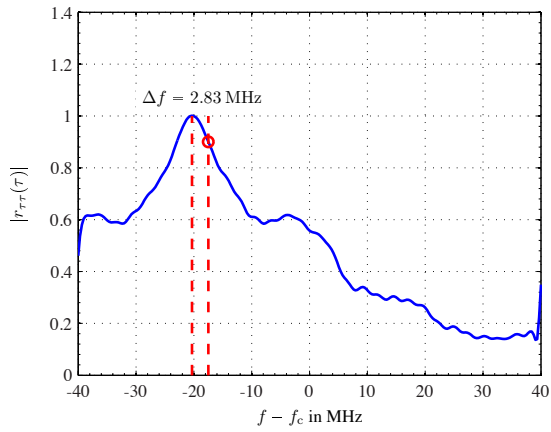
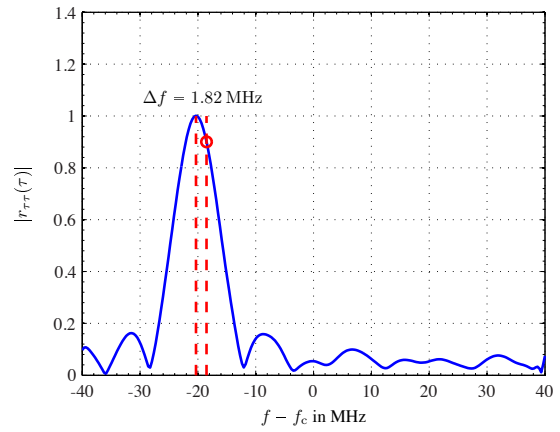


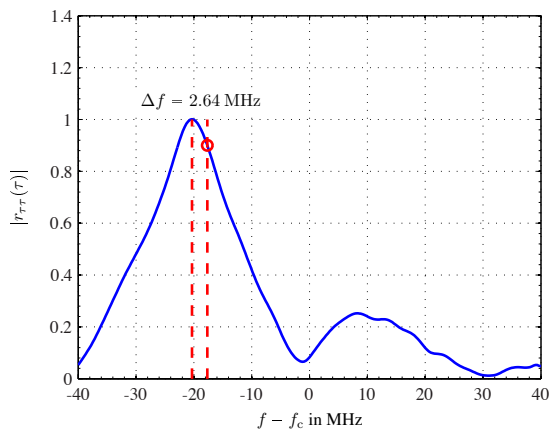
Fig. A.5: Estimated frequency correlation functions at $f = -20.32$ MHz in the open office scenario for some single-hop links.



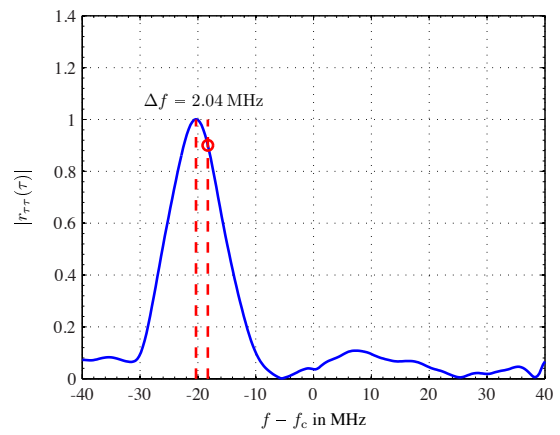
(a) From RACooN 5 via RACooN 3 to RACooN 6



(b) From RACooN 6 via RACooN 4 to RACooN 8



(c) From RACooN 7 via RACooN 2 to RACooN 5



(d) From RACooN 8 via RACooN 1 to RACooN 7

Fig. A.6: Estimated frequency correlation functions at $f = -20.32$ MHz in the open office scenario for some two-hop links.

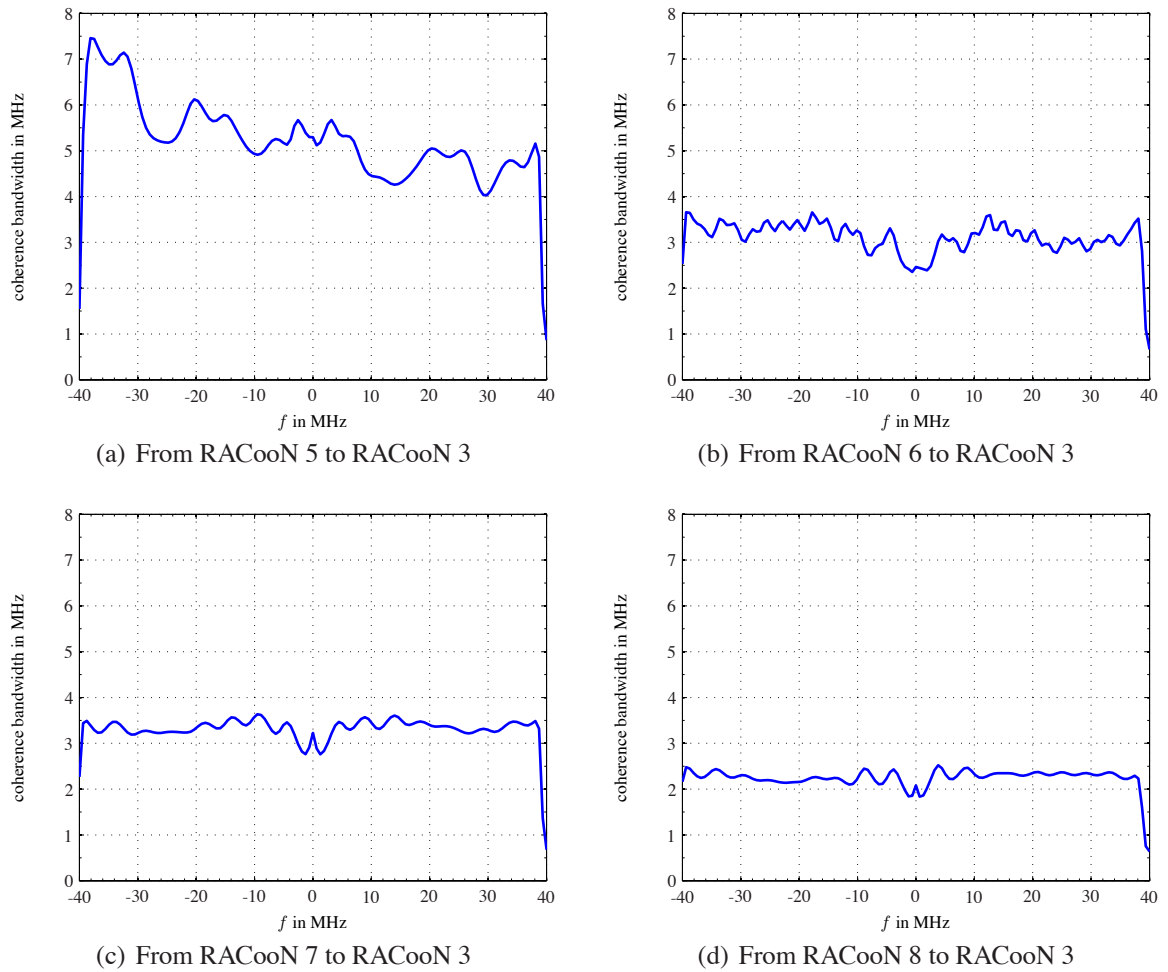
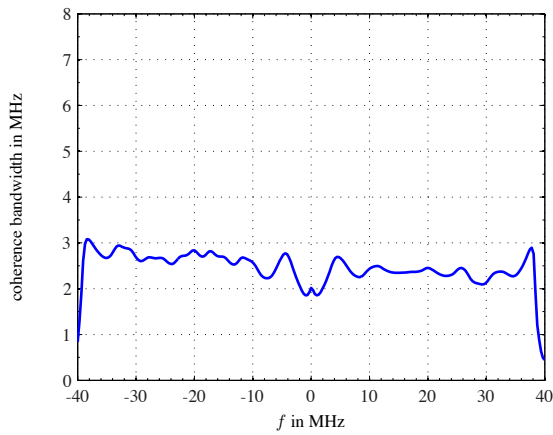
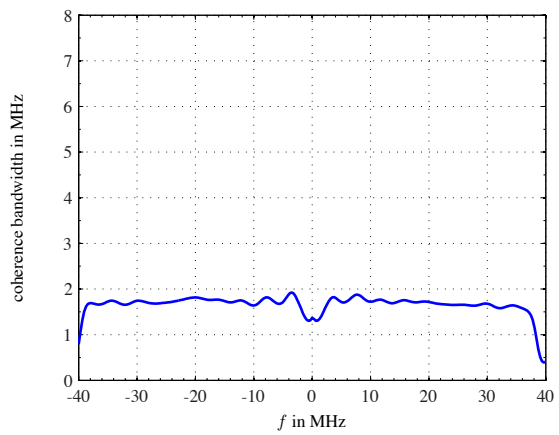


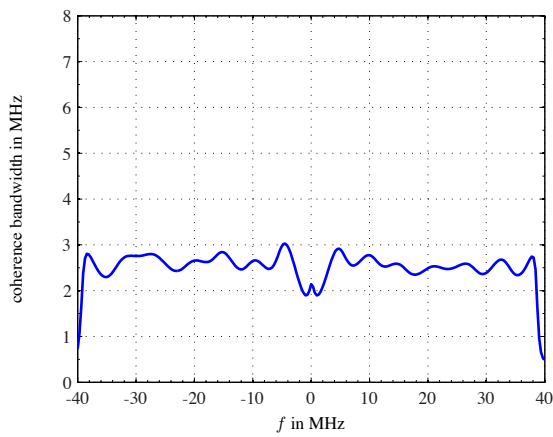
Fig. A.7: Estimated coherence bandwidth for $K = 0.9$ in the open office scenario (single-hop links).



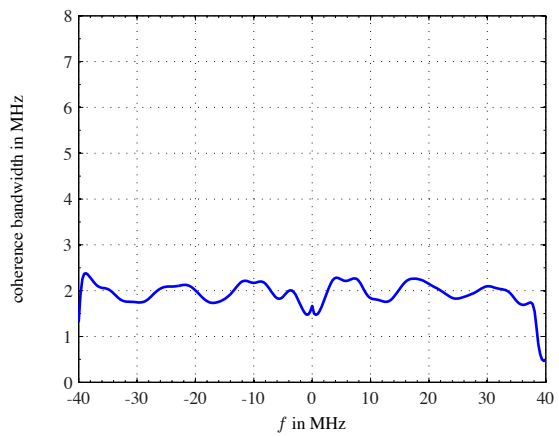
(a) From RACooN 5 via RACooN 3 to RACooN 6



(b) From RACooN 6 via RACooN 4 to RACooN 8



(c) From RACooN 7 via RACooN 2 to RACooN 5



(d) From RACooN 8 via RACooN 1 to RACooN 7

Fig. A.8: Estimated coherence bandwidth for $K = 0.9$ in the open office scenario (two-hop links).

Acronyms

Notation	Description
ADC	analog to digital converter.
AF	amplify-and-forward.
AGC	automatic gain control.
AWGN	additive white Gaussian noise.
cdf	cumulative density function.
CF	compress-and-forward.
CIR	channel impulse response.
CSI	channel state information.
DAC	digital to analog converter.
DC	direct current.
DF	decode-and-forward.
DFE	decision feedback equalizer.
DFT	discrete Fourier transformation.
DMT	diversity-multiplexing tradeoff.
EGC	equal gain combining.
FDD	frequency division duplex.
ICI	intercarrier interference.
iid	independent, identically distributed.
ISI	intersymbol interference.

Notation	Description
KKT	Karush-Kuhn-Tucker.
LDAS	linear distributed antenna system.
LinRel	linear relaying.
LNA	low noise amplifier.
LO	local oscillator.
LoS	line-of-sight.
MB	master-based.
MIMO	multiple-input multiple-output.
MISO	multiple-input single-output.
ML	maximum likelihood.
MMSE	minimum mean squared error.
MRC	maximum ratio combining.
MSE	mean squared error.
MUI	multiuser interference.
MUZF	multiuser zero-forcing.
NLoS	non-line-of-sight.
OFDM	orthogonal frequency division multiplexing.
OFDMA	orthogonal frequency division multiple access.
PA	power amplifier.
pdf	probability density function.
PLL	phase-locked-loop.
PSU	power supply unit.
RACooN	radio access with cooperating nodes.
RAM	random access memory.
RF	radio frequency.
RFU	radio frequency unit.

Notation	Description
rms	root-mean-square.
RPC	remote procedure call.
RSSI	radio signal strength indicator.
SB	slave-based.
SINR	signal-to-interference-and-noise ratio.
SIR	signal-to-interference ratio.
SISO	single-input-single-output.
SNR	signal-to-noise ratio.
STU	storage unit.
SVD	singular value decomposition.
TDD	time division duplex.
TDMA	time division multiple access.
US	uncorrelated scattering.
UWB	ultra wideband.
VCO	voltage controlled oscillator.
WSS	wide-sense stationary.
WSSUS	wide-sense stationary uncorrelated scattering.
ZF	zero-forcing.

Notation

Notation	Description
\mathbf{x}	Bold-face lower-case letters denote vectors.
$\mathbf{x} \in \mathbb{C}^a$	Denotes a vector of size $a \times 1$ with entries in \mathbb{C} .
$\mathbf{x}[i]$	Element in row i of vector \mathbf{x} .
\mathbf{X}	Bold-face upper-case letters denote matrices.
$\mathbf{X} \in \mathbb{C}^{a \times b}$	Denotes a matrix of size $a \times b$ with entries in \mathbb{C} .
$\mathbf{X}[i, j]$	Element in row i , column j of matrix \mathbf{X} .
\mathbf{X}^T	Matrix transpose.
\mathbf{X}^H	Conjugate complex transpose (hermitian).
\mathbf{X}^{-1}	Matrix inverse.
$\det(\mathbf{X})$	Matrix determinant.
$\text{tr}(\mathbf{X})$	Trace of the matrix \mathbf{X} , i.e. sum of its diagonal elements.
$\text{Null}(\mathbf{X})$	Nullspace of the space spanned by the columns of the matrix \mathbf{X} .
$\text{vec}(\mathbf{X})$	Takes the columns of matrix $\mathbf{X} \in \mathbb{C}^{a \times b}$ and stacks them on top of each other to get a vector $\mathbf{x} \in \mathbb{C}^{a \cdot b}$.
$\text{diag}(\mathbf{X})$	Takes the element of the main diagonal of the matrix $\mathbf{X} \in \mathbb{C}^{a \times a}$ and stacks them in a vector of size $a \times 1$.
$\text{diag}(\mathbf{x})$	Takes the elements of \mathbf{x} and writes them into a diagonal matrix.
\mathbf{I}_a	Identity matrix of size $a \times a$.
$\mathbf{1}_a$	Vector of all ones and dimension $a \times 1$.
\otimes	Kronecker product.
\odot	Hadamard (elementwise) product.
$\ \mathbf{x}\ _2$	Euclidean norm of the vector \mathbf{x} ; $\ \mathbf{x}\ _2 = \sqrt{\mathbf{x}^H \mathbf{x}}$.
$:=$	Definition.
$\hat{=}$	Corresponds to.

Notation	Description
\approx	Approximately corresponds to.
x^*	Conjugate complex of the scalar $x \in \mathbb{C}$.
\circledast	Convolution.
$\text{Re} \{x\}$	Real part of $x \in \mathbb{C}$.
$\text{Im} \{x\}$	Imaginary part of $x \in \mathbb{C}$.
$\angle \{x\}$	Angle $x \in \mathbb{C}$; If $x = x e^{j\varphi}$ then $\angle \{x\} = \varphi$.
$ x $	Absolute value of $x \in \mathbb{C}$.
$\max \{\mathcal{X}\}$	Maximum element in the set \mathcal{X} .
$\min \{\mathcal{X}\}$	Minimum element in the set \mathcal{X} .
$\arg \max_x f(x)$	$\arg \max_x f(x) := \{x \mid \forall y : f(y) \leq f(x)\}$.
$\arg \min_x f(x)$	$\arg \min_x f(x) := \{x \mid \forall y : f(y) \geq f(x)\}$.
$E_x [f(x)]$	Expectation with respect to x .
\log_x	Logarithm to the base of x .
$\text{erf} (x)$	Error function; $\text{erf} (x) = \frac{2}{\sqrt{\pi}} \int_0^x e^{-t^2} dt$.
$I_n (\cdot)$	Modified Bessel function of the first kind of order n .
$\mathcal{F} \{ \cdot \}$	Fourier transform.
$\mathcal{F}^{-1} \{ \cdot \}$	Inverse Fourier transform.
$\frac{\partial}{\partial x} f(x)$	Partial derivative of $f(x)$ with respect to x .
$\frac{\partial^2}{\partial x^2} f(x)$	Second order partial derivative of $f(x)$ with respect to x .
$\mathbf{Z} = \frac{\partial}{\partial \mathbf{X}} f(\mathbf{X})$	Partial derivative of the scalar function $f(\mathbf{X})$ with respect to the elements of \mathbf{X} . The result \mathbf{Z} is a matrix of the same dimension as \mathbf{X} : $\mathbf{Z}[i, j] = \frac{\partial}{\partial \mathbf{X}[i, j]} f(\mathbf{X})$.
$x \sim \mathcal{N} (m, \sigma^2)$	x is a Gaussian random variable with mean m and variance σ^2 .
$x \sim \mathcal{CN} (m, \sigma^2)$	x is a complex Gaussian random variable with mean m and variance σ^2 .
$\mathbf{x} \sim \mathcal{CN} (\boldsymbol{\mu}, \boldsymbol{\Sigma})$	\mathbf{x} is a vector with entries that are complex Gaussian random variables; mean vector $\boldsymbol{\mu} = E [\mathbf{x}]$ and covariance matrix $\boldsymbol{\Sigma} = E [\mathbf{x}\mathbf{x}^H]$.
$x \sim \mathcal{U} (a, b)$	x is uniformly distributed with support $x \in [a, b]$.
$x \sim \mathcal{VM} (\mu, \kappa)$	x is a random variable that is distributed according to von Mises distribution with location parameter μ and concentration parameter κ .

Notation **Description**

Frequently Used Symbols

Notation Description

M_{D_m} ,	Number of antennas at destination m .
M_D	Number of destination antennas.
M_{R_l}	Number of antennas at relay l .
M_R	Number of relay antennas.
M_{S_k}	Number of antennas at source k .
M_S	Number of source antennas.
N_D	Number of destinations.
N_R	Number of relays.
N_{SD}	Number of source/destination pairs.
N_S	Number of sources.
P_R	Total relay transmit power.
P_S	Total source transmit power.
\mathbf{G}	Gain matrix; $\mathbf{G} \in \mathbb{C}^{M_R \times M_R}$.
\mathbf{H}_{RD}	Second-hop channel matrix; $\mathbf{H}_{RD} \in \mathbb{C}^{M_D \times M_R}$.
\mathbf{H}_{SD}	Direct link channel matrix; $\mathbf{H}_{SD} \in \mathbb{C}^{M_D \times M_S}$.
\mathbf{H}_{SR}	First-hop channel matrix; $\mathbf{H}_{SR} \in \mathbb{C}^{M_R \times M_S}$.
Φ_X	Diagonal LO phase matrix of node \mathbf{X} ; $\Phi_X \in \mathbb{C}^{M_X \times M_X}$.
$\tilde{\mathbf{H}}_{RD}$	Equivalent second-hop channel matrix; $\tilde{\mathbf{H}}_{RD} \in \mathbb{C}^{M_D \times M_R}$.
$\tilde{\mathbf{H}}_{SD}$	Equivalent direct link channel matrix; $\tilde{\mathbf{H}}_{SD} \in \mathbb{C}^{M_D \times M_S}$.
$\tilde{\mathbf{H}}_{SRD}$	Equivalent two-hop channel matrix; $\tilde{\mathbf{H}}_{SRD} \in \mathbb{C}^{M_D \times M_S}$.
$\tilde{\mathbf{H}}_{SR}$	Equivalent first-hop channel matrix; $\tilde{\mathbf{H}}_{SR} \in \mathbb{C}^{M_R \times M_S}$.
$g_l \in \mathbb{C}$	Gain factor at relay l .

Bibliography

- [1] I. E. Telatar, “Capacity of multi-antenna Gaussian channels,” *Eur. Trans. Telecommun.*, vol. 10, no. 6, pp. 585–595, 1999.
- [2] G. J. Foschini and M. J. Gans, “On limits of wireless communications in a fading environment when using multiple antennas,” *Wireless Personal Communications*, vol. 6, no. 3, pp. 311–335, Mar. 1998.
- [3] H. Bölcskei, D. Gesbert, and A. J. Paulraj, “On the capacity of OFDM-based spatial multiplexing systems,” *IEEE Transactions on Communications*, vol. 50, no. 2, pp. 225–234, Feb. 2002.
- [4] A. J. Paulraj, R. Nabar, and D. Gore, *Introduction to Space-Time Wireless Communications*. Cambridge University Press, May 2003.
- [5] W. C. Jakes, *Microwave Mobile Communications*. Wiley-IEEE Press, 1974.
- [6] E. C. van der Meulen, “Three-terminal communication channels,” *Adv. Appl. Prob.*, vol. 3, pp. 120–154, 1971.
- [7] J. N. Laneman and G. W. Wornell, “Distributed space-time-coded protocols for exploiting cooperative diversity in wireless networks,” *IEEE Transactions on Information Theory*, vol. 49, no. 10, pp. 2415–2425, Oct. 2003.
- [8] A. Sendonaris, E. Erkip, and B. Aazhang, “User cooperation diversity – Part I: System description,” *IEEE Transactions on Communications*, vol. 51, no. 11, pp. 1927–1938, Nov. 2003.
- [9] — —, “User cooperation diversity – Part II: Implementation aspects and performance analysis,” *IEEE Transactions on Communications*, vol. 51, no. 11, pp. 1939–1948, Nov. 2003.
- [10] J. N. Laneman, D. N. C. Tse, and G. W. Wornell, “Cooperative diversity in wireless networks: Efficient protocols and outage behaviour,” *IEEE Transactions on Information Theory*, vol. 50, no. 12, pp. 3062–3080, Dec. 2004.

- [11] H. Bölcskei, R. U. Nabar, Ö. Oyman, and A. J. Paulraj, "Capacity scaling laws in MIMO relay networks," *IEEE Transactions on Wireless Communications*, vol. 5, no. 6, Jun. 2006.
- [12] A. F. Dana and B. Hassibi, "On the power efficiency of sensory and ad hoc wireless networks," *IEEE Transactions on Information Theory*, vol. 52, no. 7, pp. 2890–2914, Jul. 2006.
- [13] B. Wang, J. Zhang, and L. Zheng, "Achievable rates and scaling laws of power-constrained wireless sensory relay networks," *IEEE Transactions on Information Theory*, vol. 52, no. 9, pp. 4084–4104, Sept. 2006.
- [14] A. Sendonaris, E. Erkip, and B. Aazhang, "User cooperation diversity - part I and II," *IEEE Transactions on Communications*, Nov. 2003.
- [15] A. Wittneben, I. Hammerström, and M. Kuhn, "Joint cooperative diversity and scheduling in low mobility wireless networks," in *IEEE Global Telecommunications Conference (Globecom)*, Nov. 2004.
- [16] I. Hammerstrom, M. Kuhn, and A. Wittneben, "Channel adaptive scheduling for cooperative relay networks," in *Proc. VTC2004-Fall Vehicular Technology Conference 2004 IEEE 60th*, vol. 4, 26–29 Sept. 2004, pp. 2784–2788.
- [17] I. Hammerstroem, M. Kuhn, and A. Wittneben, "Cooperative diversity by relay phase rotations in block fading environments," in *5th IEEE Workshop on Signal Processing Advances in Wireless Communications (SPAWC)*, Jul. 2004, pp. 293–297.
- [18] I. Hammerstrom, J. Zhao, and A. Wittneben, "Temporal fairness enhanced scheduling for cooperative relaying networks in low mobility fading environments," in *Proc. IEEE 6th Workshop on Signal Processing Advances in Wireless Communications*, 5–8 June 2005, pp. 525–529.
- [19] M. Muhaidat and M. Uysal, "Cooperative diversity with multiple-antenna nodes in fading relay channels," *IEEE Transactions on Wireless Communications*, vol. 7, no. 8, pp. 3036–3046, Aug. 2008.
- [20] B. K. Chalise and L. Vandendorpe, "Outage probability analysis of a mimo relay channel with orthogonal space-time block codes," *IEEE Communications Letters*, vol. 12, no. 4, pp. 280–282, April 2008.
- [21] X. Lei and P. Fan, "Comment on "outage probability analysis of a mimo relay channel with orthogonal space-time block codes","" *IEEE Communications Letters*, vol. 12, no. 10, pp. 720–721, October 2008.

-
- [22] L. Yang and Q. T. Zhang, "Outage performance of mimo relay channels with maximal ratio transmission," *Electronics Letters*, vol. 45, no. 5, pp. 273–274, February 26 2009.
- [23] H. Min, S. Lee, K. Kwak, and D. Hong, "Effect of multiple antennas at the source on outage probability for amplify-and-forward relaying systems," *IEEE Transactions on Wireless Communications*, vol. 8, no. 2, pp. 633–637, Feb. 2009.
- [24] A. Host-Madsen and A. Nosratinia, "The multiplexing gain of wireless networks," in *Proc. International Symposium on Information Theory ISIT 2005*, 4–9 Sept. 2005, pp. 2065–2069.
- [25] A. Wittneben and B. Rankov, "Distributed antenna systems and linear relaying for gigabit MIMO wireless," in *IEEE Vehicular Technology Conference (VTC Fall 2004)*, Los Angeles, Sep. 2004.
- [26] V. I. Morgenshtern, H. Boelcskei, and R. U. Nabar, "Distributed orthogonalization in large interference relay networks," in *Proc. IEEE International Symposium on Information Theory (ISIT)*, Sep. 2005, pp. 1211–1215.
- [27] B. Rankov and A. Wittneben, "Distributed spatial multiplexing in a wireless network," in *Proceedings of the Asilomar Conference on Signals, Systems, and Computers 2004*, (Pacific Grove, CA), Nov. 2004.
- [28] P. Herhold, E. Zimmermann, and G. Fettweis, "Cooperative multi-hop transmission in wireless networks," *Computer Networks*, vol. 49, no. 3, pp. 299–324, 2005.
- [29] G. Kramer, M. Gastpar, and P. Gupta, "Cooperative strategies and capacity theorems for relay networks," *IEEE Transactions on Information Theory*, vol. 51, no. 9, pp. 3037–3063, Sep. 2005.
- [30] P. A. Anghel, G. Leus, and M. Kaveh, "Multi-user space-time coding in cooperative networks," in *Proc. of ICASSP*, vol. 4, Apr. 2003, pp. IV-73 – IV-76.
- [31] S. Barbarossa, L. Pescosolido, D. Ludovici, L. Barbetta, and G. Scuteria, "Cooperative wireless networks based on distributed space-time coding," in *International Workshop on Wireless Ad-Hoc Networks (IWVAN)*, Jun. 2004.
- [32] G. J. Foschini, "Layered space-time architecture for wireless communication in a fading environment when using multi-element antennas," *Bell Labs Technical Journal*, vol. 1, no. 2, pp. 41–59, 1996.
- [33] Y. Jing and B. Hassibi, "Distributed space time coding in wireless relay networks," *IEEE Transactions on Wireless Communications*, vol. 5, no. 12, pp. 3524–3536, Dec. 2006.

- [34] — — , “Cooperative diversity in wireless relay networks with multiple-antenna nodes,” in *Proc. International Symposium on Information Theory ISIT 2005*, 4–9 Sept. 2005, pp. 815–819.
- [35] Y. Jing and H. Jafarkhani, “Using orthogonal and quasi-orthogonal designs in wireless relay networks,” *IEEE Transactions on Information Theory*, vol. 53, no. 11, pp. 4106–4118, Nov. 2007.
- [36] X. Guo and X.-G. Xia, “A distributed space-time coding in asynchronous wireless relay networks,” *IEEE Transactions on Wireless Communications*, vol. 7, no. 5, pp. 1812–1816, May 2008.
- [37] J. Zhao, Y. Xu, and Y. Cai, “Cooperative differential space-time transmission scheme for mimo relay networks,” in *Proc. Congress on Image and Signal Processing CISP '08*, vol. 5, 27–30 May 2008, pp. 44–48.
- [38] Y. Jing and H. Jafarkhani, “Distributed differential space-time coding for wireless relay networks,” *IEEE Transactions on Communications*, vol. 56, no. 7, pp. 1092–1100, July 2008.
- [39] H. X. Nguyen, H. H. Nguyen, and T. Le-Ngoc, “Optimization of linear dispersion codes for wireless relay networks,” *IEEE Signal Processing Letters*, vol. 16, no. 5, pp. 366–369, May 2009.
- [40] A. Bletsas, A. Khisti, D. P. Reed, and A. Lippman, “A simple cooperative diversity method based on network path selection,” *IEEE Journal on Selected Areas of Communication, Special Issue on 4G*, vol. 24, no. 3, pp. 659–672, Mar. 2006.
- [41] Y. Zhao, R. Adve, and T. J. Lim, “Improving amplify-and-forward relay networks: Optimal power allocation versus selection,” in *IEEE International Symposium on Information Theory*, 2006.
- [42] — — , “Symbol error rate of selection amplify-and-forward relay systems,” *IEEE Communication Letters*, vol. 10, no. 11, pp. 757–759, Nov. 2006.
- [43] A. Bletsas, A. Lippman, and D. P. Reed, “A simple distributed method for relay selection in cooperative diversity wireless networks, based on reciprocity and channel measurements,” in *Proc. IEEE VTC'05 Spring, Stockholm*, May 2005.
- [44] A. Bletsas, H. Shin, and M. Z. Win, “Cooperative communications with outage-optimal opportunistic relaying,” *IEEE Transactions on Wireless Communications*, vol. 6, no. 9, pp. 3450–3460, Sep. 2007.

- [45] I. Krikidis, J. Thompson, S. McLaughlin, and N. Goertz, "Amplify-and-forward with partial relay selection," *IEEE Communications Letters*, vol. 12, no. 4, pp. 235–237, Apr. 2008.
- [46] Y. Zhao, R. Adve, and T. J. Lim, "Beamforming with limited feedback in amplify-and-forward cooperative networks," *IEEE Transactions on Wireless Communications*, vol. 7, no. 12, pp. 5145–5149, Dec. 2008.
- [47] F. ad Lau F. C. M. Xu, Q. F. Zhou, and D.-W. Yue, "Outage performance of cooperative communication systems using opportunistic relaying and selection combining receiver," *IEEE Signal Processing Letters*, vol. 16, no. 4, pp. 237–240, Apr. 2009.
- [48] J.-B. Kim and D. Kim, "Outage probability of opportunistic decode-and-forward relaying with co-channel interferences," in *Proc. 11th International Conference on Advanced Communication Technology ICACT 2009*, vol. 02, 15–18 Feb. 2009, pp. 919–922.
- [49] A. S. Ibrahim, A. K. Sadek, W. Su, and K. J. R. Liu, "Cooperative communications with relay selection: When to cooperate and whom to cooperate with?" *IEEE Transactions on Wireless Communications*, vol. 7, no. 7, pp. 2814–2827, Jul. 2008.
- [50] E. Beres and R. Adve, "Selection cooperation in multi-source cooperative networks," *IEEE Transactions on Wireless Communications*, vol. 7, no. 1, pp. 118–127, Jan. 2008.
- [51] A. Bletsas, A. Khisti, and M. Z. Win, "Opportunistic cooperative diversity with feedback and cheap radios," *IEEE Transactions on Wireless Communications*, vol. 7, no. 5, pp. 1823–1827, May 2008.
- [52] Z. Ding, Y. Gong, T. Ratnarajah, and C. F. N. Cowan, "On the performance of opportunistic cooperative wireless networks," *IEEE Transactions on Communications*, vol. 56, no. 8, pp. 1236–1240, Aug. 2008.
- [53] M. A. Torabi and J. F. Frigon, "Semi-orthogonal relay selection and beamforming for amplify-and-forward mimo relay channels," in *Proc. IEEE Wireless Communications and Networking Conference WCNC 2008*, March 31 2008–April 3 2008, pp. 48–53.
- [54] C. K. Lo, S. Vishwanath, and R. W. J. Heath, "Relay subset selection in wireless networks using partial decode-and-forward transmission," *IEEE Transactions on Vehicular Technology*, vol. 58, no. 2, pp. 692–704, Feb. 2009.
- [55] Y. Jing and H. Jafarkhani, "Single and multiple relay selection schemes and their achievable diversity orders," *IEEE Transactions on Wireless Communications*, vol. 8, no. 3, pp. 1414–1423, Mar. 2009.

- [56] R. Madan, N. B. Mehta, A. F. Molisch, and J. Zhang, "Energy-efficient cooperative relaying over fading channels with simple relay selection," *IEEE Transactions on Wireless Communications*, vol. 7, no. 8, pp. 3013–3025, Aug. 2008.
- [57] O. Munoz, J. Vidal, and A. Agustin, "Non-regenerative mimo relaying with channel state information [cellular example]," in *Proc. IEEE International Conference on Acoustics, Speech, and Signal Processing (ICASSP '05)*, vol. 3, 18–23 March 2005, pp. iii/361–iii/364.
- [58] X. Tang and Y. Hua, "Optimal design of non-regenerative mimo wireless relays," *IEEE Transactions on Wireless Communications*, vol. 6, no. 4, pp. 1398–1407, April 2007.
- [59] Z. Fang, Y. Hua, and J. C. Koshy, "Joint source and relay optimization for a non-regenerative mimo relay," in *Proc. Fourth IEEE Workshop on Sensor Array and Multichannel Processing*, 12–14 July 2006, pp. 239–243.
- [60] O. Munoz-Medina, J. Vidal, and A. Agustin, "Linear transceiver design in nonregenerative relays with channel state information," *IEEE Transactions on Signal Processing*, vol. 55, no. 6, pp. 2593–2604, June 2007.
- [61] W. Yang, C. Pan, Y. Cai, and Y. Xu, "A novel transmission scheme for mimo relay channels," in *Proc. 4th International Conference on Wireless Communications, Networking and Mobile Computing WiCOM '08*, 12–14 Oct. 2008, pp. 1–5.
- [62] Y. Fu, L. Yang, and Z. He, "Amplify-and-forward relaying scheme based on gsvd for mimo relay networks," in *Proc. International Conference on Neural Networks and Signal Processing*, 7–11 June 2008, pp. 506–511.
- [63] W. Guan and H. Luo, "Joint MMSE transceiver design in non-regenerative MIMO relay systems," *IEEE Communications Letters*, vol. 12, no. 7, pp. 517–519, Jul. 2008.
- [64] B. Khoshnevis, W. Yu, and R. Adve, "Grassmannian beamforming for mimo amplify-and-forward relaying," *IEEE Journal on Selected Areas in Communications*, vol. 26, no. 8, pp. 1397–1407, October 2008.
- [65] H. W. Je, B. Lee, S. Kim, and K. B. Lee, "Design of non-regenerative mimo-relay system with partial channel state information," in *Proc. IEEE International Conference on Communications ICC '08*, 19–23 May 2008, pp. 4441–4445.
- [66] B. Rankov and A. Wittneben, "Spectral efficient protocols for half-duplex fading relay channels," *IEEE Journal on Selected Areas in Communications*, vol. 25, no. 2, pp. 379–389, Feb. 2007.

-
- [67] A. Wittneben and I. Hammerstroem, "Multiuser zero forcing relaying with noisy channel state information," in *IEEE Wireless Communications and Networking Conference (WCNC)*, Mar. 2005.
- [68] A. Wittneben, "A theoretical analysis of multiuser zero forcing relaying with noisy channel state information," in *Proc. IEEE VTC'05 Spring*, Stockholm, May 2005.
- [69] — —, "Coherent multiuser relaying with partial relay cooperation," in *IEEE Wireless Communication and Networking Conference (WCNC)*, Las Vegas, NV, USA, Apr. 2006.
- [70] C. Esli, S. Berger, and A. Wittneben, "Optimizing zero-forcing based gain allocation for wireless multiuser networks," in *IEEE International Conference on Communications (ICC)*, Jun. 2007.
- [71] J. Wagner, M. Kuhn, and A. Wittneben, "Multihop-enabled orthogonalization in distributed mimo networks," in *Proc. IEEE 19th International Symposium on Personal, Indoor and Mobile Radio Communications PIMRC 2008*, 15–18 Sept. 2008, pp. 1–6.
- [72] C. Esli, J. Wagner, and A. Wittneben, "Distributed gradient based gain allocation for coherent multiuser AF relaying networks," in *IEEE International Conference on Communications (ICC 2009)*, Jun. 2009.
- [73] S. Berger and A. Wittneben, "Cooperative distributed multiuser MMSE relaying in wireless ad-hoc networks," in *Asilomar Conference on Signals, Systems, and Computers*, Pacific Grove, CA, Oct. 2005.
- [74] N. Khajehnouri and A. H. Sayed, "A distributed MMSE relay strategy for wireless sensor networks," in *Proc. IEEE 6th Workshop on Signal Processing Advances in Wireless Communications*, 5–8 June 2005, pp. 796–800.
- [75] — —, "Distributed MMSE relay strategies for wireless sensor networks," *IEEE Transactions on Signal Processing*, vol. 55, no. 7, pp. 3336–3348, July 2007.
- [76] H. Shi, T. Abe, T. Asai, and H. Yoshino, "A relaying scheme using QR decomposition with phase control for MIMO wireless networks," in *Proc. IEEE International Conference on Communications*, 2005, Seoul.
- [77] — —, "Relay techniques in MIMO wireless networks," in *Proc. IEEE VTC'05 Fall*, Dallas, Sep. 2005.
- [78] — —, "Analyses of achievable gains in half duplex MIMO relaying schemes using multiple relay nodes," *IEICE Transactions on Communications*, vol. E90-B, no. 9, pp. 2541–2551, Sep. 2007.

- [79] K. S. Gomadam and S. A. Jafar, "Optimal distributed beamforming in relay networks with common interference," in *Proc. IEEE Global Telecommunications Conference GLOBECOM '07*, 26–30 Nov. 2007, pp. 3868–3872.
- [80] C. Esli and A. Wittneben, "A cluster-based multiuser cooperative network," in *Proc. IEEE Global Telecommunications Conference GLOBECOM '07*, 26–30 Nov. 2007, pp. 3926–3931.
- [81] — —, "Distributed multiuser cooperative network with heterogenous relay clusters," in *Conference Record of the Forty-First Asilomar Conference on Signals, Systems and Computers ACSSC 2007*, 4–7 Nov. 2007, pp. 829–834.
- [82] — —, "Robust gain allocation against phase uncertainty at the relays for multiuser cooperative networks," in *IEEE Asilomar Conference on Signals, Systems and Computers*, Oct. 2008.
- [83] M. A. Torabi and J. F. Frigon, "A decomposition approach to mimo interference relay networks," in *Proc. IEEE Global Telecommunications Conference IEEE GLOBECOM 2008*, Nov. 30 2008–Dec. 4 2008, pp. 1–6.
- [84] D. S. Michalopoulos, A. S. Lioumpas, and G. K. Karagiannidis, "Low complexity amplify and forward relaying without channel amplitude estimation," in *Proc. IEEE International Conference on Communications ICC '08*, 19–23 May 2008, pp. 4295–4299.
- [85] V. Havary-Nassab, S. Shahbazpanahi, A. Grami, and Z. Q. Luo, "Distributed beamforming for relay networks based on second-order statistics of the channel state information," *IEEE Transactions on Signal Processing*, vol. 56, no. 9, pp. 4306–4316, Sept. 2008.
- [86] Z. Ding, W. H. Chin, and K. K. Leung, "Distributed beamforming and power allocation for cooperative networks," *IEEE Transactions on Wireless Communications*, vol. 7, no. 5, pp. 1817–1822, May 2008.
- [87] A. El-Keyi and B. Champagne, "Cooperative MIMO-beamforming for multiuser relay networks," in *IEEE International Conference on Acoustics, Speech and Signal Processing (ICASSP)*, Mar. 2008, pp. 2749–2752.
- [88] G. Zheng, K.-K. Wong, A. Paulraj, and B. Ottersten, "Collaborative-relay beamforming with perfect csi: Optimum and distributed implementation," *IEEE Signal Processing Letters*, vol. 16, no. 4, pp. 257–260, Apr. 2009.

- [89] A. Chowdhery and R. Mallik, "Linear detection for the nonorthogonal amplify and forward protocol," *IEEE Transactions on Wireless Communications*, vol. 8, no. 2, pp. 826–835, Feb. 2009.
- [90] R. U. Nabar, Ö. Oyman, H. Bölcskei, and A. J. Paulraj, "Capacity scaling laws in MIMO wireless networks," in *Proc. Allerton Conference on Communication, Control, and Computing*, Monticello, IL, Oct. 2003, pp. 378–389.
- [91] S. A. Jafar and S. Shamai, "Degrees of freedom region of the mimo x channel," *IEEE Transactions on Information Theory*, vol. 54, no. 1, pp. 151–170, Jan. 2008.
- [92] B. Rankov and A. Wittneben, "Spectral efficient signaling for half-duplex relay channels," in *Asilomar Conference on Signals, Systems, and Computers 2005, Pacific Grove, CA*, Nov. 2005.
- [93] — —, "Achievable rate regions for the two-way relay channel," in *Proc. IEEE International Symposium on Information Theory*, 9–14 July 2006, pp. 1668–1672.
- [94] I. Hammerström, M. Kuhn, C. Esli, J. Zhao, A. Wittneben, and G. Bauch, "Mimo two-way relaying with transmit csi at the relay," in *Proc. IEEE 8th Workshop on Signal Processing Advances in Wireless Communications SPAWC 2007*, 17–20 June 2007, pp. 1–5.
- [95] T. J. Oechtering, C. Schnurr, I. Bjelakovic, and H. Boche, "Achievable rate region of a two phase bidirectional relay channel," in *Proc. 41st Annual Conference on Information Sciences and Systems CISS '07*, 14–16 March 2007, pp. 408–413.
- [96] S. J. Kim, P. Mitran, and V. Tarokh, "Performance bounds for bi-directional coded cooperation protocols," in *Proc. 27th International Conference on Distributed Computing Systems Workshops ICDCSW '07*, 22–29 June 2007, pp. 83–83.
- [97] P. Popovski and H. Yomo, "Wireless network coding by amplify-and-forward for bi-directional traffic flows," *IEEE Communications Letters*, vol. 11, no. 1, pp. 16–18, Jan. 2007.
- [98] Y. Han, S. H. Ting, C. K. Ho, and W. H. Chin, "Performance bounds for two-way amplify-and-forward relaying," *IEEE Transactions on Wireless Communications*, vol. 8, no. 1, pp. 432–439, Jan. 2009.
- [99] T. Cui, F. Gao, T. Ho, and A. Nallanathan, "Distributed space-time coding for two-way wireless relay networks," *IEEE Transactions on Signal Processing*, vol. 57, no. 2, pp. 658–671, Feb. 2009.

- [100] M. Gastpar and M. Vetterli, "On the asymptotic capacity of gaussian relay networks," in *Proceedings of the IEEE International Symposium on Information Theory (ISIT)*, Jun. 2002, p. 195.
- [101] P. Gupta and P. R. Kumar, "The capacity of wireless networks," *IEEE Transactions on Information Theory*, vol. 46, no. 2, pp. 388–404, Mar. 2000.
- [102] — —, "Toward an information theory of large networks: An achievable rate region," *IEEE Transactions on Information Theory*, vol. 49, no. 8, pp. 1877–1894, Aug. 2003.
- [103] L.-L. Xie and P. R. Kumar, "A network information theory for wireless communication: Scaling laws and optimal operation," *IEEE Transactions on Information Theory*, vol. 50, no. 5, pp. 748–767, May 2004.
- [104] O. Lèvêque and I. E. Telatar, "Information theoretic upper bounds on the capacity of large extended ad hoc networks," *IEEE Transactions on Information Theory*, vol. 51, no. 5, pp. 858–865, Mar. 2005.
- [105] M. Grossglauser and D. N. C. Tse, "Mobility increases the capacity of ad hoc wireless networks," *IEEE/ACM Transactions on Networking*, vol. 10, no. 4, pp. 477–486, Aug. 2002.
- [106] R. U. Nabar and H. Bölcskei, "Capacity scaling laws in asynchronous relay networks," in *Proc. Allerton Conference on Communication, Control, and Computing*, Monticello, IL, Oct. 2004.
- [107] J. Wagner, B. Rankov, and A. Wittneben, "On the asymptotic capacity of the rayleigh fading amplify-and-forward mimo relay channel," in *Proc. IEEE International Symposium on Information Theory ISIT 2007*, 24–29 June 2007, pp. 2711–2715.
- [108] — —, "Large n analysis of amplify-and-forward mimo relay channels with correlated rayleigh fading," *IEEE Transactions on Information Theory*, vol. 54, no. 12, pp. 5735–5746, 2008.
- [109] S. Simoens, O. Munoz, J. Vidal, and A. Del Coso, "Capacity bounds for gaussian mimo relay channel with channel state information," in *Proc. IEEE 9th Workshop on Signal Processing Advances in Wireless Communications SPAWC 2008*, 6–9 July 2008, pp. 441–445.
- [110] — —, "On the gaussian mimo relay channel with full channel state information," *IEEE Transactions on Signal Processing*, vol. 57, no. 5, 2009.
- [111] B. Hassibi and A. F. Dana, "On the power efficiency of sensory and ad hoc wireless networks," in *Asilomar Conference on Signals, Systems, and Computers*, Pacific Grove, CA, Nov. 2002.

-
- [112] — —, “On the power efficiency of sensory and ad-hoc wireless networks,” in *Proceedings of the IEEE International Symposium on Information Theory (ISIT)*, Jun. 2003.
- [113] S. Verdu, “Spectral efficiency in the wideband regime,” *IEEE Transactions on Information Theory*, vol. 48, no. 6, pp. 1319–1343, Jun. 2002.
- [114] O. Sahin and E. Erkip, “Achievable rates for the gaussian interference relay channel,” in *Proc. IEEE Global Telecommunications Conference GLOBECOM '07*, 26–30 Nov. 2007, pp. 1627–1631.
- [115] — —, “On achievable rates for interference relay channel with interference cancellation,” in *Conference Record of the Forty-First Asilomar Conference on Signals, Systems and Computers ACSSC 2007*, 4–7 Nov. 2007, pp. 805–809.
- [116] R. Tannious and A. Nosratinia, “The interference channel with mimo relay: Degrees of freedom,” in *Proc. IEEE International Symposium on Information Theory ISIT 2008*, 6–11 July 2008, pp. 1908–1912.
- [117] I. Maric, R. Dabora, and A. Goldsmith, “On the capacity of the interference channel with a relays,” in *Proc. IEEE International Symposium on Information Theory ISIT 2008*, 6–11 July 2008, pp. 554–558.
- [118] G. Farhadi and N. Beaulieu, “On the ergodic capacity of wireless relaying systems over rayleigh fading channels,” *IEEE Transactions on Wireless Communications*, vol. 7, no. 11, pp. 4462–4467, November 2008.
- [119] J. Wagner and A. Wittneben, “Capacity scaling of (long) non-regenerative mimo multi-hop channels,” in *Proc. IEEE International Symposium on Information Theory ISIT 2008*, 6–11 July 2008, pp. 1913–1917.
- [120] L. Zheng and D. Tse, “Optimal diversity-multiplexing tradeoff in multiple antenna channels,” in *Proc. Allerton Conference on Communication, Control, and Computing, Monticello, IL*, Oct. 2001.
- [121] — —, “Diversity and multiplexing: A fundamental tradeoff in multiple-antenna channels,” *IEEE Transactions on Information Theory*, vol. 49, no. 5, pp. 1073–1096, May 2003.
- [122] K. Azarian, H. El Gamal, and P. Schniter, “On the achievable diversity-multiplexing tradeoff in half-duplex cooperative channels,” *IEEE Transactions on Information Theory*, vol. 51, no. 12, pp. 4152–4172, Dec. 2005.
- [123] N. Prasad and M. K. Varanasi, “Cth17-3: High performance static and dynamic cooperative communication protocols for the half duplex fading relay channel,” in *Proc.*

- IEEE Global Telecommunications Conference GLOBECOM '06*, Nov. 27 2006–Dec. 1 2006, pp. 1–5.
- [124] M. Yuksel and E. Erkip, “Multiple-antenna cooperative wireless systems: A diversity–multiplexing tradeoff perspective,” *IEEE Transactions on Information Theory*, vol. 53, no. 10, pp. 3371–3393, Oct. 2007.
- [125] C. Rao and B. Hassibi, “Diversity-multiplexing gain trade-off of a mimo system with relays,” in *Proc. IEEE Information Theory Workshop on Information Theory for Wireless Networks*, 1–6 July 2007, pp. 1–5.
- [126] D. Gunduz, A. J. Goldsmith, and H. V. Poor, “Diversity-multiplexing tradeoffs in mimo relay channels,” in *Proc. IEEE Global Telecommunications Conference IEEE GLOBECOM 2008*, Nov. 30 2008–Dec. 4 2008, pp. 1–6.
- [127] G. Fettweis, M. Löhning, D. Petrovic, M. Windisch, P. Zillmann, and W. Rave, “Dirty RF: A new paradigm,” *International Journal of Wireless Information Networks*, vol. 14, no. 2, pp. 133–148, Jun. 2007.
- [128] P. A. Parker, D. W. Bliss, P. Mitran, and V. Tarokh, “Adaptive frequency synchronization for collaborative communication systems,” in *Proc. 27th International Conference on Distributed Computing Systems Workshops ICDCSW '07*, 22–29 June 2007, pp. 82–82.
- [129] U. Spagnolini, N. Varanese, O. Simeone, and Y. Bar-Ness, “Distributed digital locked loops for time/frequency locking in packet-based wireless communications,” in *Proc. IEEE 19th International Symposium on Personal, Indoor and Mobile Radio Communications PIMRC 2008*, 15–18 Sept. 2008, pp. 1–6.
- [130] J. Mietzner, J. Eick, and P. A. Hoeher, “On distributed space-time coding techniques for cooperative wireless networks and their sensitivity to frequency offsets,” in *Proc. ITG Workshop on Smart Antennas*, Mar. 2004, pp. 114–121.
- [131] R. A. Iltis and R. Cagley, “Channel estimation and carrier offset control for cooperative mimo sensor networks,” in *Conference Record of the Thirty-Ninth Asilomar Conference on Signals, Systems and Computers*, Oct. 28 2005–Nov. 1 2005, pp. 210–214.
- [132] S. P. Ponnaluri and S. G. Wilson, “Cooperative relaying with carrier frequency uncertainty,” in *Proc. 41st Annual Conference on Information Sciences and Systems CISS '07*, 14–16 March 2007, pp. 370–375.

-
- [133] S. Berger and A. Wittneben, "Impact of noisy carrier phase synchronization on linear amplify-and-forward relaying," in *Proc. IEEE Global Telecommunications Conference GLOBECOM '07*, 26–30 Nov. 2007, pp. 795–800.
- [134] S.-J. Lee, J.-S. Yoon, and H.-K. Song, "Carrier frequency offset mitigation using mse-ofdm in cooperative communications," in *Proc. Australasian Telecommunication Networks and Applications Conference ATNAC 2008*, 7–10 Dec. 2008, pp. 76–79.
- [135] D. Sreedhar and A. Chockalingam, "Interference mitigation in cooperative sfbc-ofdm," *EURASIP Journal on Advances in Signal Processing*, Mar. 2008.
- [136] H. Wang, X.-G. Xia, and Q. Yin, "Distributed space-frequency codes for cooperative communication systems with multiple carrier frequency offsets," *IEEE Transactions on Wireless Communications*, vol. 8, no. 2, pp. 1045–1055, Feb. 2009.
- [137] — —, "Computationally efficient equalization for asynchronous cooperative communications with multiple frequency offsets," *IEEE Transactions on Wireless Communications*, vol. 8, no. 2, pp. 648–655, Feb. 2009.
- [138] X. Li, Y.-C. Wu, and E. Serpedin, "Timing synchronization in decode-and-forward cooperative communication systems," *IEEE Transactions on Signal Processing*, vol. 57, no. 4, pp. 1444–1455, April 2009.
- [139] Y. Mei, Y. Hua, A. Swami, and B. Daneshrad, "Combating synchronization errors in cooperative relays," in *Proc. IEEE International Conference on Acoustics, Speech, and Signal Processing (ICASSP '05)*, vol. 3, 18–23 March 2005, pp. iii/369–iii/372.
- [140] R. C. Palat, A. Annamalai, and J. H. Reed, "Upper bound on bit error rate for time synchronization errors in bandlimited distributed mimo networks," in *Proc. IEEE Wireless Communications and Networking Conference WCNC 2006*, vol. 4, 3–6 April 2006, pp. 2058–2063.
- [141] K. Raghunath and A. Chockalingam, "Cooperative OFDM with amplify-and-forward relaying with timing offset," in *Proc. IEEE Global Telecommunications Conference IEEE GLOBECOM 2008*, Nov. 30 2008–Dec. 4 2008, pp. 1–5.
- [142] J. Mietzner and P. A. Hoeher, "Distributed space-time codes for cooperative wireless networks in the presence of different propagation delays and path losses," in *Proc. Sensor Array and Multichannel Signal Processing Workshop*, 18–21 July 2004, pp. 264–268.
- [143] S. Wei, D. L. Goeckel, and M. C. Valenti, "Asynchronous cooperative diversity," *IEEE Transactions on Wireless Communications*, vol. 5, no. 6, pp. 1547–1557, June 2006.

- [144] A. O. Yilmaz, "Cooperative diversity in carrier frequency offset," *IEEE Communications Letters*, vol. 11, no. 4, pp. 307–309, April 2007.
- [145] K. Tourki and L. Deneire, "Multi-hop asynchronous cooperative diversity: Performance analysis," in *Proc. 3rd International Symposium on Communications, Control and Signal Processing ISCCSP 2008*, 12–14 March 2008, pp. 857–862.
- [146] X. Li, "Space-time coded multi-transmission among distributed transmitters without perfect synchronization," *IEEE Signal Processing Letters*, vol. 11, no. 12, pp. 948–951, Dec. 2004.
- [147] F. Ng and X. Li, "Cooperative stbc-ofdm transmissions with imperfect synchronization in time and frequency," in *Conference Record of the Thirty-Ninth Asilomar Conference on Signals, Systems and Computers*, Oct. 28 2005–Nov. 1 2005, pp. 524–528.
- [148] N. Benvenuto, S. Tomasin, and D. Veronesi, "Multiple frequency offsets estimation and compensation for cooperative networks," in *Proc. IEEE Wireless Communications and Networking Conference WCNC 2007*, 11–15 March 2007, pp. 891–895.
- [149] Z. Li and X.-G. Xia, "An alamouti coded ofdm transmission for cooperative systems robust to both timing errors and frequency offsets," *IEEE Transactions on Wireless Communications*, vol. 7, no. 5, pp. 1839–1844, May 2008.
- [150] A. Bletsas and A. Lippman, "Implementing cooperative diversity antenna arrays with commodity hardware," *IEEE Communications Magazine*, vol. 44, no. 12, pp. 33–40, Dec. 2006.
- [151] <http://www.openairinterface.org/>.
- [152] H. Anouar, C. Bonnet, F. Kaltenberger, and R. Knopp, "OpenAirMesh- an experimental platform for cooperative mesh networks," in *1st COST2100 Workshop on MIMO and Cooperative Communications, Trondheim, Norway*, Jun. 2008.
- [153] www.easy-c.com.
- [154] C. Jandura, P. Marsch, A. Zoch, and G. P. Fettweis, "A testbed for cooperative multi cell algorithms," in *TridentCom '08: Proceedings of the 4th International Conference on Testbeds and research infrastructures for the development of networks & communities*, 2008.
- [155] <http://www.3gpp.org/Highlights/LTE/LTE.htm>.
- [156] www.nari.ee.ethz.ch/wireless/research/projects/racoon/introduction.html, refer to this page for information on the RACooN testbed of the Swiss Federal Institute of Technology.

-
- [157] S. Berger and A. Wittneben, “A coherent amplify-and-forward relaying demonstrator without global phase reference,” in *IEEE International Symposium on Personal, Indoor and Mobile Radio Communications (PIMRC)*, Sep. 2008.
- [158] — —, “Impact of local-oscillator imperfections on nonregenerative TDD and FDD relaying,” in *Vehicular Technology Conference (VTC) Spring*, May 2010, to appear.
- [159] — —, “When do non-regenerative two-hop relaying networks require a global phase reference?” in *IEEE Global Communications Conference (IEEE Globecom 2009)*, Dec. 2009.
- [160] — —, “Carrier phase synchronization of multiple distributed nodes in a wireless network,” in *IEEE Workshop on Signal Processing Advances in Wireless Communications (SPAWC)*, Helsinki, Jun. 2007.
- [161] Y.-S. Tu and G. J. Pottie, “Coherent cooperative transmission from multiple adjacent antennas to a distant stationary antenna through AWGN channels,” in *Proc. IEEE VTC’02 Spring, Birmingham, Al*, vol. 1, 2002, pp. 130 – 134.
- [162] S. Berger and A. Wittneben, “Experimental Performance Evaluation of Multiuser Zero Forcing Relaying in Indoor Scenarios,” in *Proc. IEEE VTC’05 Spring, Stockholm*, May/June. 2005.
- [163] J. G. Proakis, *Digital Communications*. McGraw-Hill Series in Electrical and Computer Engineering, 2001.
- [164] M. Maróti, G. Simon, B. Kusy, and A. Lédeczi, “The flooding time synchronization protocol,” in *2nd International Conference on Embedded Networked Sensor Systems*, Nov. 2004, pp. 39–49.
- [165] R. Solis, V. S. Borkar, and P. R. Kumar, “A new distributed time synchronization protocol for multihop wireless networks,” in *45th IEEE Conference on Decision and Control*, Dec. 2006, pp. 2734–2739.
- [166] R. U. Nabar and H. Boelcskei, “Space–time signal design for fading relay channels,” in *IEEE Global Telecommunications Conference (GLOBECOM)*, vol. 4, Dec. 2003, pp. 1952–1956.
- [167] R. U. Nabar, H. Boelcskei, and F. W. Kneubuhler, “Fading relay channels: Performance limits and space-time signal design,” *IEEE Journal on Selected Areas in Communications*, vol. 22, no. 6, pp. 1099–1109, Aug. 2004.
- [168] A. Lozano and A. M. Tulino, “Capacity of multiple-transmit multiple-receive antenna architectures,” *IEEE Transactions on Information Theory*, vol. 48, no. 12, pp. 3117–3128, Dec. 2002.

- [169] M. Masegawa, T. Fukagawa, M. Mimura, and M. Makimoto, “Homodyne receiver technology for small and low-power consumption mobile communications equipment,” in *Proc. URSI International Symposium on Signals, Systems, and Electronics ISSSE '95*, 1995, pp. 259–262.
- [170] V. Manassewitsch, *Frequency Synthesizers: Theory and Design*. Wiley & Sons, 2005.
- [171] “IEEE Standard 802.11-2007, part 11: Wireless LAN medium access (MAC) and physical layer (PHY) specifications.”
- [172] A. Demir, A. Mehrotra, and J. Roychowdhry, “Phase noise in oscillators: A unifying theory and numerical methods for characterization,” *IEEE Transactions on Circuits and Systems – I: Fundamental Theory and Applications*, vol. 47, no. 5, pp. 655 – 674, May 2000.
- [173] A. Papoulis, *Probability, Random Variables and Stochastic Processes*. McGraw Hill Higher Education, 2006.
- [174] M.-D. Tsai, Y.-H. Cho, and H. Wang, “A 5GHz low phase noise differential colpitts CMOS VCO,” *IEEE Microwave and Wireless Components Letters*, vol. 15, no. 5, pp. 327–329, May 2005.
- [175] Z. Li, W. Zhihua, and C. Hongyi, “A 5-GHz CMOS VCO for IEEE 802.11a WLAN application,” in *Proceedings of the 7th International Conference on Solid-State and Integrated Circuits Technology*, vol. 2, Oct. 2004, pp. 1311–1314.
- [176] A. Mehrotra, “Noise analysis of phase-locked loops,” *IEEE Transactions on Circuits and Systems – I: Fundamental Theory and Applications*, vol. 49, no. 9, pp. 1309–1316, Sep. 2002.
- [177] D. Petrovic, W. Rave, and G. Fettweis, “Effects of phase noise on OFDM systems with and without PLL: Characterization and compensation,” *IEEE Transactions on Communications*, vol. 55, no. 8, pp. 1607–1616, Aug. 2007.
- [178] M. Debbah, J. Gil, P. Fernandes, J. Venes, F. Cardoso, L. Marques, and M. Correia, “Final report on channel models,” FLOWS project, 2004. [Online]. Available: http://www.nari.ee.ethz.ch/~berger/FLOWS_Final_Report_on_Channel_Models.pdf
- [179] A. A. Abidi, “Direct-conversion radio transceivers for digital communications,” *IEEE Journal of Solid-State Circuits*, vol. 30, no. 12, pp. 1399–1410, Nov. 1995.
- [180] B. Razavi, *RF Microelectronics*. Englewood Cliffs, NJ, USA: Prentice Hall, 1998.

-
- [181] S. Mirabbasi and K. Martin, "Classical and modern receiver architectures," *IEEE Communications Magazine*, vol. 38, no. 11, pp. 132–139, Nov. 2000.
- [182] M. Valkama, J. Pirskanen, and M. Renfors, "Signal processing challenges for applying software radio principles in future wireless terminals: An overview," *International Journal of Communication Systems*, vol. 15, no. 8, pp. 741–769, 2002.
- [183] Y. Zou, M. Valkama, and M. Renfors, "Analysis and compensation of transmitter and receiver I/Q imbalances in space-time coded multiantenna OFDM systems," *EURASIP Journal on Wireless Communications and Networking*, vol. 2008, no. 1, pp. 1687–1472, Jan. 2008.
- [184] C. S. Patel and G. L. Stuber, "Channel estimation for amplify and forward relay based cooperation diversity systems," *IEEE Transactions on Wireless Communications*, vol. 6, no. 6, pp. 2348–2356, Jun. 2007.
- [185] T. Cui, F. Gao, and A. Nallanathan, "Optimal training design for channel estimation in amplify and forward relay networks," in *IEEE Global Telecommunications Conference (GLOBECOM)*, Dec. 2007.
- [186] A. S. Behbahani and A. Eltawil, "On channel estimation and capacity for amplify and forward relay networks," in *IEEE Global Telecommunications Conference (GlobeCom)*, Dec. 2008.
- [187] T. Yoo and A. Goldsmith, "Capacity and power allocation for fading MIMO channels with channel estimation error," *IEEE Transactions on Information Theory*, vol. 52, no. 5, pp. 2203–2214, May 2006.
- [188] R. F. H. Fischer, *Precoding and Signal Shaping for Digital Transmission*. Wiley-IEEE Press, Aug. 2002.
- [189] D. J. Best and N. I. Fisher, "Efficient simulation of the von Mises distribution," *Applied Statistics*, vol. 28, no. 2, pp. 152–157, 1979.
- [190] G. Barriac, R. Mudumbai, and U. Madhow, "Distributed beamforming for information transfer in sensor networks," in *IPSN'04: Proc. of the Third International Symposium on Information Processing in Sensor Networks*, 2004, pp. 81 – 88.
- [191] R. Mudumbai, G. Barriac, and U. Madhow, "On the feasibility of distributed beamforming in wireless networks," *IEEE Transactions on Wireless Communications*, vol. 6, no. 5, pp. 1754–1763, May 2007.
- [192] D. A. Harville, *Matrix Algebra from a Statistician's Perspective*. Springer, 1997, ISBN 0-387-94978-X.

- [193] S. Boyd and L. Vandenberghe, *Convex Optimization*. Cambridge University Press, 2004.
- [194] C. Esli, “Design and optimization of distributed multiuser cooperative wireless networks,” Ph.D. dissertation, ETH Zurich, 2009.
- [195] R. Kueng, *Repeater RF Unit (RFU) Specification, Design and Test*, Elektrobit AG, 2003.
- [196] M. Wattinger, *Specification Storage Unit (STORU)*, Elektrobit AG, 2003.
- [197] — — , *User Manual - Installation, Operation and Maintenance*, Elektrobit AG, 2004.
- [198] — — , *Appendix to User Manual - STORADIO Mission Configuration*, Elektrobit AG, 2004.
- [199] — — , *Appendix to User Manual - STORADIO File Formats*, Elektrobit AG, 2004.
- [200] — — , *Appendix to User Manual - STORADIO XML-RPC Interface*, Elektrobit AG, 2004.
- [201] D. S. Baum and H. Bölcskei, “Impact of Phase Noise on MIMO Channel Measurement Accuracy,” in *Proc. IEEE VTC’04 Fall*, 2004. [Online]. Available: <http://www.nari.ee.ethz.ch/commth/pubs/p/vtcf2004>
- [202] M. Paetzold, *Mobile Fading Channels*. John Wiley and Sons, Ltd, 2002.
- [203] P. A. Bello, “Characterization of Randomly Time-Variant Linear Channels,” *IEEE Transactions on Communication Systems*, vol. 11, no. 4, pp. 360–393, Dec. 1963.
- [204] J. D. Parsons, *The Mobile Radio Propagation Channel*, 2nd ed. John Wiley & Sons, Ltd, 2000.
- [205] P. Hafezi, D. Wedge, M. Beach, and M. Lawton, “Propagation measurements at 5.2 GHz in commercial and domestic environments,” in *The 8th IEEE International Symposium on Personal, Indoor and Mobile Radio Communications (PIMRC ’97)*, vol. 2, Sep. 1997, pp. 509–513.
- [206] S. Guerin, Y. Guo, and S. Barton, “Indoor propagation measurements at 5 GHz for HIPERLAN,” in *Tenth International Conference on Antennas and Propagation*, vol. 2, Apr. 1997, pp. 306–310.
- [207] J. McDonnell, T. P. Spiller, and T. Wilkinson, “RMS delay spread in indoor LOS environments at 5.2 GHz,” *Electronics Letters*, vol. 34, no. 11, pp. 1149–1150, May 1998.

- [208] A. Poon and M. Ho, “Indoor multiple-antenna channel characterization from 2 to 8 GHz,” in *IEEE International Conference on Communications (ICC)*, vol. 5, May 2003, pp. 3519–3523.
- [209] A. Paulraj, R. Nabar, and D. Gore, *Introduction to Space-Time Wireless Communications*. Cambridge University Press, 2003.
- [210] S. Berger, M. Kuhn, A. Wittneben, T. Unger, and A. Klein, “Recent advances in amplify-and-forward two-hop relaying,” *IEEE Communications Magazine*, vol. 47, no. 7, pp. 50–56, Jul. 2009.
- [211] K. B. Petersen and M. S. Pedersen, “The matrix cookbook,” Feb. 2008. [Online]. Available: <http://matrixcookbook.com/>

Curriculum Vitae

Name: **Stefan Berger**
Birthday: June 22, 1978
Birthplace: Münster, Germany

Education

12/2003–
03/2010 **ETH Zurich**
PhD Studies in Electrical Engineering at ETH Zurich, Communication Technology Laboratory. Degree as **Dr. sc. ETH Zürich**

10/1998–
06/2003 **TU München**
Studies in Electrical Engineering. Focus on Automation and Autonomous Systems. Degree as Diplom-Ingenieur (**Dipl.-Ing.**) with overall grade 1.5 (very good).

Experience

since
10/2003 **ETH Zurich**, Research Assistant

- Research and teaching in wireless communications and signal processing.
- Organization of the annual '*International Seminar on Signal Processing*' in cooperation with TU Wien and TU München.
- Project leader of industrial project '*iTrain*' with Ascom AG (ETH: 16.5 man-months, 4 team members). Specification, evaluation and extension of key technologies for wireless train-to-ground communication.
- Participation in European cooperations in the field of scientific and technical research: COST289, COST 2100
- Reviewer for IEEE magazines, conferences, and journals.

02/2002 –
05/2002 **Fairchild Dornier**, Munich, Internship
Inspection and revision of the fire detection system, wiring, and lighting on a Dornier 728 jet. Composition of specifications.

- 10/2001 – **TU München**, Institute of Automatic Control Engineering, Project Work
02/2002 Topic: '*Multi-Fingered Haptic Sensing of Surface Textures*'
- 10/2000 – **TU München**, Institute of Automatic Control Engineering
12/2000 Student Assistant. Collaboration in the development of a tactile actuator for sensing virtual surfaces.
- 03/2000 – **Siemens**, Munich, Working Student
04/2000 Optimization of three-dimensional image capturing with a CMOS row-sensor.

Publications

1. S. Berger and A. Wittneben, “**Comparison of Channel Estimation Protocols for Coherent AF Relaying Networks in the Presence of Additive Noise and LO Phase Noise**”, EURASIP Journal on Wireless Communications and Networking, 2010.
2. S. Berger and A. Wittneben, “**Impact of Local-Oscillator Imperfections on Non-regenerative TDD and FDD Relaying**”, IEEE Vehicular Technology Conference, VTC Spring 2010, Taipei, Mai 2010.
3. S. Berger and A. Wittneben, “**When Do Non-Regenerative Two-Hop Relaying Networks Require a Global Phase Reference?**”, IEEE Global Communications Conference (IEEE Globecom 2009), Dec. 2009.
4. S. Berger, T. Unger, M. Kuhn, A. Klein, and A. Wittneben, “**Recent Advances in Amplify-and-Forward Two-Hop Relaying**”, Communications Magazine, July 2009.
5. S. Berger and A. Wittneben, “**A Coherent Amplify-and-Forward Relaying Demonstrator Without Global Phase Reference**”, IEEE International Symposium on Personal, Indoor and Mobile Radio Communications (PIMRC 08), Sept. 2008.
6. S. Berger and A. Wittneben, “**Impact of Noisy Carrier Phase Synchronization on Linear Amplify-and-Forward Relaying**”, IEEE Global Communications Conference (IEEE Globecom 07), Nov. 2007.
7. S. Berger and A. Wittneben, “**Carrier Phase Synchronization of Multiple Distributed Nodes in a Wireless Network**”, 8th IEEE Workshop on Signal Processing Advances for Wireless Communications (SPAWC), Helsinki, Finland, June 2007.
8. C. Esli, S. Berger, and A. Wittneben, “**Optimizing Zero-Forcing Based Gain Allocation for Wireless Multiuser Networks**”, IEEE International Conference on Communications (ICC 07), pp. 5825 - 5830 , June 2007.
9. M. Kuhn, S. Berger, I. Hammerström, and A. Wittneben, “**Power-Line Enhanced Cooperative Wireless Communications**”, IEEE JSAC Special Issue on Power Line Communication, July 2006.
10. S. Berger and A. Wittneben, “**Cooperative Distributed Multiuser MMSE Relaying in Wireless Ad-Hoc Networks**”, Asilomar Conference on Signals, Systems, and Computers 2005, Pacific Grove, CA, Nov. 2005.
11. I. Hammerström, J. Zhao, S. Berger, and A. Wittneben, “**Experimental Performance Evaluation of Joint Cooperative Diversity and Scheduling**”, IEEE Vehicular Technology Conference, VTC Fall 2005, Dallas, Sept. 2005.
12. S. Berger and A. Wittneben, “**Experimental Performance Evaluation of Multiuser Zero Forcing Relaying in Indoor Scenarios**”, IEEE Vehicular Technology Conference, VTC Spring 2005, May 2005.
13. M. Joham, R. Irmer, S. Berger, G. Fettweis, and W. Utschick, “**Linear Precoding Approaches for the TDD DS-CDMA Downlink**”, in Proc. WPMC’03, vol. 3, pp. 323–327, October 2003.